

Development of a Technology for Arranged Electrofusion of Mammalian Cells:
Applicability in Breast Cancer Immunotherapy

Dissertation

zur

Erlangung des Doktorgrades (Dr. rer. nat.)

der

Technischen Fakultät

der

Universität Bielefeld

vorgelegt von

Janina Schaper

aus

Bremen

Bielefeld, July 2007

Angefertigt mit Genehmigung der Technischen Fakultät
der Universität Bielefeld.

1. Referent: Prof. Dr. T. Noll
2. Referent: Prof. Dr. C. Wandrey

Tag der Promotion: 17.12.2007

In order to make an apple pie from scratch, you must first create the universe.

Carl Sagan

Acknowledgment

I'd like to thank ...

- Prof. Dr. Christian Wandrey für die paradiesischen Arbeitsbedingungen in seinem Institut und die Übernahme des Co-Referats.
- Prof. Dr. Thomas Noll für die Idee zu meiner Doktorarbeit, die Möglichkeit an einem EU-Projekt teilzunehmen und die stets offene Tür seines Büros.
- Dr. Ulrich Krühne and Dr. Leif Højslet Christensen for the brief introduction in microfluidics during my two weeks in Copenhagen and their sympathetic ears for every question concerning this topic.
- Dr. David C. Cullen for the excellent cooperation and the great support during my time in Cranfield.
- Derek Bernard Annan and Ángel Medina Vayá for a great time in Cranfield.
- Nadine Körfer, Bianca Klein und Ruth Essers für die vielen helfenden Hände und die gute Atmosphäre im Labor.
- Daniela Lowis und Björn Christians für ihr Engagement während ihrer Diplomarbeiten.
- Allen Blutspendern.
- Der ganzen Zellyfamily im Besonderen Angela Magin und Ralf Herbold für ihre Unterstützung und den Spaß in Jülich.
- Meinen Eltern für die Unterstützung während meines Studiums und den Glauben an mich.
- Ein besonderer Dank geht an Dich, Hermann. Du hast mir in jeder nur erdenklichen Weise geholfen, mit Deiner Geduld, Liebe und Deinem unverbesserlichen Optimismus.

Parts of this thesis were published previously:

- *Schaper, J.*, Bohnenkamp, H.R. and Noll, T. (2004) Microfluidics and micropatterned immobilization as a tool for improved electrofusion of dendritic cells with tumour cells. *J Immunother* 27, p30.
- *Schaper, J.*, Noll, T., Merkel, R., Offenhäusser, A., Mourzina, J. and Lowis, D. (2005) Verfahren und Vorrichtung zur Elektrofusionierung von Zellen. Patent, Deutsches Patent- und Markenamt, DE 103 59 189.
- *Schaper, J.*, Noll, T., Hubbuch, J. and Offenhäusser, A. (2005) Verfahren und Vorrichtung zur Elektrofusionierung von Zellen. Offenlegungsschrift, Deutsches Patent- und Markenamt, DE 103 59 190.
- *Schaper, J.*, Bohnenkamp, H.R. and Noll, T. (2007) New electrofusion devices for the improved generation of dendritic cell-tumour cell hybrids. *Cell technology for cell products*, ESACT Proceedings , Vol. 3 (SBN: 978-1-4020-5475-4) Springer, Dordrecht, The Netherlands, p207-216.

Poster

- *Schaper, J.*, Bohnenkamp, H.R. and Noll, T. (2005) Microfluidic upgraded electrofusion devices for mammalian cell fusion. Gordon research conference on the physics and chemistry of microfluidics, August 2005, Oxford, UK.

Lecture

- *Schaper, J., Bohnenkamp, H.R. and Noll, T. (2005) New electrofusion devices for the improved generation of dendritic cell-tumour cell hybrids. ESACT - European Society for Animal Cell Technology, Cell Technology for Cell Products, June 2005, Harrogate, UK.*
- *Schaper, J. and Noll, T. (2006) Microfluidic upgraded electrofusion devices for mammalian cell fusion. Jahrestagung "Mikrosysteme für die Biotechnologie", June 2006, Bremen, Germany.*

Abbreviations

Ab	<i>Antibody</i>	ELISA	<i>Enzyme linked immunosorbent assay</i>
a.c.	<i>Alternating current</i>	ER	<i>Endoplasmatic reticulum</i>
AICD	<i>Activation-induced cell death</i>	Eu	<i>Euler number</i>
APC	<i>Antigen presenting cell</i>	FACS	<i>Fluorescence activated cell sorter</i>
APTES	<i>3-aminopropyltriethoxysilane</i>	FCS	<i>Fetal calf serum</i>
ATCC	<i>American type culture collection</i>	FITC	<i>Fluorescein isothiocyanate</i>
AV	<i>Annexin V</i>	FNAB	<i>1-fluoro-2-nitro-4-azidobenzene</i>
BSA	<i>Bovine serum albumin</i>	Fr	<i>Froude number</i>
CAD	<i>Computer aided design</i>	FSC	<i>Forward scatter</i>
CD	<i>Clusters of differentiation</i>	GMBS	<i>N-gamma-maleimidobutyryloxy succinimide ester</i>
CFD	<i>Computational Fluid Dynamics</i>	GM-CSF	<i>Granulocyte macrophage-colony stimulating factor</i>
CLIP	<i>Class II-associated invariant chain peptide</i>	GMP	<i>Good manufacturing practice</i>
CTL	<i>Cytotoxic T-cell</i>	h	<i>Hour</i>
d	<i>Days</i>	HF	<i>Hydrofluorid acid</i>
d.c.	<i>Direct current</i>	HPLC	<i>High performance liquid chromatography</i>
DC	<i>Dendritic cell</i>	ID	<i>Inner diameter</i>
DEP	<i>Dielectrophoresis</i>	iDC	<i>Immature dendritic cell</i>
DMSO	<i>Dimethyl sulfoxide</i>	IFN- γ	<i>Interferon-gamma</i>
DNA	<i>Deoxyribonucleic acid</i>	Ig	<i>Immunoglobulin</i>
EDC	<i>1-ethyl-3-(3-dimethylaminopropyl) carbodiimide hydrochloride</i>		
EDTA	<i>Ethylene diamine tetraacetate</i>		

IL	<i>Interleukin</i>	<i>pattern</i>
IBT-2	<i>Institute of Biotechnology 2</i>	PBMC <i>Peripheral blood mononuclear cell</i>
ISG-2	<i>Institute of Thin Films and Interfaces 2</i>	PBS <i>Phosphate buffered saline</i>
LCA	<i>Leukocyte common antigen</i>	PCR <i>Polymerase chain reaction</i>
LOC	<i>Lab-on-a-chip</i>	PDMS <i>Polydimethylsiloxane</i>
LOR	<i>Lift-off resist</i>	PE <i>R-Phycoerythrin</i>
LTCC	<i>Low temperature co-fired ceramic</i>	PEG <i>Polyethylene glycol</i>
m	<i>Milli</i>	PET <i>Poly(ethylene terephthalat)</i>
μ	<i>Micro</i>	PGE ₂ <i>Prostaglandin E₂</i>
mAb	<i>Monoclonal antibody</i>	PGMEA <i>Propylene glycol monomethyl ether acetate</i>
MACS	<i>Magnetic cell sorter</i>	PI <i>Propidiumiodide</i>
MEMS	<i>Micro electro mechanical systems</i>	PMMA <i>Polymethyl methacrylate</i>
MHC	<i>Major histocompatibility complex</i>	PRR <i>Pattern recognition receptor</i>
MLR	<i>Mixed leukocyte reaction</i>	PS <i>Phosphatidylserine</i>
μ CP	<i>Micro-contact printing</i>	PTFE <i>Polytetrafluorethylene</i>
μ TAS	<i>Micro total analysis system</i>	Re <i>Reynolds number</i>
MST	<i>Microsystems technology</i>	REB <i>Reversible electrical breakdown</i>
MTS	<i>3-mercaptopropyltrimethoxysilane</i>	RNA <i>Ribonucleic acid</i>
MUA	<i>11-mercaptoundecanoic acid</i>	RPMD <i>Rapid micro product development</i>
MUC1	<i>Mucin 1</i>	rhu <i>Recombinant human</i>
n	<i>Nano or number of experiments</i>	SAM <i>Self assembled monolayer</i>
NHS	<i>N-hydroxysuccinimide</i>	SSC <i>Sideward scatter</i>
NMR	<i>Nuclear magnetic resonance</i>	SD <i>Standard deviation</i>
OD	<i>Outer diameter</i>	SDS <i>Sodium dodecyl sulfate</i>
PAGE	<i>Polyacrylamide gel electrophoresis</i>	SEM <i>Scanning electron microscopy</i>
PAMP	<i>Pathogen associated molecular</i>	TAA <i>Tumour associated antigen</i>
		TCR <i>T-cell receptor</i>
		TLR <i>Toll-like receptor</i>
		TNF- α <i>Tumor necrosis factor-alpha</i>

UV *Ultraviolet*

UVO *Ultraviolet/ozone*

WHO *World Health Organisation*

XPS *X-ray photoelectron spectroscopy*

Contents

Abbreviations	VII
1 Introduction	1
1.1 Objectives and Concept	1
2 Theory	5
2.1 Biological Background	5
2.1.1 Cancer	5
2.1.2 Breast Carcinoma	6
2.1.3 New Approaches – Targeted Cancer Treatment	7
2.1.4 The Immune System	7
2.1.5 Cancer Immunotherapy	12
2.1.6 Dendritic Cell-based Vaccines	13
2.1.7 Fusion Vaccines	14
2.1.8 Electrofusion	18
2.2 Microtechnological Background	23
2.2.1 Microsystems Technology	23
2.2.2 Microfluidics	23
2.2.3 Fluid Mechanics in the Micro Scale	24
3 Results	31
3.1 Immobilisation	38
3.1.1 Concept	38
3.1.2 Covalent Immobilisation of Antibodies	40
3.1.3 Softlithography	45
3.1.4 Optimisation of the Immobilisation Reaction for the Printing Process	57

3.1.5	Cell Binding	67
3.1.6	Cell Detachment	73
3.1.7	Electrode Integration and Chamber Assembly	76
3.1.8	New Surface Chemistry According to Design	86
3.2	Microfluidics	94
3.2.1	Concept	94
3.2.2	Geometric Definition of Microfluidic Fusion Devices	97
3.2.3	Model Based Optimisation	100
3.2.4	Fabrication of the Microstructures	115
3.2.5	Assembly of the Microchambers	124
3.2.6	Design and Assembly of the Pump Station	131
3.2.7	Validation	138
3.2.8	Redesign of the Microfluidic Chamber	149
3.2.9	Electrode Integration	165
3.3	Electrofusion	185
3.3.1	Fusion Parameters	186
3.3.2	Fusion	197
3.4	Immunological Evaluation	204
4	Patent Application	211
5	Discussion	235
5.1	Immobilisation	236
5.2	Microfluidics	238
5.3	Comparison: Immobilisation and Microfluidic Approach	241
5.4	Electrofusion	242
5.5	Immunological Evaluation	248
6	Summary & Outlook	251
7	Material and Methods	255
7.1	Immobilisation	255
7.1.1	Mask Preparation	255
7.1.2	Master Preparation	255

7.1.3	PDMS Stamp Preparation	256
7.1.4	Microcontact Printing	257
7.1.5	Inverse Microcontact Printing	257
7.1.6	Immobilisation Reaction	257
7.1.7	Ellipsometry	259
7.1.8	Lift-off Photoresist Processing and Metal Coating	259
7.1.9	Laser Processing	260
7.1.10	Immobilisation of Antibodies on Gold	261
7.1.11	XPS	262
7.2	Microfluidics	262
7.2.1	Fluid Simulation	262
7.2.2	UV Laser Micromachining	262
7.2.3	Assembly and Operation of Pump Station	263
7.3	Fusion	268
7.4	Immunological Methods	269
7.4.1	Mixed Leukocyte Reaction	269
7.4.2	Generation of lysate from MCF-7 breast carcinoma cells	270
7.4.3	Autologous T-cell Expansion Assay	271
7.5	Cell Culture and Cell Analysis	272
7.5.1	Cultivation of Human Tumour Cell Lines	272
7.5.2	Cell Counting and Viability	272
7.5.3	Ex Vivo Generation of Dendritic Cells	273
7.5.4	Cryo Storage of Cells	274
7.5.5	FACS	275
7.5.6	Apoptosis Analysis	275
7.5.7	Intracellular Staining of Mammalian Cells	277
7.6	Microscopic Methods	277
7.6.1	Scanning Electron Microscopy (SEM)	277
7.7	Solutions	278

A Pump/Valve Operation Programmes**List of Figures**

XIV

CONTENTS

List of Tables

XL

Bibliography

XLI

Chapter 1

Introduction

Hybrids of two different cell types, so-called heterologous hybrids, are of particular interest for a number of applications such as hybridoma cell lines for the production of monoclonal antibodies (KÖHLER AND MILSTEIN, 1975), somatic cell hybrids for the generation of gene databases (adapted from gene localisation experiments on chromosomes) and oocyte-skin cell fusions for the creation of human embryonic stem cells (COWAN ET AL., 2005). In recent years, besides several implementations of hybrid technologies for research purposes, also another potential use has emerged. Hybrids of antigen presenting cells (especially dendritic cells) and tumour cells may be used in cancer immunotherapy, since the initiation of anti-tumour immune responses from such hybrids has been suggested (GALEA-LAURI ET AL., 2002). However, the processes for generating heterologous hybrids by chemically induced fusion or by electrofusion are inefficient, thus severely limiting the clinical application of this technology.

1.1 Objectives and Concept

The research presented in this thesis was completed as part of a project funded by the European Commission as a component of the 5th framework programme (Project QLK3-2002-01980, <http://www.fz-juelich.de/ibt/cancer-immunotherapy>). Its research consortium is investigating the "Development of an immunotherapy for breast cancer based on dendritic cells by developing and comparing different types of tumor-specific immunogens (cancer immunotherapy)". This includes the design and constitution of new, and the improvement of existing strategies for enhanced antigen presentation by dendritic cells. In this context, the work is intended to discover dendritic cell-tumour cell hybrids and their application for breast cancer immunotherapy. The

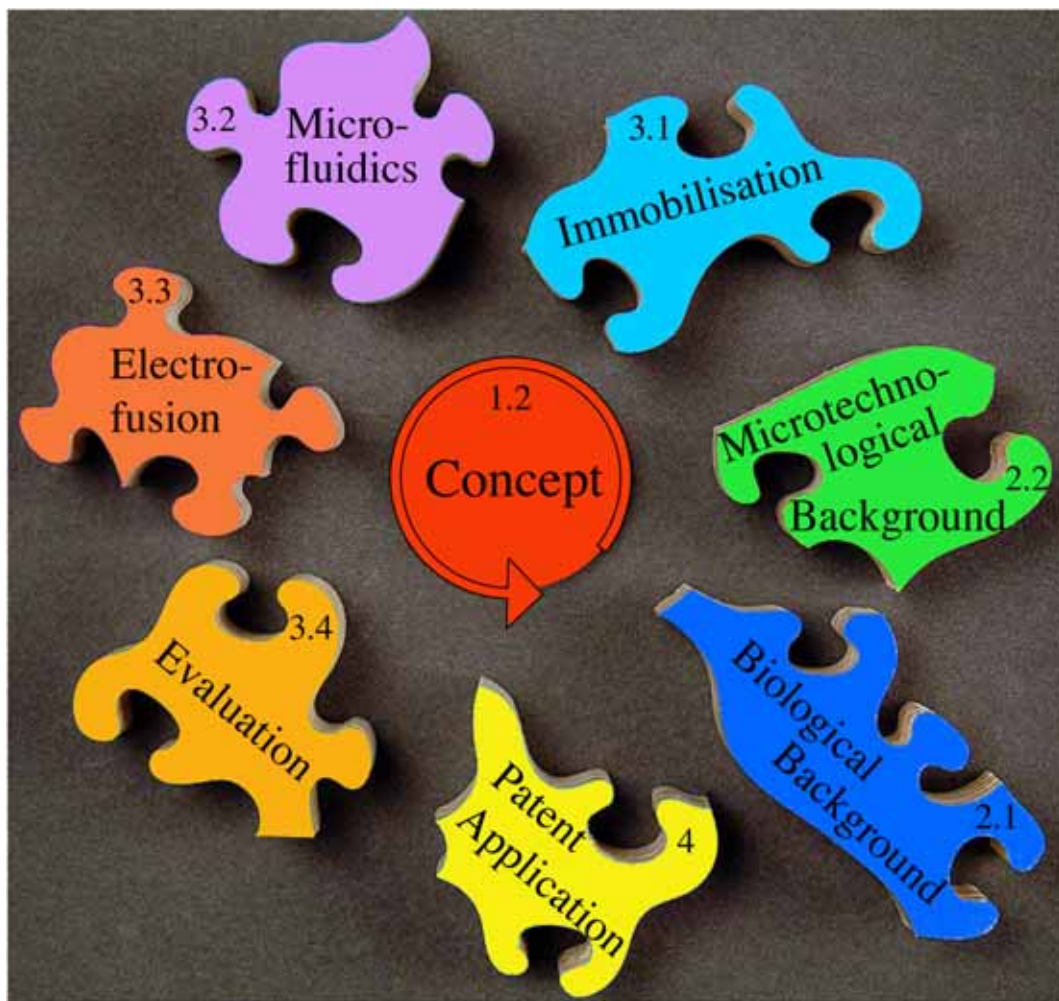


Figure 1.1: The concept of this thesis

goals of this thesis have been specified as follows:

- Process development of an optimised fusion for the generation of large numbers of viable hybrids
- Investigation of all relevant fusion parameters, addressing technical and biological problems of generating heterologous hybrids, *e.g.* development of a new fusion device
- Application of the process to dendritic cell-tumour cell fusions, thus delivering whole tumour cell information to dendritic cells
- Evaluation of the *in vitro* immune stimulatory capacity of the generated hybrids

Figure 1.1 illustrates the structure of this thesis. The theoretical background is divided into two parts, the biological and the microtechnological background in chapter 2, section 2.1 on

page 5 and section 2.2 on page 23, respectively. The former gives the reader an understanding of the nature of cancer, the immune system and the background to cancer immunotherapy, cancer vaccines and fusion vaccines in particular. The latter introduces technologies available for the development of new fusion devices. Subsequently, in chapter 3 the results are presented, structured into four sections, dealing with the development of two new fusion chambers based either on immobilisation (see section 3.1 on page 38) or microfluidics (see section 3.2 on page 94), the fusion process itself (see section 3.3 on page 185) and the immunological evaluation of the fusion products in section 3.4 on page 204.

Chapter 2

Theory

2.1 Biological Background

2.1.1 Cancer

Cancer represents a group of diseases in which the patient suffers from uncontrolled growth of abnormal cells. Normally, the division of cells take place in an orderly and controlled manner. If, for some reason, this process gets out of control, the cells will continue to divide and can accumulate in one place in the form of a tumour. Tumours can be either benign or malignant. The prefix "benign" means that the tumour cells cannot invade the normal tissue and do not spread to other parts of the body and so are not cancerous. If they continue to grow at the original site, however, they may cause a problem by pressing on the surrounding organs and damage them. A malignant tumour consists of cancer cells, which, if left untreated, may invade and destroy the surrounding tissue. Sometimes cells break away from the primary cancer and spread through the bloodstream or lymphatic system beyond the original sites to other organs in the body. When these cells reach a new site they may go on dividing and form a new tumour, often referred to as a secondary tumour or metastasis.

Numerous mutations in the genes of normal somatic cells can cause malignant proliferation in a multistage process. During carcinogenesis, mutations sequentially and collectively promote deviation from normal growth constraints and contribute to evasions of apoptosis (programmed cell death), genomic instability, tissue invasion, angiogenesis (growth of new blood vessels) and metastasis - all of which have implications for tumour formation.

As a cause of death in developed countries, cancer is second to cardiovascular disease,

with an overall cause of 13 % of all deaths in the world in 2005. While cardiovascular disease has declined, cancer deaths have remained relatively constant since 1950. Each year cancer is diagnosed in 9 million people worldwide. It causes 7.6 million deaths, which means that approximately 21,000 people die of cancer each day (FROM WORLD HEALTH ORGANISATION (WHO) STATISTICS).

2.1.2 Breast Carcinoma

Breast carcinoma (cancer in breast epithelium) is by far the most common cancer in women accounting for more than 25 % of all cancer cases. Earlier detection and better treatment helped driving down breast cancer death rates in the last few years. Most breast cancer patients now live for at least ten years after their diagnosis (FROM WHO STATISTICS).

The female breast consists mainly of milk producing epithelial glands, called lobules, of epithelial ducts and stroma. The ducts are tubes that carry the milk from the lobules to the nipples, while the stroma surrounds the ducts and lobules with fatty tissue. Carcinomas arise in epithelial cells. For breast cancer, about 80 % of cancers originate in the mammary ducts (ductal cancer), while about 20 % arise in the lobules (lobular cancers).

Two major genes, BRCA1 and BRCA2 have been associated with the susceptibility to breast cancer. Mutations in these genes affect the activity of the molecular repair kit for DNA in normal cells and result in a lifetime risk of breast cancer of between 60 and 85 percent. However, only about 5 % of all breast cancers are due to this inherited gene mutations. In the far more common nonfamilial cancer, the gene mutations are induced environmentally (WOOSTER AND WEBER, 2003).

Early detection of breast cancer is crucial. Treatment is far more likely to be successful at early stages of the disease before the tumour has had a chance to metastasise.

Treatment of Breast Cancer

Each women's treatment will be slightly different, depending on many factors such as the patient's age and the type, side and spread of the cancer. Most patients will have surgery to remove the tumour from the breast. This may be followed by radiotherapy and/or chemotherapy to kill cancer cells that might be left in the breast or surrounding areas after surgery or have spread from the breast. They can also be used before surgery, in women with large tumours, to shrink the tumour so that breast conserving surgery becomes possible. Despite its successes,

chemotherapy and radiotherapy will affect all of the patient's dividing cells, whether cancerous or not, causing weakening the patient's immune defence as well as other severe side effects both in the short term and later in life (LÓPEZ ET AL., 2005; POOLE ET AL., 2006).

Many women will also have hormone therapy using drugs such as Tamoxifen or Arimidex, since some breast cancers require the hormone oestrogen for their continued development and, if deprived of the hormone, will stop growing. Tamoxifen prevents the growth-promoting action of oestrogen on breast cells by blocking the oestrogen receptor, while Arimidex, an aromatase inhibitor, shuts down the production of oestrogen. One problem of hormone treatment is that it is only effective in a proportion of patients with tumours expressing the oestrogen receptor and, even in these, a resistant form of the disease can appear in time.

Trastuzumab (Herceptin), a humanised monoclonal antibody to the protein HER2/neu is another possible treatment (PICCART-GEBHART ET AL., 2005). It can only be used in 20-25 % of breast cancer patients, whose cancer cells are HER2/neu positive and express high levels of HER2/neu on their surface. One major risk linked to Trastuzumab is congestive heart failure (3-4 % of patients).

Altogether, a problem with many current breast cancer treatments is the occurrence of severe side effects, resistance to the used drugs and the lack of long-term protection against recurrences.

2.1.3 New Approaches – Targeted Cancer Treatment

Recent approaches in the treatment of cancer use the body's immune system, in particular immune cells for fighting the disease. Cell-based immunotherapies are thought to stimulate and activate the patient's natural immune response to eliminate cancer cells, inhibit metastasis and prevent tumour recurrence. In contrast, with traditional nonselective cancer treatments, immunotherapy targets specific molecular lesions within tumour cells and thus has the advantage of avoiding toxic side effects. Immunotherapy might soon be called the fourth leg of cancer treatment, squaring the triad of surgery, radiation and chemotherapy.

2.1.4 The Immune System

The immune system is very complex and consists of a number of components. It protects the body against pathogens such as bacteria, viruses and parasites and also attacks other foreign

entities. Therefore, the immune system has to distinguish self from nonself or foreign to mount a destructive immune response against foreign, but not against self.

In general, the immune system can be divided into innate and adaptive immunity. The innate immunity represents the first line of defence, which is triggered immediately or within several hours of encountering invaders. Conserved molecular patterns (*i.e.* pathogen-associated molecular patterns (PAMPs)), which are shared by a large group of microorganisms, are recognised by pattern-recognition receptors (PRRs) (*e.g.* Toll-like receptors (TLRs), C-type lectins) and launch the innate immune response. The innate immunity can be seen as a relatively specific first line response to evolutionary conserved molecular structures and has the purpose to confine the pathogen infection (LUSTER, 2002).

In contrast, the adaptive immunity is directed against unknown, differentiated or mutated proteins and unconserved structures of viruses, bacteria and other parasites. This adaptive immune response is mediated by lymphocytes such as T- and B-cells. They are named after their place of maturation, which is the thymus (T-cells) or the bone marrow (B-cells). The initiation of an adaptive immune response requires the recognition and binding of lymphocytes to very specific molecular sequences called antigens, which are small parts of proteins. Every nucleated cell of the body processes endogenous proteins to small fragments (antigens) and displays them bound to specific presenting proteins called Major Histocompatibility Complex class I (MHC I) on their surface. When for example a virus infects a cell, it takes over the cells protein manufacturing equipment to make viral proteins, which are assembled to new viruses. One of the defence mechanisms of the body is that the infected cell presents fragments of these viral proteins bound to MHC class I on its surface, where it can be recognised by cells of the immune system. The same applies for other intracellular pathogens. Their proteins are reduced to peptides by proteasomes, special protein complexes present in the cellular cytosol that have proteolytic function. Once the parasite proteins have been digested to small peptides, they are transported into the lumen of the endoplasmatic reticulum (ER), where they bind to the MHC class I molecule, which is being fold in the ER. The MHC class I peptide complex is then transported to the surface via the classical secretory pathway (JANEWAY ET AL., 2005).

Extracellular antigens derived from extracellular parasites like bacteria are processed through a different pathway, which combines the internalisation of extracellular antigen with the exocytosis of MHC class II molecules. Antigens are captured and internalised by antigen-presenting cells (APC). Soluble extracellular molecules are engulfed through endocytosis, bac-

terial particles and dead cells through phagocytosis, and localised to intracellular vesicles derived from the plasma membrane and are subsequently digested by proteolytic enzymes (BELZ ET AL., 2004). The MHC class II molecule is like MHC I assembled in the endoplasmatic reticulum, but their loading with the endogenous antigens present in the ER is prevented by invariant chain/CLIP (class II-associated invariant chain peptide), which occupies the binding groove of MHC II. Histocompatibility Complexes class II (MHC II) are then diverted from the classical secretory pathway into the endosomal/lysosomal system, where they fuse with vesicles containing internalised antigens. Subsequently, the release of CLIP is catalysed and exogenous antigens can bind the MHC II in a competitive displacement reaction. Thus, the role of the MHC II molecules is preserved for presentation of exogenous antigens (JANEWAY ET AL., 2005).

MHC class I:antigen complexes are recognised by cytotoxic CD8⁺ T-cells (CTLs), while the MHC class II:antigen complex activates CD4⁺ T helper cells. This two T-cell types can be distinguished by the presence of one of two leukocyte differentiation antigens or cluster of differentiation (CD), CD8 or CD4.

The primary adaptive immune response takes place in the draining lymph nodes and not in the tissue itself. Antigen is picked up by dendritic cells in the tissue and carried into regional lymph nodes.

Dendritic Cells

Dendritic cells (DCs) are often referred to as the sentinels of the immune system or the most potent antigen presenting cells (APCs) for the initiation and modulation of antigen-specific immune responses. In addition to their ability to efficiently acquire and process antigens, they express high level of both class I and class II MHC molecules as well as co-stimulatory molecules essential in antigen-presentation (SHORTMAN AND LIU, 2002).

DCs derive from bone marrow stem cells and exist in two activation stages, as immature and mature dendritic cell. The function of a DC is highly influenced by its level of maturation. Immature dendritic cells are found in nearly all tissues, especially in the skin and the mucosal surfaces. They are recruited to sites of inflammation caused by pathogens in peripheral tissues by TLR-mediated events. There, they are activated by innate stimuli and loaded with foreign antigen, which they internalise via pinocytosis or receptor-mediated endocytosis. After antigen uptake and processing, the immature dendritic cell differentiates into a mature DC, induced

by a danger signal (PAMP) such as bacterial cell wall components. During maturation the dendritic cell converts from an immature, antigen-capturing cell to a mature antigen presenting cell, expressing co-stimulatory molecules and becoming a potent stimulator of T-cells. Thus, DCs translate and integrate innate signals into adaptive immunity (REIS E SOUSA, 2004).

Furthermore, the innate immune stimuli (TLR activation) set in motion the expression of chemokines from resident tissue macrophages and dendritic cells, which modulates the expression of chemokine receptors on dendritic cells. These changes in chemokine and chemokine receptor expression trigger the migration of the antigen-loaded DCs from the tissue to secondary lymphoid organs (*e.g.* regional lymph nodes)(see figure 2.1).

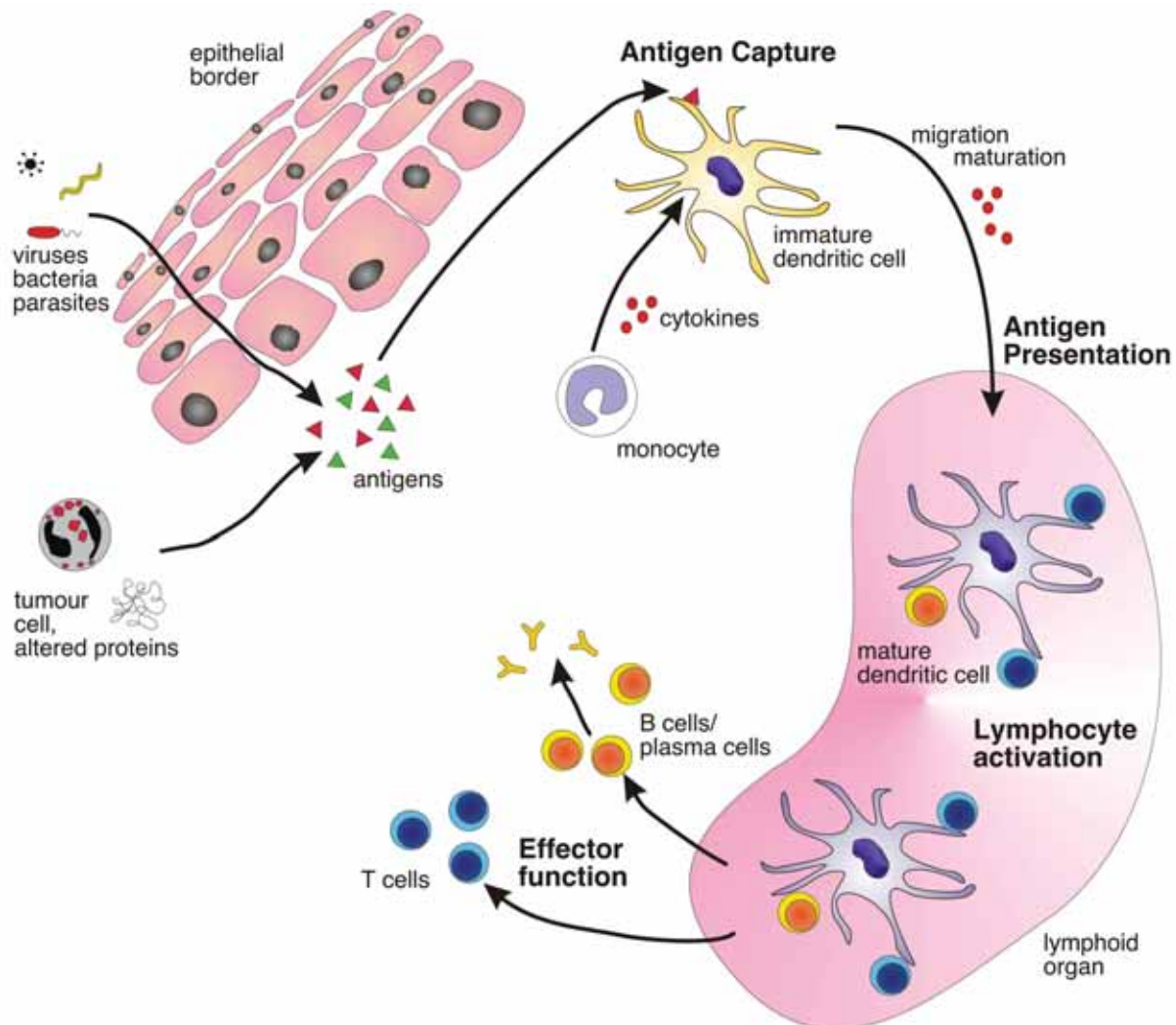


Figure 2.1: Dendritic cell life cycle: In tissue resident dendritic cells take up antigens and migrate towards lymphoid organs. During this time they get matured and are then able to activate T-cells in the lymph nodes to launch an effective immune response.

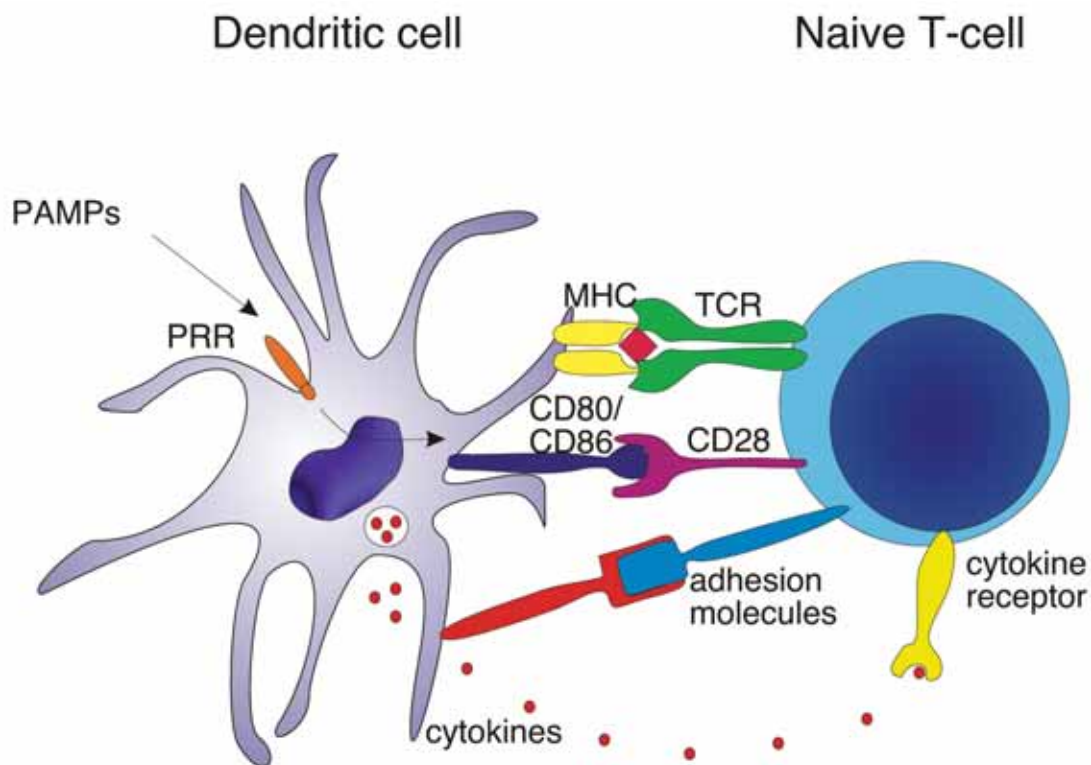


Figure 2.2: T-cell stimulation requires three dendritic cell-derived signals: MHC/TCR interaction, a co-stimulatory signal via CD28 and a signal via the cytokine receptor.

In the regional lymph nodes, the mature antigen-loaded dendritic cell activates naïve T-cells, triggering several effector pathways, including activation of B-cells and antibody production, activation of CD8⁺ cytotoxic T lymphocytes and stimulation of cytokine production by CD4⁺ T helper cells to initiate an effective, adaptive immune response.

The signals that lead to T-cell activation (see figure 2.2) are generated by the physical contact between dendritic cells and T-cells by forming an immunological synapse, which is stabilised by adhesion molecules (HUPPA AND DAVIS, 2003). The first signal is received through the T-cell receptor (TCR) after it recognises antigenic peptides displayed by MHC molecules on the surface of DCs. The consequence is an upregulation of the expression of co-stimulatory molecules. The second signal is provided by plasma membrane bound co-stimulatory molecules such as CD80 and CD86, which are present on the antigen-presenting cell and are recognised by a co-receptor on the cell surface of T-cells, called CD28 (ACUTO AND MICHEL, 2003). The receipt of the second signal results in the production and secretion of cytokines and expression of cytokine receptors on T-cells. The third signal is then provided by the secretion of cytokines,

whose nature defines the type of the activated T-cell.

The activation process is completed by proliferation and evolving of T-cells to effector cells (LANZAVECCHIA AND SALLUSTO, 2001). Helper T-cells are activated to proliferate and to secrete a variety of interleukins, supporting antibody production by activated B-cells (plasma cell) and cytotoxic T-cell responses. Target cells that carry the same class I MHC molecule and the same antigen that originally induced CTL activation are killed by activated CTLs by induction of apoptosis. Not only endogenous antigens can be presented via MHC I by dendritic cells, but also exogenous antigens by so-called cross-presentation. This unique cross-priming capacity of dendritic cells was shown to be indispensable for induction of CTL responses against viruses that do not infect dendritic cells themselves and to maintain self-tolerance against non-DC components (LIZÉE ET AL., 2003).

After activation, T-cells leave the lymph node and find their way back to the site of inflammation, guided by cytokines (BANCHEREAU AND STEINMAN, 1998).

2.1.5 Cancer Immunotherapy

Immunotherapy involving recruitment of the patient's immune system has been shown to be an alternative or addition to conventional treatments targeting tumour cells with far greater precision resulting in fewer side effects. In general, cancer vaccines are not used to induce prophylactic immunity, but to act on an existing disease, *e.g.* the tumour. However, immunisations of patients bearing established tumours have often been ineffective since the tumour may have already elicited an immune suppressive response. Thus, prior to immunotherapy, it had been necessary to reduce the tumour mass. The first clinical trials on cancer immunotherapy have indicated this form of treatment as feasible and safe. Furthermore, in some cases, objective clinical responses were observed, even in patients heavily pretreated with standard chemo- or radiotherapy approaches (BREMERS AND PARMIANI, 2000).

The target for cancer immunotherapy are tumour antigens. They can be either tumour-specific, meaning they are exclusively expressed on tumour cells, as in the case of viral antigens and mutated gene products, or tumour-associated. Tumour-associated antigens (TAA) are also expressed to a certain degree on normal tissue, but overexpressed in the tumour cells. The immune system can recognise those tumour antigens and even eliminate early stage transformed cells. One evidence of such an immune surveillance is the fact that patients with drug-induced immunosuppression after organ transplantation or due to severe immunodeficiency syndromes

develop a higher frequency of several tumours. All those tumours are virally induced, but this does not mean, that other cancer types are not under the control of immunity. The latter is proved by lymphocyte infiltration into tumours (PARDOLL, 2003).

However, most progressed human tumours are capable of evading the host immune system. They can downregulate the expression of co-stimulatory signals that are essential for T-cell activation. Presentation of antigens in the absence of co-stimulatory signals or signals that accompany tissue destruction and inflammation may lead to immunologic tolerance instead of cytotoxicity because of ignorance, anergy or physical depletion. Other immune escape mechanisms of tumours are known such as generation of a tumour microenvironment by local release of inhibitor factors, *e.g.* inhibiting maturation and migration of dendritic cells. Thus, the primary aim of cancer vaccines is to overcome immune suppression, circumvent the immune escape mechanisms of the tumour and break tolerance to the tumour (GUNZER ET AL., 2001).

In the 1890s, Coley treated cancer patients with bacterial extracts of streptococcal cultures that boosted non-specifically the general function of the immune system. Nowadays, more specific ways are used and the immune system is activated by optimising the presentation of antigens by vaccination. Since the most effective antigen presentation to a naïve immune systems occurs through antigen presenting cells, dendritic cells are the cells of choice (ARMSTRONG ET AL., 2001).

2.1.6 Dendritic Cell-based Vaccines

Dendritic cells express elevated levels of the important co-stimulatory molecules, which tumour cells lack. They can attract and recruit T-cells by chemokines and efficiently stimulate them. DCs loaded with tumour-associated antigens (TAAs) can induce immunity to tumours as shown by successful tumour vaccinations in several animal models. Studies in humans have also shown the capacity of TAA loaded DCs to prime effective antitumour immune responses. In addition, it was shown that tumour-specific CD8⁺ cytotoxic T lymphocytes (CTL) and their tumourlytic action constitute an important arm of the antitumour response (BOCCHIA ET AL., 2000).

In cancer, however, dendritic cells, although capable of efficient tumour antigen processing, may be unable to stimulate T-cells successfully, because of factors secreted by the tumour, which inhibit the maturation and migration of DCs, or the lack of a danger signal. These problems can be circumvented by loading the DCs with tumour-associated antigens and their additional activation *in vitro*. The loaded DCs are then reinfused into the patient to generate

an integrated CD4⁺ and CD8⁺ T-cell response.

Thus, DCs are used as efficient vector. As the number of immature precursors of dendritic cells in the circulating blood is very low (< 0.5 percent of all peripheral blood mononuclear cell (PBMCs)), large numbers of dendritic cells for clinical use can be generated, *e.g.* from peripheral blood monocytes. Blood monocytes differentiate *in vitro* in the presence of exogenous cytokines into immature DCs (iDCs). These iDCs possess functional characteristics typical of this differentiation status, such as phagocytosis, macropinocytosis, receptor-mediated endocytosis and antigen-processing (BOHNENKAMP AND NOLL, 2003).

Dendritic cells can then be loaded with the tumour antigens, whereas the antigenic source has to be carefully selected. Just a single tumour-associated antigen can be chosen, or the full profile of antigens expressed by a cancer cell. Nevertheless, one has to keep in mind that the tumour is heterogeneous and its cells can mutate. If a immune response is elicited against only one or a few antigens, some tumour cells can escape immune detection. In addition, for the extension to some cancer types, for which no defined tumour-associated antigens are known, the whole-tumour cell approaches are needed. They have the further potential advantage of generating a broader T-cell response on the basis of the antigens selected by the dendritic cell processing machinery.

Several methods have been devised, for successful loading of MHC molecules on dendritic cells. These methods range from pulsing DCs with peptides (THURNER ET AL., 1999), proteins (HSU ET AL., 1996), cell lysate (KUROKAWA ET AL., 2000) and apoptotic cells (JENNE ET AL., 2000), through fusion with whole tumour cells, transfection with RNA (DÖRFEL ET AL., 2005) or with viral vectors (SONG ET AL., 1997). These numerous methods for tumour antigen delivery to dendritic cells, still need further extensive investigation, addressing technical and biological problems of the loading process. The efficacies of these immunotherapeutic strategies for the loading of dendritic cells have rarely been directly compared (PARAJULI ET AL., 2004).

2.1.7 Fusion Vaccines

One promising way of delivering tumour-associated antigens to dendritic cells is the fusion of a DC with a live tumour cell resulting in a hybrid. In 1997, GONG ET AL. proposed that such fusions of dendritic cells with a murine carcinoma cell line used as a vaccine induced T-cell protective immunity against tumour challenge and immune rejection of established tumours in mice. Therefore, immature dendritic cells are generated from patient's blood monocytes *in*

vitro and fused with autologous tumour cells, which can be obtained from surgery or pleural effusions (see figure 2.3 on page 16). The use of allogeneic tumour cells or even cell lines as well as allogeneic DCs from an unrelated donor is also possible, but reduces the patient specificity of the vaccine (see table 2.1). Thereby, four different combinations are possible: fusion of autologous DCs with autologous tumour cells, autologous DCs with allogeneic tumour cells or allogeneic DCs with autologous tumour cells or selection of both fusion partners from allogeneic origin.

Table 2.1: Impact of autologous versus allogeneic fusion composition on TAA presentation

DC origin	autolog	autolog	allogen	allogen
Tumour origin	autolog	allogen	autolog	allogen
DC MHC	matching	matching	non-matching	non-matching
Tumour MHC	matching	non-matching	matching	non-matching
TAA's	all TAA's from heterologous tumour	some TAA's (if corresponding)	all TAA's from heterologous tumour	some TAA's (if corresponding)
DC function	antigen presentation, supply of co-stimulatory molecules	antigen presentation, supply of co-stimulatory molecules	supply of co-stimulatory molecules, mismatched response	supply of co-stimulatory molecules, mismatched response
Tumour function	TAA presentation and delivery	TAA delivery	TAA presentation and delivery	mismatched response

If allogeneic cells are used, the MHC complexes of either the dendritic cell or the tumour cell or both do not match with the MHC complexes of the patient, due to histocompatibility differences. The name histocompatibility complex was given because originally these proteins were found due to skin transplant rejection of different donors. Usually, different donors have a different set of MHC complexes and are recognised by a transplant recipient as foreign. MHC mismatch results in graft rejection in organ transplantations and in graft-versus-host disease in a bone-marrow transplant. Therefore, the matching of MHC complexes by skin, tissue or organ transplantation is *sine qua non*. Using allogeneic DCs for fusion vaccines results in immune responses to the mismatched MHC complexes rather than in specific immune responses to

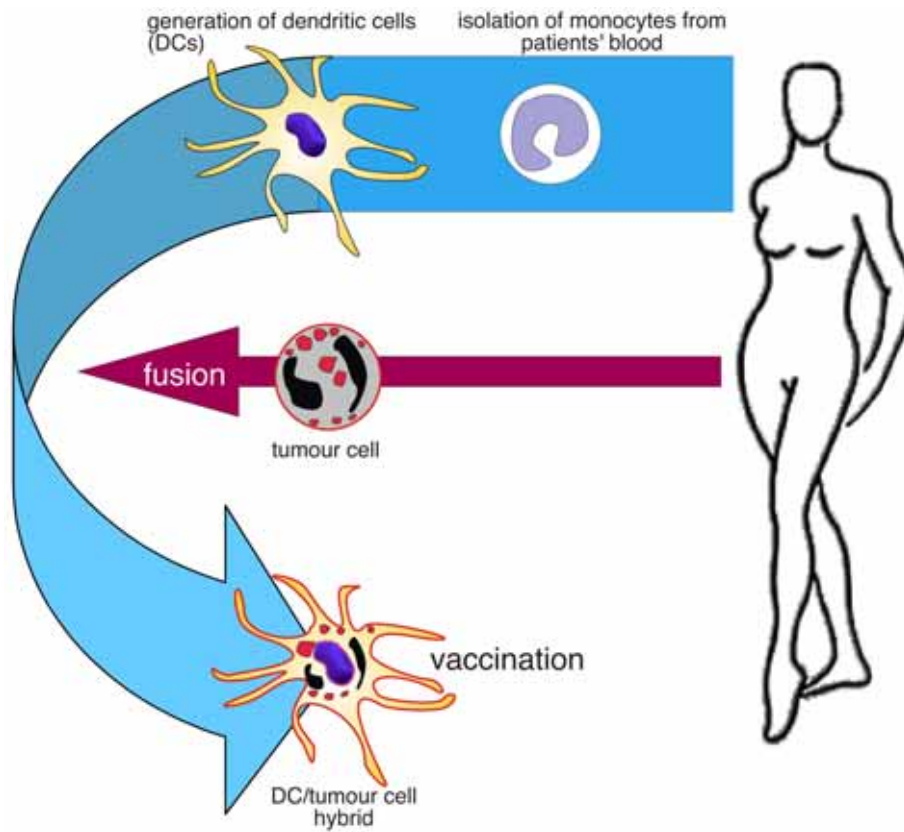


Figure 2.3: Dendritic cell/cancer cell hybrid vaccination strategy

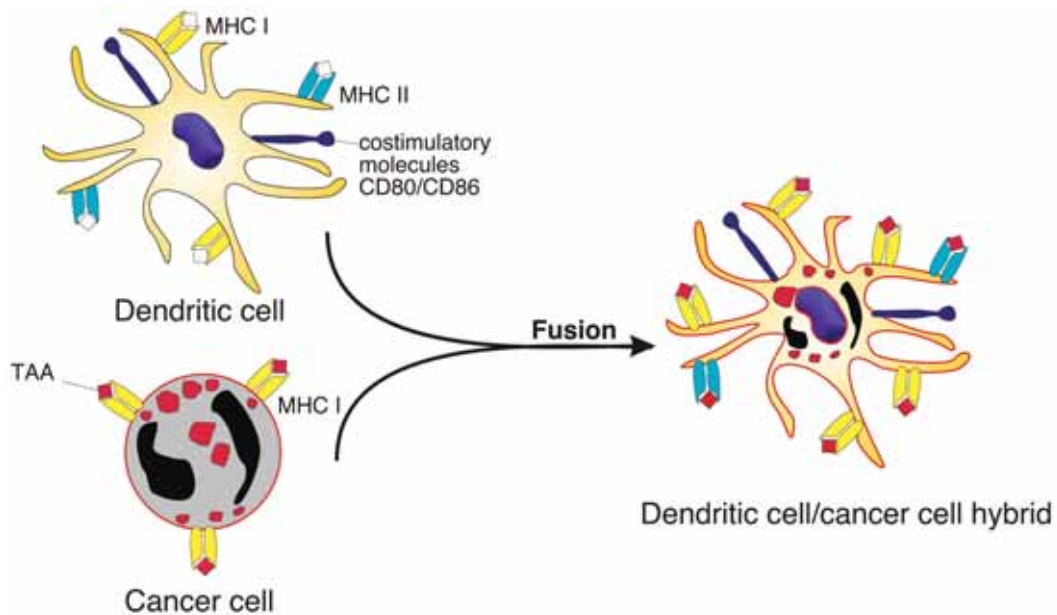


Figure 2.4: Schematic depiction of a hybrid resulting from DC/tumour cell fusion: It is hypothesised that the DC/tumour cell hybrid functions as antigen-presenting cell expressing TAAs on MHC class I and II alongside with co-stimulatory molecules.

tumour-associated antigens and should be avoided.

Cell-cell fusions share one cell membrane and all proteins. Tumour-associated as well as proteins from DC origin are comprised within the hybrid cell. It is assumed that the hybrid still functions as an antigen-presenting cell and the tumour antigens are allowed to be processed and presented as endogenous proteins by the MHC I pathway as well as cross-presented on MHC class II (see figure 2.4). For this reason, hybrids from DC/tumour cell fusions could induce both MHC class I and class II responses (ROSENBLATT ET AL., 2005). Furthermore, on the dendritic cell, TAAs are presented in the context with co-stimulatory molecules. Nevertheless, the DC loading should be followed by maturation to obtain a fully functional antigen presenting cell, which expresses high levels of co-stimulatory molecules and is able to migrate to the lymph nodes, ensuring correct antigen presentation (BARRATT-BOYES AND FIDGOR, 2004).

Several potential advantages distinguish this approach from other DC vaccine strategies. The applicability is not dependent on the identification of tumour-associated antigens (TAAs), but is based on the whole antigenic repertoire of the tumour cells, which can contain a variety of TAAs, including those that are unidentified and those specific to a particular patient. The TAAs are generated endogenously by the fusion cell resulting in a more efficient and stable antigen presentation compared to exogenous loading. In contrast to other whole-tumour cell approaches with endogenous antigen synthesis such as loading of DCs with tumour RNA or DNA, the fusion vaccine has the advantage of comprising all tumour proteins, not only those which were translated or transcribed by the tumour cell at the time of RNA/DNA extraction. However, the main limitation is the available amount of tumour material for vaccine production.

Fusion hybrids can be generated by chemically induced fusion with polyethylene glycol (PEG) or by electrofusion, whereby tumour cells and DCs are subjected to an electrical pulse. Independent from the used method, not more than 10-15 % of heterologous hybrid formation were documented (leaving out the overly optimistic interpretations of data by some authors). A low fusion yield avoids the transfer of this technique to cancer types where only small samples of tumour material are available (*e.g.* breast cancer) or to early stage disease without a significant tumour burden. For a therapeutic setup, multiple vaccinations would be needed for an effective induction of an antitumour immune response. THURNER ET AL. (1999) suggested four vaccinations with 10^7 hybrids each, resulting in a need of $2.6 \cdot 10^8$ tumour cells, if a fusion efficacy of 15 % could be achieved. The dose is based on the percentage of heterologous hybrids. Homologous DC/DC fusions and tumour/tumour cell fusion should not be considered. Never-

theless, homologous hybrids and unfused cells are normally not sorted out, leaving a need for radiation treatment of the vaccine prior to administration, because of the risk of tumour cell proliferation.

2.1.8 Electrofusion

Cell-cell fusion can be induced artificially by subjecting the cells to electric pulses. This process, known as electrofusion, is preferred to chemically induced fusion by polyethylene glycol (PEG). PEG can have toxic side effects and the method is only partly controllable and difficult to standardise (KARSTEN ET AL., 1988).

Electrical field-mediated cell fusion has found application in the formation of hybridomas for monoclonal antibody production and in animal and plant breeding. It is based on electropermeabilisation of the cell membrane achieved by exposure of the cells to a short (micro-to-milliseconds) but intense (hundreds of volts per centimetre) electrical field. The external field induces an increase in transmembrane potential, which in first approximation is proportional to the applied field strength and the cell radius. It is assumed that a membrane destabilisation occurs that is associated with aqueous pore formation, if the transmembrane potential is high enough or rather exceeds a certain threshold (TEISSIÉ AND RAMOS, 1998). In 1958, STAEMPFLI reported for the first time that electrical stimulation of cell membranes can lead to a reversible electrical breakdown of the excitable membrane. Large cells for example are more sensitive to lower electric field strengths than small cells and would not survive a high electrical field pulse.

About 50 years later the basis for pore formation still remains poorly understood. The induced pores have a lifespan in a microsecond time range (GABRIEL AND TEISSIÉ, 1999), which complicates their observation and description. Several models have been proposed, using cell models with simple shapes, which can only describe pore formation as an approximation. Recently, researchers tried to address pore formation on a molecular basis by computer simulations (TIELEMAN, 2004).

Permeabilised cell membranes allow insertion of proteins that are of biological and medical interest. They are introduced through the pores into the cell, by-passing the normally impermeable plasma membrane. When present on two or more cells, the permeabilised membranes allow cell fusion, with spontaneous merging of the two lipid cell membranes into a single continuous membrane bilayer. This associated fusogenicity has been described by ZIMMERMANN in 1982. The efficacy of electropermeabilisation and fusion strongly depends on many parameters.

It can be distinguished between parameters of the electric field such as pulse duration, number of pulses and pulse strength, and biological parameters of the cells such as cell size, shape, transmembrane potential, osmotic pressure and temperature (TEISSIÉ ET AL., 1999). Strict control of electric field parameters allows electropermeabilisation to be reversible.

Electrofusion is a multistep procedure (RAMOS AND TEISSIÉ, 2000). First of all, the cells have to be brought into close contact, before the fusion can take place. Therefore, the forces exerted by non-uniform a.c. electrical fields on cells in liquid media can be harnessed. Cells become polarised in the presence of such an electrical field with high frequency and low intensity (100V per cm). The resulting dipole is due to an ion charge separation inside the cell (see figure 2.5). The dielectrically polarised cells then experience lateral forces in the non-uniform field and move to regions of highest field intensity (see figure 2.6), a process called positive dielectrophoresis (DEP). The magnitude and direction of the dielectrophoretic force are dependent on the electric field, the size of the particles and the electrical properties of the particles relative to those of the surrounding medium (GHALLAB AND BADAWY, 2004). In a uniform field dipoles are also induced in the cells, but the cells do not move, because the forces affecting the cells are the same in both directions. The induced movement in a non-uniform field causes the cells to align at the electrodes, forming strings of cells resembling pearl chains (ZIMMERMANN ET AL., 2000). Thus, a close membrane contact is established by cell alignment through dielectrophoresis prior to fusion.

Secondly, the cells are subjected to one or more short high-voltage d.c. pulses, which cause permeation of the cell membrane and initiate cell fusion. The electrical breakdown of the cell membrane leads to induction of transient membrane pores along the field lines (SUGAR ET AL., 1987). These aqueous pores form in protein-free lipid domains of the membrane, which occurred by lateral movement of membrane proteins in the a.c. field (see figure 2.7). During healing of the membrane, the cell membranes of two cells can form bridges of lipid molecules, leading to the establishment of cytoplasmic continuity and the fusion of the cells. Thereby, all transition states are governed by forces that minimise exposure of non-polar surfaces to water (see figure 2.8).

In the third step, the post-alignment, a weak non-uniform a.c. field (as in step one) is applied for a brief period to hold the cells in place while the fused membranes mature, the fusion products round off and the cytoplasms mix, forming a cell with characteristics of both fusion partners. The fusion maturation includes large rearrangements of the cytoskeleton and

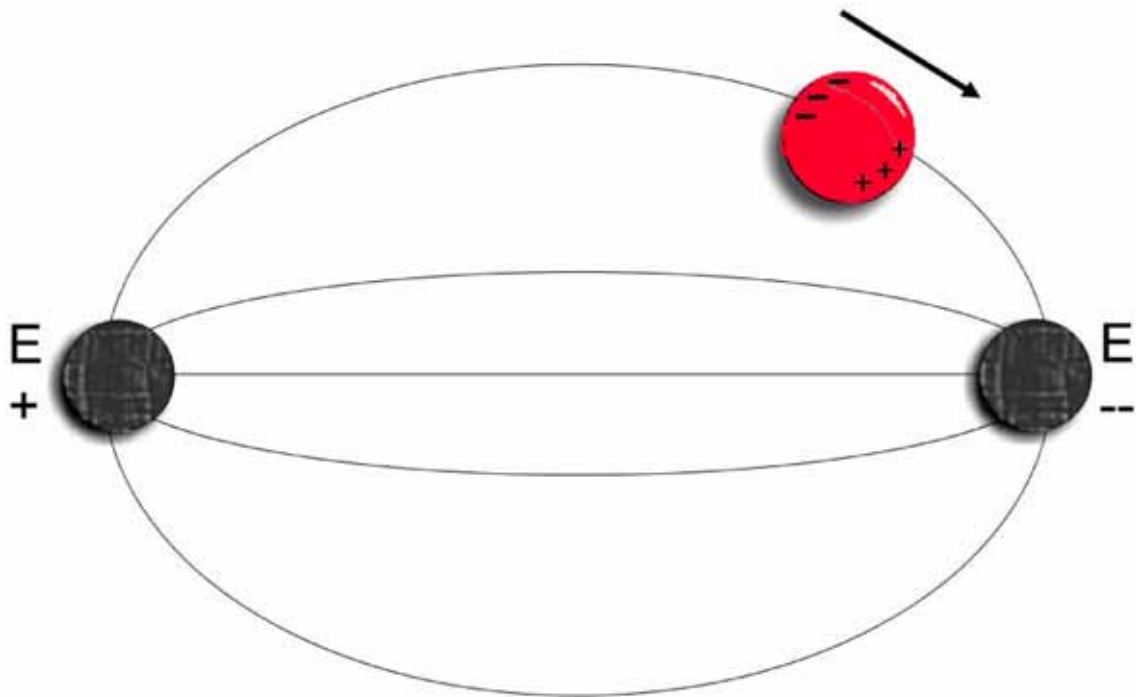


Figure 2.5: Schematic representation of an inhomogeneous electrical field between electrodes E^+ and E^- that induces a dipole in a cell.

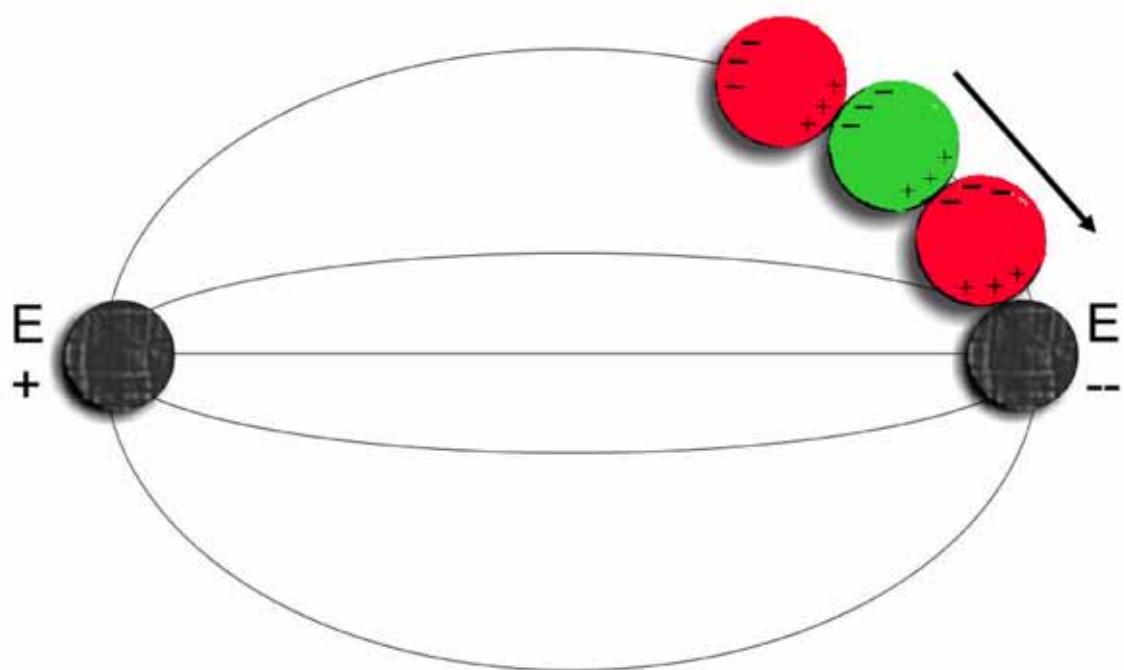


Figure 2.6: Cells in an inhomogeneous electrical field line up in pearl chains at the electrodes by dielectrophoresis

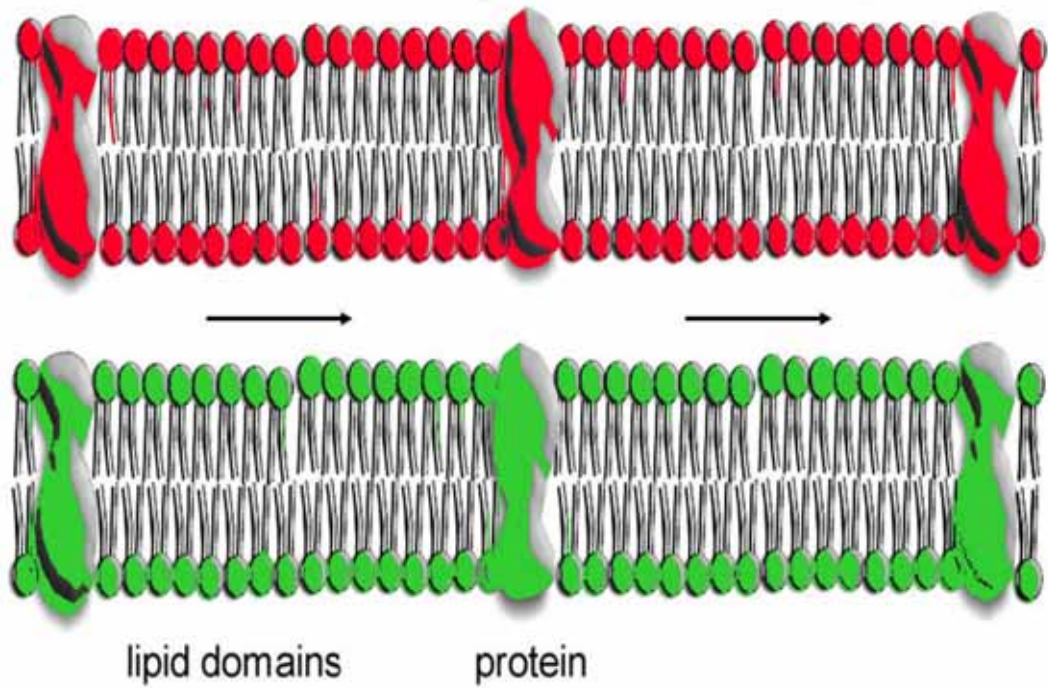


Figure 2.7: Schematic representation of two cell membranes (red and green)

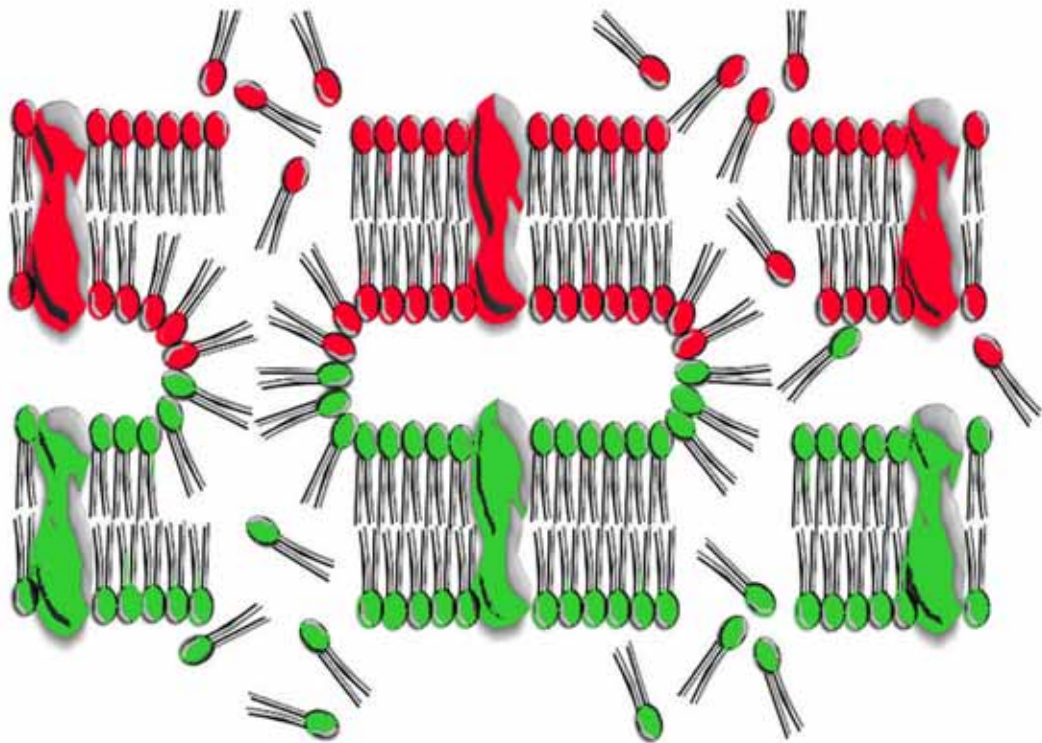


Figure 2.8: Schematic representation of the electrical breakdown and coalescence of the membranes of two adjacent cells

continues during the next minutes, thus the hybrids should not be disturbed in this time to stabilise the process.

A critical part of the whole cell fusion process is the medium in which the cells are suspended. The dielectrophoresis process for cell alignment requires a low conductivity medium to prevent excess heat build-up. Other factors must also be considered, as the requirement of millimolar levels of divalent cations, such as Mg^{2+} and Ca^{2+} (HA, 2001), which interact with negatively charged lipids and are important for membrane healing after poration. In addition, the use of a hypoosmolar buffer for mammalian cell fusion has been shown to facilitate electropermeabilisation of cell membranes due to osmotically induced membrane tension by swelling of the cell (BARRAU ET AL., 2004). The critical value of transmembrane potential needed to trigger pore formation is smaller under this osmotic stress, where membrane and cytoskeleton are temporarily loosened (SCHMITT AND ZIMMERMANN, 1989). Lots of other conditions and additives have been used to facilitate cell fusion (ABIDOR AND SOWERS, 1992; JIANG ET AL., 1999). However, only hypoosmolar fusion buffers seem to influence fusion yield positively and are nowadays applied widely.

Apart from fusion conditions and additives, the area in which electrofusion could be improved most, is the design of the cell fusion chamber. The design should allow observation of the fusion events for a quick decision for readjustment of the fusion parameters where appropriate.

2.2 Microtechnological Background

The last decade has seen a surge in the development of so called Micro Electro Mechanical Systems (MEMS), Micro Total Analysis Systems (μ TAS) or Lab-on-a-Chip (LOC) devices. This is due to the recent advances made in microfabrication technologies. The drive towards miniaturisation of existing systems spread across diverse technological disciplines, but not many devices can be found in use today.

2.2.1 Microsystems Technology

In principle, microsystems technology (MST) is an invention of nature. Each creature consists of a multitude of specialised microsystems – the cells. Since the beginning of the 90^{ths}, researchers try to harness many of the underlying principles of nature for the development of technological systems.

Microsystems are small effective systems, which satisfy many tasks better and less expensive than their bigger paragons, fabricated with conventional techniques. The microsystems technology has developed from microelectronics. It started with the effort to combine more and more functions on one device. The characteristic of MST compared to microelectronics is its systemic nature. All microsystems have in common the connection of different functions, materials, components and technologies in an integrative system. Diverse basic technologies such as mechanics, optics, fluidics and also new fields of technology are unified under the patronage of MST.

A variety of methods exist for the fabrication of microsystems such as photolithography, wet etching, reactive ion etching, soft lithography, injection molding, micromachining, replica molding, hot embossing and laser ablation. Today, MST can be seen as a key technology satisfying the growing demand for smaller, more economical and more integrated systems also in new fields like biotechnology or nanotechnology.

The techniques used in this thesis, are explained in "Technique Boxes" in the results section where applicable.

2.2.2 Microfluidics

Microfluidics is one of the major application areas of microsystems technology dealing with small quantities of fluids. It comprises design, manufacturing, handling and analysis of microsystems,

which work with fluids in channel cross-sections of $1\mu m$ up to $1mm$ in width. In practice, the average channel width used, is between $50\mu m$ and $500\mu m$ with a channel length of several millimetre up to several centimetre, depending on the application.

Although a lot of research is ongoing in the field of microfluidics, this discipline is still in its infancy. In the last decade, many microfluidic components were developed. They were either miniaturisations of existing or conventional systems, due to the usage of new effects or the search for new applications. Bioassays and biological procedures have been miniaturised into a chip format including applications such as DNA sequencing and separation, polymerase chain reaction (PCR), electrophoresis and enzymatic and immuno assays (SIA AND WHITESIDES, 2003). Microfluidic devices and systems are also useful for cell-based applications, especially as the size of cells fits very well with that of microfluidic devices (ANDERSSON AND VAN DEN BERG, 2003).

Due to the small fluid volume and in most cases also the small size of the system, the design, development and analysis of these systems show considerable differences to conventional fluidic systems. The fluid behaviour follows the scaling law and thus changes with miniaturisation. In the micro range, surface dependent effects such as interfacial tension, electrostatic and electrokinetic forces prevail, whereas in the macro world the volume-dependent effects are dominating such as vis inertiae and gravity. In general, the proportion of surface to volume rises with miniaturisation. This is the reason for the increase of surface forces, especially the viscous friction force of fluids (NGUYEN, 2004).

2.2.3 Fluid Mechanics in the Micro Scale

Scaling laws permit a rough estimation of the systems behaviour in the micro scale. The behaviour of a fluid volume is dependent on weight, surface tension and adhesive force. While the weight F_G is proportional to the volume V of the fluid, the surface tension and the adhesive force F_H are proportional to the surface A .

The proportion of F_H to F_G can be described as follows:

$$\frac{F_H}{F_G} \propto \frac{A}{V} \propto \frac{S^2}{S^3} \propto \frac{1}{S} \quad (2.1)$$

with

F_H : Adhesive force

F_G : Weight

A: Surface

V: Volume

S: Scaling factor.

For miniaturisation S is smaller than 1: $S < 1$

The equation 2.1 describes the square-cube-law, which can be illustrated in an example: Take a cup of coffee with $125mL$ of coffee. The scaling factor is set to $S = 1$. $125mL$ of coffee correspond to a volume of $5 \cdot 5 \cdot 5cm^3$. If this amount of coffee is spilt on the table, the fluid leaks over the table. With such a big volume, the weight outweighs the adhesive force and surface tension, the coffee flows over the table. If only a spoon full of coffee is taken ($V = 0.125mL$), which is the volume of a $5 \cdot 5 \cdot 5mm^3$ cube, and spilt on the table, it is unlikely to flow. From the equation it is obvious, that the proportion $\frac{F_H}{F_G}$ is 10 times higher, since $S = 0.1$. Adhesive force and surface tension alter the behaviour of the fluid volume. If the coffee volume gets even smaller *e.g.* only a drop, $0.5 \cdot 0.5 \cdot 0.5mm^3$ with a volume of $0.125\mu L$, this drop sits on the table. It does not move, even if the surface is tilted. With a scaling factor of $S = 0.01$ the proportion of $\frac{F_H}{F_G}$ is increased by 100fold. Adhesive force and surface tension define the behaviour of the fluid volume.

The scaling of physical variables is dependent on the physical effect, while the dimension or unit is independent of it (see table 2.2). This presents the real difference between scaling analysis and the dimensional analysis used in traditional fluid mechanics.

Table 2.2: Scaling derived from physical parameters (L: length, T: time, M: mass)

Parameter	Dimension	Scaling
Surface	L^2	S^2
Volume	L^3	S^3
Velocity	L/T	$1 \text{ or } S^{-2}$
Angular velocity	T^{-1}	1
Acceleration	$F/M = L/T^2$	S^{-2}, S^{-1}, S^0, S^1
Force	$M \cdot L/T^2$	S^1, S^2, S^3, S^4
Work	$M \cdot L^2/T^2$	S^2, S^3, S^4, S^5

Dimensionless numbers are introduced in the macro world, because of the dimensional ana-

lysis being a helpful tool for traditional fluid mechanics. Systems with the same dimensionless numbers are hydrodynamically similar. Therefore, scale models in different sizes/scales can rise correct conclusions about the fluid behaviour, as long as the dimensionless numbers correspond.

The influence of the scaling law on the fluid mechanics can be shown with the help of force analysis. The balance of forces in fluid mechanics is described by the Navier-Stokes equation:

$$\underbrace{\rho \frac{Dv}{Dt}} = \underbrace{-\nabla p} + \underbrace{\rho \cdot g} + \underbrace{\mu \cdot \nabla^2 \cdot v} \quad (2.2)$$

vis inertiae = pressure gradient + gravity + frictional force
with

v: Velocity vector

ρ : Density

p: Pressure

g: Acceleration vector

μ : Dynamic viscosity

The proportions between vis inertiae, pressure gradient, gravity and frictional force determine the behaviour of the fluid. In the following, the scaling law is analysed for different force proportions of a fluid.

Proportion of Vis Inertiae and Frictional Force

When assumed for the scaling that the density ρ and viscosity μ are constant (continuum requirement), the Reynolds number is proportional to the characteristic geometry.

$$\text{Re} = \frac{\text{vis inertiae}}{\text{frictional force}} = \frac{\rho \cdot u \cdot D_h}{\mu} \quad (2.3)$$

with

Re: Reynolds number

ρ : Density

u: Average fluid velocity

D_h : Hydraulic diameter (or other characteristic length)

μ : Viscosity

$$\text{Re} \propto S(\text{for } u = \text{const.}) \quad (2.4)$$

with

Re: Reynolds number

S: Scaling Factor

In the macro scale the Reynolds number is the criterion for fluid behaviour. If the fluid flow is dominated by the frictional force (small Reynolds number), the flow is laminar. When vis inertiae is much higher than the frictional force (high Re number), a turbulent flow is present. In the macro world a transition range between laminar and turbulent flow ($2000 < Re < 4000$) exists. In general, Re_{crit} is set as critical Reynolds number. The Reynolds number of microfluidic components is in most cases much smaller than Re_{crit} , because of high frictional forces due to a high surface/volume ratio of the microfluidic systems. Thus, a laminar flow is found in most microfluidic systems.

Proportion of Vis Inertiae and Gravity

$$Fr = \frac{\text{vis inertiae}}{\text{gravity}} = \frac{u}{\sqrt{g \cdot D_h}} \quad (2.5)$$

with

Fr: Froude number

u: Average fluid velocity

g: Gravitational acceleration

D_h : Channel height

The Froude number describes the relationship between flow velocity and velocity of the surface waves.

Proportion of Pressure Loss and Inertia

$$Eu = \frac{\text{pressure loss}}{\text{vis inertiae}} = \frac{\Delta p}{\rho \cdot u^2} \quad (2.6)$$

with

Eu: Euler number

Δp : Pressure loss

ρ : Density

u: Average fluid velocity

For a cylindrical capillary the pressure loss accounts to:

$$\Delta p = \int_D \cdot \frac{L}{D} \cdot \rho \cdot \frac{u^2}{2} = 32 \frac{\mu \cdot L \cdot u}{D^2} \quad (2.7)$$

with

f_D : Darcy friction factor

L: Length of the capillary

D: Diameter of the capillary

ρ : Density

u: Average fluid velocity

Consequently, the following is obtained for the Euler number:

$$\text{Eu} = 32 \frac{\mu \cdot L}{\rho \cdot D^2 \cdot u} \quad (2.8)$$

with

Eu: Euler number

μ : Viscosity

L: Length of the capillary

ρ : Density

D: Diameter of the capillary

u: Average fluid velocity

$$\text{Eu} \propto S^{-1} \quad (2.9)$$

with

Eu: Euler number

S: Scaling factor

The pressure loss in a microchannel is very high, due to the frictional force, while vis inertiae is negligible.

Please note, that for the analysis of the above dimensionless numbers, a continuum was assumed, which does not apply for gases in the submicrometre scale. In general, the continuum model applies for fluid flows, since fluids cannot withstand a shear force as a solid can. Under shear stress a fluid flows and thus loses its primary form.

The viscosity of a fluid causes a frictional force against the shear force. The dynamic viscosity μ of a fluid is defined by the following relation:

$$\tau = \mu \cdot \frac{du}{dy} = \mu \cdot \dot{\gamma} \quad (2.10)$$

with

τ : Shear stress

μ : Dynamic viscosity

u : Velocity

The variation of the velocity u over the axis y is termed shear strain $\dot{\gamma}$.

Under a constant fluid flow the shear strain and the shear stress τ rises with miniaturisation:

$$\tau \propto S^{-1} \quad (2.11)$$

In conclusion, in microchannels, the fluid flow differs fundamentally from macroscopic flows. The fluid in a microfluidic setting exhibits laminar flow and the occurrence of turbulence is prevented. This is primarily due to higher importance of molecular effects such as wall slip, because of the higher surface-to-volume ratio in microfluidic channels.

Chapter 3

Results

Overview

This chapter outlines the current problems using commercially available fusion chambers and introduces the principle idea how these problems can be solved. It then leads over to the development of two new electrofusion systems (described in section 3.1 and 3.2), which were developed in the context of this thesis.

The concept of cancer vaccines as described into detail in the 2nd chapter is the initiation of an effective immune response based on a strong stimulation of the immune system to overcome tolerance. Most of the vaccine therapies intend to stimulate T-cells that can recognise and kill tumour cells directly and/or attempt to activate professional antigen presenting cells (APC), such as dendritic cells, to specifically activate T-cells against tumour cell antigens. One way to introduce the antigen to the APCs is to form hybrid cells consisting of dendritic cells and cancer cells.

This can be achieved by chemically or electrically induced cell fusion between the respective cells. However, the electrofusion is highly preferable for clinical use. Purchasable devices offered by different companies can achieve this by the introduction of the cells into a micro fusion chamber and the subsequent application of an electrical field to the solution. Dipoles are induced within the cells, which group in pearl chains at the electrodes. This is a significant step in the procedure, since the cells need to have physical contact for the fusion. After the alignment of the cells a short electrical pulse is applied, resulting in a perforation of the cell membranes. During the membrane reorganisation the membranes of neighboured cells can fuse and a hybrid

is formed. If the damage of the membranes by the applied pulse is too substantial the cells will not survive the procedure. Otherwise, if the perforation is not wide enough, no hybrid cells will be formed.

In many cases, normal or altered electroporation cuvettes are used for cell fusion. There are, however, some systems available, which are specialised for the electrofusion of mammalian cells, *e.g.* the Eppendorf Multiporator. It can be used with standard electroporation cuvettes, but also comprises the possibility to use two special chambers for cell fusion in small and in larger scale.

The micro fusion chamber, illustrated in figure 3.1 and figure 3.2., respectively, is developed for the use under a microscope, while the helix fusion chamber (see figure 3.3) has been designed for the production of larger quantities of fusion products (fusion of up to $2.5 \cdot 10^5$ cells).

Generally, a protocol for cell fusion implies firstly a mixture of the two fusion partners in equal shares and their subsequent introduction into the fusion chamber. Figure 3.4 on page 34 shows a cell suspension in the Eppendorf micro fusion chamber and the cell alignment provoked by the application of a low alternating electrical field.



Figure 3.1: Micro fusion chamber for the Eppendorf Multiporator: It consists of a casing containing two electrodes above a transparent reservoir. Connection to the Multiporator can be established by a coaxial cable via a special insert. This micro fusion chamber allows the optimisation for cell alignment and cell fusion under microscopic control.

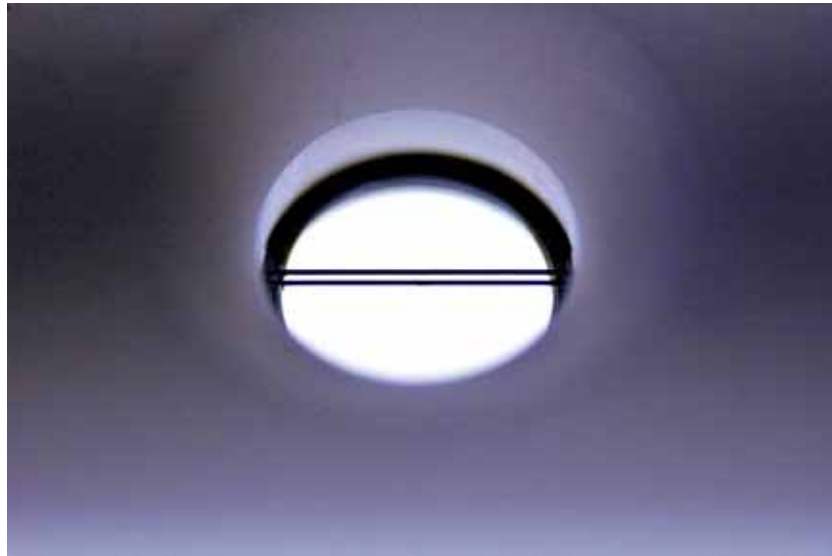


Figure 3.2: Close-up view of the electrodes from the Eppendorf micro fusion chamber: The two electrodes consist of Platinum and are $200\mu m$ apart.



Figure 3.3: Helix chamber for the Eppendorf Multiporator: It consists of a conical core that carries the parallel wrapped electrode wires and a beaker into which the cell suspension is added. The filling volume accounts to $250\mu L$. The electrode gap width of $200\mu m$ is filled by the screwing of the core into the beaker, whereupon the cell solution is pressed upwards into the gap.

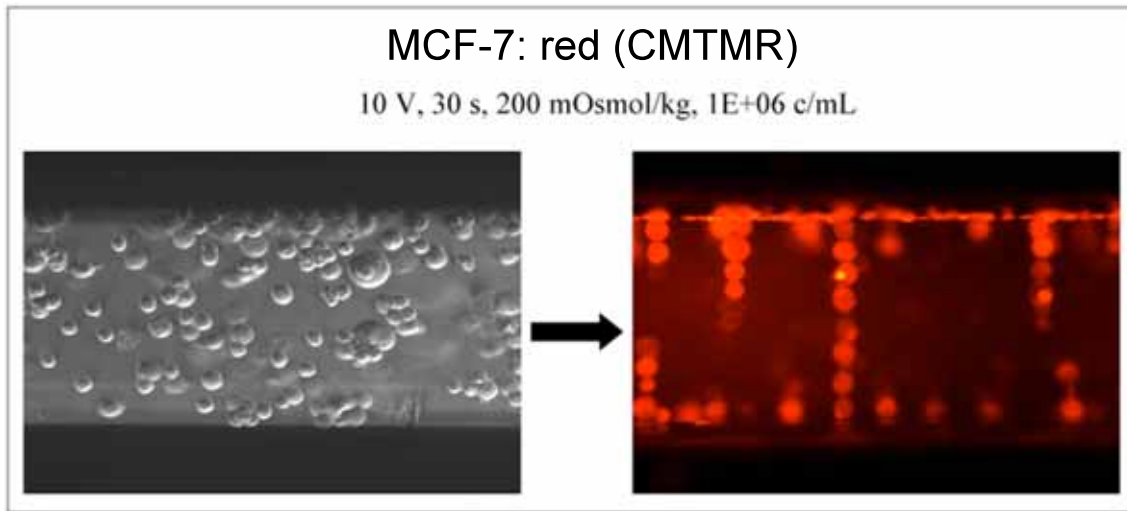


Figure 3.4: Situation in the Eppendorf micro fusion chamber filled with a cell suspension of 10^6 mL^{-1} before and after application of a low a.c. field (500 V/cm) for 30 seconds. The used breast cancer cell line MCF-7 has been stained in red using the fluorescent cytoplasmatic Celltracker CMTMR dye. [picture by H.R. Bohnenkamp]

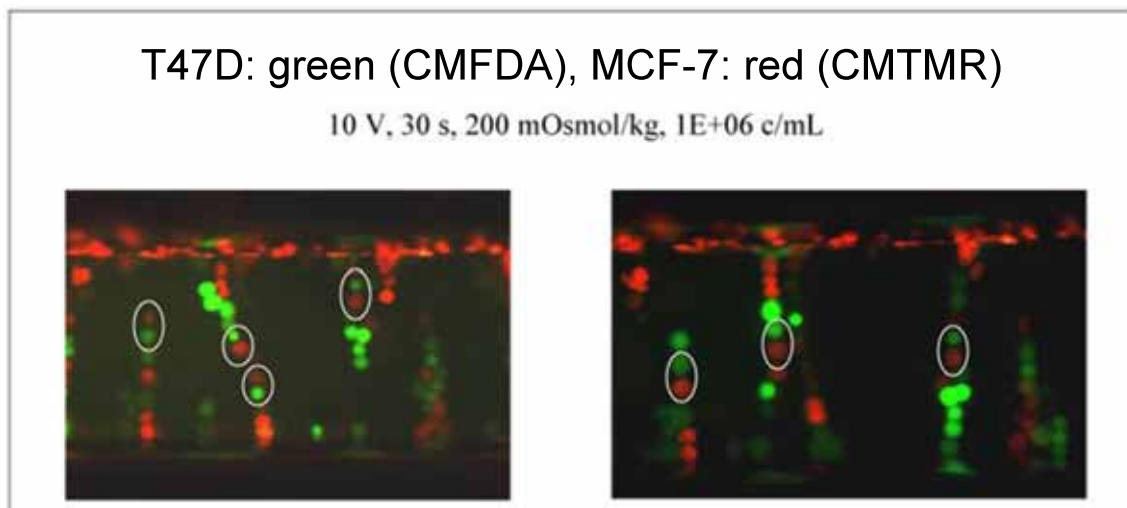


Figure 3.5: Mixture of two different breast cancer cell lines, T47D and MCF-7, stained in green with CMFDA and in red with CMTMR, respectively, in the micro fusion chamber. Many clusters of cells of the same type can be observed. However, only at sites in the cellular pearl chains, where the two cell types alternate (see marks for example) a heterologous fusion can take place. [picture by H.R. Bohnenkamp, modified]

For the investigation of the cell alignment in the fusion chamber, two different breast cancer cell lines, T47D and MCF-7, were stained with a green and a red cytoplasmic fluorescent dye and introduced into the chamber. The resulting situation in the fusion chamber after the alignment process showed a high formation of clusters of cells of the same cell type (see figure 3.5 on page 34). This phenomenon can be explained by the differential cell specific parameters of the fusion partners, such as cell size, cell shape and membrane potential. Their interaction during cell alignment triggers cluster formation in an a.c. field, thus dramatically reducing the potential fusion efficacy.

This general phenomenon, as revealed in our group, is responsible for the low yield of heterologous hybrids. The high cluster formation reduces the fusion efficacy for heterologous hybrids, as only the cells that are alternatingly aligned (red-green, see mark in figure 3.5) have a chance that a hybrid cell is formed after the application of an electrical pulse. Therefore, it can be directly understood that only a minor heterologous hybrid formation yield can be expected.

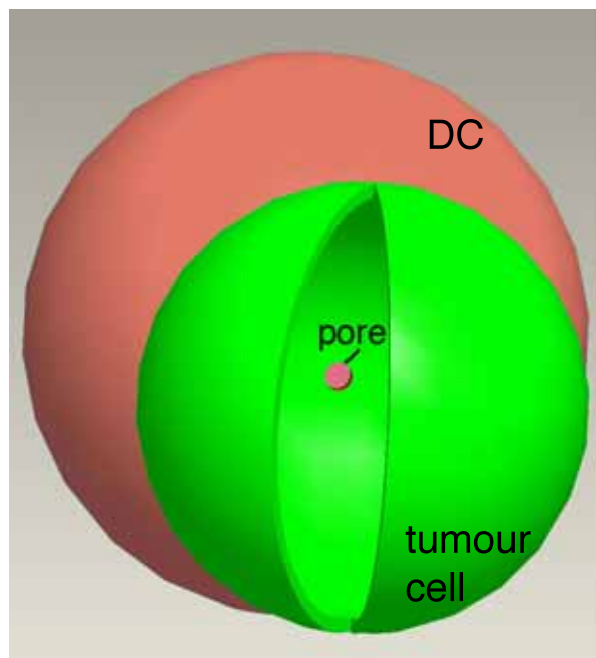


Figure 3.6: Schematic diagram of the proportion of a cancer cell (green) in comparison to a dendritic cell (red): A successful two-cell fusion requires the appearance of two holes in the membranes, one in each cell. These holes, which result from a membrane breakdown due to the applied fusion pulse, have to co-localise.

In theory, a 50 % fusion efficacy can be obtained by simply mixing the fusion partners before the application of the pulse. However, only 10-15 % of hybrid formation were achieved with the Eppendorf Multiporator. It is obvious, that the cluster formation limits the heterologous hybrid cell formation and thereby the potency for an application to a variety of cancer types (for example breast cancer), because of a limited availability of tumour material. By circumventing the cluster formation by alternating arrangement of the fusion partners, the theoretical fusion efficacy could be raised up to 100 %.

Furthermore, it has to be kept in mind, that the fusion itself is a rarely occurring event, since it requires the formation of one hole in the cell membrane of each cell, which co-localise exactly (see fig. 3.6). Even when this situation is established, the cell membranes can reorganise and close the holes without mergence. That means that extracellular fusion parameters such as fusion pulse voltage, pulse length, number of pulses and the osmolality of the fusion medium inhere a sizable influence.

Nevertheless, a straightforward improvement of the fusion efficacy would be the previous alternating arrangement of the cells in the fusion chamber before the fusion procedure. This eliminates the chance of cell cluster formation, thus boosting the fusion efficacy.

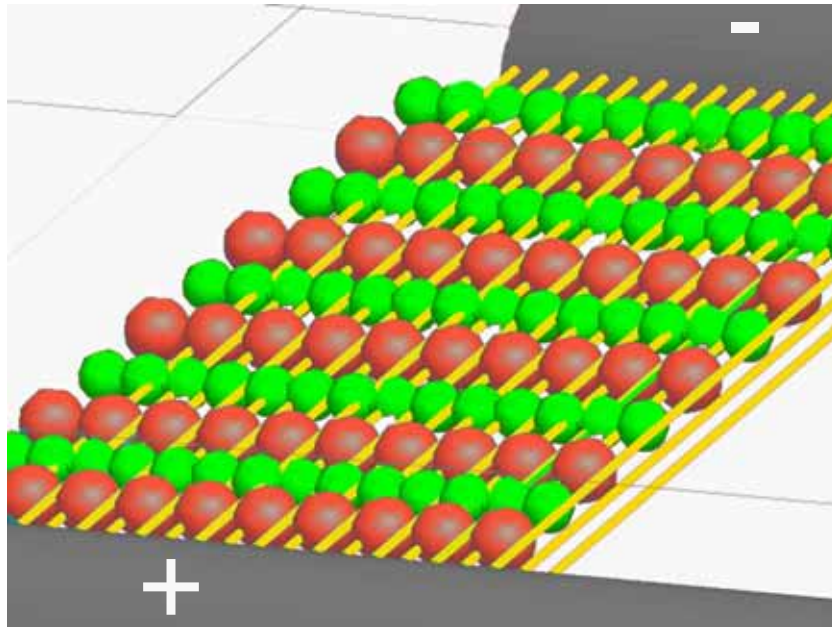


Figure 3.7: Schematic depiction of the targeted alternating cell alignment between the electrodes of the fusion chamber. The arrangement has to be adjusted alongside the field lines, depicted here in yellow.

Within the scope of this thesis, novel electrofusion systems were established on the basis of this conceptual design. The underlying principle of cell arrangement inside the fusion chamber is depicted in figure 3.7, where the cells are aligned along the field lines pictured in yellow. The development and technical engineering of such an electrofusion chamber requires a concept how particles such small as a cell can be arranged in a specific pattern. Two theoretical approaches were developed and their feasibility has been examined in this thesis. The first is based on cell immobilisation, with one fusion partner being bound to a surface in a pattern (see section 3.1). The other approach focuses on microfluidic techniques for cell arrangement and is dwelled on in section 3.2.

Summary

The technical problems with commercially available fusion chambers are:

- 1.) low achievable fusion efficacies
- 2.) cell cluster formation
- 3.) these problems prevent the application to new fields, such as cancer therapy

Thus, a novel electrofusion system has to accomplish the following requirements:

- 1.) avoidance of cluster formation
- 2.) generally applicable to different cell systems
- 3.) feasibility to vary all important fusion parameters
- 4.) integrate the principle idea of alternating cell arrangement

3.1 Immobilisation

3.1.1 Concept

Overview

The development of a fusion chamber for arranged electrofusion based on cell immobilisation is described in this section. Thereby, the concept of this approach is specified.

The first approach for the implementation of an alternating cell arrangement into a fusion chamber is based on immobilisation. One of the two cell types involved in the electrofusion process will be immobilised on lanes of monoclonal antibodies to prevent cluster formation.

The idea of immobilising cells in an alternating cell arrangement originated from the work of Prof. A. Offenhäuser (head of the Institute of Thin Films and Interfaces 2 (ISG-2) at the Research Center Jülich) and its work on neuronal networks. To refine existing neuronal models and gain deeper understanding of related processes, his research group produces artificial networks of neuronal cells on synthetic substrate surfaces (LAUER ET AL., 2001). The neuronal cell growth is thereby controlled with micropatterned structures of laminin, an extracellular matrix protein. The structural dimensions of the laminin pattern correlated with the shape of the resulting cellular network as shown in figure 3.8.

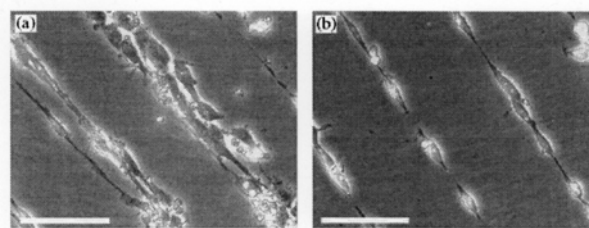
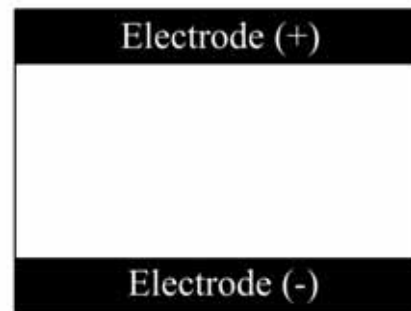


Figure 3.8: Phase contrast micrographs of PCC7-MzN mouse embryonic neuroblastoma cells on straight lines of patterned laminin. Comparison of cellular growth on different line sizes at day 4 shows that on $6\mu\text{m}$ lines cells form big clusters (a), whereas on $2\mu\text{m}$ lines monocellular lines are visible (b). Scale bar represents $100\mu\text{m}$ (pictures taken from LAUER ET AL., 2001).

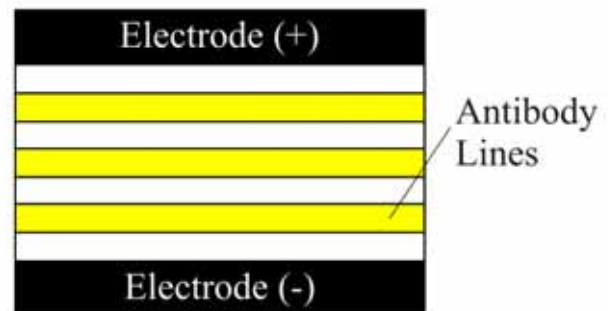
The patterning has been performed with polydimethylsiloxane (PDMS) microstamps, in a process called micro-contact printing (μCP). The transfer of this technique to the immobilisation of dendritic cells in lines forms the basis for the development of an arranged electrofusion

A) The electrofusion chamber

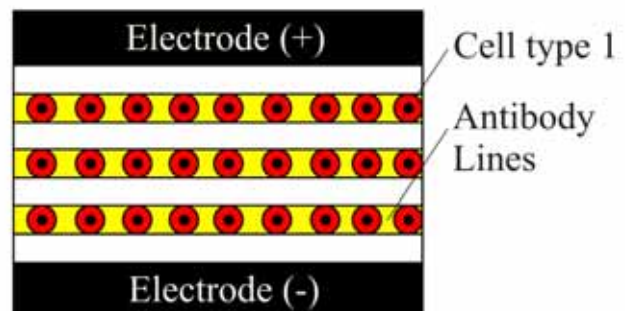
The electrofusion chamber is bordered on both sides by an electrode.

**B) Printing of antibody lines**

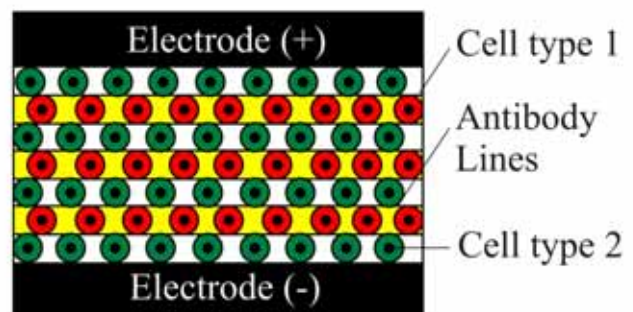
First of all, antibody lines are printed in the space between the electrodes using microcontact printing. Thereby, the antibody is bound covalently to the bottom of the fusion chamber.

**C) Adhesion of the 1st cell type**

In the second step, the first cell type, e.g. dendritic cells, are bound to the antibody lines by antigen antibody interactions. All surplus cells, which have not bound, are removed in a washing step.

**D) Addition of the 2nd cell type**

Now, the second cell type is added. These cells will locate in the space between the single cell lines of the first cell type.

**E) Alignment and fusion**

Finally, the cells are aligned by an a.c. field and are subsequently fused by a d.c. pulse.

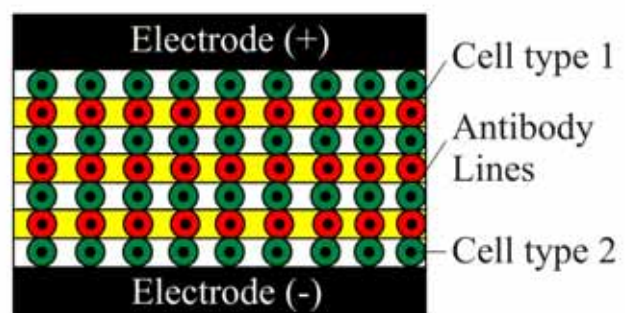


Figure 3.9: Immobilisation approach for an arranged electrofusion chamber

process based on immobilisation (see figure 3.9). In the process, the width of the antibody lines will play an important parameter. The lines should not be too small to provide good producibility, but not that wide that several cells bind over the line width and clusters are obtained.

The first step in the immobilisation procedure comprises the printing of small lanes of antibodies on the surface of the fusion chamber. These antibodies are used to immobilise the cells since mature dendritic cells are non-adherent in culture. After the first cell type is added to the chamber and the cells have bound to the antibody lines, all excessive cells are removed in a washing step. Cell type 2 is added to the chamber and the cells sediment between the immobilised cells building an alternating arrangement. The electrical field lines the cells up in pearl chains and fixates them in this arrangement until the fusion pulse is applied.

This antibody-based approach allows for the disposition of the electrofusion chamber to other fusion pairs by simply changing the printed antibody to another one who is specific for a surface protein on the chosen cell type.

Summary

For the assignment of cell immobilisation to the development of a novel electrofusion chamber the following questions have to be addressed:

- 1.) What is the best method to covalently bind an antibody to a solid surface?
- 2.) Can the antibody be printed by means of micro-contact printing using the chosen covalent binding reaction?
- 3.) Do cells *e.g.* dendritic cells bind to these antibody lines?
- 4.) What is the right width for the antibody lines that only one cell binds over the width of the lane.

3.1.2 Covalent Immobilisation of Antibodies

Overview

Different strategies were investigated to find the optimal technique for the immobilisation of antibodies. They are presented in this chapter and make up the basis for an advanced electrofusion chamber.

Adsorption

Physical adsorption was the first method that was tested. Unfortunately, adsorptive immobilisation as used for the coating of polystyrene plates with antibodies for ELISA (enzyme-linked immunosorbent assay) did not allow a structured immobilisation. At the first contact with fluid during a washing step, the antibodies adsorbed in structures were detached and spread over the complete surface. Thus, a chemical covalent binding of antibodies was mandatory.

A further advantage of a chemical binding is the oriented binding of the antibody molecule in comparison to the unoriented immobilisation of the biomolecules by physical adsorption.

Antibodies or immunoglobulins G (IgG) are a family of Y-shaped glycoproteins. The antibody molecule is a tetramer with a molecular weight of about 150 kDa. It consists of two identical heavy and two identical light peptide chains. The upper part of the heavy chains and the light chains build the variable region (Fab-region), which is unique for each antibody. These Fab fragments react with antigens to yield immune complexes. The lower part of the heavy chains is known as Fc fragment.

A covalent coupling of antibodies can be realised via the terminal amino- or carboxyl groups of the peptide chains. The mode of the antibody immobilisation will thereby determine the orientation of the antibody on the surface. An important factor for the successful antibody immobilisation is the accessibility of the Fab fragments for the interaction with the antigens, and as a result the antibody activity. In addition, the spacer length has a big influence on the immobilisation reaction. Longer spacers optimally decrease the steric interactions among large molecules such as antibodies and increase binding capacity. Thus, the activity of the antibodies needed to be proven after their covalent attachment by binding of a sample cell line.

In the following, three different routes of chemical binding of antibodies have been investigated. For all immobilisation reactions tested the antibody solution was applied as a drop on the activated surfaces.

Photolinker

The immobilisation of antibodies in a photochemical reaction was tested on polystyrene (BORA ET AL., 2002), polypropylene and polyethylene (NAQVI ET AL., 2002). The surfaces were coated by 1-fluoro-2-nitro-4-azidobenzene (FNAB) and activated by exposure to ultraviolet (UV) light. Upon UV excitation, the azido group of FNAB is transformed into a highly reactive nitrene, which inserts the C-H bonds of the polymer by a covalent linkage. A primary amino

group of the antibody is then bound to the activated polymer in a thermochemical displacement reaction of the fluoro group of FNAB, which is then part of the polymer.

Thiol-Terminal Silanes and Heterobifunctional Cross-Linkers

A covalent bond formation between a hydroxyl group of a glass surface, a thiol-terminal silane, a heterobifunctional crosslinker and the antibody was tested next (BHATIA ET AL., 1989). The modification of the surface's hydroxyl groups was accomplished with 3-mercaptopropyltrimethoxysilane (MTS). The silane is covalently attached to the hydroxylated glass surface under an inert atmosphere to protect the thiol-group of oxidation. This thiol-group can react with the maleimide group of N-gamma-maleimidobutyryloxy succinimide ester (GMBS), the heterobifunctional crosslinker. The succinimide residue of this linker is left to bind a primary amino group of the antibody through the formation of a stable amide bond.

Aminosilanes and Homobifunctional Cross-Linkers

The third method uses again a silane film for modifying the negative hydroxy groups of a glass or silica surface. 3-aminopropyltriethoxysilane (APTES) was chosen as silane, which bears the functionality for attaching an antibody via glutardialdehyde as homobifunctional cross-linker (see figure 3.10 for reaction scheme) (WANG AND JIN, 2004). First of all, silanol groups are formed on the glass surface by hydroxylation using aqueous sulfuric acid in a cleaning step. Then, the aminosilane binds to these hydroxyl groups, whereupon an ethoxy group of APTES is hydrolysed by a nucleophilic displacement resulting in a reactive silanol group, which forms a siloxane linkage to the activated glass surface. The silanisation leaves a primary amino group on the surface, which reacts with the cross-linker glutardialdehyde in an addition-elimination-reaction. A stable imine is formed containing a carbon-nitrogen double bond. This Schiff's base reaction is repeated in the last step of the immobilisation reaction, where the residual carbonyl group reacts with a primary amino group of the antibody.

Satisfying results could only be obtained with the last reaction. All other reactions were not suitable in terms of the amount of immobilised antibodies. The aminosilane/glutardialdehyde procedure gave a high density of immobilised antibodies and also maintained antibody function as determined by antigen binding in a cell-binding test. Cells of the cell line KG-1 (from human acute myeloid leukaemia) were used as model suspension cell line. They were immobilised using an antibody against the CD34-Antigen (CD = Cluster of Differentiation), which is highly

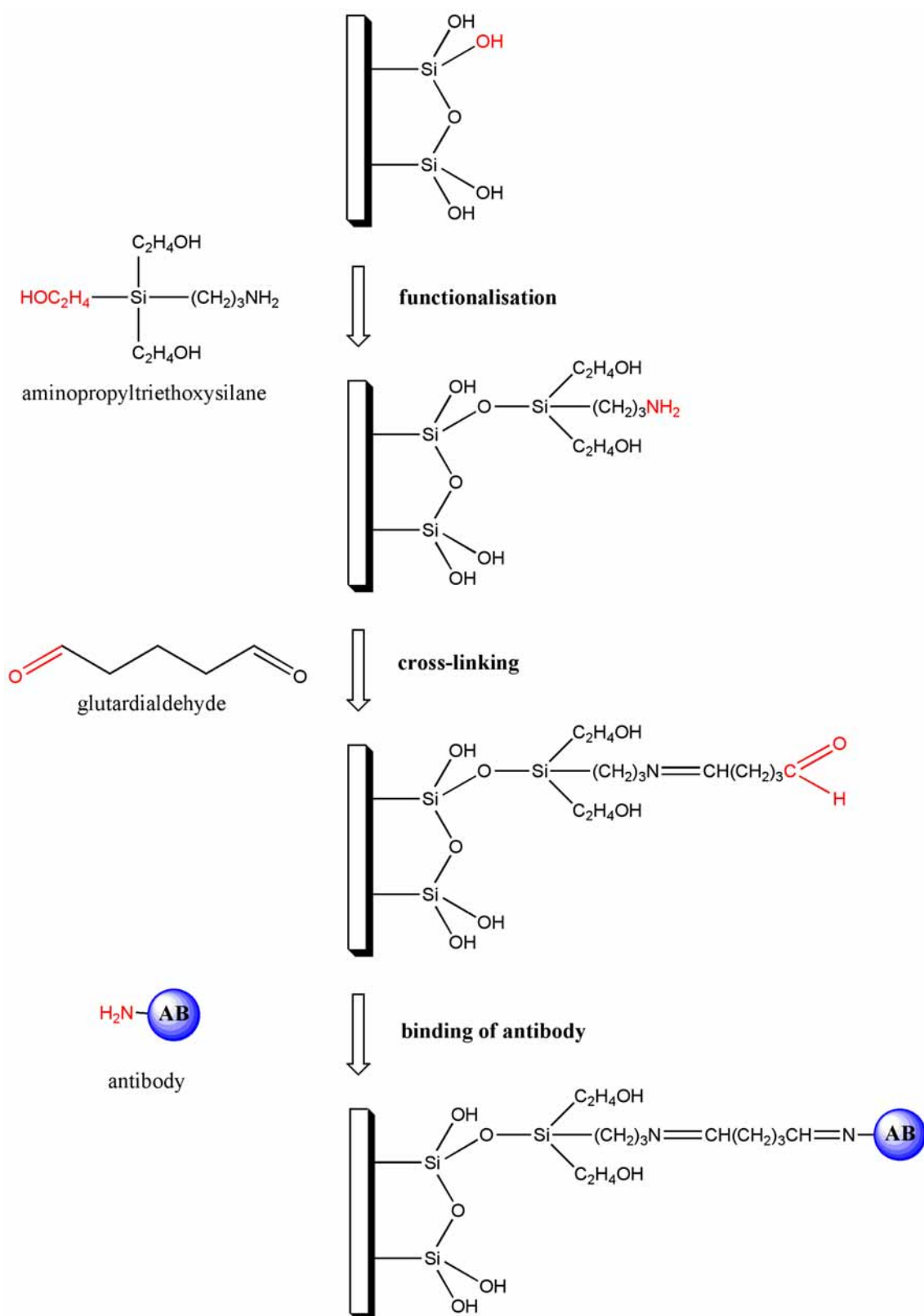


Figure 3.10: Reaction scheme for the coupling of antibodies to a glass surface by 3-aminopropyltriethoxysilane and glutaraldehyde

expressed on the surface of KG-1 cells.



Figure 3.11: Immobilisation of KG-1 cells on a APTES/glutardialdehyde-treated glass surface via a covalent coupled anti-CD34 antibody: The antibodies were immobilised in a drop shape. The picture was assembled from multiple micrographs.

The results were promising for a structured immobilisation of cells (see figure 3.11). KG-1 cells were bound circularly on the glass carrier, but it has to be noticed, that no cells were bound inside the drop shape. This suggests that the antibodies were immobilised only on the drop interface or that at least the antibody concentration was higher at this interface, resulting in cell binding. Whether this behaviour may be obstructive for the patterning of antibody lines needed to be checked in further experiments.

Summary

Four different ways for the immobilisation of antibodies on solid surfaces were investigated. Satisfying results proven in a cell-binding assay could only be obtained with one approach. The immobilisation reaction using an aminosilane and glutardialdehyde will subsequently needed to be optimised for the structured immobilisation of antibodies.

3.1.3 Softlithography

Overview

This section discusses the assignment of the approved immobilisation chemistry for the printing of antibody lines using softlithographic methods.

For the control of the cell position inside the electrofusion chamber, small lines of antibodies should be deposited on the surface of the fusion chamber. Such a line pattern can be created by softlithographic methods.

The term softlithography summarises a group of microstructuring techniques, which are based on the application of polymeric stamps. These softlithographic methods allow the generation of surface patterns in the micrometer and submicrometre range. In contrast to commonly used photolithography, no radiation is used for the pattern formation and the resolution of the pattern is not diffraction limited. Nevertheless, the production of the masters, which are needed for casting the elastomeric stamps, still requires photolithographic methods (see Technique Box on page 46).

Microcontact Printing

For a first attempt, microstamps, manufactured by the Institute of Thin Films and Interfaces 2 (ISG-2) at the Research Center Jülich (VOGT ET AL., 2003) were used to print antibody lines. The polydimethylsiloxane (PDMS) stamps were fabricated curing PDMS prepolymer in 2mL Eppendorf tubes upside down on a master with a line pattern. These stamps possessed structures in a width range of 50 μ m to 100 μ m. Obviously, antibody lines printed with these stamps would be far too wide to just bind one cell over the line width, but would give a first impression of the transferability of the aminosilane/glutaraldehyde immobilisation reaction to micropatterning.

The chosen surface chemistry for the antibody immobilisation consisted of three reaction steps: functionalisation of the glass surface with 3-aminopropyltriethoxysilane, cross-linking with glutaraldehyde and binding of the antibody. To obtain an antibody pattern in the end, it would be sufficient to pattern just the last reaction step using an microstructured elastomeric stamp, but patterning of two or all reaction steps is also conceivable. However, if all reactants

Technique Box

Softlithography (master and stamp production)

Application:

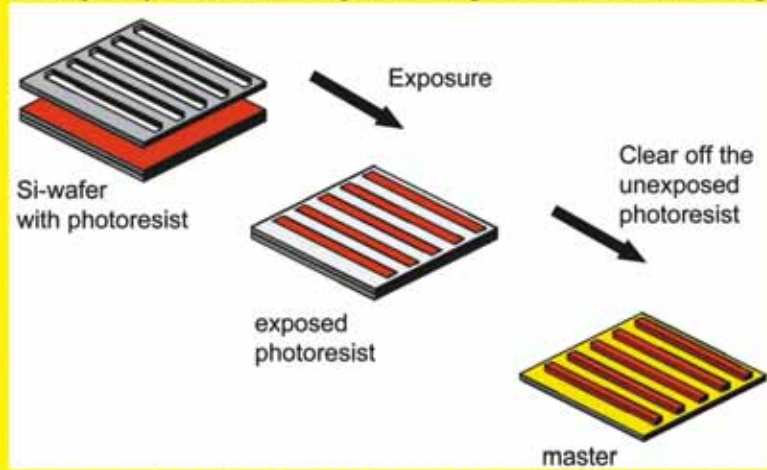
Silicium wafers with a micro-structured surface, so-called masters, are used as a negative for the casting of elastomeric stamps or devices.

Requirements:

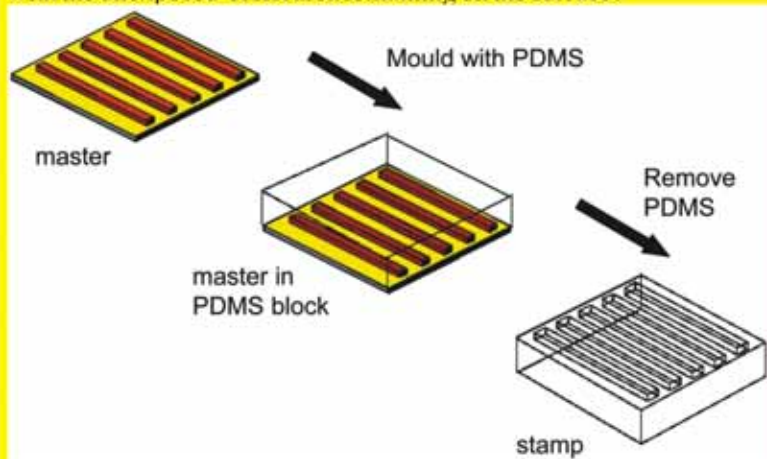
Silicium wafer, photoresist, photolithographic chrome mask, UV source, prepolymer

Method:

A spin-coat of a photoresist is applied to a clean and dry silicium surface. The thickness of the film is depending on spin speed and resist properties. After the application of the resist to the substrate, the film is soft baked on a hot plate or in a convection oven to evaporate the solvent and densify the film. Subsequently, the surface is exposed through a chrome mask to UV light.



In the case of negative photoresist (see below), the exposed resist area is cross-linked and rendered insoluble to liquid developers. After a post exposure bake, the unexposed film areas are removed with a chemical developer, and the master is completed. A positive photoresist would behave obversely, with the unexposed resist area remaining on the surface.



Stamps are moulded from the master using a mixture of elastomer precursor polydimethylsiloxane and its curing agent.

are applied to the solid surface using the stamping technique, it has to be presumed that the stamp is repeatedly contacted with the surface at exactly the same position. Therefore, the stamp can be clamped to a special instrument, which guarantees the micrometer accurate deposition.

Technique Box

Microcontact Printing (μ CP)

Application:
Microcontact printing is a versatile, non-lithographic method for the patterning of surfaces with an ink solution using an elastomeric stamp.

Requirements:
Elastomeric stamp (PDMS), inking solution (*e.g.* antibody solution), printable surface

Method:
For protein patterning, an elastic and chemical inert stamp is inked with the protein solution (*e.g.* antibody) and dried. The inked stamp is then contacted with the printable surface. Due to the high elasticity of PDMS as stamp material, a direct contact can be developed with surfaces of a roughness of 100 nm. The stamp is removed after short time leaving the pattern on the surface.

The diagram illustrates the Microcontact Printing (μ CP) process in two stages. The top stage, labeled "Wetting of the stamp with an antibody solution", shows a grey stamp with four rectangular protrusions on its bottom surface. An arrow points to the "inked stamp", where the protrusions are filled with a red liquid. The bottom stage shows the stamping process: the inked stamp is pressed onto a yellow substrate, then removed, leaving a "patterned antibody" on the substrate.

In the present case, the surface chemistry circumvented the printing of all reaction steps, since they differed strongly in the necessary reaction conditions. While the first reaction step was carried out at 60°C , the second step took place at room temperature. Thus, the substrate needed to be manoeuvrable and a clamping to a special instrument was not suitable. This left the possibility of patterning one reaction step. Preferentially, the last step, the antibody binding, offered a good point for the patterned application. Simultaneously, the printing of the

antibody reduces the amount of used antibody, since not the whole surface needs to be covered with the antibody solution, but the stamp is wetted with the antibody containing solution and then pressed onto the chemically modified surface.

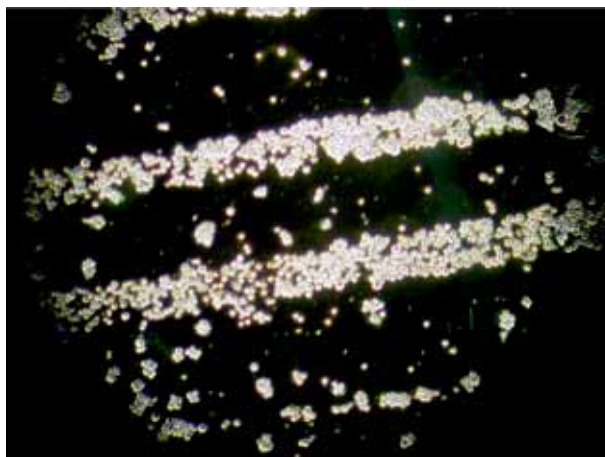


Figure 3.12: Immobilisation of KG-1 cells via anti-CD34 antibody: The antibody was applied using a microstamp to a glass surface completely functionalised with APTES/glutaraldehyde. $80\mu m$ wide antibody lines show binding of multiple cells over the line width. Cell clusters could also be observed in the space between the printed antibody lines.

The first immobilisation results as shown in figure 3.12 confirmed that the patterned immobilisation of cells is feasible. Nevertheless, the cells from the used model cell line KG-1 did not only bind to the antibody imprinted onto the surface by the contact between the stamp and the substrate, but also to the aminosilane/glutaraldehyde functionalised surface in between the lines. The latter cell binding probably came from non-specific adsorption to the long aliphatic chains of APTES. Blocking agents such as Tween 20 did not reduce this unspecific binding, but a solution to the problem could be found, using the PDMS microstamps in an inverse microcontact printing process.

Inverse Microcontact Printing

In the case of inverse microcontact printing, an elastomeric stamp is used to cover the whole substrate area except for the part where the proteins/antibodies are placed (KANE ET AL., 1999). Therefore, big stamps with a diameter of $7.5cm$ were produced, which had the size to cover a glass wafer of the same diameter. The stamps were designed to combine four different line widths 10 , 15 , 20 and $30\mu m$ on one stamp separated by a $1cm$ space. The width of the

lines were chosen to bind one dendritic cell per line width. Every line bundle covered $200\mu\text{m}$ in width (the distance between the two electrodes in the future electrofusion chamber). Obviously, depending on the line width the amount of lines per bundle varied. The distance between each line in a bundle to the next line was equivalent to the line width itself and should assign a place for the second fusion partner, the breast cancer cells. For the $10\mu\text{m}$ lines ($20\mu\text{m}$ pitch), 10 lines built a bundle, for the $15\mu\text{m}$ lines ($30\mu\text{m}$ pitch), the $20\mu\text{m}$ lines ($40\mu\text{m}$ pitch) and the $30\mu\text{m}$ lines ($60\mu\text{m}$ pitch), the bundle consisted of 7, 5 and 3 lines, respectively.

Technique Box

Inverse Microcontact Printing

Application:

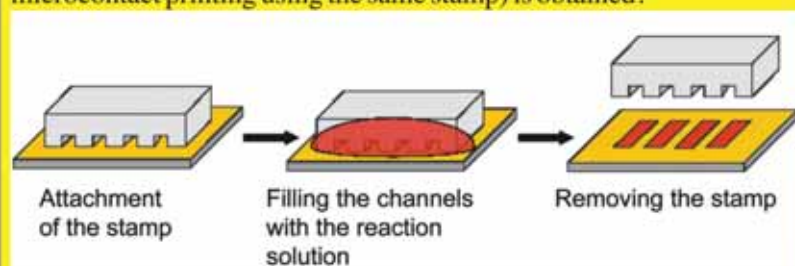
Inverse microcontact printing can be used in the same way as direct microcontact printing for the patterning of surfaces with an ink solution using an elastomeric stamp.

Requirements:

Elastomeric stamp (PDMS), inking solution (e.g. antibody solution), printable surface

Method:

In this modified way of microcontact printing, the clean elastomeric stamp is attached to the printable surface. The PDMS stamp adheres to the surface and channels are formed. These cavities can then be filled with the inking solution and an inverse pattern (compared to the one, which resulted from microcontact printing using the same stamp) is obtained.



These PDMS stamps were subsequently brought into contact with the glass substrate and by sealing the PDMS structure with the glass surface, a microfluidic network was formed, which defined the areas of inking. These channels could then guide the solutions for the immobilisation reaction over the substrate. Thereby, the elastomeric properties of stamps made of PDMS ensured conformal contact with the substrate. A watertight seal was formed via van der Waals forces between the soft PDMS silicone structure and the hard glass surface.

Mask Preparation

The layout for the stamps (as described above) were designed using an CAD (computer aided design) programme. The length of the line structure was 4cm . An electron beam writer transposed the different line pattern to a chrome mask.

Master Preparation

Stamp masters were produced under standard photolithographic conditions, using the negative photoresist SU-8 25 (after MOURZINA ET AL., 2005). SU8 25 is a high contrast, epoxy based photoresist. The exposed and subsequently cross-linked portions of the film are rendered insoluble to liquid developers. The resist was spin-coated with a layer thickness of $15\mu\text{m}$ on a 0.6 mm thick silicon wafer (this value corresponds to the height of the microfluidic channels in the PDMS replica). The film was exposed to UV light via a photomask for 33sec and pre- and postbaked following the manufacturer's instruction. After the development with PGMEA (propylene glycol monomethyl ether acetate), they were silanised with a 3 % solution of chloro(dimethyl)octadecylsilane in toluene for 1.5h for better mould release. Followed by rinsing with 2-propanol and water, the masters were dried with argon, analysed via scanning electron microscopy (see figure 3.13 on page 51) and stored.

PDMS Stamp Preparation

Elastomeric stamps were made from polydimethylsiloxane (PDMS). The elastomer and curing agent were mixed in a 10 : 1 ratio. Bubbles were removed from the mixture under vacuum in an excicator and the prepolymer mix was poured onto the master. For these purposes, the masters were clamped into a special holder (in-house production; see figure 3.14 on page 52) and 11g of prepolymer mix were applied per master. The PDMS covered masters were degassed again for 5min to remove all bubbles and were subsequently cured for 4h at 60°C , whereas the heating shortened the polymerisation time. After curing, the PDMS stamps were peeled off as a negative cast of the master and surmounting stamp parts were removed.

Moulding provided the replica that contained three of the four walls necessary to form enclosed channels. Sealing the replica to a flat surface as for inverse microcontact printing provided the fourth wall. To allow filling of the channels, after conformal contact of the stamp with the substrate surface was established, filling holes (one at every end of a channel or

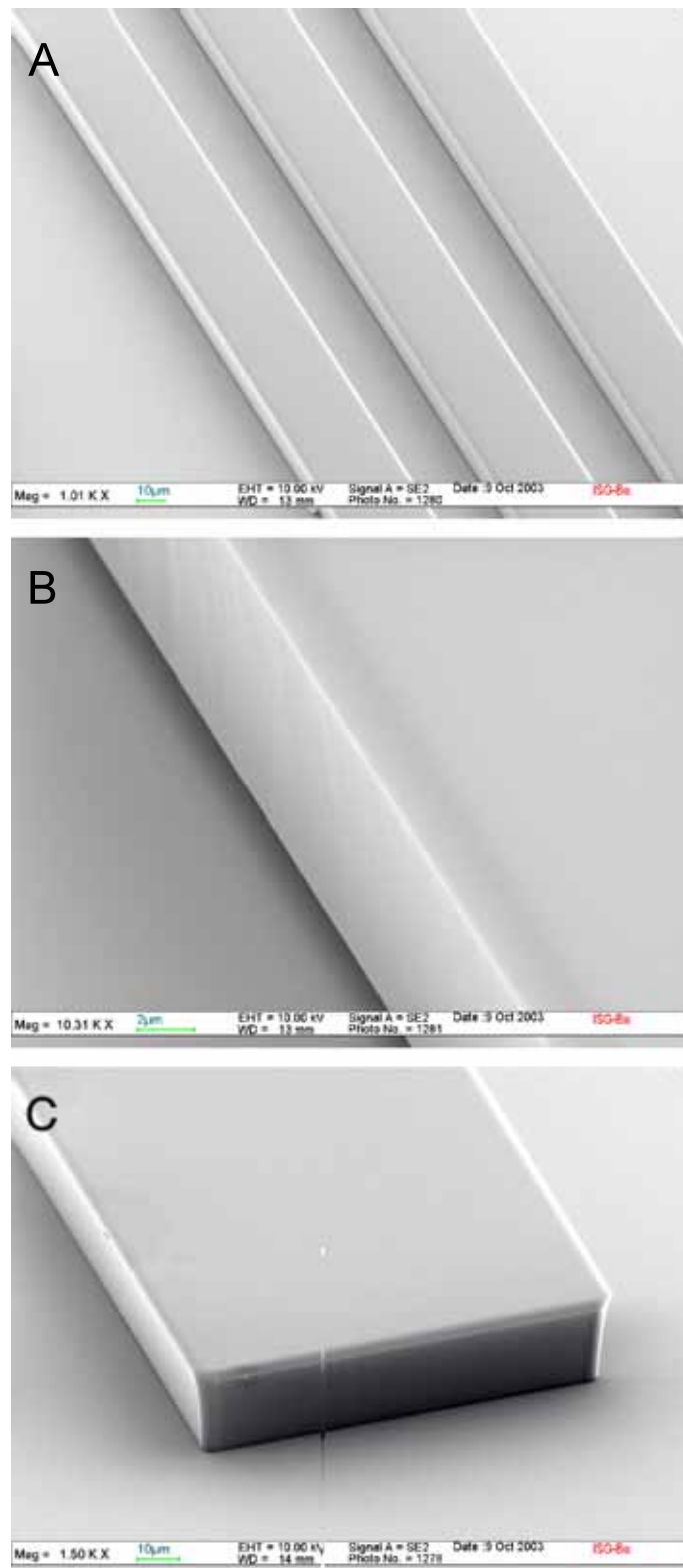


Figure 3.13: Scanning electron micrographs of master structures raised from negative photoresist SU-8 25 on a silicon master: A) three $30\mu\text{m}$ wide and $15\mu\text{m}$ high structures, B) $30\mu\text{m}$ wide, $15\mu\text{m}$ high, c) a $100\mu\text{m}$ wide and $25\mu\text{m}$ high structure. The results demonstrated that smaller structures can be obtained the thinner the spincoats are applied. Best results were obtained with a structure height of $15\mu\text{m}$.

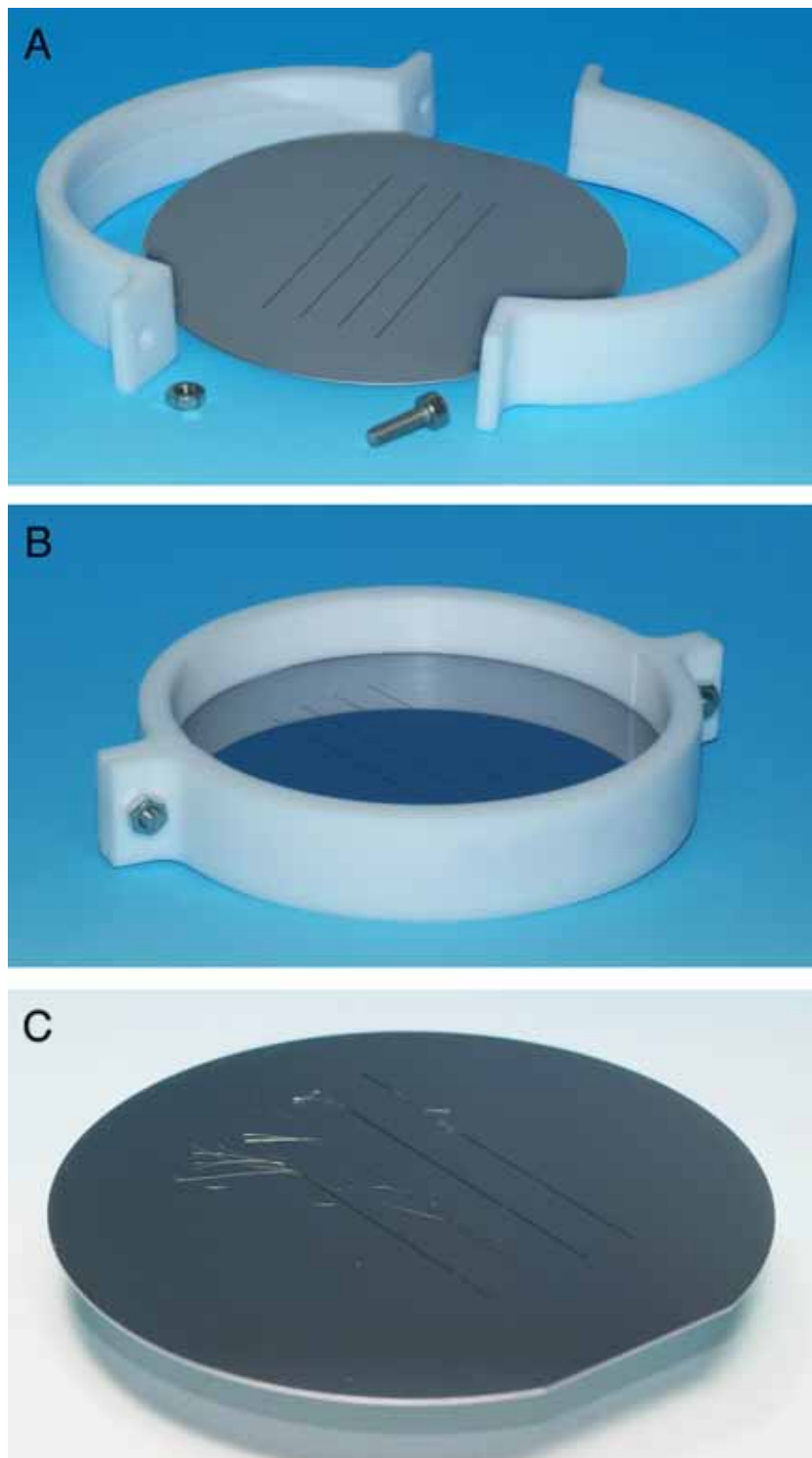


Figure 3.14: Photographs of the produced master for the PDMS stamp preparation. The master was placed into a special holder for the moulding with PDMS. A) master and holder (in-house production), B) assembled, C) defect master where the photoresist lines were detached, due to improper handling such as sonication.

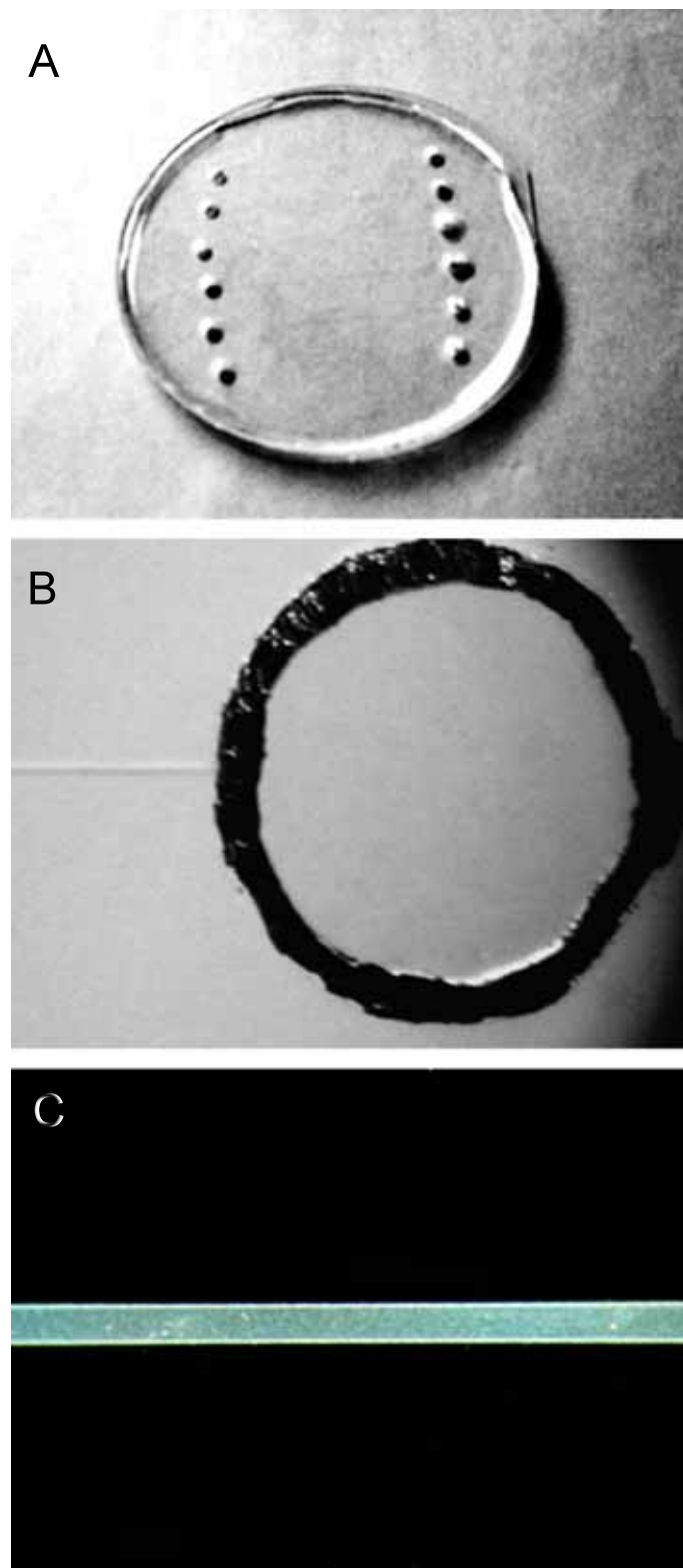


Figure 3.15: Photographs of PDMS stamps for inverse microcontact printing: A) PDMS stamp with punched holes for filling the channels, B) punched filling hole in PDMS with connection to channel, C) $15\mu\text{m}$ channel in PDMS stamp.

channel bundle) were punched with the help of a ticket-punch into the PDMS stamp (figure 3.15). Subsequently, the stamps were cleaned in 2-propanol under ultrasonication and rinsed with water. The PDMS stamps provided a hydrophobic surface. For a better filling of the PDMS channels during inverse microcontact printing, the surface was rendered hydrophilic by ultraviolet/ozone (UVO) treatment (EFIMENKO ET AL., 2002), simultaneously removing organic residues. This UVO treatment caused significant changes in the surface and near surface structure of the PDMS. The molecular oxygen and ozone created during the process interacted with the UV-modified PDMS, resulting in a large number of hydrophilic groups.

Not to loose the hydrophilic character again, the stamps were treated for 1h with a 0.1M sodiumhydroxid solution, thoroughly washed with water under ultrasonication and stored in deionised water. Just before use, the stamps were dried under a stream of air. The above protocol was also used under sterile conditions when appropriate.

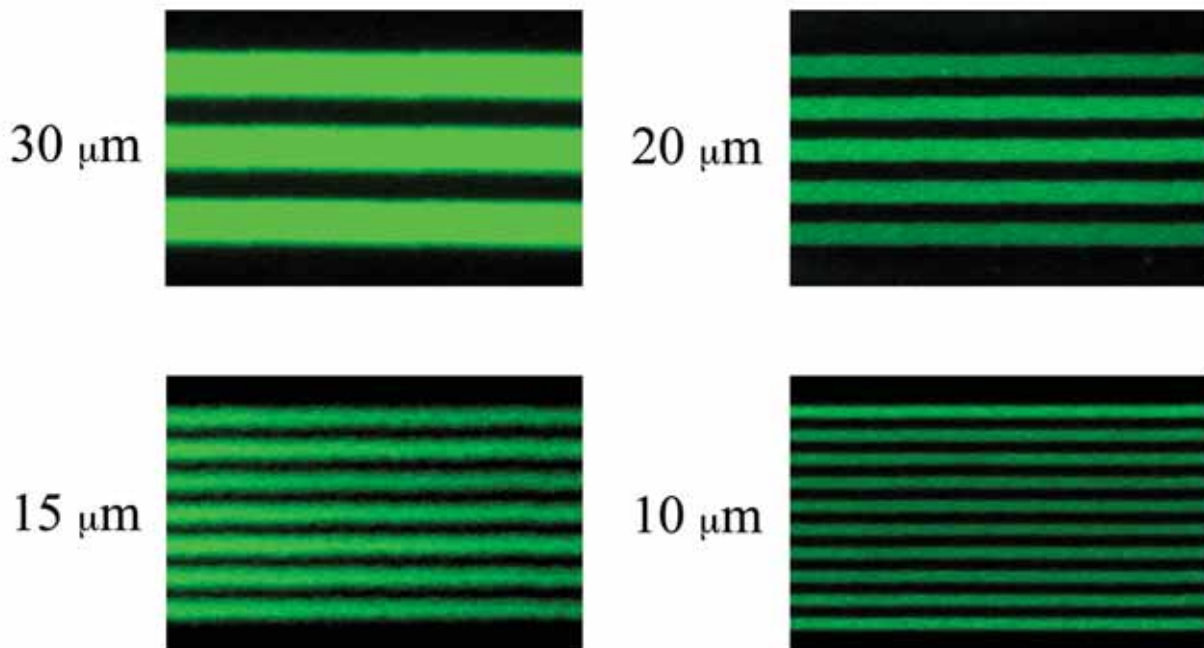


Figure 3.16: Fluorescent images of channels in PDMS stamps to examine the quality and filling: Channels of different widths from $30\mu m$ down to $10\mu m$ in a PDMS stamp filled with a green fluorescent fluid (na.fluorescein).

For the immobilisation process, the PDMS stamps were attached to a glass wafer and air bubbles, which disturbed the conformal contact were removed. The channels in the PDMS

stamp were examined for quality and filling properties (see figure 3.16). Finally, PDMS stamps with intact channels of channel widths of 10, 15, 20 and 30 μm were produced successfully.

Immobilisation Reaction

Before the immobilisation reaction, the glass wafer (borosilicate glass) were incubated together with the stamps (as described above) in a 0.1M sodiumhydroxid solution for an hour, rinsed with water and dried under a stream of air. The stamps were contacted with the substrate and the channels were formed.

Subsequently, all three steps of the immobilisation reaction took place in the microfluidic channels. Firstly, a 10 % aqueous solution of 3-aminopropyltriethoxysilane was prepared and its pH adjusted to 3.45 with 6M HCl. The microfluidic channels were filled, whereas a drop of the reaction solution was placed in the filling hole of one side of the channel and sucked through the channel by applying an vacuum with a vacuum pump at the other end. The solution reacted with the glass surface for 1.5h at 60°C in a convection oven. The oven was turned off and another 2.5 hours were given to cool the substrate down and complete the reaction. The channels were emptied with the use of a vacuum pump and washed three to four times with the next reaction solution, a 2.5 % solution of glutardialdehyde in a 0.1M sodium phosphate (pH 7). Then, channels were filled free of blowholes with the glutardialdehyde solution and left at room temperature for 2h. After depletion of the channels, a fluorescein isothiocyanat (FITC)-labelled bovine serum albumin (BSA) solution was filled in and left over-night at 4°C. In this case, the BSA was used as a model protein for immobilisation instead of the antibody, since it is cheaper and easier to detect with its higher fluorescent label per protein ratio. For analysis, the PDMS stamps were simply peeled of the glass substrate and the latter was thoroughly washed with water and dried in a stream of air.

Blocking of Channels

With the use of the fabricated PDMS stamps for inverse microcontact printing, a patterned immobilisation of FITC-labelled BSA was obtained. Nevertheless, a few drawbacks were caused by operating the whole immobilisation reaction inside the PDMS channels. The filling and depleting of the channels after each reaction step was problematic. Not every channel was emptied and filled for the next reaction step, because of blockage of the channels. Some channel showed dried up parts at the boarder of the channels (see figure 3.17 A on page 56) or were

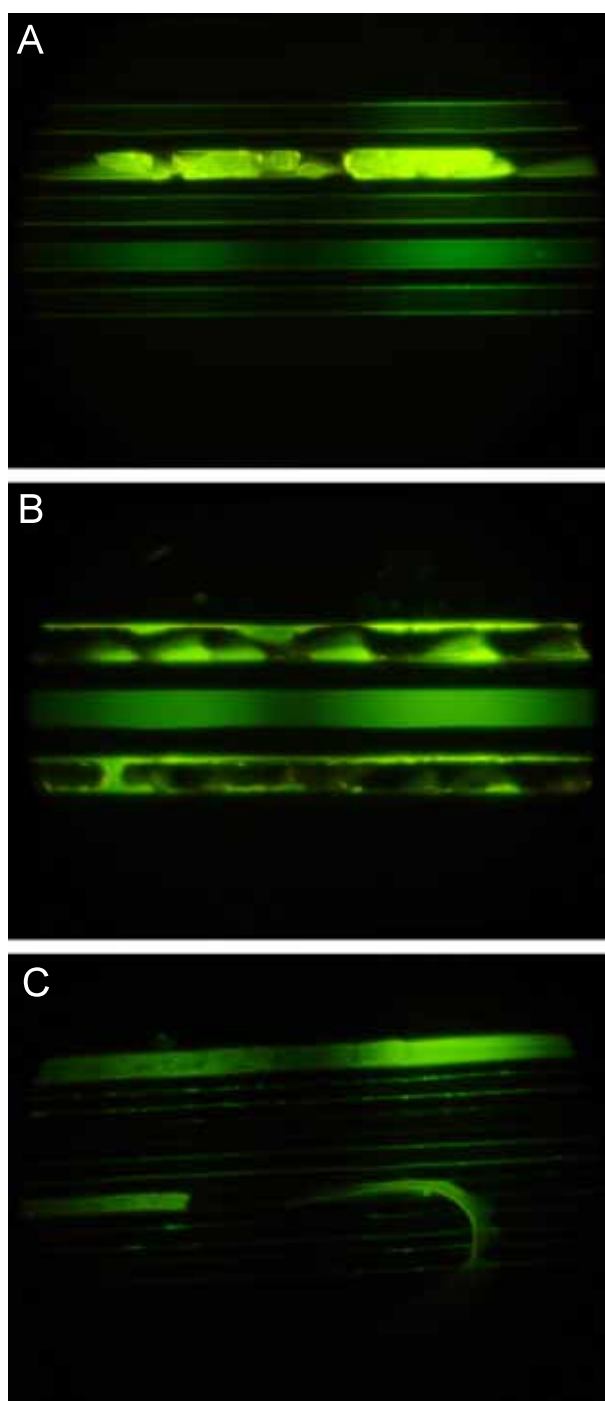


Figure 3.17: Immobilised FITC-labelled bovine serum albumin (BSA) on glass: A) Three $30\mu m$ lines of immobilised BSA are shown with only the middle line showing homogenous immobilisation. The other two protein lines show debris at the border of the line; B) Seven $15\mu m$ wide lines of immobilised BSA should be visible, but only part of the channels show protein immobilisation; C) The picture shows a curved line of immobilised FITC-labelled BSA, which probably resulted from bursting of the channel by the applied vacuum.

totally blocked (figure 3.17 B). In conclusion, a successful protein immobilisation in the desired pattern was possible, but the reaction protocol needed to be optimised for the use with PDMS stamps.

Summary

Positive and inverse microcontact printing was tested for the patterned immobilisation of proteins using the chosen aminosilane/glutaraldehyde chemistry, with promising results for the inverse μ CP approach. None the less, the immobilisation reactions needed to be optimised for the use in the small microfluidic channels of the PDMS stamps.

3.1.4 Optimisation of the Immobilisation Reaction for the Printing Process

Overview

The surface chemistry for protein immobilisation based on aminosilane and glutaraldehyde demanded optimisation for the use in inverse microcontact printing. Accomplishment and results are presented in the following section.

To avoid blockage in the microfluidic channels, which are formed between the PDMS stamp and the glass substrate in the inverse microcontact printing technique, the surface chemistry for protein immobilisation using aminosilane and glutaraldehyde was further analysed. Every single reaction step was investigated and optimised for best performance in inverse microcontact printing.

Substrate

Borosilicate glass was used as a substrate for the protein immobilisation. Glass is widely used in chemical and biological reactions. It is based on silicon dioxide (SiO_2) and is built of oxygen tetrahedra around Si^{4+} ions with the tetrahedra being linked together to form a random network. As all commercial glasses, it contains small amounts of water in form of hydroxyl ions (OH^-). The hydroxyl groups of the glass surface are used as starting point for the immobilisation reaction. They are converted to stable oxane bonds by reaction with a silane.

First Reaction Step: Functionalisation with Silane

3-Aminopropyltriethoxysilane was utilised as a silane-coupling agent. Generally, silanes with three alkoxy groups are used as a starting point for substrate modification. 3-Aminopropyltriethoxysilane combines the organic chemistry of an amino group with the inorganic chemistry of silicates to bridge the hydrophilic interface between mineral substrates and organic molecules. This aminosilane is water-soluble and the resulting solutions have unlimited stability over a wide range of concentrations. Trialkoxysilanes hydrolyse step wise in water to give the corresponding silanols, which ultimately condense with silanol groups of the glass surface to form siloxane linkages without altering the amino group. At a pH of 3 to 4, as adjusted for the used 10 % aminopropyltriethoxysilane solution in water, the initial hydrolysis is relatively rapid and may be considered complete to the triol in 1 to 30 minutes. The stability of the solution was examined over 2 hours by means of nuclear magnetic resonance (NMR), since the silanol groups can condense and become unavailable for bonding with the substrate surface. Figure 3.18 shows the spectrum of the aminosilane. The solution was stable over the contemplated time. No conversion of the aminosilane was observed and only the five characteristic peaks of the C atoms of aminosilane can be seen in the NMR spectrum.

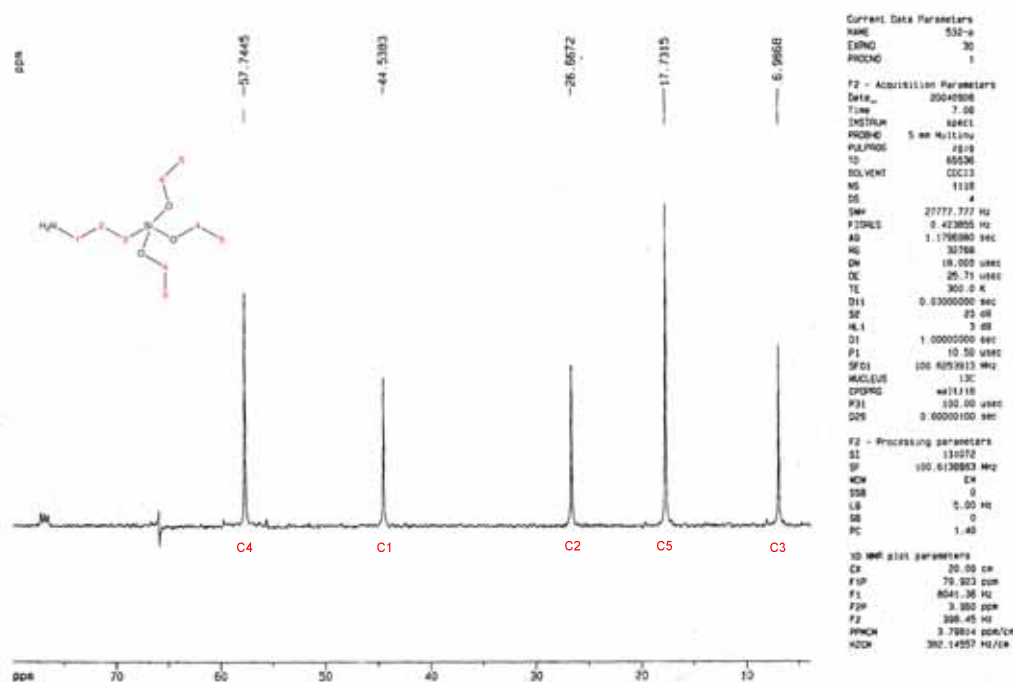


Figure 3.18: ^{13}C nuclear magnetic resonance spectrum of 3-aminopropyltriethoxysilane

The heating of the first reaction step to 60°C for $2h$ insured the silanol condensation at the surface, but simultaneously caused blocking problems, when the small PDMS channels ran dry. To solve this blocking problem, different reaction times ($1h$, $2h$ and over night incubation) and conditions (60 , 100 and 120°C) were tested (data not shown), in parallel with different solvents such as ethanol, toluol and water for the aminosilane solution. The reaction was analysed by imaging ellipsometry (see figure 3.19 on page 60) to assist the selection of the optimal reaction parameters. Lower concentrations of aminosilane were also assayed regarding an effect on the amount of blocked channels after the first reaction step (data not shown).

The results indicated, that the exchange of the solvent to ethanol or toluol did not decrease desiccation and showed worse functionalisation of the glass surface as imaged with ellipsometry. Furthermore, the toluol was not compatible with the use of the PDMS stamp in inverse microcontact printing. It spread under the stamp, thus disturbing the patterning.

Finally, the blocking of the PDMS channels in the first reaction step was avoided by reducing the reaction time to $1h$. Additionally, the reaction was carried out in a convection oven with humidified atmosphere and filling holes of the stamp were sealed with adhesive tape to avoid desiccation. Thereby, all channels were refillable after the first reaction step. The covering of the stamp's filling holes with adhesive tape was retained also for the other reaction steps.

Second Reaction Step: Cross-Linking with Glutardialdehyde

Subsequently, the aminosilane-functionalised glass surface is cross-linked with glutardialdehyde. A 2.5 % aqueous glutardialdehyde solution in $0.1M$ sodium phosphate buffer was used and reacted with the amine-containing matrix for $2h$ at room temperature. Again, extensive blockage of the PDMS channels was observed. Covering of the filling holes with adhesive tape did not lead to satisfying results. There was evidence that the blockage was related to the use of $0.1M$ sodium phosphate buffer as a solvent for the 2.5 % glutardialdehyde solution (pH 7). A reduction of the salt concentration was tested by using a $0.01M$ or $0.001M$ phosphate buffer, respectively, but the subsequent protein immobilisation was not successful when using these buffers with lower salt concentrations. An explanation for this observation was found in the character of the addition/elimination reaction on the carbonyl group and the factors affecting the reaction kinetics. In the presence of a strong nucleophil such as a primary amine, the nucleophil adds to the carbonyl group forming a tetrahedric intermediate, followed by the transmission of a proton and the condensation to the imine. In such a system, the total reaction rate is diminished by

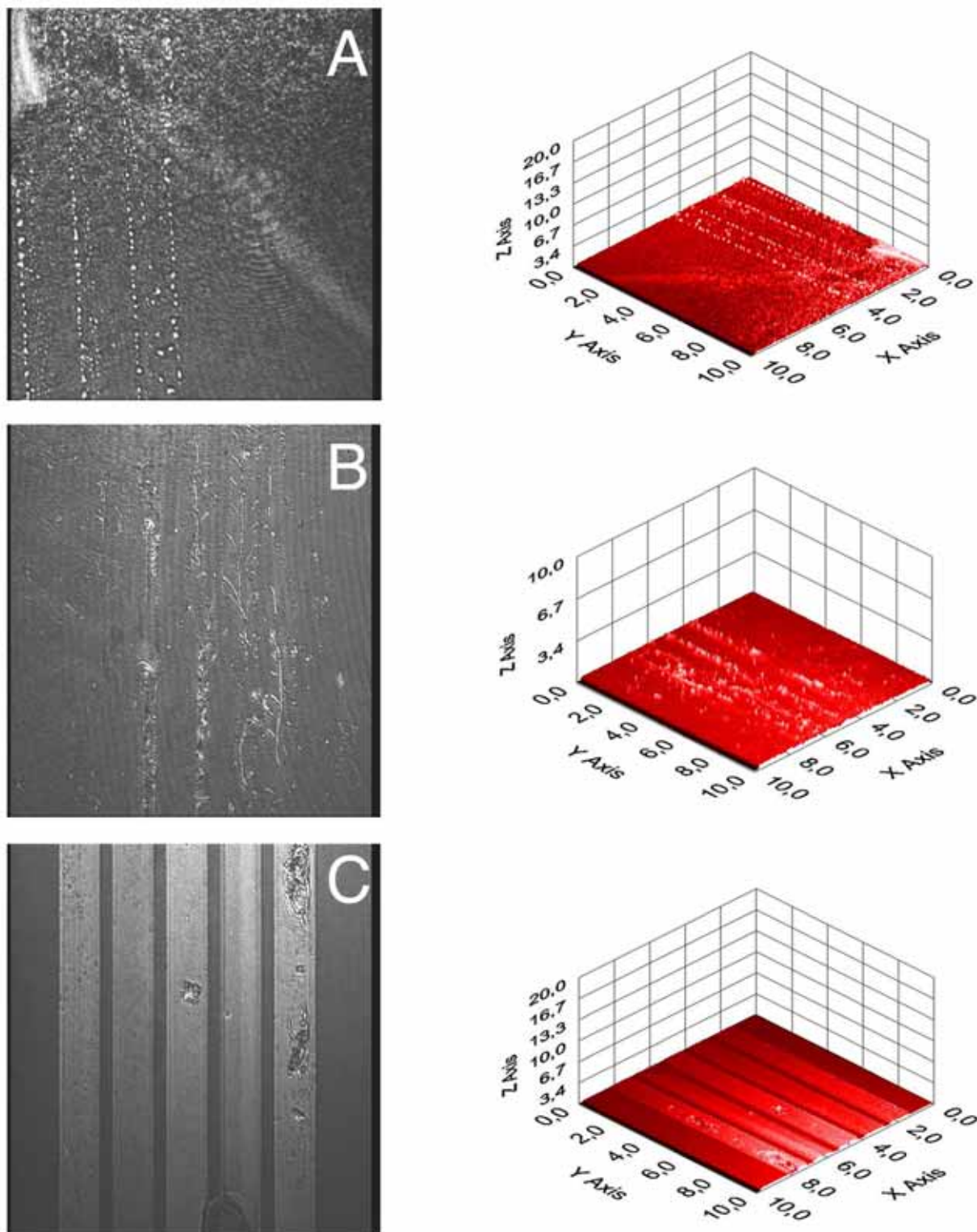


Figure 3.19: Live Images and 3D maps of aminopropyltriethoxysilane functionalised lines on glass. A 10 % aminosilane solution in different solvents was reacted for 1h at 60°C with the substrate: A) 85 % ethanol (pH 4.5-5.5), B) toluol (pH not adjusted), C) in water (pH 3.45)

Technique Box

Imaging Ellipsometry

Application:

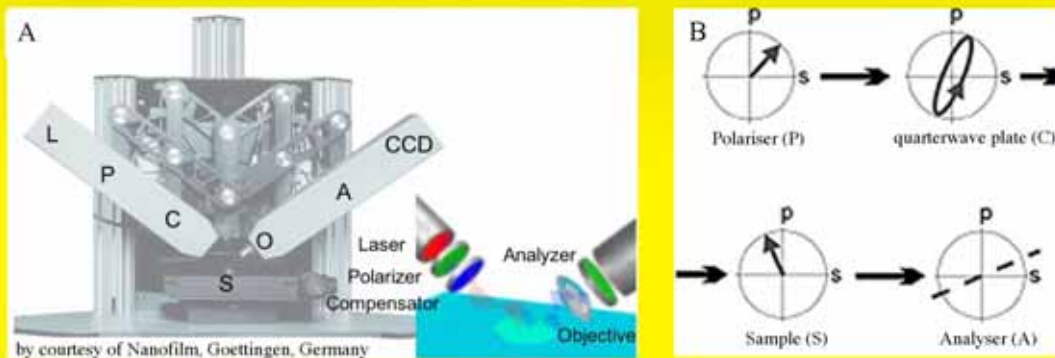
Non-destructive characterisation/imaging of thin films (analysis of thickness and optical properties)

Requirements:

Ellipsometer (high resolution microscope, light source (multiple laser wavelengths), motorised goniometer for accurate angle-of-incidence adjustments, software)

Method:

Imaging ellipsometry makes use of the fact that the polarisation state of light may change when the light beam is reflected from a surface. If the surface is covered by a thin film (or a stack of films), the entire optical system of film and substrate influences the change in polarisation. It is therefore possible to deduce information about the film properties, especially the film thickness. The name "ellipsometry" derives from the elliptical state of polarisation, where the electrical field vector travels along an ellipse when observed at a fixed point in space.



The imaging ellipsometer operates on the principle of classical null ellipsometry and real-time ellipsometric contrast imaging. The laser beam is elliptically polarised after it passes through a linear polarizer (P) and a quarter-wave plate (C). The elliptically polarised light is then reflected off the sample (S) into an analyser (A) and imaged onto a CCD camera through a long working distance objective. In this PCSA configuration, the orientation of the angles of P and C is chosen in such a way that the elliptically polarised light is completely linearly polarised after it is reflected off the sample.

As shown in figure B, the ellipsometric null condition is obtained when A is perpendicular with respect to the polarisation axis of the reflected light, *i.e.*, the state at which the absolute minimum of light flux is detected at the CCD camera. The angles of P, C and A that determine the null condition are related to the ellipsometric parameters Δ and Ψ . The tangent of the angle Ψ gives the ratio of amplitude change for the polarisation components, while Δ denotes the relative phase shift of these polarisation components upon reflection. Reduction of the measured Δ and Ψ with computerised optical modeling leads to a deduction of the optical properties of the sample (complex refractive indices) and the film thickness.

proton donors, since the amount of nucleophilic for the reaction is reduced. Thus, the reaction of primary amines is not catalysed by acid, because the ammonium groups, which would result from protonation, are not nucleophilic towards the carbonyl group, and the carbonyl group cannot compete against the primary amine for protonation. Using the 0.01M and 0.001M sodium phosphate buffer, the buffer capacity, which is already low because of the low salt concentration, was exceeded. Residues of the aminosilane solution with a pH of 3.45 are left in the PDMS channels after the first reaction step. By washing with the next reaction solution, most of it is removed, but a good buffer capacity is still needed to keep a neutral pH for the second reaction step. In the case of the use of lower salt concentration for the phosphate buffer, an acidic condition is present in the second step, which slows down the reaction, because of the reasons given above.

Analysis of the buffer revealed a high number of particles ($3.5 \cdot 10^6$ particles) with an average size of $4.74\mu\text{m}$. Two filtration cycles using an aseptic filter (pore size: $0.22\mu\text{m}$) reduced the number of particles by 97.2 %. Removing those particles, which probably were insoluble impurities from the sodium phosphate, solved the problem of channel blockage.

Third Reaction Step: Binding of Protein (*e.g.* Antibody)

The optimisation of the two preceding reaction steps solved the blockage problem. The PDMS stamp was removed after the third step. In this step, the protein (*e.g.* an antibody) was immobilised via its primary amino groups in a Schiff's base reaction with the second carbonyl group of the glutardialdehyde of the previous cross-linking step.

As a test system, the monoclonal antibody anti-CD34-FITC and FITC-labelled BSA were immobilised successfully in lines of different width by inverse micro contact printing (see figure 3.20). The use of a FITC-labelled BSA solution with a concentration of $200\mu\text{g}/\text{mL}$ resulted in a homogenous immobilisation of the protein over the width and length of the PDMS channels (as shown in figure 3.20 A and B). The immobilised antibody (Ab) lines (Ab concentration: $6\mu\text{g}/\text{mL}$) looked inhomogeneous and less dense. To analyse the immobilised protein lines, each reaction step was examined by imaging ellipsometry, a sensitive optical method of quantifying thin layers (see Technique Box on page 61).

The immobilised antibody (anti-CD34-FITC) and immobilised BSA lines (FITC-labelled) were analysed qualitatively by ellipsometry of an $0.4 \cdot 0.6\text{mm}^2$ area with a spatial resolution of $2\mu\text{m}$. Figure 3.21 on page 64 shows a live image and an image with inverted ellipsometrical

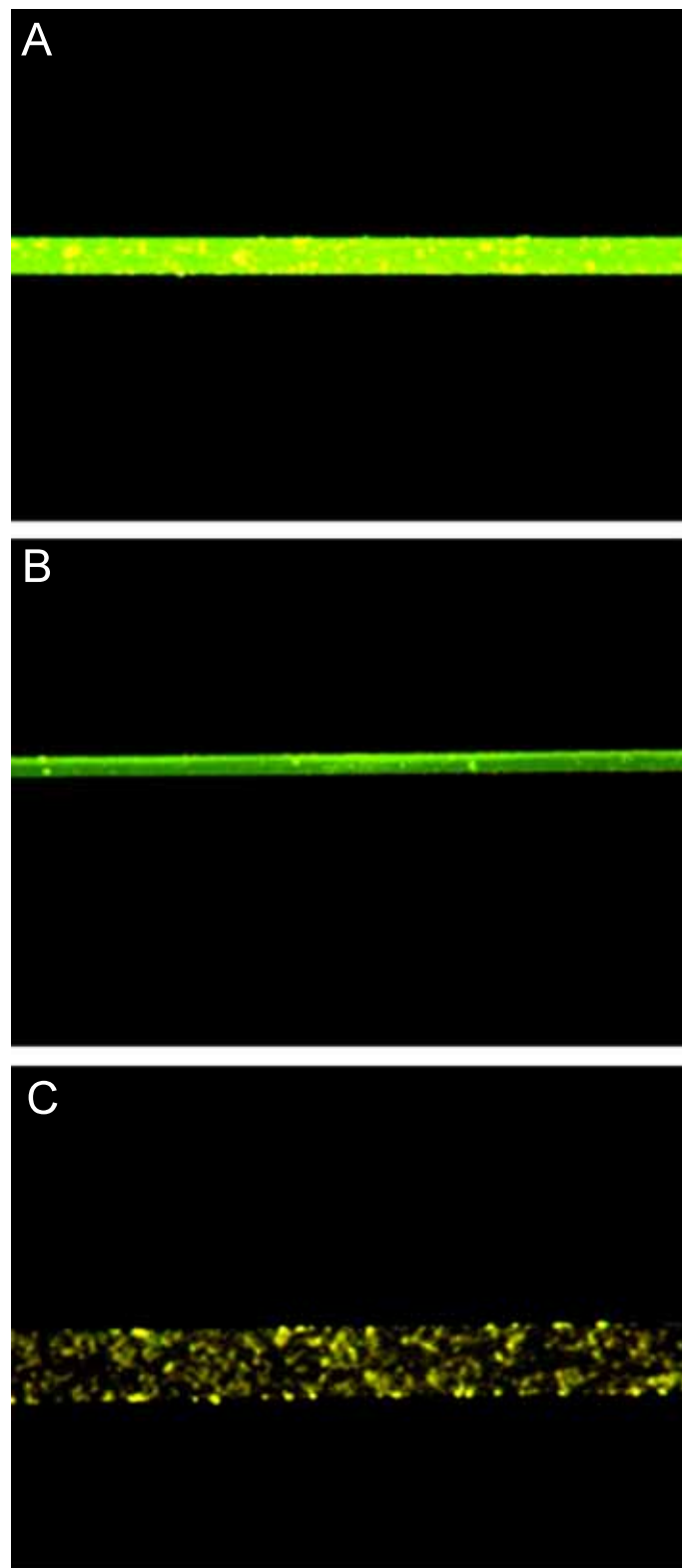


Figure 3.20: Fluorescence micrographs of immobilised proteins on glass via aminopropyltriethoxysilane and glutardialdehyde: A) BSA-FITC in a $50\mu m$ channel; B) BSA-FITC (bovine serum albumin) in a $30\mu m$ channel; C) anti-CD34-FITC antibody in a $80\mu m$ channel.

contrast of both samples. The ellipsometrical contrast was inverted to verify that the structure shown in the live image was not due to interferences. The ellipsometrical images of the antibody line confirmed the inhomogeneity, which already had been observed via fluorescence microscopy. Generally, the lines of immobilised protein are clearly silhouetted against the background.

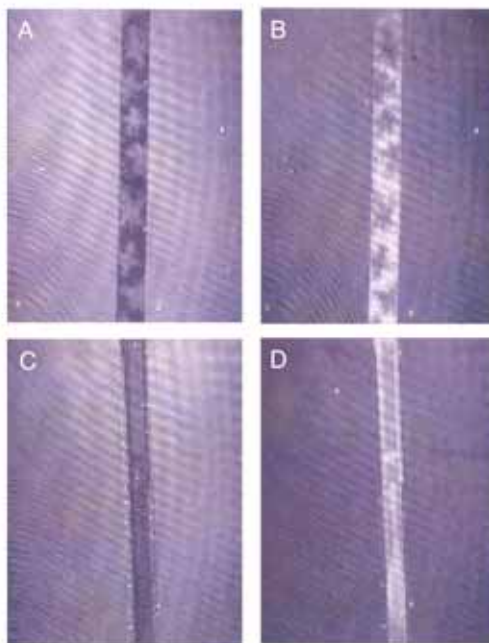


Figure 3.21: Live images (A and C) and ellipsometrical contrasts (B and D) of an immobilised antibody line (anti-CD34-FITC) (A and B) and an immobilised FITC-labelled BSA line (C and D)

In a subsequent quantitative measurement the film thickness and refractive index were determined. First of all, the optical parameters of the substrate were measured in the surrounding of the protein line. To obtain a higher accuracy, the number of the measured parameters were increased by recording a spectrum of the angle of incidence. Data for the ellipsometrical angles Delta and Psi were measured near the Brewster angle from 55° to 57.5° in 0.2° steps. From these data, the optical constants of the substrate were defined, which were then applied for the determination of film thickness of the protein lines.

With the help of an optical model the film parameters were calculated. Therefore, the measured data for Delta and Psi were fitted to the model (see figure 3.22 on page 65 for an example). The measured data showed a good compliance with the fitted data.

A refractive index of 1.495 and 1.513 was obtained for the antibody line and the BSA line,

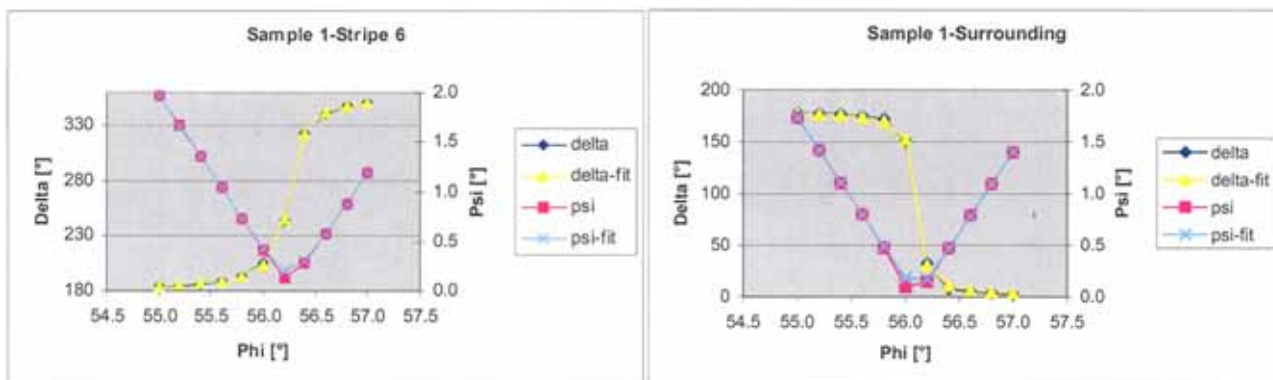


Figure 3.22: Measured and fitted Delta and Psi data for the glass substrate (surrounding) and an FITC-labelled BSA line (named stripe 6).

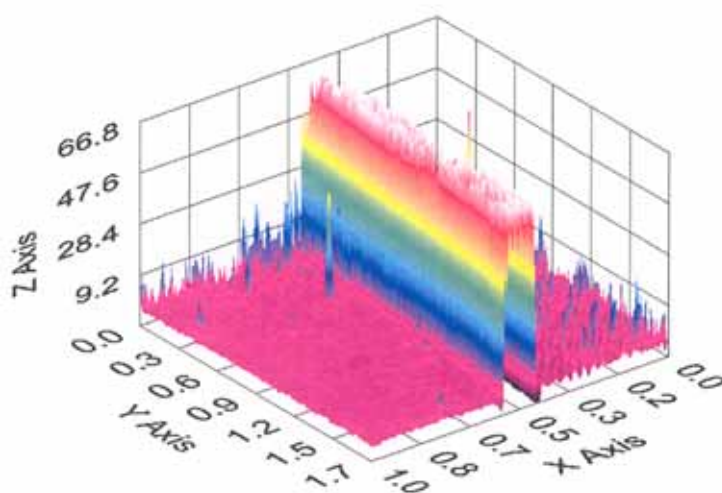


Figure 3.23: 3-dimensional film thickness map of an immobilised FITC-labelled BSA line. The z-axis gives the film thickness in nm, x- and y-axis are random units.

respectively, which is a typical value for biomolecules. The film thicknesses were averaged over the inhomogeneity of the protein lines, resulting in $80.9nm$ for the anti-CD34-FITC antibody line and in $68.2nm$ for the FITC-labelled bovine serum albumin line, respectively. The BSA line with a height of $68.2nm$ was also displayed as a 3-dimensional thickness map in figure 3.23 on page 65.

To check the reproducibility of the measurements, 10 measurements were conducted exemplarily on one position of the substrate and also on ten different positions on the substrate. A reproducibility of $0.05nm$ at the same position and $1nm$ at different positions of the substrate arised from the measurements.

One reason for the inhomogeneity of the anti-CD34-FITC antibody line could be due to the low concentration ($6\mu g/mL$) of the commercially available antibody, thus not enough antibody was present to form an homogenous film. Unfortunately, this antibody was not available in higher concentrations. Therefore, an unlabelled anti-CD34 antibody, which was available in a concentration of $55\mu g/mL$, was tested. The ellipsometrical live image (see figure 3.24) showed a homogenously immobilised antibody in a line.



Figure 3.24: Ellipsometrical live image of an anti-CD34 antibody line

Summary

The surface chemistry for the immobilisation of antibodies had to be optimised for the use with inverse micro contact printing. All three reaction steps were analysed and changed to avoid blockage in the small PDMS channels. In the end, a test antibody was immobilised homogenously.

3.1.5 Cell Binding

Overview

After the successful immobilisation of antibodies in small lines from 10 to 30 μm has been shown, the binding of cells to these antibody lines was investigated. Therefore, the model cell line KG-1 and primary dendritic cells were tested to bind immobilised antibodies.

Using antibody lines for the binding of cells in an electrofusion chamber, the specificity of the antibody determines the type of cell, which can bind to these lines. For a broader application to various cell systems and different fusion partners, the immobilisation of a linker protein, such as streptavidin could be used (see figure 3.25). This would allow binding of every cell type, which is coupled to an individual biotinylated antibody, to the streptavidin line.

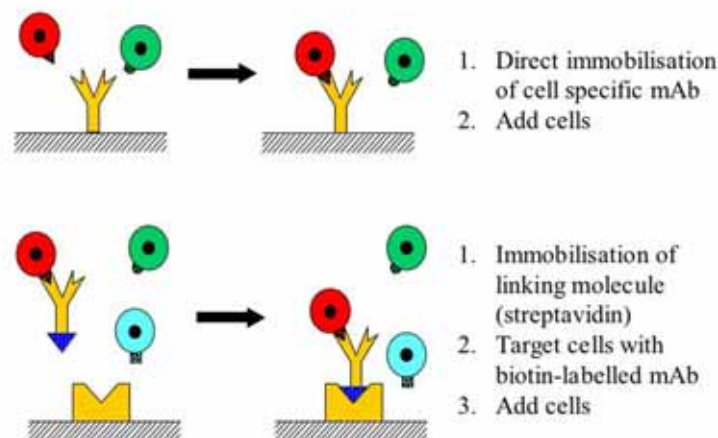


Figure 3.25: Diagram of direct binding of cells to antibodies and indirect binding via streptavidin/biotin linkage

The streptavidin/biotin system was tested successfully with inverse μCP and streptavidin was immobilised homogenously as proven by ellipsometry (data not shown). Using this system extends the number of reaction steps by one. For this reason, the direct immobilisation via covalently bound antibodies was used for all subsequent experiments.

In previous experiments described in section 3.1.3 and 3.1.4, the cell line KG-1 was bound to an anti-CD34 antibody. To transfer this approach to primary dendritic cells, an antibody

specific for surface proteins expressed by DCs needed to be chosen.

The selection of an antibody for DC binding was determined by its required properties: A blockage of receptors important in immunological reactions such as co-stimulation by CD80 or CD86 had to be avoided and the antibody should be usable with primary DCs as well as with the cell line KG-1. Therefore, the antibody anti-CD45 was chosen. It is expressed on both the cell line KG-1, an erythroleukemia cell line, which shares morphological and physiological properties with myeloid DCs, and primary DCs. The CD45 antigen is a tyrosine phosphatase also known as leukocyte common antigen (LCA). It is expressed on all human cells of haematopoietic origin, except erythroid cells, platelets and their precursor cells.

Firstly, KG-1 was used for the binding experiments of a cell to the anti-CD45 antibody, which is shown in figure 3.26. The cell line was attached to antibody lines in $10\mu m$, $15\mu m$ and $20\mu m$ width. As demonstrated in figure 3.26C, KG-1 cells bound to the $10\mu m$ lane of immobilised anti-CD45 in a monocellular chain. The figure shows clearly that the arrangement of cells in chains is determined by the cell diameter and therefore by the width of the antibody lanes. In the next experiments, primary DCs were bound to the anti-CD45 antibody. The antibody was immobilised in $10\mu m$, $15\mu m$ and $20\mu m$ lanes and DCs were incubated. Figure 3.27 on page 71 demonstrates the results analysed by scanning electron microscopy (SEM). As the diameter of DCs was bigger compared with KG-1 cells ($20\mu m$ compared to $15\mu m$), $15\mu m$ lanes showed that the cells bound over the width of the antibody line (figure 3.27A). The dendritic cells stretched along the line (figure 3.27B) and the extensions of the DCs did not exceed the antibody lane (figure 3.27C). In figure 3.28, multiple lines of immobilised antibody were used to bind primary DCs. The cells line up along the lines, but the preparation of the biological specimen for the SEM analysis removed some of immobilised cells due to dehydration and gold sputtering.

The human anti-CD45 antibody was used in all subsequent experiments and produced in two continuous fermentations of up to $10L$ of the hybridoma cell line CF10H5 (data not shown).

After the binding of the cell line KG-1 and the primary DCs, the alternating arrangement of the fusion partners was tested. KG-1 cells were stained with the cytosolic CellTracker dyes CMTMR (red) and CMFDA (green), respectively. The red KG-1 cells were bound to the anti-CD45 antibody lines with a width of $10\mu m$. After removing the excess of cells by washing, the green KG-1 cells were added (see figure 3.29 on page 73). The green KG-1 cells settled in the spaces between the red bound cells and an alternating arrangement of red and green KG-1 cell lines was obtained. In the following section, the detachment of bound cells was investigated. In

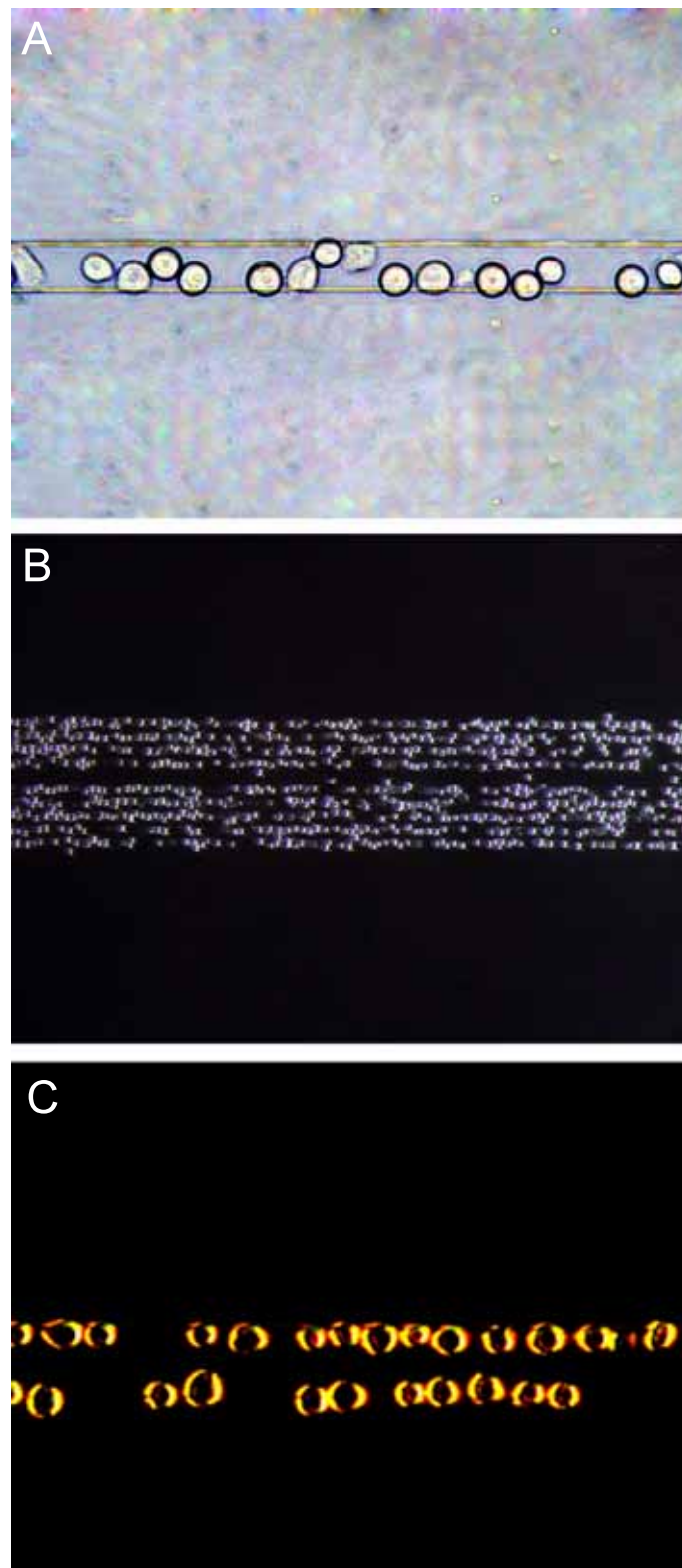


Figure 3.26: Light microscopy pictures of the immobilisation of KG-1 to antibody lines: A) This picture shows a $20\mu\text{m}$ wide antibody line. This line is too wide for the binding of KG-1, thus the cells do not line up in a chain; B) shows binding of the cells to nine parallel antibody lines ($15\mu\text{m}$); C) the picture shows the alignment of cells in a chain bound to antibody lanes with a width of $10\mu\text{m}$.

Technique Box**Ex vivo generation of monocyte-derived dendritic cells (moDCs)****Application:**

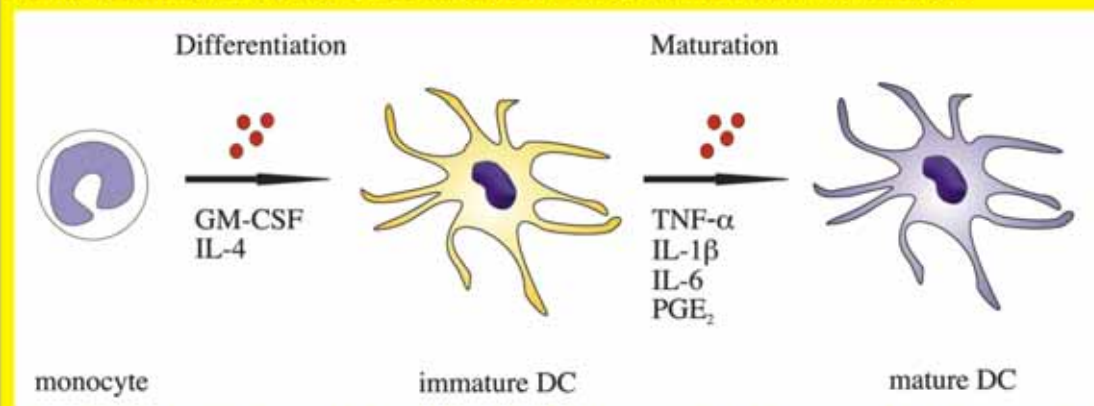
In vitro experiments such as cell binding assays, T cell stimulation, etc.

Requirements:

Ficoll-Paque, magnetic cell separation column, magnetic beads, serum-free cell culture medium, cytokines

Method:

Immature dendritic cells can be generated from blood monocytes by cultivation with special cytokines, such as granulocyte macrophage-colony stimulating factor (GM-CSF) and interleukin 4 (IL-4), and subsequently matured with inflammatory cytokines like tumor necrosis factor alpha (TNF- α), interleukin 1 beta (IL-1 β), interleukin 6, (IL-6) and prostaglandin E₂ (PGE₂). The process of maturation enables the DCs to evolve from antigen-capturing to antigen-presenting cells. Not only the function, but also the phenotyp of dendritic cells is dependent on the maturation stage.



An optimised protocol was developed within the EU project (Bohnenkamp and Noll, 2003) for the generation of monocyte derived dendritic cells in a clinical scale to GMP standard. Highly viable DCs ($94 \pm 2\%$) can be produced from CD14⁺ monocytes enriched via immunomagnetic beads in a high yield ($28 \pm 6\%$).

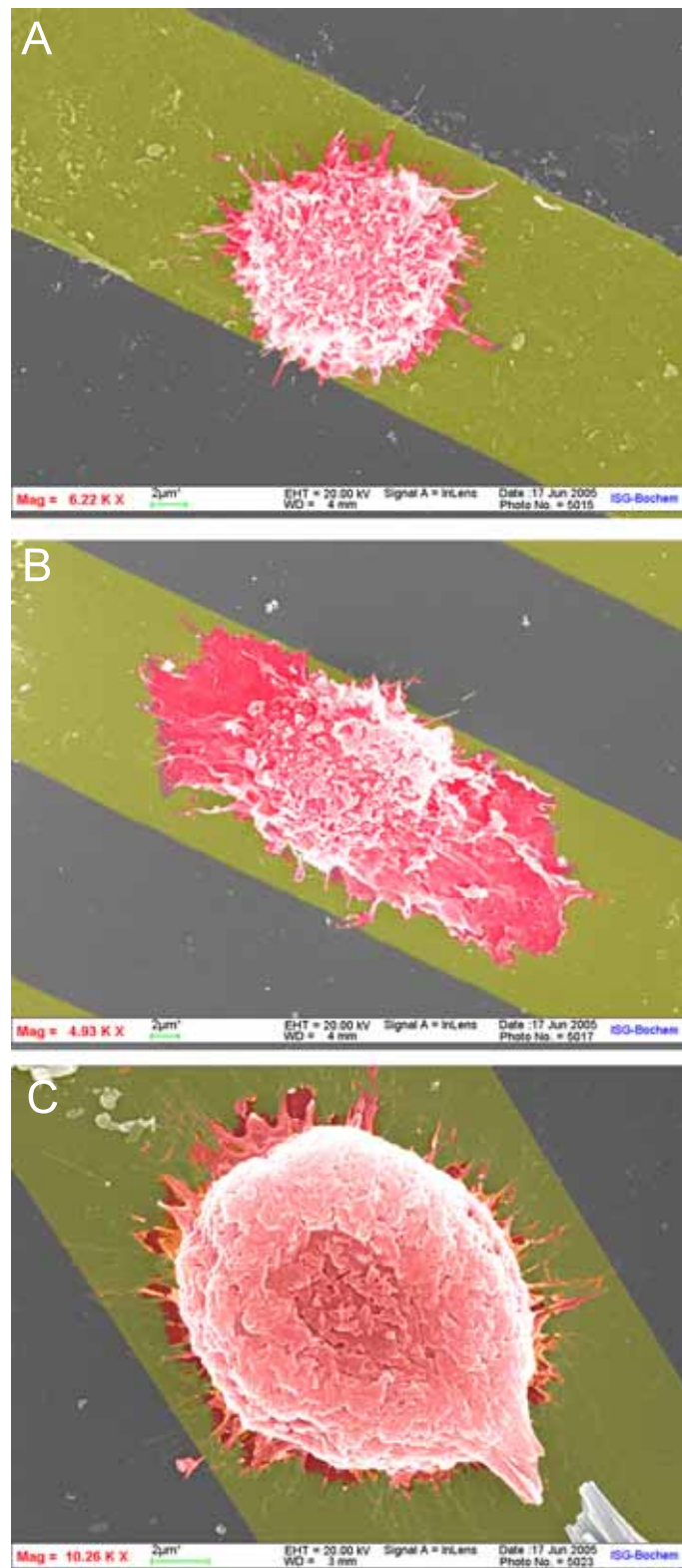


Figure 3.27: Coloured SEM pictures of single dendritic cells bound to an antibody line: A) shows that the chosen size of $15\mu\text{m}$ for the antibody line correlates with the size of the dendritic cell; B) shows a dendritic cell stretching along an antibody line; C) shows that the extensions of the DC do not protrude over the edge of the antibody line.

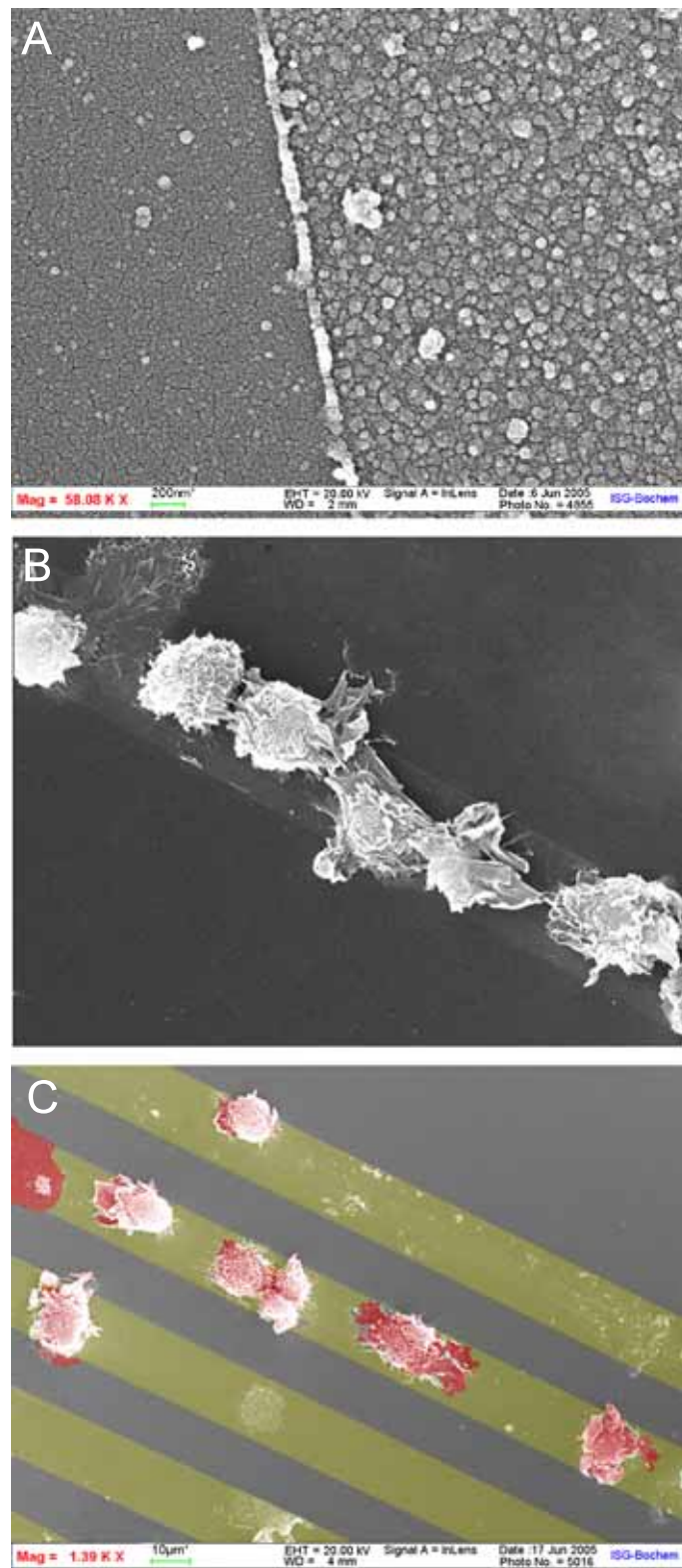


Figure 3.28: Scanning electron micrographs of immobilised antibody stripes and dendritic cells bound to it: A) The micrograph shows part of an immobilised antibody stripe on the right and the glass substrate on the left; B) Dendritic cells bound side by side on an antibody line; C) Coloured photo of dendritic cells on antibody lines ($15\mu m$).

a fusion process, DCs are bound to antibody lines that are covalently immobilised to the glass surface and fused to an unbound fusion partner. After the fusion process, the cell-antibody connection has to be broken up to yield a fusion product.

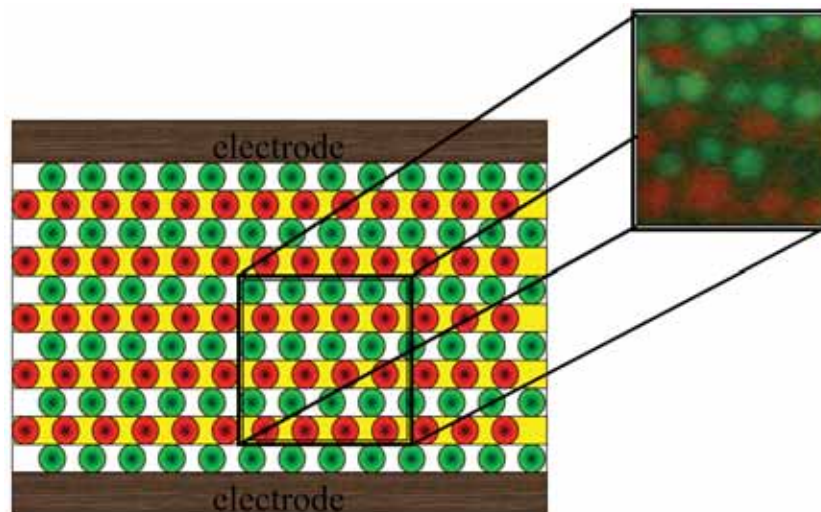


Figure 3.29: Alternating arrangement of red and green KG-1 cells, stained with CMTMR (red) or CMFDA (green), respectively, opposed to the schematic representation.

Summary

In conclusion, the cell line KG-1 and the primary dendritic cells were bound to an immobilised anti-CD45 antibody. Furthermore, an alternating arrangement of two fusion partners was realised.

3.1.6 Cell Detachment

Overview

The detachment of cells, which are bound to antibody lines, is addressed in the following section. The detachment is needed for harvesting the hybrids after the fusion process, since the hybrids will be immobilised to the antibody lines due to the fact, that one of their parts (the first fusion partner) was immobilised.

The binding of the cells to the antibody micropattern resulted in immobilised hybrids after the fusion process. The disruption of the antigen-antibody-complex is needed for harvesting the

hybrids. Mild conditions are preferred not to damage the cells. Pepsin (from porcine stomach), papain, trypsin, high salt concentration and pH shift were tested as displacement agent for the immobilised cells. The first three are proteases, which cleave protein at defined amino acids. Especially papain and pepsin are known to cleave antibodies near the hinge region and separates F_c and F_{ab} fragments from each other. All five approaches were tested for the detachment of antibodies from the bound cells, either by cleavage of the antibody or by detachment of the antigen-antibody binding. The best results were obtained using a pH-shift from a neutral pH to an acidic pH of 2 (see figure 3.30).

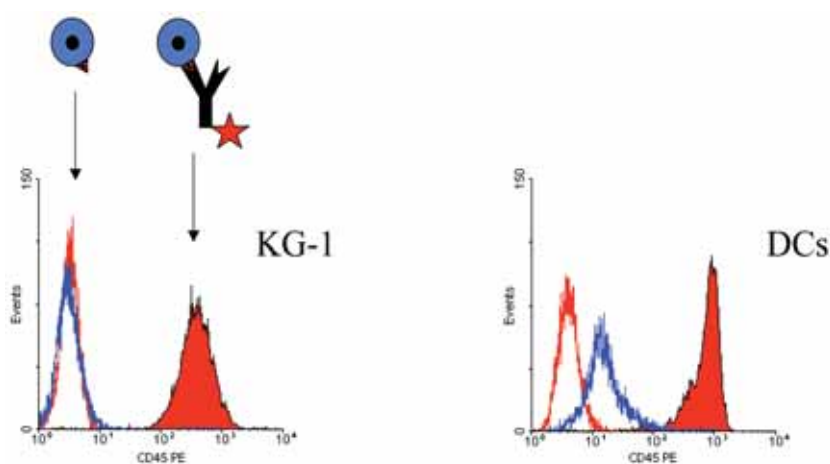


Figure 3.30: Detachment of an anti-CD45 antibody from KG-1 or dendritic cells by a short drastic shift of the pH from pH 7.4 to pH 2. The unlabelled cell peak is outlined in blue (negative controlled), the stained cell peaks are depicted in red (before treatment with pH 2 (red filled) and after treatment (red outlined)).

In the first step, the cell detachment analysis were performed using FACS (fluorescent activated cell sorting). The cells were labelled with an anti-CD45-PE antibody and measured in a flow cytometer using unlabelled cells as negative control. The labelled cells, which bound the antibodies to their surface (CD45-antigen), were then treated with a 25 % v/v solution of hydrochloric acid for 30sec and immediately neutralised with a great volume of saline phosphate buffer (PBS) with neutral pH. The results (figure 3.30) showed, that all anti-CD45 antibodies bound to KG-1 cells could be removed by this treatment. When transferring this technique to dendritic cells, it was observed, that more antibodies bound per cell and that not all of them could be removed with the pH shift. Whether this would be sufficient for the detachment of immobilised cells from the substrate was tested in subsequent experiments and was successful.

Technique Box**Fluorescence-Activated Cell Sorting (FACS)****Application:**

Measurement of cell surface and intracellular antigens and receptors, cell cycle status, intracellular ion flux and cell proliferation

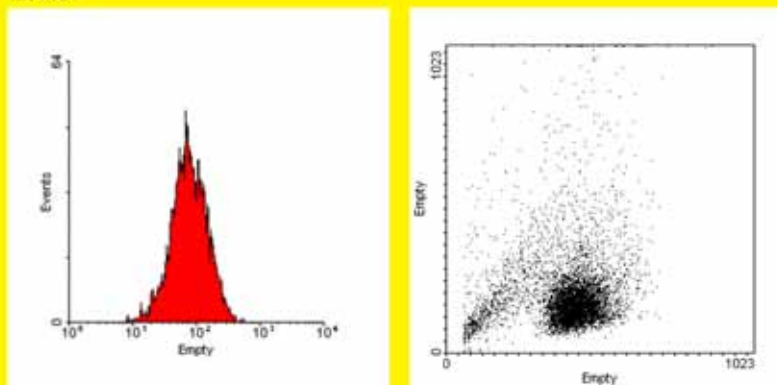
Requirements:

Flow cytometer, cells, fluorescent labelled antibody or other fluorescent dyes

Method:

Fluorescence-activated cell sorting is a type of flow cytometry. Flow cytometry uses laser light to excite fluorescent labelled molecules (such as antibodies or proteins) attached to or located inside cells and subsequently detects the emitted fluorescent light on cells passing in single file in a fluid stream. Multiple characteristics of single cells can be measured simultaneously at a rapid rate. In addition to the relative fluorescence intensity (FL-1, FL-2 and FL-3) of the cells, their relative size (Forward Scatter - FSC) and relative granularity (Side Scatter - SSC) can be measured in line with the laser beam or perpendicular to it.

FACS data are commonly presented as one-dimensional histograms or two-dimensional displays (dot plots) with logarithmic axes that extend over a 'four- to five-decade' range, representing cells with fluorescence values that differ 10,000- to 100,000-fold between the lower and upper ends of the scale.



In addition, the occurrence of apoptosis, or programmed cell death, was monitored, using the Annexin V-FITC apoptosis detection kit II for flow cytometry from BD Biosciences following the manufacturer's instruction. Apoptosis in its early stages can be detected by Annexin V, which binds with high affinity to phosphatidylserine (PS). In normal cells PS is situated on the inner leaflet of the plasma membrane, but during the early stages of apoptosis, PS is translocated to the outer layer of the cell membrane. Because PS is exposed in the early stages

of apoptosis when the cell membrane still remains intact an Annexin V assay coupled with a dye exclusion test (propidium iodide) can discriminate between apoptotic and necrotic cells (VERMES ET AL., 1995).

No apoptosis induction was observed in the detached cells, neither for KG-1 nor for dendritic cells (data not shown). For KG-1 cells the result was verified by monitoring the growth curve of pH 2 treated KG-1 in comparison to untreated cells over 14 days. No difference was observed. Thus, both the cells and the antibodies survived the short subsidence of the pH. The latter has been proven successfully by the reuse of the detached antibodies for cell binding. For DCs, the results were verified by a wash-out-test additionally. After the differentiation from monocytes to immature dendritic cells for six days and maturation for another two days, all differentiation and maturation cytokines were removed and the DCs cultured for 48h in serum-free medium. No differences in cell number or viability were observed for cells treated by pH 2 on day 6 compared with untreated cells.

Summary

A method was found for the reliable detachment of cells from antibodies, which immobilised the cells to a solid substrate. Furthermore, it was proven that the used pH-shift did not harm the cells or antibodies, if neutralised after 30 seconds.

3.1.7 Electrode Integration and Chamber Assembly

Overview

The following section shows how the electrofusion chamber is assembled around the antibody lines and electrodes are integrated into the system to obtain a fully functional electrofusion chamber.

The next step in the development of a cell fusion chamber supporting the immobilisation methods was the integration of electrodes and the build-up of the fusion chamber. According to the commercially available fusion chamber by Eppendorf, it was aimed to integrate Platinum wires with a diameter of $200\mu m$. However, a positioning of the wires parallel to the antibody lines was not possible and stretching the wires over the glass surface proved to be difficult, as well.

As an interim solution, electrodes were used, which were applied as conductor paths on a $400\mu\text{m}$ thick low temperature co-fired ceramic (LTCC) slab (see figure 3.31). The electrodes were manufactured by a cut-out of $200\mu\text{m}$ width and 4 cm length in a AgPd conductor path at Viaelectronic (Hermsdorf, Germany).

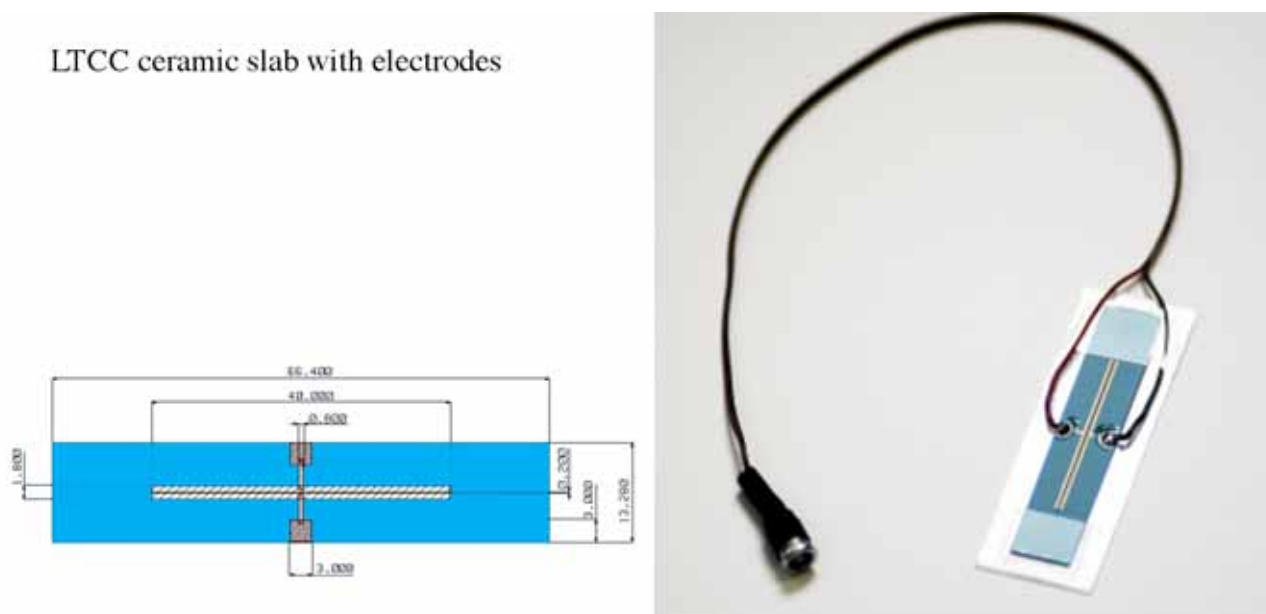


Figure 3.31: Schematic depiction and photograph of LTCC ceramic slab with electrodes for the usage as fusion chamber in the immobilisation approach

Nevertheless, with the LTCC slab, the electrodes had to be positioned manually under microscopic surveillance to run parallel to the antibody lines. With other approaches such as the application of electrodes by vacuum deposition (*e.g.* gold electrodes), the same problem persisted. The PDMS stamp had to be placed on the glass substrate with the electrodes in that way, that the channels were formed parallel to the evaporated electrodes. In either way, the positioning had to be accurate to a micrometer, which in principle was considered to be difficult, and the instruments needed were not available.

Therefore, a method was developed, which avoided this positioning step. The electrodes and lines for the antibody immobilisation were applied simultaneously by gold evaporation onto a glass substrate. The applied structure combined the two electrodes with a width of $200\mu\text{m}$ and a length of 10 mm, their contact patches for impressing a voltage, and lines for antibodies, which were applied in the $200\mu\text{m}$ space between the electrodes (see figure 3.32). This approach was developed and realised at the university in Cranfield, UK in the research

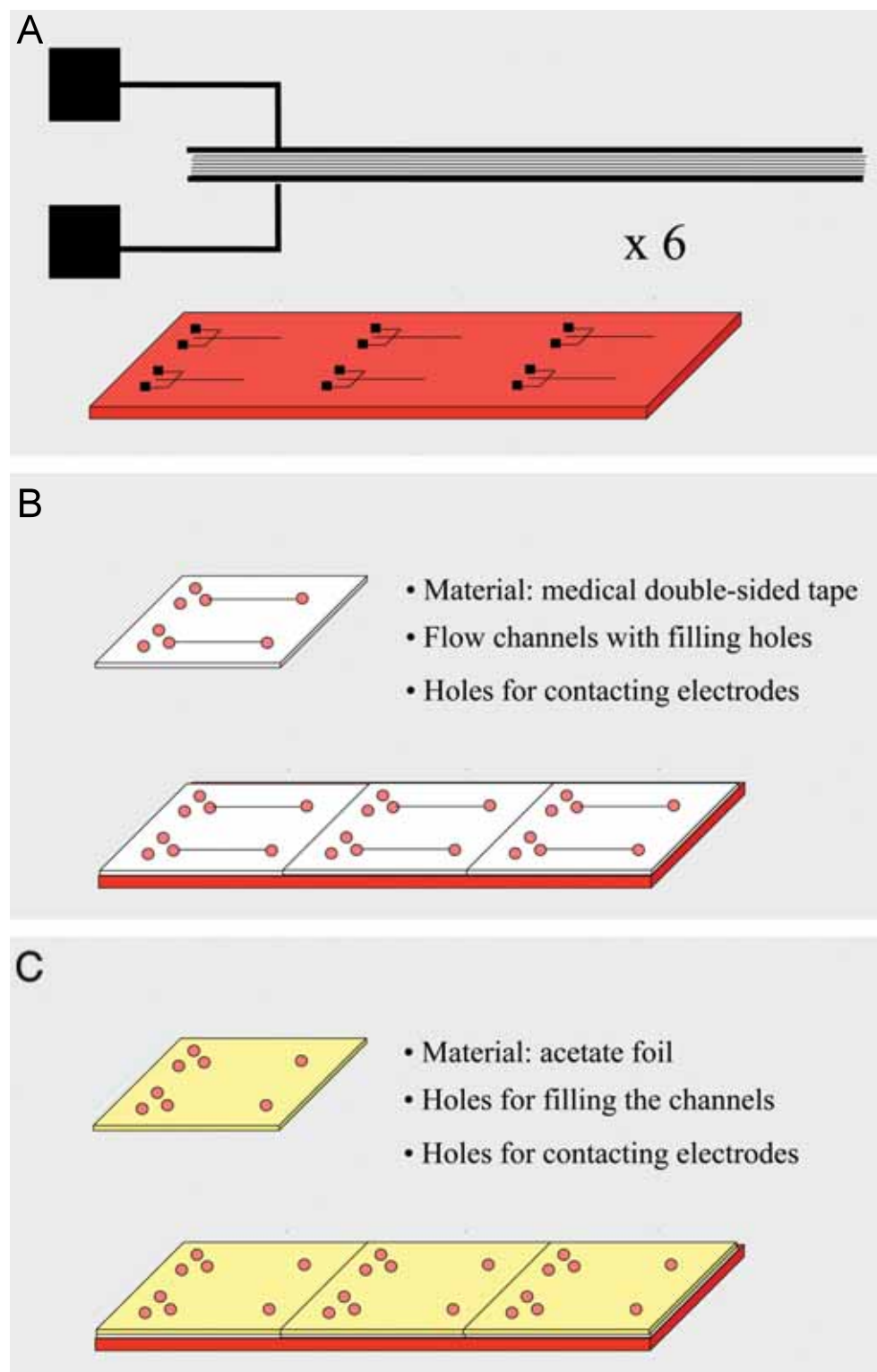


Figure 3.32: Schematic diagram of the electrofusion chamber assembly: A) A gold structure, which comprises electrodes and lines for antibody immobilisation, is evaporated six times onto a glass substrate, the size of a microscope slide; B) A bonding layer, made of double-sided tape, is applied on top of the gold structure; C) The chamber is sealed with a acetate foil top layer.

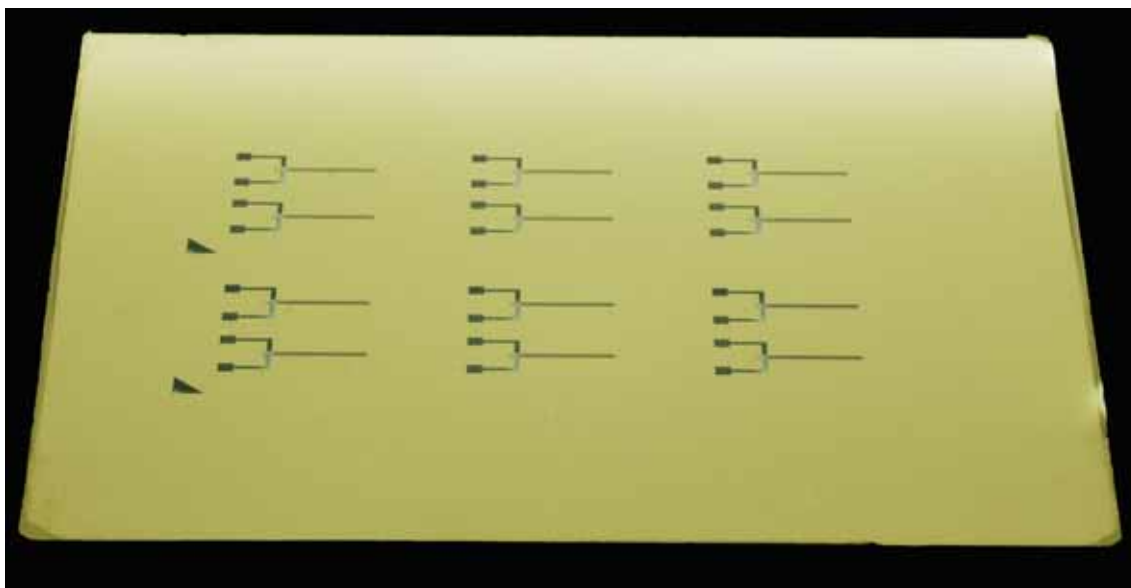


Figure 3.33: Photolithographic chrome mask with two times six gold structures: Three different photolithographic masks were manufactured, which differ in the width of the lines for the antibodies (not visible macroscopically).

group of Dr. Dave Cullen. The optical alignment of different structures were avoided and only one photolithographic mask (see figure 3.33) was needed.

The photolithographic chrome mask was used with a photoresist lift-off process (see Technique Box on next page) to create the desired gold structures on a glass wafer. Three masks were produced, which differ in the width of the lines for the antibodies from $5 - 15\mu\text{m}$. The line widths and spacing (from $15 - 35\mu\text{m}$) were varied to ensure to find the right combination of line size and spacing for the fusion partners, dendritic cells and breast cancer cells.

LOR 3B was used as lift-off resist with the positive imaging resist S1813 to create a bi-layer reentrant profile (see figure 3.34 on page 81). Thereby, the height of the lift-off resist needed to be at least 1.2-1.3 fold the height of the desired metal film. It was aimed for a gold film of 200nm height, plus a 2nm tick layer of chrome as adhesion mediator. Thus, the LOR spin-coat should have a minimum of 262nm (see figure 3.34 B). The whole structure (LOR3B + S1813) had a height of about 1200nm .

The undercut rate is another important parameter. If the undercut is too big, the whole photoresist structure can collapse (see figure 3.35). The undercut rate is mainly influenced by the prebake temperature, followed by other parameters such as prebake time, exposure dose of imaging resist, choice of developer and developing time. In general, it is recommended

Technique Box**Lift-Off Resist (LOR)****Application:**

Creation of re-entrant profiles in bi-level processes; generation of metallic patterns on a substrate

Requirements:

substrate, lift-off resist, positive imaging resist, photolithographic mask, UV source, developer, remover

Method:

Lift-off processing is a simple and easy method for patterning deposited metal films using photoresists.

1.) A spin-coat of lift-off resist (LOR) is applied onto a clean and dry substrate and prebaked. The layer should be about 1.2 - 1.3 fold thicker than the desired metal film.

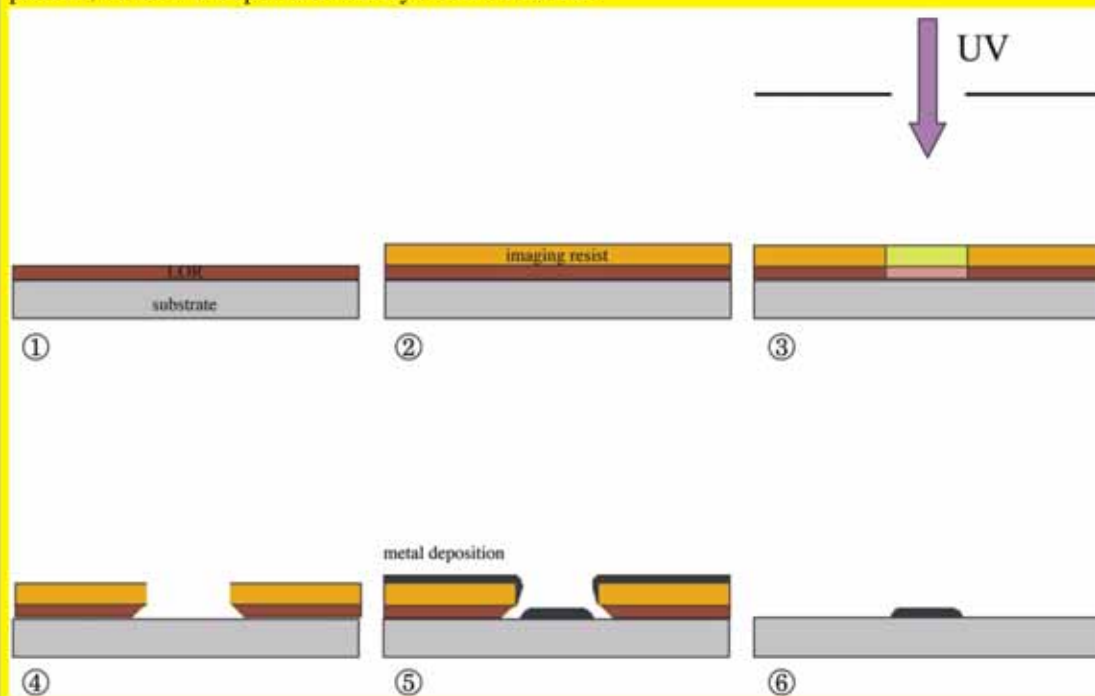
2.) A layer of imaging photoresist is spun onto the baked LOR and prebaked.

3.) The photoresist bi-layer (imaging photoresist & LOR) is patterned by exposure to UV light through a lithographic mask.

4.) The imaging photoresist & LOR are developed, whereupon the developer clears the exposed imaging resist areas, but also etches away the lift-off photoresist (LOR). LOR develops isotropically, creating a bi-layer reentrant sidewall profile or untercut. This re-entrant profile prevents sidewall deposition in the next step.

5.) A metallic film is deposited all over the substrate by evaporation, covering the photoresist and the areas in which the photoresist has been cleared. The metal film is discontinuous due to the bi-level sidewall profile.

6.) A remover is used to lift-off the photoresist taking the metal film with it and leaving only the metal pattern, which was deposited directly on the substrate.



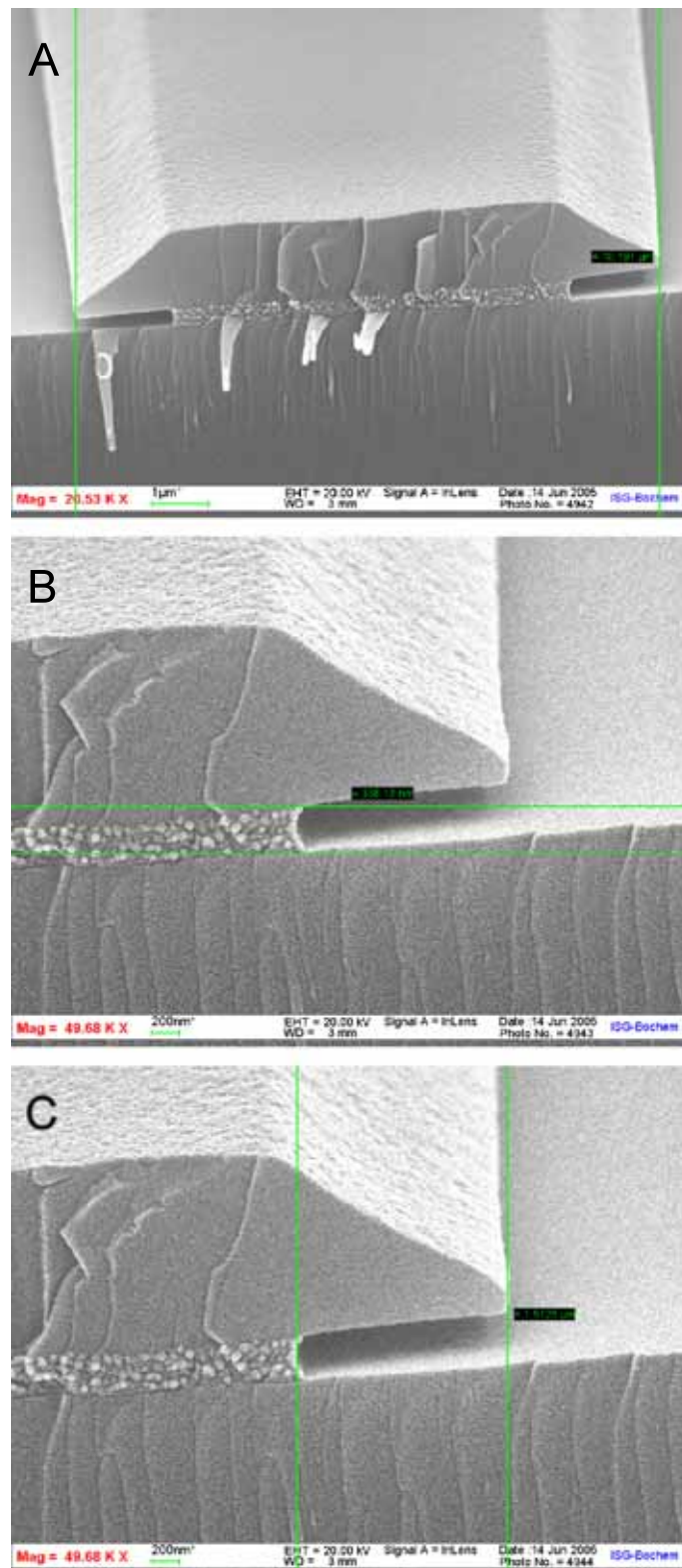


Figure 3.34: Cross sections of a bi-layer reentrant sidewall profile with LOR 3B and S1813 as imaging resist. A) The width of the photoresist structure determines the distance of the structure elements *e.g.* lines within the whole gold structure. B) The height of the lift-off resist needs to be 1.2 - 1.3 fold thicker than the metal film, which will be deposited, to obtain a discontinuous metal film. C) Undercut of the lift-off resist.

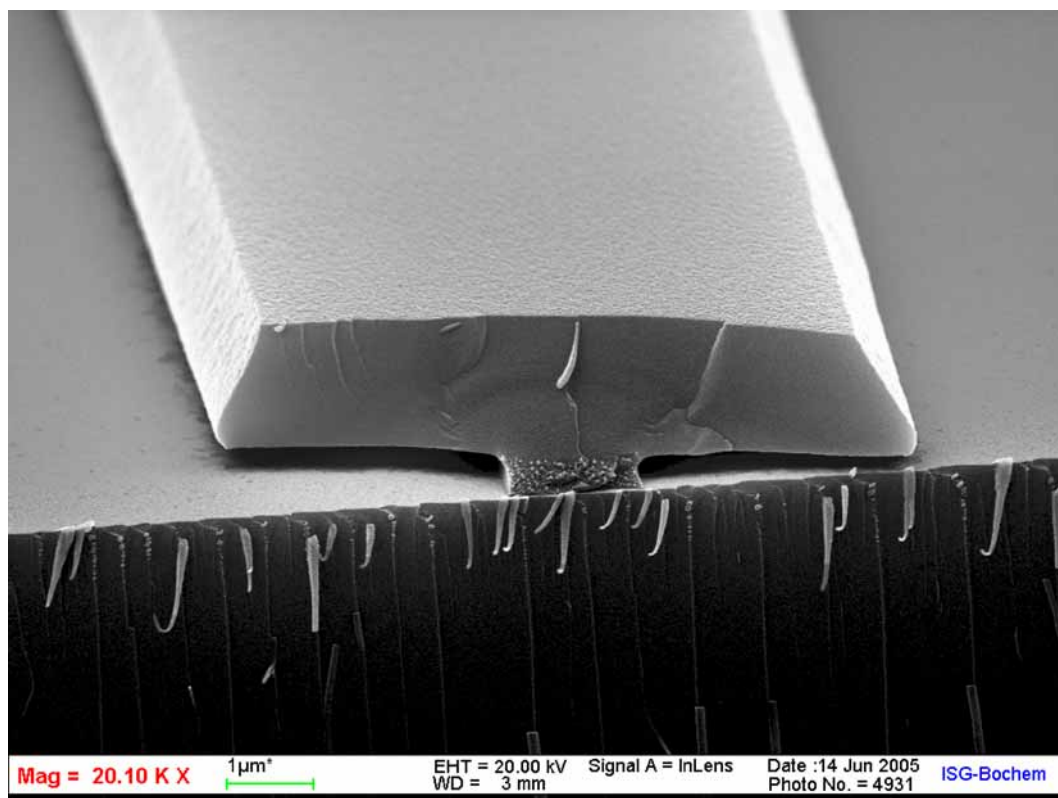


Figure 3.35: Cross section of a bi-layer reentrant sidewall profile with LOR 3B and S1813. The exposure dose was too high, with 10sec exposure time, leaving only a small rest of the lift-off resist. The photoresist structure nearly collapsed.

to keep the development time constant and adjust the exposure time as necessary to meet critical dimension requirements. The best results for the given dimensions were obtained with a exposure time of 8sec (UV light) and a development time of 40sec with the MF-319 developer.

After the right exposure and development settings were found, the metal film was deposited on top of the photoresist structure. Due to the bi-layer reentrant sidewall profile, the applied gold film was discontinuous. In the following step, the photoresist was removed with SVC-14 positive photoresist stripper, lifting-off most of the gold film, leaving only the desired gold pattern on the glass surface (see figure 3.36). Twelve gold structures, each the basis for an electrofusion chamber, fit on the size of a 14cm glass wafer, whereby a group of six could be cut out, resulting in a glass slide with the size of a microscope slide.

A single gold structure comprises electrodes, contact patches and lines for the antibodies. The antibody immobilisation to the gold surface will be described later on page 86. To avoid immobilisation of the antibodies on the other gold structures such as electrodes and contact

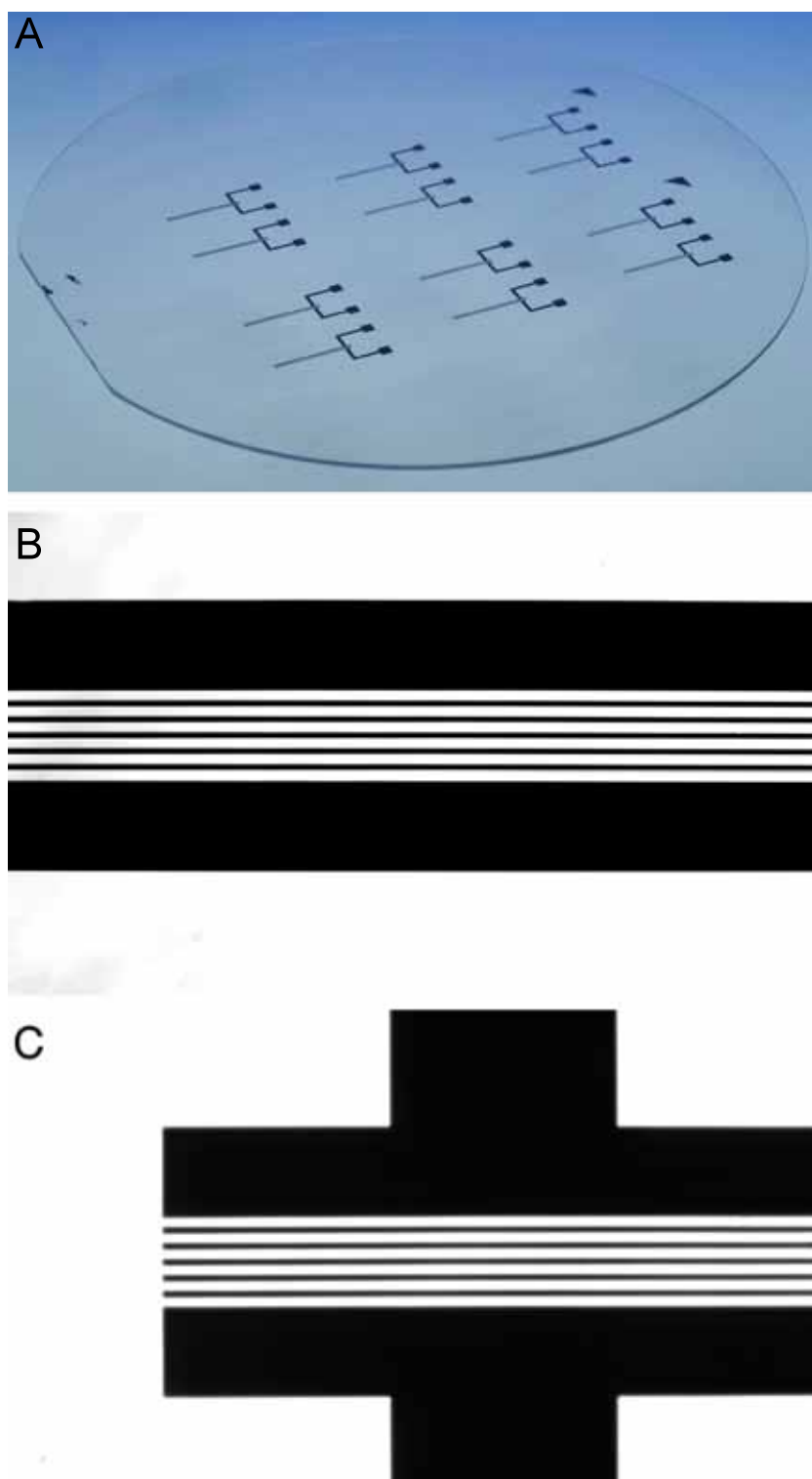


Figure 3.36: Gold structures on glass: A) Two times six structures of electrodes and lines for antibodies of gold on a 140mm glass wafer; B) Micrograph of the 200µm wide electrodes with five 10µm wide lines for antibodies in the space between the electrodes; C) Micrograph of the same structure than in B, showing the branching to the contact patches.

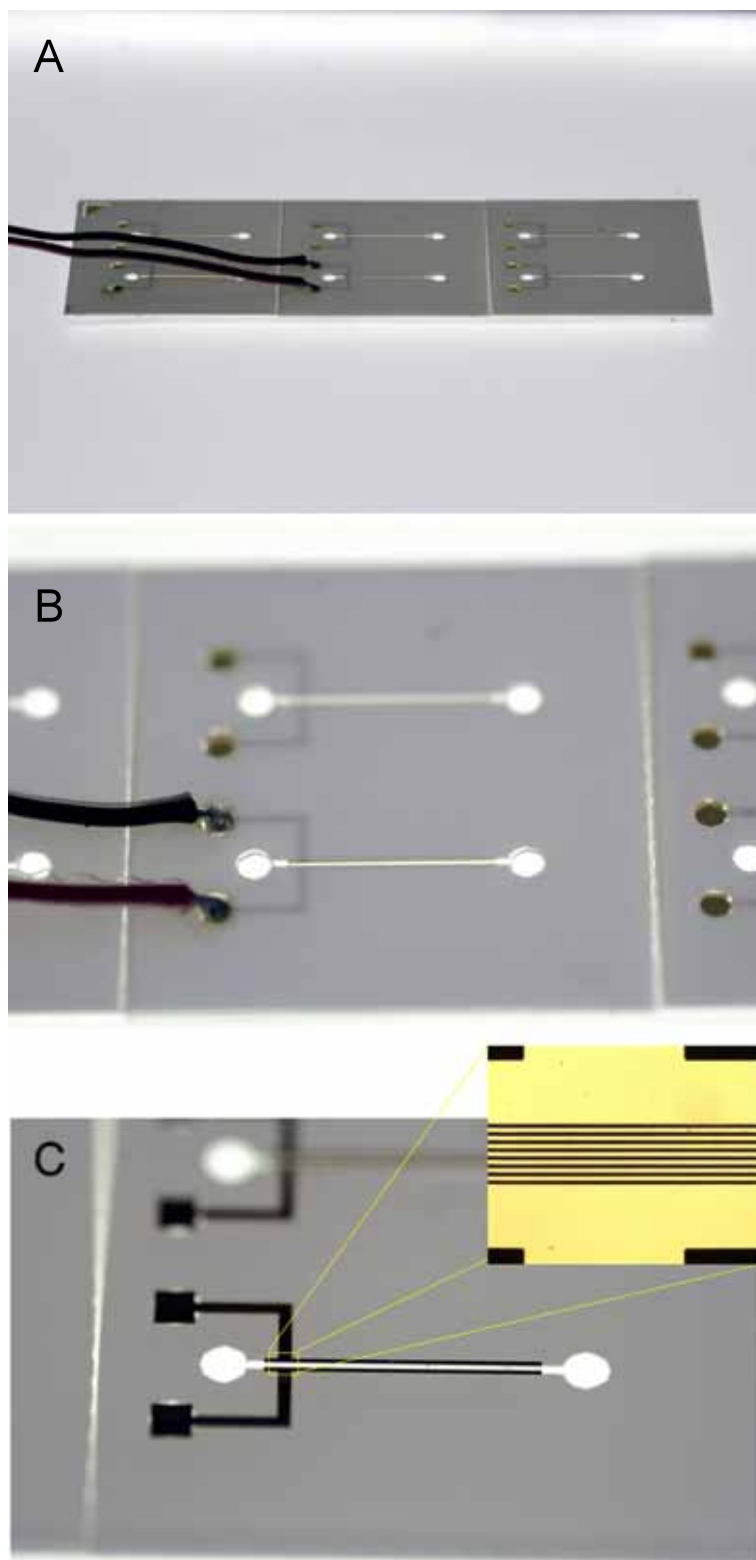


Figure 3.37: Assembly of the chamber for the immobilisation approach. The goldstructure was applied 6 times on the size of a microscope slide and the electrode structures where covered by the build-up of the electrofusion chamber: A) Microscope slide with six electrofusion chambers. B) Each electrofusion chamber can be connected and operated individually. C) Multiple gold lines for the immobilisation of the antibodies were deposited inside the electrofusion chamber.

patches, they were subsequently covered by the build-up of a chamber on top of the gold structure.

The parts for the chamber build-up were cut out of double-sided tape and acetate foil using a CO_2 laser (see figure 3.38). The three parts for the binding layer were cut out of double sided tape and comprised holes for contacting the gold electrodes, a channel, which forms the electrofusion chamber, and holes for filling the chamber. The self-adhesive parts were attached to the glass surface and air bubbles were smoothed out. The structure was sealed with a top layer of acetate foil, which comprised only the holes for filling the chamber and contacting the electrodes.

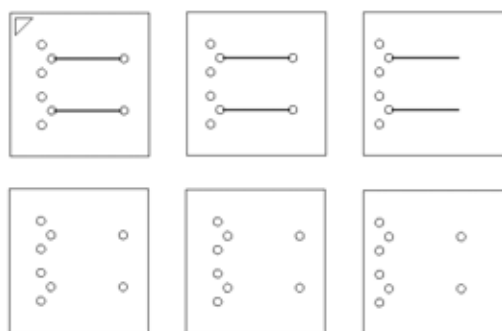


Figure 3.38: Design drawing of the six pieces, which were used for the build-up of the electrofusion chamber. Top row: These three pieces are cut with a CO_2 laser out of double-sided tape. Bottom row: Holes for filling the electrofusion chamber and contacting the electrodes are comprised in the pieces, which seal the chamber.

The six pieces for the build up of the chamber fit accurately on a standard microscope slide. An optical parallel positioning of the channel to the gold electrodes and gold lines for the antibody immobilisation was not necessary, since the pieces were aligned by the outer dimensions.

Summary

For the integration of electrodes into the electrofusion chamber the antibody printing and electrode evaporation step were combined. Thus, the optical alignment of two structures was avoided and only one lithographic mask was needed. The chamber assembly on top of the gold structure accomplished the electrofusion chamber.

3.1.8 New Surface Chemistry According to Design

Overview

Due to the redesign of the electrofusion chamber, which was described into detail in the last chapter, a new surface chemistry for the immobilisation of the antibodies was needed. The antibodies will be immobilised on the small evaporated gold lines within the electrofusion chamber.

For the immobilisation of antibodies on the gold lines a new surface chemistry based on self-assembled monolayers (SAMs) were used. SAMs form spontaneously by chemisorption and self-organisation of functionalised long-chain organic molecules on appropriate substrates. The most widely studied systems have been SAMs formed by chemisorption of alkane-thiols on metal surfaces such as gold and silver.

For the immobilisation of antibodies on the gold lines within the electrofusion chamber, the gold surfaces were covered with a self-assembled monolayer of 11-mercaptoundecanoic acid (MUA), an alkane-thiol with a terminal carboxy group (see figure 3.39 on page 87 for reaction scheme). Therefore, the gold surfaces were immersed into an ethanolic solution of 1mM MUA for 48h. Upon removal, the wafer were rinsed with absolute ethanol and soaked in water for 5min before drying under a stream of nitrogen. The well-ordered monolayers formed by this alkane-thiol on the gold lines were carboxylic acid terminated. These functionalities of the SAM were used to form an amide bond with primary amino groups of the antibodies.

To activate the SAM for the antibody immobilisation 1-ethyl-3-(3-dimethylaminopropyl) carbodiimide hydrochloride (EDC), a water-soluble carbodiimide, was used, which activated the carboxylic acid groups forming an unstable O-urea derivate (step is not shown in figure 3.39). Subsequently, N-hydroxysuccinimide (NHS) esters were formed by exposure of the activated monolayer to an aqueous solution of NHS for 1h at RT. These succinimidyl esters are susceptible to nucleophilic attack by primary amines and form stable amid bonds in the presence of these groups. The immobilisation occurs by the displacement of the NHS group by amino residues of the antibody. Thus, the activated gold lines were exposed to an antibody solution where free amine groups on the antibody surface nucleophilically attacked the succinimidyl-terminated SAM, thus giving covalent attachment of the antibody.

The immobilisation of the antibodies were assessed using X-ray photoelectron spectroscopy (XPS). XPS is widely applied to characterise the composition and chemistry of surfaces (see

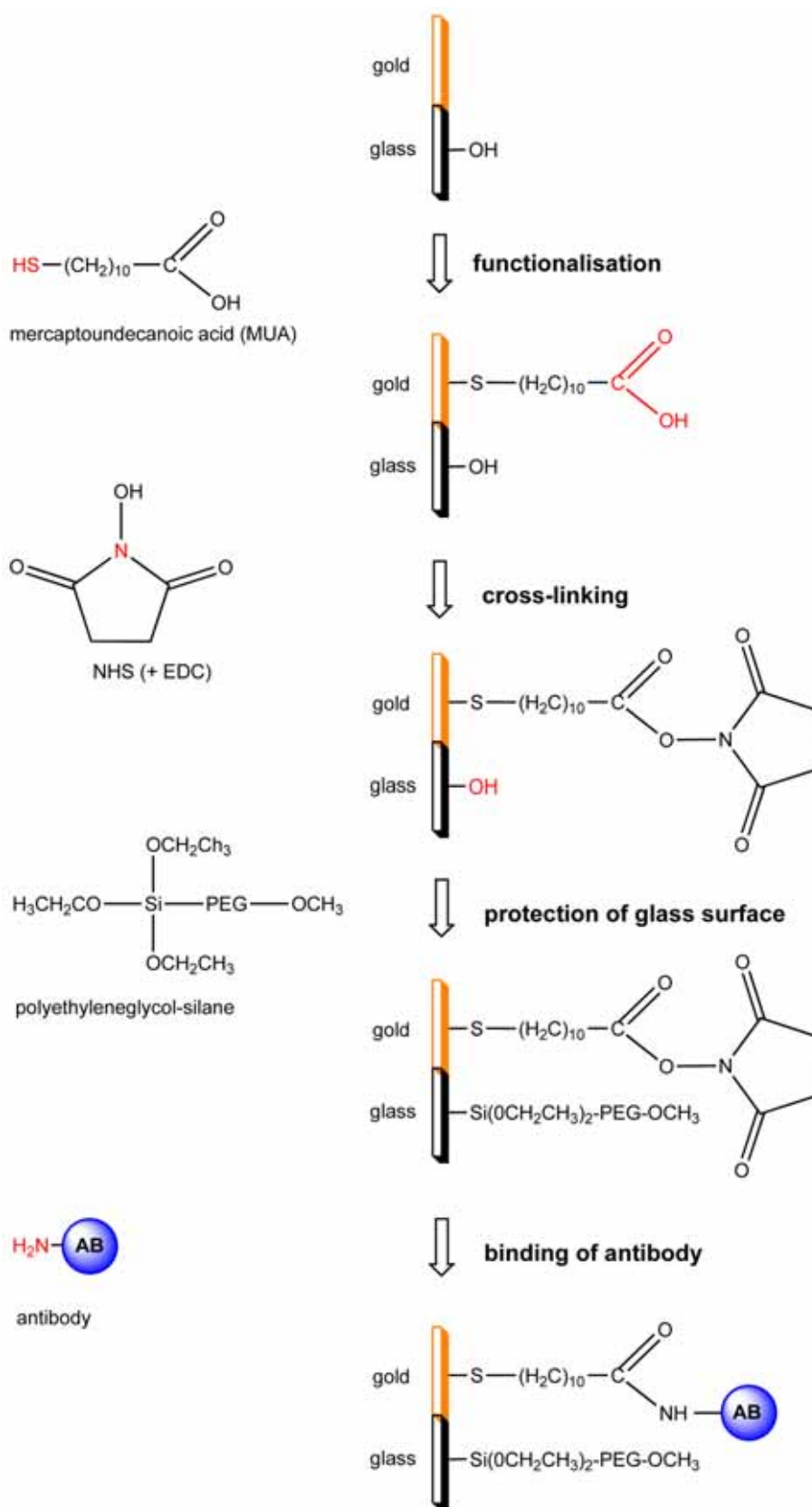


Figure 3.39: Strategy for the immobilisation of antibodies onto gold lines functionalised with carboxylate-terminated SAMs

Technique Box**X-Ray Photoelectron Spectroscopy (XPS)****Application:**

X-Ray Photoelectron Spectroscopy also known as Electron Spectroscopy for Chemical Analysis (ESCA) is used to study the composition and electronic state of the surface region of a sample. In addition to chemical identification and quantification of the elements present, this non-destructive technique also provides information about the chemical state or functionality of elements at the surface of solids. The letter is useful in studying oxidation/corrosion, adsorption, catalysis, adhesion failure and thin film growth processes.

Requirements:

XPS spectrometer, monochromatic X-ray source

Method:

XPS uses a soft X-ray beam (200-2000 eV) to cause the emission of electrons from the surface of the sample. Thus, photoelectron spectroscopy is based upon a single photon in/electron out process. The energy of a photon is given by the Einstein relation:

$$E = h \cdot \nu$$

Where h is the Planck constant ($6.62 \cdot 10^{-34}$ Js) and ν is the frequency (Hz) of the radiation. For XPS analysis only monochromatic radiation sources are used, i.e. photons of fixed energy. The photon is absorbed by an atom in a molecule or solid, leading to ionization and the emission of a core (inner shell) electron. The kinetic energy distribution of the emitted photoelectrons is measured. The process of photoionisation can be described as:



Conservation of energy then requires:

$$E(A) + h\nu = E(A^+) + E(e^-)$$

Since the electron's energy is present solely as kinetic energy (KE) this can be rearranged to give the following expression for the KE of the photoelectron:

$$KE = h\nu - (E(A^+) - E(A))$$

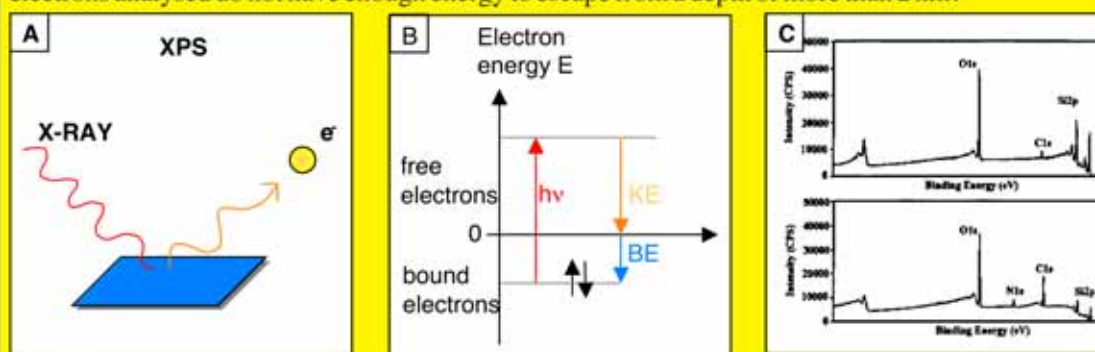
The final term in brackets, representing the difference in energy between the ionised and neutral atoms, is generally called the binding energy (BE) of the electron, an atomic characteristic.

This leads to the following equation:

$$KE = h\nu - BE$$

The measurement of the energy spectrum of the emitted electrons can then be plotted as number of counts over kinetic or binding energy. Survey energy spectra help to estimate the composition of the sample (see Fig. C, from Nehilla et al. 2004) analyzing peak position and peak area, while high-resolution spectra (within 10-20 eV) provide information about the chemical bonds of the elements by analyzing peak position and peak shape.

The sensitivity of this technique is about 0.3 at% and the analysis is inherently surface, since the electrons analysed do not have enough energy to escape from a depth of more than 2 nm.



Technique Box on page 88) and can be used for monitoring the process of surface modification and control the binding of antibodies to a solid surface.

The XPS spectra for MUA monolayer activated with NHS/EDC (sample name: BC1) and covalently bound antibodies to the MUA monolayer (BC2) are presented in figure 3.40. Four different spectra regions for oxygen (O1s), nitrogen (N1s), carbon (C1s) and gold (Au4f) are shown. Differences between sample BC1 and BC2 were particularly observed in the spectra for nitrogen and carbon, since these two atoms are comprised within the amide bond, which was formed when the antibodies were immobilised. This indicated that the reaction had taken place.

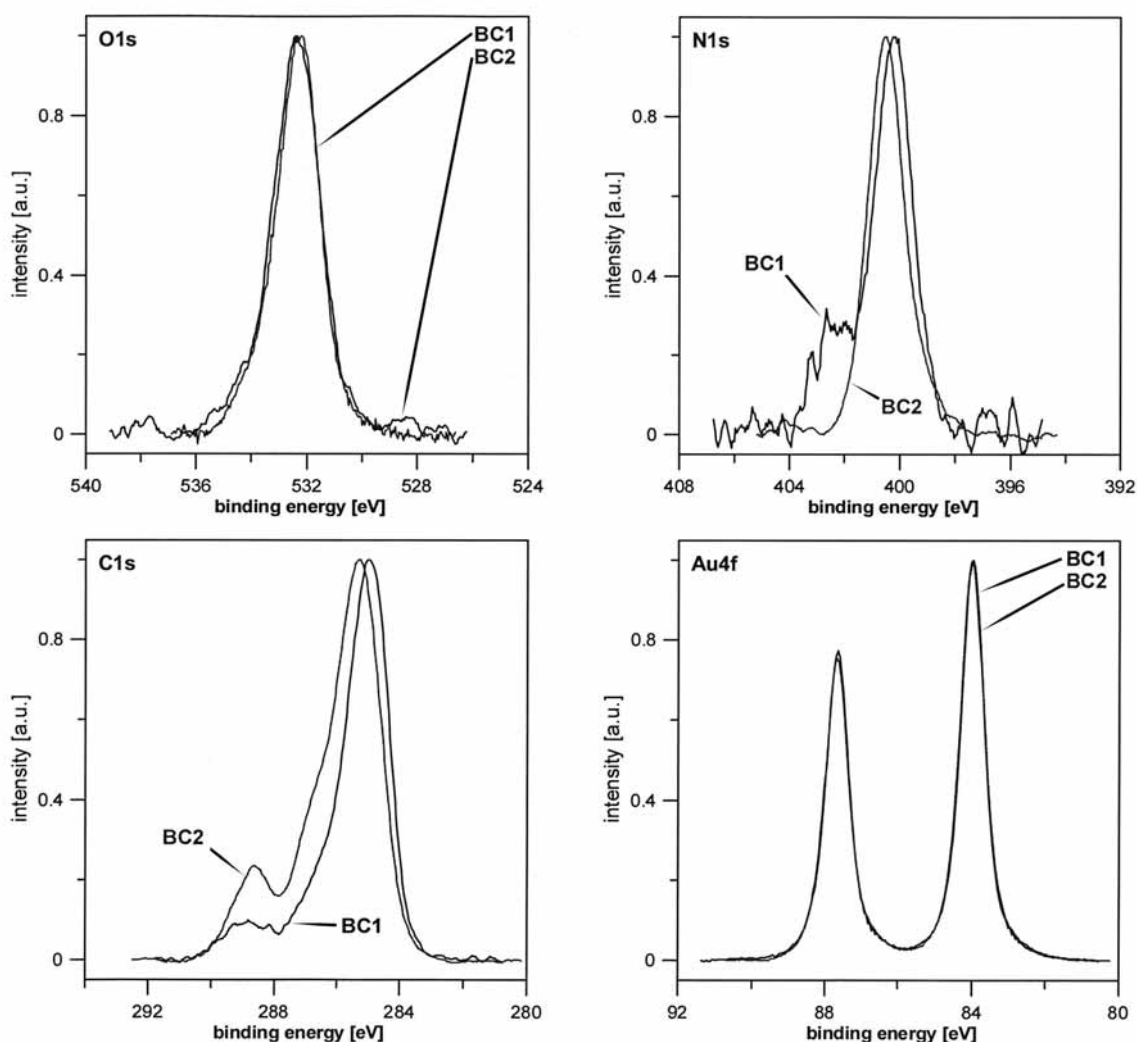


Figure 3.40: High-resolution XPS peaks for four spectral regions on activated MUA monolayers (BC1) and immobilised antibodies on MUA (BC2)

In figure 3.41 the two regions, N1s and C1s, are shown at higher magnification.

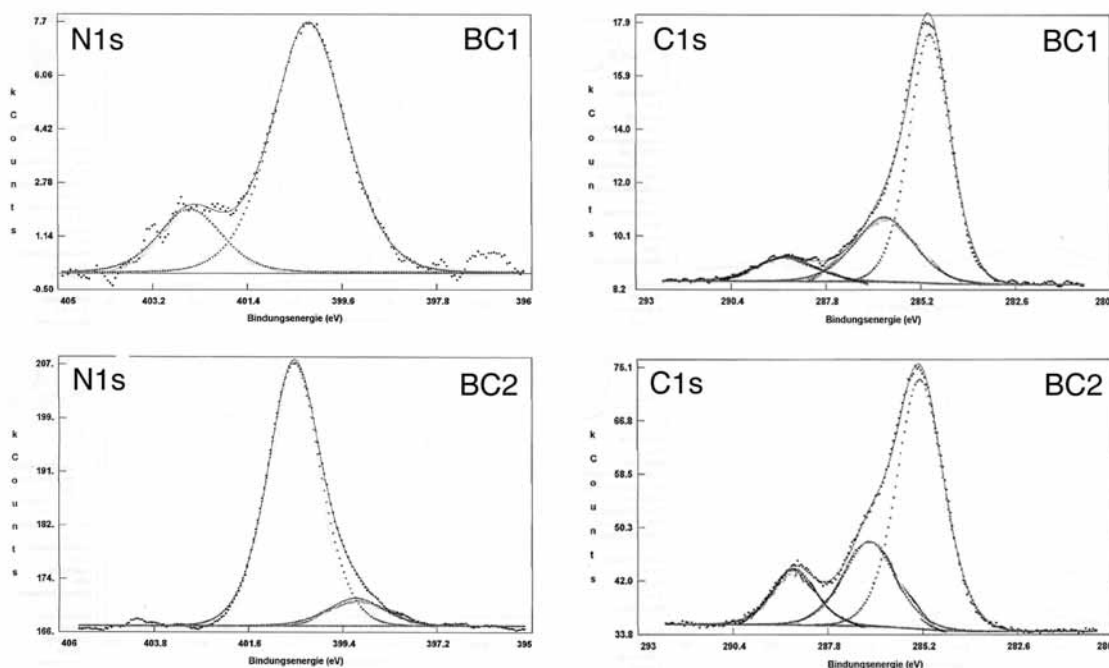


Figure 3.41: High-resolution N1s (left) and C1s (right) spectra for activated MUA monolayers (top) and immobilised antibodies on MUA (bottom). Peaks were fitted to the obtained spectrum using Unifit for Windows, Version 32-32.

The presence of antibodies immobilised on the surface of the MUA SAM could be confirmed by changes of peaks in N1s and C1s region attributed to the presence of an amide bond.

In the N1s spectra the peak at 402.5 eV corresponded to the nitrogen atom of the heterocycle of NHS. This peak completely disappeared in the spectrum for the immobilised antibodies on MUA (bottom panel), whereas the big peak at 400.5 eV corresponded to the nitrogen atoms present in the amide bond. In addition, the small peak at 399.1 eV was related to amino groups of the antibodies.

The high resolution C1s data obtained from the activated MUA surface showed three peaks at 284.9, 286.2 and 288.9 eV, which were assigned to aliphatic carbons of the alkylchains (C-H), carbons bound to sulfur and the acid group ($\text{CH}_2\text{-S}$ and $\text{CH}_2\text{-COOH}$), and the carbon of the ester group (O-C=O), respectively. The surface with the immobilised antibodies revealed the same peak for C-H, but the third peak has been shifted from 288.9 to 288.7 eV, representing the C atom of the amide group.

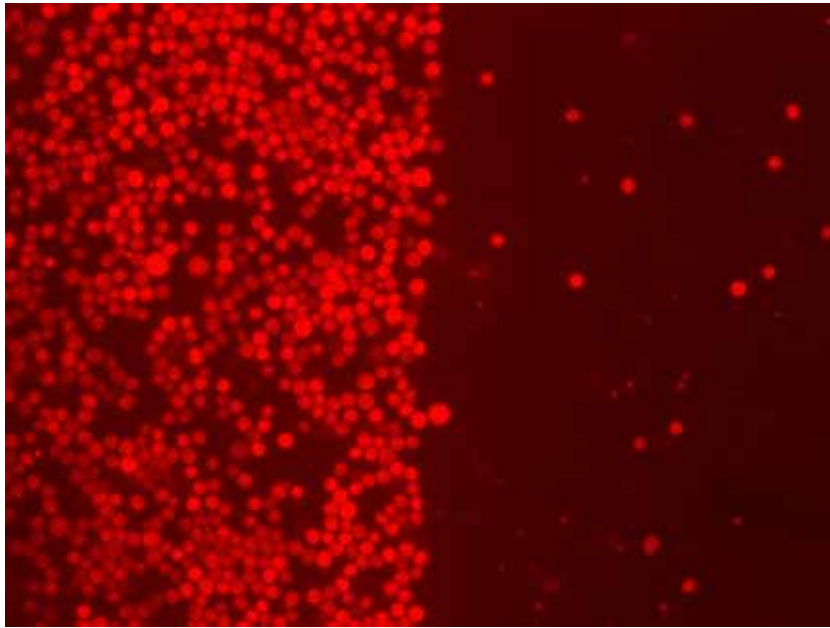


Figure 3.42: Immobilisation of KG-1 cells stained with CMTMR (red) on a gold surface. The left half of the gold surface was treated with MUA and the SAM layer was activated with NHS/EDC. The right half was left untreated. Cells only bound to the functionalised part of the gold surface.



Figure 3.43: The completed electrofusion chamber can be connected via a push-pull self-latching connection system to the voltage generator from Eppendorf.

In addition to the XPS measurements, which proved that the immobilisation reaction was successful, KG-1 cells were bound via the immobilised antibody to the gold surface (see figure 3.42). These immobilisation reaction could furthermore be transferred to the immobilisation on the small gold lines within the electrofusion chamber. Nevertheless, the glass surface should be protected before the antibodies are added in the last reaction step (see reaction scheme on page 87). PEG silane was used for avoiding adsorption or binding of antibodies to the glass surface.

Therewith, the development of the electrofusion chamber was completed. The chamber can be connected via a push-pull self-latching connection system to the voltage generator from Eppendorf (see figure 3.43).

Summary

The last step for the completion of the electrofusion chamber based on the immobilisation approach was the adjustment of the surface chemistry for the immobilisation of antibodies on gold lines. By the successful adjustment of the immobilisation reaction, the development of the electrofusion chamber for arranged electrofusion of mammalian cells was completed and the chamber was then fully functional.

3.2 Microfluidics

3.2.1 Concept

Overview

The development of a microfluidic approach for the fabrication of a fusion chamber for arranged electrofusion is described in this section. Thereby, the ideas, which triggered the evolution of this basic concept and the concept itself, are described.

The second approach for the implementation of an alternating cell arrangement into a fusion chamber is based on microfluidics. The handling of liquids and/or gases in small volumes or small sizes is understood by this term.

The idea of using microfluidics for cell arrangement was aroused by the work of Prof. A. Offenhäuser, who is in charge of the Institute of Thin Films and Interfaces 2 (ISG-2) at the Research Center Jülich. In former projects, he worked on the development of a microfluidic device for localised drug application to cell cultures (THIÉBAUD ET AL., 2002).

The system was used for manipulating the growth of neuronal cell. It is displayed in figure 3.44 on page 95. This microfluidic device was fabricated using PDMS technologies. Two parts, an array of micro-injectors and a base-flow channel, are assembled to form a system, which allows the formation of eight independent and sharply defined lines of liquids. The published results demonstrate that the application of different pharmaceutical components to cells of only one culture can be performed.

The eight independent laminar flow lines possess a cross section of $100 \cdot 200 \mu m^2$. Notably, no mixing occurred between the individual flow lines. Although not cells themselves were streamed, but an extracellular matrix protein (laminin), which guided the neuronal growth afterwards. If it is possible to stream cells in laminar flows without mixing, this would be a starting point for the development of an fusion chamber for arranged electrofusion based on microfluidics.

So far, the streaming of cells in laminar flows has not been published. In many cases, both microfluidics and laminar flows are used to overflow adherent cells to either study cell adhesion or cell behaviour to flow conditions. They are also used to apply diverse pharmaceutical components to distinct parts of a cell culture simultaneously.

Thus, the laminar flow of cells in microfluidic channels was tackled for the development of

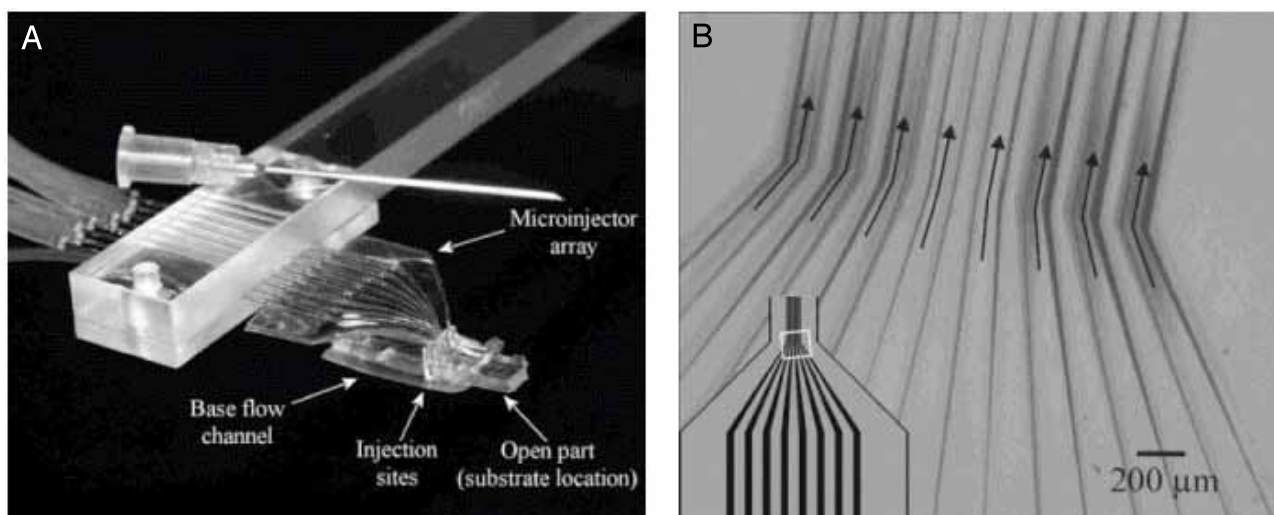
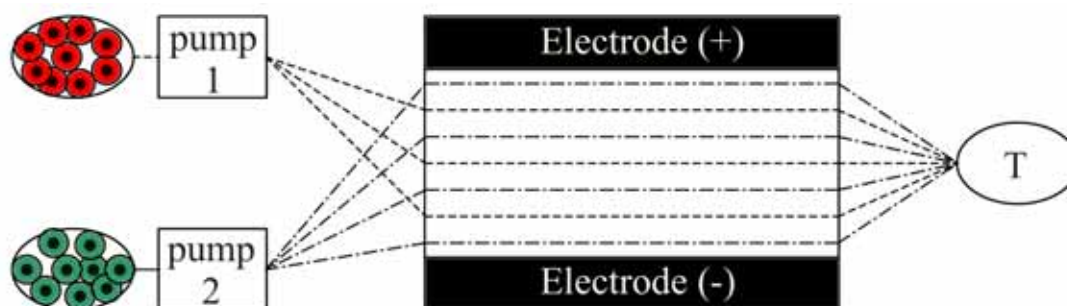


Figure 3.44: Microfluidic Device for patterned application of microfluids to neuronal cells developed by Thiébaud et al.: A) Photograph of the device compared with a syringe needle; B) Micrograph of the PDMS microinjector top plate. The grooves of the eight injection channels of the device are highlighted with arrows. The location of the picture frame in respect to the entire device is shown in the insert (pictures taken from THIEBAUD, P. ET AL., 2002).

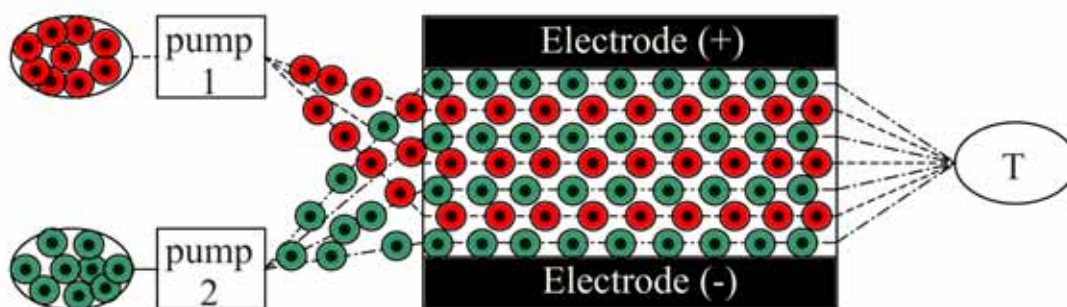
a novel fusion chamber. This device should be designed in that way, that several small single-cell flows will be streamed through a fusion chamber, which consists of a microchamber with two electrodes (see figure 3.45 for graphic account). The streams are excited by two pumps, which each deliver one cell type/fusion partner. An alternating cell arrangement arises from the cogging of multiple flows. The further course of action envisions the stoppage or reduction of the flows, the subsequent application of an electrical field to align the cells in pearl chains and the fusion of the cells by an electrical pulse.

The development of such a flow-through electrofusion chamber requires the evidence, that laminar flows from cell suspensions can be established. The laminar flow of molecular solutions is well acquainted, but the behaviour of a fluid with particles, which are deformable, is neither described nor can be easily predicted. Furthermore, the dimension of the microfluidic fusion chamber has to be dramatically reduced in size compared to the microfluidic device presented above. A cross section of $100 \cdot 200 \mu\text{m}^2$ would allow several cells to cluster and still pass the channel. It is obvious that homologous fusions would be favoured. Therefore, the aim was to scale down the cross section of an individual channel to $50 \cdot 50 \mu\text{m}^2$. The average diameter of a dendritic cell is about $25 \mu\text{m}$ (see chapter 3.3). Thus, a $50 \mu\text{m}$ wide channel admits enough safe



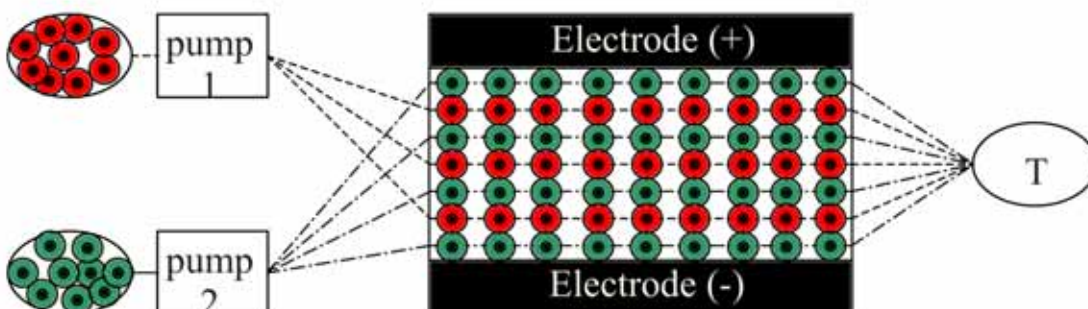
A) The electrofusion chamber

Electrodes narrow the electrofusion chamber on two sides. A single cell suspension of each cell type is provided in two reservoirs, which are connected via pumps with the chamber. At the outlet of this microfluidic chamber a collecting tank (T) is placed.



B) Filling of the microfluidic chamber

The empty microfluidic chamber is filled with single cell flows by dint of the two pumps due to hydrodynamic focussing. The arising laminar flows stream over the total length of the chamber without mixing, delivering the different cell types in lanes.



C) Alignment and fusion

Finally, the flow is stopped or reduced and the cells are aligned by an a.c. field, followed by a d.c. pulse for hybrid formation. Afterwards, the pumps are turned on again, replacing the fused cell suspension containing the desired hybrids, by new single cell suspensions of the fusion partners. The hybrids are collected in the intercepting tank.

Figure 3.45: Microfluidic approach for an arranged electrofusion chamber

distance for the cell, so that the channel walls would not harm the cells, but should prevent the simultaneous transition of two cells or even bigger clusters.

Summary

The cognitions from literature research are:

- 1.) Microfluidics can be used to generate small laminar flows, which do not mix.
- 2.) Microfluidics are used for patterned delivery of pharmaceutical components to cell cultures.
- 3.) No expertise is present in laminar flow of cell suspensions.

For the assignment of microfluidics to the development of a novel electrofusion chamber the following questions have to be addressed:

- 1.) Is it possible to generate laminar flows of cell suspensions?
- 2.) Can the flows be reduced to a size, which imports only one cell per cross section?

3.2.2 Geometric Definition of Microfluidic Fusion Devices

Overview

Starting from two presettings, graphical models for an microfluidic fusion chamber were designed. This section introduces two different model systems, which asserted themselves, and possess the potential to fulfil the requirements.

In close cooperation with the Centre for Microtechnology and Surface Analysis of the Danish Technology Institute the development of such a device, which allows the alternating cell arrangement prior to the fusion process using microfluidic flows, commenced.

Different systems were designed taking two presettings into account: First of all, the fusion devices had to allow for laminar flow inside the chambers. Secondly, a $50\mu\text{m}$ wide space should be admitted for each single-cell flow. To realise these demands, elements such as channels or trenches were integrated to guide the laminar flows in direction. In the end, two systems were followed up.

System 1

The first system contains channels, which end in a collective chamber. Figure 3.46 shows the appearance of the microfluidic device. The system exhibits two levels. Cell solution A enters the chamber via the cross section labelled in blue and is subsequently divided into four partial flows. These flows ascend through standpipes entering the channels in the upper level. Cell solution B is channelled through the red access area into a distributor, which divides the stream into five partial flows. Covering a short distance in the channel system, the flows end up in the big collective chamber.

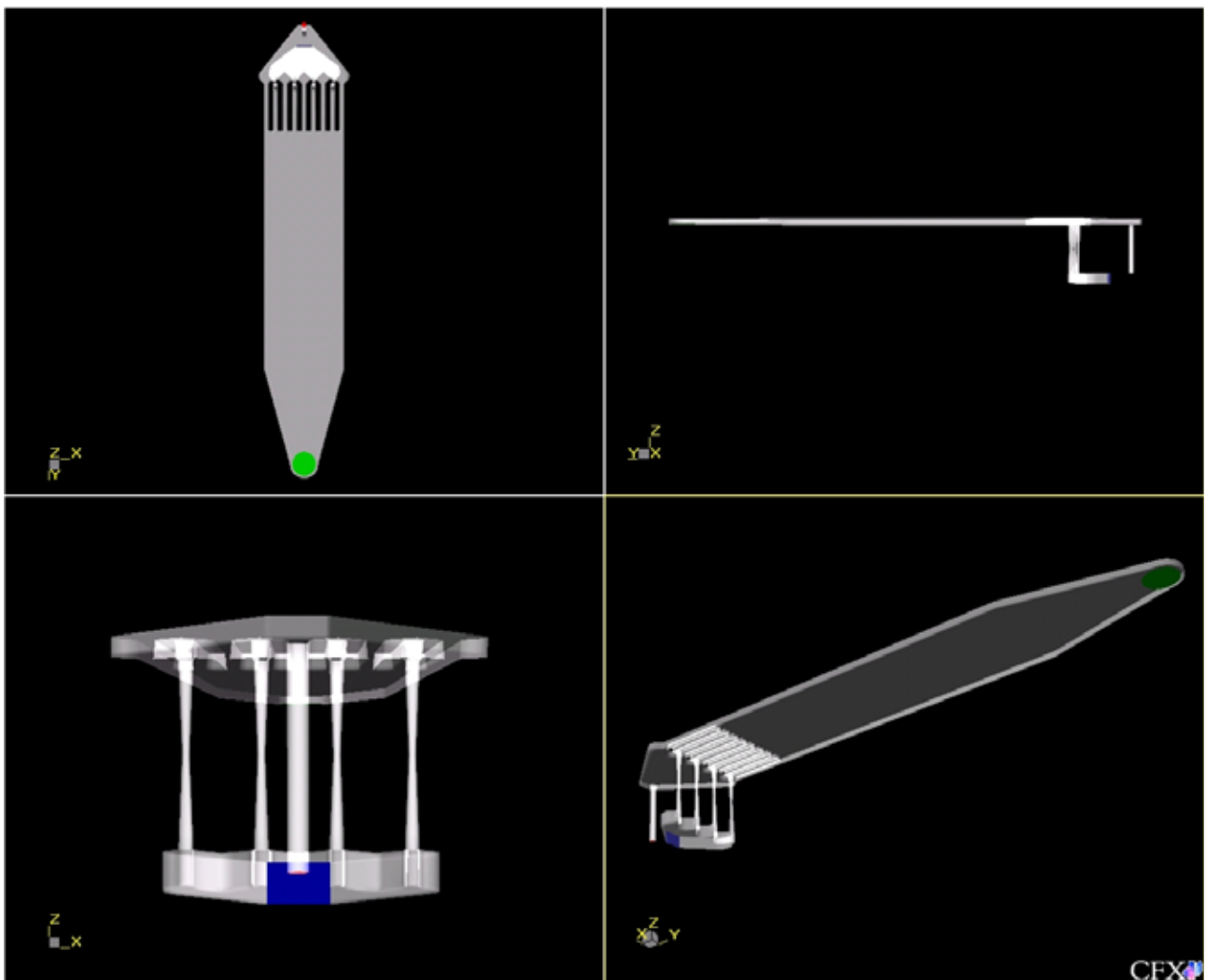


Figure 3.46: Microfluidic system 1: It contains channels, which end in a collective chamber. The red area highlights feed A (the input for cell solution A), blue marks feed B (cell solution B, respectively) and the output is displayed by a green mark. Neither microfluidic feed lines nor adapters for electric components are illustrated.

System 2

The second system features trenches or rather implied channels, which end in a collective chamber. The distribution systems for the single cell flows is identical to the one used in microfluidic system 1, thus it is not depicted in figure 3.47. After the distribution of the cell suspensions, the nine discrete flows run alongside the trenches through the joint chamber right up to the outlet.

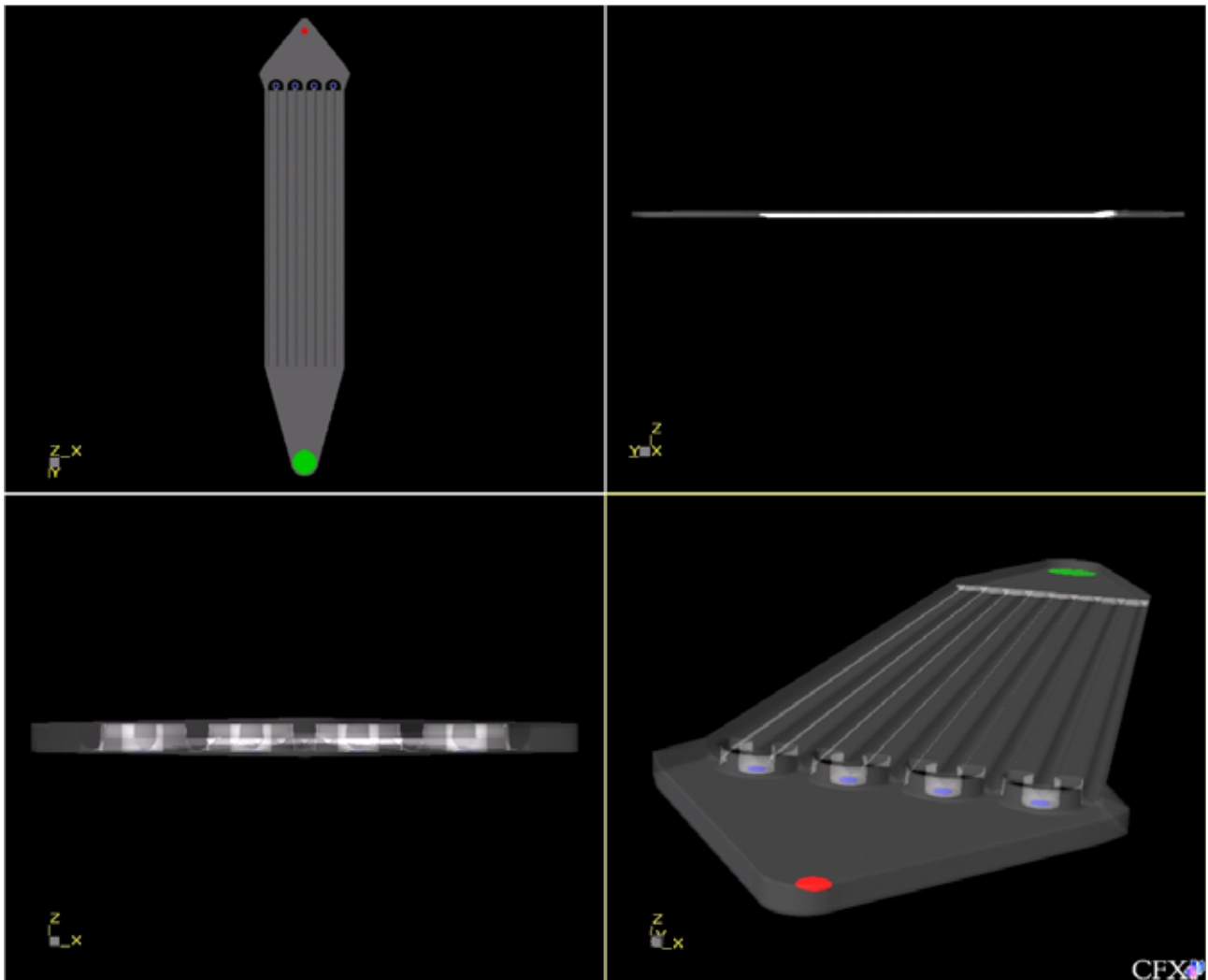


Figure 3.47: Microfluidic system 2: It contains implied trenches in the bottom plate. The red area highlights feed A (cell solution A), blue marks feed B (cell solution B) and the output is displayed by a green mark. Neither microfluidic feed lines nor adapters for electric components are illustrated.

The software Pro-Engineer was used for the 3D design of the microdevices. The basical design of two microfluidic systems was completed and these models were subsequently optimised

using computer aided flow simulation (see next section for results). Dimensioning the in- and output cross sections and the chamber length will depend on the outcome of the simulations.

Summary

Two graphical models were developed, which fulfil the requirements specified as:

- 1.) laminar flow
- 2.) $50\mu m$ wide space for every single-cell flow

Both systems exhibit analogue functional elements:

- 1.) distribution system for the generation of nine distinct partial flows
- 2.) guiding elements for the single-cell flows
- 3.) an open chamber, where the different single-cell flows can interact, to admit fusion

3.2.3 Model Based Optimisation

Overview

This section discusses how to predict the fluid dynamic behavior of these new and innovative microfluidic structures using Computational Fluid Dynamics (CFD). Thus, it was possible to shortcut some of the refinement steps necessary in standard design methods of microfluidic flow structures.

The first evaluation of the two different designs of the microfluidic electrofusion chamber was carried out in “virtual experiments” using computational fluid dynamics (CFD; see Technique Box on page 101 for more information), thus avoiding time and cost intensive experimental set-ups. A brief simulation study was performed for the analysis of the streamlines and velocities in both microfluidic chambers using CFX software.

Dependent on the outcome of this virtual prototyping and the required flow conditions it might be appropriate to re-design the flow chamber according to the desired constraints of the system.

Technique Box

Computational Fluid Dynamics (CFD)

Application:

Computational Fluid Dynamics are used to produce information about the ways in which fluids flow in given situations. A few examples for application areas are aircraft industry (lift and drag of aircraft), automotive (air flow inside internal combustion engines), electrical and civil engineering (flow of cooling air inside electrical equipment), weather forecast and micro-electrical-mechanical systems (MEMS).

Requirements:

High-end computer (the storage capacity and the speed of the computer can effect the accuracy of the prediction), computational fluid dynamic software

Method:

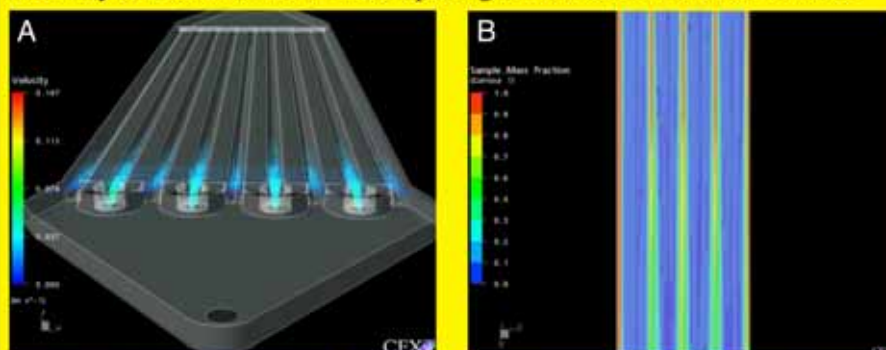
First of all, for computational fluid dynamic modeling the geometric data of a device is imported from a CAD program (computer-aided design program). Then, the part of the structure, where the fluid flows, the so-called fluid domain, is defined using the CFD software.

The equation that govern fluid motion are well known for viscous and incompressible fluids, hence most of the CFD packages solve this type of flow. Furthermore, many industrial flow problems are such slow speed flows, where the fluid is not compressed and features such as shock waves do not occur. The equation describing such flows of fluids are partial differential equations, which are not amenable to analytical solution except for very simple cases.

Therefore, a mesh is generated, that splits the fluid domain into smaller portions, which are made up of geometric primitives such as hexa- or tetrahedra. This mesh generation can be done with a geometric semi-automatic program, included in most CFD software packages. The partial differential equations are solved inside each of the resulting subvolumes (elements) by converting them in n-thousand general/linearized differential equations. The continuity of the solution have to be ensured across the interfaces of all elements. If this is respected, a complete picture of fluid flow in the entire fluid domain will arise, when all elements are put together.

Prior to the solving of the differential equations, boundary conditions for the n variables (such as temperature, velocity, geometric walls, inlets and outlets) have to be determined (preprocessing). The set of partial differential equations can then be converted in to solvable linear differential equations, which fulfill the convergence criterion.

Convergence is the ability of a set of numerical equations to represent the analytical solution to a problem, if such a solution exists. The equations are said to converge if the numerical solution tends to the analytical solution as the mesh spacing or element size reduces to zero.



Streamlines, velocities (see fig. A), pressure profiles, mass fractions (see fig. B) or other relevant flow parameters can be displayed by computational fluid dynamic modeling.

Fluid Simulation

The main emphasis for the fluid simulation was the appropriability of the designed systems for the generation of laminar flows alongside the chamber. Both microfluidic systems admit two modes of operation:

1. Suction of the cell suspensions via one pump that is connected to the outlet
2. Pumping of the cell suspensions via two independent pumps.

For reasons of economy the solution with one pump was favoured and as a result tested primarily. In the model based optimisation of the designs substantial parameters such as shear stress, velocity and pressure loss were considered. The analysis searched for conspicuities regarding pressure, shear stress and velocity profiles. The run of the streamlines had been examined in particular, since it is of great importance for the cell arrangement.

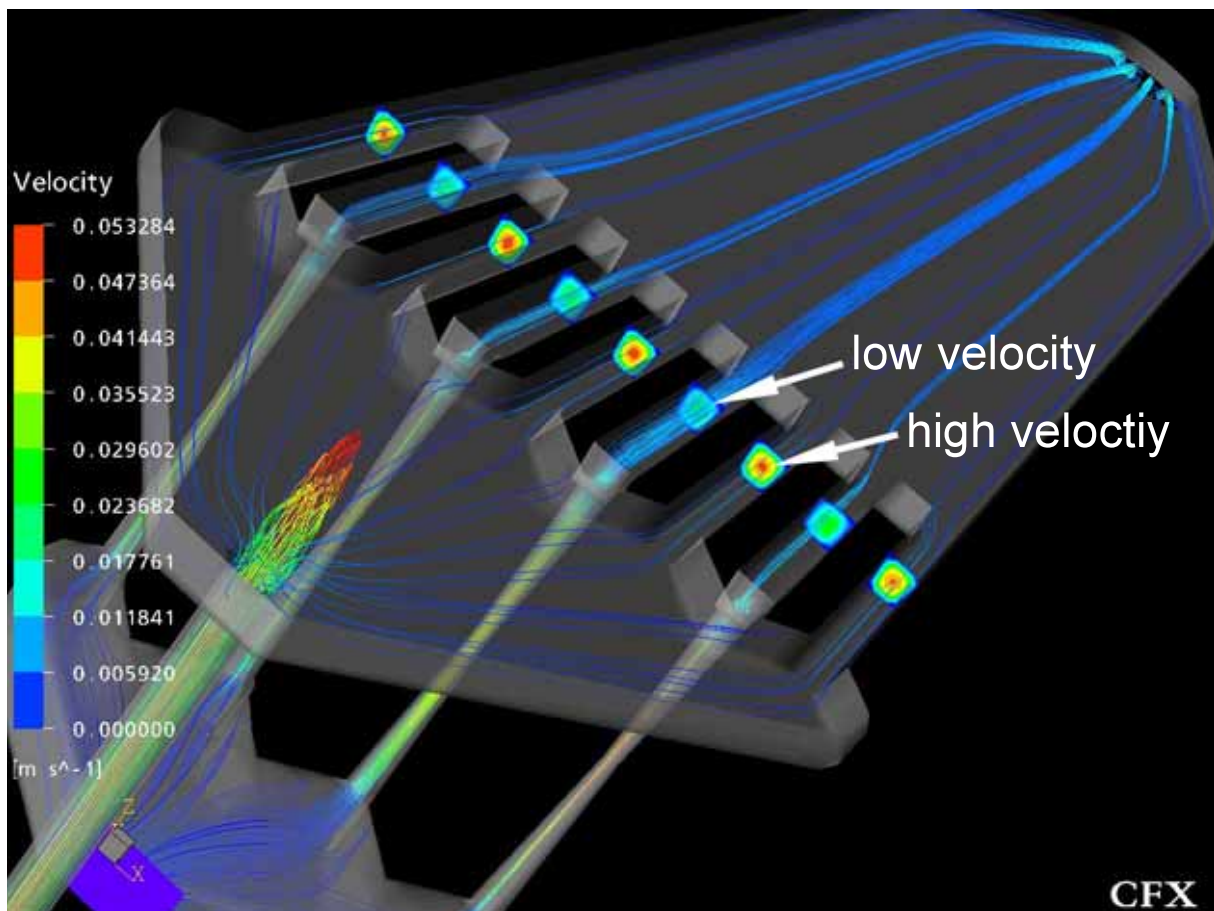


Figure 3.48: Microfluidic system 1: Partial flows with different flow velocities caused by invalid dimensions of the input cross sections.

Figure 3.48 shows the stream gradient, which arises, if one pump sucks the cell suspensions and the input cross sections have invalid dimensions. Different pressure losses arise from the badly selected input cross sections, which provokes that (in the pictured case) those partial flows, which are not obliged to pass through the standpipes, are sucked superiorly. It has to be noticed, that the number of streamlines do not necessarily correlate with the stream widths. To be precise, in this case some of the partial flows would feature bigger cross sections than the others. This could result in an increased homologous cell fusion, since the streams would be wide enough, that two cells of the same cell type can flow side by side. This needed to be circumvented.

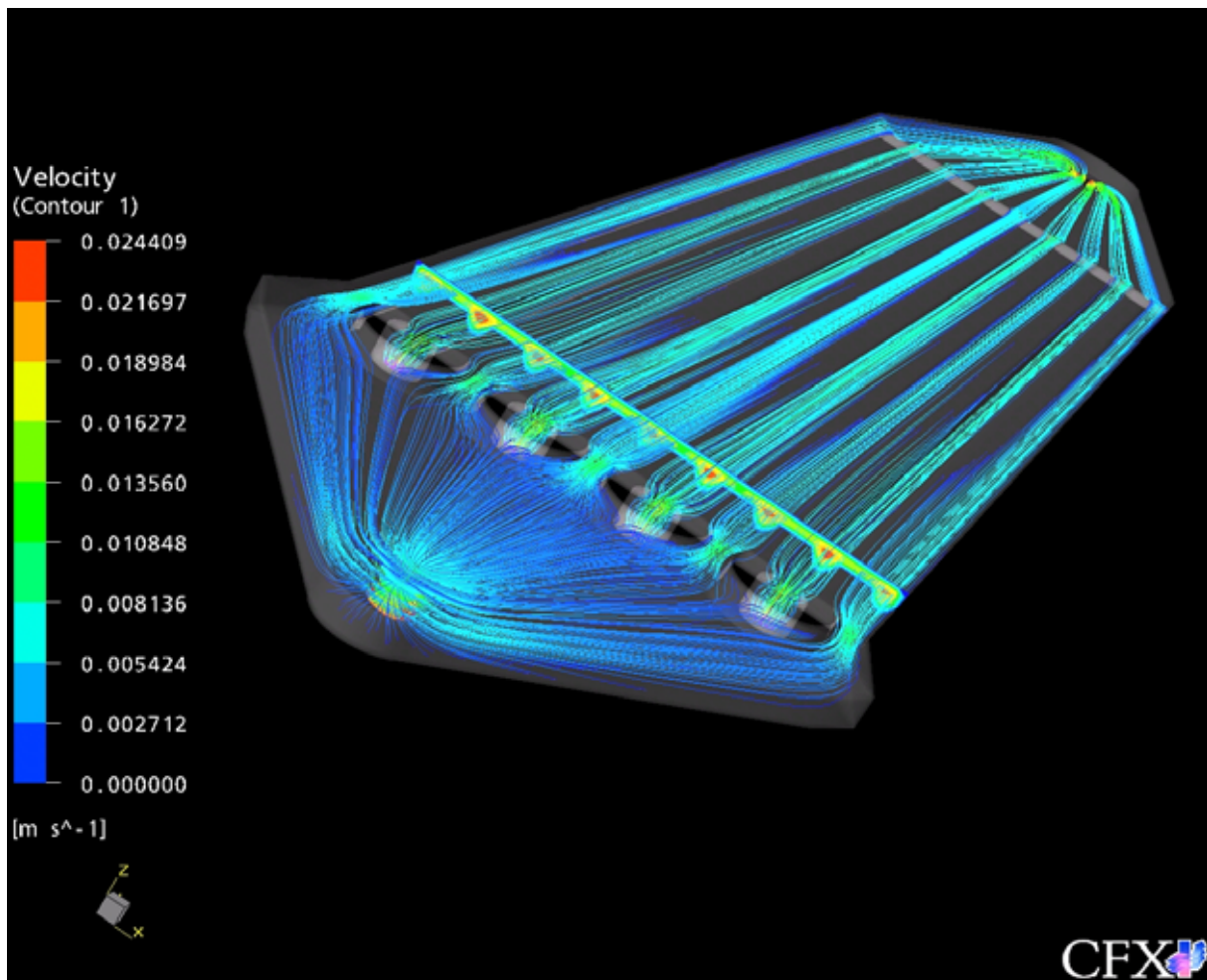


Figure 3.49: Microfluidic system 2: Run of the streamlines with 2-pump-operation modus

Nonetheless, it is possible, that such a flow situation with un-balanced partial flows can occur in the validation phase of a fabricated chamber, since the channels can only be fabricated with a certain precision. Under these circumstances, the operation mode has to be changed. The

cell suspensions can be pumped through the chamber via two independent pumps as illustrated in figure 3.49. The volumetric currents were adjusted as desired. Thus, the bad dimensioning of the input cross sections is irrelevant, since the effectiveness of the Hamilton pumps (chosen for the pump station; see section 3.2.6) delivers fluids independently from pressure loss.

However, it is delicate to predict on the basis of a simulation, if an alternating cell arrangement can be achieved. This has to be tested in real experiments.

A further example for the high influence of the pressure inside the chamber and especially of pressure losses at inlet, outlet and standpipes, is displayed in figure 3.50.

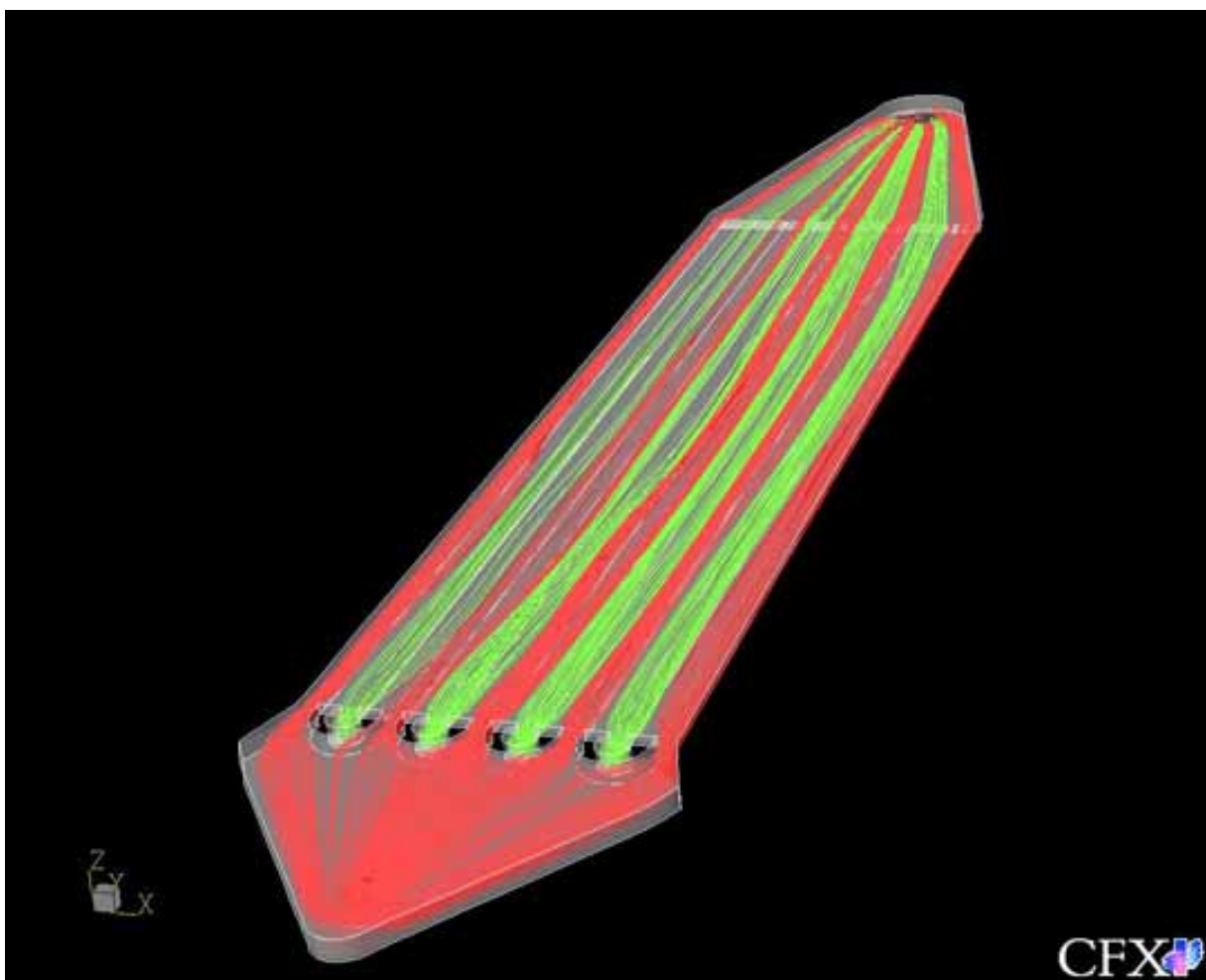


Figure 3.50: Microfluidic system 2: The simulated streamlines, coloured in red for cell suspension 1 and green for cell suspension 2, start to trundle, due to pressure rise towards the end of the chamber.

The simulated streamlines start to trundle, thus a laminar flow is not given anymore. This phenomenon results from the pressure rise towards the end of the chamber. The increase in

pressure is explained by the tapered form of the chamber's rear part. In consequence of the increased pressure, the flow velocity rises. Via the Reynolds number (Re), it appears that a rise in flow velocity results in a higher Re number, indicating a transition in flow from a laminar to a turbulent nature. For the chamber geometry on hand, a Re number of about 1 is required for laminar flow. A turbulent flow will exist for $Re > 10$. The trudging of the streamlines can be seen more easily, if only one inlet is used in the simulation (see figure 3.51). It is obvious that such a flow situation will result in some mixing between the two different solutions, which shall be introduced into the chamber. If the flow situation develops further, it can result in a turbulent flow.

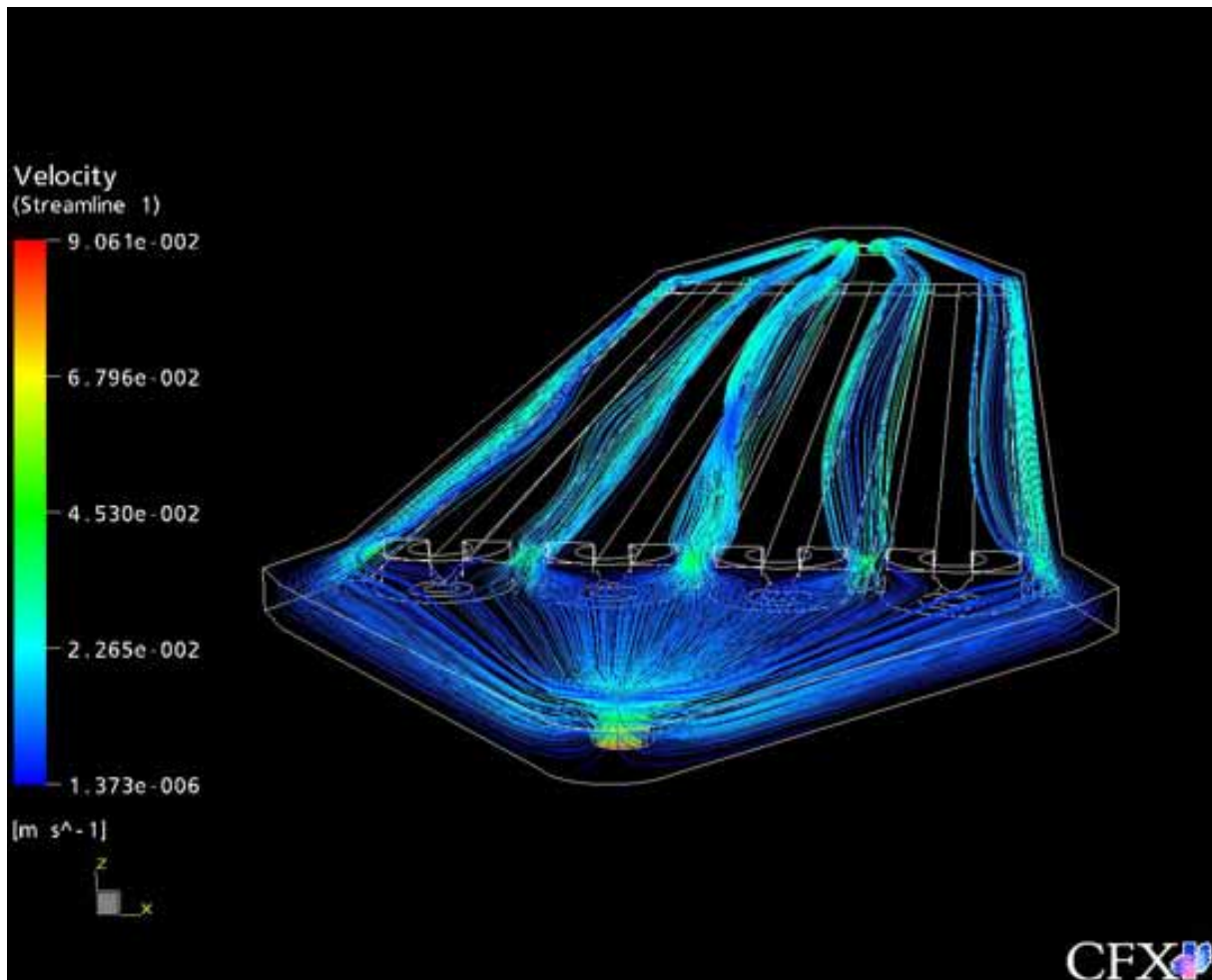


Figure 3.51: Microfluidic system 2: The simulated streamlines enter the microfluidic chamber via inlet A. The other streamlines, resulting from the fluid entering via inlet B have been left out to clarify the flow situation.

The presented situations appeared in both chamber designs, since the designs do not differ in this elementary items. Such problems were solved in simulation studies using a two-pump operation modus and doubling the radius of the outlets from $50\mu m$ to $100\mu m$. The detailed dimensions are specified in the section "Fabrication of the microstructures" on page 115. Accordingly, the desired flow pattern was obtained in both chamber designs. The simulated streamlines run parallel and do not mix.

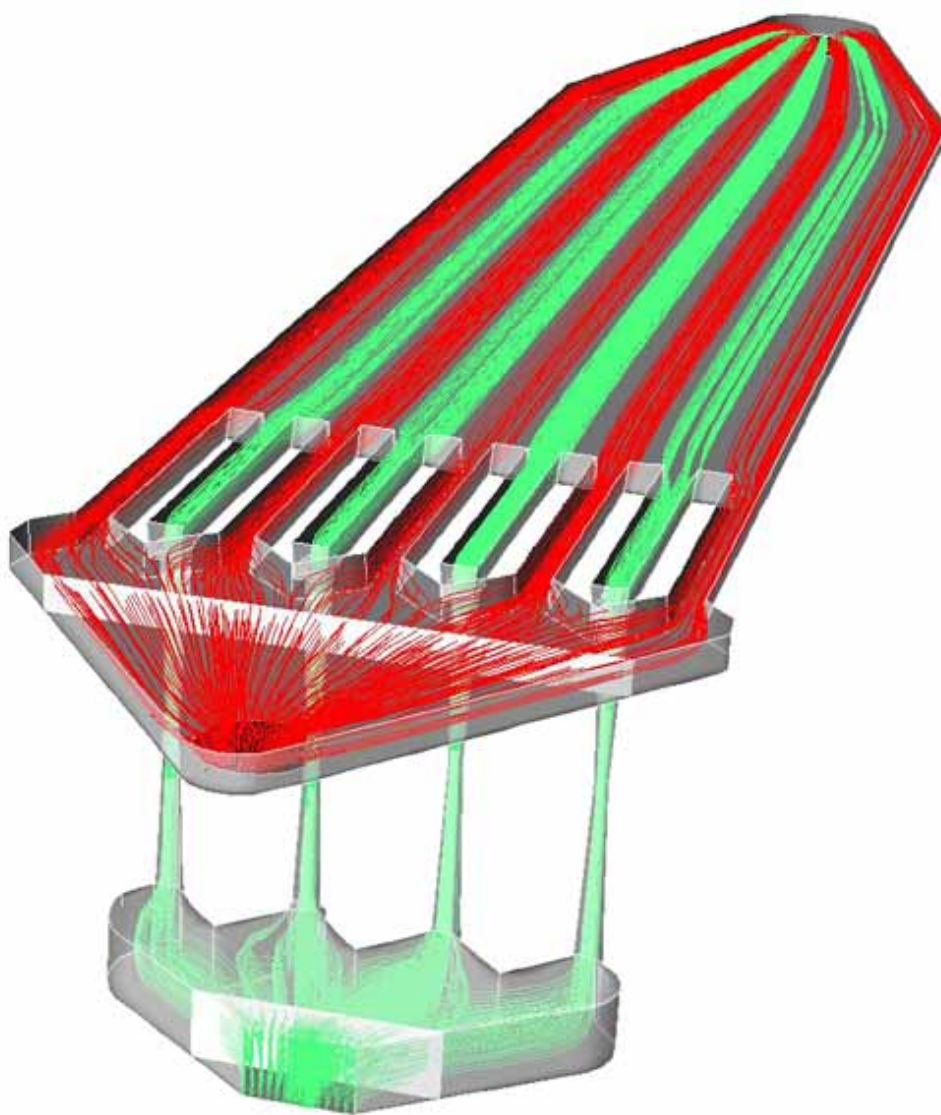


Figure 3.52: Microfluidic system 1: The coloured streamlines represent cell solution 1 (red) and cell solution 2 (green). They show a laminar flow pattern alongside the whole chamber.

The final results from the simulation studies have been captured on film (see figure 3.53 and 3.54). The corresponding movies can be found on the enclosed DVD.



1. The microfluidic system 1 is shown in 3D from different perspectives.
2. The guiding system of nine parallel channels is magnified to point out their geometry and the connection to the standpipes.
3. A fluid flow through the microfluidic chamber is simulated. A red fluid enters via inlet A, a green fluid via inlet B.
4. The fluids pass through the distribution and guiding systems, thus resulting in nine parallel laminar flows.
5. The flows alternate in colour and run through the whole chamber without mixing.

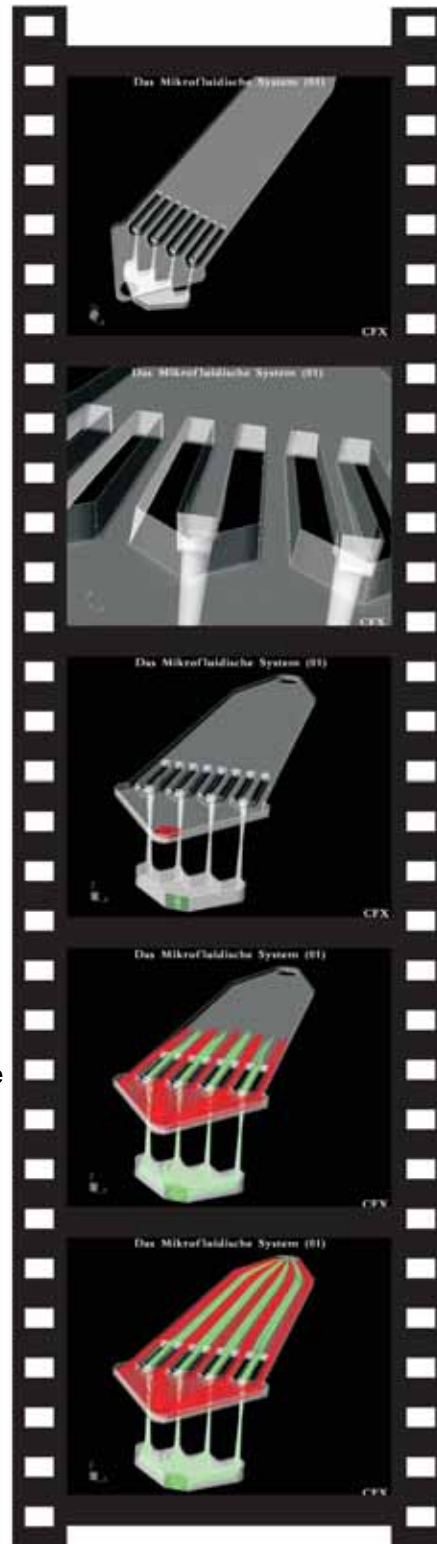


Figure 3.53: Microfluidic system 1: The selected pictures have been extracted from a movie, which presents the final design of the microfluidic system 1, showing the chamber in 3D and the flow of the streamlines. This movie is available on the enclosed DVD.



1. The microfluidic system 2 is shown in 3D from different perspectives.
2. The guiding system consists of nine trenches in the chamber bottom. It is magnified to point out their geometry. The distribution system resembles the one from the first system, thus it is not shown.
3. A fluid flow through the microfluidic chamber is simulated. A red fluid enters via inlet A, a green fluid via inlet B. The latter is not shown, but the holes, which are connected to the standpipes are depicted.
4. The fluids pass through the distribution and enter simultaneously the open chamber with the trenches.
5. The flows alternate in colour and run through the whole chamber without mixing.

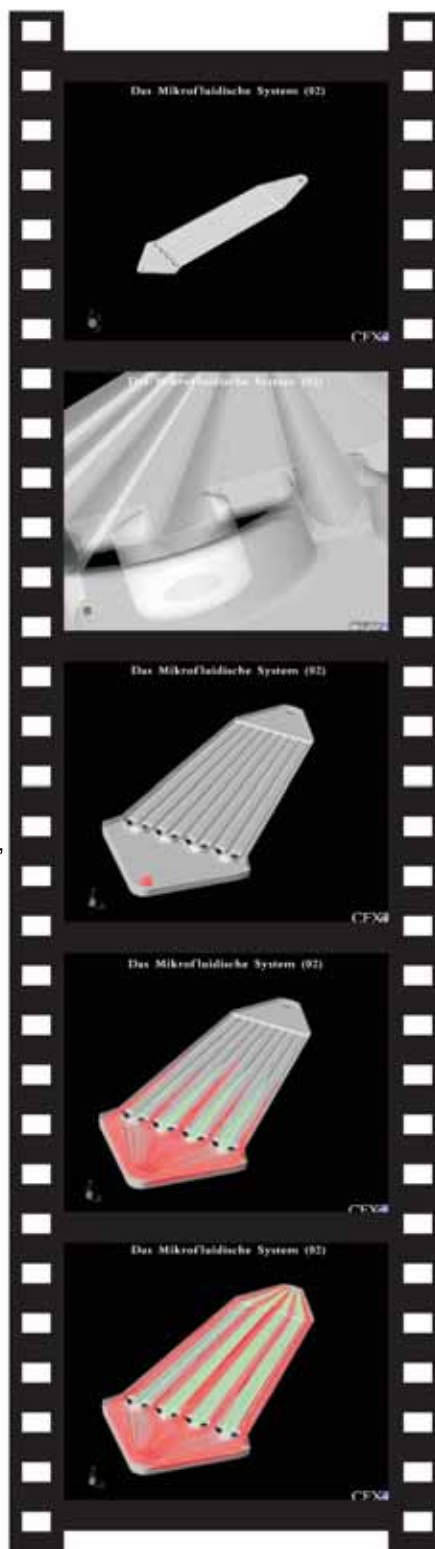


Figure 3.54: Microfluidic system 2: The selected pictures have been extracted from a movie, which presents the final design of the microfluidic system 2, showing the chamber in 3D and the flow of the streamlines. This movie is available on the enclosed DVD.

The velocity and pressure conditions turned out to play a decisive role for the restriction to laminar flow conditions inside the microfluidic chambers. Thus, a more precise simulation analysis was carried out, picturing the velocities with the help of vector graphics.

An overview of the flow velocity conditions inside the microfluidic system 1 is shown in figure 3.55. The highest velocities can be found in the channels, which guide the flow in direction, and at the outlet. A close-up of these arrays is shown in figure 3.56 and 3.57 on page 110.

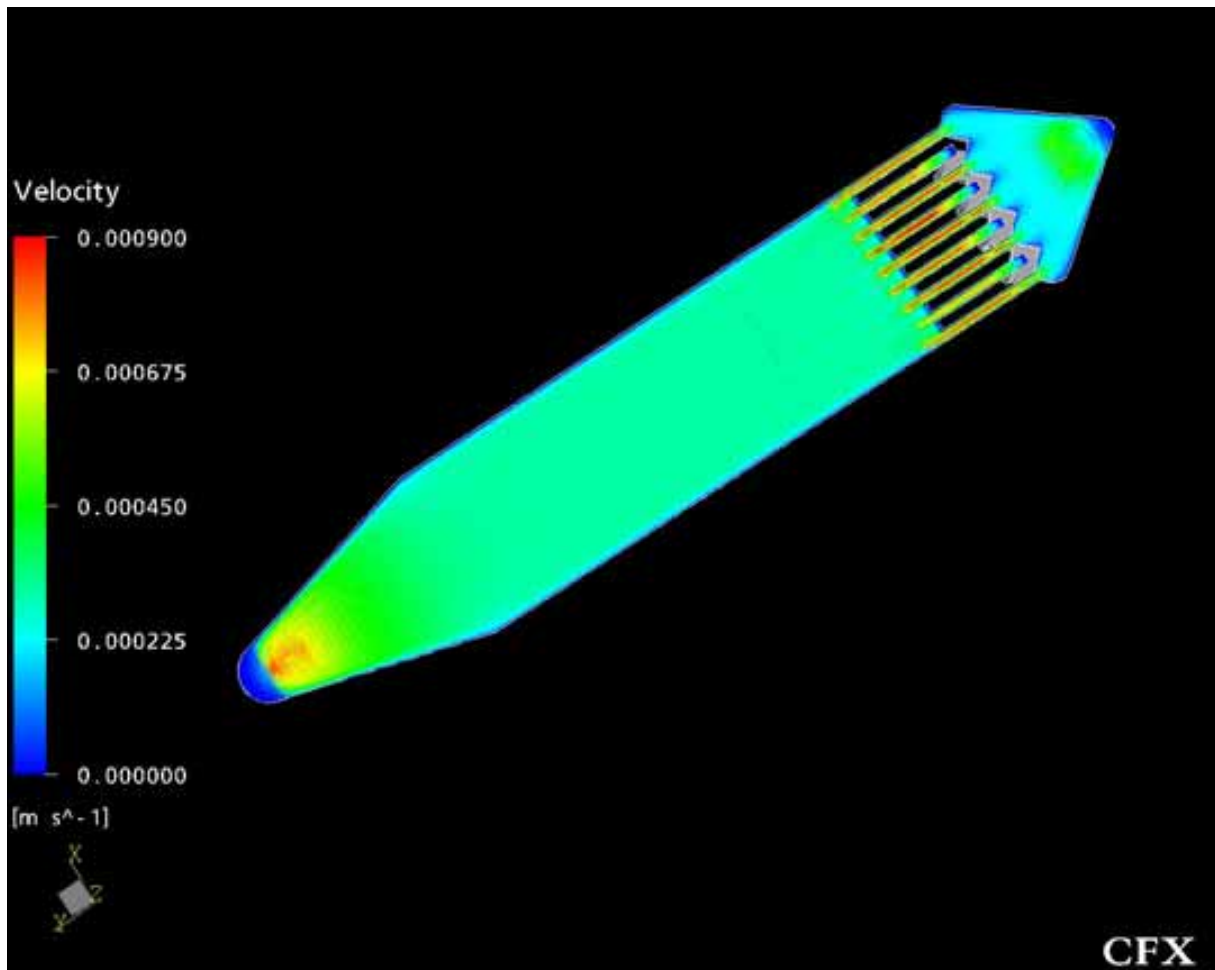


Figure 3.55: Overview of the flow velocity inside the microfluidic system 1: The highest velocities are found in the channels and at the outlet, indicated in red.

The law of continuity applies to this situation. The mass (volume) of a fluid, which flows through different cross section per time unit, is constant. Assuming that the fluid is incompressible (simplification), the total pressure is always constant.

To transport the same mass in the very same time through a smaller cross section, the flow velocity consequently increases in smaller cross sections. For incompressible fluids applies

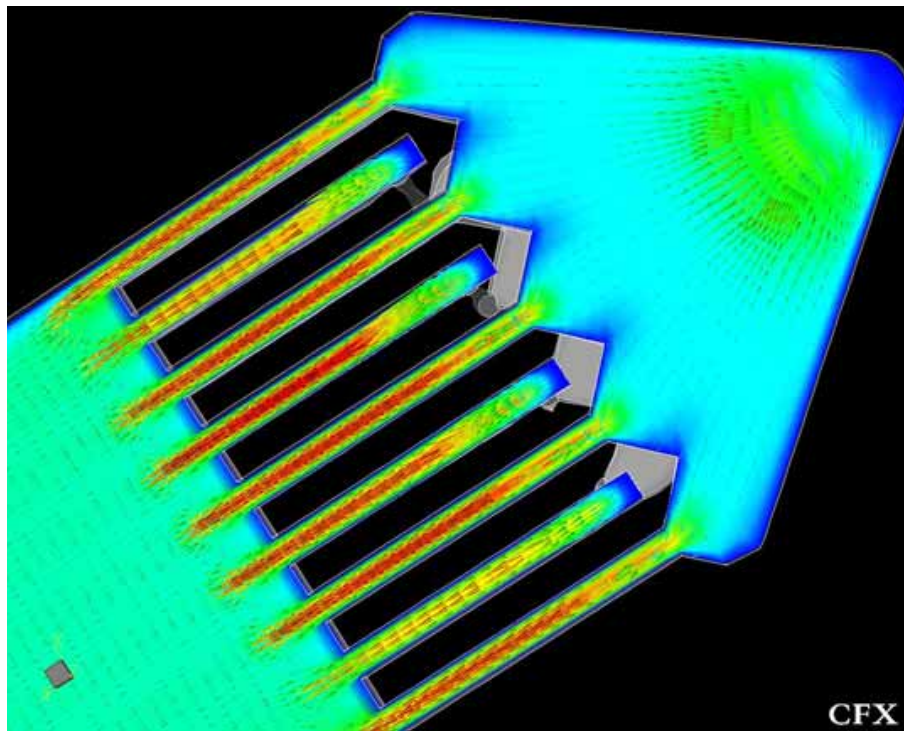


Figure 3.56: Close-up from figure 3.55 showing the channels of the microfluidic system 1, which guide the laminar flows in the right direction.

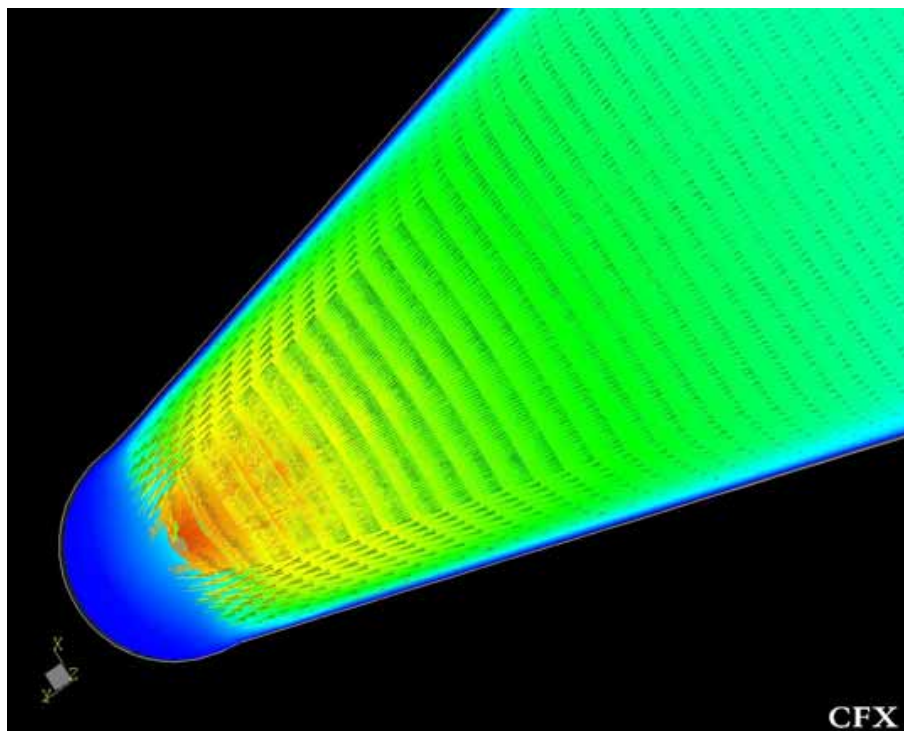


Figure 3.57: Close-up from figure 3.55 showing the outlet of the microfluidic system 1 as vector graphic.

the Venturi effect: The ratio of both flow velocities is reciprocally proportional to the ratio of the cross-sectional areas. A bigger cross section surface means a lower velocity, and a higher velocity results from a smaller cross sectional surface.

The areas with the smallest cross sections of the designed microfluidic systems are the inlets, outlets and for system 1 the guiding channels. Figure 3.58 shows a simulated inflow of a fluid in microfluidic system 2.

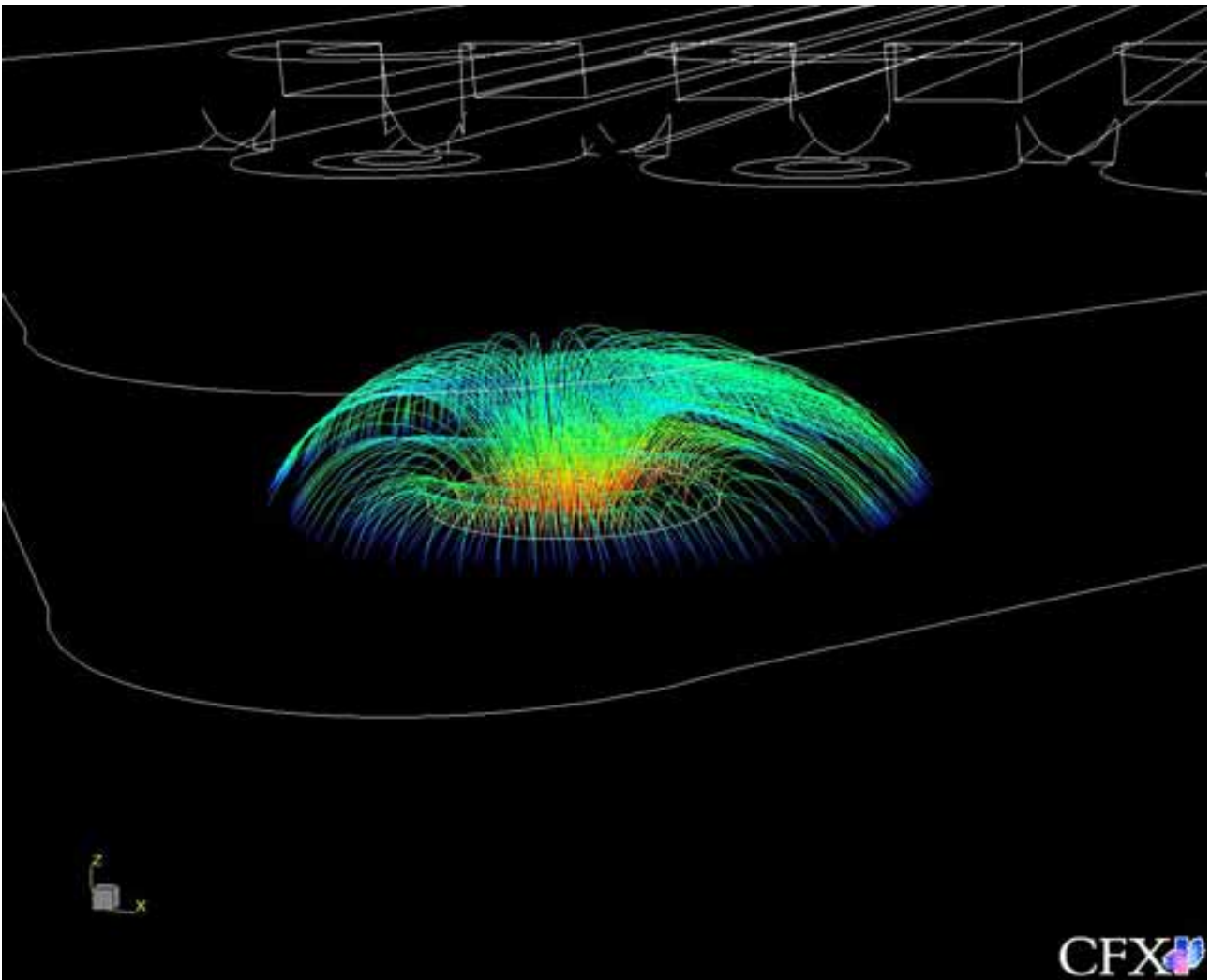


Figure 3.58: Simulated inflow of a fluid into the microfluidic system 2: The fluid arrives with high velocity at inlet A and is decelerated by entering the chamber.

As in the case of the simulated fluid inflow, every cross sectional area and the flow velocity, which prevails in this section, can be pictured individually as vector graphic. This is presented in figure 3.59 for the first system and 3.60 for the second system on page 112 and 113, respectively.

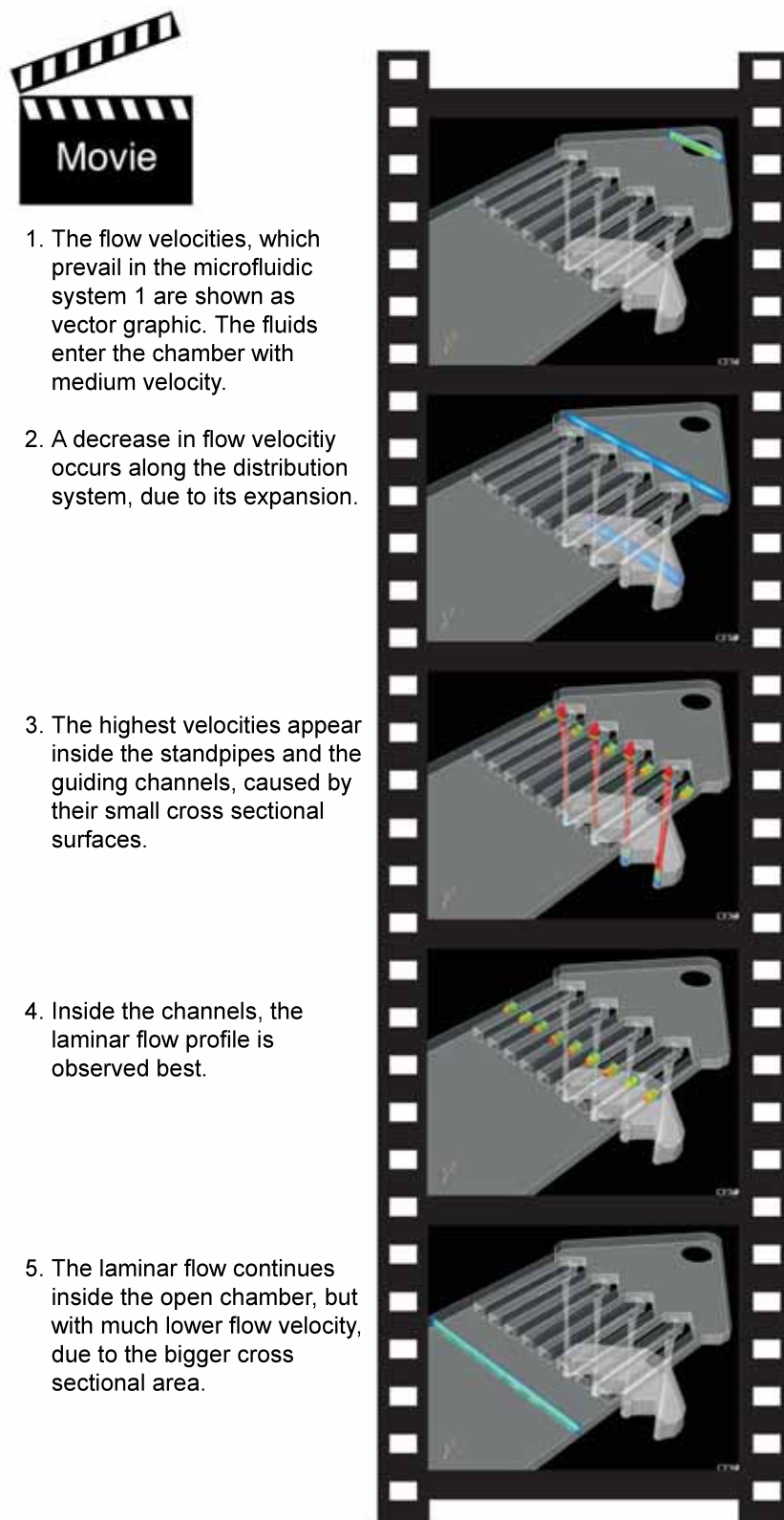


Figure 3.59: Vector graphics system 1: The selected pictures have been extracted from a movie, which presents the flow velocity pictured as vector graphic. An animation of all cross sectional areas is shown. This movie is available on the enclosed DVD.



1. The flow velocities, which prevail in the microfluidic system 2 are shown as vector graphic. The fluids enter the chamber with medium velocity.
2. A decrease in flow velocity occurs along the distribution system, due to its expansion.
3. The highest velocities appear inside the standpipes (not shown) and at the junction to the open chamber, caused by their small cross sectional surfaces.
4. Inside the open chamber, the flow velocity in the trenches is higher than above the trench walls. It is also higher than the flow velocities found in the microfluidic system 1.
5. The laminar flow profile can be observed inside the trenches.

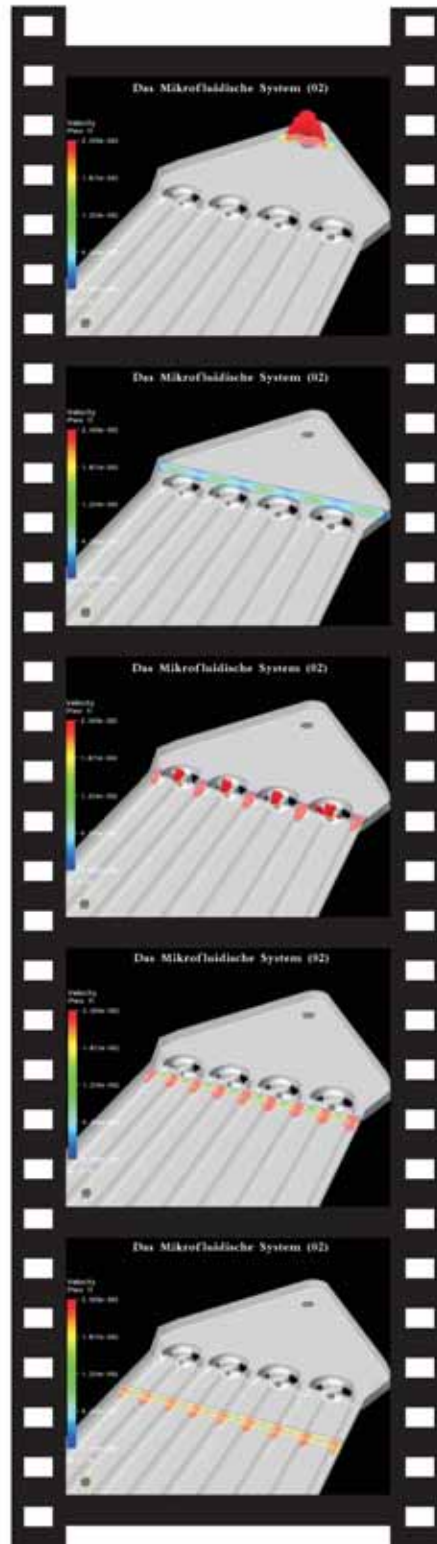


Figure 3.60: Vector graphics system 2: The selected pictures have been extracted from a movie, which presents the flow velocity pictured as vector graphic. An animation of all cross sectional areas is shown. This movie is available on the enclosed DVD.

The laminar flow profile of a cross sectional area within the guiding channels in the microfluidic system 1 can be observed in figure 3.61. The velocity varies from zero at the walls to a maximum along the center of the flow stream, resulting in a parabolic flow profile.

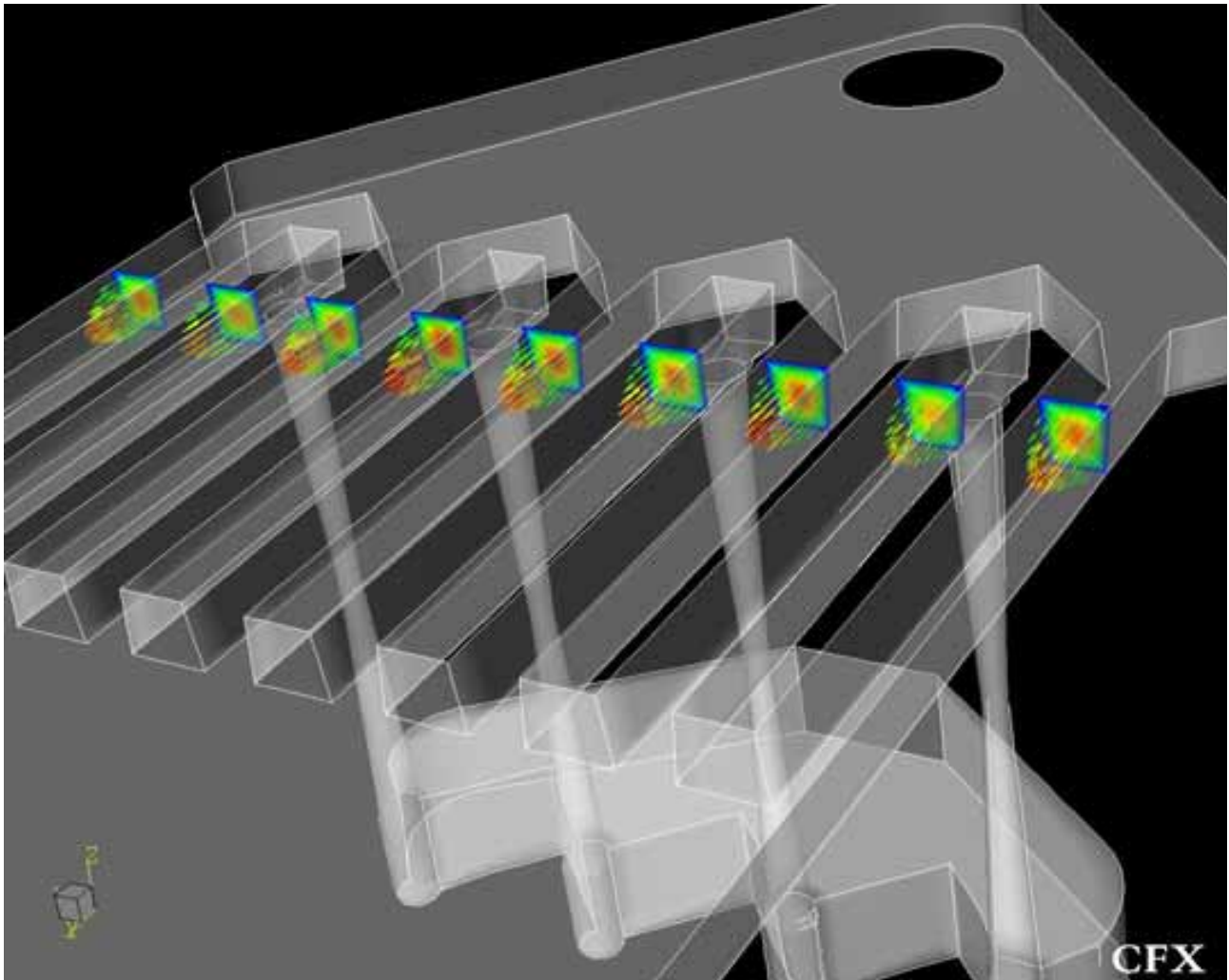


Figure 3.61: Flow velocity profile in a cross sectional area situated inside the channels of microfluidic system 1, which guides the laminar flows in direction. The gradient of velocity is parabolic, which is typical for a laminar flow. Thereby, the highest flow velocity, indicated in red, can be found in the center of the channel.

All simulations in this section are based on a two-pump operation modus (except for figure 3.48). Furthermore, the underlying mass flow rates of the fluids entering the chambers have been set to $4 \cdot 10^{-9} \text{ kg/s}$ for inlet A and $5 \cdot 10^{-9} \text{ kg/s}$ for inlet B due to the higher pressure loss.

Summary

The simulation studies avoided cost intensive experiments and indicated necessary refinements:

- 1.) enlargement of the outlet by doubling the radius to $100\mu\text{m}$.
- 2.) a two-pump operations modus had to be applied, when the partial flows which enter the chamber via inlet A, differed in magnitude from those entering through the standpipes.

Including this changes, a laminar flow inside the chambers should be feasible.:

3.2.4 Fabrication of the Microstructures

Overview

The microfluidic systems, whose development and design have been described on the last pages, were cut with an excimer laser into a glassy polymer. Accomplishment and results are presented in the following section.

The designed chambers were fabricated using a Krypton-Fluor (KrF) excimer laser (Micro-Master, Optec), operated in the Centre for Microtechnology and Surface Analysis in Denmark. The term EXCIMER derives from EXCited DIMERs and refers to the chemical gain medium of the laser, which is a gas mixture, typically containing a noble gas such as krypton (Kr) and a halogen such as fluor (F). Noble gases are highly inert and do not usually form chemical bonds. However, in an excited state, induced by an electrical discharge, they form temporary bonds with themselves (dimers) or with halogens (complexes). The resulting molecules such as KrF possess only a short lifetime of a few nanoseconds (ns). Pulses with those ns time span are emitted by the laser in the UV at a wavelength of 248nm . The interaction between the UV photons and polymers allows structures to be made with negligible thermal damage to the surroundings. Polymers can be finely micromachined at this wavelength by photo-ablative decomposition. The large molecules typical of polymers are broken into smaller fragments by electronic excitation. The resulting smaller molecules take up a bigger space, thus the irradiated volume expands rapidly and ejects the surface layers of the polymer. Additionally, most of the excess energy is carried away in the form of kinetic energy by the ejected material. Therefore, the process is relatively cool, which is important for thermally delicate materials.

With this so-called laser micromachining, it is possible to create microstructures with minimum dimensions in the order of $2\mu m$.

Selection of Material

Following some pilot studies, the choice was made for polymethyl methacrylate (PMMA), since a long in-house experience has been gained using this polymer with laser micromachining.

PMMA is a vinyl polymer, made by free radical vinyl polymerisation from the monomer methyl methacrylate. It is an amorphous transparent thermoplastic with excellent optical properties, such as high light transmittance. Best known under its common trade name Plexiglas, this hard and rigid acrylic is widely used. Prolonged exposure to moisture, or even total immersion in water, does not significantly effect the mechanical or optical properties of acrylic. With its high UV-absorbing properties, it is well suited for laser machining. Nevertheless, it possesses some restrictions, such as a sensitivity against certain solvents, *e.g.* ethanol, stress crack sensibility and a low continuous utilisation temperature at about $115^{\circ}C$. The latter and the mild solubility in ethanol circumvents sterilisation with 70% ethanol or autoclaving, but leaves room for other sterilisation techniques such as irradiation.

Biocompatibility Test

The chosen material PMMA was subjected to a biocompatibility test. Therefore, polymer samples with an excimer laser machined area of $20mm \cdot 20mm$ were brought into contact with cells. The laser-machined area has not been cleaned in any manner and represented a "worst case" scenario with much ablation material remaining on the surface. Normally, the excess ablation material would be washed off with a mild detergent solution.

A growth curve of the model cell line KG-1 was surveyed over 3 days both with direct contact to PMMA and with PMMA conditioned medium (medium, which was incubated with a PMMA sample for 24h at $37^{\circ}C$ and the polymer was removed thereafter). The cell line was cultured with IMDM + 10% FCS at $37^{\circ}C$ in a T flask. No influences on their proliferation ability or toxic effects were recognised in comparison with an untreated KG-1 culture (data not shown). To further test the material for the use with dendritic cells, fresh matured monocyte-derived DCs (d8) were incubated for 24h with a PMMA sample under culture conditions and compared with the non-treated culture. Their phenotyp was analysed before and after the test (see figure 3.62) by FACS, focussing on four specific surface markers: MHC-II, CD80, CD83 und CD86.

PMMA showed no effect on the expression levels of the analysed surface markers after one day of co-culture. The only difference was found relating to CD83, a surface molecule, which can be regarded as maturation marker for dendritic cells. The results showed upregulation of CD83 on day 9 of about 20% in both cultures, DCs cultured with and without PMMA. The cells were left in the medium, they were generated in, which still contained cytokines from the maturation cocktail, thus advancing their maturing. Altogether, a higher CD83 level can be observed on day 9, but no differences due to the contact to PMMA.

Therefore, the material has been rated as appropriate to the use in electrofusion chamber development.

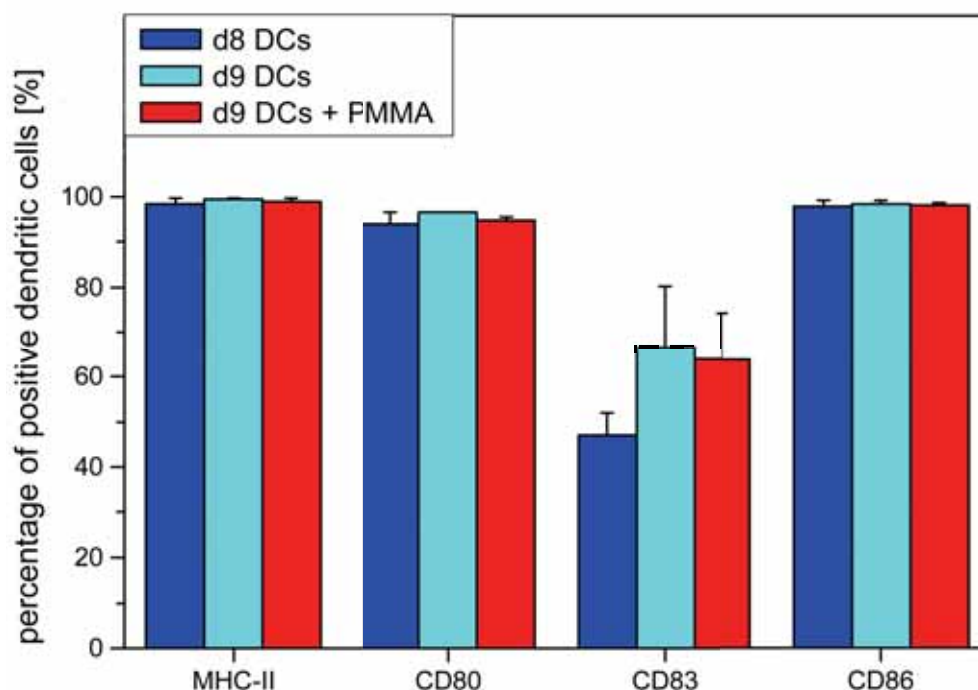


Figure 3.62: Phenotypical analysis of matured DCs either brought into contact with an PMMA sample for 24h or left untreated. Shown are results of surface antigen expression after 1 day incubation (d9) compared to the expression levels on day 8 (d8). The values are presented with a mean standard deviation (SD) resulting from 3 measurements.

System 1

For the fabrication of the microstructures in PMMA with an excimer laser, the 3D design had to be flattened to 2D and brought into a format compatible with the laser software. This was

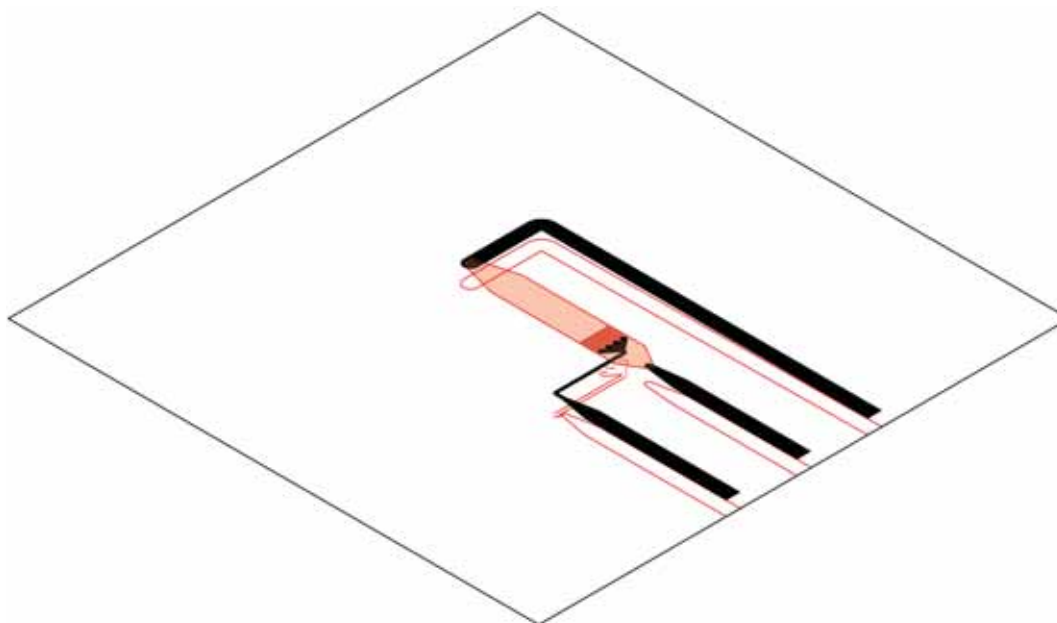


Figure 3.63: Positioning of the microfluidic system on a $15\text{mm} \cdot 15\text{mm}$ polymer piece

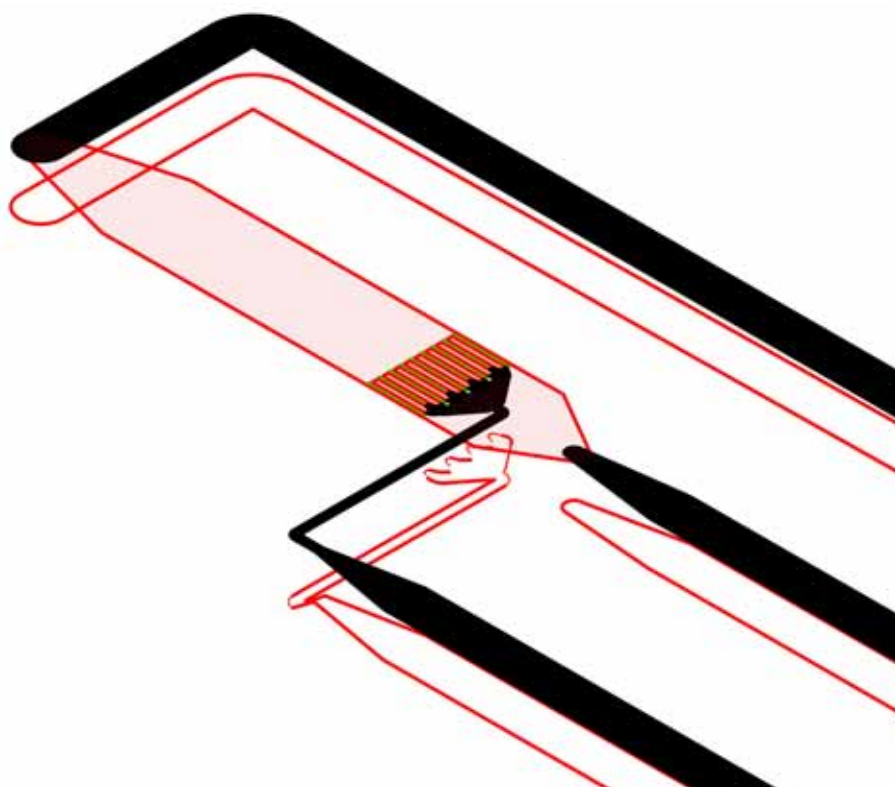


Figure 3.64: Close-up of figure 3.63: The 2D design of the microfluidic system 1 was drawn with the software AutoCAD showing the chamber with feedlines for inlet A, inlet B and the outlet (from left to right).

realised using AutoCAD software. The flattened design is shown in figure 3.63 and figure 3.64 on page 118.

To obtain a 3D structure in PMMA from the 2-dimensional design, the chamber was burned from the upper side and all feedlines and distribution systems from the bottom side into a polymer piece of $15\text{mm} \cdot 15\text{mm}$. The cut lines are pictured in red, with the black areas representing the projection of the feedlines onto the up side. Both sides are connected via through-holes, which are visualised in figure 3.65.

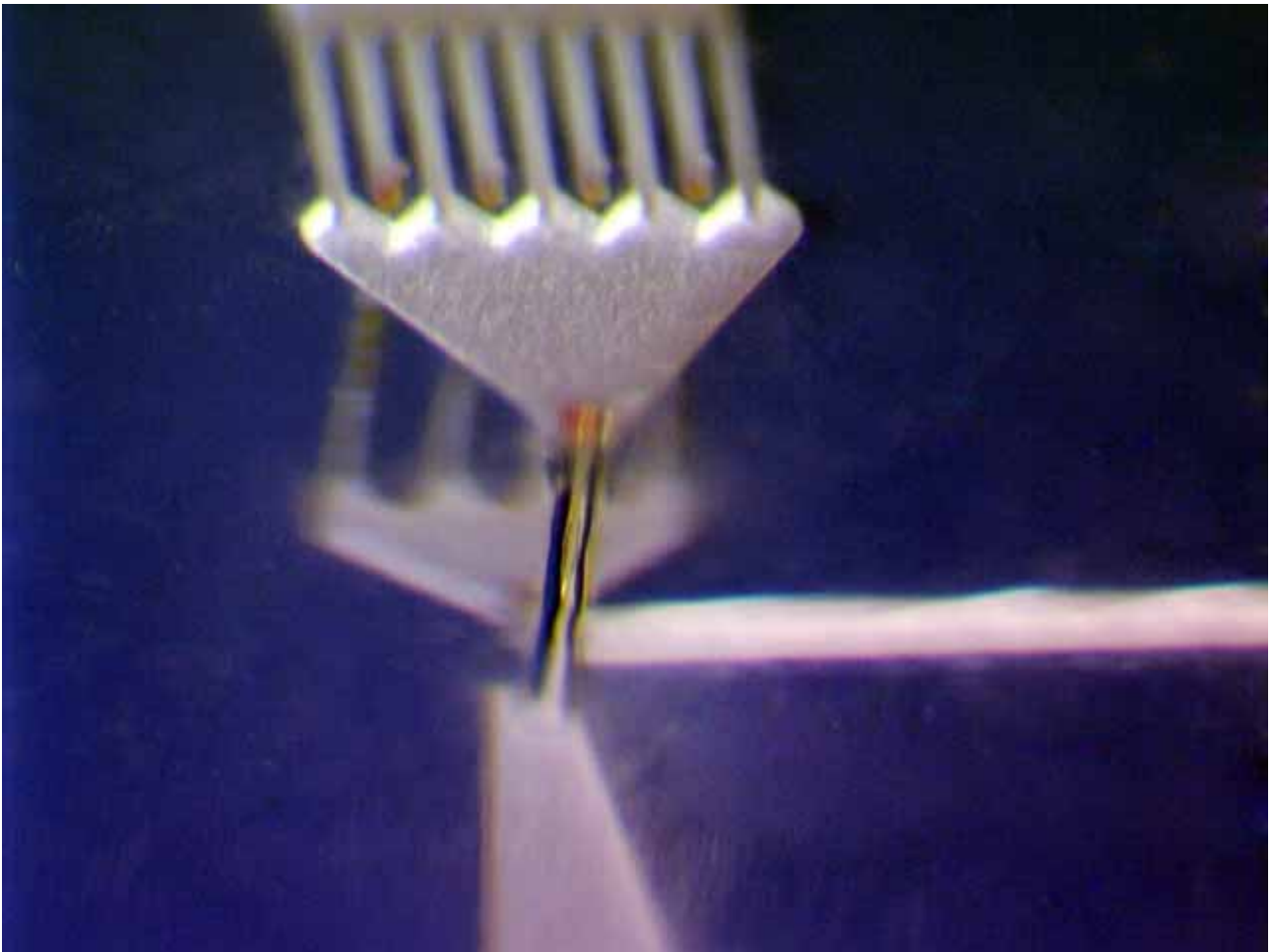


Figure 3.65: Picture of the front part of the microfluidic system 1 burned into PMMA with the use of an excimer laser: The through holes are visible, which connect the feedlines from the bottom side with the chamber on the Top.

The generation of these 3-dimensional structures required an alignment step during laser micromachining, since the micromachined features of the upper side had to be aligned to the features on the bottom side. This was done, relying on the visual identification of features,

which served as alignment point. Minimum two of those reference points were needed, to align all other features accordingly. In the present case the through holes were used as reference points, since they are visible from both sides and six in number, more than enough to admit a good orientation on the polymer piece.

Hence, those holes were established first and all other features were aligned with respect to the existing through holes on the part to be processed. A resulting 3D structure is shown in figure 3.66 and 3.67, respectively. More detailed pictures of the chamber, which reveal the rasterised ablation of the surface layers, can be seen in figure 3.68 on page 122.

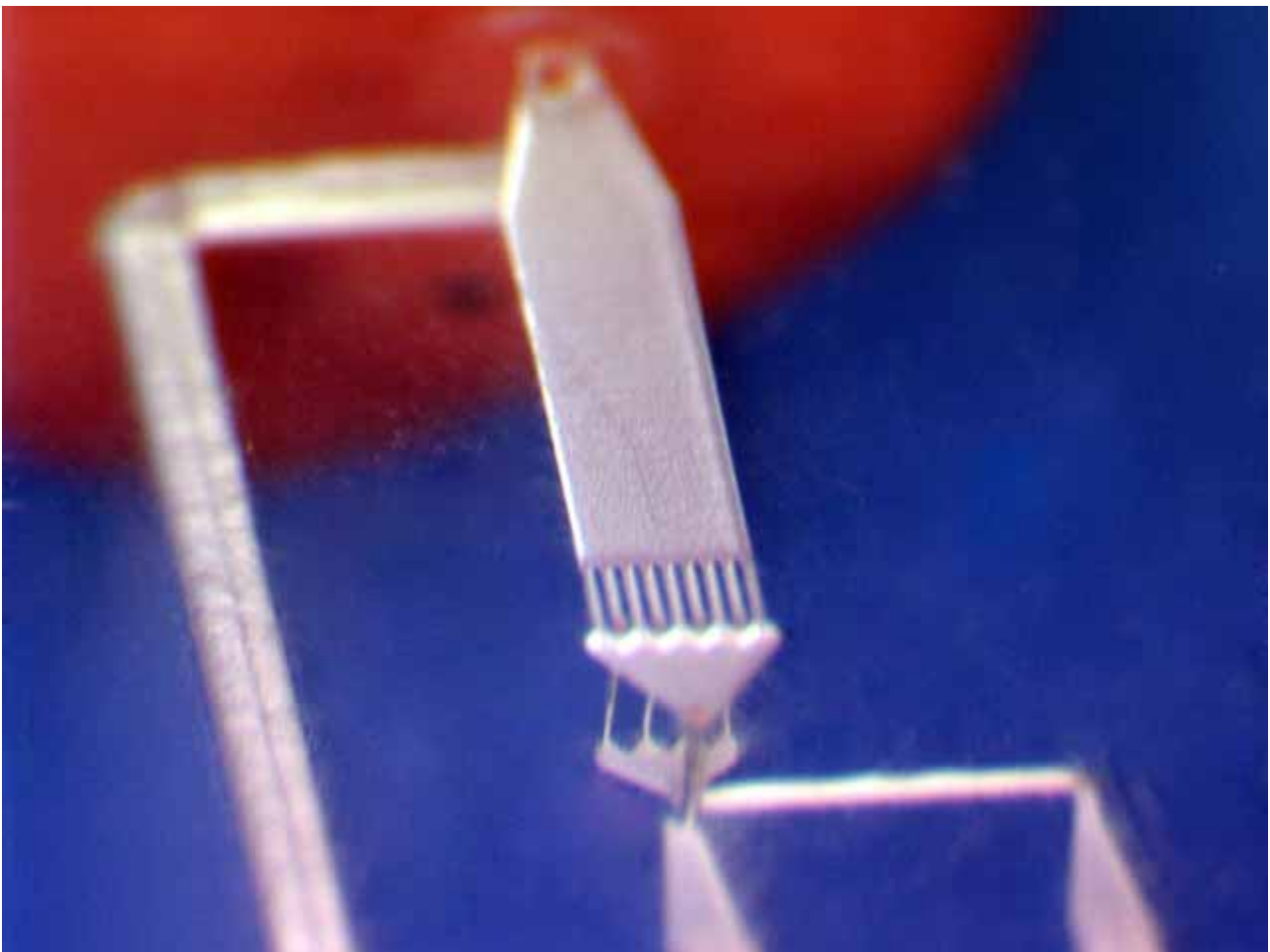


Figure 3.66: Sloped oversight of the microfluidic system 1 using a binocular microscope

To avoid crack propagation by mechanical stress of the handling, all processed microfluidic systems were reheated after fabrication and chilled slowly. Initial frictions were due to thermally induced stress during the laser micromachining process, anyhow energy densities of around 20 J/cm^2 at repetition rates up to a few hundred Hz were applied. However, the stress was relieved

by the mentioned method.

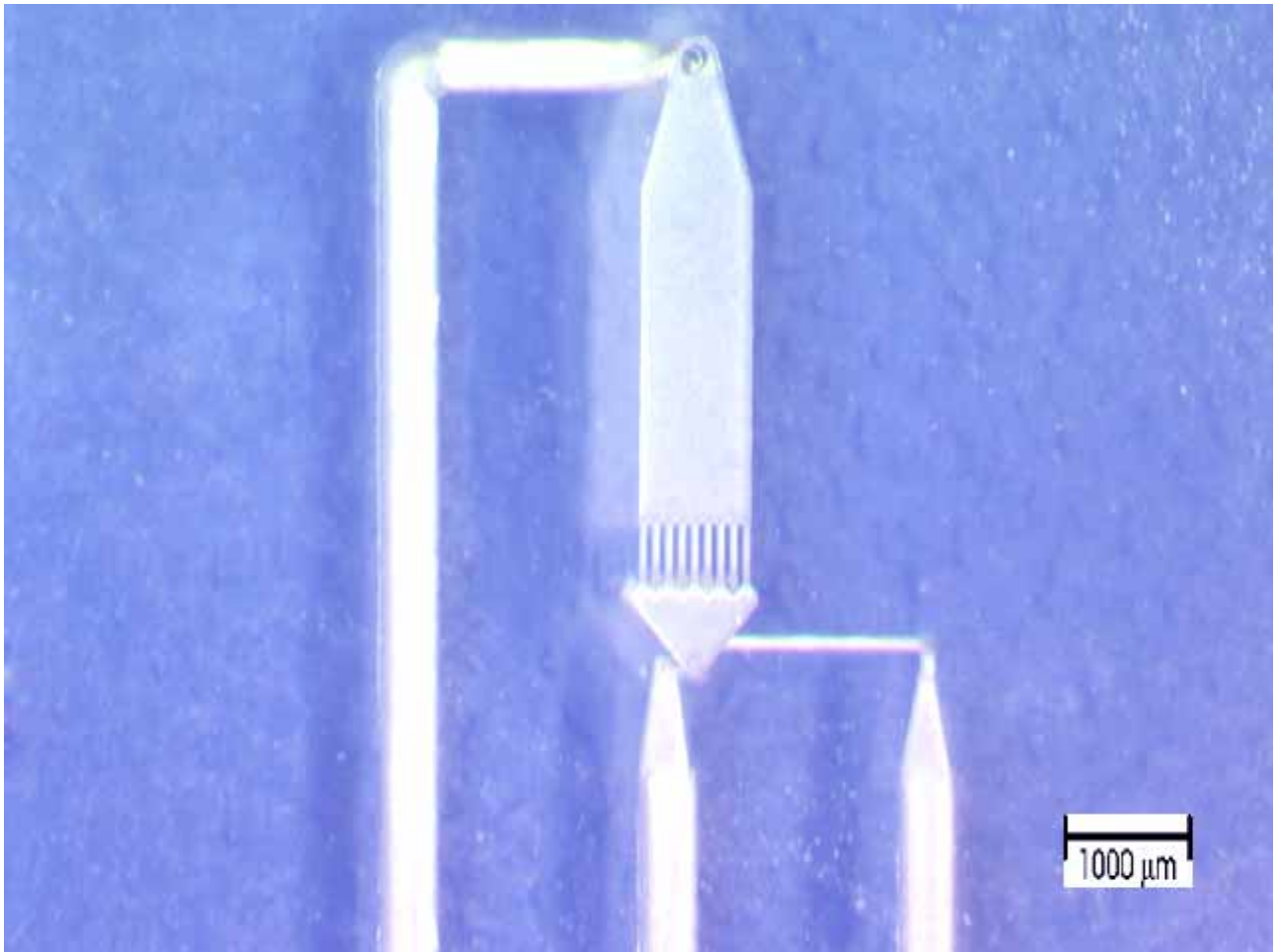


Figure 3.67: Plan view of the microfluidic system 1 using a binocular microscope

System 2

The second microfluidic system was cut the same way into PMMA as described for system 1. Only one thing had to be considered. During the fabrication of the trenches in the bottom of the microfluidic chamber, attention had to be paid to emission of material at the sides of the trenches. These bulging needed to be kept low, so not to hamper the contact of the cells during the alignment for the electrofusion process or to affect the laminar flow. The specification of those trenches can be examined in figure 3.69 on page 123, which shows pictures from the microfluidic system 2 using a light microscope.

At last, the developed chambers in their 3-dimensional set-up are an open system. Both, the upper and bottom side needed to be sealed with a cover in order to obtain a utilisable

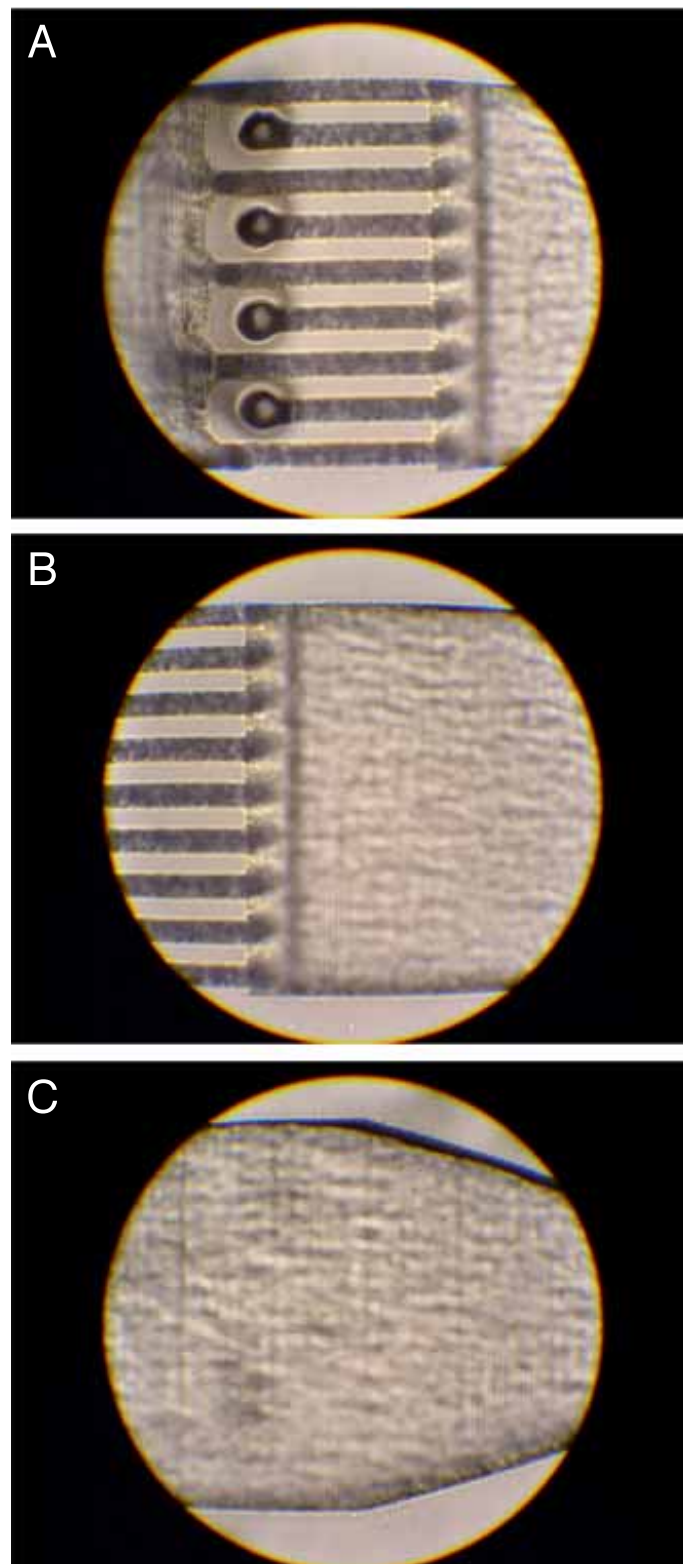


Figure 3.68: Microfluidic system 1: Photographs from the inlets B (A), the middle (B) and rear part (C) of the chamber taken using a light optical microscope.

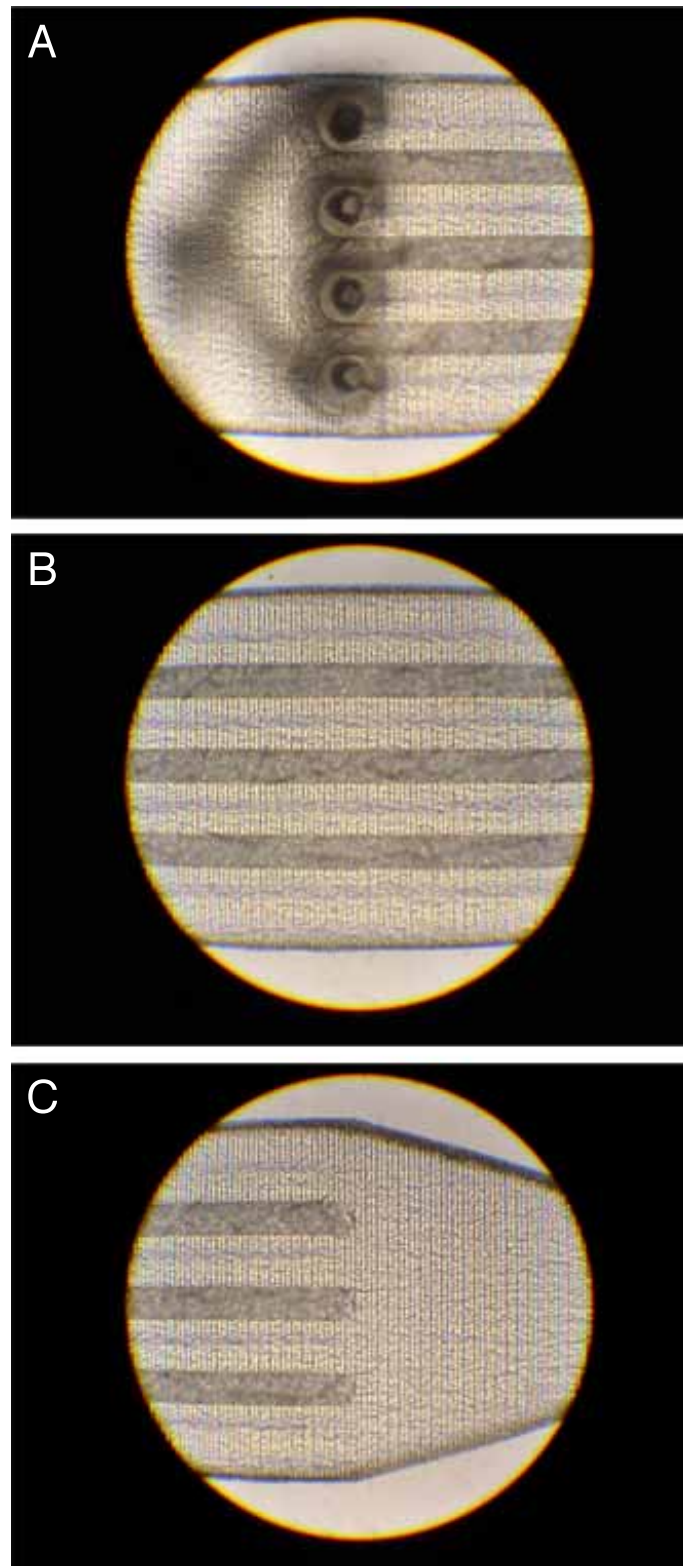


Figure 3.69: Microfluidic system 2: Photographs from the inlets B (A), the middle (B) and the rear part (C) of the chamber taken using a light optical microscope.

microfluidic chamber, which is discussed in chapter 3.2.5.

Summary

The microfluidic systems were fabricated using the following process specifications:

- 1.) laser micromachining process using an KrF excimer laser
- 2.) polymethyl methacrylate as raw material (Plexiglas), a polymer with proven biocompatibility for the use with the designated cell systems

3.2.5 Assembly of the Microchambers

Overview

The laser-machined microstructures in PMMA need to be sealed to obtain a functional microfluidic systems. Sealing attempts by direct bonding with PMMA substrates and the final sealing procedure are described in this section.

To obtain a functional microfluidic structure, the laser-machined PMMA slides were connected to non polar fused silica capillaries, which allowed the subsequent connection of the microfluidic chip to a pump station. In addition, sealing of the open structure with a top and a bottom plate was required.

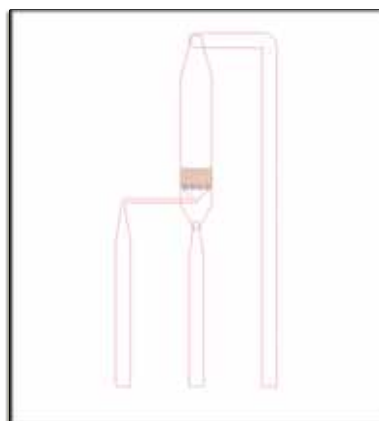


Figure 3.70: Schematic depiction of the microfluidic chip for the microsystem 1

The silica capillaries with an inner diameter (ID) of 0.25mm were glued into the microfluidic chip. Therefore, small channels were drilled into the PMMA slide, which bridged the gap from the beginning of the microfluidic channel structure to the border of the PMMA slide (see figure 3.71). In this connection to the outside the capillaries were entered and fastened by a glue, which cures under UV light (depicted in figure 3.71). This gluing was done under microscopic observation, since a penetration of the glue into the inserted capillary had to be avoided.

The experience showed, that a penetration of the glue into the capillary was likely to occur, if the glue was not hardened fast enough. In practice, it appeared reasonable to drill the holes, insert and glue the capillaries in the PMMA slides before the microfluidic structure is cut, as the latter procedure is the time-consuming and expensive one.

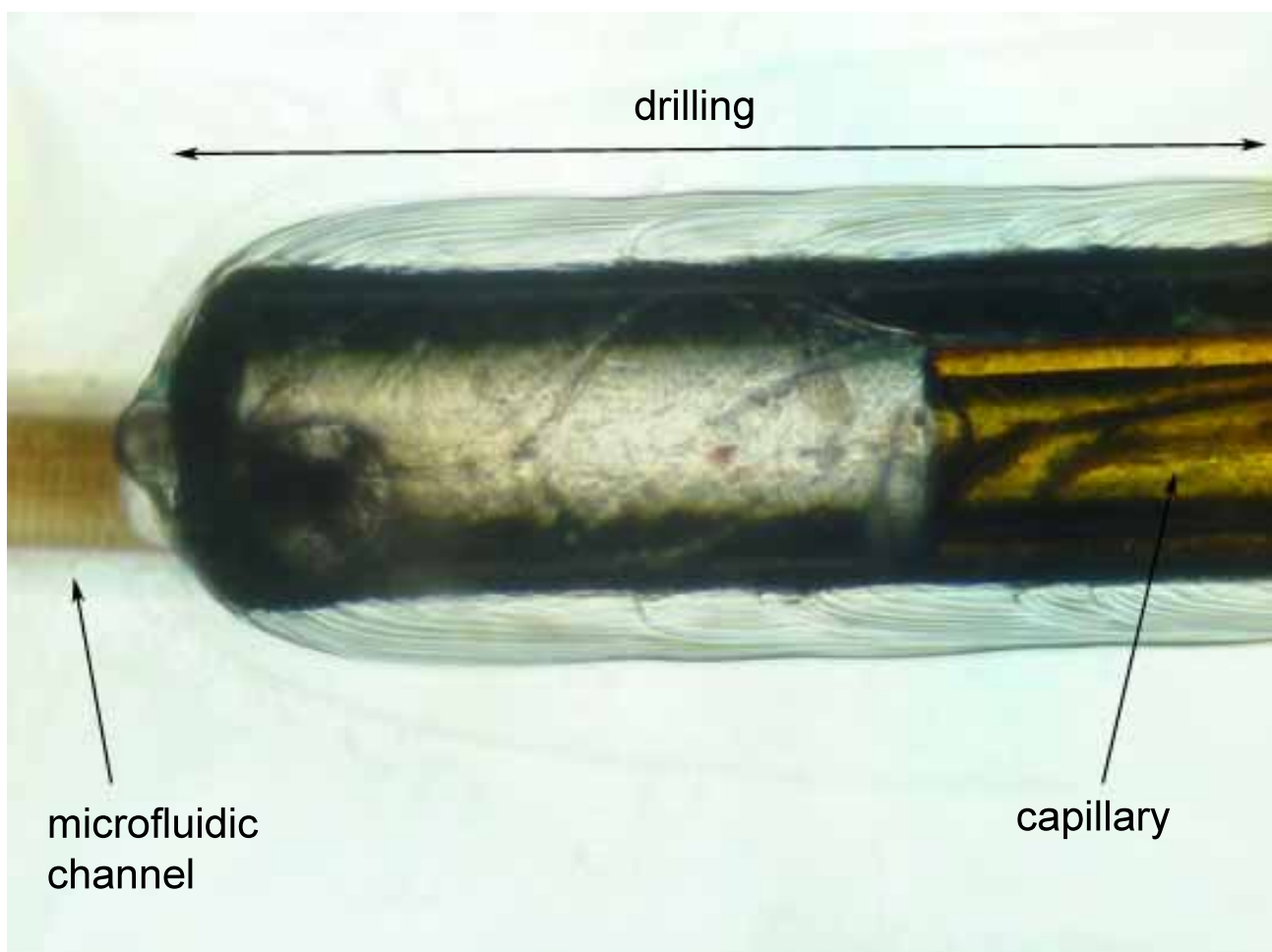


Figure 3.71: Light-Micrograph of a capillary with an ID of 0.25mm glued into a drilling, thus connecting the microfluidic channels of the microstructure with outer apparatus, such as pumps.

For batch production of the microfluidic chip it would be an advantage to find a way to reversible connect and disconnect the standard operating polymeric microfluidic units, *e.g.* the supply chains. The solution of this problem is discussed in section 3.2.9.

Bonding

The last step of the assembly of the microchamber was the sealing of the open microstructure. Polymer slides of PMMA had to be bonded as top and as bottom to the microfluidic chip to make a functional system. Thereby, the adhesion between different polymer layers was achieved by thermal compression.

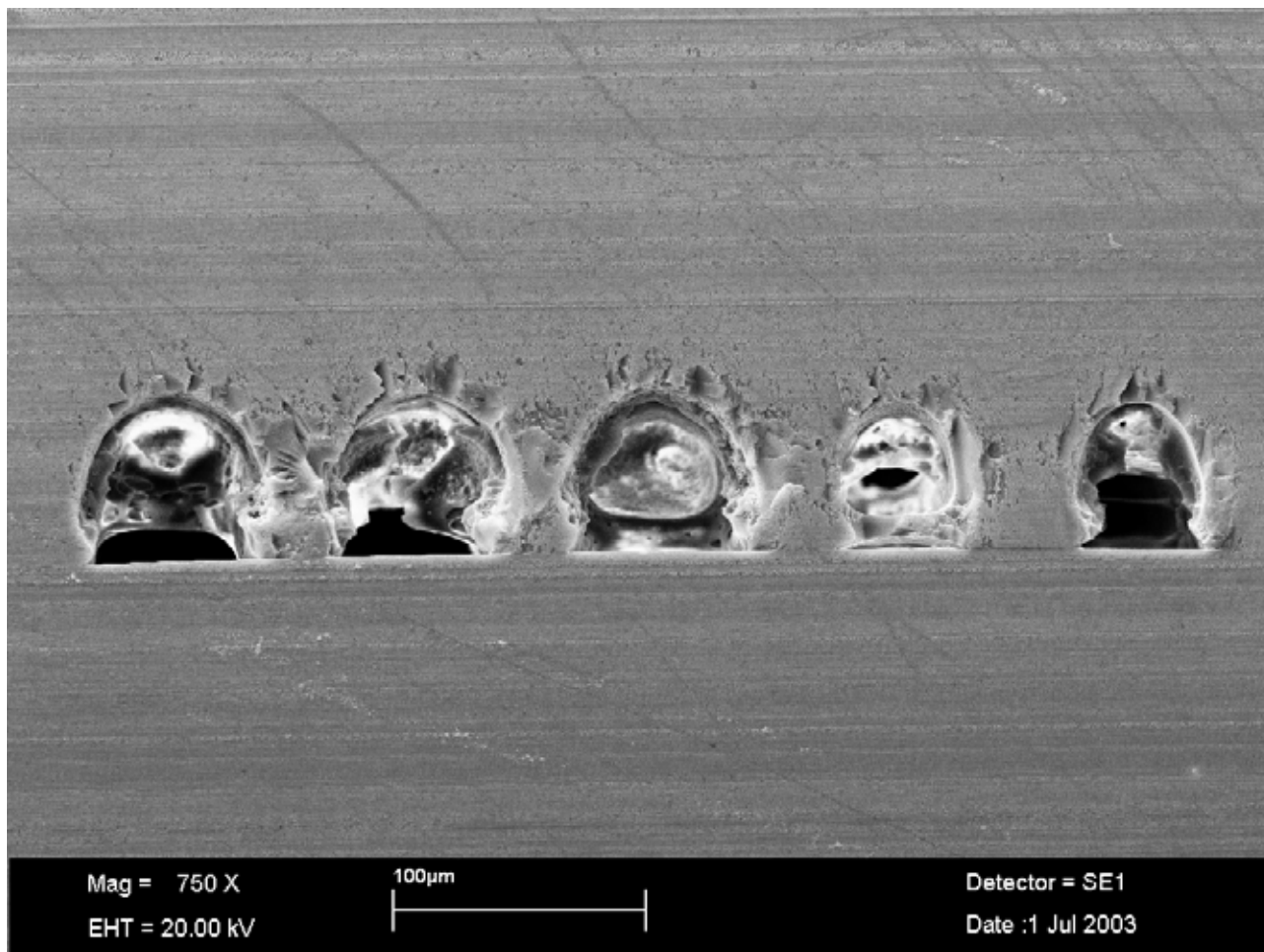


Figure 3.72: Cross section through a bonded microfluidic structure: A test series of channels with different widths and depths were cut with an excimer laser in PMMA. Subsequently a PMMA cover was welded on top of the microstructure under specific process conditions.

The adversely affect of this process, called bonding, is the occurrence of global and localised

geometric deformation, if the parameters such as pressure, temperature or residence time are chosen wrongly. Since PMMA cannot withstand a high bonding temperature, a low temperature bonding of the microfluidic structure was carried out.

The biggest problem arose from the determination of the process parameters for this assembly of the PMMA components. The process was empirical and iterative. The results of the pilot studies on PMMA bonding can be seen in the pictures of scanning electron microscopy (see figure 3.72 and 3.73).

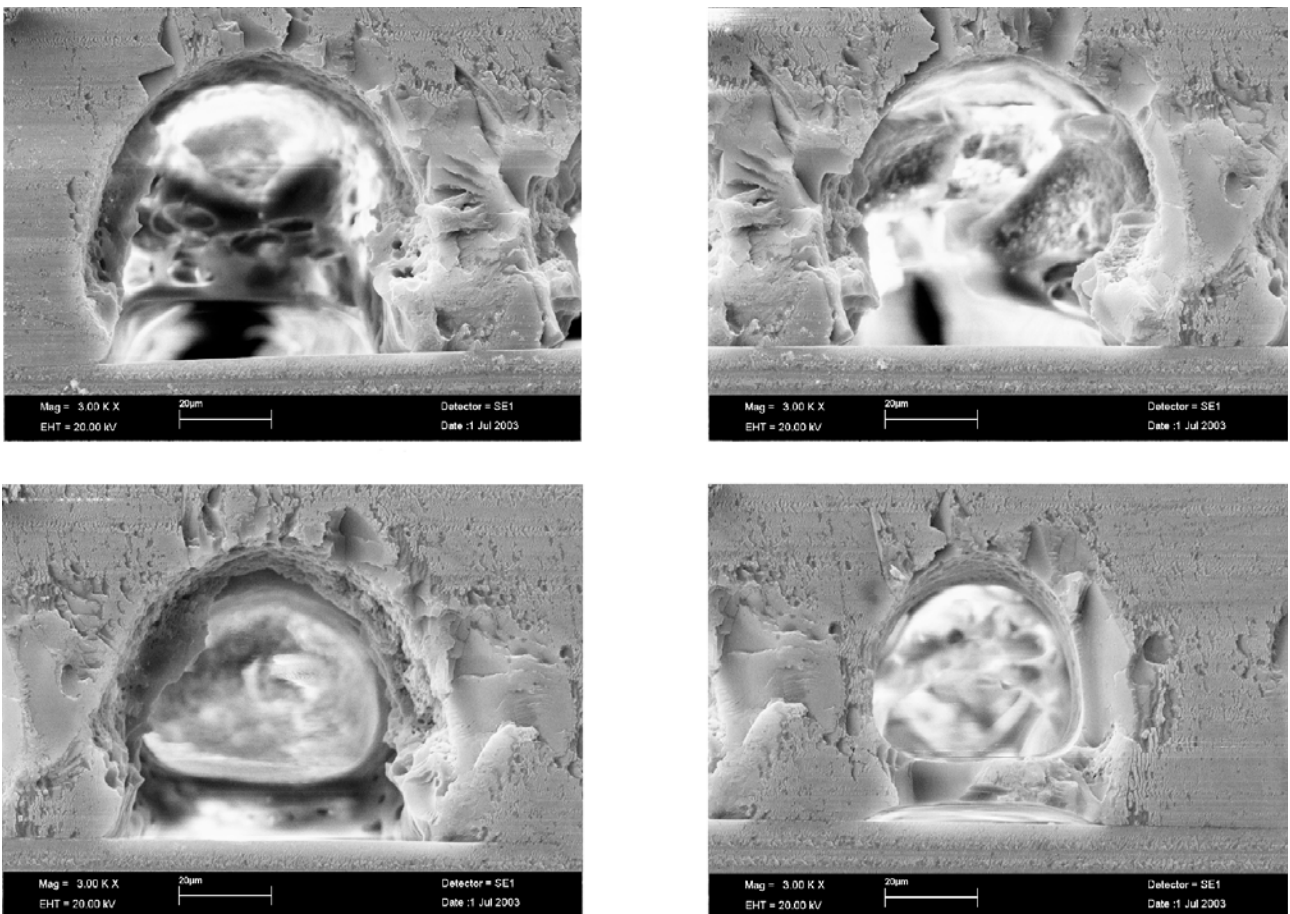


Figure 3.73: Partial records of the channels of figure 3.72

The following effects can be recognised in the channels shown in the SEM pictures:

- Spallings as a result of the manufacturing process, which were of little importance for the application.
- The channels seemed to be blocked, since items were spotted in the background of the channels. However, this was primarily an optical issue: Channel walls were seen in the

background of the channels, which did not actually extend into the run of the channel. In addition, static charges of the polymeric material occurred (see white faces), which gave the impression of blocked channels.

- The channel surfaces possessed a certain roughness, which might affect the flow of the cells through the channels.

In total, the channel outcome and the bonding were applicable for the use in the described system. Whether the channel roughness had any negative effect on the streamed cells needed to be determined in the validation phase (see chapter 3.2.7 for results). None the less, it was not possible to transfer the bonding process to the designed microfluidic systems, because of the system containing both small channels with only $50\mu\text{m}$ in diameter and big cross sectional areas like the open chamber. Bonding parameters, which applied for both were not found. Usually, geometric deformation occurred, which were tolerable for channels in the range from millimetres to a few hundred microns, but not for micron sized channels. The significant material deformation distorted the microchannel geometry and consequently destroyed the microfluidic structure.

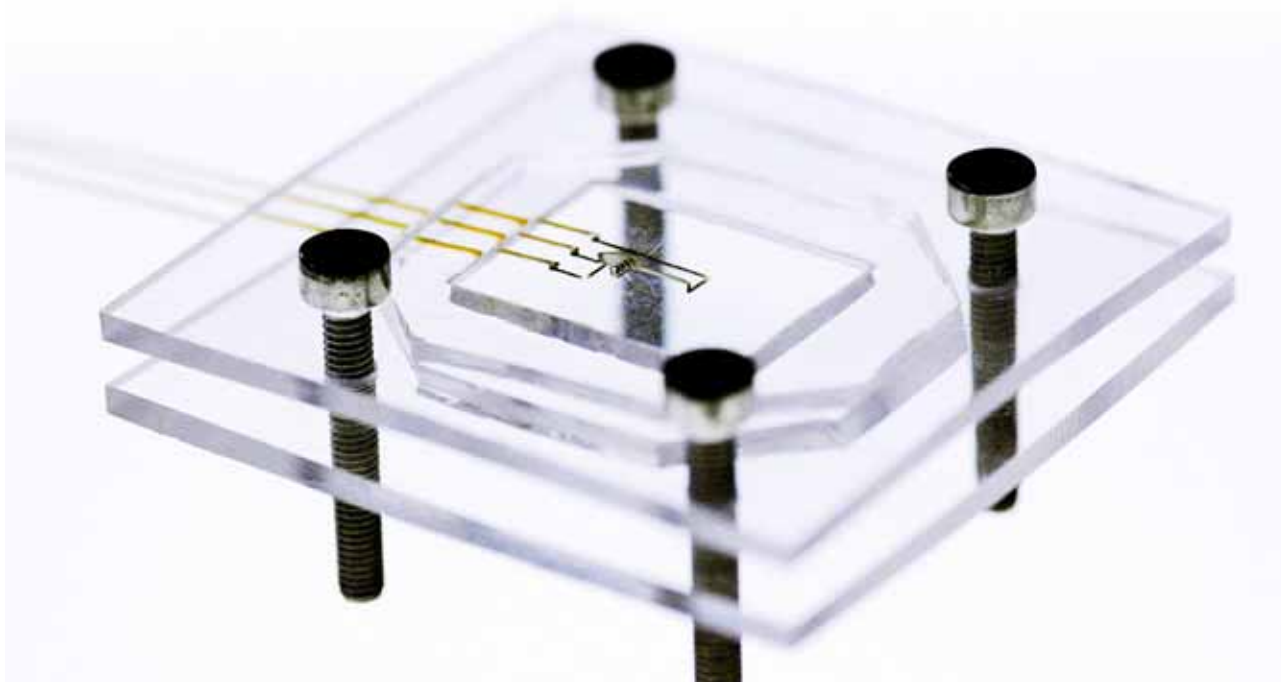


Figure 3.74: Solution for the sealing of the microfluidic chambers instead of bonding

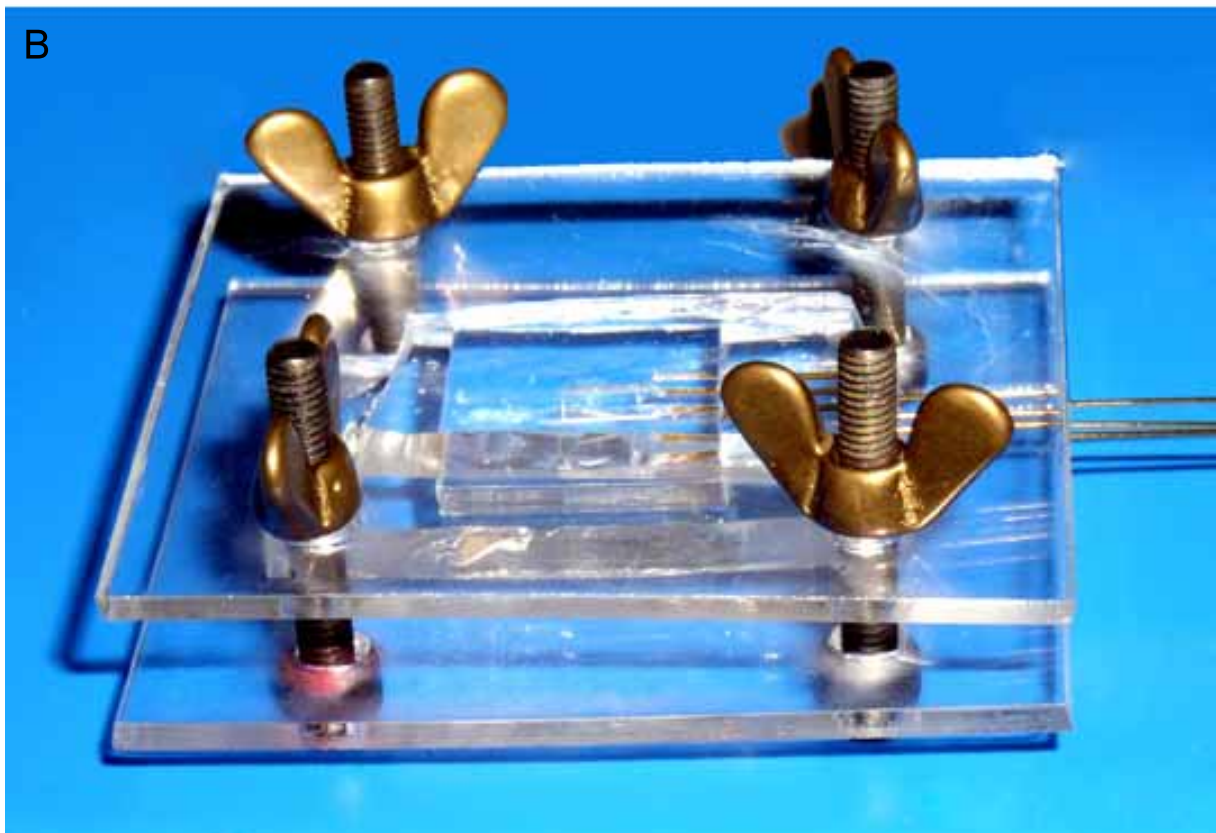
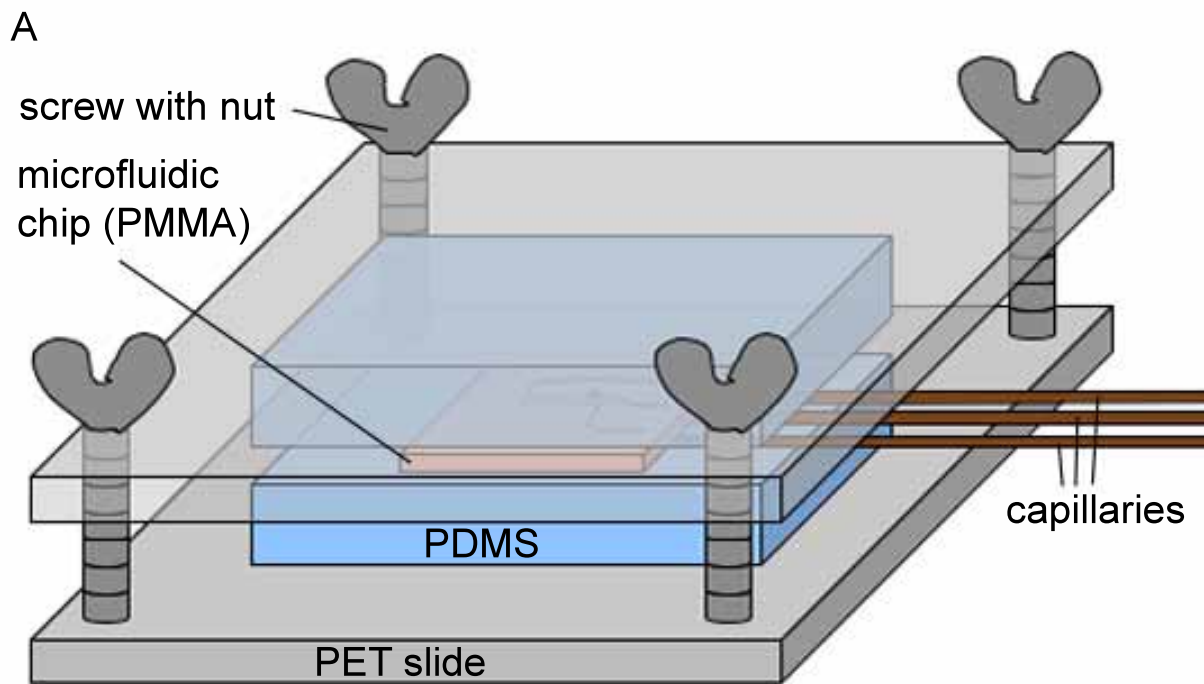


Figure 3.75: Schematic (A) and real (B) view of the sandwich technique used for sealing the microfluidic chambers.

As a solution, the chambers were sealed by two polydimethylsiloxane (PDMS) slides, which were pressed onto the microfluidic PMMA structure by two poly(ethylene terephthalate) (PET) slides held together by screws and nuts. This sandwich assembly is shown in figure 3.74 and described on page 129 in figure 3.75. In its subsequent development, the nuts were replaced by windings, which were integrated in the holes of the PET slides. This set up was used under an inverted microscope as shown in figure 3.76.

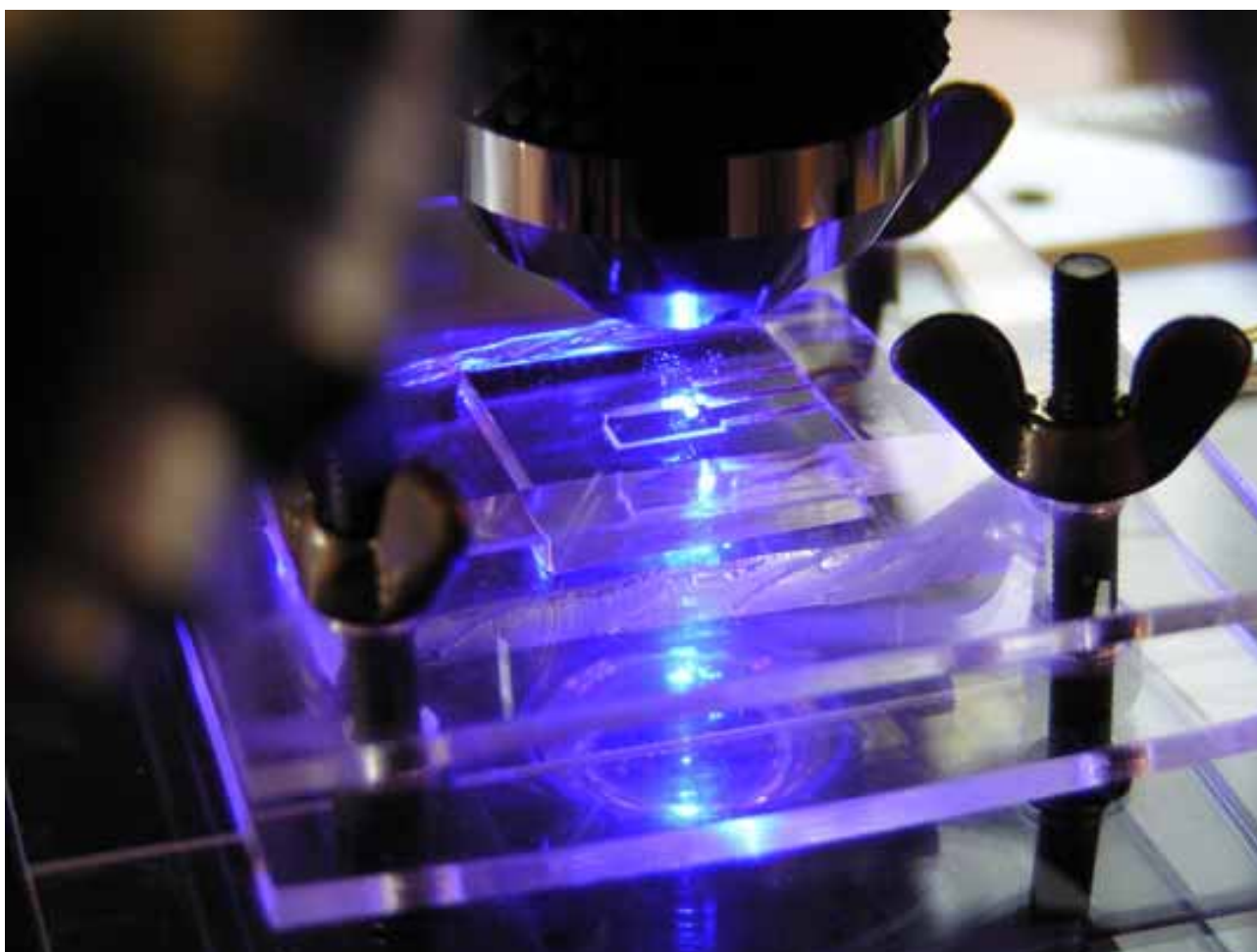


Figure 3.76: Sealed microfluidic chamber placed under an inverted microscope for the examination of the fusion process. The UV light is turned on to track fluorescent labelled cells (see validation section 3.2.7 for specification).

Thus, elastomeric polymer slides of PDMS sealed the chamber and avoided a direct bonding process. Their biocompatibility was proven (data not shown) and with their transparent nature they possessed a good alternative to direct bonding.

Summary

The microfluidic systems were sealed using a sandwich setup, where PDMS slides account for the sealing and PET slides and screws hold them in place. Consecutively, the closed chamber can be connected to a pump system via the silica capillaries, which have been glued into the microsystem.

3.2.6 Design and Assembly of the Pump Station

Overview

The assembly of the pump station, which is needed for the appliance of the microfluidic structures, is described in the following section. Pumps, valves and interconnecting tubing are combined to form a pump station, which is fully programmable by an external computer.

Generally, a pump station is needed to operate the microfluidic chip. The handling of different fluids at certain flow rates requires a pump station with several pumps, valves and connecting tubing. For the initial experiments a ready-to-use pump station was utilised, which was available at the Danish Technology Institute (see figure 3.77). Later on, an analogue system was assembled in Jülich (see figure 3.78).

Syringe pumps instead of hose or flexible-tube pumps were chosen for the pump station, since they deliver a constant volume per time independent from pressure loss. Furthermore, the used syringe pumps produce lower pump waves than a hose pump and the volume to be delivered can easily be determined by the syringe size, the resolution settings and the pump motion (direction and number of steps, in which the plunger is moved).

Three of those syringe pumps (XL 3000 modular digital pumps, Cavro) were integrated in the system. They are fully programmable and designed to automate pipetting, diluting, and dispensing operations in the $5\mu L$ to $50mL$ range with excellent precision and accuracy. They provide a wide range of plunger speeds, from 0.8 seconds to 20 minutes per stroke. Additionally, the pumps are available in different configurations with a variety of syringes ranging up to $50mL$. The syringes are driven by a stepper motor, which drives a precision lead screw, thus moving in half steps or microsteps depending on the resolution setting of the pump.

The three high resolution pumps, which are contained in the pump station, use a default of 3,000 half steps per full stroke ($60mm$) and through a firmware command they can provide up

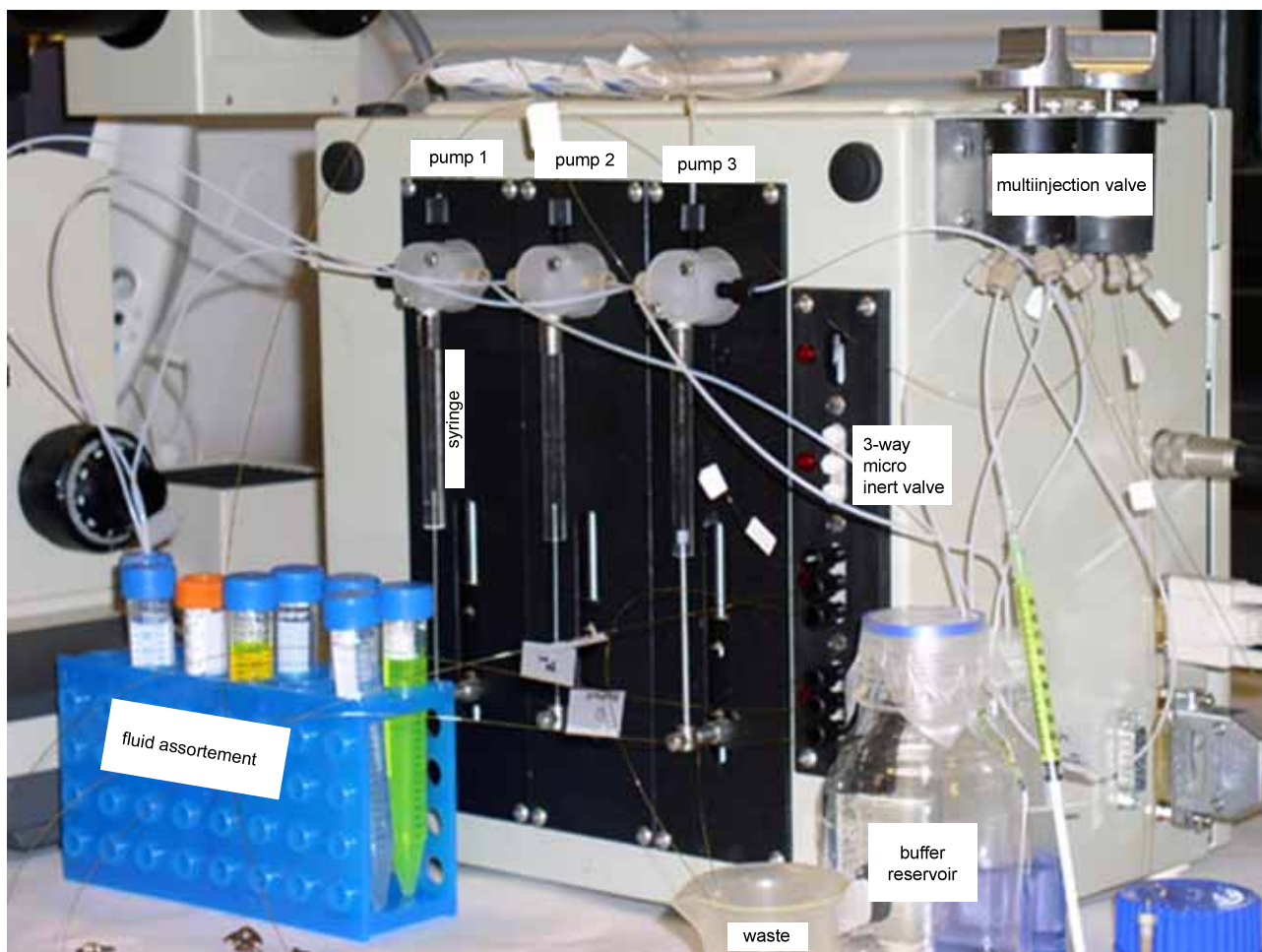


Figure 3.77: Pump station for fluid handling in combination with the microfluidic chips: The main components (pumps and valves) are controlled by an external computer (not shown).

to 24,000 microsteps per stroke. Two of them were chosen with a 3-port distribution valve (3+ valve), one with a normal 3-port valve. The 3-port distribution valve has an additional valve position, which allows to bypass the pump.

The pumps and their valves are operated from a single 24 volt power supply and are controlled by an external computer or microprocessor. They are programmable through an RS-232 or RS-485 interface and communicate through either an OEM or Data terminal protocol, whereas up to 15 pumps can be addressed separately from the same source.

For the assembly of the pump station, three syringe pumps were installed in an upright position, as advised by the manufacturer, to avoid problems in priming the system. In addition, a multiinjection valve of the same series (XL series smart valve (SV6+), Cavro) and two 3-way-micro inert valves (MIV, The Lee company) were integrated. The Cavro Smart Valve is a

compact, stepper motor driven module for OEM liquid handling applications, which possesses a 6-port valve and uses the same communication characteristics as the Cavro XL 3000 Modular Digital Pumps, a RS-232 or RS-485 interface and a choice of 2 communication protocols. The inert valves possess three inlets. The upper is always opened and usually connected to the bottom one. By switching the valve, the middle inlet, which is normally closed, is opened and connected to the upper inlet, whereas the bottom one is closed in return. All modules were connected to a single 24 volt (d.c.) power supply.



Figure 3.78: An analogue pump station was assembled in Jülich: The SV 6-port valve is to the fore, whereas the inert valves cannot be seen.

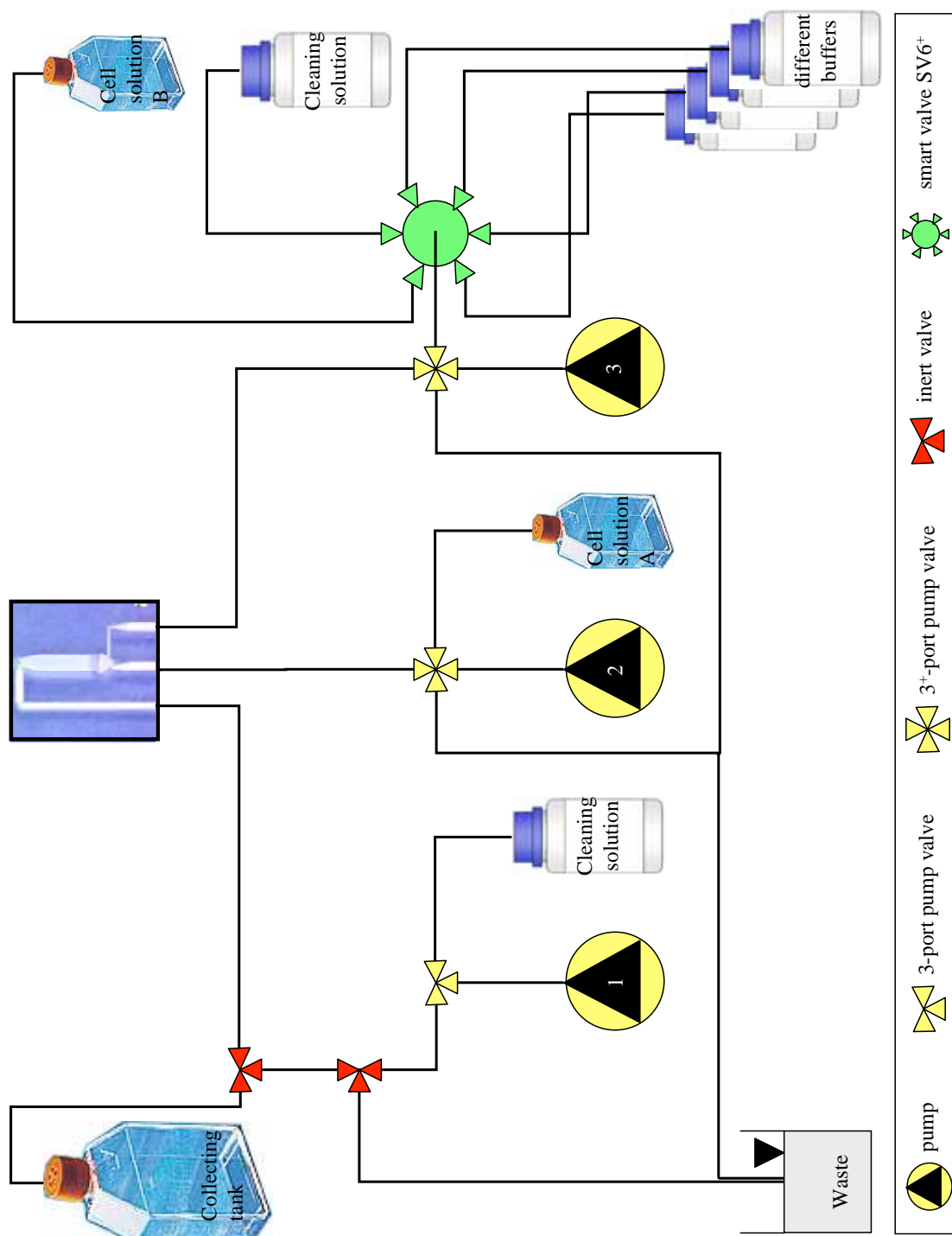


Figure 3.79: Flowsheet of the pump station illustrating the connection of the pumps and valves to the microfluidic chip.

The communication with the components was done from an RS-232 port. Therefore, one device in the chain required an RS-232 interface board. This board was plugged into the mother board of pump 1. It converts the signal into RS-485. From then on all devices in the chain communicate through RS-485.

The various components had to be connected with capillaries and tubing to allow fluid flow (see flowsheet in figure 3.79). As described previously, nonpolar fused silica capillaries (ID 0.1mm) were glued into the microfluidic chip. For the connection of these capillaries to the pumps and valves, which possess standard $1/4 \times 28$ coned ports intended for $1/16$ " OD (outer diameter) tubing, PTFE (polytetrafluorethylen, Teflon) tubing with an ID of 0.25mm and an OD of $1/16$ " is used. The PTFE tube acts as a sealtight sleeve: It expands when heated, thus the fused silica capillary insertion is facilitated, and encases the capillary tightly when cooled afterwards. For the interconnecting tubing between pumps, valves, buffer reservoirs and collecting tanks a PTFE tube ($1/16$ ") with an inner diameter of either 0.25mm or 0.5mm was used dependent on the desired flow rate. Flangeless ferrules and flangeless nuts, normally used in chromatography such as HPLC, together with unions, replaced flange fittings and facilitate replacement and rearrangement of the set-up. Furthermore, so-called frit-in-a-ferrules were used, where buffers or cleaning solutions enter the microfluidic system. These special ferrules incorporate a frit in their body, which filters the pumped solutions inline. $2\mu\text{m}$ filters avoid blocking of the microfluidic channels by dirt.

Pump and valve operation programmes were written with LabVIEW to operate all components from an external computer. LabVIEW is a graphical programming language, which is primarily used for metrological tasks. The graphical dataflow language and block diagram approach allows viewing and easily modification of data or control inputs. With its help and in combination with the intern pump software, a communications driver was written for the use with the OEM protocol. Full particulars of the programming work can be found in the appendix.

Figure 3.80 and 3.81 show screen shots of two programmes, called "sample only" and "pump rate ctrl", which have been programmed at the Danish Technology Institute and were usually used for the operation of the pump station. The sample only programme allows the easy operation of only one pump at a time. The syringe of the selected pump is repeatedly filled and emptied at the chosen speed and for the number of repetitions. Contrary to this programme, the pump rate control programme enables the user to operate all three pumps, the 6-port smart

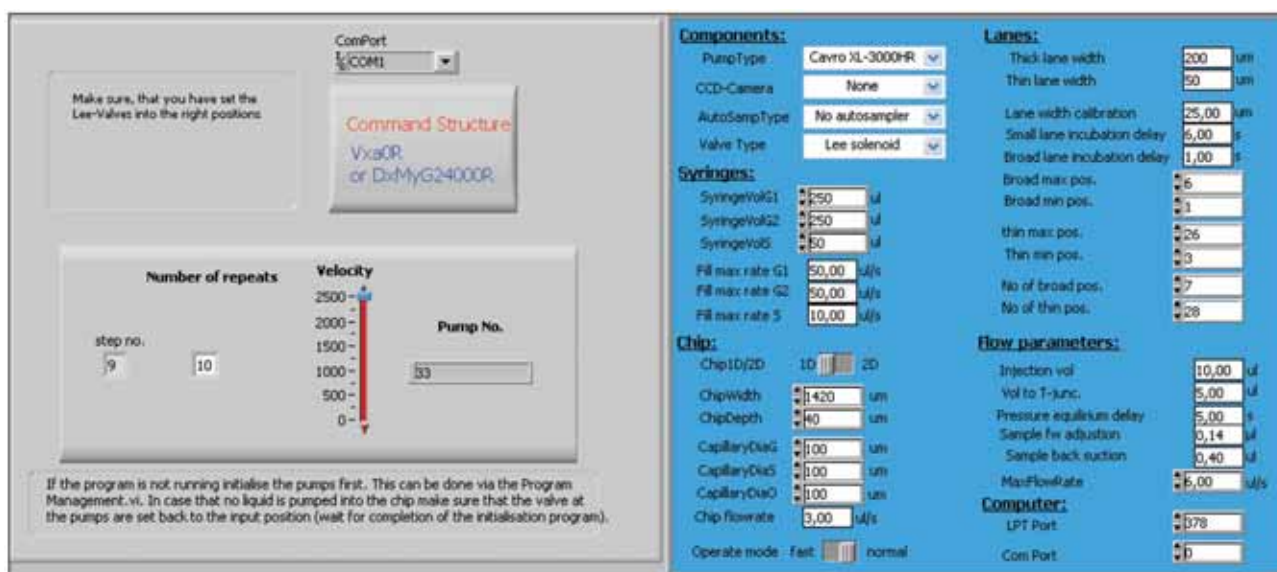


Figure 3.80: Screen shot of the sample only programme: This programme is an easy to use programme for the operation of only one pump at a time. The pump, pump velocity and the number of repeats are the only variables, which have to be chosen. The selected pump will then fill and empty its syringe via valve position inlet for the number of times chosen.

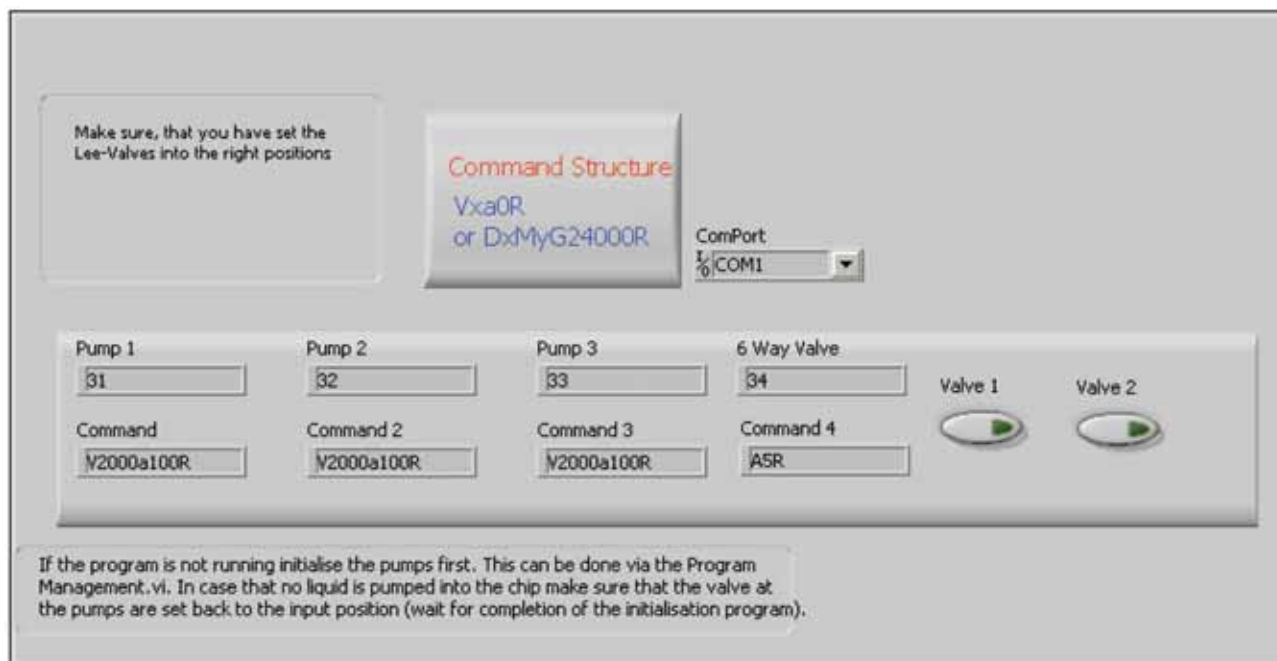


Figure 3.81: Screen shot of the pump rate ctrl programme: This programme allows the simultaneous operation of all three pumps, the 6-port smart valve and both inert valves. The knowledge of pump and valve commands and command structures are required for this programme.

valve and both inert valves simultaneously. However, pump and valve commands and command structures need to be used, which were not required with the sample only programme (see section 7.2.3 in Material and Methods for tables of the most important pump and valve commands). Thus, the latter provides the user with a wide range of possible operation procedure.

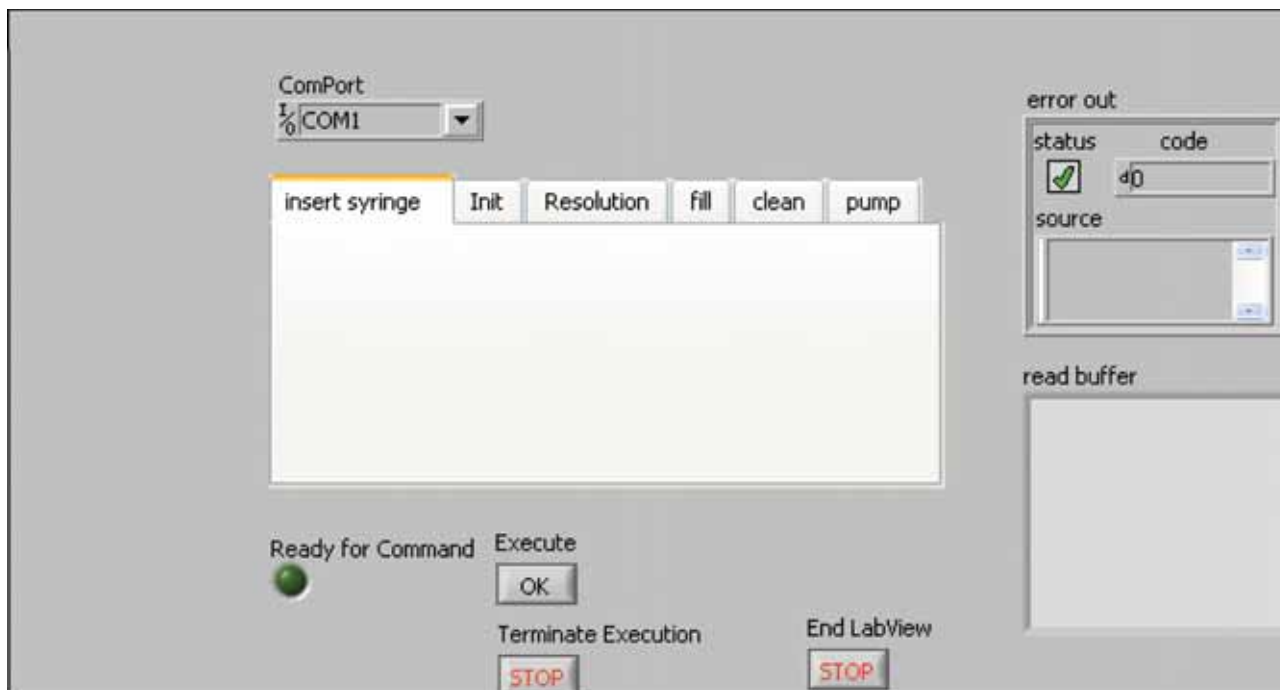


Figure 3.82: Screen shot of the Labview pump software programmed in Jülich: This easy-to-use system combines all important operation procedures.

A more user-friendly version was programmed in the IBT-2 at the Research Center Jülich (see figure 3.82), which combines all operation procedures needed for operating the pump station such as insertion of syringes, initialisation of the pumps and valves, setting the resolution of the pumps, filling pumps, cleaning and pump and valve operation without the knowledge of their internal software commands.

Summary

A pump station was assembled, which consists of three syringe pumps, a 6-port valve and two inert valves, thus providing a system to operate the microfluidic chip. The connection of all components among each other and the programmed software were introduced.

3.2.7 Validation

Overview

The following section shows how the microfluidic systems are validated using fluorescent dyes and particles to ascertain that a laminar flow situation exists inside the microfluidic chambers.

For the fluid dynamic analysis of the microfluidic structure, fluorescent tracer, fluorescent polymer particles, which act as model cells, and KG-1 cells were used.

Tracer

A fluorescent tracer, Natrium-Fluorescein, was used to stain one of the inlet flows, resulting in either four or five stained partial flows respectively in the open microfluidic chamber depending of the utilised inlet.

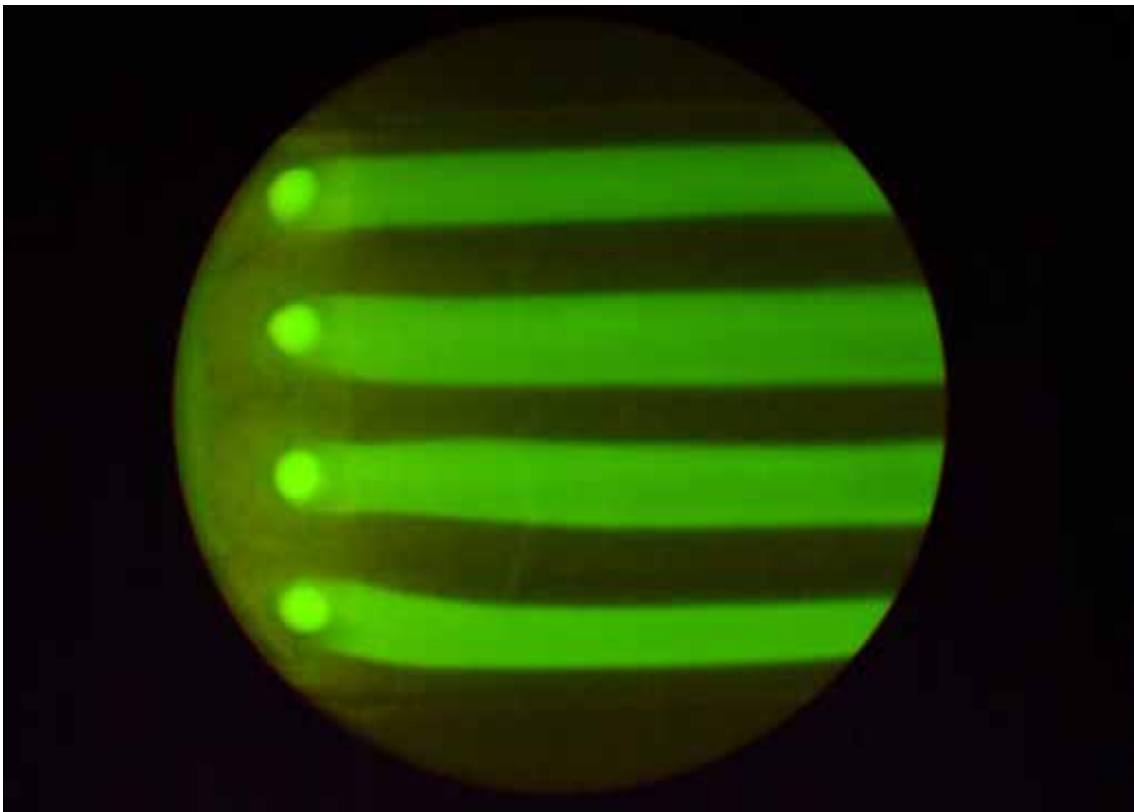


Figure 3.83: Microfluidic system 2: Light microscope picture of the laminar flows. One of the streams (inlet B) is stained with Na-Fluorescein.

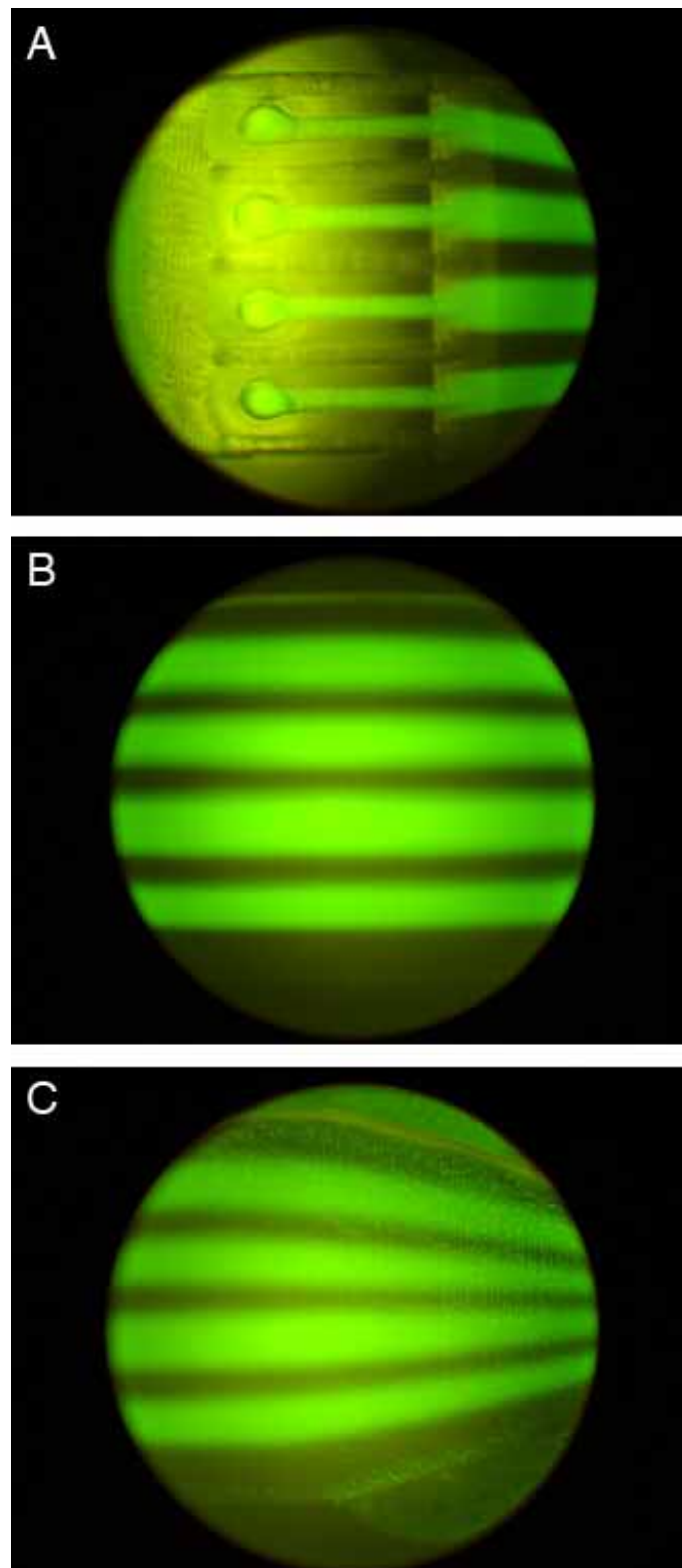


Figure 3.84: Microfluidic system 1: The solution, which enters the microfluidic structure through inlet B, is stained with Na-Fluorescein. The pictures represent the laminar flow situation, as apparent by the distinct flows, at the entrance of the open chamber (A), in the middle of the chamber (B) and near the outlet, where the streams converge (C).

These tracer experiments indicated the flow situation inside the microfluidic structure. Figure 3.83 shows the laminar flow situation in the microfluidic system 2, which is demonstrated by nine distinct laminar flows, whereas four of them were stained green by the tracer.

The same typical flow pattern resulting from the laminar separation was found in the microfluidic system 1, if inlet stream B was stained with Na-Fluorescein. The separation of the streams could be recognised clearly (see figure 3.84).

Particles

This flow pattern was also validated in experiments with fluorescent particle suspensions. These polymer particles acted as a model system for cells, with their size ($15-19\mu m$) correlating to the size of a breast cancer cell (such as T47D, MCF-7 or MDA-MB-231). If the fluorescent particles were streamed with a high velocity, the single cell could not be spotted, but a fluorescent line was captured by the camera due to motion blur (see figure 3.85), with the resulting line representing a flow line. Thus, fast moving particles gave an idea of the stream lines analogue to a tracer experiment. Only when the cell were streamed slowly (see figure 3.86) the taken pictures showed the discrete particles.

Cells

In the subsequent experiments the fluorescent particles were replaced by fluorescent labelled cells of the KG-1 cell line. These cells acted as a model cell for breast cancer cells, but in comparison with the polymer particles comprise features such as deformability, an important parameter for the microfluidic experiments. KG-1 cells were used instead of breast cancer cells, since they are suspension cells, thus easy to culture and are also easy to stain. Their flow attitude resembled the behaviour of the polymer particles, when streamed. However, the fluorescence intensity of the cells stained with Celltracker CMFDA (see Material and Methods) was insufficient to capture moving cells with the digital colour picture camera used, even though the highest dye concentration for this cytosol staining of cells was tested. For further experiments with cells a monochromatic digital camera with higher sensitivity had to be purchased.

Further difficulties were faced as depicted in figure 3.87 and figure 3.88: Air bubbles and cell clusters, which blocked the inlets, disturbed the flow situation inside the microfluidic chamber

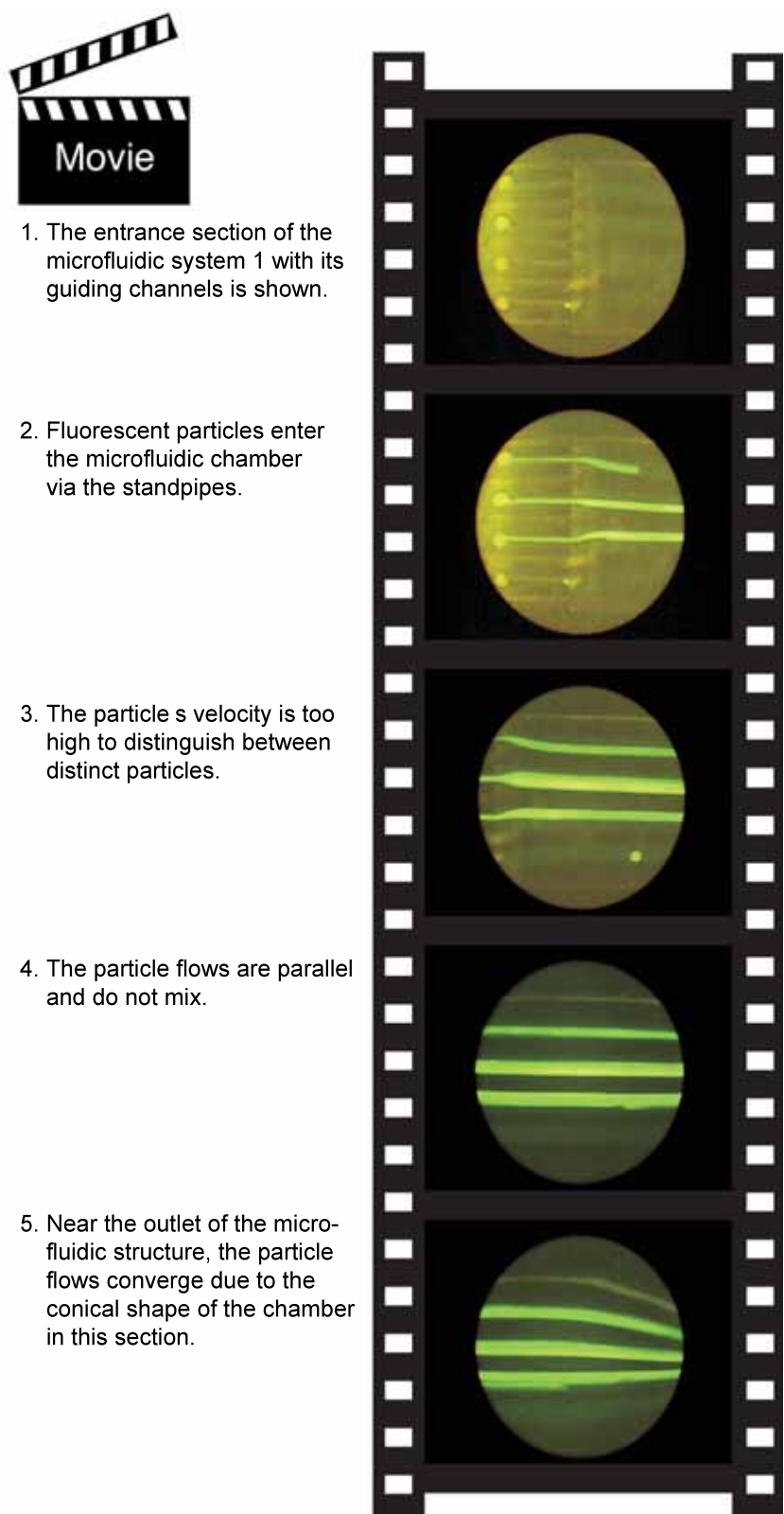


Figure 3.85: Particle flow system 1: The selected pictures have been extracted from a movie, which shows how fluorescent particles are streamed through the chamber with high speed, thus the single cell cannot be spotted. This movie is available on the enclosed DVD.

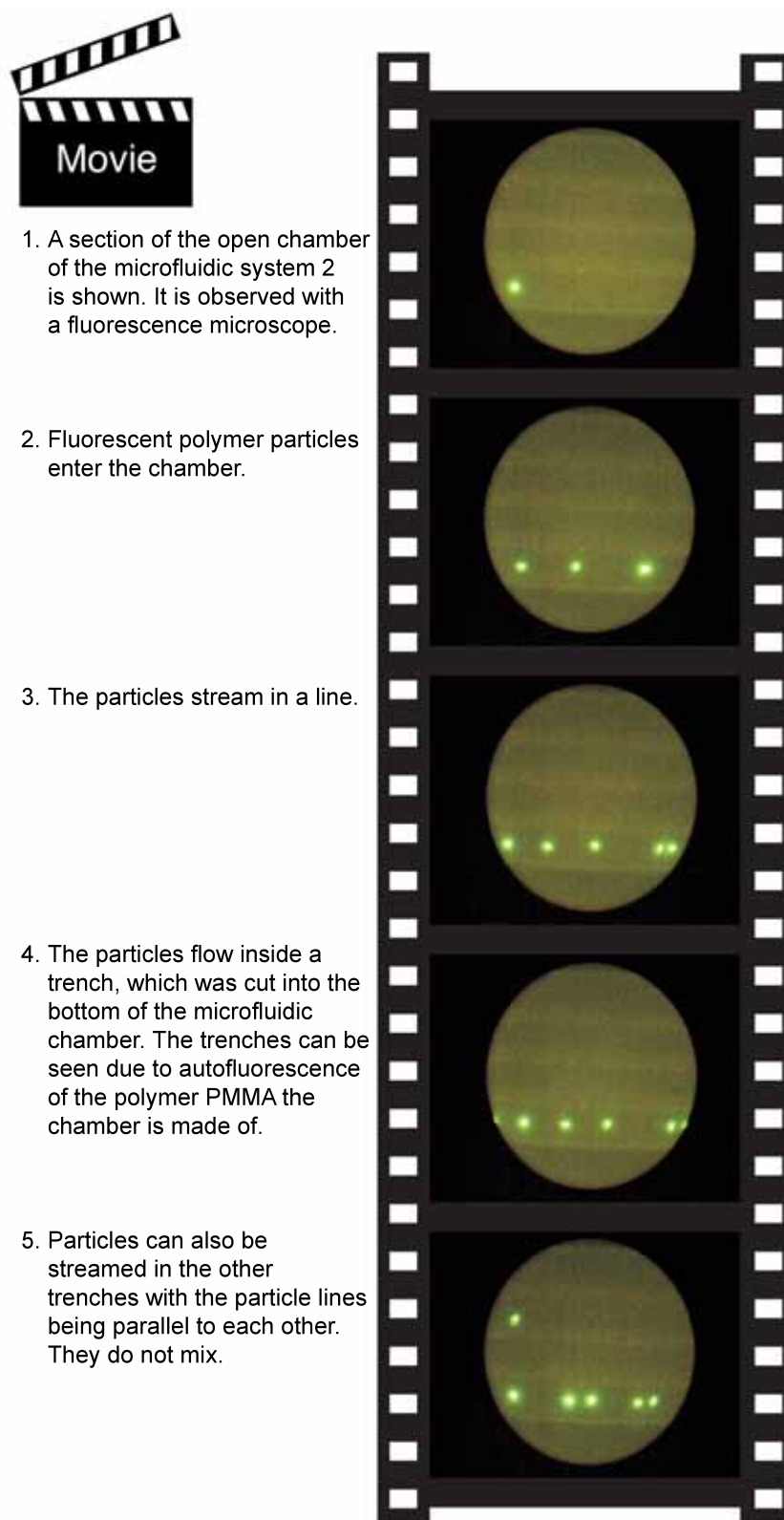


Figure 3.86: Particle flow system 2: The selected pictures have been extracted from a movie, which shows how fluorescent particles are streamed through the chamber at lower speed than in figure 3.85. This movie is available on the enclosed DVD.

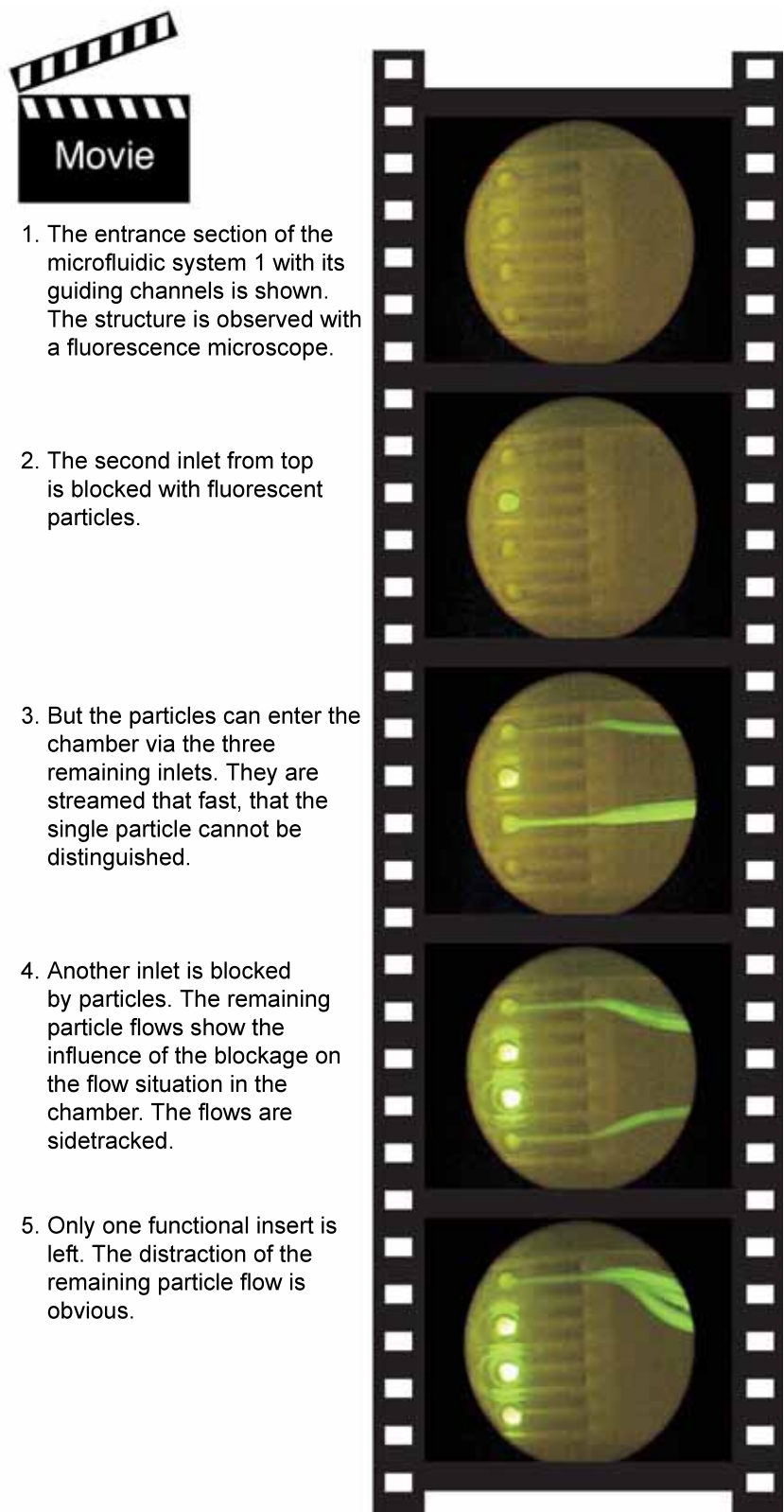


Figure 3.87: Trouble-shooting 1: The selected pictures have been extracted from a movie, which shows how the standpipes of the microfluidic system 1 are plugging. This movie is available on the enclosed DVD.

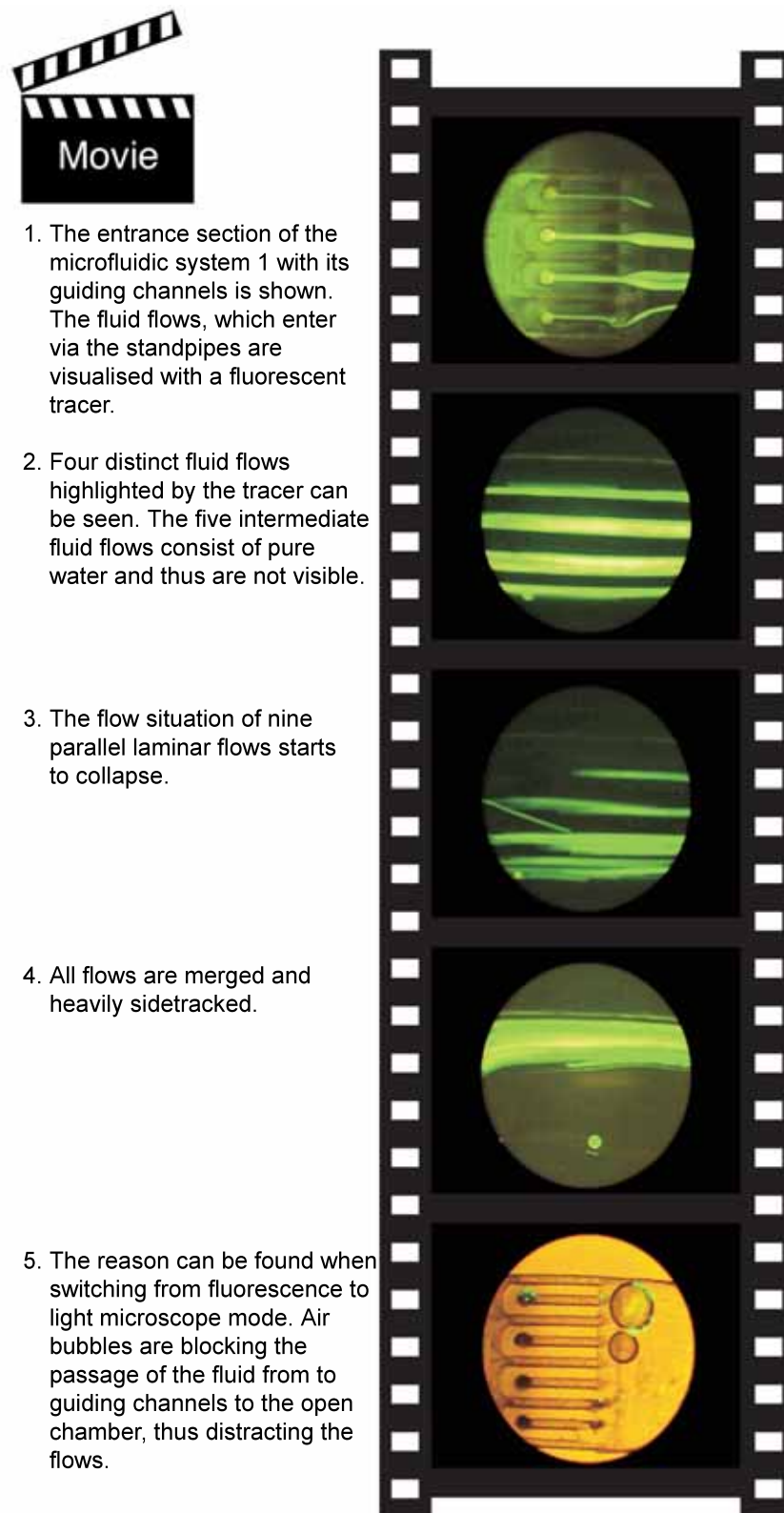


Figure 3.88: Trouble-shooting 2: The selected pictures have been extracted from a movie, which shows the breakdown of the laminar flow situation with nine parallel flows in the microfluidic system 1 due to the incidence of air bubbles. This movie is available on the enclosed DVD.

and destroyed the arrangement of nine parallel fluid and/or cell flows.

A solution to the air bubble problem was easily found. The outgassing of all buffers and solutions used with the microfluidic chip together with an extensive flushing of the chip before usage avoided the entrance or formation of air bubbles. Furthermore, it had to be considered, whether the use of outgased solutions affected the cells, but no influence was noticed.

The blockage of the $50\mu\text{m}$ wide channel inlets or the standpipes, respectively was scrutinised. Clusters of tens to hundreds of cells were found (see figure 3.89), which usually could not be eliminated by rising the flow velocity or reversing the flow direction. The cells sometimes gave the impressions that they were sticking together.

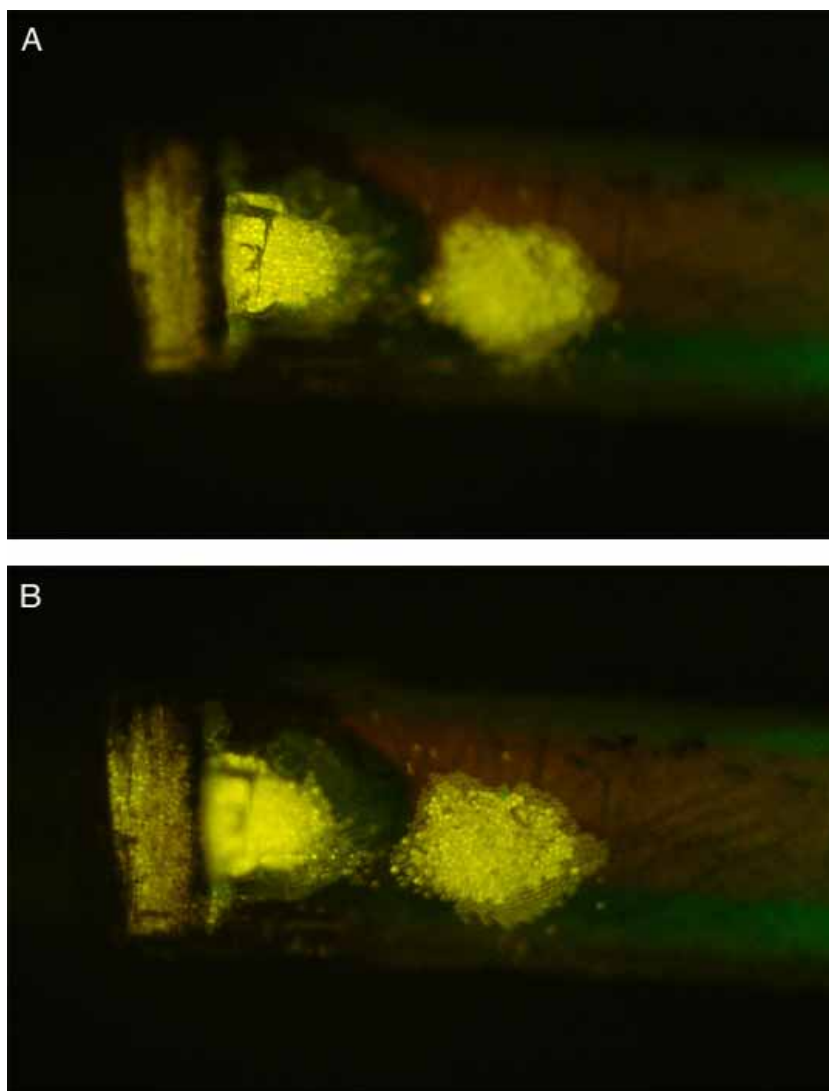


Figure 3.89: Plugging in the feed and standpipes: The pictures show plugging of fluorescent particles in a standpipe (in focus in A) and in a feed pipe (in focus in B)

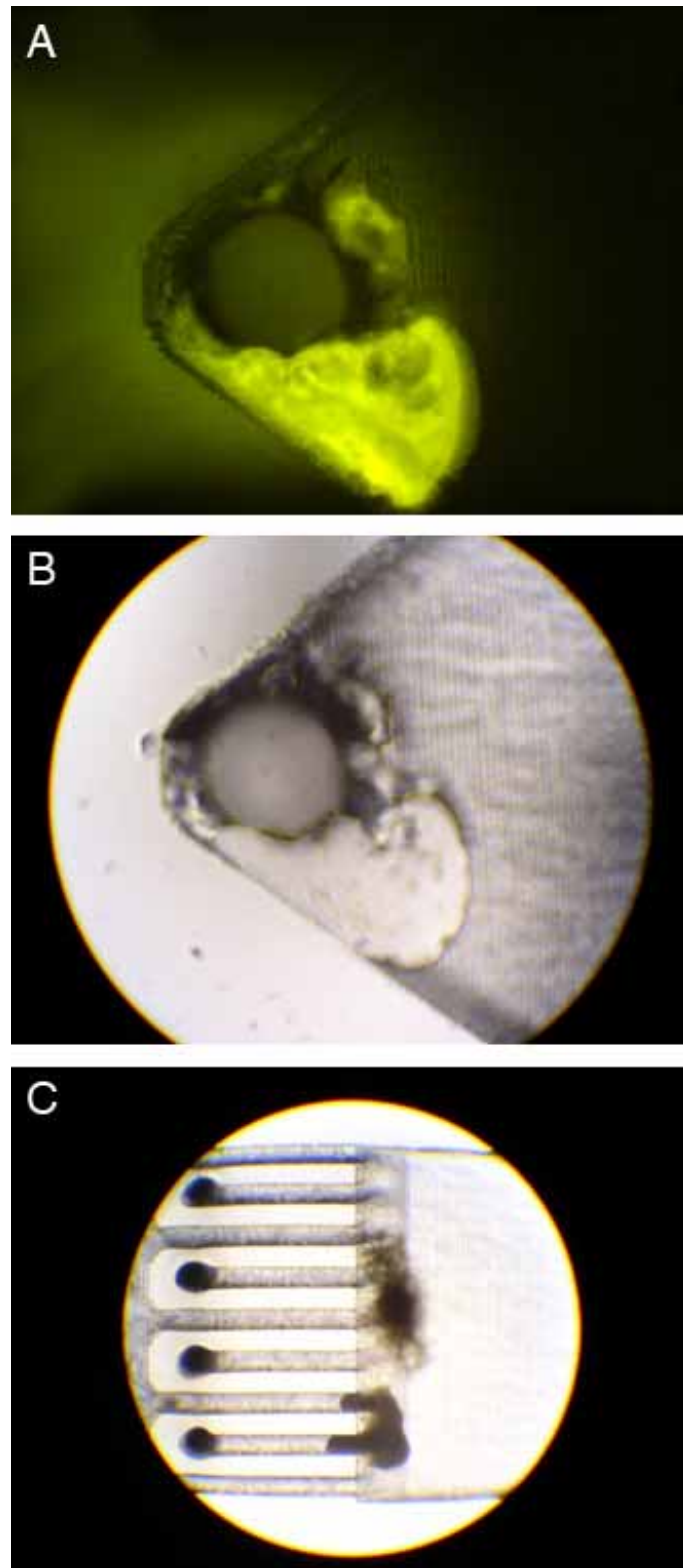


Figure 3.90: Ablation material, which is characterised by a high self fluorescence (A), is found near the inlets (B) and sometimes is plugging the channels (C).

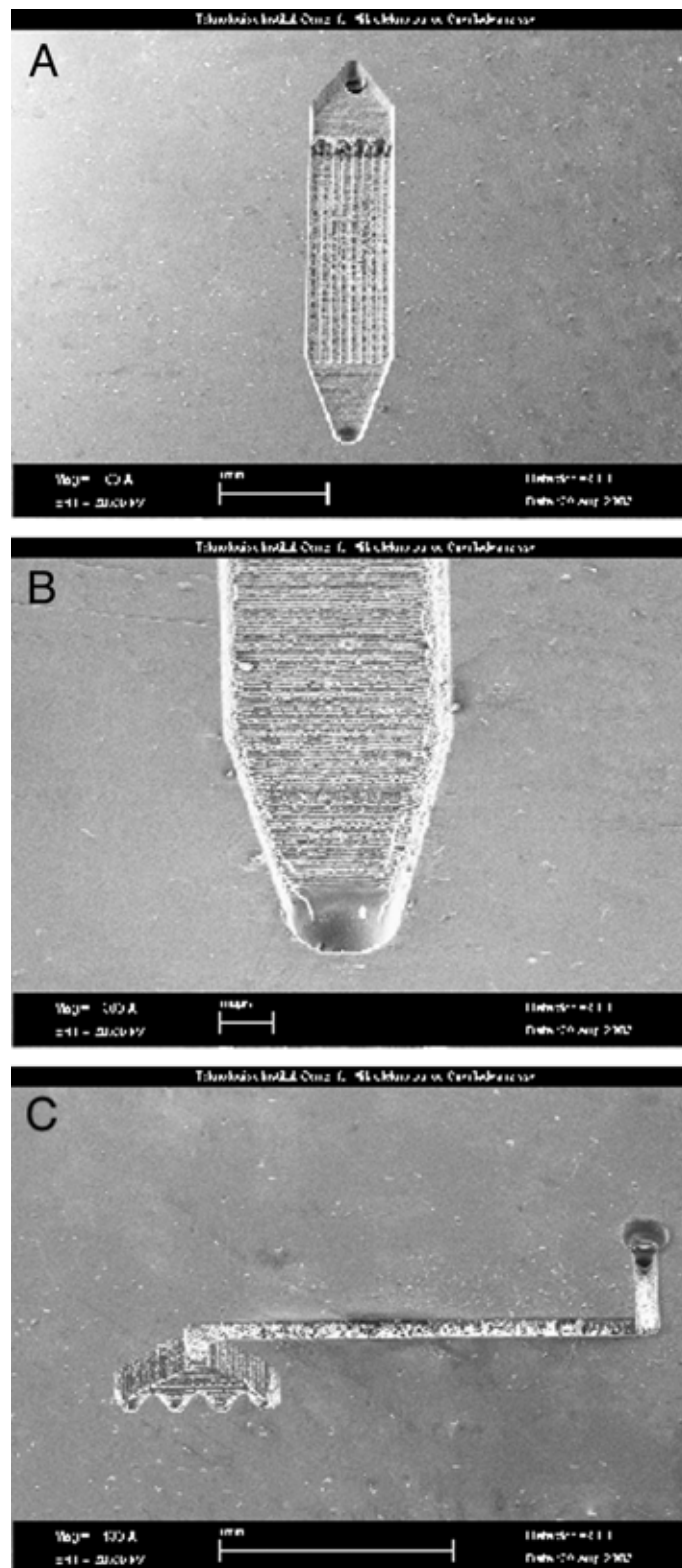


Figure 3.91: Scanning electron microscope pictures of the microfluidic system 2: The top part of the laser-manufactured structure (A), a close-up of the outlet (B) and the distribution system of inlet B (C) can be seen.

Usually, the plugging of particles was observed in the inlets and in the standpipes, where a sticky material could be observed (see figure 3.90). It was assumed, that this adhesive material was not related to the glue used, but to the chamber material itself. During the laser machining process ablation material was left inside the chamber, inlets and standpipes. It was shown that this material accumulated preferably in the feed and standpipes when the chamber was flushed with water for the first time and coalesced with the fluid to form a sticky compound.

A chemical removal of this ablation material was not possible without inflicting damage on the whole microfluidic structure. Although, a mechanical removal was feasible, it also led to minor detriments of the chamber (see figure 3.91 and 3.92). However, modifications of the chamber due to normal usage were not recognised.

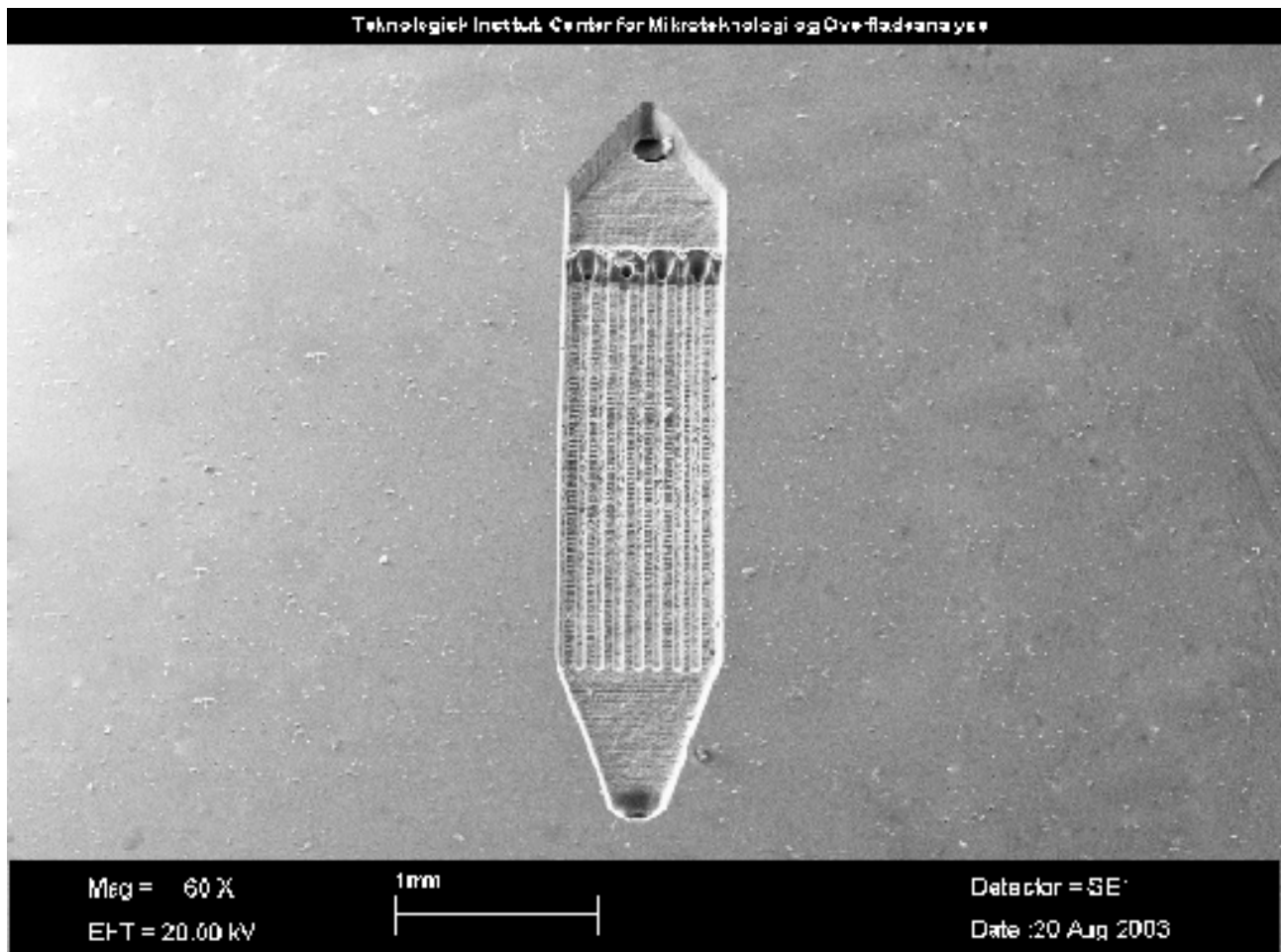


Figure 3.92: Microfluidic system 2: SEM picture of the top part of the laser-manufactured structure. It should be mentioned here that the chamber has been extensively used before the micrograph was taken and ablation material was removed mechanically from the blocked inlets.

The accumulated and swollen ablation material found primarily in the feeds and standpipes necessitated the change of the material used for the laser-machining process. In addition, an expansion of the inlet wholes and standpipes would contribute also to a better particle flow inside the chamber.

Summary

A laminar flow was proven inside the microfluidic chambers with fluids, particle or cell suspensions, which results in 9 parallel discrete flows. Although the microfluidic structures are functional, some minor revisions should be implemented to optimise the fluid flow and avoid blockage.

3.2.8 Redesign of the Microfluidic Chamber

Overview

The reasonable redesign of the microfluidic structures is explained in the following section. This resign comprises geometrical changes as well as a change of the chamber material, thus achieving an optimisation of the microfluidic chamber performance.

So far, it could be shown that the microfluidic chips, both system 1 and system 2, are functional and thus have the ability to generate 9 parallel laminar partial flows with a total width of about $850\mu m$. To further optimise the performance of those chips, some changes to the geometry and the chamber material had to be implemented.

Geometric Redesign

A necessary 3D redesign was the increase of the inflow dimensions. The channel diameters were increased to $200\mu m$ to optimise particle and cell flow (see figures 3.93 and 3.95 for design model and realisation, respectively).

Thereby, the geometry of the front part of the chamber was changed. The widened channel and inlet diameters needed more space, thus the chamber was in this part enlarged from $850\mu m$ to $1800\mu m$ (see figure 3.94 for engineering drawing). If the chamber width is kept at that size over the full length of the chamber, the width of the resulting 9 parallel flows would be inappropriate for the target use. Thus, in the run of the chamber its width had to be reduced

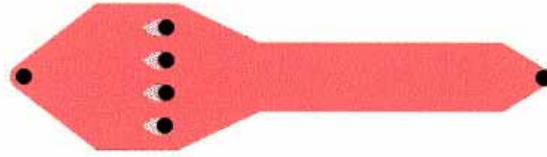


Figure 3.93: Open Chamber of the microfluidic system 3 characterised by enlarged inflow channels and standpipes.

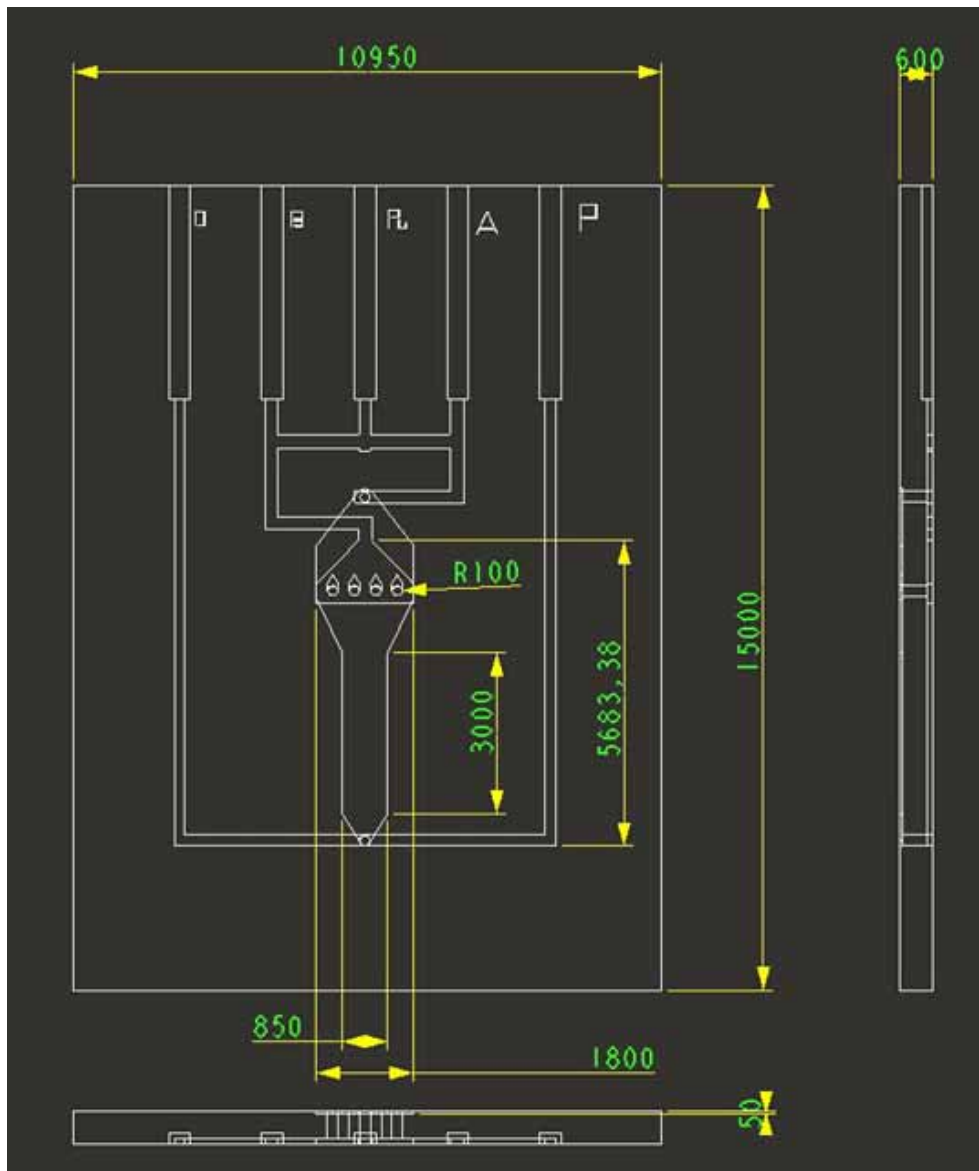


Figure 3.94: Engineering drawing of the microfluidic chamber 3. All data is given in μm .

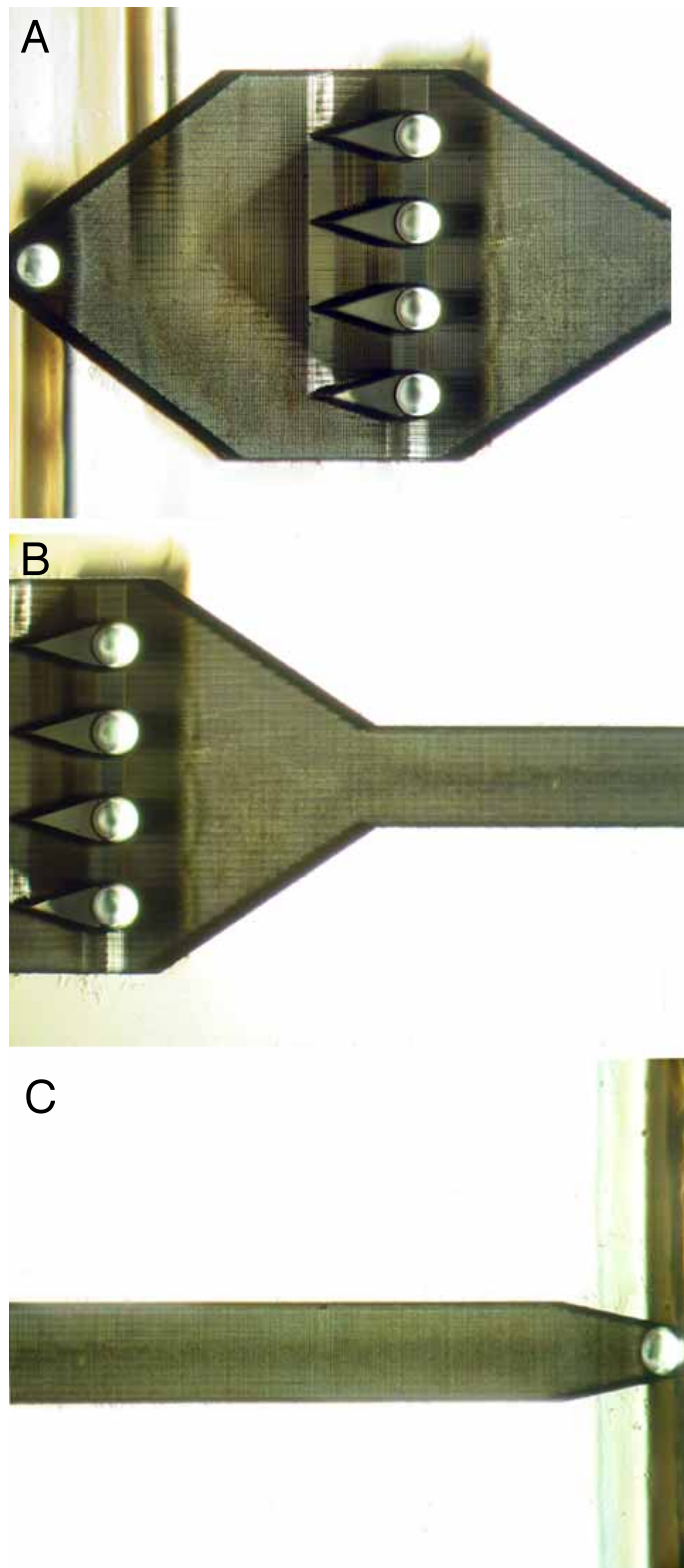


Figure 3.95: Microfluidic system 3: Photographs from the inlets (A), the middle (B) and rear part (C) of the chamber.

back to the size, which was proved appropriate for the microfluidic system 1 and 2. The reduction of the chamber width to $850\mu m$ resulted in a size reduction of the distinct flows.

Consequently, the focussing of the partial flows to the designated channel widths was achieved by hydrodynamic focussing. Due to the laminar nature of the flow inside this microfluidic structure, the partial flows did not mix during the hydrodynamic focussing, which has been demonstrated using a fluorescent tracer as shown in figure 3.97 on page 153 .

Change of the Chamber Material

Even though the inlet and channel dimensions were expanded, the blockage problems were not solved. Occasionally, particles still got trapped inside the standpipes and other inlets and the same grease related to ablation material of PMMA (as described in chapter 3.2.7) was found, when these blockages were further analysed. Due to this resisting obstructions as shown in figure 3.96, the decision was made to change the chamber material to Polyethylenterephthalat (PET). PET has better ablation characteristics, with much less debris, and is structurally tougher compared with PMMA.

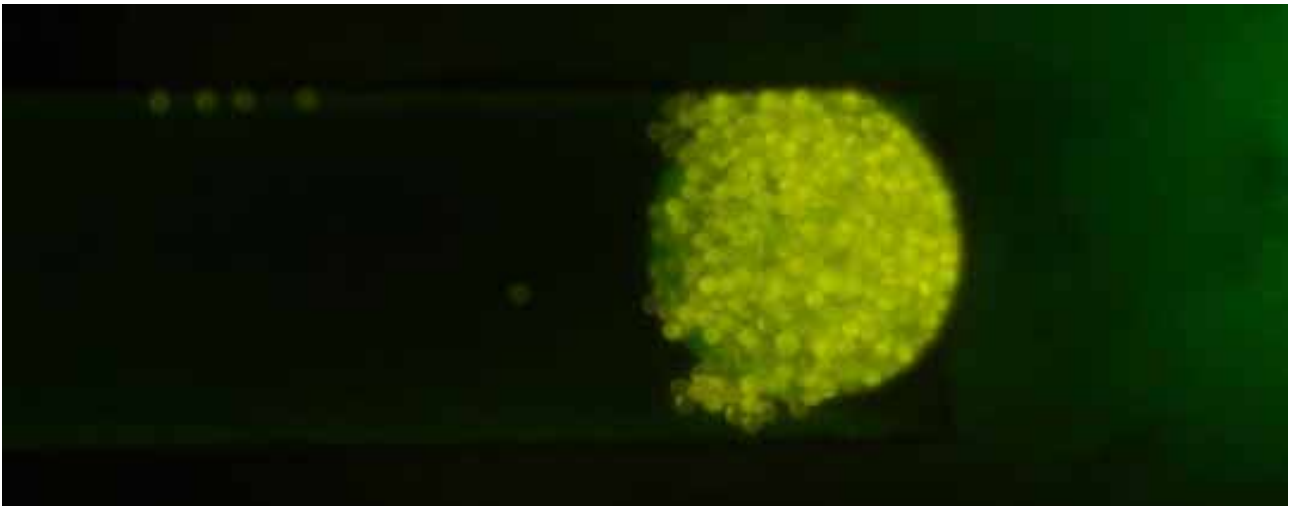


Figure 3.96: Blockage of a channel inlet by fluorescent particles.

As shown before, the PMMA microfluidic structure was damaged in its functional parts, when the blockage was removed mechanically (see figure 3.98). With the change to PET as chamber material these problems were solved.

However, the change of the material to PET also entailed some minor disadvantages, such as a higher self fluorescence than PMMA (see figure 3.99). This property indeed hampered the

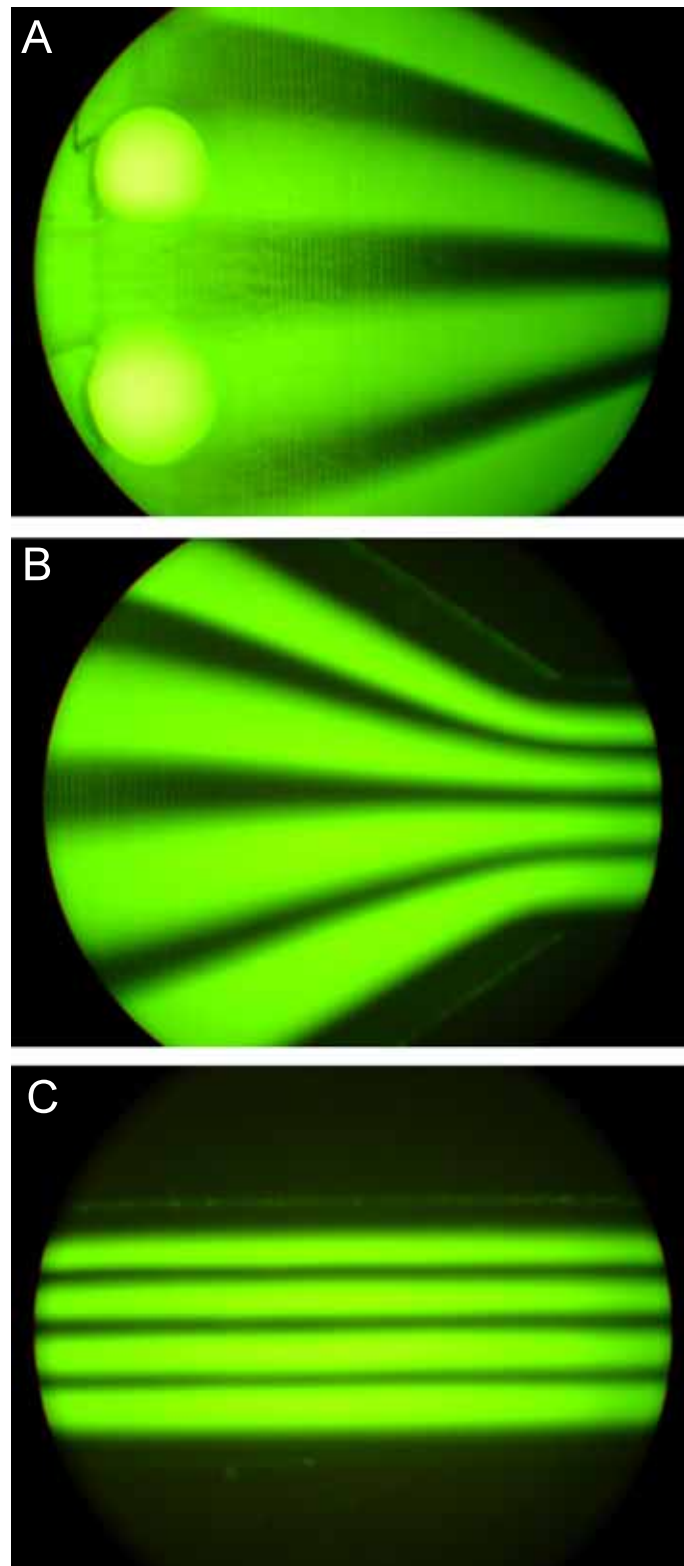


Figure 3.97: Microfluidic structure 3: The hydrodynamic focussing of the laminar flows is visualised by the addition of Na-Fluorescein into the solution, which enters the microfluidic structure via inlet B.

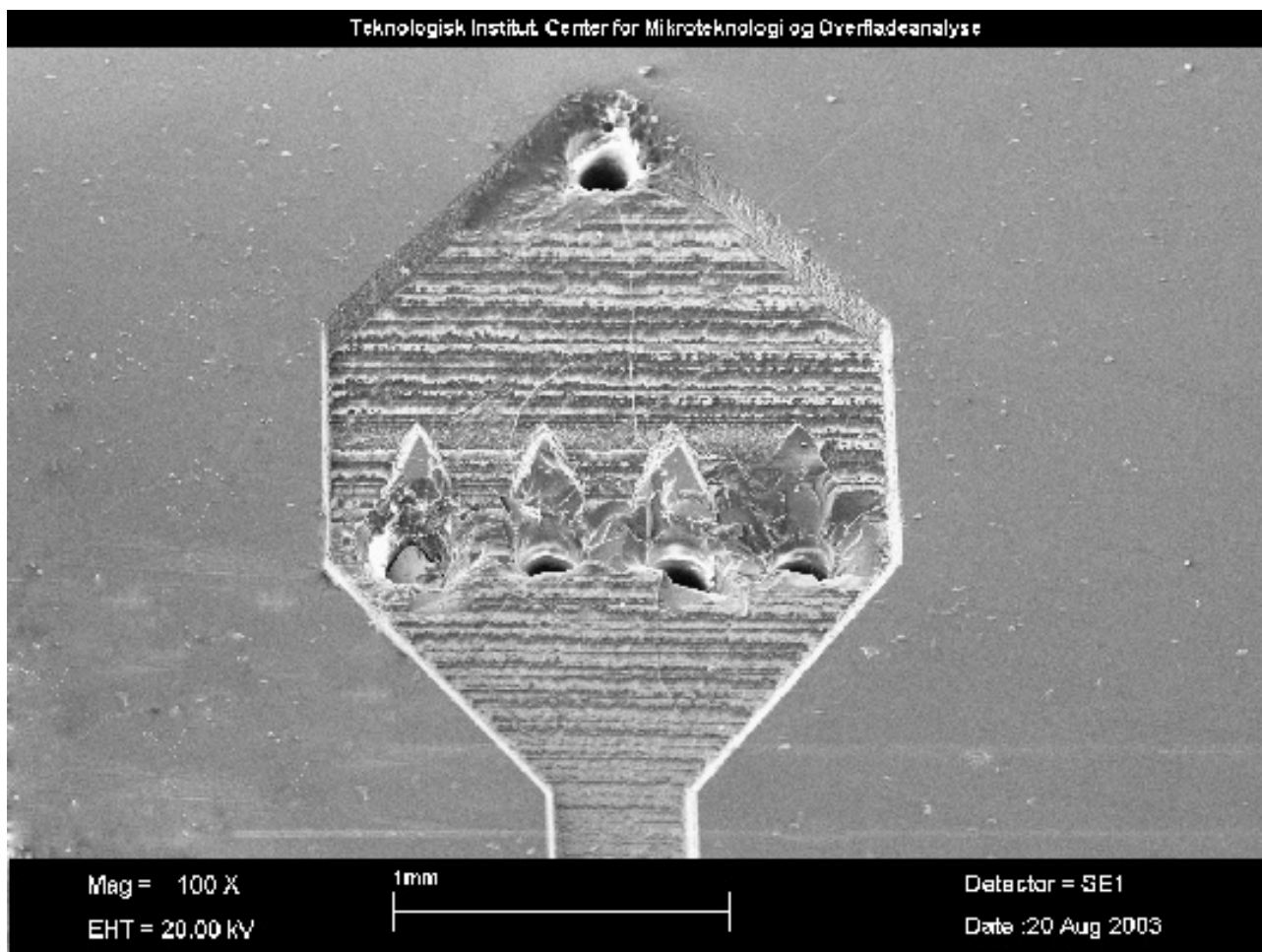


Figure 3.98: SEM picture showing extensive damage caused to the microfluidic structure 3 by mechanical removing of blockages

visualisation of fluorescent stained cells inside the microfluidic chamber, but did not have any impact on the functionality of the microfluidic system. In addition, fluorescent particles were found, which clinged to the channel walls probably due to electrostatic interactions between both polymers (see figure 3.100). This phenomenon was never observed when the chamber was used with cells, thus it is extraneous.

Altogether, the advantages of PET as chamber material outweigh the higher autofluorescence. PET has a better chemical resistance to solvents and a much higher melting temperature of 225°C compared with PMMA. This means that the use of PET leaves more options for the sterilisation of the microfluidic chamber as ethanol as well as autoclaving can be used. Anyway, PMMA was chosen as material in the first place, since it was well known from long in-house experience and was considered adequate.

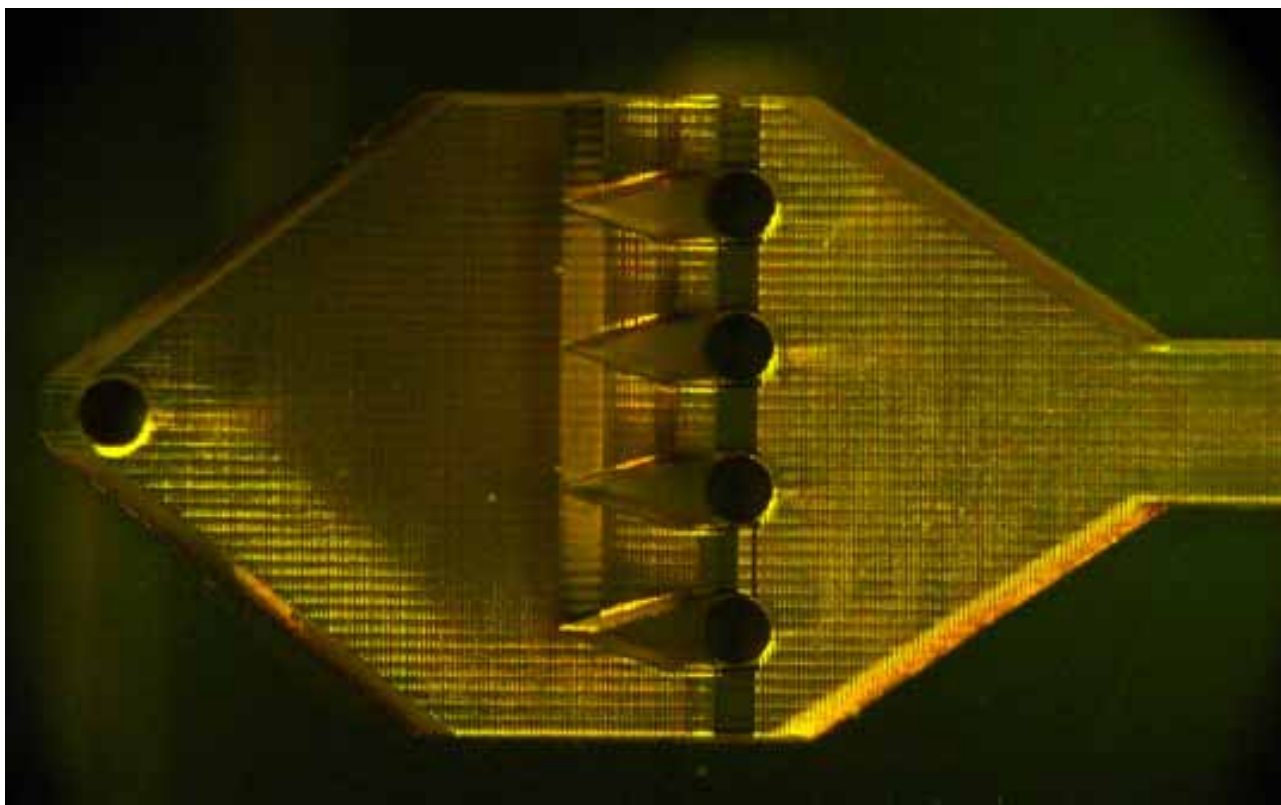


Figure 3.99: Microfluidic system 3 cut in PET, which shows a higher autofluorescence compared with PMMA.

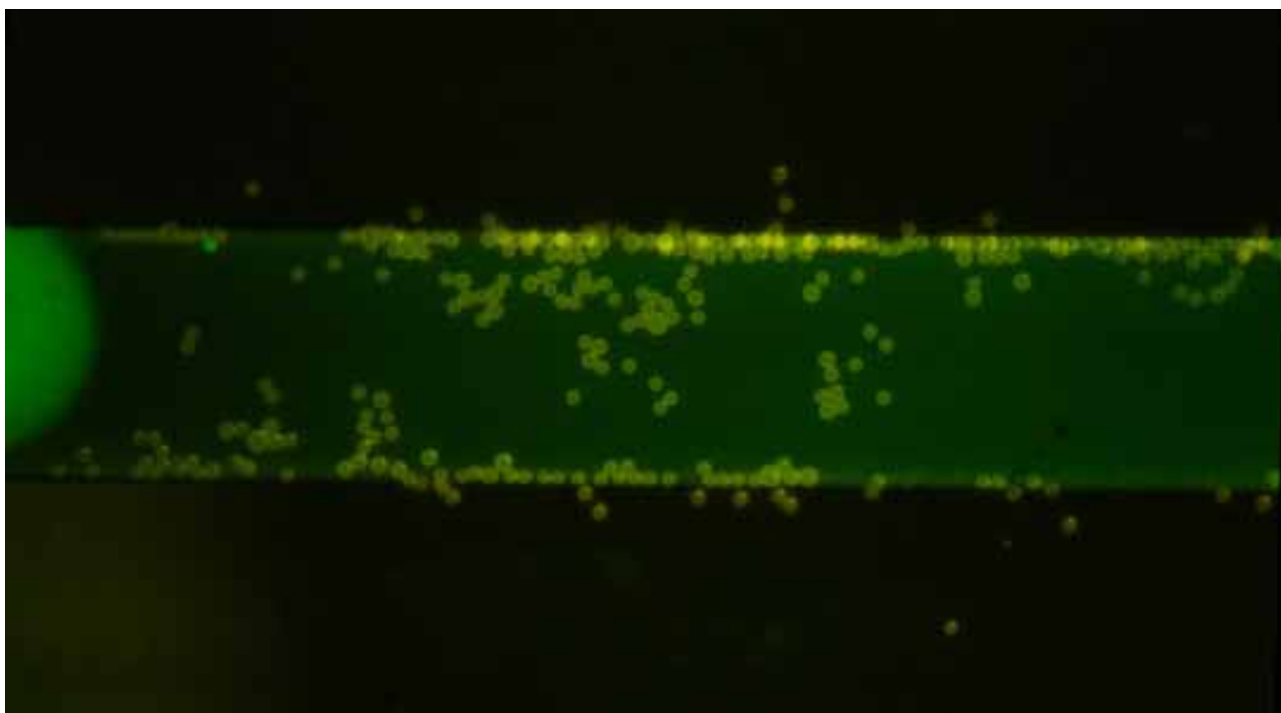


Figure 3.100: Fluorescent polymer particles sticking to the walls of the microfluidic structure.

Introduction of a Purge Line

The introduction of additional microchannels, acting as a purge line (see figure 3.101), provided the opportunity to flush the whole microfluidic system more flexible, thus preventing or eliminating blockage of channels. For example, the outlet channel of the system can be flushed with the use of the purgeline, bypassing the microfluidic chamber. This would represent an advantage for the cleaning of the passage between the laser-machined structure and the drillings, where the silica capillaries were glued in (see figure 3.102).

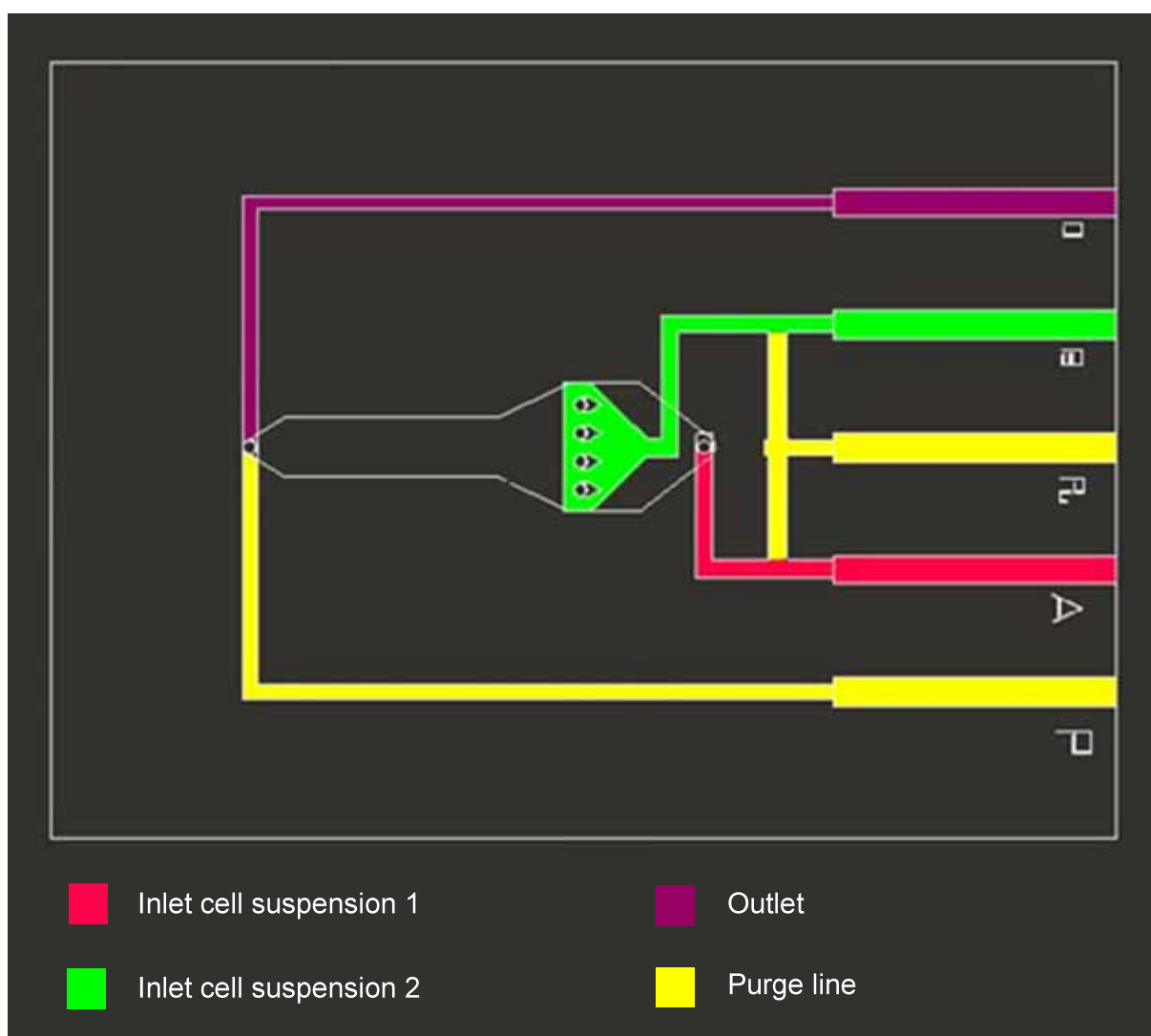


Figure 3.101: Microfluidic structure 3: A purgeline (shown in yellow) was introduced to provide more flexibility for flushing the system.

The realisation of the microfluidic structure 3 with purgelines is shown in figure 3.103 and figure 3.104 on page 158 or page 159, respectively.

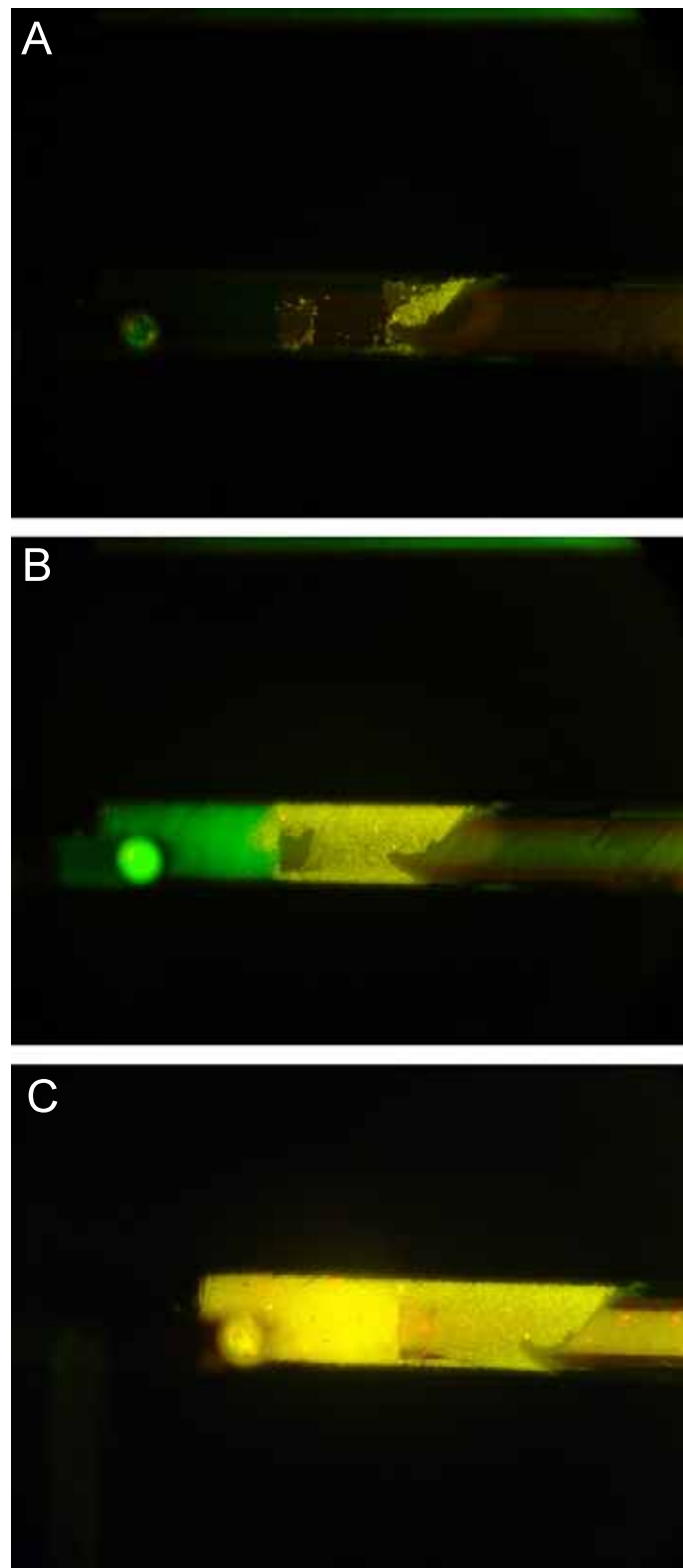


Figure 3.102: The pictures show the connection of the laser-machined area of the microfluidic structure to the boreholes, where the capillaries are inserted. The glue does not approximate to the entrance of the capillary. Otherwise, the risk exists that the capillary is sealed by the glue. Thus, particles can accumulate in this passage, which need regular flushing.

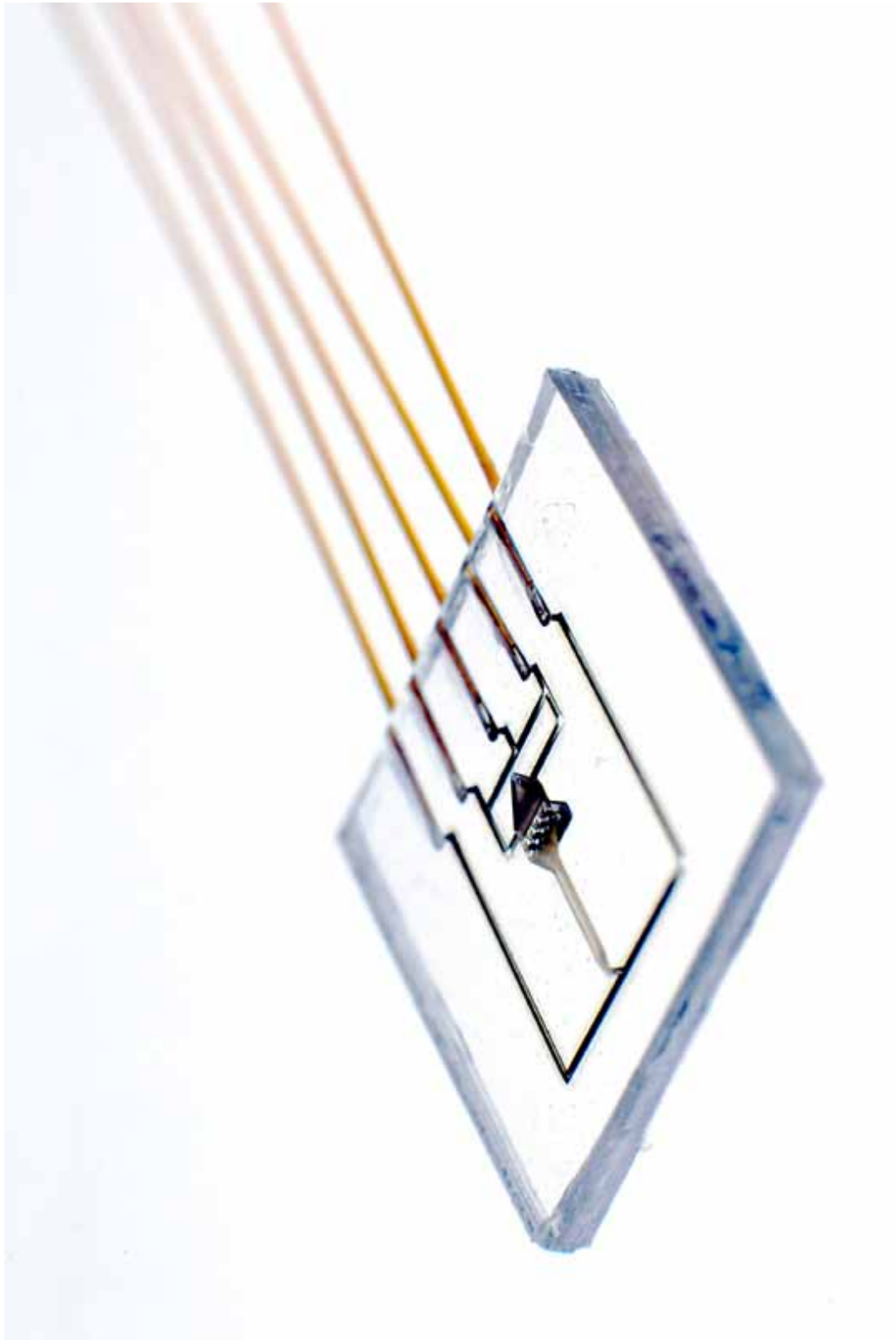


Figure 3.103: Microfluidic system 3 with purge line: The microfluidic structure is cut in PET and before usage will be sealed with PDMS.

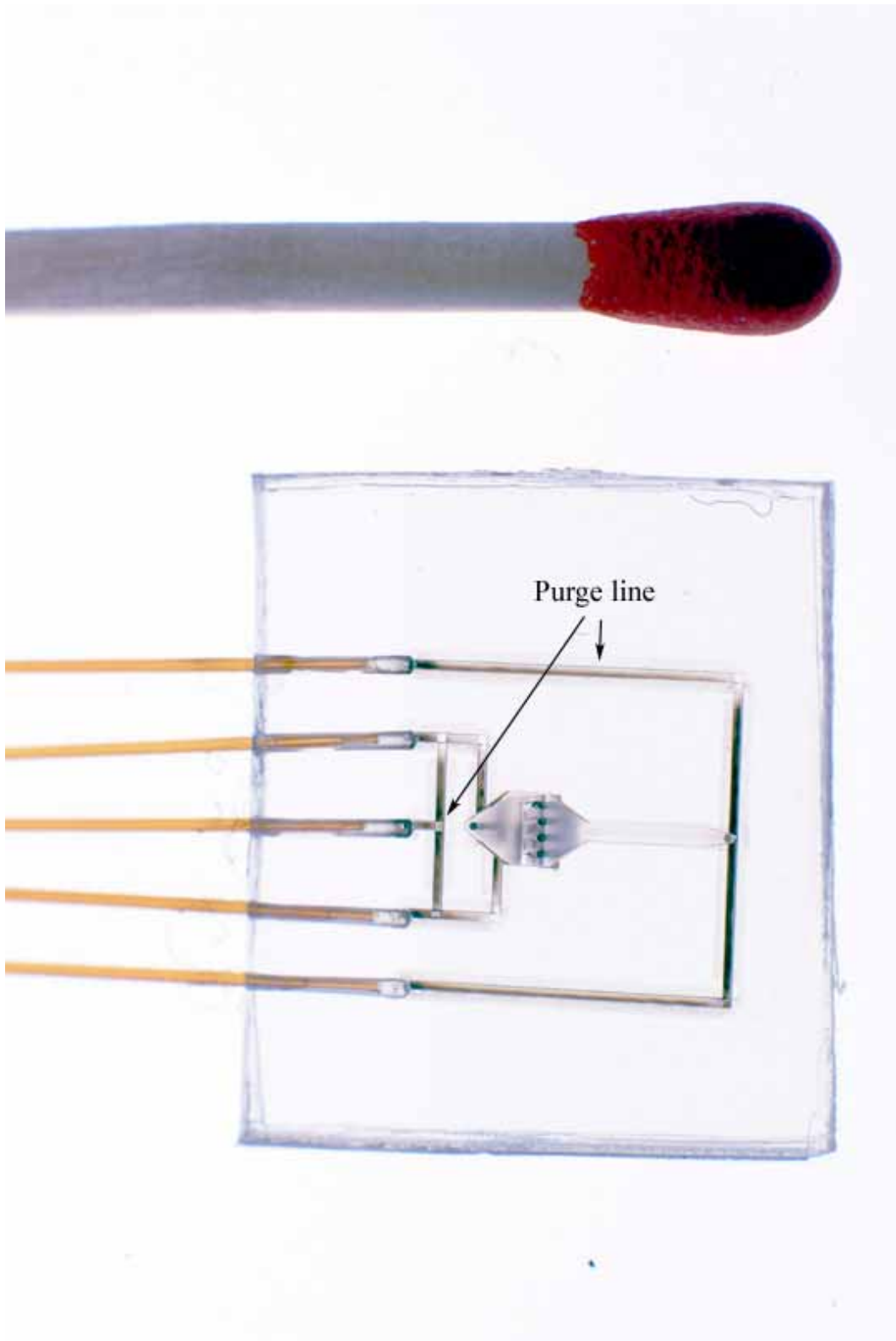


Figure 3.104: Microfluidic system 3 with purge line: The picture shows the proportions of the microfluidic system in comparison to a match.

However, the purge line could not live up to expectations. The integration of the purge line should provide an opportunity to better flush all connection sections between the laser-machined structure and the drillings. This also comprised a connection between inlet A and inlet B (see figure 3.101) to clean the inlets bypassing the microfluidic chamber.

This connection of the inlets was the area where problems arose in the first tracer experiments with the microfluidic structure 3 with integrated purgeline. Short-circuit flows occurred, which hindered the development of nine alternating parallel flows (see figure 3.106, picture B and C). Cross-circuits as such, which led to mixing of the inlet flows A and B, had been considered before the integration of the purge line, but due to the usage of pressure-independent pump systems, were not expected. In contrast, a clear boundary between fluid A and fluid B (as shown in figure 3.106A) were estimated.

Thus, all changes to the microfluidic system were kept expect the integration of the purgeline. The resulting design is shown in figure 3.105.

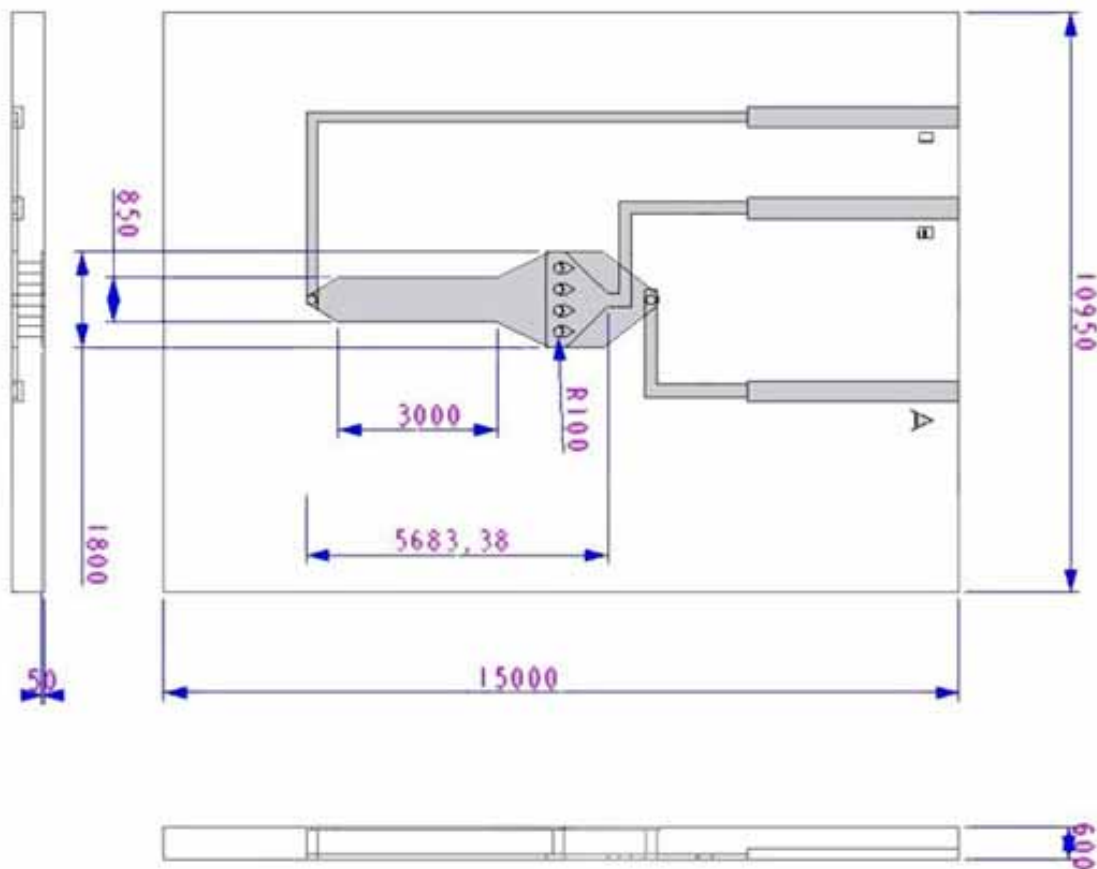


Figure 3.105: Final design of the microfluidic structure 3 with dimensions in μm .

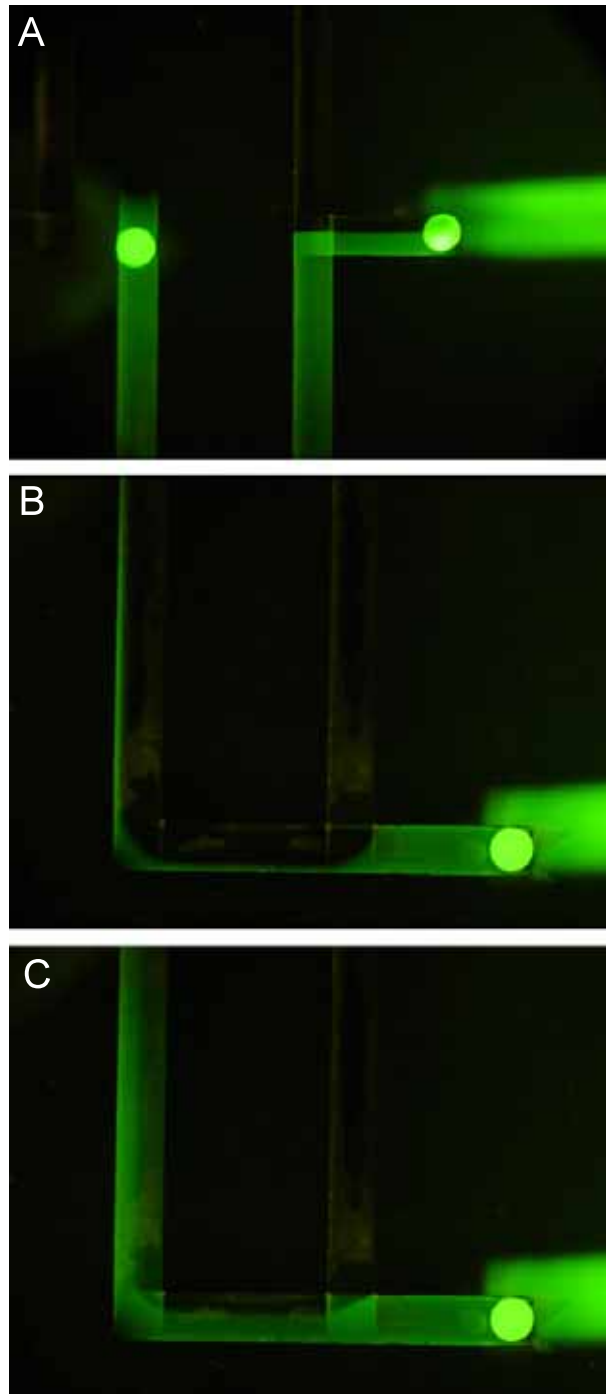


Figure 3.106: Purgeline between inlet A and B. The fluid entering the system via inlet A is stained with Na-Fluorescein (green). In the normal operation mode of the microfluidic system, a flow situation with a distinct boundary (A) should prevail. However, such a stable flow situation could not be obtained and more (B) or less (C) strong cross-circuit flows were present.

The microfluidic system 3 (as shown in figure 3.107) is continued to seal with the help of PDMS, since no satisfying results were obtained from bonding experiments. This sealing method is also of advantage, since it allows the chamber to be opened for cleaning.

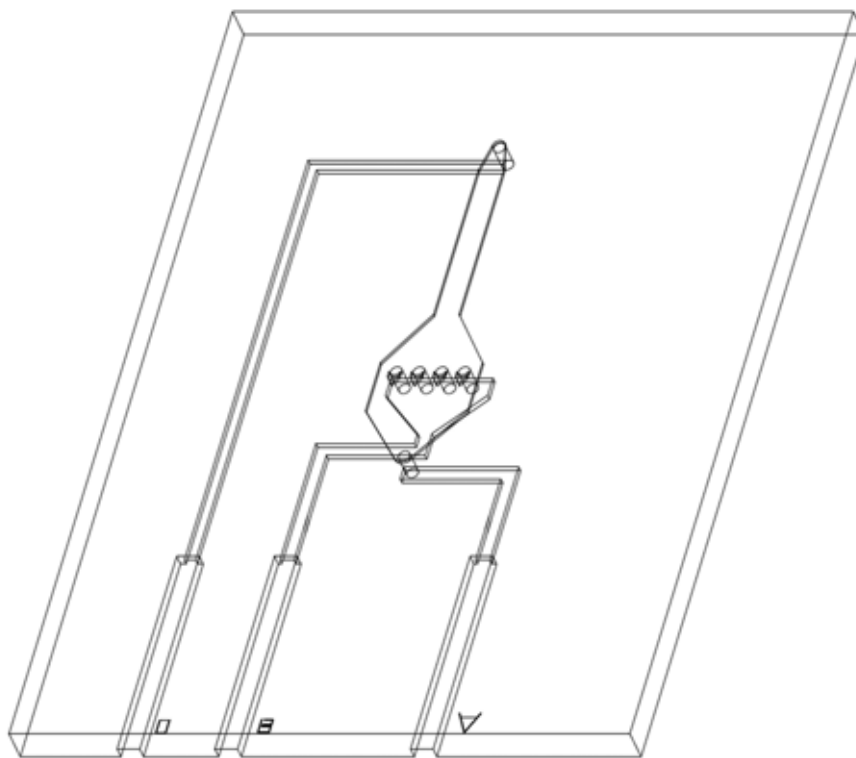


Figure 3.107: 3D-model of the microfluidic system 3

The fluid flow inside the redesigned microfluidic system still corresponds with the ones observed in the previous microfluidic systems except for the inclusion of a hydrodynamic focussing section in the front of the open chamber. Nine parallel partial flows are found inside the microfluidic chamber, which are visualised in figure 3.108 by the addition of Na-Fluorescein into the fluid of inlet B. Furthermore, the pictures of figure 3.108, which are taken out of a movie sequence, show, that the distinct flows appear immediately after the pumps are turned on. They persist until the pumps are turned off and subsequently mix due to diffusion.

However, during the operation of the pumps no diffusion of the dyes from one partial flow into the other took place, which could be visualised even better, if both inlet flows were stained with a fluorescent dye (see figure 3.109 on page 164).

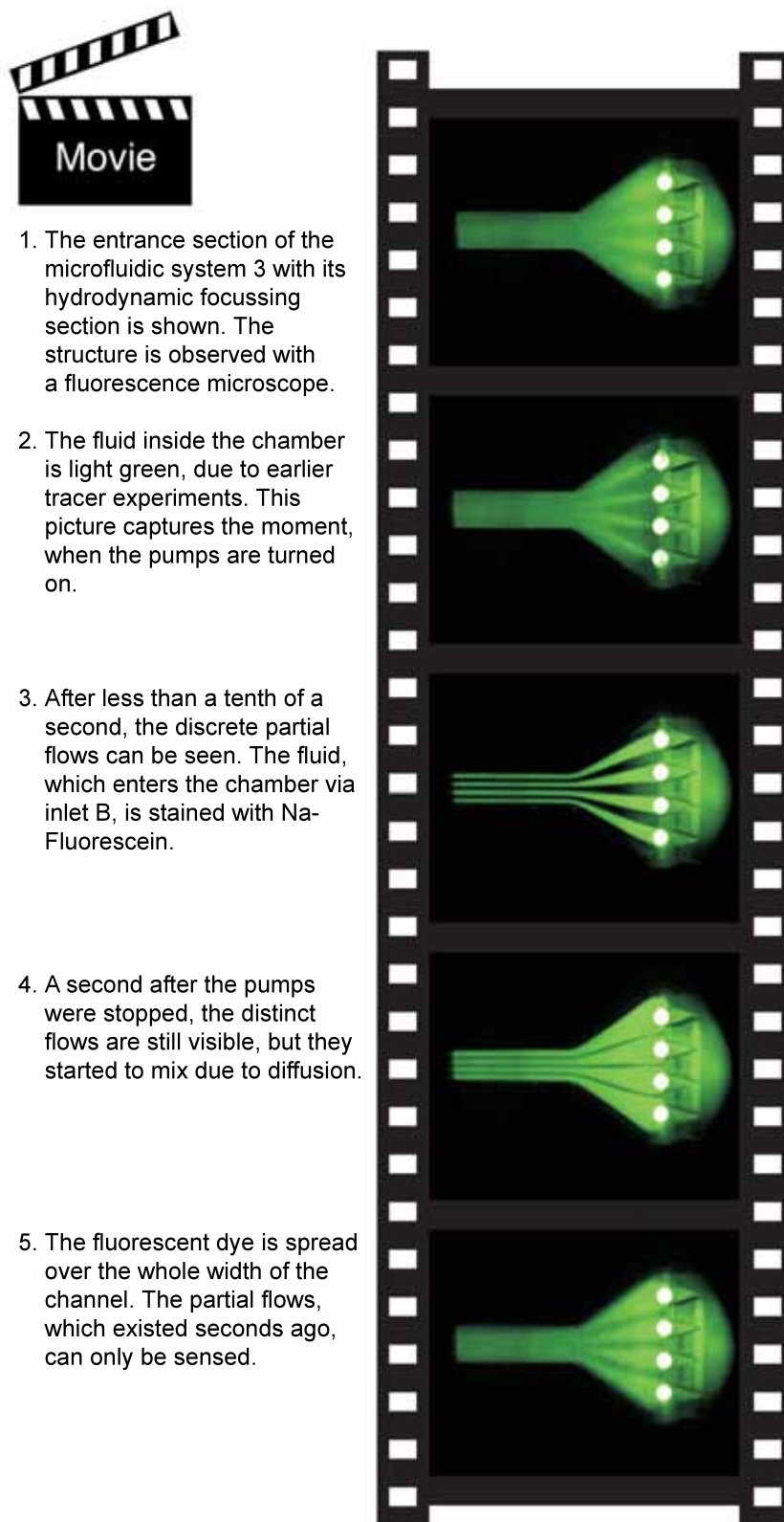


Figure 3.108: Tracer experiment system 3: Na-Fluorescein adds a green fluorescence to the fluid, which enters the microfluidic chamber via inlet B. With the start of the pump system, the partial flows can be observed immediately, while they disappear, when the pumps are switched off and the fluids mix by diffusion.

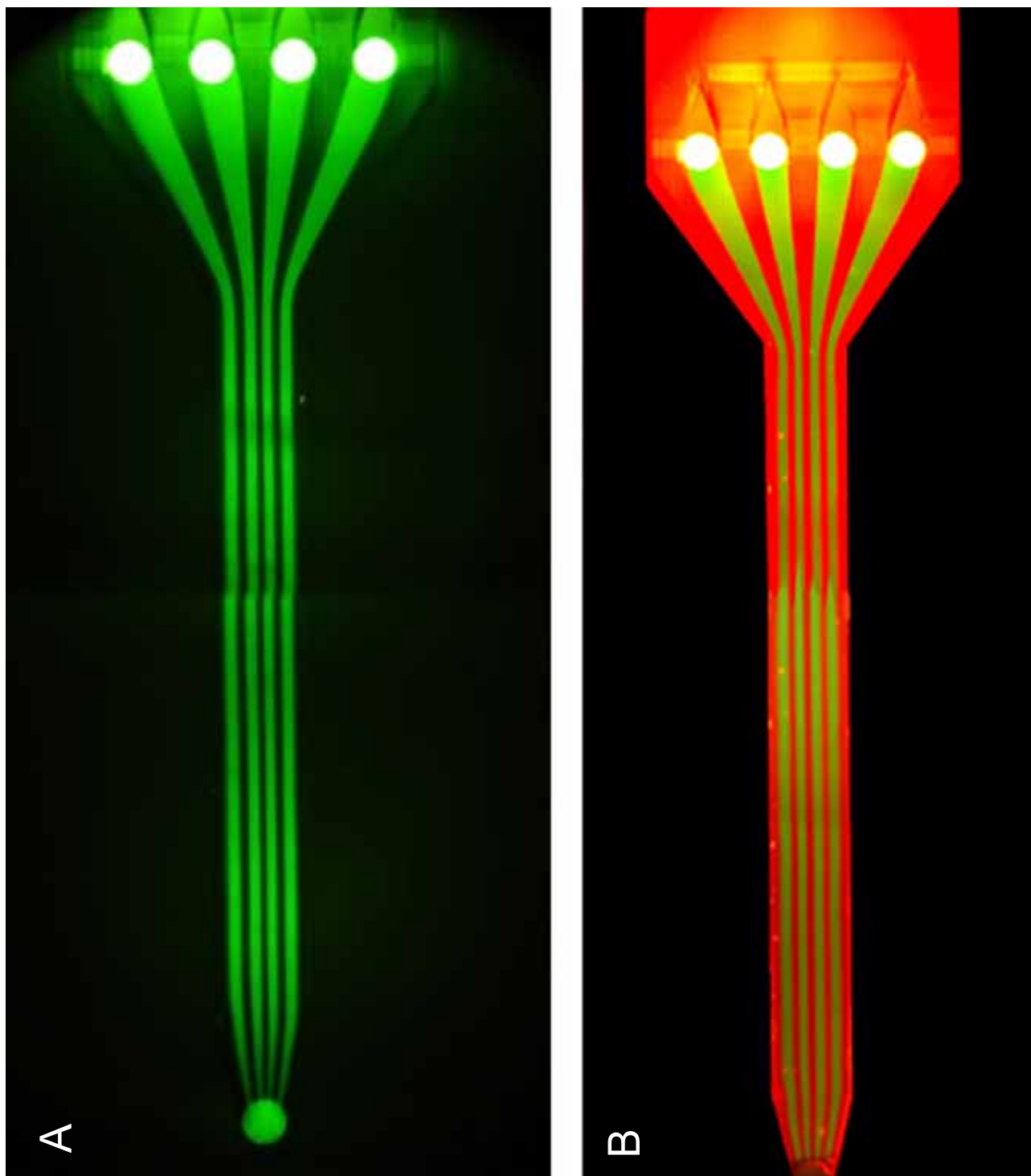


Figure 3.109: Microfluidic system 3: The fluid flow of inlet B is stained with Na-Fluorescein (A) and in addition, the second fluid is stained with CMTMR (B) resulting in an alternating flow of red and green partial flows.

Summary

Two changes have been introduced to the design of the microfluidic system:

1. Increase of all inflow dimension, thus expanding the whole front part of the microfluidic chamber
2. Change of the chamber material from PMMA to PET

The microfluidic chamber is now fully functional. In the next step, the electrodes for the fusion process need to be integrated to obtain an electrofusion chamber in the end.

3.2.9 Electrode Integration

Overview

This section describes the last step, which is needed to obtain a functional electrofusion chamber, the integration of electrodes into the microfluidic system. For the alignment of the cells (by dielectrophoresis) before fusion and for the fusion itself an inhomogeneous electrical field is needed.

The last step for obtaining a functional electrofusion chamber was to implement the electrodes into the design of the microfluidic system. Following the design concept of the Eppendorf electrofusion chamber for bulk electrofusion, it was aimed for an integration of Platinum wires, $200\mu\text{m}$ in diameter (see figure 3.110 and figure 3.111 respectively).



Figure 3.110: Sketch of the microfluidic system 3 with positioning of two Platinum wires as electrodes alongside the microfluidic chamber

The identification of a possible strategy for the introduction of those electrodes into the

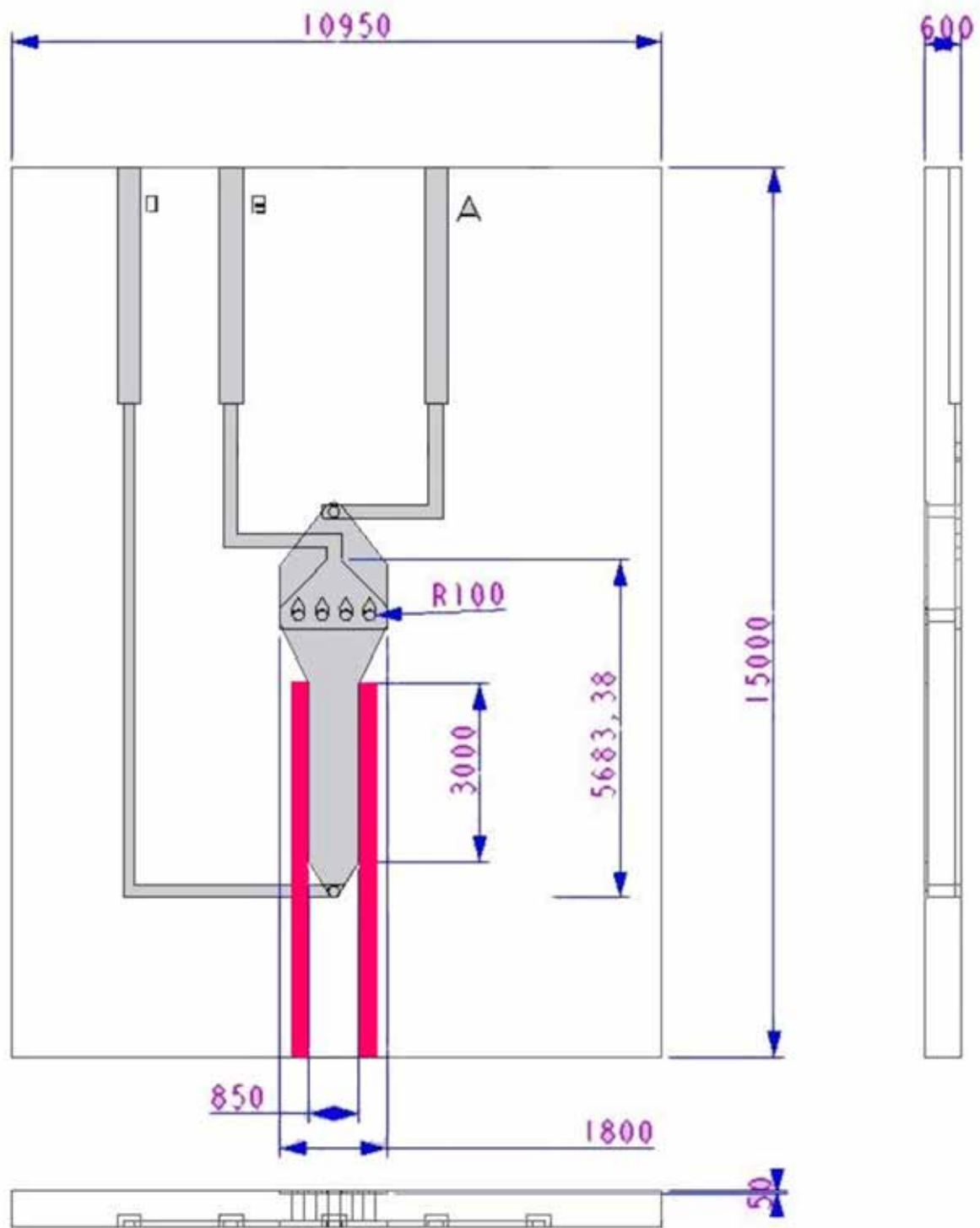


Figure 3.111: Engineering drawing of the microfluidic system 3 including electrodes. All dimensions are given in μm .

already designed fluidic chamber turned out to be difficult. An irreversible implementation of the electrodes was conceivable, using the UV glue, which was already used for the integration of the capillaries. However, the chamber could not be sealed using this approach and leakages occurred in the area of electrode integration. Even robot assisted microdispensing (also called micro adhesive bonding) of the glue could not solve this problem and a reversible electrode implementation by O-ring fabrication for electrode assembly had not been proven feasible in surface leakage studies (data not shown).

The search for an integration strategy was expanded, considering other manufacturing processes for the microfluidic chamber, such as injection moulding, hot embossing and new rapid micro product development (RMPD) techniques such as one step production and assembly using UV-cured polymers. However, none of these techniques could provide a solution for the system in hand. Throughout all approaches either a positioning of the electrodes in micrometer range was not possible or sealing problems occurred. Furthermore, the integration of wires as electrodes entailed the appearance of dead zones, where either particle or air was trapped. Since both, new manufacturing processes and new sealing and bonding techniques (*e.g.* laser beam welding of polymers), failed, the integration of electrodes by coating was considered. This led to the collaboration with Micronit Microfluidics, a Dutch company.

Micronit Microfluidics is specialised in customised glass micromachining (*i.e.* to produce microfluidic devices) from prototyping up to high volumes. By a combination of their core technologies, such as micropowderblasting, wet etching, direct bonding and integration of electrodes they were capable of producing the required micro device. In general, they produce microelectrophoresis chips, microtiterplates, micro reactor chips and customised chips. They provide the knowledge of electrode integration from their electrophoresis chips, where electrodes are integrated inside the separation channel for amperometric detection.

Since Micronit specialises in glass micromachining, the chamber material of the final electrofusion chamber was chosen to be Borofloat glass, which is the most commonly used glass type for microdevices. The benefits of glass compared to plastic are the stable hydrophilic properties, the optical superiority and proven inertness. Furthermore, no special type of glass was required for this application, because of the detection of the cells and hybrids inside the chamber was done by fluorescence in the normal visible spectrum (VIS). Other assumptions were the possible connection of the chip to capillaries and pumps and the adoption of the chamber design of the microfluidic system 3 with its enlarged front part of the chamber, followed by an area

for hydrodynamic focussing.

The through-holes of the chamber should have a minimum diameter of $100\mu m$ at entry side, but the exact diameter is not critical and could slightly be more. This made the powderblasting process applicable, which was used to generate semi-transparent holes with sloped sidewalls at an angle of around 70° .

The chamber and the channels were fabricated using hydrofluorid acid (HF) etching, to obtain 100 % optically clear structures with a surface roughness of $0.1\mu m$. The predetermined dimensions of the channels by the HF etching technique (minimum channel width of $5\mu m$, a minimum channel depth of half the channel width (aspect ratio 2:1) and a maximal channel depth of $100\mu m$) were consistent with the required channel geometry.

Technique Box

Micropowderblasting

Application:

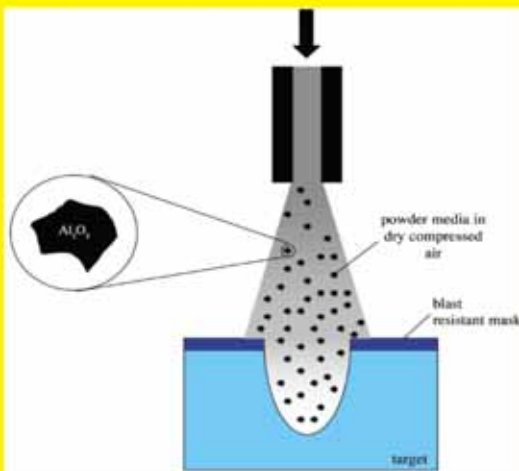
Micropowderblasting or abrasive jet machining (AJM) technique is a fast, cheap and accurate method for the creation of holes, channels and cavities in brittle materials such as glass or ceramics.

Requirements:

Glass or ceramic target, powder blaster, compressed air, powder media, blast resistant mask (e.g. metal mask)

Method:

The powderblasting technique is based on the erosion of substrate by physical impact. The desired structure is patterned with the help of a protection mask (metal or polymer layer). Subsequently, a particle jet of small Aluminiumoxid particles is blasted out of a moving nozzle towards the target for mechanical material removal. This method provides high etching rates, whereas the quality of the mask influences the accuracy of the powderblasting process. Furthermore, the control of parameters like pressure, angle of incidence of the powder beam, distance between nozzle and substrate, determine the speed of the eroding particles and also the properties of the structures. The minimum feature size is $50\mu m$, with an aspect ratio of the resulting hole/cavity of 3:1. The surface roughness of this technique amounts to $1.0\mu m$, but the surfaces of the substrate remain undamaged, so bonding it to another substrate can still be achieved without the need of polishing.



Schematic presentation of the micropowderblasting process

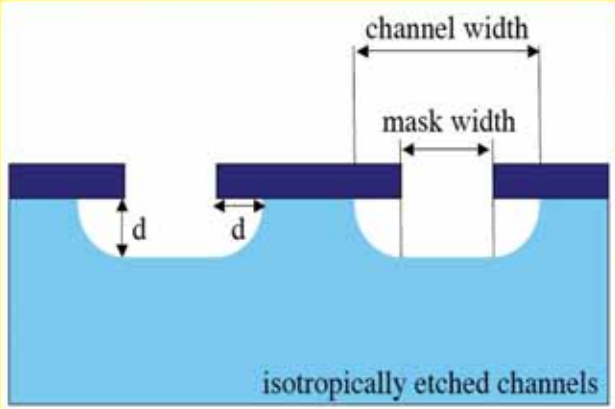
Technique Box

Hydrofluorid acid (HF) etching

Application:
HF etching is accounted to be the best way of making optically clear and smooth channel structures in glass in a fast and cost-effective way.

Requirements:
lithographic mask, HF solution, glass target

Method:
A photoresist film is coated on top of the target material and processed by UV illumination through a mask and development to obtain a protection mask for the etching process.



HF etching is an isotropical etching technique. Isotropic etchants attack the material being etched at the same rate in all directions. Thus, the lateral etch rate is about the same as the vertical etch rate and material is removed horizontally under the etch mask (undercutting). Using this chemical wet etching technique for glass the width of the resulting channels is more than twice the depth of it, and the corners are rounded. The bottom of the channel will stay smooth (surface roughness is $0.1 \mu\text{m}$) and optically transparent.

Schematic depiction of isotropically etched channels

The direct adoption of the design of the microfluidic system 3 would result in a triple stack glass layer (sandwich structure) with electrodes. The bonding of three thin glass layers is a very complex and time intensive process and thus is very expensive. To reduce the costs and enhance the connectivity, the design was adapted to suit the standard $45 \cdot 15\text{mm}$ dimension and standard hole pattern of Micronit's microfluidic chips (10 holes per chip, five on each side; see figure 3.112).

Instead of a triple layer stack a dual layer stack was used, minimising costs and resulting in a better yield (number of chips resulting from one glass wafer). All channels and the electrofusion chamber were designed to lay in one surface and had the same depth, while the electrodes were integrated between the layers, but inside the chamber, with the connections for electrodes and capillaries placed on top of the system. Nine of the ten access holes of the microfluidic chip

were used as inlets in an alternating manner, the remaining one as outlet (see figure 3.112).

Furthermore, the adapted design was suitable for the high pressure chipholder, provided by Micronit, which allowed to connect the microfluidic chips to the outer periphery with near zero dead volume and was capable of withstanding high pressures at these microfluidic interconnections.

In this design an additional chip was needed for splitting the two inputs, which came from one pump each (conterminously cell suspension 1 and 2), into four and five partial flows, respectively. This splitter chip was needed to enable an alternating arrangement of the partial flows in a double layer stack with a two-and-a-half dimensional (2.5D) design. In machining the term 2.5D refers to a surface, which is a projection of a plane into the third dimensions, which applies to this case, since the height of the microfluidic structure (channels as well as chamber) is constant and they all lay in one surface.

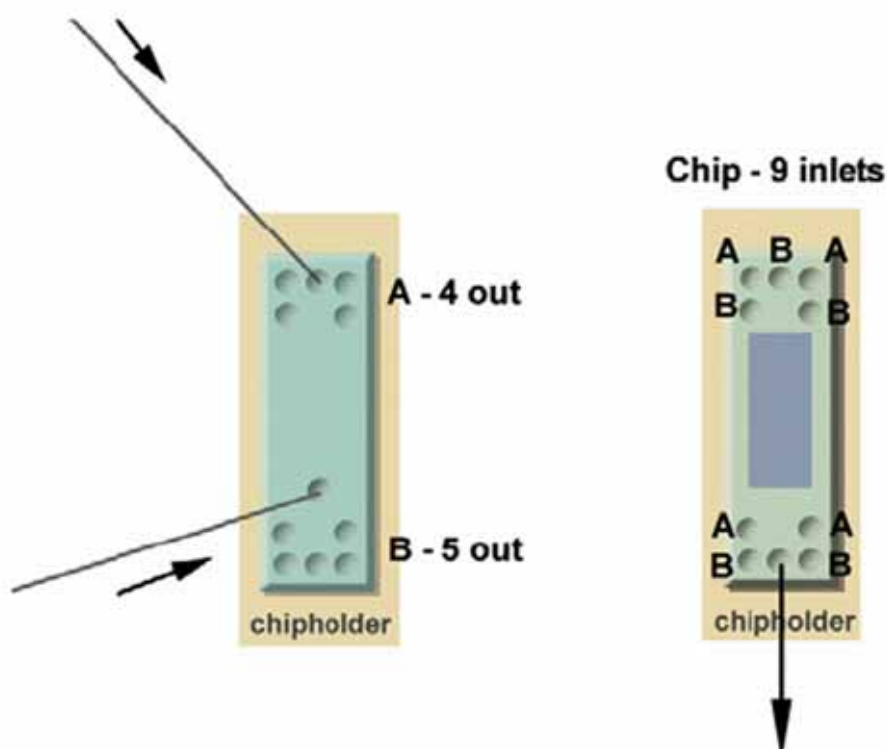


Figure 3.112: Left: Concept of the splitter chip for the use with the microfluidic chip (on the right), to reduce the number of required pumps from nine to two. Right: Concept of the microfluidic chip based on Micronit's standard hole pattern, where nine of the ten access holes are used as inlets (in an alternating manner B-A-B) and one as outlet

Thus, the new solution consisted of one splitterchip and two different electrofusion chips. All chips were produced from one 4" square wafer, resulting in 12 chips of $45 \cdot 15\text{mm}$ (five electrofusion chips with 9 inlets and 1 outlet, five electrofusion chips with 2 inlets and 1 outlet and two splitter chips with 2 inlets and 9 outlets, divided as 1 · 4 and 1 · 5 outlets).

In the design of the 9in-1out-chip the width of the chamber, where all channels come together, amounts to $1800\mu\text{m}$ (see figure 3.113 for engineering drawing). All input channels have a width of $110\mu\text{m}$, while the outlet channel is $190\mu\text{m}$ wide to avoid blockage by hybrids after the fusion process.

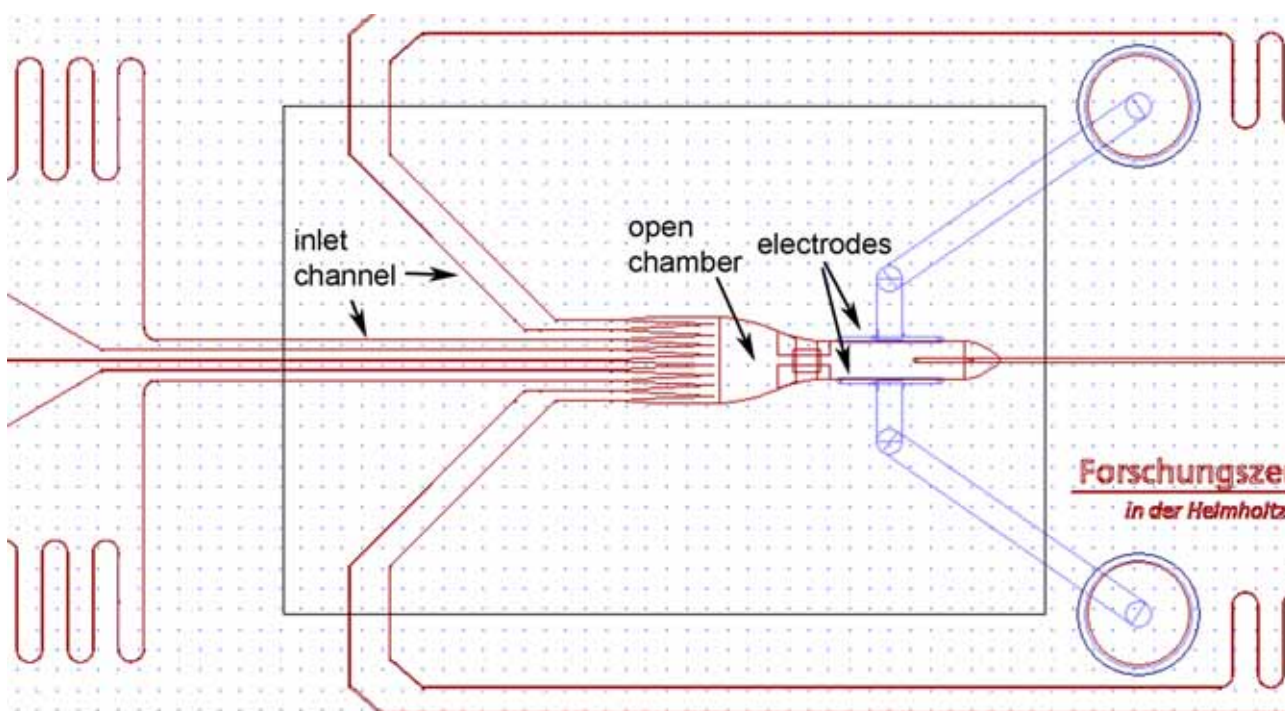


Figure 3.113: Engineering drawing of the electrofusion chamber of the microfluidic system 4: Nine individual channels enter the chamber, each channel gives rise to one partial flow. The nine parallel flows are subsequently reduced in size by hydrodynamic focussing and enter the part of the chamber, which is flanked by electrodes (depicted in blue). The electrodes are leading to patches, where the connection to the power supply can take place. The black rectangle with a dimension of $1 \cdot 1.5\text{cm}^2$ indicates, which part of the chip will be accessible for visual inspection.

The inlet channels approach the chamber from various directions, since they are connected to the access holes of the microfluidic chip, which are placed on the chip in Micronit's standard hole pattern. Thus, five of the 9 inlet holes are situated on the left side and the remaining four are found on the right side of the chip. This situation would lead to different channel length

from access hole to chamber entrance, which had to be avoided as it would cause different pressure losses in the channels. Therefore, some channels have integrated wiggly lines to adjust the channel to the right length. Electrodes are flanking the rear part of the chamber, where the electrofusion process shall take place. They are $200\mu\text{m}$ wide with $500\mu\text{m}$ wide feed lines.

Although, the aim of the electrofusion chamber development was to enable an optimised fusion process for the generation of large numbers of viable hybrids, a reduced version of the above microfluidic electrofusion chip was designed. This 2in-1out-chip (see figure 3.114) can only harbour two laminar parallel flows and was used for the improvement and the understanding of the electrofusion process of mammalian cells itself. In this design, the entrance part of the chamber possesses a width of $320\mu\text{m}$, which increases to a width of $450\mu\text{m}$ at the site of the electrodes. All channels are $110\mu\text{m}$ wide.

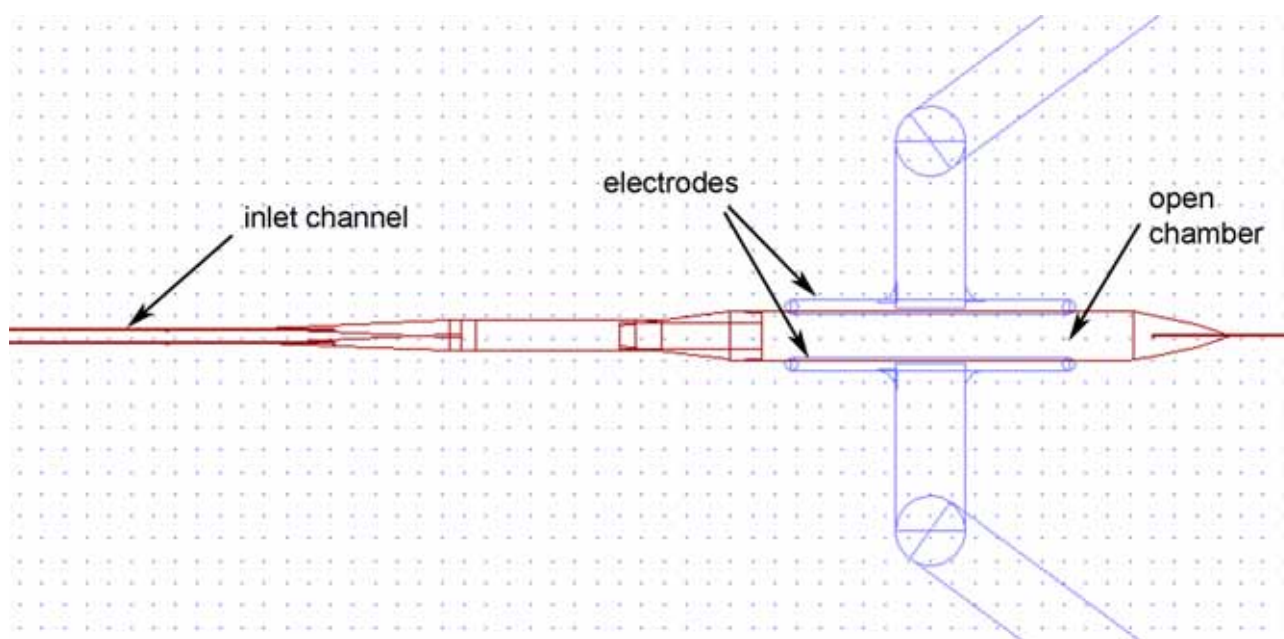


Figure 3.114: Engineering drawing of the 2in-1out microfluidic chip. In this design only two channels enter the chamber, resulting in two parallel laminar cell flows inside the electrofusion chamber.

The full design of all three microfluidic chips (9in-1out chip, 2in-1out-chip and splitter chip) can be seen in the figures 3.115, 3.116 and 3.117 on page 173. Their realisation is shown in the figures 3.118, 3.119 and 3.120 on page 174ff.

The chips with an outer dimension of $45 \cdot 15\text{mm}$ are made of Borofloat glass. Both layers (top and bottom layer) are $1100\mu\text{m}$ high and bonded together by direct bonding without the

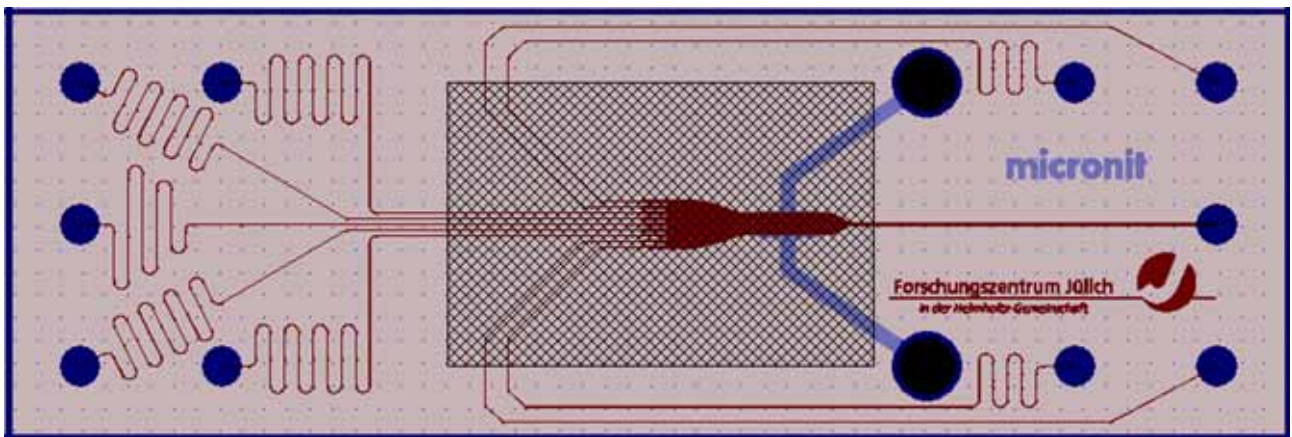


Figure 3.115: Schematic depiction of the microfluidic system 4 with two integrated electrodes (9in-1out).

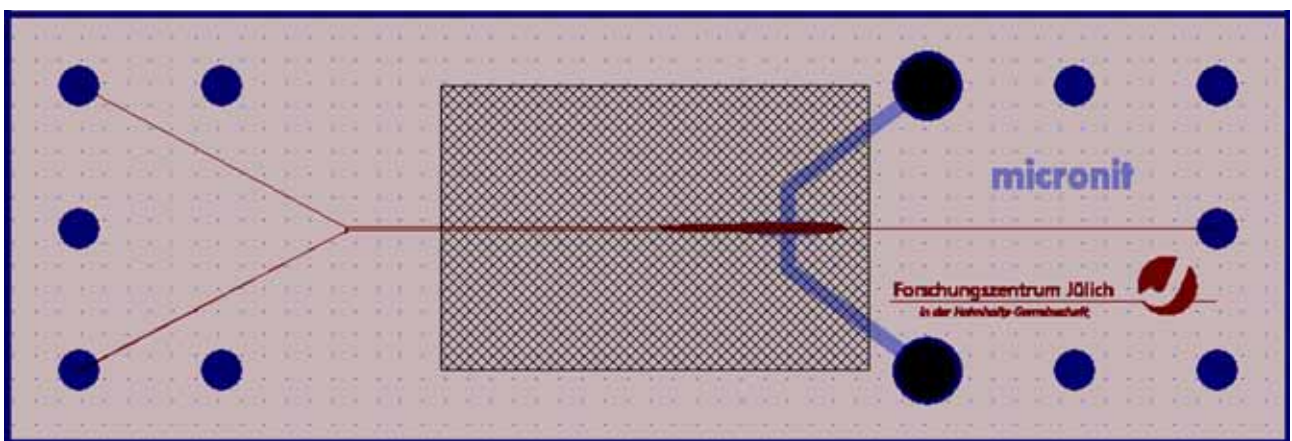


Figure 3.116: Schematic depiction of the reduced version of the electrofusion chip (2in-1out).

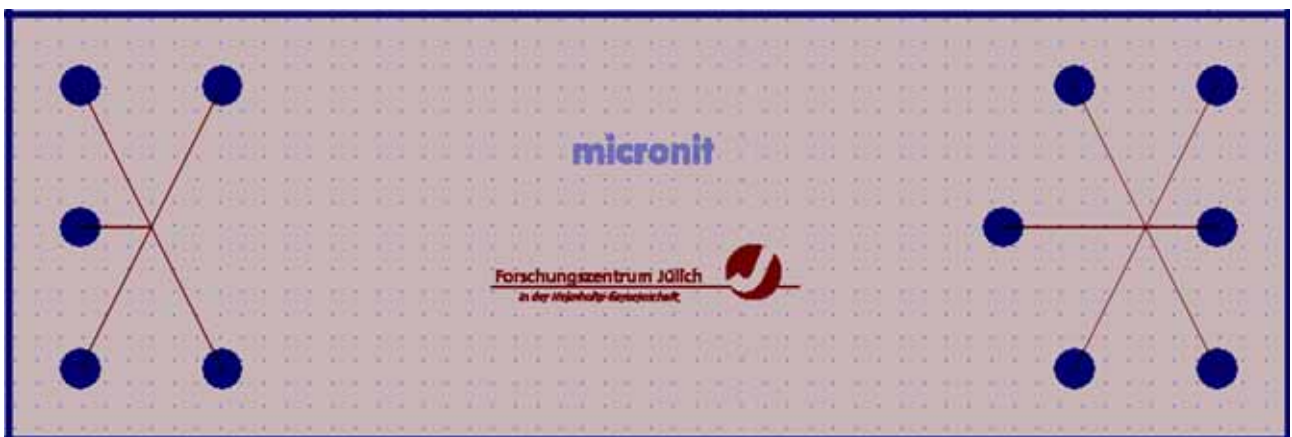


Figure 3.117: Schematic depiction of the splitter chip (1in-4out (left) and 1in-5out (right)).



Figure 3.118: Microfluidic electrofusion chip with nine inlets, one outlet and two electrodes (with feed line to contact patches) alongside the rear part of the chamber for the generation of large numbers of hybrids.



Figure 3.119: Reduced version of the microfluidic electrofusion chip for the study of the fusion process of mammalian cells.



Figure 3.120: Splitter chip for the use with the microfluidic electrofusion chip to reduce the number of required pumps from nine to two.

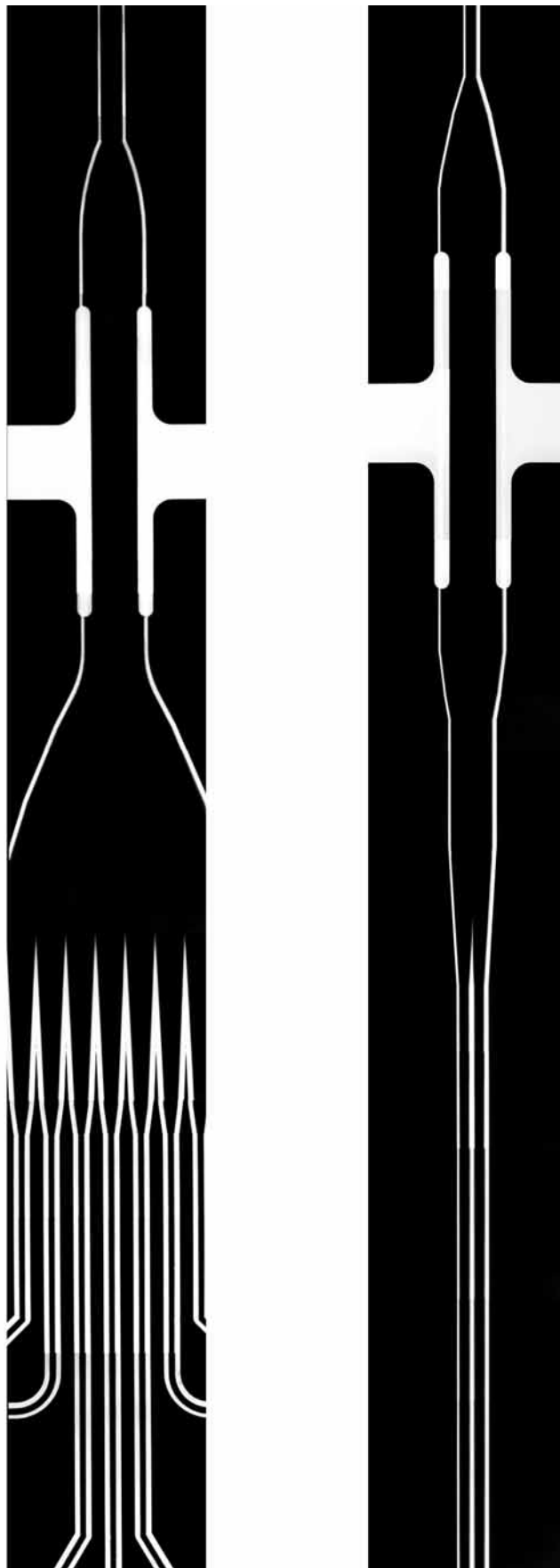


Figure 3.121: Inverted photographs of the electrofusion chamber in the 9in-1out chip (left) and 2in-1out chip (right).

use of glue or other adhesives with an alignment accuracy of $10\mu\text{m}$. All access holes and the holes for connecting the electrodes were manufactured using the powderblasting process. The inlet and outlet holes possess a bottom diameter of $600\mu\text{m} \pm 50\mu\text{m}$, resulting in a top diameter of $1400\mu\text{m} \pm 100\mu\text{m}$ due to the natural slope of the walls with powderblasting of approximately 73° . The holes for electrode connection are bigger with a top diameter of $2400\mu\text{m} \pm 100\mu\text{m}$. The microfluidic channels and chamber were etched into the glass using hydrofluoric acid (HF). All structures are $20\mu\text{m} \pm 2\mu\text{m}$ deep. The wet etching process was used to obtain a 100 % clear chamber with an average surface roughness of about $0.1\mu\text{m}$. The integrated electrodes consist of Platinum (Pt). A close up of both electrofusion chambers is shown in figure 3.121. Silver past was used to connect the electrodes via the contact patches to wires. Micronit's chipholder (see figure 3.122 and figure 3.123) was used to connect the microfluidic electrofusion chip to the macroworld.

At that time, Micronit was still working on a better solution for connection. In their latest version a screw thread is integrated into a chipholder, which keeps the wire in place. No glue in terms of silver past is needed anymore.

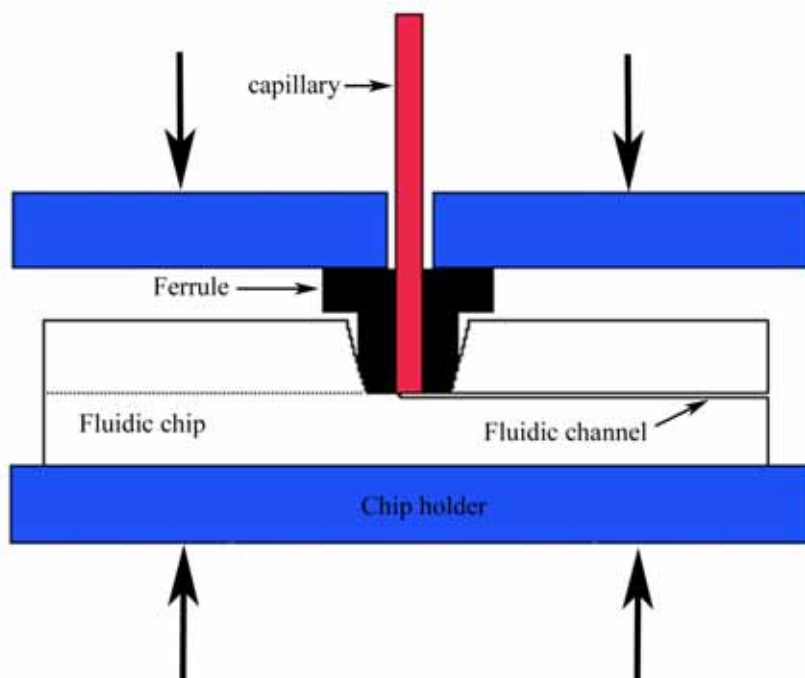


Figure 3.122: Schematic depiction of the cross sectional area of the chipholder including a ferrule (sealing rubber).

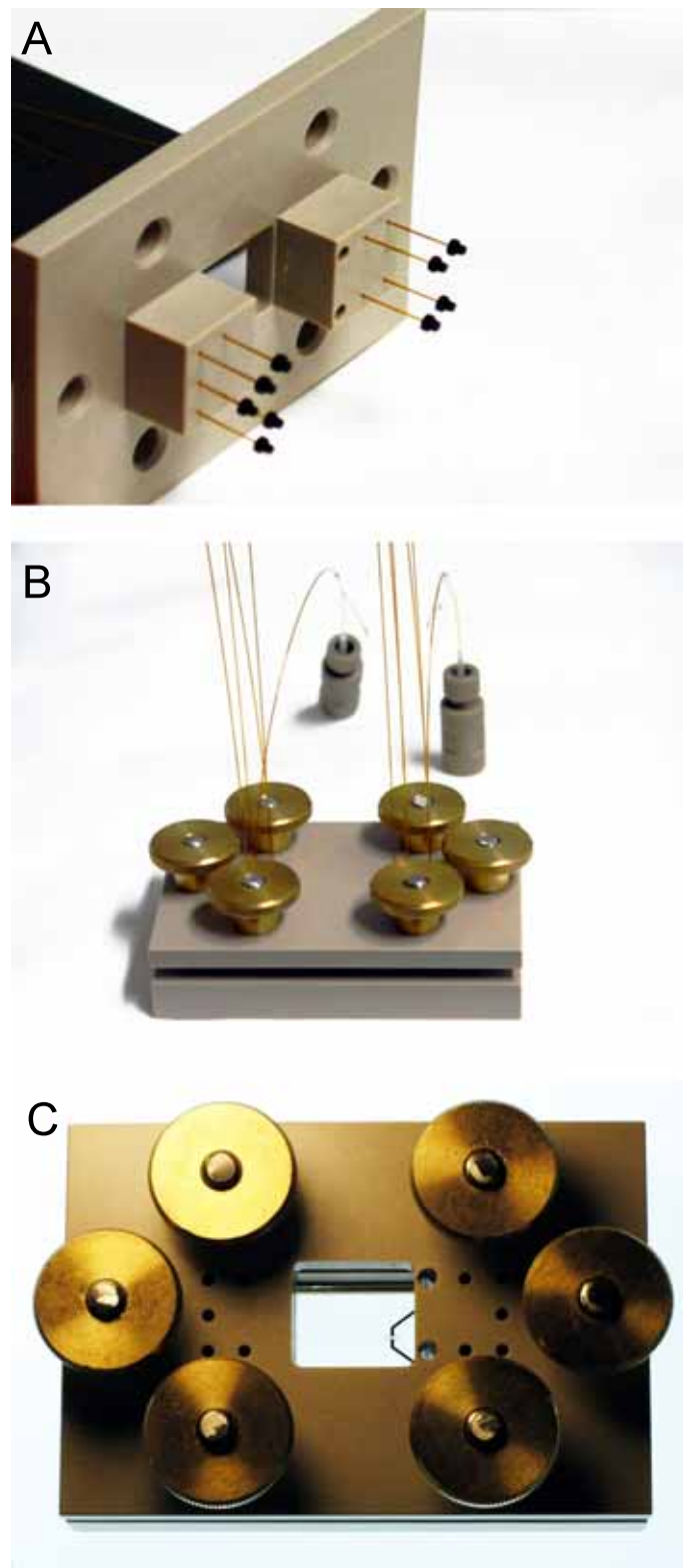


Figure 3.123: Chipholder from Micronit: A) The capillaries were threaded through the top plate of the chipholder and received a ferrule at their ends. B) The assembled chipholder for the splitter chip has two inlets and 9 outlets. C) Micronit's chipholder was customised for the application with electrofusion chips and received a see-through window for observation of the fusion process.

Micronit's microfluidic chipholder provided the sought-after plug and play solution for the connection of the chip to the capillaries and thus to the pump system. It establishes a fast and easy interconnection with a very low dead volume 20–100nL, which withstands a high pressure up to 80 bar. It works with Micronit's standard chips with a dimension of $45 \cdot 15 \cdot 2.2\text{mm}$ and 10 access holes.

This chipholder was adapted to suit the customised microfluidic chips. An optical area was made above the reaction chamber, allowing optical inspection of the chamber and detection of hybrids using fluorescence microscopy (see figure 3.123C on page 179). For the microfluidic electrofusion chip, two contact holes for the electrodes were created, and in case of the splitter chip an additional hole.

The chipholder with the inserted electrofusion chips can be used with an inverted microscope (figure 3.124) or a normal microscope, respectively. The electrodes were connected to the high voltage power supply of the Eppendorf Electroporator via a push-pull self latching connection system as used for the immobilisation approach.



Figure 3.124: The electrofusion chip with chipholder can easily be placed on an inverted microscope, whereas the splitterchip can be placed elsewhere.



Figure 3.125: Overview of the set-up for electrofusion experiments.

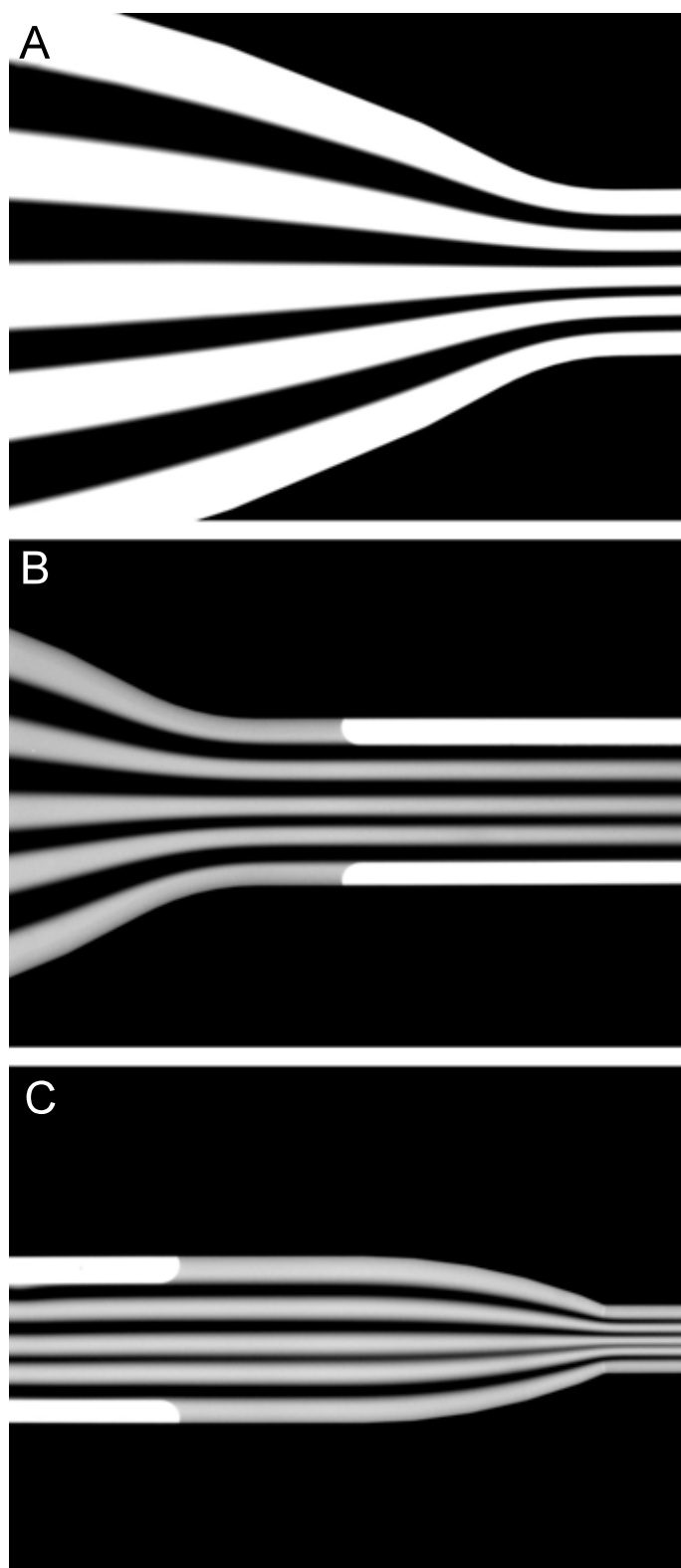


Figure 3.126: Fluorescent micrographs of the laminar flow situation inside a 9in-1out electrofusion chip. The electrodes in the middle of the fusion chamber appear in white, due to reflection on the gold surface.

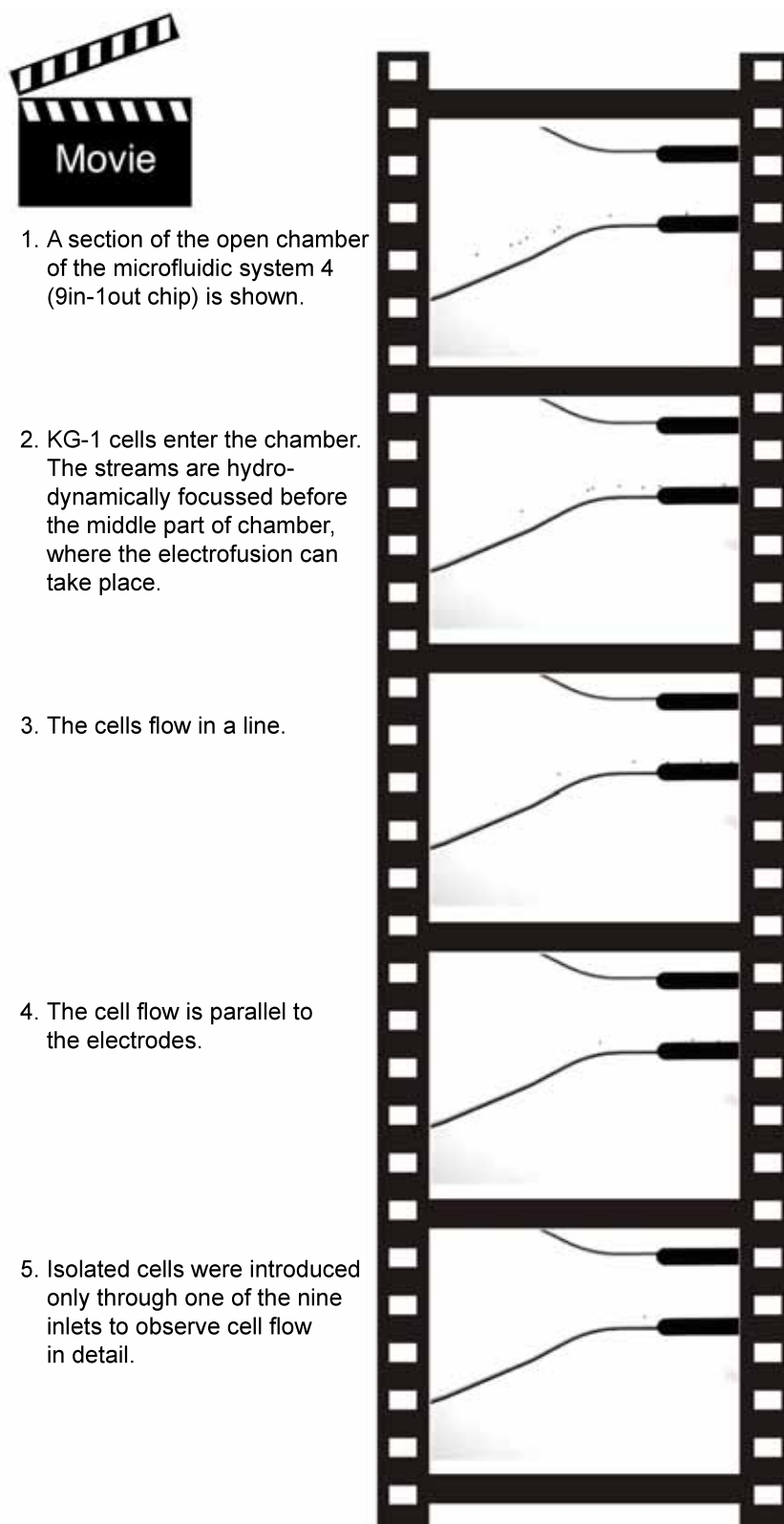


Figure 3.127: Cell flow system 4: The selected pictures have been extracted from a movie which shows the cell flow within a 9in-1out electrofusion chip. This movie is available on the enclosed DVD.

The completed electrofusion chambers were connected via these chipholders to the macro-world (see figure 3.125 on page 181 for the setup). The flow situation inside the fusion chambers were tested with the use of fluorescent tracers (figure 3.126) and the cell flow was recorded (figure 3.127). Laminar flows and single cell flows were observed, which are the requirements for a functional electrofusion chamber.

Summary

The last step for the completion of the electrofusion chamber based on the microfluidic approach was the integration of electrodes into the microfluidic chamber. Therefore, the chamber design had to be changed a last time. In the end, the development of the electrofusion chamber for arranged electrofusion of mammalian cells is completed and the chamber now fully functional.

3.3 Electrofusion

Overview

This section deals with the electrofusion process and its parameters influencing the fusion yield. The fusion of dendritic cells and breast cancer cells is addressed and the newly developed electrofusion chambers are applied.

Cell electrofusion is a multi-step procedure. Firstly, the cells are brought into close contact with each other via dielectrophoresis. This process uses a high frequent, non-uniform alternating electric field (a.c.), which induces dipoles within the cells, causing them to align in pearl chains. The second step is the fusion of the aligned cells by one or several short high-voltage pulses with field intensities in the range of kV/cm , which cause permeation of the cell membrane and the formation of pores. This may lead to the fusion of adjacent cell membranes, forming a hybrid. Subsequently, a post fusion a.c. voltage is provided in order to stabilise the process and hold the cells in alignment while they mature.

The permeabilisation of cell membranes by external electrical fields is also known as electroporation. Nowadays, this is a standard technique to introduce foreign molecules into a cell. Nevertheless, the exact mechanism, which causes the increase in permeability, is not well understood. This is due to the fact that electroporation is a very rapid membrane phenomenon, which occurs at time scales and spatial dimensions outside the reach of direct observation. Due to this lack of experimental observation of the mechanism of electroporation, several theories have been put forward.

It is accepted theory now that high-voltage d.c. electric field pulses induce a reversible destabilisation of the plasma membrane resulting in temporary depolarisation and pore formation. This process, known as electrical breakdown of the cell membrane, occurs if the total membrane potential exceeds a critical value of approximately $1V$ (at $25^{\circ}C$). The electrical breakdown is reversible and provides, for a short time, passage for all sorts of molecules to enter the cell (ZIMMERMANN ET AL., 2000). It is also the requirement for the occurrence of fusion events, thus electrofusion is sometimes described as electroporative fusion.

The applied electrical field has to be strong and long enough to induce the reversible electrical breakdown (REB), but not too strong to rupture the cell's membrane irreversibly, causing the death of the cell. Besides the electrical parameters many other influences have to be taken

into account, such as temperature, physiologic condition of the cells and osmolarity of the fusion buffer. Sometimes also membrane active agents such as bivalent cations and proteases are used to facilitate fusion (HARITOU ET AL., 2000; OHNO SHOSAKU AND OKADA, 1984).

Summary

Although electroporation and electrofusion of cells is used widely today, the underlying principals are not well understood. The dependence of the fusion process and fusion yield from various parameters will be adressed in the next section.

3.3.1 Fusion Parameters

Overview

Several different parameters, such as electrofusion buffer and electrical alignment settings were investigated to find the optimal preconditions for a fusion of dendritic cells and breast cancer cells. The findings are presented in this section. All parameters have been adjusted to the newly developed electrofusion chambers.

Apart from the used electrofusion chamber with its electrodes, electrode material and electrode geometry, the fusion process is depending on several different parameters. The principal field factors, influencing the electrofusion process, are the field strength and the pulse duration. But other parameters play an equally important role, including the cell species, physical properties of the cell membrane, fusion medium and alignment process by dielectrophoresis. The important parameters for the fusion process, *i.e.* the electrofusion buffer, the alignment and the biological parameters, such as cell type and cell size, were analysed in this thesis.

Electrofusion Buffer

A critical part of the cell fusion process is the medium, in which the cells are suspended during cell fusion. Both, the fusion process and the previous cell alignment require a low conductivity medium with high resistance to prevent excess heat build-up. Usually sugar solutions, *e.g.* glucose, sorbital or sucrose, are used since they possess a low ionic strength.

Specific membrane active agents are typically added to enhance fusion yields. Millimolar levels of divalent cations, mainly Ca^{2+} and Mg^{2+} , are used as additives (HARITOU ET AL.,

2000; HA, 2001). They influence the fusion process in a positive way by facilitating pore sealing and cell recovery after the fusion has taken place. The buffer has to be chosen that way that an optimal balance of high resistance and the presence of divalent cations is provided.

A commercially available hypoosmolar sorbital electrofusion buffer was used throughout all experiments. It is a low-conductive ($120\mu S/cm \pm 10\%$ at $23^\circ C$), calcium and magnesium acetate-based buffer ($0.1mM$ and $0.5mM$, respectively) with BSA and a pH value of 7.0 ± 0.2 . Due to the low osmolarity of this buffer ($90mOsmol/kg$) compared with culture medium or physiological buffer solutions, the cells adsorb water and swell (see figure 3.128).

The swelling of the cells in the hypoosmolar buffer detaches the cell membrane from the cytoskeleton and stretches the membrane. The osmotic pressure, which prevails in the cell, then facilitates the development of pores in the electrofusion process (PERKINS ET AL., 1991).

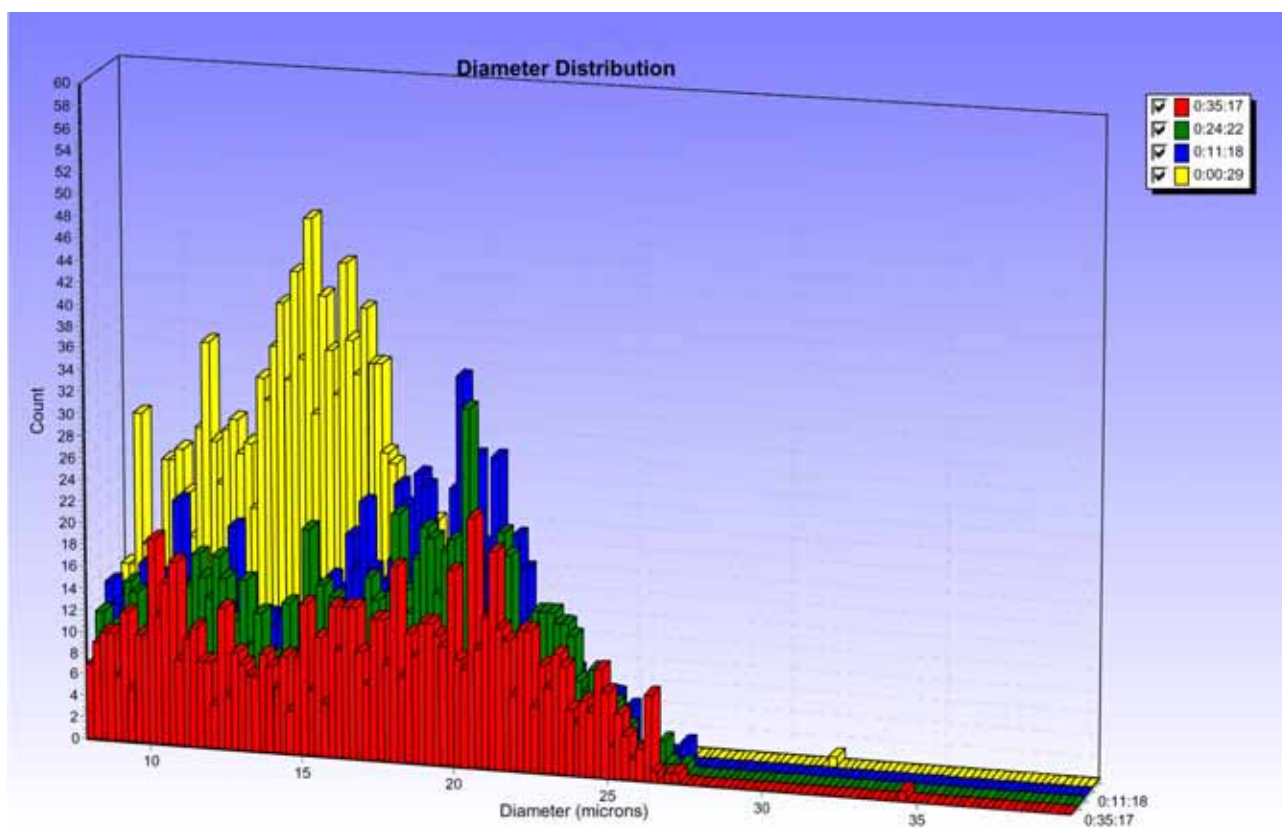


Figure 3.128: Size distribution of MCF-7 cells: The size distribution represented a Gauss curve (yellow) with a mean cell diameter of about $15\mu m$. After different time intervals of incubation in hypoosmolar buffer ($90mOsmol/kg$) the size of the cells increased and the distribution curves were shifted to the right.

Before a hypoosmolar fusion buffer is used, all cell types needed to be tested for tolerance

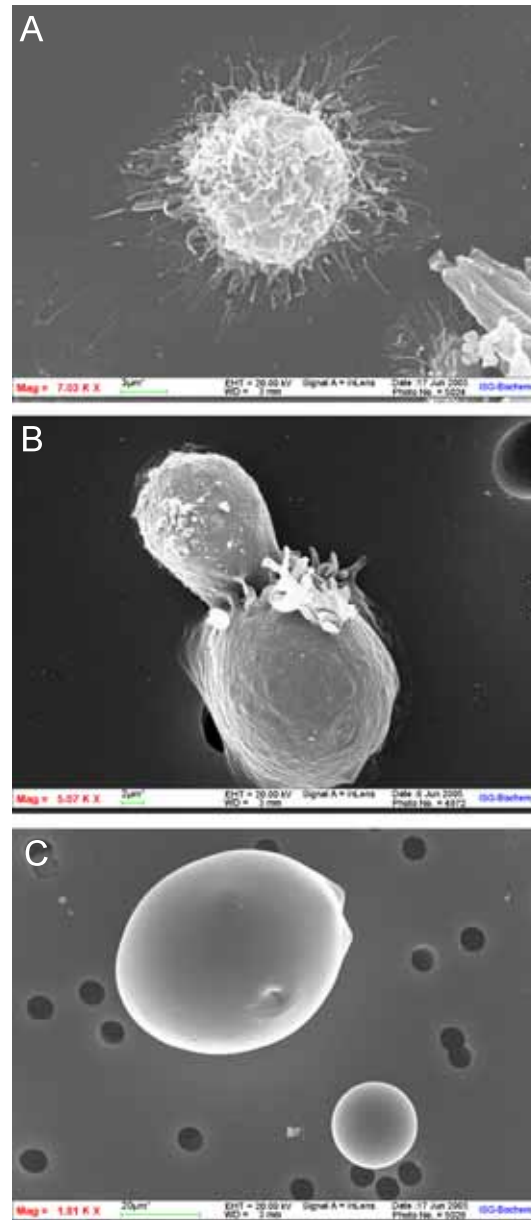


Figure 3.129: SEM pictures of dendritic cells incubated for different time intervals in hypoosmolar buffer: A) shows a dendritic cell in an isoosmolar solution. B) After an incubation of 30 minutes in a hypoosmolar buffer (90mOsmol/kg) the dendritic cells lost their dendrites and obtained a smoother surface. C) After 120 minutes of incubation the DCs were heavily swollen and assumed a rounded form.

to hypoosmolar conditions. Therefore, the survival rate of the cells was determined by viability staining with trypan blue after the cells were incubated for 30 min in the hypoosmolar buffer. After incubation, the tested cell types KG-1, MDA-MB-231, MCF-7, T47D and DCs demonstrated a good viability of more than 90 % (data not shown). The reduction of the viability during the incubation time amounted to maximal 8 %.

The four tested cell lines exhibited an increase in cell diameter of about 20 %, while the dendritic cells only increased in cell diameter by 5 % (see table 3.1).

Table 3.1: Increase in cell size by incubation in hypoosmolar buffer with an osmolarity of $90mOsmol/kg$ for 30 minutes. The increase in cell volume is calculated from the cell diameter.

Cell type	cell diameter after 30 min incubation	Increase in diameter (in %)	Increase in volume (in %)
KG-1	$14.21\mu m$	19.84 ± 0.84	72.14 ± 3.62
MDA-MB-231	$14.95\mu m$	21.21 ± 1.13	78.11 ± 5.00
MCF-7	$15.43\mu m$	22.33 ± 0.62	83.07 ± 2.77
T47D	$15.52\mu m$	21.04 ± 1.45	77.39 ± 6.38
DCs	$21.62\mu m$	5.63 ± 1.25	17.90 ± 4.18

To investigate the reason, the behaviour of dendritic cells in hypoosmolar buffer was analysed carefully by means of scanning electron microscopy (SEM) (see figure 3.129 on page 188). The pictures show that during incubation in hypoosmolar buffer, the dendrites were reformed and the cell assumed a round form with a smooth surface.

Alignment

The close membrane contact between the fusion partners is the prerequisite for successful electrofusion. This contact is established by cell alignment via positive dielectrophoresis.

For all alignment and fusion processes the Eppendorf Multiporator was used as voltage generator. Different settings for the alignment process were tested, varying the voltage between $50 - 500V/cm$ in $5V$ steps and the alignment time from $5 - 95sec$ in increments of $5sec$. The optimal alignment conditions for the used cell lines and/or a breast cancer cell/dendritic cell pair was found for a current of $500V/cm$, applied for $30sec$ (see alignment of KG-1 in figure 3.130 on page 190 as example). During alignment the cells form pearl chains with the chains

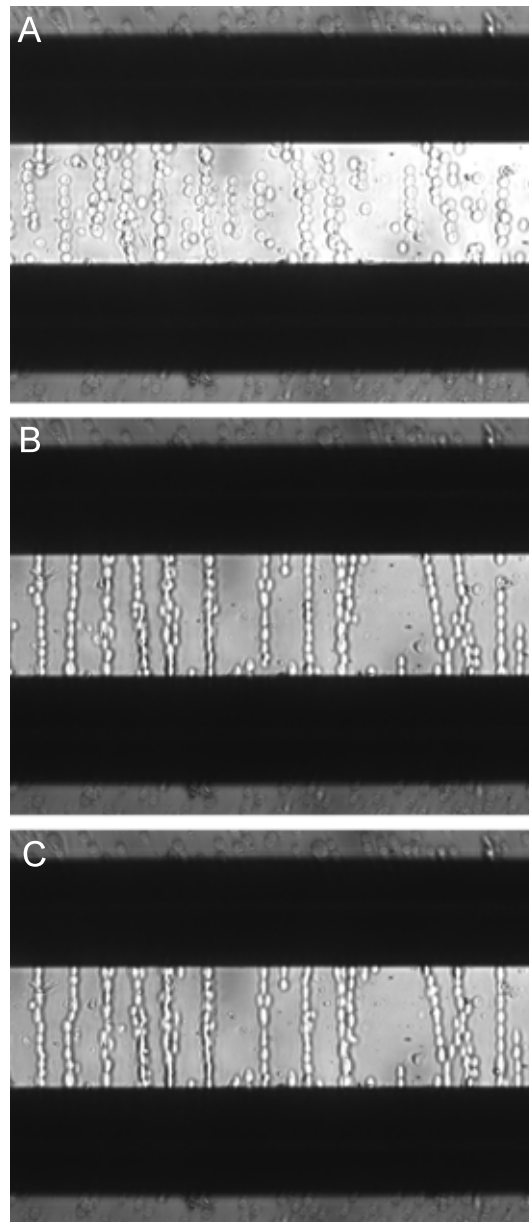


Figure 3.130: Cell alignment of KG-1 cells in a standard electrofusion chamber with two electrodes with a separation distance of $200\mu m$: A) The cells were aligned by an alternating field ($500V/cm$ for $30sec$). B+C) Subsequently, a d.c. pulse of $1.8kV/cm$ is applied for $20\mu s$ and the pearl chains are stretched by the electrode deformation force. Upon removal of the field, the pearl chains assume their original shape.



1. The cells are introduced into the space between the two electrodes.

2. An alternating current is applied between the two electrodes. The inhomogeneous electrical field causes the build up of dipoles within the cells and the cells start to align.

3. The first pearl chains are formed.

4. The pearl chains are growing and contacting the electrodes.

5. The alignment is finished and the fusion pulse can be applied.

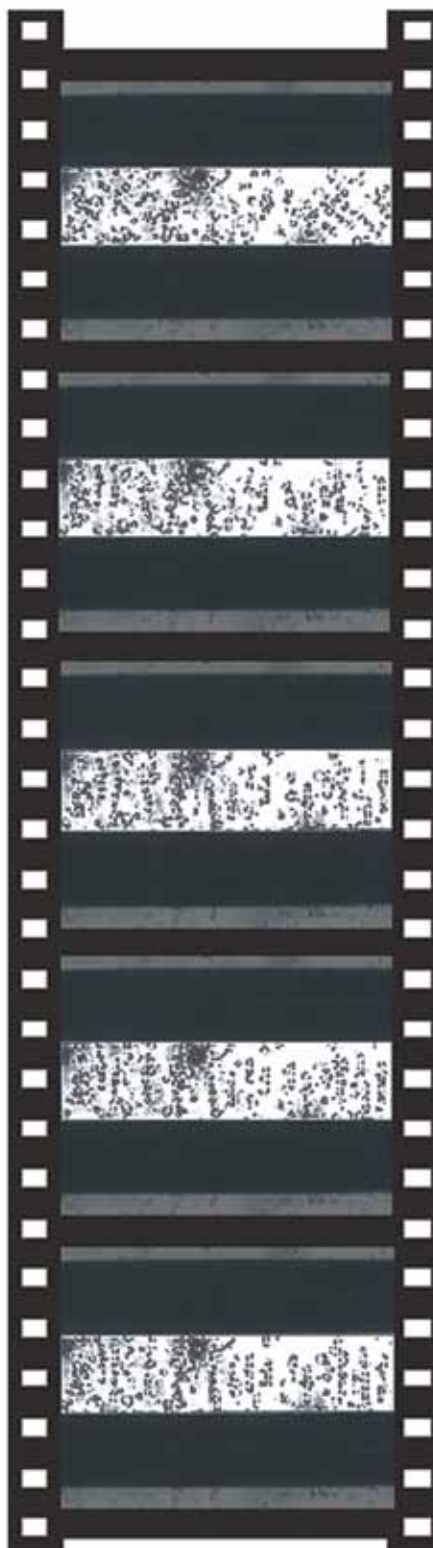


Figure 3.131: Cell alignment (KG-1) by dielectrophoresis in a standard electrofusion chamber with two Platinum electrodes with a separation distance of $200\mu m$: The selected pictures have been extracted from a movie, which shows the alignment of the cells in pearl chains. This movie is available on the enclosed DVD.

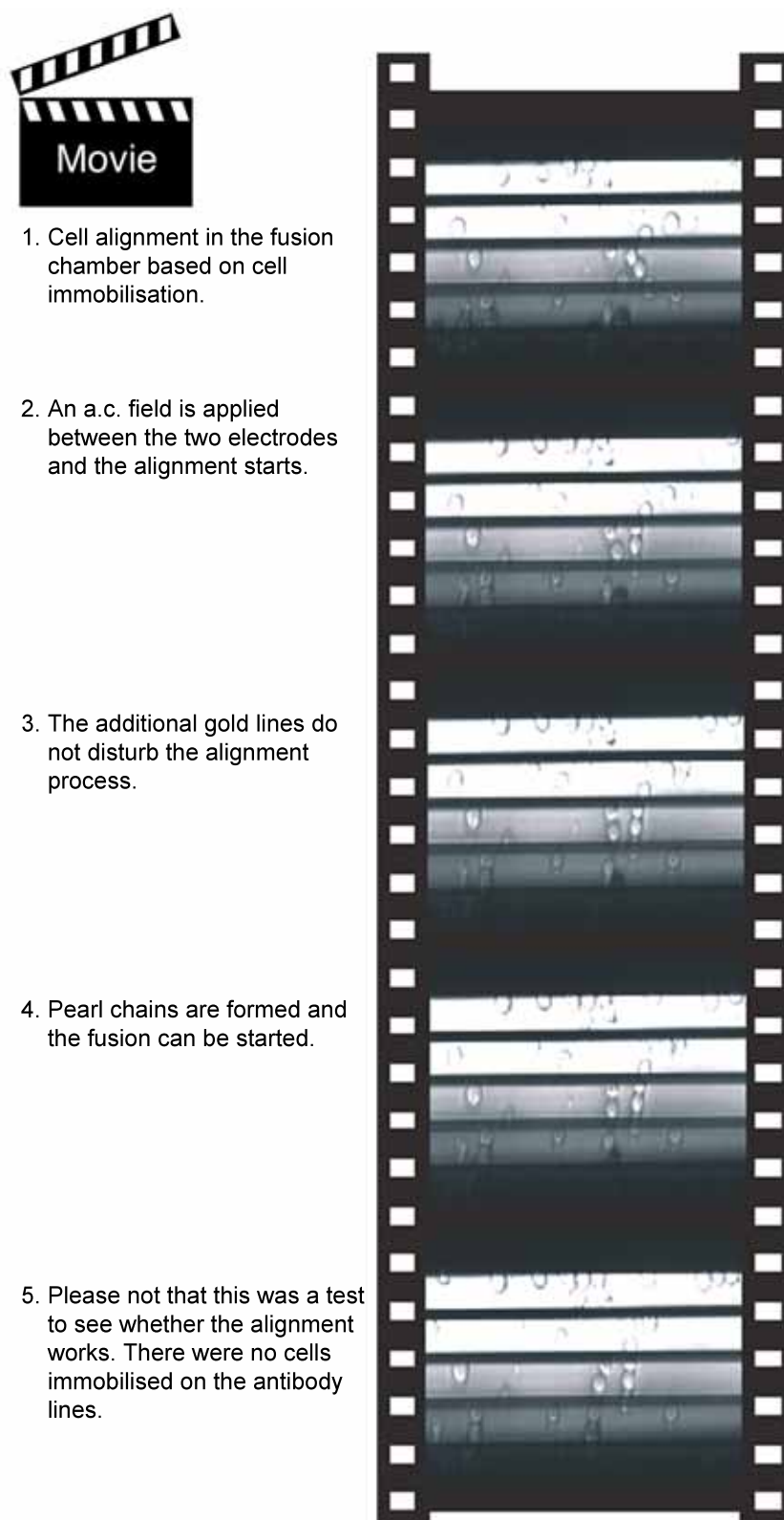


Figure 3.132: Cell alignment (KG-1) by dielectrophoresis in the newly developed electrofusion chamber based on immobilisation: The selected pictures have been extracted from a movie, which shows that cell alignment was successful. This movie is available on the enclosed DVD.

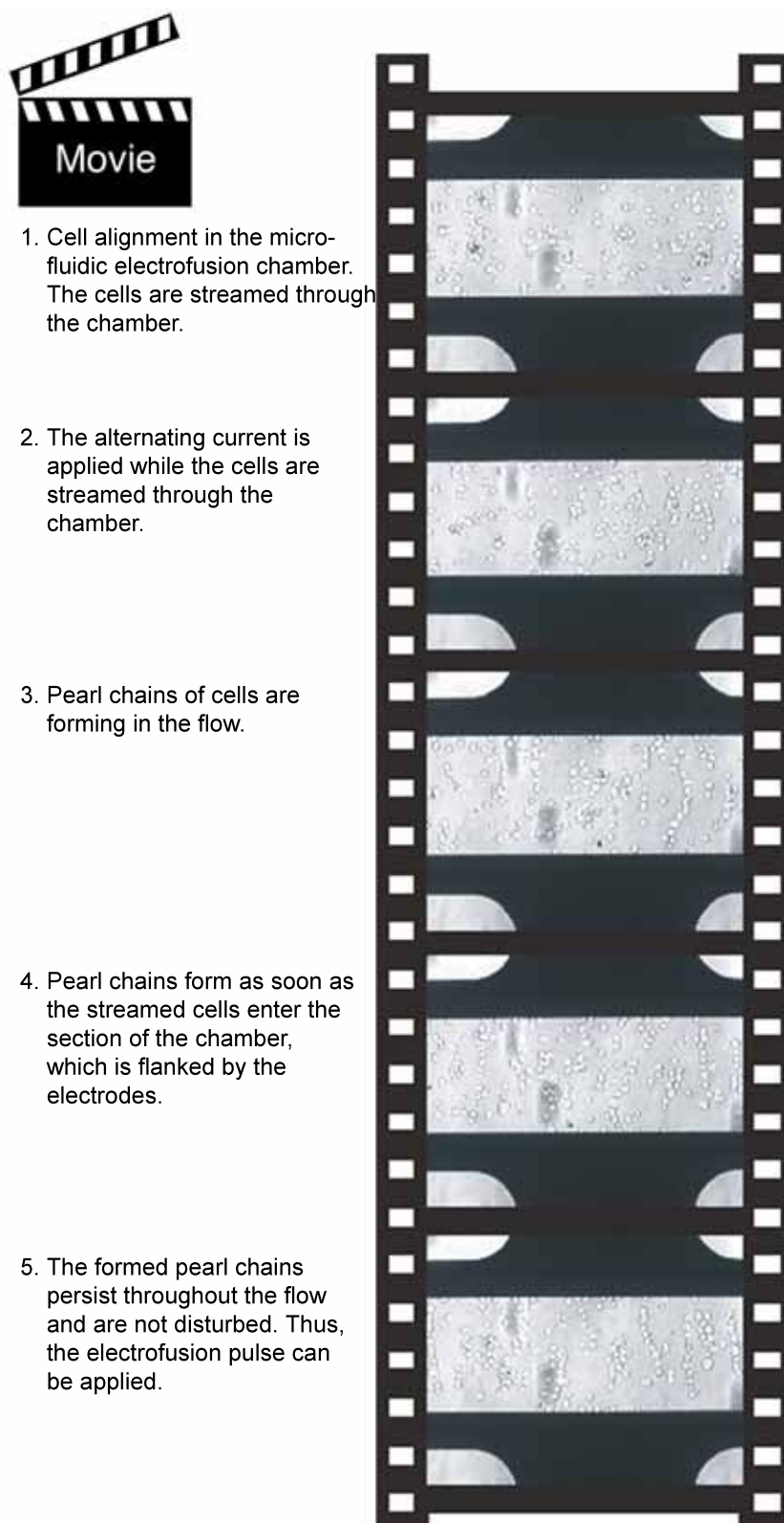


Figure 3.133: Cell alignment (KG-1) by dielectrophoresis in the newly developed microfluidic electrofusion chamber: The selected pictures have been extracted from a movie, which shows the alignment of cells in flow. This movie is available on the enclosed DVD.

having no contact or contact to just one electrode (see figure 3.130A). When, subsequently, the fusion pulse (d.c.) is applied, the pearl chains are stretched (figure 3.130B) until they have contact with both electrodes (figure 3.130C). This electrode deformation force has been described by ZIMMERMANN and colleagues (ZIMMERMANN ET AL., 2000). It arises from the electrostatic interaction of the generated cell dipoles with the applied field and is thought to be responsible for an enhanced electroporation of mammalian cells. With the same settings as used in the last experiment (500V/cm for 30sec), the alignment process has been shown in a standard, an immobilisation based and a microfluidic electrofusion chamber (see figure 3.131, 3.132 or 3.133 on page 191 to 193, respectively).

Biological Parameters

The cell type, cell size and the properties of the cell membrane severely affect the choice of the electrical parameters for fusion and the fusion yield.

For the detection of hybrids after the fusion process, it is common technique that the fusion partners are stained with different fluorescent dyes before the fusion, enabling the detection of dual-fluorescent hybrids by FACS after the fusion has taken place (see figure 3.134). Widely-used vital cell dyes for this purpose are CellTracker probes (Molecular Probes, Eugene, USA), such as CMFDA (green) and CMTMR or CMRA (both orange).

Some of the experiments for this thesis gave reason to analyse, whether those dyes influence the fusion efficacy and thus the fusion process itself. Six different dyes were tested, including two dyes staining the cytosol of viable cells, two lipophilic dyes staining the membrane and two nucleic acid dyes staining the nucleus: CellTracker CMFDA (green) and CMRA (orange) freely diffuse into the cell. They are nonfluorescent until cytosolic esterases cleave off their acetate groups, producing membrane-impermeant brightly fluorescent products, which accumulate in the cytosol. Vybrant DiO (green) and DiI (orange) are long-chain dialkylcarbocyanines, which stain the cell membranes due to their lipophilic character. SYTO11 (green) and SYTO17 (orange) are cell-permeant nucleic acid stains that show a large fluorescent enhancement upon binding nucleic acids, thus staining the nucleus.

The influence of those dyes of the membrane permeabilisation of MCF-7 cells in comparison to a unstained negative control were determined by electroporative dye uptake (NEUMANN ET AL., 1998) and are shown in table 3.2. The cells were pulsed twice (n=2) with a 20 μ s long pulse of a voltage of 1.8kV/cm in the presence of trypan blue. Trypan blue is an established

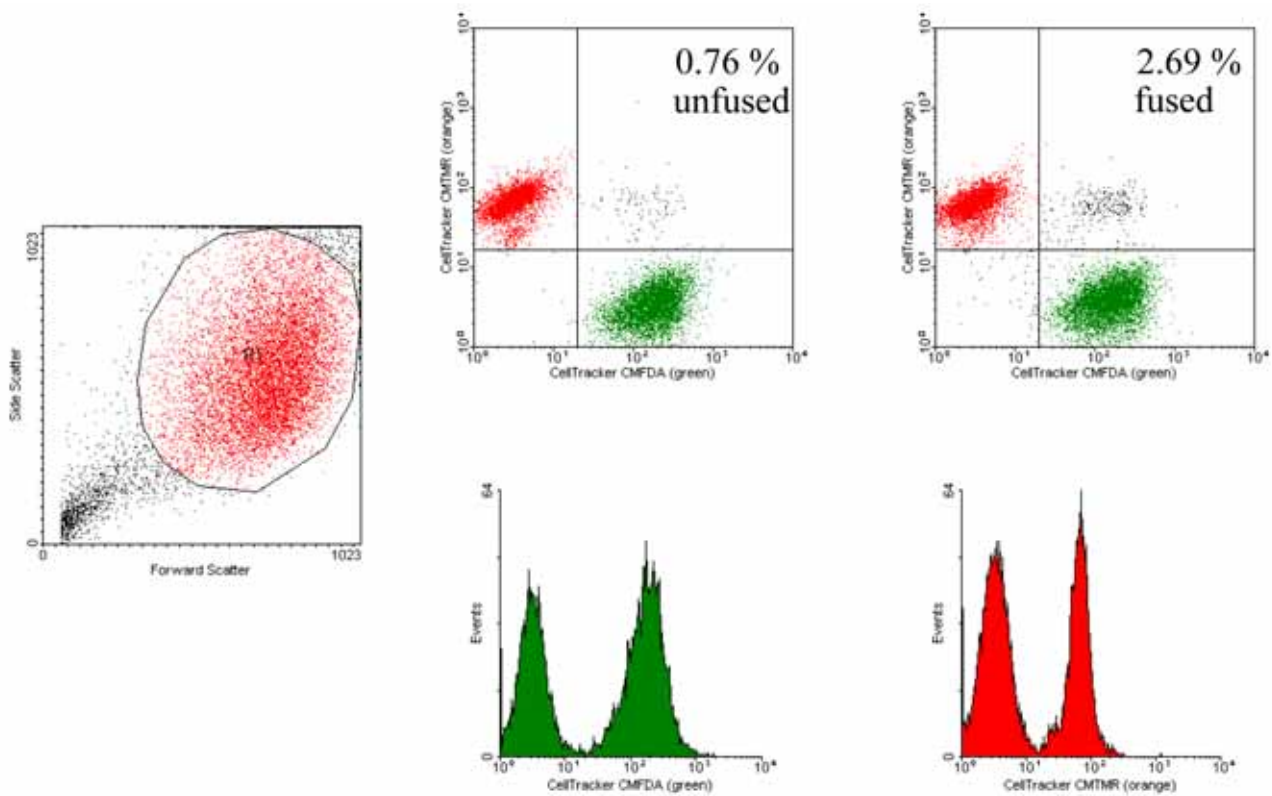


Figure 3.134: FACS analysis of a fusion process. Measurements before and after fusion pulse application are shown. The fusion partners are stained with CMFDA green and CMTMR orange to distinguish the two populations by means of FACS.

Table 3.2: Permeabilisation of MCF-7 cells as subject to different cellular stains

Dye	Stained compartment	Colour spectrum	percentage of permeabilised cells	Viability after pulse (in %)
CMFDA	cytosol	green	16.6	85.3
CMRA	cytosol	orange	0.4	78.0
DiO	membrane	green	28.4	74.6
DiI	membrane	orange	5.9	64.9
SYTO11	nucleus	green	14.5	41.8
SYTO17	nucleus	orange	1.3	58.9
Neg. Ctrl	-	-	22.4	96.0

protein dye that does not penetrate intact cell membranes. After the pulse application the cell solution was incubated for a 10 min period at room temperature. Subsequently, the number N_c of coloured cells of the population was determined. To estimate the number of transiently permeabilised cells by pulse application, the number of stained cells had to be reduced by the number N_{irrev} of cells, which were irreversibly damaged by the applied electrical pulse. Therefore, another batch of cells were subjected to the pulses in the absence of trypan blue, and the dye was added after the incubation period of 10 min. The percentage of reversible permeabilised cells could then be calculated by the ratio of $N_c - N_{irrev}$ to N_t , the total number of the cell population.

The results showed that most of the used dyes reduced the poration yield. This could be explained by the fact that every substance, which interacts or penetrates the cell membrane, disturbs the regular bilayer structure, thus modifying membrane properties. For this reason, for the analysis of fusion processes, the fusion partners should be stained with cell type-specific antibodies after the fusion has taken place. Therefore, two antibodies were chosen, which selectively bind either dendritic cells or a breast cancer cell line. For MFC-7 and MDA-MB-231 anti-CD71/anti-HLA-DR were chosen as antibody pair (see figure 3.135).

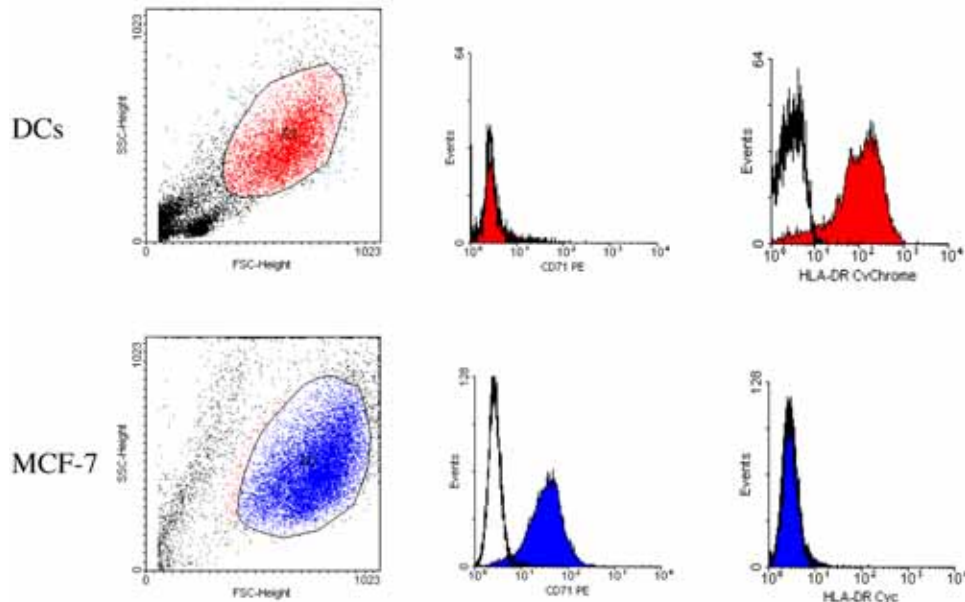


Figure 3.135: FACS analysis of DCs and the breast cancer cell line MCF-7. An antibody pair was found (CD71 and HLA-DR), which can be used after fusion to distinguish between the two fusion partners and hybrids by means of FACS.

The anti-CD71 antibody was used to stain the breast cancer cell lines, while dendritic cells are negative for CD71, and the anti-HLA-DR antibody was used to stain the DCs independently from their maturation status, but does not stain the breast cancer cells. This allows for the undisturbed fusion of the cells without the negative influence of intracellular staining.

Summary

Three important parameters for electrofusion were analysed and optimised to assure an optimal, undisturbed fusion process for the electrofusion of dendritic cells and breast cancer cells.

3.3.2 Fusion

Overview

This section discusses the optimisation of the electrofusion process and its parameters. It relates to the special application of fusing dendritic cells and breast cancer cells.

The experimental parameters for cell electrofusion comprise field strength, pulse length, number of pulses and cell concentration. For the fusion efficacy a complex dependence on field strength, pulse length and number of pulses is suggested. The optimisation of all those parameters is essential. If, for example, the strength, duration or number of fusogenic pulses is chosen wrongly, cell lysis instead of cell fusion can occur, due to an irreversible breakdown of the cell membrane (see figure 3.136). If, in contrast, the parameters are chosen in the right way, cell fusion of two or more cells can be observed (see figure 3.137 and figure 3.138 on page 198 and 199).

The progression of the fusion process between two adjacent KG-1 cells after the application of a single pulse (field strength and pulse duration) was monitored under a light microscope. The different phases of the fusion process, such as alignment, formation of fusion point and fusion neck, establishment of cytoplasm continuity (plasmogamy) and rounding of the hybrid during post-alignment were observed.

The ideal fusion parameters such as field strength, pulse duration and number of applied pulses, vary according to the cell type, and especially the cell diameter, and must be determined

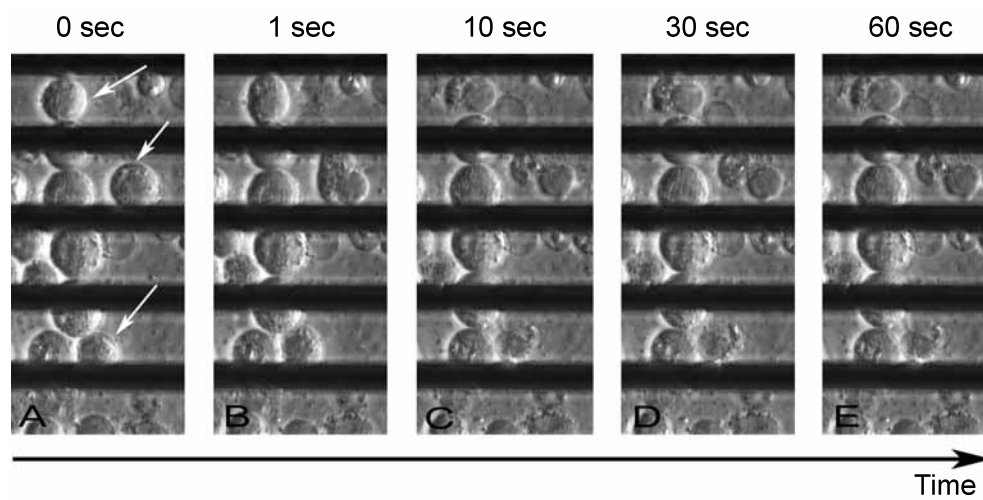


Figure 3.136: Series of pictures taken within 1min , which show the lysis of KG-1 cells in the electrofusion chamber based on immobilisation. The white arrows in A) mark the cells, which were lysed by the application of one pulse of $2.5\text{kV}/\text{cm}$ for $25\mu\text{s}$

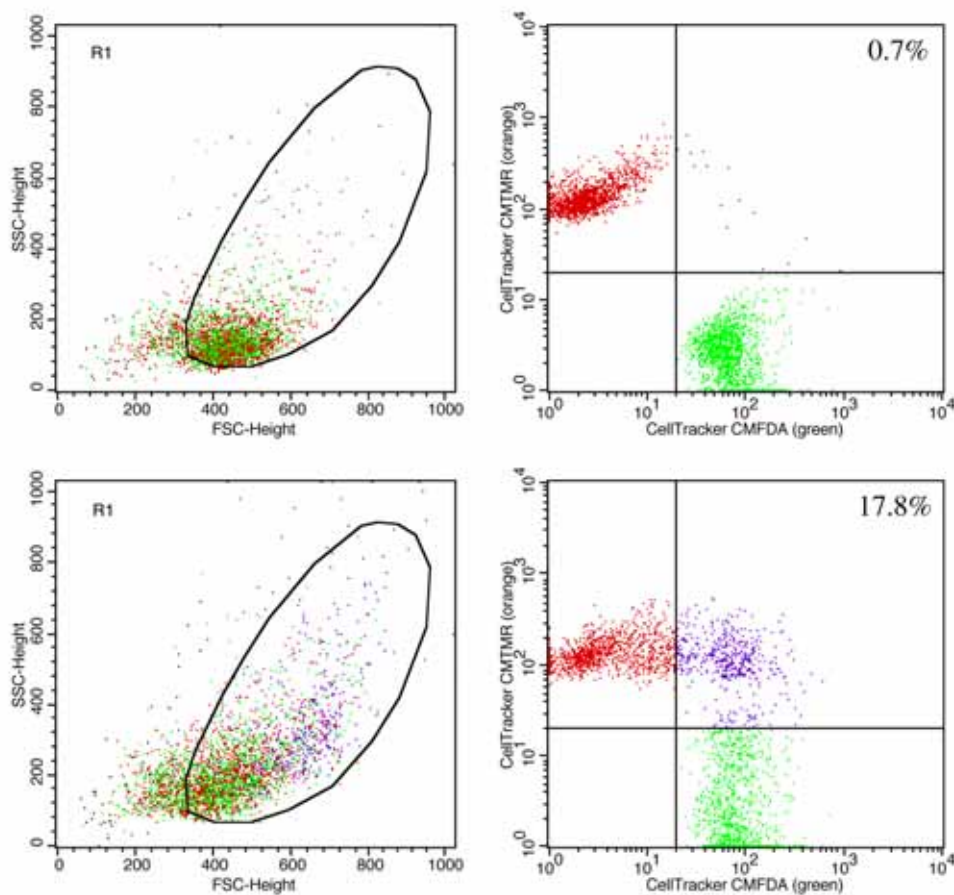


Figure 3.137: Homologous fusion of T47D breast cancer cells

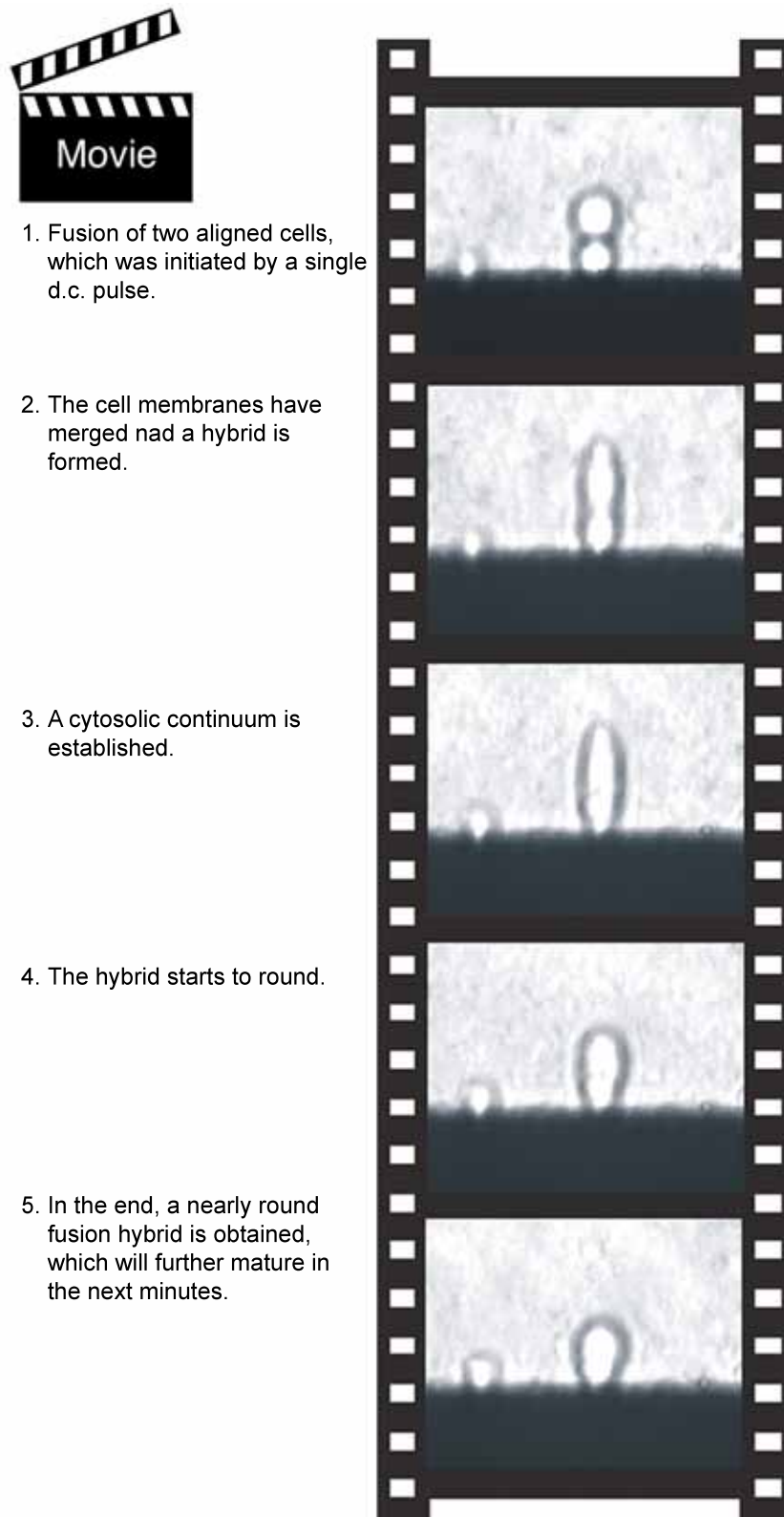


Figure 3.138: Fusion Phases: The selected pictures have been extracted from a movie, which shows the evolution of the fusion process between two adjacent KG-1 cells. Details from a series of images captured at times of 1 to 60sec after pulse application. This movie is available on the enclosed DVD.

by experiment. An empirical formula is often used as a starting point for the optimisation of the electrical parameters (see Manual Multiporator from Eppendorf):

$$E_C = \frac{V_C}{0.75 \cdot d} \quad (3.1)$$

with

E_C : Critical field strength (V/cm)

V_C : Permeation voltage (for eukaryotic cells: 1V at 25°C)

d : Cell diameter (cm)

With the help of this formula, the critical field strength for permeating the membrane of spherical cells can be estimated. The critical field strength is defined as the voltage at which the cell membranes are permeated at points of the cell membrane, which are vertical to the field lines. The parameters needed for the calculation are the cell diameter and the permeation voltage of the cell membrane. The latter can be assumed as 1 V for a single membrane and 2 V for membranes that are arranged in series. The cell diameter has to be determined under hypoosmolar conditions for a correct calculation of the critical field strength.

In general, small cells require much higher field pulses than cells with a bigger cell diameter to permeate the membrane by inducing an reversible electrical breakdown of the cell membrane. This local perforation of the cell membrane enables two or more cells to fuse, if the pre-requisite, a direct contact between the cells, has been established. Again, the number of cells that can be fused depends on the type and size of the cells, the field strength of the electrical pulse and on the osmolar conditions of the fusion buffer.

After the formation of a local fusion point within the cell membranes that are in contact, the primary fused membrane sections expand, resulting in a so-called plasmogamy. This is followed by the rounding off the fusion products. The time required for the various fusion stages is depending on many parameters such as cell size, the condition of the cytoskeleton, the temperature, the ion environment (Mg^{2+} , Ca^{2+}) and probably the extent of the primary fused membrane section as well. In general, it is advised to leave the cells undisturbed for a 5 to 10 minute post-fusion cultivation period.

Using the equation 3.1 for the calculation of the fusion voltage, the obtained parameter was used as a basic value for the optimisation of the fusion parameters. The voltage was varied in a range from 250 V to 15 kV with a pulse length from 10 to 300 μs . The cells were subjected to 1 to 10 electric field pulses.

More than 200 different combinations of experimental fusion conditions were quantified using FACS and dye penetration assays for analysis (see Material and Methods). No fusion of dendritic cells and breast cancer cells was obtained. The optimised electrical parameters for pore formation in these cell types confirm the findings (see table 3.3). The fusion parameters for DCs and breast cancer cells are differing too much to allow a fusion to take place. If the fusion parameters for breast cancer cells are chosen for the heterologous fusion of DCs and breast cancer cells, the DCs are not perforated. Without pores being induced in the cell membranes of both fusion partners, no heterologous hybrids can be obtained. On the other hand, if the fusion parameters are chosen to electropermeate the dendritic cells, the pulse voltage is far too high for breast cancer cells to survive.

Table 3.3: Optimised fusion parameters for different cell types

Cell type	fusion voltage (in kV/cm)	pulse length (in μs)	number of pulses
MCF-7	1.8	20	1
MDA-MB-231	1.8	20	2
DCs	8.5	65	4

Although no DC-breast cancer hybrids were obtained, due to the discrepancy in the electrical parameters, sometimes dual fluorescent events could be observed by FACS. The occurrence of dual fluorescent events should not be used as exclusive argument for the existence of heterologous hybrid cells, since cell aggregates can occur as double fluorescent events in FACS, as well. This results in wrong outcomes, if the upper right quadrant in a dual fluorescent FACS dot plot is used to quantify the percentage of hybrid formation.

In addition to the occurrence of double fluorescent events due to cell aggregates, a shifting of cell populations in FACS dot plots was found, due to electrical effects on the cells. The effect is intensified the higher the applied voltage (see figure 3.139). The cell populations migrate into the upper right quadrant of the FACS dot plot.

The displacement of the cell populations, which was observed independently from the type of fusion buffer or the used cell staining method, would lead to a wrong quantification of the formation of hybrids during electrofusion, if the upper right quadrant in a double fluorescent dot plot is used for analysis. To avoid this miscalculation, either another analysis method such as microscopy should be used in parallel, or the FACS analysis can be adjusted to take the

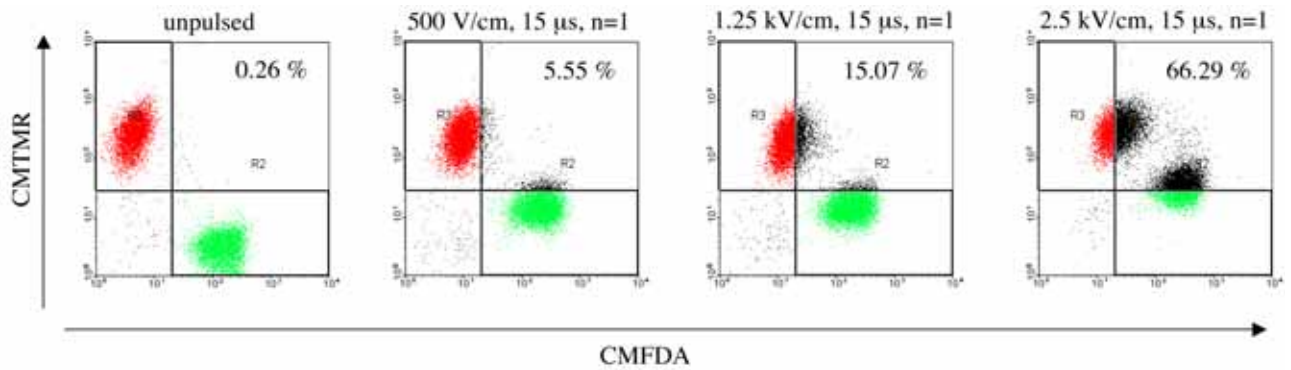


Figure 3.139: Shifting of cell populations in connection with the treatment with a fusion pulse. The displacement of the populations in the FACS dot plot increases with the applied voltage.

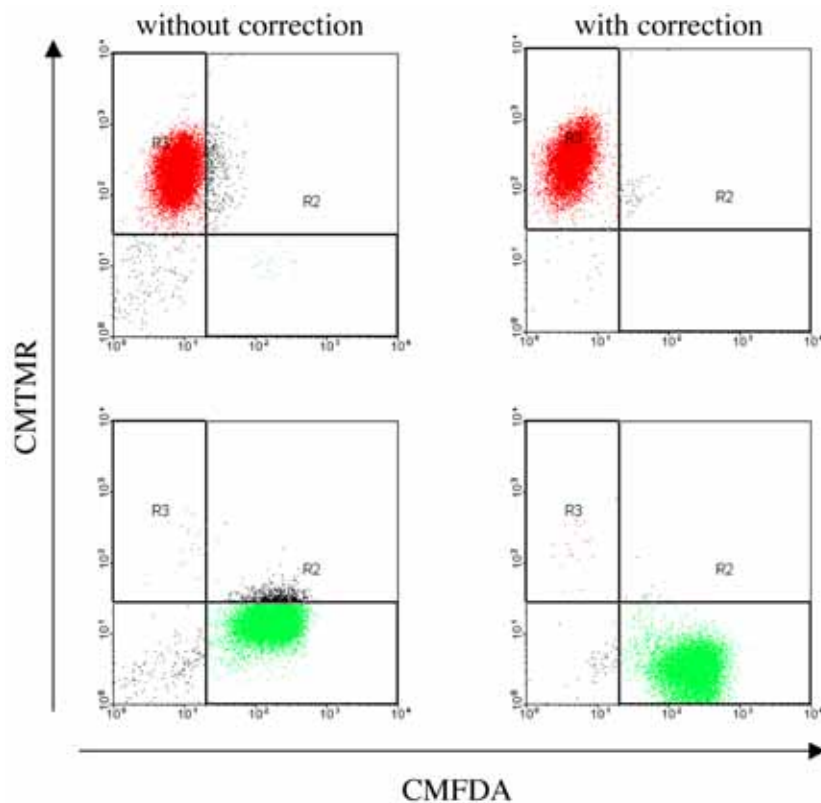


Figure 3.140: Correction of the cell population displacement by adjusting the dot plot quadrants according to a pre-fused negative control

shifting into calculation (see figure 3.140).

In general, for the fusion evaluation, the quadrants of the dot plot are arranged in that way that the two starting populations are placed inside the upper left and lower right quadrant. To avoid the displacement of the populations into the quadrant of evaluation after the fusion process, the quadrant adjustment should be based on a pre-fused negative control. This would mean that not only a mixture of the fusion partners is used, but a mixture of the two cell types, which, each for itself, was subjected to the fusion pulse.

Summary

The fusion of dendritic cells and breast cancer cells could not be realised, since a big discrepancy in the electrical parameters exist. Nevertheless, dual fluorescent events could be observed in FACS analysis, which are partly due to cell aggregates and partly due to the shifting of the cell populations in the FACS dot plot.

3.4 Immunological Evaluation

Overview

The cell detachment using an acid solution with a pH of 2, which was used in the immobilisation approach, required an analysis by immunological methods to ensure that the functions of a dendritic cell are not effected in a negative way. In addition, the immunological effect of the outcome of the accomplished fusions was determined and is presented in this section.

After the development of the electrofusion chambers one remaining task was to control, whether the immunostimulatory capacity of the dendritic cells was not affected negatively by the cell detachment procedure used in the immobilisation approach. The detachment by applying an acid solution of a pH of 2 could for example influence protein integrity, such as the MHC molecules on the cell surface. For this reason the allostimulatory capacity of pH 2 treated DCs was tested in a mixed leukocyte reaction (see figures 3.141 and 3.142 on page 205).

Technique Box

Mixed Leukocyte Reaction (MLR)

Application:

In this case: Test for the immunostimulatory capacity of dendritic cells

Requirements:

Dendritic cells and leukocytes from different individuals with MHC mismatch (allogeneic leukocytes), flow cytometer for analysis

Method:

A mixed leukocyte reaction can be used as readout of the dendritic cell allostimulatory capacity. This means that DCs are able to activate T-lymphocytes based on a difference in MHC phenotypes. Therefore, dendritic cells of one individual are co-cultivated in different ratios with T-cells from a second individual with MHC mismatch. The allogeneic T-cells recognise the MHC molecules of the DCs as nonself, which causes activation and proliferation. The recognition of the MHC molecules by the T-cells can take place in two ways. The T-cell receptor can either bind to the MHC molecules through a peptide, which is bound by the allogeneic MHC molecule (peptide-dominant binding) or bind directly to distinctive features of the non-self MHC molecule (MHC-dominant binding) (JANEWAY et al., 2001).

In general, the T-cell stimulation by cross-reactive recognition is larger the more MHC complexes and co-stimulatory molecules are expressed by the dendritic cells. The T-cell activation is determined by measurement of their proliferation and their expression of proliferation markers, such as CD25 (interleukin-2 α chain) and CD71 (transferrin receptor) (NGUYEN et al., 2003).

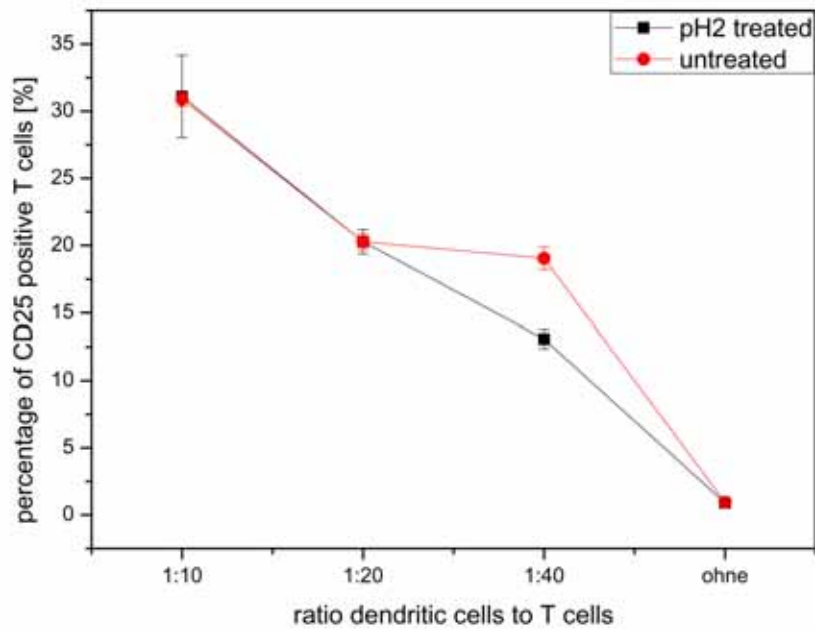


Figure 3.141: Activation of positive T-cells (CD3) was assessed by CD25 (α -chain of the IL-2 receptor) staining after 4 days of co-cultivation in a MLR. Shown is one representative donor out of two. The experiments were made in triplicates and results are presented as mean \pm SD.

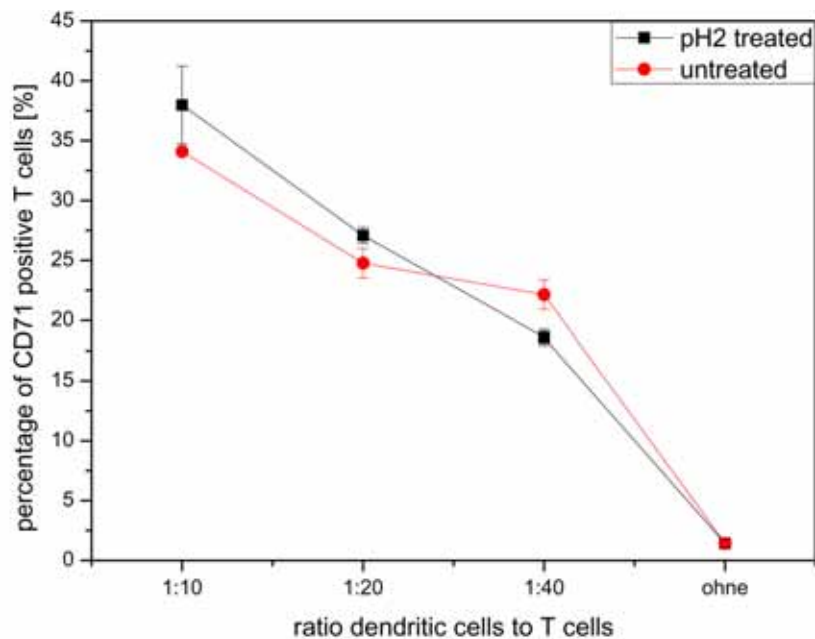


Figure 3.142: Activation of positive T-cells (CD3) was assessed by CD71 (transferrin receptor) staining after 4 days of co-cultivation in a MLR. Shown is one representative donor out of two. The experiments were made in triplicates and results are presented as mean \pm SD.

The pH 2 treated dendritic cells were compared in a mix leukocyte reaction with untreated dendritic cells. The activation of T-cells in the MLR was assessed by the analysis of CD25 and CD71 activation marker expression on T-cells after four days of co-cultivation with DCs at different ratios (1:10, 1:20 and 1:40, respectively). Both, CD25 and CD71 expression analysis did not reveal any significant differences of pH2 treated DCs compared with untreated DCs. Differences of the percentage of positive CD25 and CD71 T-cells might be due to different expression kinetics of both surface proteins.

A further task was the analysis of the obtained hybrids for the stimulation of T-cells in an autologous stimulation reaction (see Technique Box on page 207 for explanation of the method). Thereby, the biological activity of the hybrids for the generation of tumour-specific T-lymphocytes was tested. Since the generation of hybrids by electrofusion could not be validated, the fusion outcomes were used for this assay. Dendritic cells, which were subjected to four 65 μ s long fusion pulses with a pulse strength of 8.5 kV/cm in the presence of MCF-7 tumour cells in a ratio of 1:1 were compared in their immune stimulatory efficacy *in vitro* with MCF-7 lysate-pulsed dendritic cells (see figure 3.143).

By the application of the four fusion pulses with the chosen fusion parameters most of the MCF-cells were destroyed as described in section 3.3.2. To further explore this situation another approach was included in the autologous T-cell stimulation assay: dendritic cells were loaded with MCF-7 cell debris, which was obtained by the application of four fusion pulses with the above defined parameters (dendritic cells loaded with pulsed MCF-7).

The results showed that an expansion of the T-cells could be obtained in every approach, whereas the dendritic cells loaded with pulsed MCF-7 cell debris performed best and resulted in a 14.1-fold expansion. The expansion factors of the other approaches were accounted as 6.5-fold and 3.9-fold for the pulsed mixture of DCs and MCF-7 breast cancer cells and the DCs loaded with MCF-7 lysate, respectively.

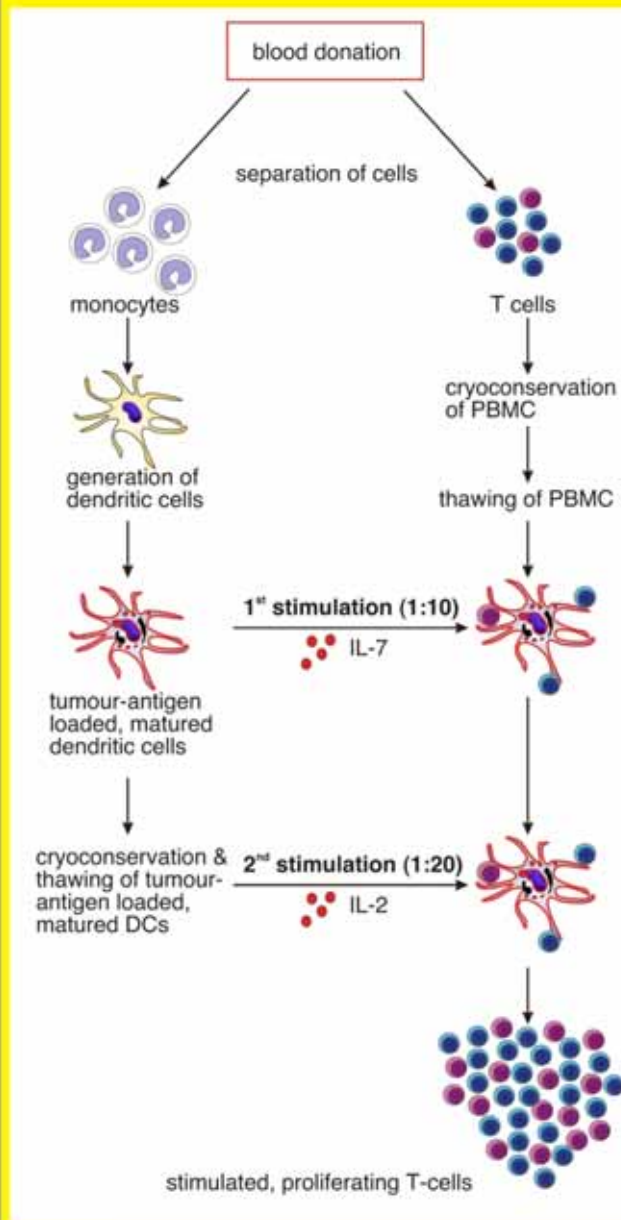
The expanded T-cells were further analysed by flow cytometry. The cytotoxic T-cells (CD8⁺) were divided into four subsets: naïve, central memory (CM), effector memory (EM) and effector memory RA (EMRA) T-cells. These subsets were identified based on cell surface markers, in particular the expression of CCR7, a molecule that mediates homing to lymph nodes through endothelial venules, and CD45. The latter is expressed in various isoforms, which differ in their relative molecular mass. The isoform with the highest molecular mass is called CD45RA, the one with the lowest CD45RO.

Technique Box**Autologous T-cell stimulation****Application:**

Test for the specific immune stimulatory capacity of dendritic cells

Requirements:

Dendritic cells and T-cells from the same donor (autologous), cell counting device, flow cytometer for further analysis of the stimulated T-cells

**Method:**

The picture on the left shows a scheme of the autologous stimulation of T cells with tumour-antigen, loaded dendritic cells. Before stimulation, the dendritic cells can be loaded with tumour-associated antigens by various strategies such as lysate-pulsing or fusion.

Dendritic cells are loaded with tumour-associated antigens and are co-cultured with autologous PBMCs at a ratio of 1:10 in the presence of IL-7.

After 7 days the PBMCs are re-stimulated with thawed tumour-antigen loaded, mature dendritic cells at a ratio of 1:20 in fresh medium containing IL-2.

The stimulated and proliferating T-cells are analysed seven days after the 2nd stimulation. The cell number is determined and the different T cell subsets can be analysed by flow cytometry.

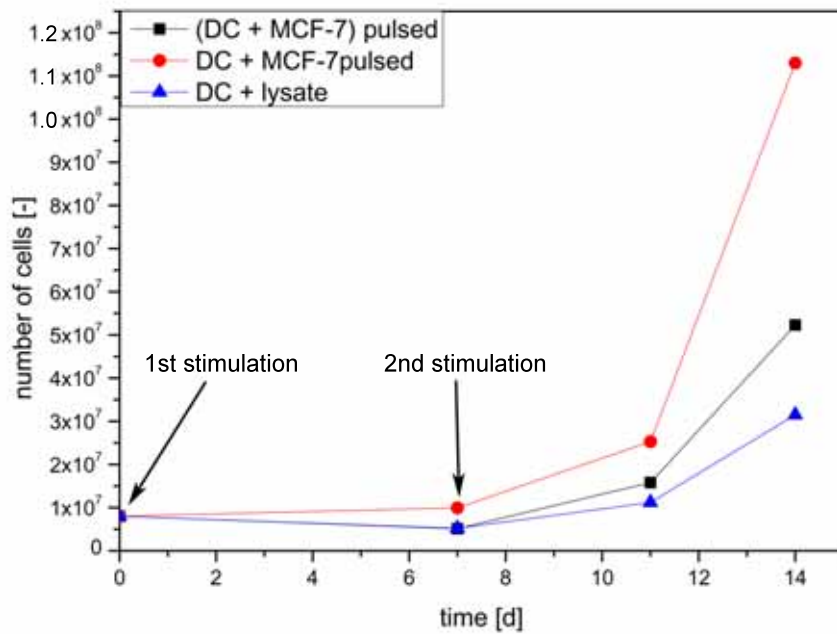


Figure 3.143: Proliferation of autologous T-cells stimulated with DCs pulsed together with MCF-7 cells or DCs loaded with pulsed MCF-7. Dendritic cells loaded with a MCF-7 lysate were used as control. Shown is one representative donor out of two.

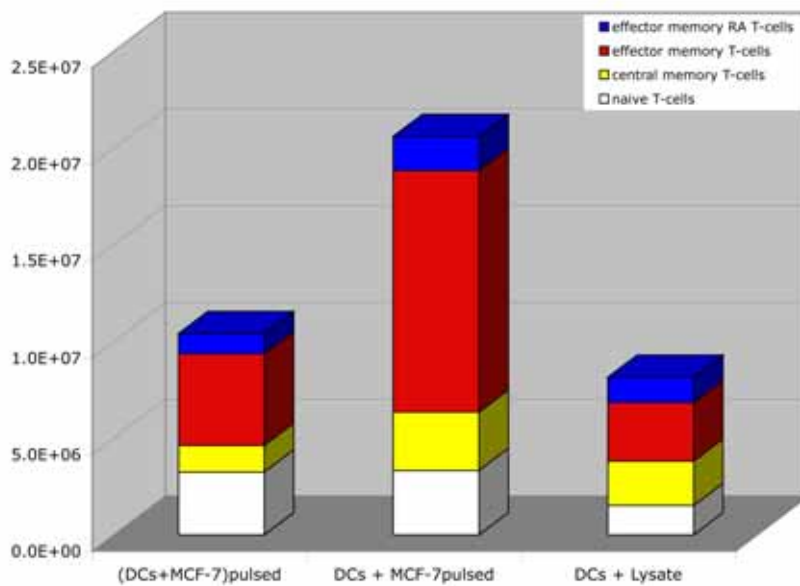


Figure 3.144: Expansions of different cytotoxic T-cell (CTL, CD8⁺) subsets obtained from autologous T-cell stimulation (see figure 3.143).

Human naïve T-cells are CCR7⁺ and CD45RA⁺. When stimulated, they can undergo clonal expansion, culminating in a higher frequency of antigen-specific T-cells with more rapid effector function. These antigen-specific T-cells belong to the memory T-cell pool, which functions as a dynamic source of antigen-experienced T-lymphocytes that accumulate over the lifetime of an individual. Antigen-specific or memory T-cells can be divided into two subpopulations, CCR7⁺ CD45RO⁺ central memory T-cells (T_{CM}) and CCR7⁻ effector memory T-cells. The latter are further sub-divided into CD45RO⁺ effector memory cells (T_{EM}) and CD45RA⁺ effector memory cells (T_{EMRA}) (see table 3.4).

Table 3.4: Memory T-cell subsets

	T_{naive}	T_{CM}	T_{EM}	T_{EMRA}
CCR7	+	+	-	-
CD45RO	-	+	+	-
CD45RA	+	-	-	+

Effector memory T-cells form the protective memory of the immune system. They are able to migrate to inflamed peripheral tissues and display immediate effector function. Central memory T-cells in contrast home to secondary lymphoid organs and have no effector function, but may proliferate and differentiate into effector cells in response to antigenic stimulation (SALLUSTO ET AL., 2004).

The expanded cytotoxic T-cells from the autologous T-cell stimulation assay were analysed by flow cytometry for the different T-cell subset, such as naïve, central memory, effector memory and effector memory RA T-cells (see figure 3.144 on page 208). The results from the phenotypical analysis of the proliferation assay showed that the most effector T-cells were obtained when the T-cells were stimulated with dendritic cells, which were loaded with pulsed MCF-7 cells.

Summary

The outcome of the fusion experiments showed immunostimulatory capacity with a proven expansion of cytotoxic effector cells in an autologous T-cell stimulation assay. Additionally, the obtained T-cell expansion was superior to the stimulation with lysate-pulsed dendritic cells.

Chapter 4

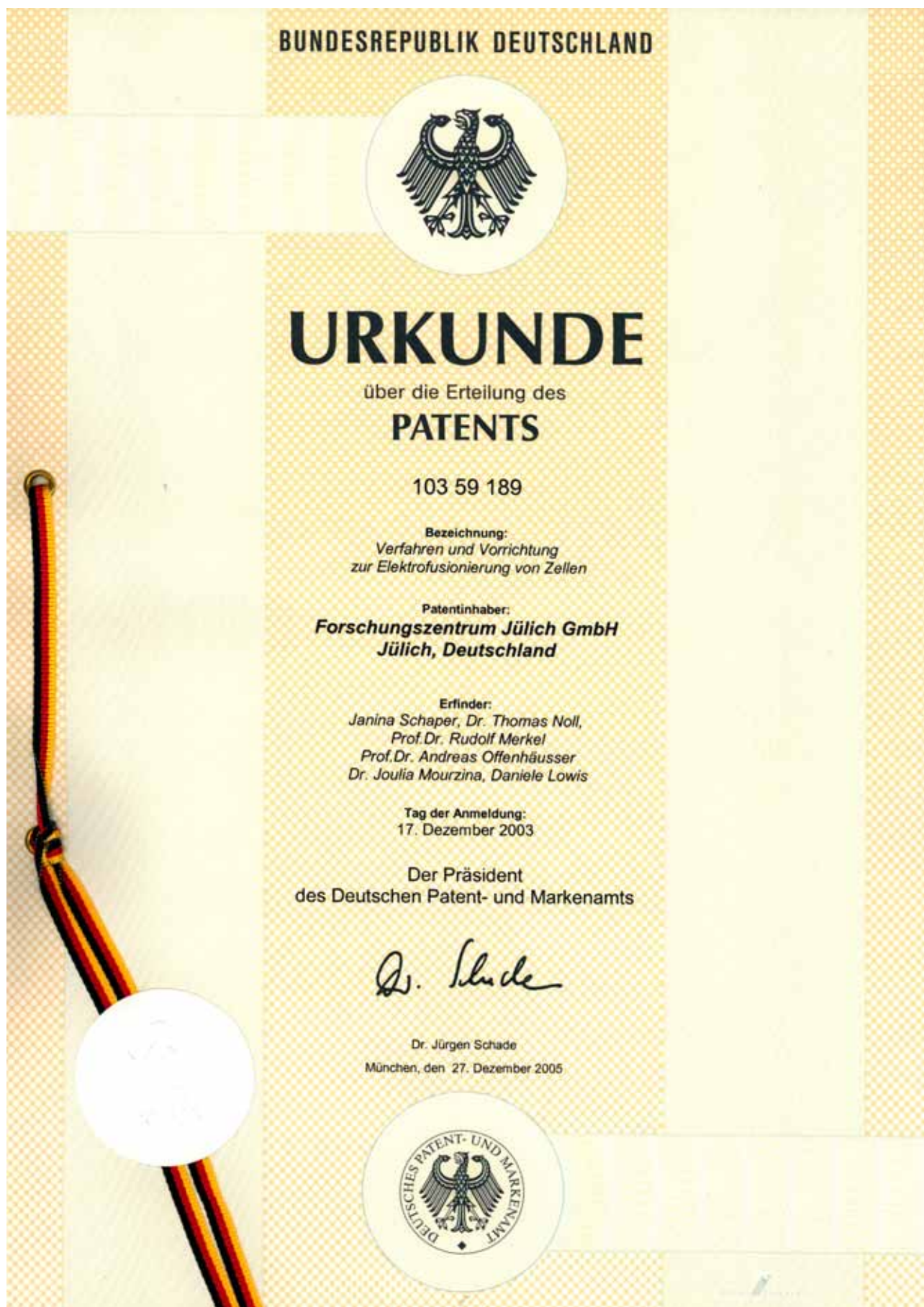
Patent Application

The developed electrofusion chambers for arranged electrofusion of mammalian cells as described in sections 3.1 and 3.2 were both filed as patents. The patent applications were handed in on 12th December 2003 at the German Patent Office and were published 18 months later.

For the electrofusion chamber based on immobilisation seven citations, mostly patent applications from Japan (see patent specification on page 213), were taken into account for the assessment of the patent capability. The immobilisation approach was compared with other fusion methods, where the cells were adsorped onto electrodes, attached to cultivation sheets or seperated by suction during the fusion process. In the end, all citations could be debilitated and the patent was granted on the 22nd December 2005 (DE 103 59 189). No objections were raised within the period for objection.

For the microfluidic electrofusion chamber only three Japanese patent applications were asserted as citations, but they mostly represent methods for single cell fusion. For the microfluidic approach the patent application is still pending.

In the following, the patent specification for the immobilisation approach and the published patent application for the microfluidic approach, respectively, are displayed.





(19)
Bundesrepublik Deutschland
Deutsches Patent- und Markenamt

(10) **DE 103 59 189 B4 2005.12.22**

(12)

Patentschrift

(21) Aktenzeichen: **103 59 189.3**
 (22) Anmeldetag: **17.12.2003**
 (43) Offenlegungstag: **28.07.2005**
 (45) Veröffentlichungstag
 der Patenterteilung: **22.12.2005**

(51) Int Cl.⁷: **C12M 1/42**
C12N 13/00

Innerhalb von drei Monaten nach Veröffentlichung der Patenterteilung kann nach § 59 Patentgesetz gegen das Patent Einspruch erhoben werden. Der Einspruch ist schriftlich zu erklären und zu begründen. Innerhalb der Einspruchsfrist ist eine Einspruchsgebühr in Höhe von 200 Euro zu entrichten (§ 6 Patentkostengesetz in Verbindung mit der Anlage zu § 2 Abs. 2 Patentkostengesetz).

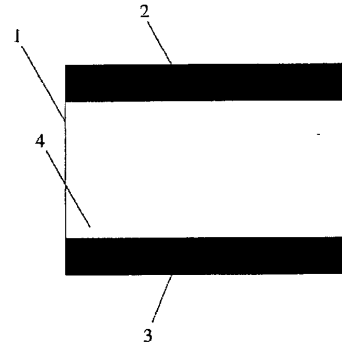
(73) Patentinhaber:
Forschungszentrum Jülich GmbH, 52428 Jülich, DE

(72) Erfinder:
Schaper, Janina, 52428 Jülich, DE; Noll, Thomas, Dr., 52428 Jülich, DE; Merkel, Rudolf, Prof. Dr., 52428 Jülich, DE; Offenhäusser, Andreas, Prof. Dr., Eynatten, BE; Mourzina, Joulia, Dr., 52428 Jülich, DE; Lowis, Daniele, 52249 Eschweiler, DE

(56) Für die Beurteilung der Patentfähigkeit in Betracht gezogene Druckschriften:
US 62 38 909 B1
WO 96/39 417 A1
JP 63-2 14 185 A
JP 60-2 51 876 A
JP 02-2 83 272 A
JP 01-2 15 274 A
JP 0223-32 A

(54) Bezeichnung: **Verfahren und Vorrichtung zur Elektrofusionierung von Zellen**

(57) Hauptanspruch: Verfahren zur Elektrofusion von heterologen Zellen
 dadurch gekennzeichnet,
 dass folgende Schritte durchgeführt werden:
 – in Kontakt bringen einer mit Haftstreifen (5) ausgestatteten Oberfläche (4) mit einer ersten Zellart (6),
 – Abspülen der nicht an den Haftstreifen (5) anhaftenden Zellen mit einer Flüssigkeit,
 – in Kontakt bringen der so behandelten Oberfläche (4) mit einer zweiten Zellart (7), wobei die zweite Zellart (7) auf Haftstreifen (5a) aufgebracht wird, die zwischen den Haftstreifen (5) für die erste Zellart (6) angebracht sind
 – Anlegen einer Spannung auf der Ebene der Haftstreifen (5), die senkrecht zu den Haftstreifen (5) verläuft,
 – Applizieren eines elektrischen Fusionspulses.



DE 103 59 189 B4 2005.12.22

Beschreibung

[0001] Die Erfindung betrifft ein Verfahren und eine Vorrichtung zur Elektrofusionierung von Zellen nach dem Oberbegriff des Anspruchs 1.

Stand der Technik

[0002] In den letzten Jahren ist der Fusion von Zellen zur Herstellung heterologer Hybride immer mehr Bedeutung zugekommen. Die Fusionsprodukte finden Anwendung in der Krebstherapie (Hybride aus dendritischen Zellen und Tumorzellen), bei der Herstellung von monoklonalen Antikörpern (Hybridomazellen), in der Reproduktionstechnologie (Hybride aus Eizellen und Spermazellen) und in vielen anderen Gebieten.

[0003] Für die Erzeugung von Zellhybriden stehen grundsätzlich drei Methoden zur Auswahl: Die Fusion der Zellen kann entweder chemisch (mittels Polyethylenglycol), rezeptorvermittelt oder elektrisch induziert werden, wobei im Hinblick auf die spätere klinische Anwendung die Methode der Elektrofusion eindeutig von Vorteil ist.

[0004] Die Standardmethode der Elektrofusion sieht vor, dass die beiden Fusionspartner (Zelltyp 1 und Zelltyp 2) gemischt und in eine Fusionskammer gegeben werden. Eine solche Kammer besteht aus zwei Elektroden, die in einem definierten Abstand angeordnet sind. In den so entstehenden Zwischenraum wird die Zellsuspension (Mix aus Zelltyp 1 und Zelltyp 2) gegeben. Durch Anlegen eines schwachen elektrischen Gleichstrom-Feldes werden die Zellen in engen Kontakt miteinander gebracht. Bei diesem sogenannten Alignment werden durch Anlegen des Feldes Dipole innerhalb der Zellen induziert. Die Zellen wandern dann in den Bereich der höchstens Feldintensität und reihen sich dabei in einer sogenannten „Perlenkette“ an. Anschließend werden die Zellen durch einen kurzen Puls fusioniert.

[0005] Wenn die Aneinanderreihung der beiden Zelltypen in der Perlenkette statistisch verteilt erfolgen würde, läge bei einer 1:1-Mischung der Zelltypen die maximale theoretische Bildung von heterologen Hybriden bei 50 %. Real wurden bisher nur 10–20 % erreicht, da zum einen nicht alle Zellen fusionieren und zum anderen homologe Fusionen gegenüber heterologen bevorzugt werden. Des Weiteren ist zu beobachten, dass schon in der Aufreihung der Zellen keine statistische Verteilung vorliegt, sondern sich Zellen gleichen Zelltyps (auf Grund ähnlicher Zell-eigenschaften) anhäufen.

[0006] Dadurch treten die ungewollten homologen Fusionen gehäuft auf.

[0007] Zur Lösung dieses Problemes gab es in den

letzten Jahren grundsätzlich nur drei Ansätze. Jaroszeski et al. versuchten bei der „mechanisch vereinfachten Zell-Zell-Fusion“ (Biophys. J. 1994, 67: 1574–1581) die beiden Zelltypen in Monoschichten auf einem Filter anzuordnen und diese beiden Filter dann mechanisch miteinander in Kontakt zu bringen. Die mit dieser Methode erreichte maximale Fusions-effizienz lag bei 10 %.

[0008] Die Arbeiten von Strömberg et al. (Anal. Chem. 2001, 73: 126–130), die Einzelzellen microfluidisch anordneten, oder von Bakker Schut et al. (Biophys. J. 1993, 65(2): 568–72), die die beiden Fusionspartner durch eine Avidin-Biotin-Brücke aneinander banden, um dann die so gekoppelten Zellen in einem umgebauten Durchflusszytometer zu fusionieren, brachten bessere Ergebnisse bezüglich der Fusions-effizienz, sind aber nur für Einzelzellfusionen konzipiert. Für die Herstellung einer grossen Menge an vitalen Hybriden sind diese Methoden somit nicht ausgelegt.

[0009] Aus dem Abstract JP 02-2332 ist ein Verfahren zur Zellfusion bekannt, bei dem eine mit einem Haftstreifen ausgestattete Oberfläche mit einer ersten Zellart in Kontakt gebracht wird, die nicht haftenden Zellen mit einer Flüssigkeit abgespült werden, die so behandelte Oberfläche mit einer zweiten Zellart in Kontakt gebracht wird und dann die Zellfusion erfolgt.

[0010] Die Verfahren nach dem Stand der Technik führen zu niedrigen Fusionsausbeuten oder sind lediglich geeignet kleine Zellmengen zu fusionieren.

Aufgabenstellung

[0011] Es ist daher die Aufgabe der Erfindung ein Verfahren und eine Vorrichtung zu schaffen, mit denen Zellen, vorzugsweise verschiedenartige Zellen mit einer höheren Ausbeute fusioniert werden können. Es soll auch die Möglichkeit geschaffen werden, möglichst viele Zellen in kurzer Zeit zu fusionieren.

[0012] Ausgehend vom Oberbegriff des Anspruchs 1 wird die Aufgabe erfindungsgemäß gelöst mit den im kennzeichnenden Teil des Anspruchs 1 angegebenen Merkmalen. Weiterhin wird die Aufgabe durch die Vorrichtung nach Anspruch 13 gelöst.

[0013] Mit dem Verfahren und der Vorrichtung können nunmehr Fusionen, vorzugsweise heterologe Fusionen, mit einer hohen Ausbeute und in kurzer Zeit durchgeführt werden.

Ausführungsbeispiel

[0014] Im Folgenden soll die Erfindung beispielhaft erläutert werden. Die Figuren zeigen den schematischen Aufbau der erfindungsgemäßen Vorrichtung

DE 103 59 189 B4 2005.12.22

sowie Darstellungen von verschiedenen Stadien des erfindungsgemäßen Verfahrens.

[0015] Fig. 1: Eine Fusionskammer.

[0016] Fig. 2: Eine Fusionskammer mit Streifen von Haftmitteln.

[0017] Fig. 3: Eine Fusionskammer mit Zellen, die auf den Haftmitteln angebracht sind.

[0018] Fig. 4: Eine Fusionskammer in der zwei Zelltypen eingebracht sind.

[0019] Fig. 5: Eine Fusionskammer mit zwei Zelltypen, die in einem elektrischen Feld ausgerichtet sind.

[0020] Fig. 6a, b, c: Verschiedene Arten der Haftung von Zellen an einer Oberfläche.

[0021] Fig. 7a: Eine Ausführungsform ohne Haftstreifen.

[0022] Fig. 7b: Eine Ausführungsform mit einem breiten Haftstreifen.

[0023] Fig. 7c: Eine Ausführungsform mit einem breiten Haftstreifen, an dem Zellen der ersten Zellart anhaften.

[0024] Fig. 7d: Die Ausführungsform nach Fig. 7b bei der die erste und die zweite Zellart aufgebracht wurde.

[0025] Fig. 7e: Die mit den beiden Zellarten beschickte Ausführungsform gemäß Fig. 7b bei der ein elektrisches Feld angelegt ist.

[0026] In Fig. 1 ist eine Elektrofusionskammer 1 mit zwei Elektroden 2 und 3 dargestellt, die eine Oberfläche 4 der Elektrofusionskammer 1 begrenzen. Die Elektroden 2, 3 sind parallel zueinander an zwei gegenüberliegenden Seiten der Elektrofusionskammer 1 angebracht.

[0027] In den folgenden Figuren haben die selben Vorrichtungsmerkmale die gleichen Bezugszeichen.

[0028] Fig. 2 zeigt Haftstreifen 5, die parallel zu den Elektroden 2, 3 in im wesentlichen äquidistanten Abständen angeordnet sind.

[0029] Fig. 3 zeigt eine Elektrofusionskammer 1 bei der Zellen einer ersten Zellart 6 auf den Haftstreifen 5 aufgetragen sind.

[0030] Fig. 4 zeigt die Elektrofusionskammer 1 in einem Zustand, in dem bereits eine zweite Zellart 7 eingebracht ist.

[0031] In Fig. 5 ist die Elektrofusionskammer 1 dargestellt, die mit Zellen 6, 7 beschickt ist und bei der ein elektrisches Feld angelegt ist.

[0032] Fig. 6a zeigt eine Oberfläche 4 auf der ein Haftmittel als Haftstreifen 5 angebracht ist, sowie die Zellen 6, 7 und zellspezifische Oberflächenmoleküle 8a, 8b.

[0033] Fig. 6b zeigt zusätzlich zu Fig. 6a zellspezifische Antikörper 9, die an die Zellen gebunden sind und an den Haftstreifen binden.

[0034] Fig. 6c zeigt Adaptermoleküle 10, die an die zellspezifischen Antikörper 9 angehängt sind und die an das Haftmittel des Haftstreifens 5 binden.

[0035] Die erfindungsgemäße Vorrichtung und das erfindungsgemäße Verfahren können grundsätzlich für die Fusion aller möglichen Zellen eingesetzt werden. Es können gleiche Zelltypen aber auch verschiedene Zelltypen fusioniert werden. Vorzugsweise werden verschiedene Zelltypen miteinander fusioniert. Das Fusionieren von verschiedenartigen Zellen birgt nach den Verfahren nach dem Stand der Technik besondere Probleme, da sich gleichartige Zellen bei den Elektrofusionsverfahren nach dem Stand der Technik bevorzugt aneinander lagern. Grundsätzlich können beliebige Zellkombinationen fusioniert werden. Die Wahl der zu fusionierenden Zellen richtet sich nach der jeweiligen Problemstellung. So können beispielsweise Krebszellen mit Immunzellen, z.B. dendritische Zellen, Antikörper produzierende Zellen und Tumorzellen fusioniert werden. Grundsätzlich ist es auch denkbar Eizellen mit Samenzellen zu befruchten.

[0036] Erfindungsgemäß sollen mindestens zwei im wesentlichen parallel zueinander angeordnete Reihen heterologer Zellen der Zellart 6 und 7 im wesentlichen parallel zu den Elektroden 2, 3 angeordnet werden. Dabei werden Haftstreifen 5 parallel zu den Elektroden 2, 3 aufgebracht, die eine Zellart binden können.

[0037] Der Anbindemechanismus kann, wie in den Fig. 6a-c dargestellt, erfolgen.

[0038] Im Beispiel gemäß Fig. 6a besteht das Haftmittel 5 aus einem zellspezifischen Antikörper, an den zellspezifische Oberflächenmoleküle 8a binden, die selektiv in den zellspezifischen Antikörper passen. Auf diesem Weg können die gewünschten Zellen der ersten Zellart 6 selektiv an die Haftstreifen 5 angehängt werden.

[0039] In dem Beispiel nach Fig. 6b sind an die Zellen 6, die an den Haftstreifen angehängt werden sollen, über zellspezifische Oberflächenmoleküle 8a an zellspezifische Antikörper 9 gebunden, welche

DE 103 59 189 B4 2005.12.22

wiederum selektiv in dem Haftvermittler **5** eingepasst werden, der in diesem Fall aus einem sekundären Antikörper besteht.

[0040] Fig. 6c zeigt einen Mechanismus, bei dem der zellspezifische Antikörper **9**, der an das zellspezifische Oberflächenmolekül **8a** der Zelle **6** gebunden ist, mittels eines Adaptermoleküls **10** in den Haftstreifen **5** eingreift, der in diesem Fall aus einer daran anbindenden Verbindung besteht. Als Adaptermolekül **10**/Haftstreifen **5** – Kombination kann zum Beispiel Biotin/Streptavidin eingesetzt werden.

[0041] Vorzugsweise werden die Haftstreifen **5** mit einem chemischen Linker mit der Oberfläche **4** verbunden. Dadurch wird der Haftstreifen **5** besser gegen ein Verrutschen oder Wegspülen beim Abspülen überschüssiger Zellen geschützt. Als Linker können verschiedene Verbindungen eingesetzt werden. Beispielsweise kann mindestens eine Komponente aus der Gruppe der Verbindungen Aminosilane, oder Dialdehyde, wie beispielsweise Glutardialdehyd eingesetzt werden.

[0042] Bei der Fusion wird entweder eine Elektrofusionskammer **1** ohne Haftmittel mit einem Haftmittel streifenförmig beschickt (Haftstreifen **5**, **5a**) oder es wird eine fertige Elektrofusionskammer **1** mit mindestens einem Haftstreifen **5**, oder **5**, (**5a**, wie weiter unten beschrieben) verwendet. Diese Elektrofusionskammer **1** wird mit einer Lösung der ersten Zellart **6** in Kontakt gebracht. Dabei haften bzw. binden die Zellen **6** an den oder die Haftstreifen **5** an, und kommen natürlich auch mit den nicht mit Haftstreifen **5** versehenen Stellen der Oberfläche **4** oder gegebenenfalls mit den Haftstreifen **5a** (nicht in den Figuren abgebildet) in Kontakt. Der Haftstreifen **5a** ist in diesem Fall so ausgestaltet, dass er die Zellen der ersten Zellart **6** nicht bindet, sondern nur die Zellen der zweiten Zellart **7**. Sind die Zellen an die Haftstreifen **5** angebunden, so wird die, die Zellen **6** enthaltene Flüssigkeit entfernt und die Oberfläche nochmals abgespült. Dabei haften die Zellen **6** an dem Haftmittel **5** an, während sie von den Zwischenräumen abgespült werden.

[0043] Zum Auftragen der Zellen **6** kann als Flüssigkeit ein Kulturmedium, Fusionslösung, Puffer, Salzlösung, Kohlehydratlösung verwendet werden, die beispielsweise als isotone oder hypoosmolare Lösungen vorliegen können.

[0044] Zum Abspülen der überzähligen Zellen **6** kann beispielsweise ein Kulturmedium, Fusionslösung, Puffer, Salzlösung oder Kohlehydratlösung verwendet werden, die beispielsweise als isotone Lösungen vorliegen können. Hier ist die Verwendung von hypoosmolaren Lösungen bevorzugt.

[0045] In einem weiteren Schritt wird eine Lösung

der zweiten Zellart **7** auf die Oberfläche **4** der Elektrofusionskammer **1** aufgebracht. Als Flüssigkeit zum Auftragen der Zellen kann hier ein Fusionspuffer dienen, wenn ein Haftstreifen **5a** vorhanden ist. Liegt eine Ausführungsform vor, bei der lediglich Haftstreifen **5** und keine Haftstreifen **5a** vorhanden sind, so ist die Verwendung eines Fusionspuffers für das Aufbringen der zweiten Zellart **7** notwendig.

[0046] Für die zweite Zellart **7** ist kein weiterer Haftstreifen **5a** zwingend nötig, da sich die Zellen **7** zwischen den Haftstreifen **5** anordnen. Es müssen keine überschüssigen Zellen **7** abgespült werden, jedoch ist es zu bevorzugen, dass mit der Lösung, die die Zellen **7** enthält im Wesentlichen die gleich Anzahl von Zellen eingebracht wird, wie bereits an den Haftstreifen **5** anhaften.

[0047] Bei einer alternativen Ausführungsform kann der Bereich zwischen den Haftstreifen **5** für die erste Zellart **6** auch mit weiteren Haftstreifen **5a**, die in den Figuren nicht dargestellt sind, für die zweite Zellart **7** beschichtet sein, an die zweite Zellart **7** anbinden kann.

[0048] Bei diesen Haftstreifen **5a** kann es sich analog wie im Fall der Haftstreifen **5** für die erste Zellart **6** um die gleichen Haftverbindungsbestandteile handeln. Es gelten also die gleichen Grundsätze, wie beim Befestigen der ersten Zellart **6** jedoch dürfen die Haftstreifen **5a** keine Verbindungsmittel sein, an die die Zellen der ersten Zellart **6** anhaften können.

[0049] Die Haftstreifen **5**, **5a** können im wesentlichen die gleiche Breite annehmen, wie die an ihnen zu befestigenden Zellen **6**, **7**. Es reicht aber auch noch aus, wenn die Breite der Haftstreifen **5**, **5a** 25% der Breite der zu befestigenden Zellen beträgt.

[0050] Wenn die Haftstreifen **5**, **5a** eine Breite besitzen, die größer ist als die Zellbreite, beispielsweise die dreifache Zellbreite, so tritt ein besonderer Effekt auf, der in den Fig. 7b–e dargestellt ist. Die Zellen lagern sich dann nämlich bevorzugt am Rand der Haftstreifen an. Wird die zweite Zellart **7** aufgetragen, so ordnen sich diese Zellen sowohl zwischen den Haftstreifen, als auch in der Mitte der Haftstreifen an, ohne dabei besonders an dem Haftmittel des Haftstreifens **5** anzuhängen. Es entstehen wiederum alternierende Reihen von Zellen **6** und **7**. In diesem Fall ist es besonders bevorzugt, wenn die Haftstreifen **5** im wesentlichen einen Durchmesser haben, der dem **2** bis **5** fachen der Zellart **6** besitzt. Vorzugsweise entspricht dann der Abstand der Haftstreifen **5** von Rand zu Rand im wesentlichen der Breite der Zellart **7** oder etwas mehr. Die Breite der Haftstreifen **5**, **5a** kann in einer Größenordnung von 5 bis 100 µm liegen.

[0051] Die Abstände zwischen den Haftstreifen **5** für eine Zellart sind im wesentlichen äquidistant in einem

DE 103 59 189 B4 2005.12.22

Abstand angeordnet, der gemessen von der Mitte des Haftstreifens vorzugsweise zwei Zellbreiten beträgt, wenn der Haftstreifen **5** im Wesentlichen die Breite der Zelle besitzt oder schmaler ist. Der Abstand zwischen zwei Streifen die für die gleiche Zellart vorgesehen sind kann dann zwischen 10 und 200 μm , vorzugsweise zwischen 10 μm und 20 μm liegen.

[0052] Die Haftstreifen **5**, **5a** können beispielsweise durch Stempeltechnik oder mikrofluidisch auf die Oberfläche **4** aufgetragen werden.

[0053] Vorzugsweise befinden sich 100, bis 500 Haftstreifen **5** für eine Zellart nebeneinander, es können aber auch 1 bis 2000 Haftstreifen **5** sein. Beim Vorliegen zweier verschiedener Haftstreifen **5**, **5a**, verdoppelt sich vorzugsweise die Anzahl der Haftstreifen, die insgesamt vorliegen.

[0054] Nach Auftragen der zweiten Zellart **7** kann in der Ausführungsform mit zwei verschiedenen Haftstreifen **5**, **5a** wiederum überschüssige Zellen mit einer Flüssigkeit abgespült werden. Diese Flüssigkeit kann beispielsweise mindestens eine Komponente aus der Gruppe der nach dem Stand der Technik bekannten Lösungen für die Elektrofusion sein.

[0055] Spätestens mit dem Einbringen der Zellart **7** muß eine für die Elektrofusion geeignete Flüssigkeit in das System eingebracht werden. Diese sind aus dem Stand der Technik bekannt.

[0056] Nachdem die beiden Zellarten **6** und **7** auf die Oberfläche **4** aufgebracht wurden, wird zwischen den Elektroden **2**, **3** eine Spannung angelegt, die ein Alignment, also eine Ausrichtung der Zellen **6** und **7** entlang der Feldlinien bewirkt, wobei die verschiedenen Zellarten **6**, **7** entlang der Feldlinien alternieren.

[0057] Das anzulegende elektrische Feld ist dem Fachmann bekannt und entspricht grundsätzlich der Größenordnung, wie sie aus anderen Elektrofusionsverfahren bekannt ist. Beispielhaft können elektrische Felder einer Stärke von 100 bis 500 Volt/cm angegeben werden.

[0058] Nach dem Alignment wird ein Fusionspuls appliziert wodurch es zu einer Verschmelzung der Zellen **6** und **7** kommt.

[0059] Wurden die Zellen so ausgerichtet, dass die Ketten in Flussrichtung so nebeneinander liegen, dass sich entlang der elektrischen Feldlinien ebenfalls Ketten, im Fall der heterologen Fusion alternierender Zellen, ausbilden, so wird ein elektrischer Fusionspuls erzeugt, mit dem die Elektrofusion bewirkt wird. Die Stärke des elektrischen Fusionspulses liegt in der gleichen Größenordnung wie bei bekannten Elektrofusionsverfahren und beträgt 250 bis 3000

Volt/cm.

[0060] Die Dauer des Pulses liegt wie bei anderen Elektrofusionsverfahren in einem Bereich der sich von 1 μs bis 1000 ms erstreckt.

[0061] Die erfindungsgemäße Vorrichtung kann aus verschiedenen Materialien bestehen. So kann sie beispielsweise die Materialien Glas, Kunststoff, PP, Polycarbonat, PMMA sowie PET umfassen. Dies gilt auch für die Oberfläche **4**, auf welche die Haftmittel **5**, **5a** aufgebracht sind.

[0062] Durch die Elektrofusion der nach dem erfindungsgemäßen Verfahren zusammengeführten Zellen wird eine höhere Raum-Zeit-Ausbeute an heterolog fusionierten Zellen erreicht als nach dem Stand der Technik. Während die Elektrofusion nach dem Stand der Technik bei einer theoretischen Ausbeute von 50 % lediglich eine praktische Ausbeute von 10 bis 20 % erreicht wird, beträgt die theoretische Ausbeute für die heterologe Fusion nach dem erfindungsgemäßen Verfahren 100%. Da es zu keiner Agglomeration von gleichen Zellen kommt, verringert sich die Zahl der heterolog fusionierenden Zellen nicht, wie bei dem Verfahren nach dem Stand der Technik. Es kann daher mit einer Ausbeute von > 50% gerechnet werden.

Patentansprüche

1. Verfahren zur Elektrofusion von heterologen Zellen

dadurch gekennzeichnet,

dass folgende Schritte durchgeführt werden:

- in Kontakt bringen einer mit Haftstreifen (**5**) ausgestatteten Oberfläche (**4**) mit einer ersten Zellart (**6**),
- Abspülen der nicht an den Haftstreifen (**5**) anhaftenden Zellen mit einer Flüssigkeit,
- in Kontakt bringen der so behandelten Oberfläche (**4**) mit einer zweiten Zellart (**7**), wobei die zweite Zellart (**7**) auf Haftstreifen (**5a**) aufgebracht wird, die zwischen den Haftstreifen (**5**) für die erste Zellart (**6**) angebracht sind
- Anlegen einer Spannung auf der Ebene der Haftstreifen (**5**), die senkrecht zu den Haftstreifen (**5**) verläuft,
- Applizieren eines elektrischen Fusionspulses.

2. Verfahren nach Anspruch 1, dadurch gekennzeichnet, dass die zweite Zellart (**7**) mittels eines Fusionspuffers aufgebracht wird.

3. Verfahren nach Anspruch 1 oder 2, dadurch gekennzeichnet, dass die Haftstreifen (**5a**) für die zweite Zellart ein Haftmittel aufweisen, das von dem Haftstreifen (**5**) für die erste Zellart verschieden ist.

4. Verfahren nach einem der Ansprüche 1 bis 3, dadurch gekennzeichnet,

DE 103 59 189 B4 2005.12.22

dass als Haftmittel für die Haftstreifen (5,5a) folgende Stoffe eingesetzt werden:

- a) ein zellspezifischer Antikörper gegen ein zellspezifisches Oberflächenmolekül Molekül (8a) der zu bindenden Zelle und/oder
- b) ein sekundärer Antikörper, der an einen Antikörper (9) anbindet, welcher über ein zellspezifisches Oberflächenmolekül 8a an die zu bindende Zelle angeschlossen ist und/oder
- c) eine Verbindung, an die ein Adaptermolekül (10), welches an einem zellspezifischen Antikörper (9), der sich an einem zellspezifischen Oberflächenmolekül (8a) der zu bindenden Zelle befindet, anhaftet.

5. Verfahren nach einem der Ansprüche 1 bis 4, dadurch gekennzeichnet, dass die Haftstreifen (5, 5a) mit einem Linker auf der Oberfläche (4) befestigt sind.

6. Verfahren nach Anspruch 5, dadurch gekennzeichnet, dass als Linker mindestens eine Komponente aus Aminosilanen und/oder Dialdehyden und/oder Glutardialdehyd eingesetzt wird.

7. Verfahren nach einem der Ansprüche 1 bis 6, dadurch gekennzeichnet, dass folgende Zellarten fusioniert werden:

- Krebszellen mit Immunzellen,
- Krebszellen mit dendritischen Zellen,
- Antikörper produzierende Zellen mit Tumorzellen und/oder
- Eizellen mit Samenzellen.

8. Verfahren nach einem der Ansprüche 1 bis 7, dadurch gekennzeichnet, dass die Zellen der ersten Zellart (6) auf Haftstreifen (5) mit äquidistanten Abständen aufgebracht werden.

9. Verfahren nach einem der Ansprüche 1 bis 8, dadurch gekennzeichnet, dass Haftstreifen (5) eingesetzt werden, die die Breite von einer Zellbreite der Zellen der ersten Zellart (6) bis 25 % dieser Breite besitzen.

10. Verfahren nach einem der Ansprüche 1 bis 8, dadurch gekennzeichnet, dass Haftstreifen (5) eingesetzt werden, deren Breite größer ist als die der Zellen der ersten Zellart (6).

11. Verfahren nach Anspruch 10, dadurch gekennzeichnet, dass die Breite der Haftstreifen (5) die zwei- bis fünffache Breite der Zellen der ersten Zellart (6) ist.

12. Verfahren nach einem der Ansprüche 10 oder 11, dadurch gekennzeichnet, dass die Haftstreifen (5) in einem Abstand angeordnet sind, der einer Zellbreite der zweiten Zellart (7) entspricht oder der größer ist.

13. Vorrichtung zur Elektrofusion von Zellen mit einer Elektrofusionskammer mit Elektroden, dadurch gekennzeichnet, dass die Elektrofusionskammer (1) an zwei gegenüberliegenden Seiten Elektroden (2, 3) besitzt, zwischen denen eine Spannung angelegt werden kann, und dass parallel zu den Elektroden Haftstreifen (5) angebracht sind, die Zellen an sich binden, wobei sich die Haftstreifen (5) in äquidistanten Abständen befinden und dass zwischen den Haftstreifen (5) weitere Haftstreifen (5a) in alternierender Reihenfolge zu den Haftstreifen (5) angebracht sind, die eine zweite Zellart (7) an sich binden.

14. Vorrichtung nach Ansprüche 13, dadurch gekennzeichnet, dass bis 2000 der Haftstreifen (5) auf der Oberfläche (4) angebracht sind.

15. Vorrichtung nach einem der Ansprüche 13 oder 14, dadurch gekennzeichnet, dass die Haftstreifen (5, 5a) eine Breite von 5 bis 100 µm besitzen.

16. Vorrichtung nach einem der Ansprüche 13 bis 15, dadurch gekennzeichnet, dass die Haftstreifen (5) eine Breite besitzen, die die Breite der Zellen der ersten Zellart (6) bis 25 % dieser Breite beträgt.

17. Vorrichtung nach einem der Ansprüche 13 bis 15, dadurch gekennzeichnet, dass die Breite der Haftstreifen (5) größer ist als die Breite der Zellen der ersten Zellart (6).

18. Vorrichtung nach Anspruch 17, dadurch gekennzeichnet, dass die Breite der Haftstreifen (5) zwei- bis fünfmal größer ist als die Breite der Zellen der ersten Zellart (6).

19. Vorrichtung nach einem der Ansprüche 13 bis 18, dadurch gekennzeichnet, dass die Abstände zwischen den Haftstreifen (5) gemessen von deren Rändern der Breite der Zellen der zweiten Zellart (7) entsprechen oder größer sind.

20. Vorrichtung nach einem der Ansprüche 13 bis 19, dadurch gekennzeichnet, dass als Haftmittel für die Haftstreifen (5, 5a) folgende Stoffe vorhanden sind:

- a) ein zellspezifischer Antikörper gegen ein zellspezifisches Oberflächenmolekül Molekül 8a der zu bindenden Zelle und/oder
- b) ein sekundärer Antikörper, der an einen Antikörper (9) anbindet, welcher über ein zellspezifisches Oberflächenmolekül 8a an die zu bindende Zelle angebunden ist und/oder
- c) eine Verbindung, an die ein Adaptermolekül (10), welches an einem zellspezifischen Antikörper (9), der sich an einem zellspezifischen Oberflächenmolekül (8a) der zu bindenden Zelle befindet, anhaftet.

21. Vorrichtung nach einem der Ansprüche 13 bis 20, dadurch gekennzeichnet, dass die Haftmittel der

DE 103 59 189 B4 2005.12.22

Haftstreifen (5) und (5a) verschiedene Zellarten binden.

22. Vorrichtung einem der Ansprüche 13 bis 21, dadurch gekennzeichnet, dass die Haftstreifen (5, 5a) mit einem Linker auf der Oberfläche (4) befestigt sind.

23. Vorrichtung nach Anspruch 22, dadurch gekennzeichnet, dass als Linker mindestens eine Komponente aus Aminosilanen und/oder Dialdehyden und/oder Glutardialdehyd eingesetzt wird.

Es folgen 8 Blatt Zeichnungen

DE 103 59 189 B4 2005.12.22

Anhängende Zeichnungen

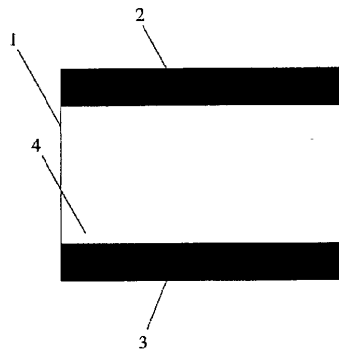


Fig.1

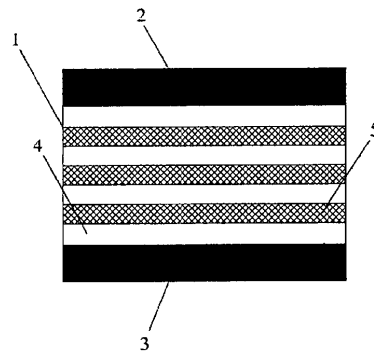


Fig.2

DE 103 59 189 B4 2005.12.22

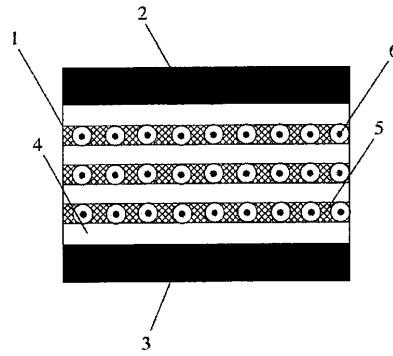


Fig.3

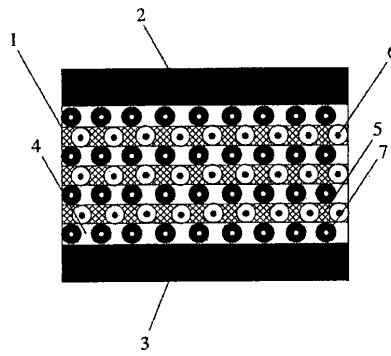


Fig.4

DE 103 59 189 B4 2005.12.22

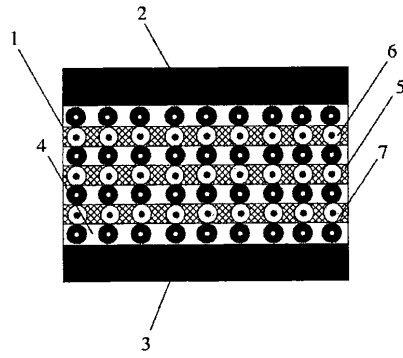


Fig:5

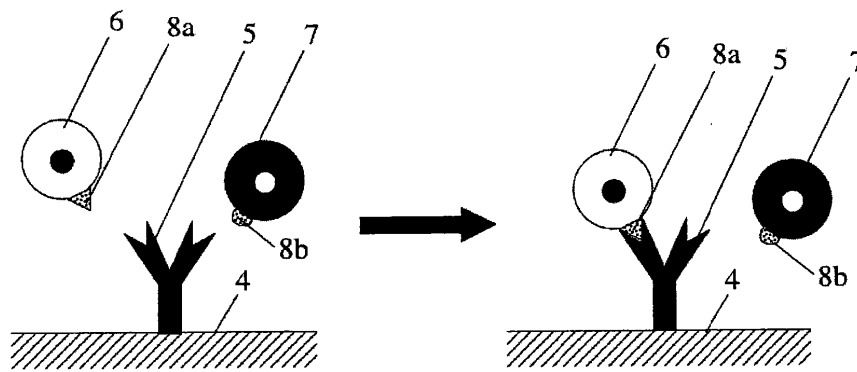


Fig. 6a

DE 103 59 189 B4 2005.12.22

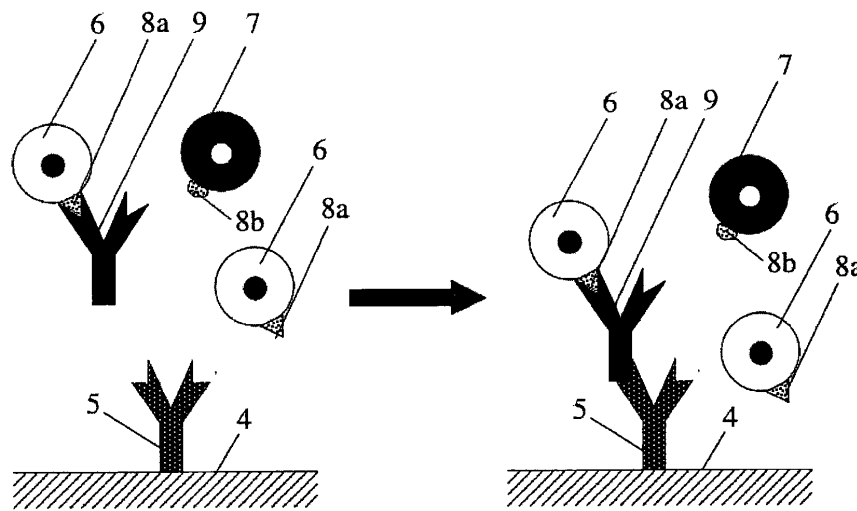


Fig. 6b

DE 103 59 189 B4 2005.12.22

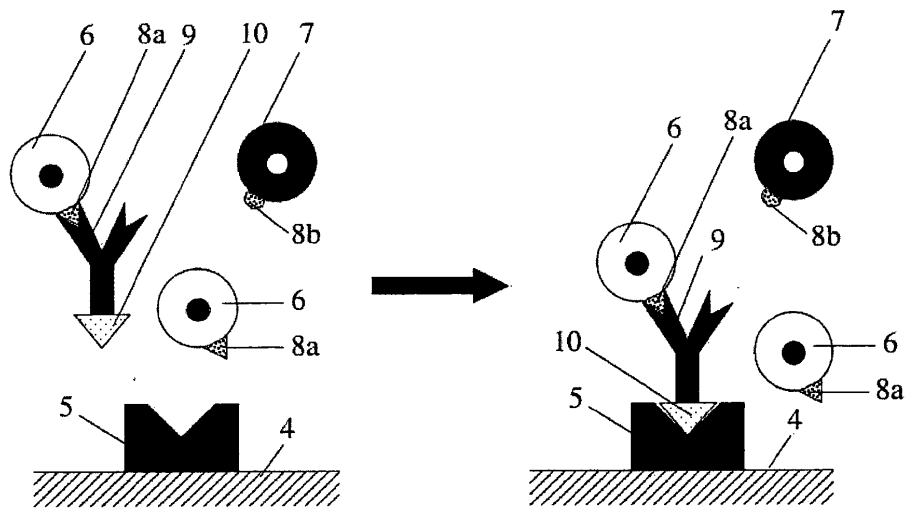


Fig. 6c

DE 103 59 189 B4 2005.12.22

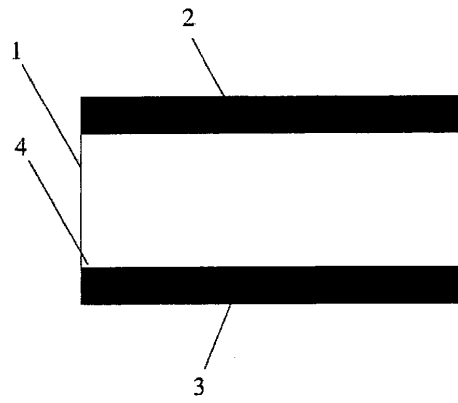


Fig. 7a

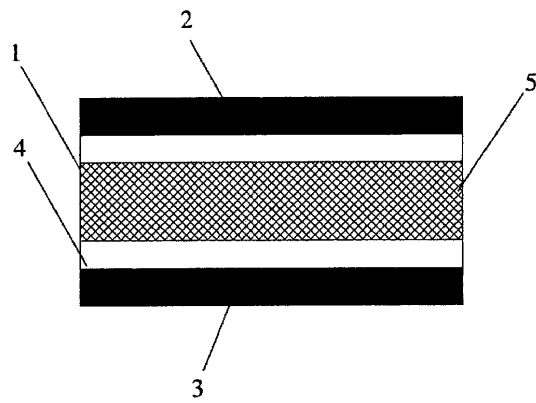


Fig. 7b

DE 103 59 189 B4 2005.12.22

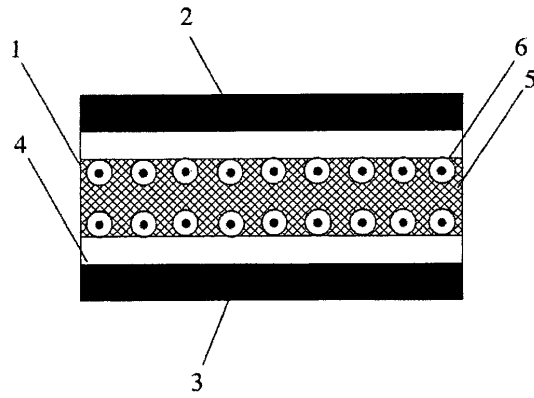


Fig. 7c

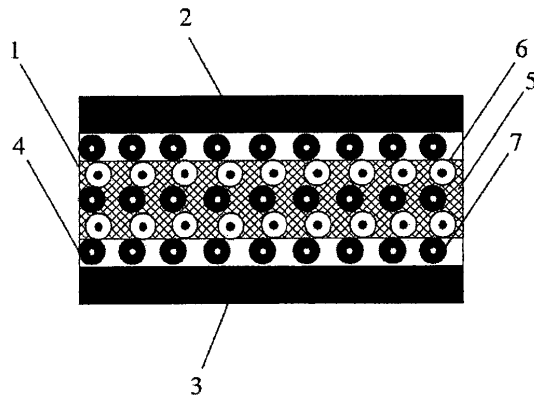


Fig.7d

DE 103 59 189 B4 2005.12.22

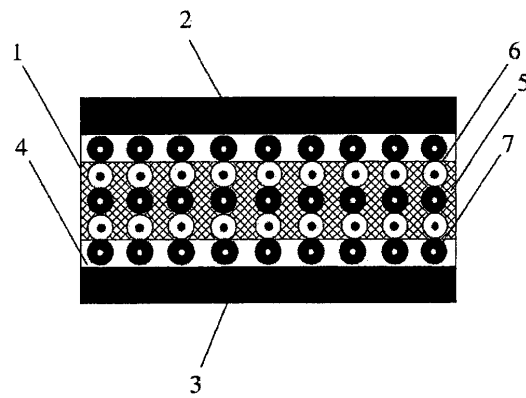


Fig. 7e



(19)
Bundesrepublik Deutschland
Deutsches Patent- und Markenamt

(10) **DE 103 59 190 A1** 2005.07.14

(12)

Offenlegungsschrift

(21) Aktenzeichen: **103 59 190.7**
(22) Anmeldetag: **17.12.2003**
(43) Offenlegungstag: **14.07.2005**

(51) Int Cl.⁷: **C12M 1/42**
C12N 13/00

(71) Anmelder:
Forschungszentrum Jülich GmbH, 52428 Jülich, DE

(72) Erfinder:
Schaper, Janina, 52428 Jülich, DE; Noll, Thomas, Dr., 52428 Jülich, DE; Hubbuch, Jürgen, Dr., 52064 Aachen, DE; Offenhäusser, Andreas, Prof. Dr., Eynatten, BE

(56) Für die Beurteilung der Patentfähigkeit in Betracht gezogene Druckschriften:
JP 01-3 04 876 A
JP 01-2 15 274 A
JP 63-63 372 A

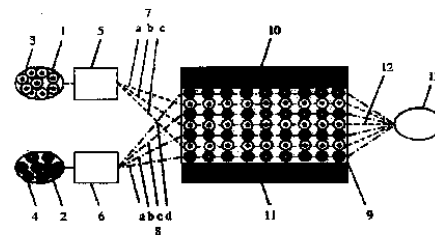
Die folgenden Angaben sind den vom Anmelder eingereichten Unterlagen entnommen

Prüfungsantrag gemäß § 44 PatG ist gestellt.

(54) Bezeichnung: **Verfahren und Vorrichtung zum Elektrofusionieren von Zellen**

(57) Zusammenfassung: Die Erfindung betrifft ein Verfahren und eine Vorrichtung zum Elektrofusionieren von Zellen.

Erfindungsgemäß werden Zellfusionen dadurch herbeigeführt, dass die Zellen in parallelen Strömen, in denen die einzelnen Zellen in einer Kette hintereinander angeordnet sind, in eine Elektrofusionskammer (9) eingeführt werden, wobei die Ketten im Fall der heterologen Fusion alternierend angeordnet sind, senkrecht zur Fließrichtung durch ein elektrisches Feld in ein Alignment gebracht werden und anschließend mit einem elektrischen Fusionspuls fusioniert werden.



DE 103 59 190 A1 2005.07.14

Beschreibung

[0001] Die Erfindung betrifft ein Verfahren und eine Vorrichtung zum Elektrofusionieren von Zellen nach dem Oberbegriff des Anspruchs 1.

Stand der Technik

[0002] In den letzten Jahren ist der Fusion von Zellen zur Herstellung heterologer Hybride immer mehr Bedeutung zugekommen. Die Fusionsprodukte finden Anwendung in der Krebstherapie (Hybride aus dendritischen Zellen und Tumorzellen), bei der Herstellung von monoklonalen Antikörpern (Hybridomazellen), in der Reproduktionstechnologie (Hybride aus Eizellen und Spermazellen) und in vielen anderen Gebieten.

[0003] Für die Erzeugung von Zellhybriden stehen grundsätzlich drei Methoden zur Auswahl: Die Fusion der Zellen kann entweder chemisch (mittels Polyethylenglycol), rezeptorvermittelt oder elektrisch induziert werden, wobei im Hinblick auf die spätere klinische Anwendung die Methode der Elektrofusion eindeutig von Vorteil ist.

[0004] Die Standardmethode der Elektrofusion sieht vor, dass die beiden Fusionspartner (Zelltyp 1 und Zelltyp 2) gemischt und in eine Fusionskammer gegeben werden. Eine solche Kammer besteht aus zwei Elektroden, die in einem definierten Abstand angeordnet sind. In den so entstehenden Zwischenraum wird die Zellsuspension (Mix aus Zelltyp 1 und Zelltyp 2) gegeben. Durch Anlegen eines schwachen elektrischen Gleichstrom-Feldes werden die Zellen in engen Kontakt miteinander gebracht. Bei diesem sogenannten Alignment werden durch Anlegen des Feldes Dipole innerhalb der Zellen induziert. Die Zellen wandern dann in den Bereich der höchstens Feldintensität und reihen sich dabei in einer sogenannten „Perlenkette“ an. Anschließend werden die Zellen durch einen kurzen Puls fusioniert.

[0005] Wenn die Aneinanderreihung der beiden Zelltypen in der Perlenkette statistisch verteilt erfolgen würde, läge bei einer 1:1-Mischung der Zelltypen die maximale theoretische Bildung von heterologen Hybriden bei 50 %. Real wurden bisher nur 10-20 % erreicht, da zum einen nicht alle Zellen fusionieren und zum anderen homologe Fusionen gegenüber heterologen bevorzugt werden. Des weiteren ist zu beobachten, dass schon in der Aufreihung der Zellen keine statistische Verteilung vorliegt, sondern sich Zellen gleichen Zelltyps (auf Grund ähnlicherer Zelleigenschaften) anhäufen.

[0006] Dadurch treten die ungewollten homologen Fusionen gehäuft auf.

[0007] Zur Lösung dieses Problems gab es in den

letzten Jahren grundsätzlich nur drei Ansätze. Jaroszeski et al. versuchten bei der „mechanisch vereinfachten Zell-Zell-Fusion“ (Biophys. J. 1994, 67: 1574-1581) die beiden Zelltypen in Monoschichten auf einem Filter anzuordnen und diese beiden Filter dann mechanisch miteinander in Kontakt zu bringen. Die mit dieser Methode erreichte maximale Fusions-effizienz lag bei 10 %.

[0008] Die Arbeiten von Strömberg et al. (Anal. Chem. 2001, 73: 126-130), die Einzelzellen microfluidisch anordneten, oder von Bakker Schut et al. (Biophys. J. 1993, 65(2): 568-72), die die beiden Fusionspartner durch eine Avidin-Biotin-Brücke aneinander banden, um dann die so gekoppelten Zellen in einem umgebauten Durchflusszytometer zu fusionieren, brachten bessere Ergebnisse bezüglich der Fusions-effizienz, sind aber nur für Einzelzellfusionen konzipiert. Für die Herstellung einer grossen Menge an vitalen Hybriden sind diese Methoden somit nicht ausgelegt.

[0009] Die Verfahren nach dem Stand der Technik führen zu niedrigen Fusionsausbeuten oder sind lediglich geeignet kleine Zellmengen zu fusionieren.

Aufgabenstellung

[0010] Es ist daher die Aufgabe der Erfindung ein Verfahren und eine Vorrichtung zu schaffen, mit denen Zellen, vorzugsweise verschiedenartige Zellen, mit einer höheren Ausbeute fusioniert werden können. Es soll auch die Möglichkeit geschaffen werden, möglichst viele Zellen in kurzer Zeit zu fusionieren.

[0011] Ausgehend vom Oberbegriff des Anspruchs 1 wird die Aufgabe erfindungsgemäß gelöst mit den im kennzeichnenden Teil des Anspruchs 1 angegebenen Merkmalen.

[0012] Mit dem Verfahren und der Vorrichtung können nunmehr Fusionen, vorzugsweise verschiedener Zelltypen, mit einer hohen Ausbeute und in kurzer Zeit durchgeführt werden.

[0013] Im Folgenden soll die Erfindung beispielhaft erläutert werden.

Ausführungsbeispiel

[0014] Die Figuren zeigen den schematischen Aufbau der erfindungsgemäßen Vorrichtung sowie Darstellungen von verschiedenen Stadien des erfindungsgemäßen Verfahrens.

[0015] Es zeigt:

[0016] **Fig. 1:** Eine erfindungsgemäße Vorrichtung

[0017] **Fig. 2:** Die Vorrichtung gemäß **Fig. 1** mit ein-

DE 103 59 190 A1 2005.07.14

strömenden Zellen.

[0018] **Fig. 3:** Die Vorrichtung gemäß **Fig. 1** mit Zellen bei einem angelegten elektrischen Feld.

[0019] **Fig. 1** zeigt eine erfindungsgemäße Vorrichtung mit Vorratsbehältern **1** und **2** für zu fusionierende Zellen **3** und **4**. Die Vorratsbehälter **1** und **2** sind mit einer Zuleitung an Pumpen **5** und **6** angeschlossen. Beide Pumpen **5**, **6** haben mindestens eine Zuleitung **7a**, **7b**, **7c**, **8a**, **8b**, **8c**, **8d** zu einer Elektrofusionskammer **9**, die an zwei gegenüberliegenden Seiten mit Elektroden **10**, **11** ausgestattet ist. Die Zuleitungen **7a**, **b**, **c**, **8a**, **b**, **c**, **d** münden dabei nebeneinander alternierend in die Elektrofusionskammer **9**. Auf der, der Seite mit der Zuleitung gegenüberliegenden Seite, befindet sich mindestens eine Ableitung **12** für die fusionierten Zellen sowie ein Auffangbehälter **13** für die fusionierten Zellen. Die Elektrofusionskammer **9** ist durch eine Bodenplatte und eine Deckplatte abgeschlossen, welche in der Figur nicht abgebildet sind. Die Elektrofusionskammer **9** bildet daher bis auf die Zu- und Ableitung einen geschlossenen Raum.

[0020] In den **Fig. 2** und **Fig. 3** besitzen die selben Vorrichtungsmkmale die gleichen Bezugszeichen.

[0021] Bei Betrieb werden in die Vorratsbehälter **1**, **2** zu Fusionierende Zellen **3**, **4** gegeben, die mit den Pumpen **5**, **6** über die Zuleitungen **7a**, **b**, **c** und **8a**, **b**, **c**, **d** in die Elektrofusionskammer **9** gefördert werden. Die zu fusionierenden Zellen bilden in der Elektrofusionskammer **9** Reihen von zu fusionierenden Zellen, die beispielhaft in **Fig. 2** dargestellt sind. In der Elektrofusionskammer **9** wird über die Elektroden **10**, **11** eine Spannung angelegt, welche bewirkt, dass sich die Zellen **3**, **4** idealerweise gemäß **Fig. 3** in einer Linie anordnen (Alignment), so dass die verschiedenen Zelltypen im Fall der heterologen Fusion entlang der Richtung der Feldlinien alternieren. Haben die Zellen **3**, **4** diese Anordnung erreicht, so wird ein Strompuls appliziert, bei dem die Elektrofusion stattfindet.

[0022] Die erfindungsgemäße Vorrichtung und das erfindungsgemäße Verfahren kann grundsätzlich für die Fusion aller möglichen Zellen eingesetzt werden. Es können gleiche Zelltypen aber auch verschiedene Zelltypen fusioniert werden. Vorzugsweise werden verschiedene Zelltypen miteinander fusioniert, die sich in den verschiedenen Vorratsbehältern **1** und **2** befinden. Das Fusionieren von verschiedenartigen Zellen birgt nach den Verfahren nach dem Stand der Technik besondere Probleme, da sich gleichartige Zellen bei den Elektrofusionsverfahren nach dem Stand der Technik beim Anlegen einer Spannung bevorzugt aneinander lagern. Grundsätzlich können beliebige Zellkombinationen fusioniert werden. Die Wahl der zu fusionierenden Zellen richtet sich nach der jeweiligen Problemstellung. So können beispiels-

weise Krebszellen mit Immunzellen, z.B. dendritische Zellen, Antikörper produzierende Zellen mit Tumorzellen fusioniert werden. Grundsätzlich ist es auch denkbar Eizellen mit Samenzellen zu befruchten.

[0023] Die zu fusionierenden Zellen **3** und **4** liegen in den Vorratsbehältern **1**, **2** in einer Flüssigkeit, Fusionspuffer oder isotonische Kohlenhydratlösung oder allgemeiner isotonischer Lösung vor mit der sie in die Elektrofusionskammer **1** eingebracht werden. Es können die für die Elektrofusion von Zellen bekannten Flüssigkeiten eingesetzt werden. Vorzugsweise können hypoosmolare Lösungen verwendet werden, da die Zellen bei deren Verwendung aufquellen und so noch besser fusionieren.

[0024] Die zu fusionierenden Zellen aus den Vorratsbehältern **1** und **2** werden über Pumpen **5** und **6** in die Zuleitungen **7a**, **b**, **c**, und **8a**, **b**, **c**, **d** gefördert. Die Pumpen **5**, **6** sowie die Zuleitungen **7** und **8** dienen als Mittel zum Zuführen von im wesentlichen parallel in der Elektrofusionskammer **9** vorliegenden Ketten bzw. Reihen von Zellen, die im Folgenden als Einzelzell-Ströme bezeichnet werden.

[0025] Die Anzahl der Zuleitungen **7a**, **b**, **c** und **8a**, **b**, **c**, **d** ist variabel und kann beispielsweise bei **8** Zuleitungen für jede Zellsorte liegen. Eine Begrenzung wird lediglich durch physikalische Parameter gegeben. Pro Vorratsbehälter **1** und **2** können bis zu **100** Zuleitungen **7**, **8**, vorzugsweise **1-20** besonders bevorzugt **5-10** Zuleitungen in die Elektrofusionskammer **9** führen. Die Zuleitungen **7a**, **b**, **c** und **8a**, **b**, **c**, **d** können sich in der Elektrofusionskammer **9** ein Stück fortsetzen.

[0026] Für eine besonders effektive Elektrofusion münden die Zuleitungen **7**, **8** mit den verschiedenen Zelltypen alternierend in einer Ebene in die Elektrofusionskammer **9**.

[0027] Die Zuleitungen **7**, **8** sind vorzugsweise so ausgebildet, dass ihr Durchmesser den Durchtritt vom im wesentlichen einer Zelle ermöglicht, so dass pro Zuleitung eine Kette von einzelnen Zellen gefördert wird, die dann in die Elektrofusionskammer **9** eintritt. Der Durchmesser der Zuleitungen **7**, **8** kann bei variierenden Zellen durchaus verschieden sein. Er kann in einem Bereich von beispielsweise **5-200** μm , vorzugsweise **10-100** μm , besonders bevorzugt **40-60** μm liegen.

[0028] Die Zuleitungen **7**, **8** können den gleichen oder einen unterschiedlichen Durchmesser besitzen.

[0029] In einer bevorzugten Ausführungsform sind die Zuleitungen **7** und **8** so angeordnet, dass sie in einer Ebene in die Elektrofusionskammer **9** einmünden, jedoch aus verschiedenen Richtungen zugeführt werden. So können die Zuleitungen **7** beispiels-

DE 103 59 190 A1 2005.07.14

weise von oben und die Zuleitungen **8** von unten zugeführt werden. Es sind aber auch Zuführrichtungen von oben oder unten in einer Kombination mit einer Zuführrichtung denkbar, die mit der Strömungsrichtung in der Elektrofusionskammer **9** eine im Wesentlichen gerade Linie bildet. Der Vorteil eine Zuführung der verschiedenen Zellen aus verschiedenen Richtungen besteht darin, dass die Herstellung einer derart ausgestalteten Vorrichtung einfach zu realisieren ist.

[0030] Durch die Pumpen **5, 6** und die Zuleitungen **7, 8** werden die Zellen in die Elektrofusionskammer **9** eingebracht.

[0031] Die Elektrofusionskammer **9** kann verschiedene Abmessungen haben. Als Tiefe wird die Länge in Fließrichtung verstanden. Die Breite ist die Länge, auf der die Einzelzellströme nebeneinander angeordnet sind und die Höhe ist die Abmessung, die senkrecht zu der Fließrichtung und der Breite angeordnet ist. Die Abmessungen liegen bei einer Höhe von mindestens 10 µm bis 250 µm und bevorzugt 15 bis 150 µm. Die Breite kann beispielsweise bei 1 cm liegen, ist jedoch in sehr weiten Bereichen variabel und hängt im wesentlichen von der Anzahl der Einzelzellströme ab. Die Tiefe kann beispielsweise 1 bis 10 cm bevorzugt 2 bis 6 cm betragen. Länge und Breite bestimmen die Anzahl der zu einem Zeitpunkt zu elektrofusionierenden Zellen. Die Höhe soll so ausgelegt sind, dass die Zellen ungestört fließen können, das heißt, die Höhe soll die Zelldicke nicht unterschreiten.

[0032] Dabei werden vorzugsweise Parameter gewählt, die dazu führen dass die Zellen in der Elektrofusionskammer **9** in einer laminaren Strömung geführt werden. Wie in **Fig. 2** dargestellt, bilden sich bei dieser Prozessführung Einzelzell-Ströme von gleichartigen Zellen aus, die parallel zueinander alternierend vorliegen.

[0033] Wie **Fig. 2** zu entnehmen ist, ordnen sich die Ketten aus den Zellen nach dem Zufallsprinzip an, wobei die zu fusionierenden Zellen zumindest teilweise nicht so zueinander vorliegen, dass eine Elektrofusion möglich ist.

[0034] Im nächsten Schritt wird ein elektrisches Feld angelegt. Hierdurch werden die Zellen in eine Position gebracht, bei der die Zellen der Einzelzell-Ströme entlang des elektrischen Feldes wiederum Ketten bilden die sich aus alternierenden Zelltypen zusammensetzen, wie es in **Fig. 3** dargestellt ist. Dieser Vorgang wird als Alignment bezeichnet.

[0035] Das anzulegende elektrische Feld ist dem Fachmann bekannt und entspricht grundsätzlich der Größenordnung, wie sie aus anderen Elektrofusionsverfahren bekannt ist. Beispielfhaft können elektri-

sche Felder einer Stärke von 100 bis 500 Volt/cm angegeben werden.

[0036] Beim Anlegen des elektrischen Feldes kann der Förderstrom verringert oder ganz abgestellt werden, so dass sich die Zellketten, die aus den Zuleitungen **7, 8** zugeführt werden in ihrer Geschwindigkeit verlangsamen oder dass sie zum Stillstand kommen. Dies hat den Vorteil, dass eine besonders gute Anordnung der zu fusionierenden Zellen hergestellt wird. Das elektrische Feld kann allerdings auch angelegt werden, wenn der Förderstrom nicht verringert wird.

[0037] Würden die Zellen so ausgerichtet, dass die Ketten in Flussrichtung so nebeneinander liegen, dass sich entlang der elektrischen Feldlinien ebenfalls Ketten, im Fall der heterologen Fusion alternierender Zellen, ausbilden, so wird ein elektrischer Fusionspuls erzeugt, mit dem die Elektrofusion bewirkt wird. Die Stärke des elektrischen Fusionspulses liegt in der gleichen Größenordnung wie bei bekannten Elektrofusionsverfahren und beträgt 250 bis 3000 Volt/cm.

[0038] Die Dauer des Pulses liegt wie bei anderen Elektrofusionsverfahren in einem Bereich der sich von 1 µs bis 1000 ms erstreckt.

[0039] Die Ableitung **12** kann verschiedenartig ausgestaltet sein. Vorzugsweise werden die Einzelzellströme in einer Ableitung **12** abgeführt, deren Breite zwischen der Breite der durch die Elektroden **10, 11** begrenzten Innenraum der Vorrichtung vorgegeben ist oder bei 25% der Breite dieses Innenraums liegt. Es sind auch noch Breiten von 5% der Breite dieses Innenraums möglich. Alternativ, aber weniger bevorzugt, ist eine Ableitung **12**, bei der mindestens zwei unabhängige Ströme an fusionierten Zellen abgeführt werden.

[0040] Die erfindungsgemäße Vorrichtung kann aus verschiedenen Materialien bestehen. So kann sie beispielsweise die Materialien Glas, Kunststoff, PP, Polycarbonat, PMMA sowie PET umfassen.

[0041] Durch die Elektrofusion der nach dem erfindungsgemäßen Verfahren zusammengeführten Zellen wird eine höhere Raum-Zeit- Ausbeute an heterolog fusionierten Zellen erreicht als nach dem Stand der Technik. Während die Elektrofusion nach dem Stand der Technik bei einer theoretischen Ausbeute von 50 % lediglich eine praktische Ausbeute von 10 bis 20 % erreicht wird, beträgt die theoretische Ausbeute für die heterologe Fusion nach dem erfindungsgemäßen Verfahren 100%. Da es zu keiner Agglomeration von gleichen Zellen kommt, verringert sich die Zahl der heterolog fusionierenden Zellen nicht, wie bei dem Verfahren nach dem Stand der Technik. Es kann daher mit einer Ausbeute von >

DE 103 59 190 A1 2005.07.14

50% gerechnet werden.

Patentansprüche

1. Verfahren zum Elektrofusionieren von Zellen, **dadurch gekennzeichnet**, dass die Zellen, die fusioniert werden sollen in mindestens zwei nebeneinander verlaufenden Strömen, in denen die Zellen im Wesentlichen hintereinander angeordnet sind, in gleicher Fließrichtung in einer Ebene geführt werden, wobei im Falle der Fusion verschiedener Zellen die Zellströme der verschiedenen Zellen über die Breite der Ebene alternieren, dass zur Bildung eines Alignments in der Ebene, die durch die Zellen gebildet wird im wesentlichen senkrecht zur Fließrichtung eine elektrisches Feld angelegt wird, und dass ein Elektrofusionspuls appliziert wird.

2. Verfahren nach Anspruch 1, dadurch gekennzeichnet, die Fließgeschwindigkeit der zu fusionierenden Zellen vor dem Zuschalten des elektrischen Feldes in ihrem Fluss gestoppt oder in der Fließgeschwindigkeit verringert werden.

3. Verfahren nach Anspruch 1, dadurch gekennzeichnet, dass die Fließgeschwindigkeit beim oder vor dem Anlegen des Elektrofusionspulses in ihrem Fluss gestoppt oder in der Fließgeschwindigkeit verringert werden.

4. Verfahren nach einem der Ansprüche 1 bis 3, dadurch gekennzeichnet, dass die Zellen in einer isotonischen oder hypoosmolaren Lösung gefördert werden.

5. Verfahren nach Anspruch 3, dadurch gekennzeichnet, dass die Zellen in einem Fusionspuffer oder in einer Kohlenhydratlösung gefördert werden.

6. Verfahren nach einem der Ansprüche 1 bis 4, dadurch gekennzeichnet, dass folgende Zellen miteinander fusioniert werden:

- Krebszellen mit Immunzellen
- Krebszellen mit dendritischen Zellen
- Antikörper produzierende Zellen mit Tumorzellen
- Eizellen mit Samenzellen.

7. Verfahren nach einem der Ansprüche 1 bis 6, dadurch gekennzeichnet, dass die Zellen in einer laminaren Strömung geführt werden.

8. Vorrichtung zum Elektrofusionieren von Zellen umfassend eine Elektrofusionskammer mit zwei gegenüberliegenden Elektroden, dadurch gekennzeichnet, dass die Elektrofusionskammer (9) an zwei gegenüberliegenden Seiten mit Elektroden (10) (11) ausgestattet ist und dass an der zwischen den Elektroden (10) (11) liegenden Seite mindestens zwei Zuleitungen (7a, b, c,) (8a, b, c, d) auf einer Ebene in die Elektrofusionskammer (9) einmünden, die über Pum-

pen (5) (6) mit Vorratsbehältern (1)(2) in Verbindung stehen.

9. Vorrichtung nach Anspruch 8, dadurch gekennzeichnet, dass mindestens eine Zuleitung (7a, b, c) aus dem Vorratsbehälter (1) und mindestens eine Zuleitung (8a, b, c, d) aus dem Vorratsbehälter (2) nebeneinander auf einer Ebene in die Elektrofusionskammer (9) eintreten, die alternierend im Hinblick auf die Herkunft bezüglich der Vorratsbehälter (1),(2) in die Elektrofusionskammer angeordnet sind.

10. Vorrichtung nach einem der Ansprüche 8 oder 9, dadurch gekennzeichnet, dass sie zwei bis hundert Zuleitungen (7, 8) pro Vorratsbehälter (1, 2) umfasst.

11. Vorrichtung nach einem der Ansprüche 8 bis 10, dadurch gekennzeichnet, dass die Zuleitungen (7, 8) einen Durchmesser in einem Bereich zwischen 5 bis 200 µm besitzen.

12. Vorrichtung nach Anspruch 11, dadurch gekennzeichnet, dass die Zuleitungen (7, 8) einen Durchmesser besitzen, der im Wesentlichen dem Durchmesser der zu fördernden Zellen entspricht.

13. Vorrichtung nach einem der Ansprüche 8 bis 12, dadurch gekennzeichnet, dass die Zuleitungen (7) und die Zuleitungen (8) aus verschiedenen Richtungen in die Elektrofusionskammer (9) eintreten.

14. Vorrichtung nach einem der Ansprüche 8 bis 12, dadurch gekennzeichnet, dass die Zuleitungen (7,8) aus der gleichen Richtung in die Elektrofusionskammer (9) eintreten.

15. Vorrichtung nach einem der Ansprüche 8 bis 14, dadurch gekennzeichnet, dass die Elektrofusionskammer (9) eine Höhe von 10 µm bis 250 µm besitzt.

16. Vorrichtung nach Anspruch 15, dadurch gekennzeichnet, dass die Elektrofusionskammer (9) eine Höhe besitzt, die im Wesentlichen der Dicke der Zellen entspricht bzw. etwas größer ist, so dass die Zellen störungsfrei strömen können.

17. Vorrichtung nach einem der Ansprüche 8 bis 16, dadurch gekennzeichnet, dass die Elektrofusionskammer (9) eine Tiefe von 1 bis 10 cm besitzt.

Es folgen 2 Blatt Zeichnungen

DE 103 59 190 A1 2005.07.14

Anhängende Zeichnungen

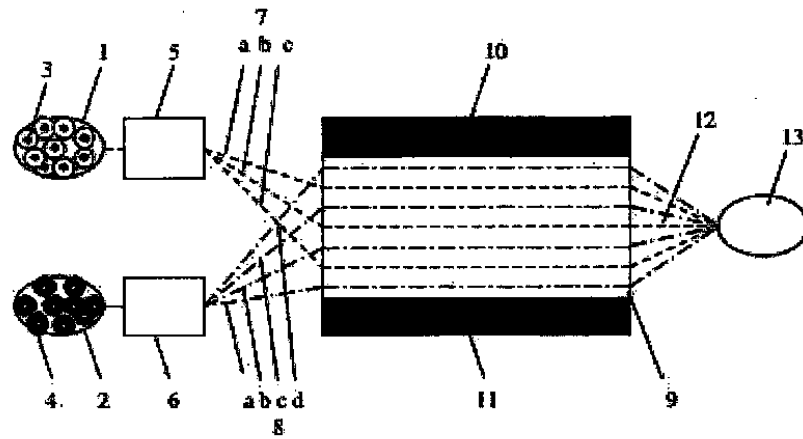


Fig.1

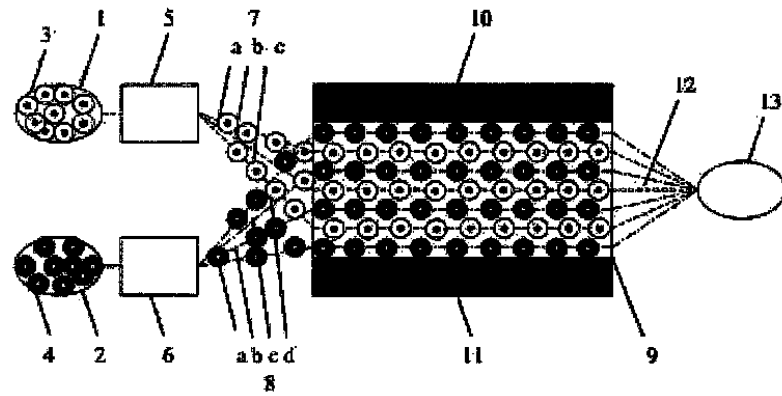


Fig.2

DE 103 59 190 A1 2005.07.14

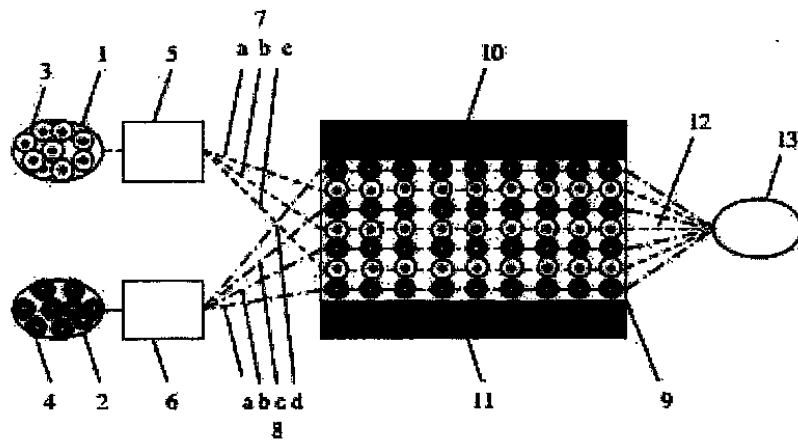


Fig.3

Chapter 5

Discussion

Since fusion hybrids play a central role in biotechnology, especially in monoclonal antibody production (hybridomas), cloning and immunotherapy (hybrid vaccines), some approaches to avoid homologous fusion events have already been developed in the last years. JAROSZESKI ET AL. (1994) tried to deposit both fusion partners in monolayers on filters, which serve as a matrix for mechanically contacting the cell layers. With this "mechanically facilitated cell-cell electrofusion" a maximal fusion efficacy of 10 % was obtained.

The work of STRÖMBERG and colleagues (1999 and 2001), who arranged cells at single-cell level by optical trapping or by adhesion to an ultramicroelectrode, and the chemical approach of BAKKER SCHUT ET AL. (1993), who used an avidin-biotin complex to couple the fusion partners together, were other approaches to an arranged electrofusion process. They resulted in better fusion efficacies than Jaroszeski's approach, but are only designed for single-cell fusions and not laid-out for the generation of large quantities of vital hybrids, especially not in a clinical setting.

To satisfy the requirement for high-throughput cell fusion towards clinical application two different electrofusion devices for the improved generation of mammalian cell hybrids were developed in the context of this thesis. The underlying ultimate principle of these devices is the alternating arrangement of the fusion partners inside the fusion chamber by either antibody-based immobilisation of the cells in micropattern or parallel microfluidic single-cell flows.

5.1 Immobilisation

The development of an electrofusion chamber for arranged mammalian cell fusion, as described in section 3.1, was a multi-step procedure. Starting off with a basic idea of printing antibody lines to immobilise one fusion partner, over the testing of different surface chemistries, the down-sizing of the whole process to cell dimension and thus micrometer scale, the actual build-up of the electrofusion chamber and the application to dendritic cells - knowledge from diverse science backgrounds was needed throughout all stages.

The work combines knowledge from the fields of cell culture and immunology, with inorganic chemistry, liquid handling and microfabrication technology. Many methods for example are descended from the field of electrotechnology and chip design. Altogether, it can be defined as a "real" biotech project, since biotechnology has often been described as an interdisciplinary science.

In the first step of the electrofusion chamber development a surface chemistry for the direct immobilisation of cells was sought. After the test of several alternatives, a method based on the functionalisation of a glass surface by 3-aminotriethoxysilane and cross-linking by glutardialdehyde was chosen to immobilise antibodies via their primary amino groups in a Schiff's base reaction. The choice was made based on a test, where monoclonal antibodies were immobilised in a drop shape. Apart from the APTES/GDA method no other chemistry turned out positive for the application, but this application was critical for a patterned deposition of antibodies in small lines as designated for the electrofusion chamber.

After the selection of the immobilisation chemistry, soft lithographic methods, such as direct and inverse microcontact printing were tested to deposit the antibodies in the desired pattern. The technique of microcontact printing was used in the group of Prof. Dr. A. Offenhäuser at the Institute of Thin Films and Interfaces 2 (ISG-2) at the Research Centre Jülich, where it was used to generate neuronal networks on synthetic substrate surfaces by providing a laminin pattern to which the neuronal cells bind.

Microcontact printing is a state-of-the-art technique for patterning cells. It is a soft lithographic method, which uses a soft elastomeric material, *e.g.* a PDMS stamp, for pattern transfer of the material of interest (*e.g.* cell-adhesion protein) onto the substrate surface. In addition to laminin polylysine, fibronectin or collagen are commonly used by researchers as cell adhesion proteins. These proteins all permit cells to specifically bind to the pattern that is printed with

these proteins on a surface, to which cells would not bind. In this way, the cells specifically bind to the pattern, but the cells need to be adherent growing cells by nature. Suspensions cells do not bind to a pattern of such adhesion molecules.

Since in the context of the electrofusion chamber development, dendritic cells should be bound to small protein lines, different "adhesion" proteins needed to be chosen. The obvious choice were antibodies, due to their ability to bind cells specifically via different surface molecules. The printing and covalently binding of antibodies to patterns in a micrometer scale has not been investigated before. The microcontact printing method was successfully adapted to print antibody lines and dendritic cell binding to these cells was achieved.

The experiments were started using the APTES/GDA cross-linking reaction to immobilise the monoclonal antibodies, but the chemistry needed to be switched due to problems with the integration of the electrodes into this attempt. No facilities were at hand, which would permit the positioning of electrodes (either as wires or by vacuum deposition) in parallel to the antibody lines present on the surface. Even a reverse way of applying the electrodes first and then printing the antibody lines accurate to a micrometer was not possible. For this reason, a new concept for electrode integration into the fusion chamber was developed with the help of Dr. David C. Cullen, reader of Biophysics & Biosensors, at the Biotechnology Centre of the Cranfield University, UK. In this collaboration, a method was developed that avoided the positioning step and combined electrode and antibody line deposition in one step. Additionally, all further parts for chamber assembly were manufactured by laser techniques at the Cranfield institute.

This change in chamber assembly entailed a change in immobilisation chemistry, since in the final design the antibodies are immobilised on small gold lines. Thus, self-assembled monolayers (SAMs) of 11-mercaptoundecanoic acid (MUA) were formed on the gold lines. The carboxyl groups of MUA were activated with a mixture of N-hydroxysuccinimide (NHS) and 1-ethyl-3-(dimethylamino-propyl)carbodiimide (EDC) and the resulting succinimide ester-activated monolayer could then be reacted with primary amino groups on the antibodies to give a peptide bond.

In conclusion, a microdevice for arranged electrofusion of mammalian cells with the use of immobilisation was fabricated using a combination of laser, photolithographic and metal-film-deposition techniques. The dimensions of the device have been chosen to correlate sizes of the cells and allow fusion of large number of cells simultaneously. Due to the alternating

arrangement of the cells within the fusion chamber cluster formation and homologous fusion events are prevented. For the examination of the fusion process, the chamber permits direct visualisation through a transparent top.

Furthermore, the chamber is easy to use and as a disposable device would fulfil clinical requirements. By now, it has been tailored for the electrofusion of dendritic cells with tumour cells, but could be upgraded for use with all cell types by replacing specific antibody binding with a streptavidin/biotin binding step. Instead of covalently bound antibodies, streptavidin would be immobilised. This allows for the binding of every cell type by biotin-labelled antibodies.

In December 2003, an application for a patent was filed for this electrofusion chamber. Seven citations were invalidated and the patent finally granted in December 2005 (see section 4 for the patent specification), which emphasises the novelty of this invention.

5.2 Microfluidics

In parallel to the immobilisation approach, a second electrofusion device was developed that is based on microfluidics (see section 3.2). The development process shows certain similarities to the development of the fusion device based on cell immobilisation. Apart from the fact that it was a matter of several steps to obtain a fully functional device and that microfabrication technology was used, the first contact to microfluidics was made via Prof. Dr. A. Offenhäuser and his research group at the Institute of Thin Films and Interfaces 2 (ISG-2) at the Research Centre Jülich. A microfluidic device was used in his group for localised drug application to adherent cell cultures of neuronal cells to manipulate their growth (THIÉBAUD, P. ET AL., 2002). The device found additional application in the immobilisation of laminin in lines on a substrate, whereas the laminin solution was streamed in small lines over the surface using the microfluidic device.

These two application areas of microfluidic devices in combination with cell culture were found throughout the literature, but no publication could be identified at the time of research, which described the streaming of cells by means of controlled pressure driven liquid flows in microfluidic devices. Although, at that time, microtechnology allowed the fabrication of microfluidic devices with channel sizes that were comparable to the size of biological particles such as cells, only very few cell-based lab-on-a-chip applications have been published.

In the field of electrofusion, or electroporation in the broader sense, two publications were found, which report the design of electrofusion devices. LEE AND COLLEAGUES (1995) developed a cell fusion device only for the fusion of two cells at a time, while TRESSET AND TAKEUCHI (2004) could only show fusion of liposomes, synthetic lipid-bilayer vesicles, in their device. Furthermore, both devices cannot be used for continuous electrofusion of cells, since the feed of the fusion partners is done manually by pipetting, and the microfluidic channels are filled by capillary forces.

The only work, which was promising in terms of continuous cell flow in a microfluidic electrofusion device, was the one from Lin and colleagues, which developed electroporation microchips for continuous gene transfection (LIN ET AL., 1995). Nevertheless, the dimension of the channel, in which the cell flow and cell manipulation by an electric field takes place, was not as such microfluidic, since the channel was 5 mm wide. Thus, the streaming of cells in single cell flows through microfluidic channels needed to be explored first, before the development of a functional electrofusion device came into reach.

With the help of Computational Fluid Dynamics (CFD) the development of a microfluidic electrofusion device was started off. This model based optimisation was accomplished with the help of Dr. Ulrich Krühne from the Centre for Microtechnology and Surface Analysis of the Danish Technology Institute. Based on two different designs for a microfluidic device, the chambers were optimised in regard to the fluid flow and pressure profiles inside the microfluidic structure, therewith circumventing several iterative development steps.

Following the geometric definition and model based optimisation, the microstructures were fabricated in PMMA using an EXCIMER laser, which allows for a relatively cool process. To obtain a functional microfluidic device, capillaries for in- and outflow into the microfluidic chip and a bottom and a top plate were added. A bonding of a PMMA plate as top and bottom plate to the PMMA structure could not be established and no publication was found at that time, which reported a method for PMMA bonding. It was not until December 2005 that Chinese researchers (Chow et al., 2006) published a way to bond two PMMA slides by PDMS-interface bonding. They used a small PDMS spin-coat as adhesive layer between the PMMA slides, which allowed them to bond the PMMA slides without the use of high temperatures or pressures. Therefore, a sandwich structure with PDMS was used as a provisional solution for sealing of the PMMA structure.

In that way, the microstructures could be evaluated in regard to fluid and particle flow inside

the electrofusion chamber. A laminar fluid flow was demonstrated with the use of fluorescent tracers. This flow pattern was also validated with polymer particles and cells showing a laminar single-cell flow. For the use with these microfluidic electrofusion devices a pump station was designed, which comprised three syringe pumps and several valves to deliver the fluids and cell suspensions to the microfluidic chips. This pump station was controlled via a computer and programmed to automatically handle the fluid flow in the microfluidic devices.

Some problems had to be faced during the development, which arose from air bubbles and clogging of microchannels with trapped particles. These are the common problems with microfluidic devices for applications in cellomics. They are the reason, why up to now, only few products have made it to the market. In the development of a microfluidic electrofusion chamber, these problems were avoided in the end by choosing a functional material and expanding all in and outlet diameters to a wider extend. Microfluidic dimensions, which are comparable with cell sizes were realised by hydrodynamic focussing.

The coupling of the microfluidic structure with the necessary equipment entailed the same problems as in the immobilisation approach. It was not possible to completely seal the chamber with the techniques used before. A redesign was needed, where with the help of the Dutch company Micronit the chamber design was reduced to a 2.5-dimensional, simpler design and electrodes were integrated by means of metal deposition techniques. The same laminar flow patterns and particle flows were obtained in the final chamber, since the chamber dimensions were adopted from the previous designs. Furthermore, with two functional microelectrodes, it was possible to generate electrical fields, which enabled cell alignment by dielectrophoresis and cell fusion.

Microfluidics has three main advantages over macroscale operations, which are its small sample volume, the high surface to volume ratio and the possibility to integrate multiple on-board functions (NGUYEN, 2004). For the first two reason, microfluidics are a favoured tool for chemical applications such as chromatography, electrophoresis, mixing and chemical reaction analysis. The possibility to integrate various fluid manipulation components such as pumps, valves, sorters and filters in one chip, would allow for hybrids generated in an microfluidic electrofusion chamber, to be subsequently sorted by means of FACS, counted and suspended in culture medium - all on board of a single chip.

These lab-on-a-chip devices are known throughout the land, and it is modern to downsize everything, even though it does not bring any advantages. However, in the case of the micro-

fluidic electrofusion chamber described here, the inclusion of microfabrication provides unique process advantages to promote this biological application and make it suitable for parallelisation and automation.

A patent application for the developed microfluidic electrofusion chamber was filed in December 2003. The application is still pending, but only 3 citations were adduced.

5.3 Comparison: Immobilisation and Microfluidic Approach

Two different electrofusion chambers for arranged electrofusion of mammalian cells were developed, which are based on two different techniques, immobilisation or microfluidics. They were developed for the fusion of dendritic cells with tumour cells for breast cancer immunotherapy and both have their advantages in regard to their application in a clinical setting or the use in a different application area (see table 5.1).

While the electrofusion chamber based on immobilisation is in its assembled state an easy to use system, the microfluidic device requires a certain amount of technical understanding from its user, but nevertheless comprises the potential to evolve into a fully automated system where a layperson only needs to press the start button.

In terms of the manufacturing costs the immobilisation approach also can be offered for moderate costs, whereas for the microfluidic electrofusion device a higher investment is needed due to the high technical demands such as the purchase of a pump station and the fundamentally higher costs of microchip production. Hence, the fusion device based on immobilisation is preferable for a single use clinical application.

Table 5.1: Comparison of Immobilisation and Microfluidic approach

	Immobilisation	Microfluidics
\oplus	<ul style="list-style-type: none"> • easy to use • moderate costs • single use (clinical application) 	<ul style="list-style-type: none"> • automatable • independent from cell line • no binding of mAbs to cells
\ominus	<ul style="list-style-type: none"> • mechanical/chemical stress on cells • limited chamber size 	<ul style="list-style-type: none"> • high technical demands • high costs (in case of single use)

Nevertheless, the microfluidic electrofusion device has the big advantage that it can be used independently from cell lines. No monoclonal antibodies are bound to the cells as in the immobilisation approach and therefore the cells are not exposed to additional stress by detachment from the antibodies after fusion.

5.4 Electrofusion

The fusion of mammalian cells by means of electrical fields is nowadays an established method. However, it is not possible to fuse every fusion pair. The fusion is so much the simpler when the physical properties of the fusion partners such as cell size and membrane stability are identical or at least similar. This is given for homologous fusions, hence homologous fusion events occur easier than heterologous fusions.

Also, the hybrid detection method is of paramount importance. As shown in this thesis, the staining of cells with membrane, cytosolic or nuclear dyes alter the physical properties of the cells and therewith the cell's fusion parameters. The cell fusion parameters, however, can be very different by nature, as in the case of dendritic cells and breast cancer cells, and thereby preventing cell fusion. A more than 4-fold higher electrical field was needed to temporarily electroporate dendritic cells in comparison to the breast cancer cell lines MCF-7 and MDA-MB-231. This finding might be due to a very stable membrane structure of dendritic cells, which is needed to maintain the special shape of dendritic cells with all its dendrites. It has been presented in this work that fusion between dendritic and breast cancer cells is not feasible and fusion events described in literature might only be due to false analysis and over-optimistic interpretation of data.

The fusion of dendritic cells and cancer cells for the generation of a cancer vaccine has occupied researchers over the last years. The first two papers reporting fusions of human dendritic cells with tumour cells have been published in the year 2000 (SCOTT-TAYLOR ET AL. (2000), KUGLER ET AL. (2000)). Since then, further 10 articles about dendritic cell/tumour cell fusions were published until and including November 2005. They are compared and analysed in regard to the used fusion partners, parameters and results in the table on page 244 and 245. The excitement about dendritic cell/tumour cell hybrids as cancer vaccine reached its height in 2003/2004 with 8 published articles in 18 months.

All publications refer to the very first article in this field (SCOTT-TAYLOR ET AL.(2000))

published in *Biochimica et Biophysica Acta* and/or to the work of KUGLER AND COLLEAGUES (2000) published in *Nature Medicine* in the same year. Appallingly, the results of both papers are not reproducible.

Prof. A.G. Dalgleish, in whose group Scott-Taylor conducted his research, acknowledged that they "gave up working on the fusion" approach, because they "could not get the required numbers consistently" and the hybrids "do not divide" (personal communication). Thereafter, the group changed their strategy and loaded dendritic cells with irradiated cells and lysates.

In the article of Kugler and colleagues (2000), the generation of tumour cell-dendritic cell hybrids and the use of this hybrid in a vaccination strategy for cancer patients with renal cell carcinoma has been reported. The university of Göttingen, where Kugler conducted his research, and the German Research Foundation (DFG) both launched an investigation after allegations were raised that a picture of a dendritic cell/tumour cell hybrid that Kugler had declared its own and used in his thesis and another publication, was downloaded from the internet. The picture did not even show a fusion hybrid of a dendritic cell and a tumour cell, but a hybrid of a homologous tumour cell fusion. In addition, the research presented in the *Nature* paper was strongly criticised by Prof. Ulrich Zimmermann (University of Würzburg), a specialist in the field of cell fusion. He wrote a letter to the Göttingen faculty, in which he claims that the cell hybrids used in the Kugler et al. experiments cannot be live because of the long pulses used for fusion and may even be dangerous for patients, due to high amounts of aluminium ions in the vaccine, which were solubilised from the electrodes upon fusion (FRIEDRICH ET AL. (1998)). Furthermore, other scientists from the University of Göttingen or the Medical University Clinic Tübingen, where the vaccination trial took place, were not able to reproduce the tumour vaccine generation. Finally, three and a half years after publishing, the article in *Nature Medicine* was retracted. The following explanation was given: "The authors unanimously wish to retract this paper, because of several incorrect statements and erroneous presentation of primary data, results and conclusions". The authors were found guilty of negligence and were admonished. They have admitted that they falsified the primary data, which made it a precarious case, especially if one bear in mind that patients were involved.

Both lead authors, Scott-Taylor and Kugler, must have been aware of the fact, that data from FACS analysis alone, do not suffice to proof the generation of fusion hybrids. Scott-Taylor wrote: "Membrane fragmentation and amalgamation are common effects of electric pulses to cells and are well known to distort estimations of cell fusion"..."and makes surface staining

No.	Author	Year	Source of tumour cells	Fusion Yield	Viability	Comments
1	Scott-Taylor et al.	2000	<ul style="list-style-type: none"> LNCaP (prostate carcinoma) MCF-7 (breast carcinoma) 	9-24%	n.d.	<ul style="list-style-type: none"> FACS analysis shows problems in compensation no microscopic analysis
2	Kugler et al.	2000	<ul style="list-style-type: none"> renal cell carcinoma 	10-15%	n.d.	<ul style="list-style-type: none"> FACS analysis no microscopic analysis
3	Jantscheff et al.	2002	<ul style="list-style-type: none"> Me15neo+ (melanoma) 	3-18%	59-86%	<ul style="list-style-type: none"> no FACS analysis no microscopic analysis data from two DC/tumour cell fusions mixed with data from 6 other fusions
4	Gottfried et al.	2002	<ul style="list-style-type: none"> ROT129 (renal cell carcinoma) Mel Im (melanoma) Mel 108 (melanoma) 	5%	50-95%	<ul style="list-style-type: none"> only FACS data of Mel Im shown microscopy data not shown
5	Goddard et al.	2003	<ul style="list-style-type: none"> B cell chronic lymphocytic leukaemia (B-CLL) 	9%	20%	<ul style="list-style-type: none"> FACS analysis not shown no microscopic analysis
6	Parkhurst et al.	2003	<ul style="list-style-type: none"> 888mel (melanoma) 	12-52%	n.d.	<ul style="list-style-type: none"> FACS analysis microscopy no comparison before/after fusion fusion yield is given as yield in adherent cell fraction
7	Trefzer and Walden	2003	<ul style="list-style-type: none"> melanoma 	5-20%	> 50%	<ul style="list-style-type: none"> FACS analysis shows shifting of populations, resulting in wrong determination of fusion yield no microscopic analysis
8	Trevor et al.	2004	<ul style="list-style-type: none"> A549 (lung cancer) U251 (glioma) MCF-7 (breast carcinoma) Colo 829 (melanoma) 	8-10%	85-95%	<ul style="list-style-type: none"> FACS analysis microscopy compensation problem for MCF-7/DC fusion
9	Haenssle et al.	2004	<ul style="list-style-type: none"> melanoma 	7-13%	50%	<ul style="list-style-type: none"> FACS analysis microscopy
10	Weise et al.	2004	<ul style="list-style-type: none"> head and neck squamous cell carcinoma (HNSCC) 	15-25%	55-81%	<ul style="list-style-type: none"> FACS analysis with inexplicable score and shifting of the cell population microscopic analysis
11	Barbuto et al.	2004	<ul style="list-style-type: none"> metastatic melanoma renal cell carcinoma 	15-30%	30-100%	<ul style="list-style-type: none"> no FACS data shown no microscopic analysis
12	Imura et al.	2004	<i>article only in Japanese</i>			

Figure 5.1: Comparison of papers reporting tumour cell/DC fusion

Ratio DC : FP2	Fusion medium	cell concentration	Chamber	Alignment	Fusion Pulse	post-fusion	Analysis
1:1	0.3 M sodium sucrose solution	1.3E+06 ml ⁻¹	0.4 cm wax laminated electroporation cuvette	60 v/cm, 5 s	100-300 V/cm	5 min rest	• CellTracker
1:1	0.3 M glucose solution	?	wax laminated electroporation cuvette	100 V/cm, 5-10 s	1200 V/cm	-	• CellTracker
1:1/ 2:1	RPMI 1640 + 10% FCS	1.0E+08 ml ⁻¹	0.2 cm electroporation cuvette	-	900 V/cm, n=1	removed immediately from cuvette	• GFP expr. (tumour) • anti-HLA-DR (DC)
1:1	5% glucose solution	?	0.4 cm electroporation cuvette	50-100 V/cm, 5 s	1000 V/cm, n=1	-	• CellTracker
1:1	0.3 M sodium sucrose solution	5.0E+05 ml ⁻¹	electroporation cuvette	-	500 V (?), 8.7 ms	-	• anti-CD20 (tumour) • anti-CD86 (DC)
1:1	5% glucose solution	1.0E+07 ml ⁻¹	pecially designed concentric fusion chamber	150 V/cm, 10 s	1200 V/cm, 25 µs	5 min rest	• CellTracker (tumour) • anti-CD11c/CD40/CD80/CD86/CD83 or HLA-DR (DC)
1:1	5% glucose solution	2.0E+07 ml ⁻¹	0.4 cm wax laminated electroporation cuvette	125 V/cm, 10 s	1000 V/cm, n=1	5 min rest, transfer to relaxation buffer (KCl, NaCl, EDTA, PIPES, ATP)	• CellTracker
1:1	Cytofusion Medium C (sorbital fusion medium from Cyto Pulse Sciences, Columbia, MD, USA)	2.0E+07 ml ⁻¹	6mL coaxial electrofusion chamber (4mm gap) (Cyto Pulse Sciences, Columbia, MD, USA)	100 V/cm, 10 s; or 187.5 V/cm, 10 s	2000 V/cm, 40 µs, n=4	post-alignment 112.5 V/cm, 55 sec; 30 min rest	• CellTracker (MCF-7, Colo 829, U251) • anti-Keratin (A549) • anti-HLA-DR (DC)
1:1	Ringer solution/5% glucose solution	5.0E+07 ml ⁻¹	electroporation cuvette	20 V (?) continuous	500 V (?), n=1/n=3	-	• CellTracker
1:1	5% glucose solution	2.0E+07 ml ⁻¹	0.4 cm wax laminated electroporation cuvette	75 V/cm, 10 sec	750 V/cm, 10 µs, n=1	5 min rest	• anti-HEA (human epithelial antigen) (tumour) • anti-HLA-DR (DC)
1:1	5% glucose solution	1.0E+07 ml ⁻¹	electroporation cuvette	62.5 V/cm, 15 s	1000 V/cm, n=1	2 min rest, 5 min relaxation buffer	• CellTracker

Figure 5.2: Continuation of Table from figure 5.1

a flawed method of assessing the proportion of hybrid cells". He therefore used cytoplasmic CellTracker dyes to stain the fusion partners before fusion. Dual-fluorescent events detected by FACS in the negative control (incubation without pulsing) were identified as aggregates of individually stained cells by fluorescence microscopy. What Scott-Taylor did not allow for, was the additional formation of hybrids due to the fusion process. Thus, the only possibility how to validate cell fusion, and why Kugler was in need of a picture of a hybrid, is an analysis by microscopy. For this reason, microscopic data are of paramount importance, even if articles are published in high-ranking journals.

For the evaluation of a cell solution after the fusion process, the cells should be analysed by FACS and confocal microscopy. Therefore, a specific monoclonal antibody should be available for each fusion partner to allow distinction between the fusion partners. The cells would be labelled after the fusion has taken place, so that the membrane properties are not altered due to the staining before the fusion process. The double positive events are determined by FACS, whereas it is important not to gate the whole upper right (UR) quarter of a dot plot as it can often be found shown in the representative fusion analysis in figure 5.3. The obtained fusion efficacies by this kind of data analysis are misleading and not related to the actual fusion efficacy. As shown in figure 5.3, it is very obvious that most of the events shown in the UR quarter are due to the shifting of the original populations into this quarter of the dot plot. This shifting of populations as described in section 3.3.2 appears after pulse application and is probably due to changes in the self-fluorescence of the cells caused by exposure to the electrical field. As shown in this thesis, the shifting of the cell populations is intensified the higher the applied field strength. In general, for FACS analysis of fusion processes, the hybrid populations should be searched and detected in fluorescent dot plot regions that have the single fluorescent magnitudes approximately equal to those of the unfused cells, as described by JAROSZESKI AND COLLEAGUES (1993). The double positive cells found in this plot region should then be sorted with the help of a FACSorter and further analysed by means of fluorescent microscopy to determine between real hybrids and cell aggregates or cell fragments.

Confocal microscopy would be the best choice to analyse the potential hybrid cells. Each hybrid should at least contain two nuclei and the cell membrane should be a mixture of the membranes of the two fusion partners. The latter can be observed by staining the cell membrane after the fusion using monoclonal antibodies specific for each fusion partner. Prelabelling of the cells with discrete fluorochromes prior to fusion should be avoided.

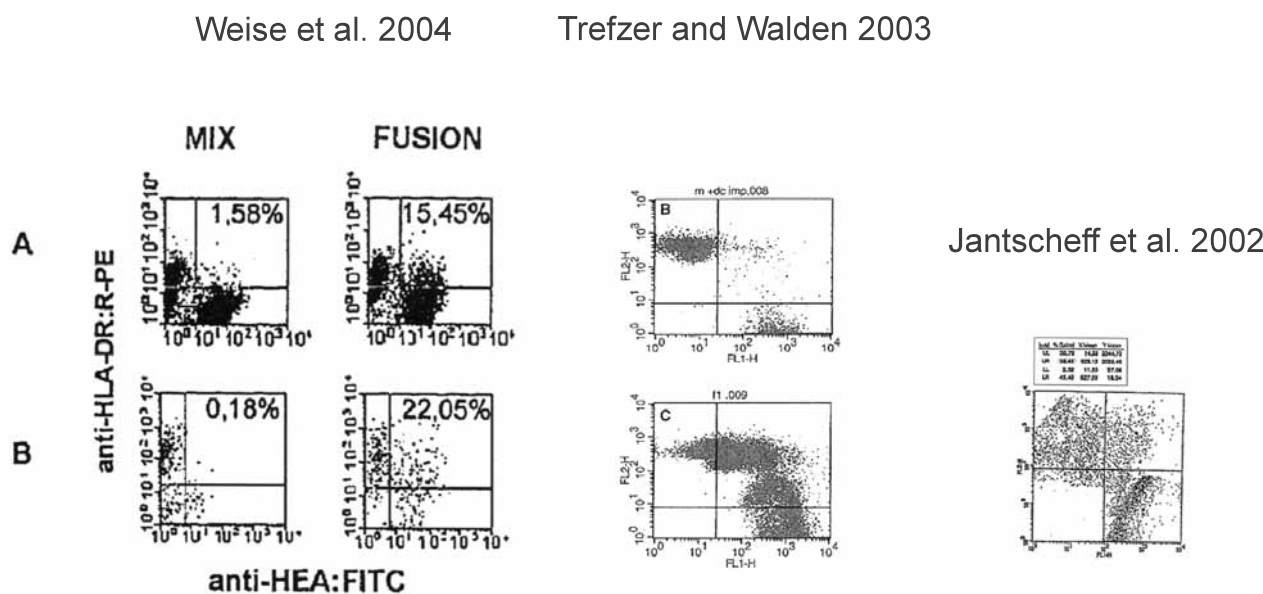


Figure 5.3: Three representative dot plots of FACS analysis of fusion processes.

Furthermore, it is essential to determine the viability of potential fusion hybrids and the integrity of the cell membrane. As criticised by Zimmermann in regard to the Kugler paper: "Dead (hybrids) do not migrate" (BÄR (2001)) - and do not process or present tumour-associated antigens.

Regarding the electrofusion chambers some precautions should be taken to provide an optimal fusion environment. Electroporation chambers (especially those with Aluminium electrodes) should not be diverted from their intended use. Due to their big electrode distance, the cell solution is considerably heated up when the chamber is used with field strength of more than 1 kV/cm, which can damage the cells. The wax, which is applied by some researchers to one electrode of the electroporation cuvette to obtain a non-uniform electrical field, could detach during the fusion process. Its influence on the fusion process itself and the effect when injected into patients with the rest of the cell vaccine is unknown. Thus, a fusion chamber should be used, which was only designed for this purpose. With the development of the fusion chambers for arranged electrofusion of mammalian cells, which is presented in this thesis, homologous fusions, which are normally favoured over heterologous fusions, are avoided.

The above "rules" for the fusion process and its analysis applies for every mammalian cell fusion, but for each fusion pair the electrofusion parameters need to be determined separately, since they are dependent on the cell radius and the other cell-specific properties. In the case of dendritic cells and breast cancer cells, no fusion parameters were found, which would allow for

the fusion of these two cell types. Four $65\mu s$ electrical pulses of 8.5 kV/cm would be needed to electroporate and subsequently fuse dendritic cells, while at this field strength all breast cancer cells would be lysed. If in contrast the optimal parameters for breast cancer cell would be used (1.8 kV/cm , $20\mu s$, $n=1$ or 2), not a single dendritic cell would be permeabilised. With these physical parameters of monocyte-derived dendritic cells and tumour cell lines from breast cancer patients, the fusion process is not feasible. As seen in the discussed literature, the published data and personal communication with other researchers in this field do not argue the converse. Additionally, after the excitement had reached its height in 2003/2004, the successional articles in 2005 did not report dendritic cell/tumour cell fusion, but investigated the effect of the electrofusion process on the immunogenicity of allogeneic human cells (HOCK ET AL. (2005)) and the impact of electrical charge on the viability and physiology of dendritic cells (HILPERT ET AL. (2005)). This underlines that few was known about the biophysical properties of DCs when earlier publications claimed the generation of DC/tumour cell hybrids.

Furthermore, huge differences in the fusion parameters might also exist for other DC/tumour cell fusion pairs, because of a high membrane stability of dendritic cells. Discussions of strategy and results with the workgroup of Prof. Dr. E. Neumann of the Physical and Biophysical Chemistry Department at the University of Bielefeld, especially with PhD student Marco Schmeer, arrived at the conclusion that a search for other fusion pairs should be started for the field of cancer immunotherapy. B-cell/tumour cell fusions might be feasible due to a similar cell size of the fusion partners.

5.5 Immunological Evaluation

Although the generation of dendritic cell/tumour cell hybrids by electrofusion have not been proven in literature and the difference in fusion parameters as presented in this thesis are significant and should not allow an electrofusion, several papers reported induction of anti-tumour immunity *in vivo* and *in vitro*. For this reason, the fusion outcome of experiments accomplished in this thesis were employed in *in vitro* expansion assays of effector cells.

T-cells from healthy donors were amplified in an autologous stimulation by cocultivation with dendritic cells at a ratio of 10:1. The dendritic cells were either subjected to an electrofusion process together with MCF-7 cells, were mixed with MCF-7 cells, which were subjected to the fusion pulse, or loaded with MCF-7 tumour cell lysate. The latter approach was chosen as

a reference for the hybrids, since it is widely used in dendritic cell based immunotherapy of cancer.

The quantitative and qualitative changes in T-cell number were measured over time and showed a very strong proliferative response with an overall expansion of 14.1-fold of autologous CD4⁺ and CD8⁺ T-cells stimulated with DCs that were mixed with pulsed MCF-7 cells. A lower, but still strong proliferation (6.54-fold) was observed when T-cells were stimulated with DCs, which were subjected to 4 fusion pulses together with MCF-7 cells. The lowest expansion (expansion factor: 3.94-fold) was found for the DCs loaded with MCF-7 tumour cell lysate. Nevertheless, the latter expansion factor was still in the expected range, as shown by other researchers for lysate-pulsed dendritic cells in mixed leukocyte reactions (BOHNENKAMP ET AL. (2004)).

However, the "fusion" approach showed a much better result with an 6.54-fold increase in T-cell number. Although no hybrids could be detected, the "fusion" outcome still showed a strong immunestimulatory effect. An explanation would be the uptake of MCF-7 cell debris by dendritic cells, either due to endocytosis or via the pores, which are formed during the electroporation/electrofusion process. The bits and pieces of the tumour cells were then processed internally and presented on the MHC complexes on the cell surface of the DCs. In this connexion, the uptake of small parts of tumour cell membrane could have been an advantage over the lysate approach, where after several freeze/thaw cycles the insoluble cell debris such as membrane fractions and organelles were removed by filtration. This might result in a lower concentration of membrane proteins. BOHNENKAMP tried to load DCs with tumour cell lysate containing also the insoluble parts of the lysate, but had to find that this resulted in a reduced number of viable dendritic cells with a phenotype that did not show high expression of DC markers such as CD80, CD86 and CD83 (Bohnenkamp, personal communication). The "fusion" approach seems to be a better approach to load DCs also with insoluble tumour cell fragments. It is also the more physiologic approach, as DCs are loaded with whole tumour cells or the debris of whole tumour cells and not with artificially produced lysate where an unknown part of the cells is removed by filtration.

The third approach, which used dendritic cells loaded with the cell debris of MCF-7 cells, which results from the subjection of the tumour cells to four electrofusion pulses (with parameters tailored for DCs), did perform even better. The difference in comparison to the "fusion" pulse is, that in this approach higher numbers of viable dendritic cells can be expected, since

the DCs themselves are not subjected to the fusion pulses. If cells are subjected to electrical pulses, which render them temporarily permeable, a small percentage of cells is lost due to necrosis.

Furthermore, the analysis of the CD8⁺ T-cell subset showed a strong expansion of memory T-cells, which normally function as constitutive immune memory and form in concert with antibody responses the basis for protective immunity against infection and disease. According to the signal strength model for T-cell differentiation and memory T-cell generation (SALLUSTO ET AL., 2004), the strength of signalling received by T-cells is a major factor that determines T-cell differentiation. Priming of CD8⁺ cells by a signal of suboptimal strength may induce CD8⁺ T-cell proliferation, but the cells fail to upregulate antiapoptotic molecules and receptors for homeostatic cytokines and will die by neglect. Only large numbers of mature DCs carrying high doses of antigen would promote a massive proliferation of antigen-specific T-cells, which will persist as effector memory cells. If the DC/T-cell ratio is low or the stimulation is brief, central memory T-cells will be generated preferentially. A too prolonged and strong proliferation may on the other hand lead to activation-induced cell death (AICD) of the T-cells. However, the used method of loading DCs with cell debris, which was originated by the electrical pulsing of tumour cells, seemed to deliver a stimulation signal with exactly the right strength to produce a large amount of effector memory T-cells.

Chapter 6

Summary & Outlook

Cellular immunotherapy of cancer is a hot topic ever since the discovery that the immune system is capable of recognising tumour cells. Dendritic cells (DCs) are the professional antigen presenting cells that are best suited for cell-based immunotherapy and therefore *ex vivo* generated DC cancer vaccines are currently applied in clinical trials. Several methods have been devised for the loading of DCs with tumour information. Instead of identifying, characterising and targeting only a single tumour-associated antigen (TAA), dendritic cells can also be loaded with whole-cell tumour information. In the majority of cases, identifying a TAA is a tedious process and targeting only a single antigen is not likely to succeed unless that antigen is necessary for the function and survival of cancer cells. For this reason, a whole tumour cell approach has several advantages.

The fusion of dendritic cells with tumour cells is used as such a whole tumour cell loading strategy and the application of the fusion outcomes, e.g. possible hybrids cells, have been shown to induce anti-tumour immunity in several cancer models and clinical studies (Orentas et al. 2001, Hayashi et al. 2002, Rosenblatt et al. 2005). Nevertheless, the absence of a reliable and reproducible fusion method, the poor fusion efficacies and the limitation of autologous tumour material for some tumour types were thought to prevent a broad application as cancer vaccine.

This study aimed for the development of new fusion devices to overcome these limitations. Cluster formation, which typically takes place in commercially available electrofusion chambers during cell alignment owing to similar electrophysical parameters (such as cell size, shape and transmembrane potential), was found to be a major limitation of heterologous mammalian cell fusion. The formation of cell clusters and homologous fusions can be avoided by a so-called arranged electrofusion process, where two fusion partners are subjected to an alternating ar-

rangement inside the fusion chamber. This alternating arrangement was realised in two newly developed electrofusion chambers by means of micropatterning and microfluidics, whereas clinical requirements have been considered throughout the whole process development. Both electrofusion chambers were also dimensioned to produce a sufficient amount of hybrid cells at once, thus satisfying the requirement for high-throughput cell fusion.

The electrofusion chambers were fabricated using a combination of several microtechnological methods such as photolithography, metal-film deposition, laser and glass etching technologies. These microdevices included up to 9 alternating cell lanes preventing cluster formation and homologous fusion events by this alternating cell arrangement. Additionally, all dimensions had been chosen to correlate sizes of cells and to allow fusion of large numbers of cells simultaneously. Direct visualisation of the fusion procedure was also permitted in both lab-on-a-chip approaches, allowing for fusion evaluation by means of fluorescent microscopy.

Inside the first electrofusion chamber, the alternating cell arrangement was implemented by the immobilisation of cells onto $15\mu\text{m}$ wide covalently-bound antibody lines. Self-assembled monolayers (SAMs) of 11-mercaptoundecanoic acid (MUA) were formed on evaporated gold lines, activated by a mixture of N-hydroxysuccinimide (NHS) and 1-ethyl-3-(dimethylamino)propylcarbodiimide (EDC), and used to covalently bind monoclonal antibodies via their primary amino groups forming a peptide bond. By the subsequent integration of electrodes, the build up of the framing chamber and the connection to the electrical equipment for cell fusion, a functional microelectrofusion device was established.

The second electrofusion device was based on microfluidics and the alternating cell arrangement inside the fusion chamber was realised by laminar single-cell flows. Also in this case, an alternating cell arrangement was demonstrated and formation of hybrid cells was achieved for test cell lines.

The deployment of microfabrication technologies for the electrofusion chamber development provided unique process advantages to promote this biological application and was not only used because microdevices are in and nice to have. It furthermore made these lab-on-a-chip applications suitable for parallelisation and automation.

After fusion could be proven in model cell lines, both chambers were applied for the formation of dendritic cell/tumour cell hybrids for breast cancer immunotherapy. Thereby, all relevant fusion parameters such as fusion buffer, alignment process by dielectrophoresis, field intensity, pulse duration and number of pulses were investigated for their influence on fusion efficacy.

It turned out that a fusion event between monocyte-derived dendritic cells and breast cancer cells from tumour cell lines is very unlikely due to huge differences in the physical properties and therewith in the needed electroporative electrofusion pulse. Dendritic cells need a more than four times higher fusion pulse and several subsequent pulses instead of just a single fusion pulse, to reversibly form membrane pores. Under these conditions, all tested breast cancer cell lines were lysed and no heterologous hybrid formation was observed.

These results query other reports about DC/tumour cell hybrid formation, while erroneous fusion analysis encourages this assumption. Nevertheless, the fusion outcomes were applied to an immunological evaluation by *in vitro* expansion of effector cells, which showed high stimulatory capacity of dendritic cells loaded by means of fusion or better to say electrical field treatment. The expansion of memory cytotoxic T-lymphocytes (CTLs), potent killer cells, were demonstrated and significantly better results were obtained compared with the widely used lysate-pulse approach for the loading of dendritic cells.

Hence, the developed electrofusion chambers represent functional devices for a new loading strategy of dendritic cells based on electrical field manipulation. Furthermore, the devices can also facilitate other real fusion applications such as hybridoma production, where a high-through-put cell fusion device is a benefit for the production and identification of a good producer of antibodies. Additionally, the famous case of Dolly, the cloned sheep, would not have been possible without fusion. Thus, several application areas are available and new might be discovered in future, which may benefit from the electrofusion chambers for arranged electrofusion of mammalian cells, developed in this project. Thereby, the low productions costs of the electrofusion chamber based on immobilisation would be an asset for medical disposables for clinical use on the one hand. On the other hand, the microfluidic electrofusion chamber holds the possibility for automation and the on-chip integration of additional units for fusion hybrid detection, by optical or impedimetric methods, units for cell sorting by FACS.

In this way and with the new findings about dendritic cell/tumour cell fusion, a project, which was primarily focussed on breast cancer, can have benefits for other areas, as well. Dendritic cell-based immunotherapy, for example, is a generally applicable approach, and the tools and methods for DC loading, which were developed in the project, are widely applicable to other types of cancer further enhancing the relevance of this project.

Nevertheless, all forms of DC-based therapies are still experimental and not approved for use as a standard treatment, but are already being tested against a variety of cancer types in ongoing

clinical trials. Much still needs to be learned regarding antigen loading, maturation, route of administration and migration of DC-based vaccines. The administration route of the vaccine needs to be investigated such as intradermal, intravenous, intralymphatic or by direct injection into the lymph node. Most delivery methods are dependent on the migration of antigen-bearing DCs from peripheral tissue to the lymph nodes, thus require viable cells.

Tumour-specific immunotherapy will not be available tomorrow, but the lessons learned from this study can now be applied to the development of therapeutic breast cancer vaccines and vaccines against other cancer types.



Figure 6.1: Three representative dot plots of FACS analysis of fusion processes.

Collaboration is an incredibly important aspect of research and being within an institute like the Research Centre Jülich, collaboration is facilitated. In this project, the key to being successful was multidisciplinary. A broad skill base was needed to understand all the different aspects of cell culture, immunology and microtechnology. The combined skills, expertise and resources of several collaboration partners at the Research Centre Jülich, the Danish Technology Institute, the Cranfield University and from companies inland and abroad succeeded in two new electrofusion chambers for arranged electrofusion, which were both filed as patents and partly already granted.

Chapter 7

Material and Methods

7.1 Immobilisation

7.1.1 Mask Preparation

The layout of the photolithographic mask was designed by the means of the AutoCAD LT 2000i software. The chrome masks were manufactured by e-beam lithography or purchased from J.D. Photo Tools Ltd. (Oldham, UK).

Table 7.1: Materials for the mask preparation

Software	AutoCAD LT 2000i	Autodesk, Munich, Germany
E-beam writer	EBPG 5HR	Leica Microsystems, Wetzlar, Germany

7.1.2 Master Preparation

The master stamp was prepared on a Si-wafer. A spin-coat of the negative photoresist SU-8 25 was applied with a height of 25 micrometer. The film was exposed to UV light via a photomask for 33sec and processed according to the manufacturer's recommendations. For a better redeemableness of the PDMS stamps after the moulding, the master was silanised with a solution of dichlormethyloctadecylsilane in toluene for 4h at 65°C and was then thoroughly washed with 2-propanol and water. In the end, the master was dried with argon and stored.

Table 7.2: Materials for the master preparation

Si wafer		MEMC Electronic Materials, St. Peters, USA
Negative photoresist	SU-8 25	Micro resist technology, Berlin, Germany
Spin coater		
Dichlormethyloctadecylsilane		Sigma, Deisenhofen, Germany
Convection oven		Heraeus, Hanau, Germany
2-propanol		Merck, Darmstadt, Germany

7.1.3 PDMS Stamp Preparation

A silicon solution of Sylgard 184 was prepared, whereas the two components (prepolymer and curing agent) were mixed at the ratio 10 : 1. Bubbles were removed under vacuum in an excicator and the mix was poured onto the master. The polymerisation time was shorten by heating at $60^{\circ}C$ for $4h$. When the stamps were cured, they were peeled off the master and surmounting stamp parts were removed. A "ticket-punch" was used to make small holes into the stamp, one at every end of a channel or channel bundle. Subsequently, the stamps are cleaned in 2-propanol under ultrasonication and rinsed with water, followed by a $2min$ ultraviolet/ozone (UVO) treatment. Not to loose the hydrophilic character again, the stamps were treated for $1h$ with a $0.1M$ sodiumhydroxid solution, thoroughly washed with water under ultrasonication and stored in deionised water. Just before use, the stamps were dried under a stream of air. The above protocol was also used under sterile conditions when appropriate.

Table 7.3: Materials for the PDMS stamp preparation

PDMS prepolymer	Sylgard 184	Troller Kunststoffe, Jegenstorf, Schweiz
PDMS curing agent	Sylgard 184	Troller Kunststoffe, Jegenstorf, Schweiz
Convection oven		Heraeus, Hanau, Germany
2-propanol		Merck, Darmstadt, Germany
UVO cleaner	model 42-220	Jelight, Irvine, USA
Sodiumhydroxid		Merck, Darmstadt, Germany
Ultrasonic bath		Köttermann Labortechnik, Uetze, Germany

7.1.4 Microcontact Printing

A PDMS stamp was inked with a 10 % aminosilane solution in water and dried. The inked stamp was dried in a stream of nitrogen and pressed to the substrate for 30sec.

Table 7.4: Materials for direct microcontact printing

3-aminopropyltriethoxysilane		Sigma, Deisenhofen, Germany
Glass wafer	Pyrex, optically polished on both surfaces with ground standard flat 7.5cm in diameter thickness 0.5 + 0.005mm	Barloworld Scientific, Stone, UK

7.1.5 Inverse Microcontact Printing

For inverse microcontact printing, the cleaned and dried PDMS stamps were contacted with the glass substrate. The subsequent immobilisation reactions were carried out in the microchannels, which were formed between the PDMS stamp and the substrate.

Table 7.5: Materials for inverse microcontact printing

Glass wafer	Pyrex, optically polished on both surfaces with ground standard flat 7.5cm in diameter thickness 0.5 + 0.005mm	Barloworld Scientific, Stone, UK
-------------	--	----------------------------------

7.1.6 Immobilisation Reaction

A 10 % aqueous solution of 3-aminopropyltriethoxysilane was prepared and its pH was adjusted to 3,45 with 6M HCl. The solution was reacted with the glass surface for 2h at 60°C in a

convection oven. The oven was turned off and another 2,5 hours are given to cool the substrate down and complete the reaction. The channels were emptied with the use of a vacuum pump and washed three to four times with the next reaction solution, a 2,5 % solution of glutardialdehyde in a phosphate buffer. The 0.1M sodium phosphate buffer had a pH of 7 and was produced by mixing 30.5mL of a 0.1M Na_2HPO_4 solution with a pH of 8.5 with 19.5mL of a 0.1M NaH_2PO_4 with a pH of 4.7. The glutardialdehyde solution was reacted with the silanised glass surface for 2h at room temperature.

Table 7.6: Materials for immobilisation reaction

3-aminopropyltriethoxysilane		Sigma, Deisenhofen, Germany
<i>HCl</i>		Merck, Darmstadt, Germany
Convection oven		Heraeus, Hanau, Germany
Glutardialdehyde	50 % aqueous solution	Sigma, Deisenhofen, Germany
Vacuum pump		Oerlikon Leybold Vacuum Cologne, Germany
Bovine serum albumin	FITC-labelled	Sigma, Deisenhofen, Germany

Table 7.7: Antibodies used for immobilisation

Antibody reacts with	Clone	Isotype	Conjugate	Manufacturer
CD34	581	Mouse IgG ₁ , κ	FITC	Becton Dickinson
CD34	581	Mouse IgG ₁ , κ	unlabelled	Becton Dickinson
CD45	HI30	Mouse IgG ₁ , κ	FITC	Becton Dickinson
CD45	HI30	Mouse IgG ₁ , κ	Biotin	Becton Dickinson
CD45	HI30	Mouse IgG ₁ , κ	unlabelled	Becton Dickinson

Subsequently, the channels were emptied using the vacuum pump and filled with a protein solution, of the protein, which should be immobilised in lines. For a first test, FITC-labelled bovine serum albumin was used. Later on, different antibodies were immobilised (see table 7.7 on page 258). The last reaction step took place at 4°C over night.

During the optimisation of the immobilisation reaction for the use with inverse microcontact printing, the reaction time of the first reaction steps were reduced to 1h and the filling holes of the PDMS stamp were covered with adhesive tape during all immobilisation reactions to avoid blockage of the channels by drying.

7.1.7 Ellipsometry

For the ellipsometrical analysis of the thin films, applied on a glass wafer, an Imaging Ellipsometer was used. Local measurements of layer thickness and recording of a thickness map were performed by recording a map of Delta and Psi from which the map of the thickness is calculated. In addition, live-contrast-images were obtained, where the layer thickness is correlated with the greyscale.

Table 7.8: Materials for ellipsometry

Imaging Ellipsometer	<i>EP</i> ³	Nanofilm, Goettingen, Germany
Objective	10x	Nanofilm, Goettingen, Germany
Software for optical modelling	<i>EP</i> ³ View	Nanofilm, Goettingen, Germany

7.1.8 Lift-off Photoresist Processing and Metal Coating

A 100mm glass wafer was coated with 2.5mL LOR 3B photoresist for 45sec at 3000rpm and prebaked on a hot plate for 5min at 170°C. The spin-coat should have 1.2 - 1.3fold the thickness of the desired metal film. S1813 was used as imaging resist. 2.5mL of this positive photoresist were spun on top of the LOR (45sec, 4000rpm). A prebake step was following on a hot plate for 2min at 115°C. The obtained bi-layer stack was exposed to UV light for 8sec and subsequently developed using the Microposit MF-319 developer in an immersion mode for 40sec. The wafer was rinsed with deionised water using an overflow setup and dried with air. For the deposition of the gold film a 2µm thick chrome layer was applied first as adhesive agent. Subsequently, a 200nm high gold layer was applied under high vacuum of approximately $1 - 2 \cdot 10^{-6}$ mbar. The deposition is controlled via a film thickness monitor, which measures the nominal thickness of deposited films. The thickness and deposition rate can then be calculated from user-supplied data on density and acoustic impedance of the film material.

The reentrant profile of the resist ensures discontinuous film deposition and allows the lift-off of the bi-layer resist stack, leaving only the desired gold film. SVC-14 positive photoresist stripper is used for the lift-off process. Two stripping tanks of SVC-14 were set up and the solvent tank temperatures were set between $70 - 90^{\circ}\text{C}$ (80°C % baseline). The glass wafer with LOR bilayer and deposited gold film were placed in bath 1 for $5 - 20\text{min}$ under sonic agitation until the biggest part of the unwished gold film was removed. Then, the wafer was transferred to bath 2 for additional $5 - 20\text{min}$. After stripping, the wafer was rinsed with deionised water (quick dump rinse) for 6-8 cycles and dried under a stream of nitrogen.

Table 7.9: Materials for LOR processing

Spincoater	P-6708D	Speciality Coating Systems Indianapolis, USA
Hot plate		Stuart Scientific
Lift-off resist	LOR 3B	Microchem, Newton, USA
Positive Photoresist	S1813	Rohm and Haas, Coventry, UK
Developer	Microposit MF-319	Rohm and Haas, Coventry, UK
Positive Photoresist Stripper	SVC-14	Rohm and Haas, Coventry, UK
Gold wire	99.995 % purity	Aldrich Chemicals, Wisconsin, USA
Vacuum Coater		BOC Edwards, London, UK
Film deposition monitor	IL 150	Intellectrics Ltd, Glasgow, UK

7.1.9 Laser Processing

A CO_2 laser with a wavelength of $10.6\mu\text{m}$ was used to cut 6 different parts for the build-up of the electrofusion chamber (based on the immobilisation approach). The parts for the bonding layer were cut into Arcare 8939. Arcare 8939 is a white, thin and flexible plastic film coated on both sides with an acrylic medical-grade pressure-sensitive adhesive. It is 3mm thick and suitable for bonding. The parts for the top layer were cut into Melinex polyester film. The structures were drawn using the drawing editor of the WinMark laser marking software. The following parameters and materials were used for laser processing.

Table 7.10: Parameters for laser processing

Pline Start Delay Base	400 μ s
Pline End Delay Base	400 μ s
Interseg Delay Base	0 μ s
Off Vector Delay Base	0 μ s
Off Vector Velocity	2000mm/s
Laser power	100 %
Laser Cutting Velocity	400mm/s

Table 7.11: Materials for laser processing

Fenix laser marker		Synrad, Mukilteo, USA
Laser marking software	WinMark Lite	Synrad, Mukilteo, USA
Double-sided tape	Arcare 8939	Adhesive Research Inc., Glen Rock, USA
Acetate foil	Melinex ST725	Dupont, Hopewell, USA

7.1.10 Immobilisation of Antibodies on Gold

The glass wafers with the vapour-deposited gold structures were immersed into 1mM 11-mercaptoundecanoic acid in absolute ethanol (previously vortexed 30min) for 48h. Upon removal, the wafers were rinsed via dipping twice into absolute ethanol and soaked in water for 5min before drying under a stream of nitrogen. NHS esters were formed by exposure of the MUA SAM to an aqueous solution of 1-ethyl-3-(3-dimethylaminopropyl) carbodiimide (EDC) and NHS 75mM and 15mM respectively (1h, 20°C). The glass surfaces of the sample were immersed in a 10mg/mL PEG-silane solution in anhydrous toluene. After removal from the PEG-silane solution, the residual PEG was removed by washing in toluene under sonication for 5min and rinsing with ethanol and distilled water. Subsequently, the NHS ester monolayers were reacted for with an antibody-solution (0.5mg/mL) for 24h at 4°C.

For immobilisation of antibodies under sterile conditions, the glass wafers were sterilised in 70 % ethanol and all reaction steps were accomplished under sterile conditions.

Table 7.12: Materials for laser processing

11-mercaptoundecanoic acid	95 %	Sigma, Deisenhofen, Germany
EDC		Sigma, Deisenhofen, Germany
N-hydroxysuccinimide		Sigma, Deisenhofen, Germany
Polyethylenglycol-silane	MW 5000	Shearwater Polymers, Huntsville, USA
CD45 unlabelled	HI30, Mouse IgG ₁ , κ	Becton Dickinson

7.1.11 XPS

XPS measurements were made on an XPS spectrometer Physical Electronics 5600 with a monochromatised Al Kr X-ray source (1486.6eV photons) with a pass energy of 20eV. High resolution spectra of C1s, O1s, N1s and Au4f regions were obtained and peaks fitted using the Unifit for Windows software (version 32-32). The analysed surface areas were $2mm \cdot 5mm$ big.

7.2 Microfluidics

7.2.1 Fluid Simulation

3D models of the microfluidic devices were developed using a computer-aided design programme (CAD) called Pro-Engineer (Parametric Technology Corporation (PTC), Needham, USA). For the subsequent computational fluid dynamics the CFX software (Ansys Inc, Canonsburg, USA) was used.

7.2.2 UV Laser Micromachining

For the fabrication of microstructures in either PMMA or PET the Krypton-Fluor (KrF) excimer laser MicroMaster (Optec, Frameries, Belgium) was utilised. To obtain a 3-dimensional structure the structures were burned from the upper and the bottom side of the polymer slide and posses through holes to connect both sides with each other. In this setup, the through holes function as alignment points, to place the microstructures in the right direction.

7.2.3 Assembly and Operation of Pump Station

The pump station is established from the components listed in table 7.13. It contains several pumps to pump or suck fluids through the microfluidic chambers. For the connection of these pumps with the microfluidic chip, tubing and valves are needed.

Table 7.13: The Components of the Pump Station

Quantity	Component	Manufacturer
2	Cavro XL 3000 3+ High resolution pumps	Tecan Systems Inc, San Jose, USA
1	Cavro XL 3000 High resolution pump	Tecan Systems Inc, San Jose, USA
1	Cavro XL series smart valve (1 input, 6 outputs)	Tecan Systems Inc, San Jose, USA
2	3-way-micro inert Valves	The Lee company, Essex, USA
1	edge connector for RS232 control	Tecan Systems Inc, San Jose, USA
20	P200 flangeless ETFE ferrules 1/16" OD	Upchurch Scientific, Oak Harbor, USA
20	P235 short flangeless PEEK nuts	Upchurch Scientific, Oak Harbor, USA
10	P272 flangeless frit-in-a-ferrule with 2 μ m filter	Upchurch Scientific, Oak Harbor, USA
10	P702 PEEK union for 1/16" OD tubing	Upchurch Scientific, Oak Harbor, USA
1	P712 1/16" PEEK tee	Upchurch Scientific, Oak Harbor, USA
2	50 μ L syringe	Tecan Systems Inc, San Jose, USA
3	100 μ L syringe	Tecan Systems Inc, San Jose, USA
2	500 μ L syringe	Tecan Systems Inc, San Jose, USA
30 m	non-polar fused silica, 0.25mm ID	Supelco, Bellefonte, USA
3 m	non-polar fused silica, 0.10mm ID	Supelco, Bellefonte, USA
10 m	Teflon tube PTFE, 1/16" · 0.25mm	Mikrolab Aarhus, Hojbjerg, Denmark
10 m	Teflon tube PTFE, 1/16" · 0.50mm	Mikrolab Aarhus, Hojbjerg, Denmark

Cavro XL 3000 Digital Pump

Single or multiple commands can be sent to the pump. For example a single command such as A3000R moves the plunger to position 3000. Commands can also be combined to form a programme string such as IA3000OA0R. This string moves the valve to the input position, moves the plunger to position 3000, turns the valve to the output position and finally returns the plunger to position 0. The pump contains a command buffer of 256 characters. If a command has been sent without $\langle R \rangle$ (execution) command, it is placed into the buffer without being executed. If a new command is sent before the first command is executed, the new command will overwrite the first command. Once a command is executed, the pump will answer immediately. New commands are not accepted until the sequence has been completed.

Table 7.14: Initialisation and valve commands for Cavro digital pump

Command	Description	Variable
Znn	Initialises plunger drive and sets valve output to the right (when viewed from the front of the pump)	nn = 0 (full plunger force) nn = 1 (half plunger force) nn = 2 (quarter force)
Ynn	Initialises plunger drive and sets valve output to the left (when viewed from the front of the pump)	nn = 0 (full plunger force) nn = 1 (half plunger force) nn = 2 (quarter force)
I	moves valve to $\langle I \rangle$ input position. The absolute position is dependent on the initialisation command $\langle Z \rangle$ or $\langle Y \rangle$.	
O	moves valve to $\langle O \rangle$ output position. The absolute position is dependent on the initialisation command $\langle Z \rangle$ or $\langle Y \rangle$.	
E	moves valve to $\langle E \rangle$ xtra position (only for 3-port distribution valves).	
B	moves valve to $\langle B \rangle$ ypass position. This connects the input and output positions bypassing the syringe (only in combination with $\langle Y \rangle$ initialisation).	

Before starting the operation the pumps have to be initialised. During the initialisation the plunger moves upward until it contacts the top of the syringe, thus defining the null position. Additionally, the valves are controlled and set. The force at which the plunger presses against the top of the syringe can be controlled by using special parameters (see table 7.14). Smaller syringes should use a lower initialisation force and larger syringes should use higher initialisation force. A constant speed (500) is applied for initialisation. Using half plunger force is recommended for $250\mu L$ and $500\mu L$ syringes and quarter plunger force for $100\mu L$ syringes and smaller. Further important commands for the operation of the Cavro digital pump are summarised in table 7.15.

Table 7.15: Important commands for Cavro digital pump

Command	Description	Variable
Nnn	Fine Positioning off/on. This command determines the resolution of the plunger travel ($60mm$).	nn = 0 (off; 3000 increments/full stroke) nn = 1 (on, 24000 increments/full stroke)
Ann	moves plunger to the < A >bsolute position nn.	nn = 0..max
Vnn	sets the < V >elocity. It can also be changed on the fly.	nn = 5..5800 Hz (half-steps/second)
X	repeats command: this command repeats the last executed command or programme string.	
Gnn	repeats command sequence. this command repeats a command or programme string nn times.	nn = 0..30000
g	marks the start of a repeat sequence and is used in conjunction with the < G > command. Instead of repeating a whole command sequence the < g > command marks the beginning of a loop. Both the < g > and the < G > commands can be used to nest up to 10 loops.	
Mnn	Delay in < M >illiseconds, delays the execution of a command in milliseconds	n = 5..30000

Cavro Smart Valve

Single or multiple commands can be sent to the Smart Valve. A single command such as A2R turns in the valve in the default (clockwise) or programmed direction to port number 2. Commands can also be combined to form a programme string such as Y2A1M50A2R. This string tells the valve to turn counter-clockwise to port 1, wait 50 milliseconds then continue turning counter-clockwise to port 2. All commands must be followed by an $\langle R \rangle$ (execution) command. Once a command is executed, new commands are not accepted until the sequence has been completed. The Smart Valve contains a command buffer of 256 characters.

Table 7.16: Overview of important commands for Cavro Smart Valve

Command	Description	Variable
Znn	Identifies number of ports on valve and initialises it to port 1	nn = 6
Ynn	Sets valve direction	nn = 1 (clockwise) nn = 2 (counter-clockwise)
Ann	Moves to selected port in direction $\langle Y \rangle$	nn = 1..6
R	Run command, executes a previously sent command	
X	Repeat command	
Gnn	Repeat Command Sequence, repeats a command or programme string nn times	nn = 0..30000
g	marks the start of a Repeat Sequence, is used in conjunction with the ;G; command	
Mnn	Delay in $\langle M \rangle$ milliseconds, delays the execution of a command in milliseconds	nn = 5..30000

Connection of the Components

The three syringe pumps, the SV6+ multiinjection valve and two inert valves were integrated into the pump station. All modules were connected to a single 24 volt (d.c.) power supply and the communication with these components was done from an RS-232 port. Therefore, pump 1 obtained a RS-232 interface board, which was plugged into its mother board. It converts the

signal into RS-485. From then on all devices in the chain communicate through RS-485. In addition, the various components had to be connected with capillaries and tubing to allow fluid flow.

For the prototypes (Microfluidic chamber 1-3):

Nonpolar fused silica capillaries (ID 0.1mm) were glued into the microfluidic chip with the help of UV light curing glue. A carbon cutter (Sigma-Aldrich) was used to cut the fused silica tubing. For the connection of these capillaries to the pumps and valves, which possess standard $1/4 \times 28$ coned ports intended for $1/16$ " OD (outer diameter) tubing, PTFE (polytetrafluorethylen, Teflon) tubing with an ID of 0.25mm and an OD of $1/16$ " was used. Thereby, the PTFE tube acted as a sealtight sleeve: It was expanded by heating over a flame, the fused silica capillary was inserted, and the PTFE tube encased the capillary tightly when cooled afterwards. For the interconnecting tubing between pumps, valves, buffer reservoirs and collecting tanks a PTFE tube ($1/16$ ") with an inner diameter of either 0.25mm or 0.5mm was used dependent on the desired flow rate. Flangeless ferrules and flangeless nuts, normally used in chromatography such as HPLC, together with unions, replaced flange fittings and facilitate replacement and rearrangement of the set-up. Furthermore, so-called frit-in-a-ferrules were used, where buffers or cleaning solutions enter the microfluidic system. These special ferrules incorporate a frit in their body, which filters the pumped solutions inline. $2\mu\text{m}$ filters avoid blocking of the microfluidic channels by dirt.

For the final microfluidic electrofusion chamber (manufactured by Micronit):

The connection of the final microfluidic electrofusion chamber to the macroworld was done with the help of Micronit's chipholder. The microfluidic chip was placed flat on the bottom of the chipholder. The capillaries were entered in the top plate of the chipholder from above. Subsequently, a conic sealing rubber was put on the capillary by sliding it over the capillary's end. The conic side of the sealing rubber needed to be equal to the tip of the capillary. The chip holes were filled with distilled water and the top layer of the chip holder was adjusted. Thereby, the sealing rubbers were pressing the water out of the holes. This excluded the appearance of air bubbles in the connection. In the last step, the bolts were put on the threads and finger tighten. The electrodes were contacted via the contact patches. Small wires were glued to the contact patches by filling the holes at half height with conducting silver paste (see table 7.17 for supplier information).

All parts of the pump station were cleaned and maintained following the supplier's instruc-

tions. The used fluids were filtered before use, apart from the cell solution, and the microfluidic system flushed extensively after each experiment. When unused, the system was filled with a 3 v/v % solution of Mucosal for disinfection.

Table 7.17: Additives for the connection of the microfluidic chip to the pump station and power supply

Glue	Dymax 628	Diatom, Hvidovre, Denmark
Conducting silver		Kemo-Electronic, Langen, Germany
Mucosal		Merz, Frankfurt, Germany

Evaluation by Particle Flow

SPHERO fluorescent polymer particles in the range from 10 to 19 μm (see table 7.18) were used to visualise the flow inside the microfluidic chip.

Table 7.18: SPHERO fluorescent particles

SPHERO, Nile red	10-14 μm	Spherotech Inc., Libertyville, USA
	Excitation 500nm	
	Emission 560nm	
SPHERO, Yellow	15-19 μm	Spherotech Inc., Libertyville, USA
	Excitation 450nm	
	Emission 480nm	
Mucosal		Merz (Frankfurt, Germany)

7.3 Fusion

Before fusion, both fusion partners were harvested by centrifugation, counted and mixed in a ratio of 1:1. The cells were washed twice with hypoosmolar fusion buffer, resuspended in hypoosmolar fusion buffer at different cell densities and introduced into the electrofusion chambers. Electrofusions were always induced by the Eppendorf multiporator regardless of the used chamber (Eppendorf electrofusion chamber, developed microfluidic electrofusion chamber or electrofusion chamber based on immobilisation).

Close contacts between cells were induced by dielectrophoresis. The cells were aligned dielectrophoretically by the application of a low electrical alternating field (5 - 500V/cm) for 5-95sec. After the alignment process, short (10 - 300 μ s) field pulses with field strengths from 250 to 1500V/cm were applied to achieve fusion. Then, the alternating field was applied again for 5-95sec to keep the cells in close contact during the fusion process. Following fusion, the cells were left untreated for 5 minutes at room temperature and subsequently analysed or transferred to cell culture. The content of the electrofusion chambers was rinsed out by using distilled water from a spray bottle, followed by washing with 70 % non-denaturated ethanol.

Table 7.19: Components for the electrofusion of mammalian cells

Hypoosmolar electrofusion buffer	Eppendorf, Hamburg, Germany
Multiporator	Eppendorf, Hamburg, Germany

The electrofusion chambers were also used for dye penetration assays, analysing, which fusion conditions are needed to provide a transient permeabilisation of the membrane allowing electroporative dye uptake. Therefore, cells were pulsed in the presence of trypan blue. After the pulse application the cell solution was incubated for a 10 min period at room temperature. Subsequently, the number N_c of coloured cells of the population was determined. To estimate the number of transiently permeabilised cells by pulse application, the number of stained cells had to be reduced by the number N_{irrev} of cells, which were irreversibly damaged by the applied electrical pulse. Therefore, another batch of cells were subjected to the pulses in the absence of trypan blue, and the dye was added after the incubation period of 10 min. The percentage of reversible permeabilised cells could then be calculated by the ratio of $N_c - N_{irrev}$ to N_t , the total number of the cell population.

7.4 Immunological Methods

7.4.1 Mixed Leukocyte Reaction

For the mixed leukocyte reaction, $1 \cdot 10^6 \frac{1}{mL}$ allogeneic T-cells with known MHC mismatch were co-cultured with matured dendritic cells ($1 \cdot 10^5 \frac{1}{mL}$ (1:10), $5 \cdot 10^4 \frac{1}{mL}$ (1:20), $2.5 \cdot 10^4 \frac{1}{mL}$ (1:40) or without dendritic cells, respectively) in AIM-V medium for 4 days in 6-well plates at 37°C in a humidified 5% CO₂ containing atmosphere. On day 4, the T cell proliferation

was analysed by flow cytometer using characteristic surface markers. The expression of the surface markers CD25 (Interleukin-2 α -chain) and CD71 (transferrin receptor) on day 4 of the mixed leukocyte reaction gives insight into specific cell subsets and T cell responses in the presence of dendritic cells (NGUYEN ET AL., 2003). These markers are involved in activation and proliferation of (allogeneic) T cell responses. T-cell samples were stained for CD3, CD25 and CD71 and compared to corresponding isotype controls.

Table 7.20: Mixed leukocyte reaction

AIM-V medium		Gibco, Carlsbad, USA
6-well plates	4mL	NUNC, Wiesbaden, Germany
anti-CD3-ECD antibody		NUNC, Wiesbaden, Germany
anti-CD25-FITC antibody		NUNC, Wiesbaden, Germany
anti-CD71-PE antibody		NUNC, Wiesbaden, Germany

7.4.2 Generation of lysate from MCF-7 breast carcinoma cells

Table 7.21: Materials for the preparation of tumour cell lysate

Versene	0.05% in EDTA / PBS	Biochrom, Berlin, Germany
Ultrasonic bath	U50	Ultrawave, Cardiff, UK
BCA assay		Pierce, Perbio Science, Tattenhill, UK

To generate tumour lysate, confluent MCF-7 cells were harvested by the addition of 3mL of 0.05% versene in 0.02% EDTA solution and incubated for 10 min at 37°C. The cells were washed twice with Phosphate Buffer Saline (PBS), resuspended $1 \cdot 10^7 \frac{1}{mL}$ in PBS and frozen at -80°C. Disruption of cells was carried out by five freeze/thaw cycles. Cells were thawed by 10min sonication at 4°C in an ultrasonic bath and subsequently frozen at -80°C. The supernatant was collected after centrifugation (1000g / 15min / 20°C) and passed through a 0.2 μ m filter. The protein concentration was determined by a BCA assay according to the manufacturer's instructions (WIECHELMAN ET AL., 1988).

7.4.3 Autologous T-cell Expansion Assay

Monocyte-derived dendritic cells were harvested after 6 days of differentiation. These immature DCs were either loaded with MCF-7 cell lysate ($100\mu\text{g} \frac{1}{\text{mL}}$) or electrically pulsed MCF-7 cells (ratio 1:1), or submitted to four fusion pulses of a length of $65 \mu\text{s}$ and a pulse strength of 8.5 kV/cm in the presence of MCF-7 cells (ratio 1:1). After the loading procedure, the DCs were matured for two additional days in the presence of $\text{TNF-}\alpha$ ($1000 \frac{\text{U}}{\text{mL}}$) and PGE_2 . In the case of lysate-pulsed dendritic cells $1 \frac{\mu\text{g}}{\text{mL}}$ ($0.003\mu\text{M}$) PGE_2 were added for maturation, whereas for the other two approaches $18 \frac{\mu\text{g}}{\text{mL}}$ ($0.051\mu\text{M}$) PGE_2 was used.

On day 8, the mature dendritic cells were subjected to a co-cultivation assay with autologous PBMCs. $1 \cdot 10^5 \frac{1}{\text{mL}}$ DCs were mixed with $1 \cdot 10^6 \frac{1}{\text{mL}}$ PBMCs and $2400 \frac{\text{U}}{\text{mL}}$ IL-7 in a volume of 4mL (triplicates) AIM-V medium and cultured in 6 well plates for 14 days. During this time, the cells were fed according to proliferation and the cell density of PBMCs was kept between $5 \cdot 10^5 \frac{1}{\text{mL}}$ and $1 \cdot 10^6 \frac{1}{\text{mL}}$ to avoid substrate limitations such as glucose and glutamine (see also BOHNENKAMP ET AL., 2002). The PBMCs are restimulated after one week of culture with thawed tumour antigen-loaded dendritic cells at a ratio of 1:20 with fresh medium and $20 \frac{\mu\text{g}}{\text{mL}}$ IL-2. All cells were harvested on day 14 and analysed for CD3, CD4, CD8, CCR7, CD45RO and CD45RA expression by FACS.

Table 7.22: Materials utilized for the autologous stimulation of T cells with lysate-pulsed dendritic cells

AIM-V		Gibco, Carlsbad, CA, USA
TNF- α	$1000 \frac{\text{U}}{\text{mL}}$	R&D, Wiesbaden, Germany
PGE_2	1 or 18 $\frac{\mu\text{g}}{\text{mL}}$	Sigma, Deisenhofen, Germany
rhuIL-7	$2400 \frac{\text{U}}{\text{mL}}$	R&D, Wiesbaden, Germany
rhuIL-2	$20 \frac{\text{U}}{\text{mL}}$	R&D, Wiesbaden, Germany
6 well plates	4mL	NUNC, Wiesbaden, Germany

7.5 Cell Culture and Cell Analysis

7.5.1 Cultivation of Human Tumour Cell Lines

MCF-7, MDA-MB-231 and T47D are three human breast carcinoma cell lines used in this thesis. These breast carcinoma cell lines were cultivated in Iscove's modified Dulbecco's medium (IMDM) supplemented with 10% heat-inactivated (56°C , 30min) fetal calf serum in standard tissue culture flasks (75cm^2) at 37°C and 5% CO_2 . Cells were detached by addition of versene, subcultivated at a ratio of 1:5 and maintained at low passage number (5 to 20). In addition, two leukaemia cell lines, KG-1 and K-562, were used as model cells for several experiments, since they are suspension cells. They were culture as described for the breast carcinoma cell lines.

Table 7.23: Materials for the cultivation of breast carcinoma cell lines

MCF-7	human breast adenocarcinoma cell line	ATCC Number: HTB-22
MDA-MB-231	human breast adenocarcinoma cell line	ATCC Number: HTB-26
T47D	human breast adenocarcinoma cell line	ATCC Number: HTB-133
KG-1	human acute myeloid leukaemia cell line	ATCC Number: CCL-246
K-562	human chronic myeloid leukaemia cell line	ATCC Number: CCL-243
Medium	IMDM	Biochrom, Berlin, Germany
Serum	10% fetal calf serum	Biochrom, Berlin, Germany
Versene	0.05% in EDTA / PBS	Biochrom, Berlin, Germany
Cultivation	Tissue culture flask, 75cm^2	NUNC, Wiesbaden, Germany

7.5.2 Cell Counting and Viability

Cell counting and viability determination was performed using a haemocytometer with standard trypan blue dye exclusion and a CASY 1 TT particle counting system (Schaerfe System, Reutlingen, Germany).

The cell concentration with a haemocytometer is determined with the term:

$$\frac{\text{number of cells}}{\text{mL}} = \frac{\text{number of cells in 4 quadrants}}{4} \cdot 10^4 \cdot \text{dilution factor} \quad (7.1)$$

The viability (trypan blue dye exclusion method) is calculated by utilising the following formula:

$$\text{viability} = \frac{\text{viable cells}}{\text{total number of cells}} \cdot 100 \quad (7.2)$$

7.5.3 Ex Vivo Generation of Dendritic Cells

Peripheral blood mononuclear cells (PBMC) were obtained from buffy coat preparations from healthy donors (kindly provided by Dr. T. Tonn, Blutspendedienst Hessen, Germany) by standard density gradient centrifugation on Ficoll separating solution. 15mL of Ficoll separating solution were filled into Leucosep tubes and the tubes were centrifuged for 30 seconds at 1000g and room temperature (RT). Subsequently, 15 to 20mL of buffy coat were poured directly from the blood sampling bag carefully into the Leucosep tubes and centrifuged for 15min at 1000g and RT. The brakes of the centrifuge were switched off. During centrifugation, lymphocytes and PBMC's are separated from the unwanted erythrocytes and granulocytes on the basis of their density and enriched in an interphase above the separation medium. The plasma (supernatant) was discarded and the enriched cell fraction were harvested and transferred into a new 50mL tube. The cells were washed twice with 50mL of PBS-EDTA (centrifugation for 10 minutes at 400g and RT) and resuspended in 50mL PBS and counted. CD14⁺ monocytes were affinity-purified utilising the MACS CD14 isolation kit following the manufacturer's instructions. Briefly, PBMC were incubated in recommended buffer with MACS CD14 MicroBeads for 15min at 4°C, centrifuged and resuspended in PBS buffer. Subsequently, the cells were passed through a positive selection column. This step was repeated to obtain highly purified CD14 positive cells.

The enriched cells were counted and disseminated in 30mL AIM-V medium in 75cm² tissue culture flasks with a cell density of $1.3 \cdot 10^6 \text{ cells/mL}$. After 1h of incubation at 37°C 400U/mL rhuGM-CSF and 1500U/mL IL-4 were added and the cells were cultivated for 6 days at 37°C and 5 % CO₂. Immature dendritic cells were obtained from the CD14 positive monocytes after 6 days of cultivation. For maturation of these DCs a differentiation cytokine cocktail is added on day 6 and the cells were cultivated for two additional days. The following four cytokines were used in the differentiation cocktail: 1000U/mL TNF-alpha, 1000U/mL IL-1beta, 1000U/mL IL-6 and 1µg/mL PGE2.

Table 7.24: Materials for DC generation and maturation

Ficoll separating solution	Biocoll	Biochrom, Berlin, Germany
Leucosep tubes	50mL	Greiner, Solingen, Germany
Tubes	50mL	Greiner, Solingen, Germany
Tubes	15mL	Greiner, Solingen, Germany
MACS CD14 isolation kit		Miltenyi, Bergisch Gladbach, Germany
MACS column small (MS)	(up to $2 \cdot 10^8$ cells)	Miltenyi, Bergisch Gladbach, Germany
MACS column big (LS)	(up to $2 \cdot 10^9$ cells)	Miltenyi, Bergisch Gladbach, Germany
Filter	3M	Miltenyi, Bergisch Gladbach, Germany
Micro-beads	CD14 ⁺	Miltenyi, Bergisch Gladbach, Germany
Magnet	MIDI cell sorting kit	Miltenyi, Bergisch Gladbach, Germany
Tissue culture flasks	75cm ²	Greiner, Solingen, Germany
AIM-V		Heraeus, Hanau, Germany
rhuGM-CSF	400 $\frac{U}{mL}$	R&D, Wiesbaden, Germany
rhuIL-4	2000 $\frac{U}{mL}$	R&D, Wiesbaden, Germany
TNF- α	1000 $\frac{U}{mL}$	R&D, Wiesbaden, Germany
IL-1 β	1000 $\frac{U}{mL}$	R&D, Wiesbaden, Germany
IL-6	1000 $\frac{U}{mL}$	R&D, Wiesbaden, Germany
PGE ₂	1 $\frac{\mu g}{mL}$ (0.003 μM)	Sigma, Deisenhofen, Germany

7.5.4 Cryo Storage of Cells

For the cryopreservation of dendritic cells and PBMC, the cells were centrifuged ($200g / 10min / 20^\circ C$) and resuspended at a cell density of $1 \cdot 10^7 \frac{1}{mL}$ (PBMCs) and between $1.1 \cdot 10^6$ and $3.5 \cdot 10^6 \frac{1}{mL}$ (mature dendritic cells) in autologous plasma. The plasma was obtained after Ficoll-Paque centrifugation, heat-inactivated at $56^\circ C$ for $30min$, centrifuged at $1000g$ and $20^\circ C$ for $10min$ and passed through a $2\mu m$ filter before use. 10 % DMSO were added as an anti-freezing agent before the cells were frozen at $-80^\circ C$ in a polystyrene box that allowed a freezing rate of $1^\circ C$ per minute until $-70^\circ C$ is reached. Below $-70^\circ C$ the tube can be immersed in liquid nitrogen, placed in the gas phase of liquid nitrogen or in a mechanical freezer at a storage temperature below $-130^\circ C$.

For thawing, the cells were suspended in icecold medium as soon as all ice was melted. Subsequently, the cells were harvested by centrifugation ($200g / 10min / 20^{\circ}C$) and resuspended preheated medium at $37^{\circ}C$.

Table 7.25: Materials and solutions used for the cryopreservation of primary cells

Medium	AIM V	Gibco, Carlsbad, CA, USA
Cryovials	1.8mL	NUNC, Wiesbaden, Germany
Dimethyl sulfoxide	DMSO	Sigma, Deisenhofen, Germany
Tubes	50mL	Greiner, Solingen, Germany

7.5.5 FACS

For analysing of cell populations by means of FACS, several directly conjugated monoclonal Abs against surface molecules (see table 7.25 on page 275) were used to stain the cells. $2 \cdot 10^5$ cells per specimen were suspended in $85\mu L$ of ice-cold PBS and incubated with $5\mu L$ of corresponding mAb for $15min$ at $4^{\circ}C$. After staining, the cells were washed once with ice-cold PBS and fixed in $200\mu L$ of 0.5% paraformaldehyde (Sigma, Deisenhofen, Germany) in PBS. Appropriate isotype controls were used. FACS analysis was performed using a FACSCalibur and CellQuest 3.1 software (both Becton Dickinson, Erembodegem, Belgium).

7.5.6 Apoptosis Analysis

For the analysis, if DCs or KG-1 cells undergo early programmed cell death after a short treatment with a PBS solution at a pH2, an annexin V – propidiumiodide apoptosis detection kit (Becton Dickinson, Heidelberg, Germany) was used. The analysed cells were washed once in PBS and resuspended in the provided binding buffer. FITC-conjugated Annexin V and propidiumiodide were added and incubated for $15min$ at room temperature in the dark. Immediate flow cytometric analysis was performed using a FACSCalibur and CellQuest 3.1 software (both Becton Dickinson, Erembodegem, Belgium).

Table 7.26: Antibodies used for surface protein analysis

Antibody reacts with	Clone	Isotype	Fluorochrome	Company
CD1a	HI149	Mouse IgG ₁ , κ	CyChrome	Becton Dickinson
CD3	UCHT1	Mouse IgG ₁ , κ	CyChrome	Becton Dickinson
CD4	RPA-T4	Mouse IgG ₁ , κ	FITC	Becton Dickinson
CD8	RPA-T8	Mouse IgG ₁ , κ	PE	Becton Dickinson
CD14	M5E2	Mouse IgG _{2a} , κ	PE	Becton Dickinson
CD16	3G8	Mouse IgG ₁ , κ	FITC	Becton Dickinson
CD19	HIB19	Mouse IgG ₁ , κ	PE	Becton Dickinson
CD25	M-A251	Mouse IgG ₁ , κ	PE	Becton Dickinson
CD34	581	Mouse IgG ₁ , κ	FITC	Becton Dickinson
CD45	HI30	Mouse IgG ₁ , κ	FITC	Becton Dickinson
CD40	5C3	Mouse IgG ₁ , κ	FITC	Becton Dickinson
CD54 (ICAM-1)	HA58	Mouse IgG ₁ , κ	PE	Becton Dickinson
CD71	M-A712	Mouse IgG _{2a} , κ	PE	Becton Dickinson
CD80	BB1	Mouse IgM, κ	FITC, PE	Becton Dickinson
CD83	HB15e	Mouse IgG ₁ , κ	FITC	Becton Dickinson
CD86	FUN-1	Mouse IgG ₁ , κ	FITC, PE	Becton Dickinson
CCR7	3D12	Rat IgG _{2a} , κ	PE	Becton Dickinson
HLA-A,B,C	G46-2.6	Mouse IgG ₁ , κ	FITC	Becton Dickinson
HLA-DR	G46-6	Mouse IgG _{2a} , κ	CyChrome	Becton Dickinson
Isotype control	MOPC-21	Mouse IgG ₁ , κ	all	Becton Dickinson

7.5.7 Intracellular Staining of Mammalian Cells

Vital fluorescent dyes were used for staining different compartments (membrane, cytosol or nucleus) of the cells (see table 7.27). The cells were stained following the manufacturer's instructions.

Table 7.27: Dyes used for the intracellular labelling of mammalian cells

CellTracker CMFDA	green	cytosolic dye	Molecular Probes, Eugene, USA
CellTracker CMTMR	orange	cytosolic dye	Molecular Probes, Eugene, USA
CellTracker CMRA	orange	cytosolic dye	Molecular Probes, Eugene, USA
Vybrant DiO	green	lipophilic dye	Molecular Probes, Eugene, USA
Vybrant DiI	orange	lipophilic dye	Molecular Probes, Eugene, USA
Syto11	green	nucleic dye	Molecular Probes, Eugene, USA
Syto17	orange	nucleic dye	Molecular Probes, Eugene, USA

7.6 Microscopic Methods

Fluorescence images were obtained with an Axiovert 200 inverted microscope (Zeiss, Jena, Germany) equipped with optical filters (FITC and Texas Red) and an AxioCam HR camera (Zeiss, Jena, Germany). The images were analysed by the LSM 5 software (Zeiss, Jena, Germany).

7.6.1 Scanning Electron Microscopy (SEM)

The scanning electron microscopy characterisation of the master structures (sputtered with a 5nm gold layer) was performed using a scanning electron microscope.

Particularly, the Scanning Electron Microscopy (SEM) serves for the representation of surfaces. Therefore, the object of interest have to fulfil the following conditions: The object needs to be clean, free of dust and water-free, must not be gassing out in the vacuum and the surface needs to be electroconductive. For this reason, biological surfaces are sputtered with gold. The specimen were overlaid with a 2.5% glutaraldehyde solution for 1 day, washed twice with PBS and dehydrated with an increasing acetone concentration (from 20% up to 100% for 1h each).

Finally, the objects were incubated for 1 day in 100% acetone, subjected to critical point drying and sputtered with gold.

Table 7.28: Materials for scanning electron microscopy

scanning electron microscope	LEO GEMINI 1550	Zeiss, Oberkochen, Germany
gold wire		

7.7 Solutions

Phosphate Buffered Saline

Table 7.29: Formulation of phosphate buffered saline (PBS), which is an isotonic solution and not nutritionally complete. The pH was adjusted to 7.3. The solution was autoclaved for 30min.

Distilled water	1L	
$NaCl$	$8.00 \frac{g}{L}$ (137mM)	Sigma, Deisenhofen, Germany
KCl	$0.20 \frac{g}{L}$ (27mM)	Sigma, Deisenhofen, Germany
Na_2HPO_4	$1.25 \frac{g}{L}$ (8mM)	Sigma, Deisenhofen, Germany
KH_2PO_4	$0.20 \frac{g}{L}$ (15mM)	Sigma, Deisenhofen, Germany

EDTA Buffer

Table 7.30: Formulation of EDTA buffer. The pH was adjusted to 7.3. The solution was autoclaved for 30min.

PBS	1L	
$Na_2EDTA \cdot 2H_2O$	$0.74 \frac{g}{L}$ (2mM)	Sigma, Deisenhofen, Germany

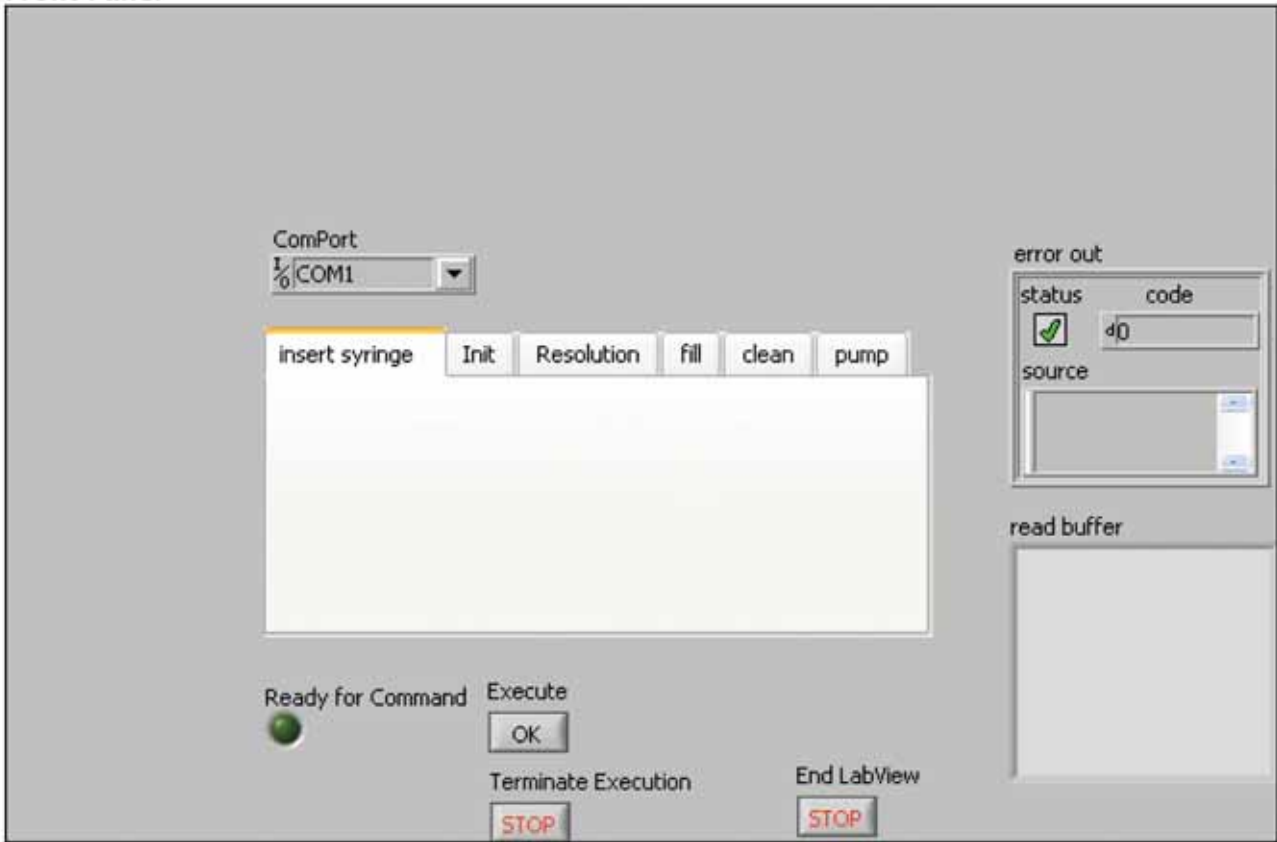
Appendix A

Pump/Valve Operation Programmes

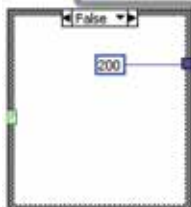
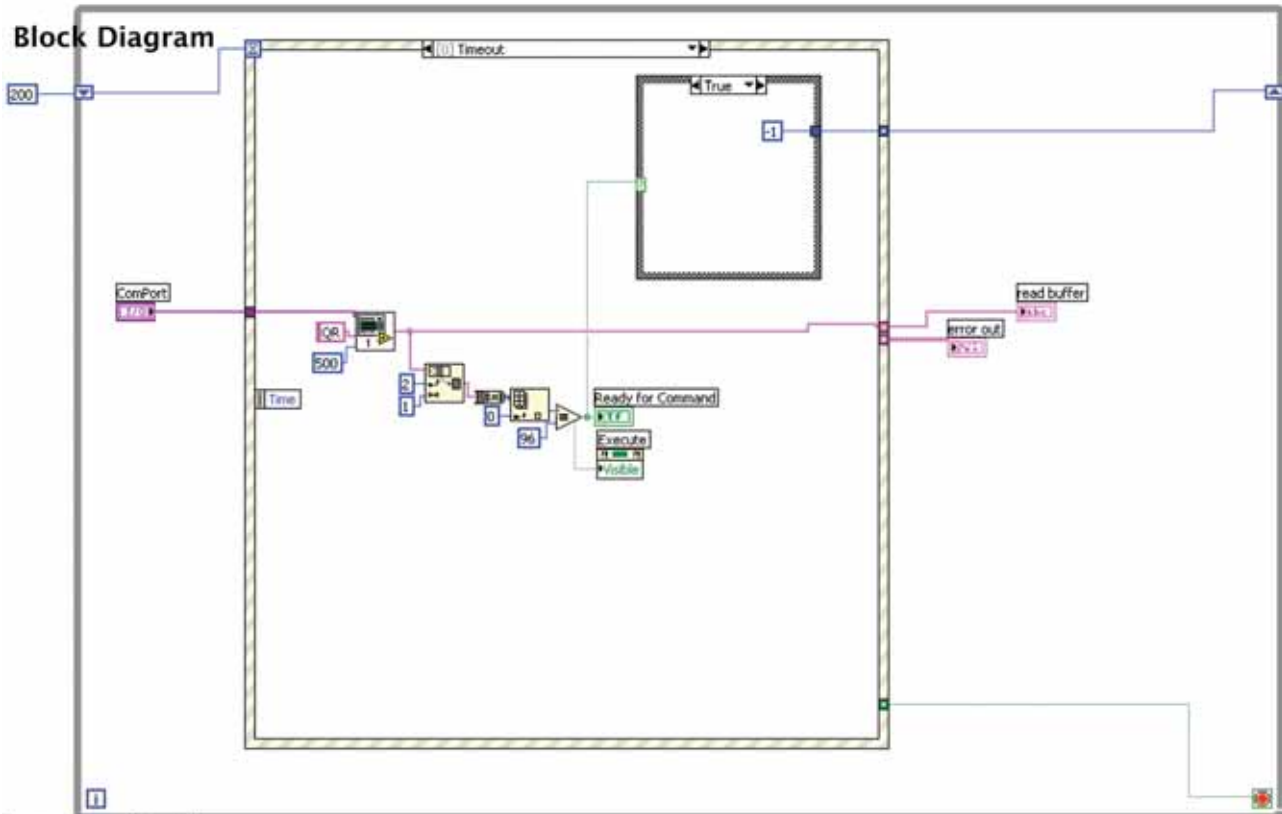
The pump and valve operation programmes, which were written for this project with LabVIEW to operate all components from an external computer are shown in the following. LabVIEW is a graphical programming language, which is primarily used for metrological tasks. The graphical dataflow language and block diagram approach allows viewing and easily modification of data or control inputs.

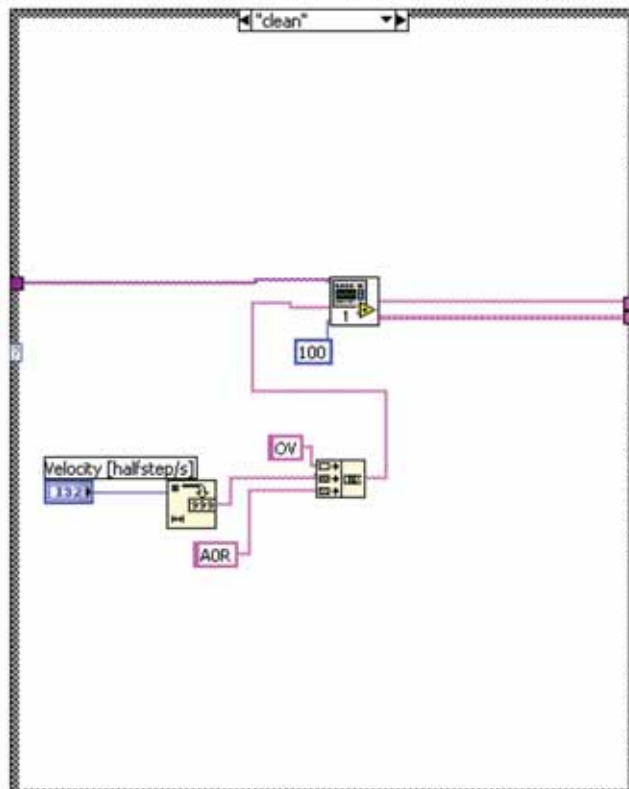
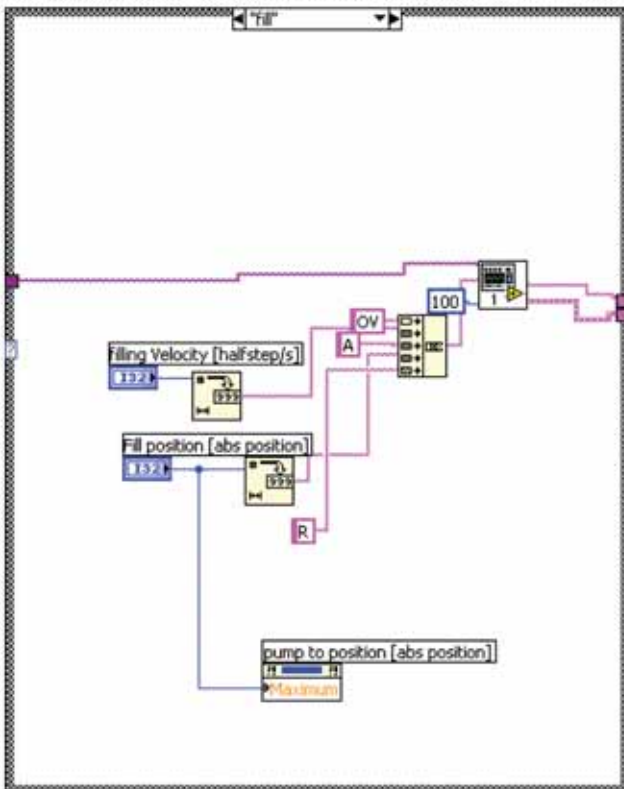
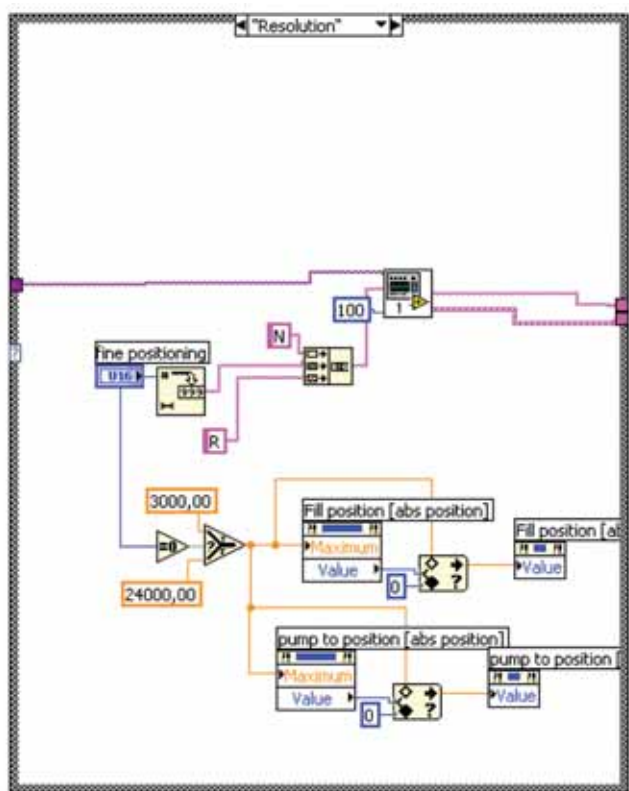
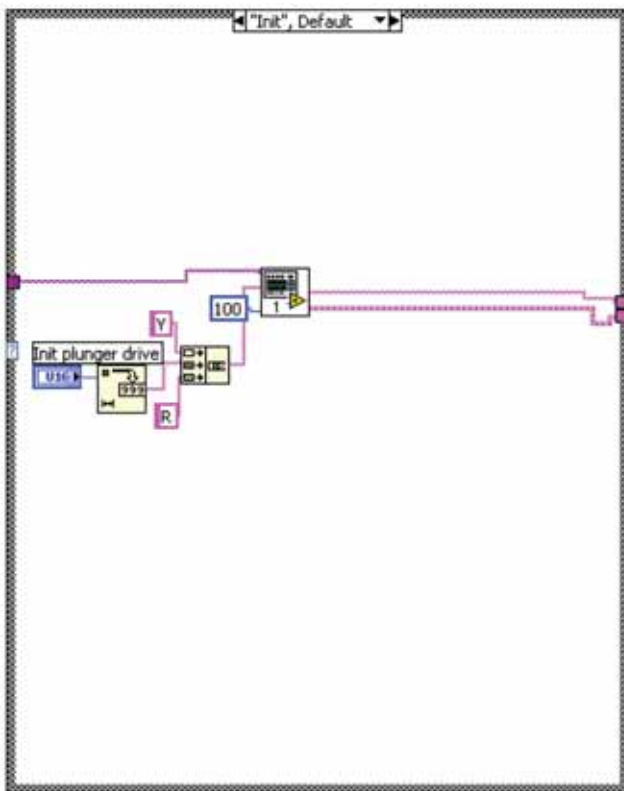
Control Cavro 3000.vi

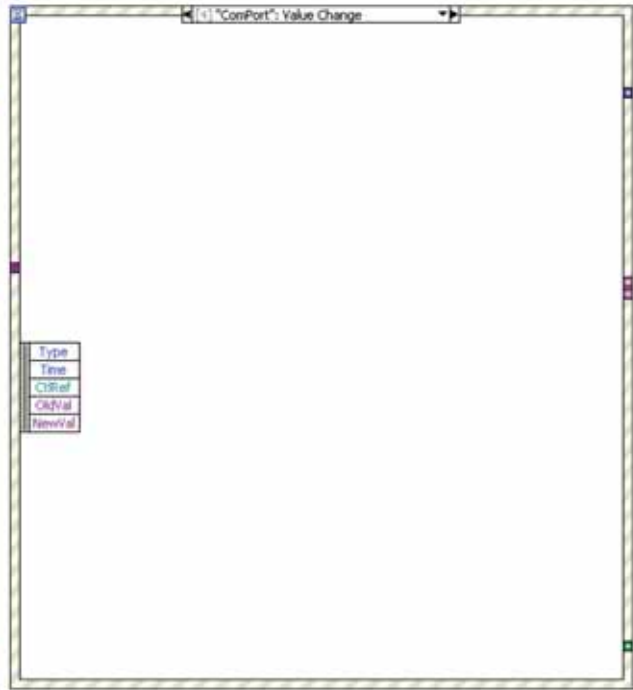
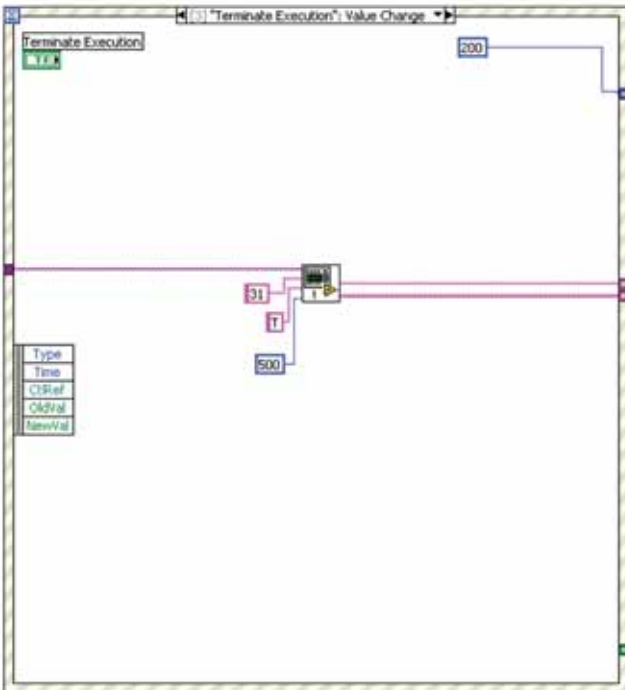
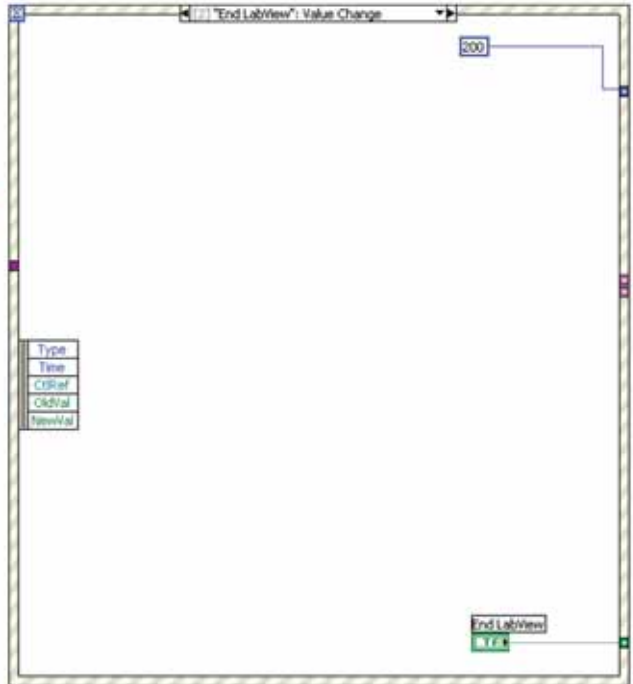
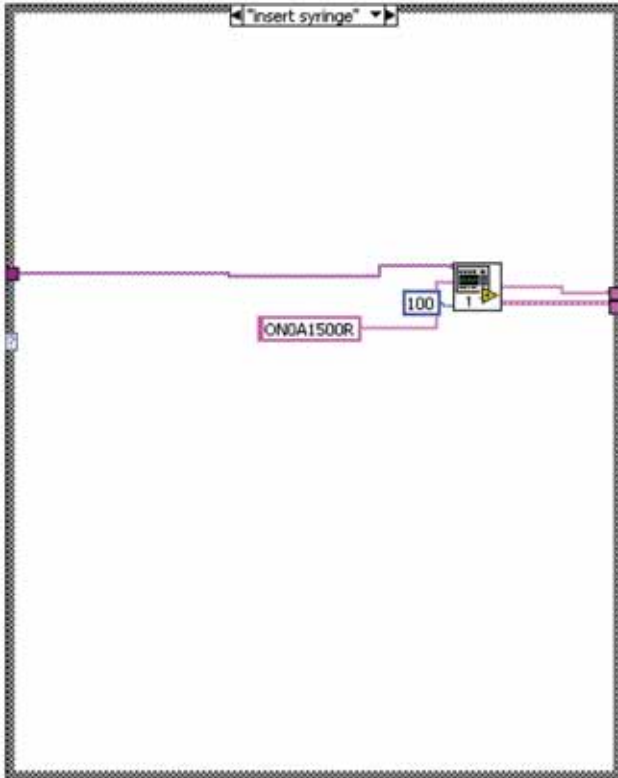
Front Panel

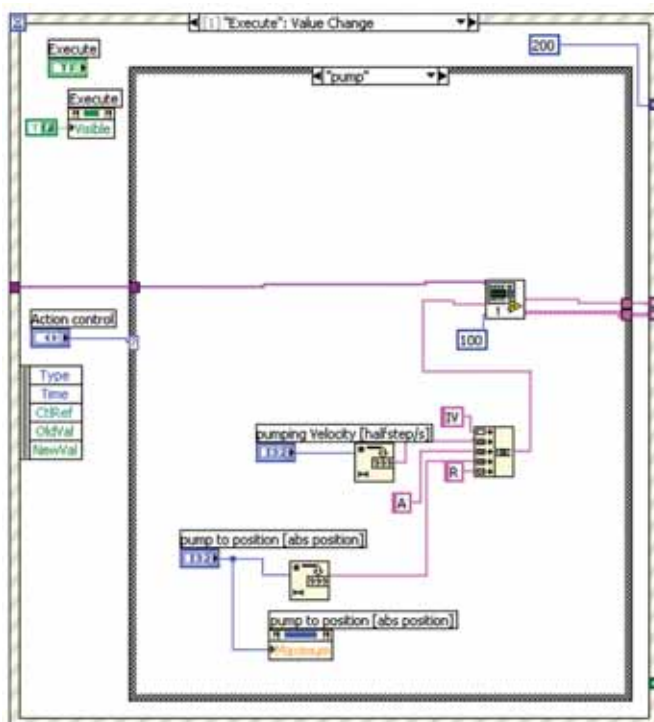


Block Diagram









sampleonly.vi

Connector Pane



Front Panel

ComPort
COM1

Make sure, that you have set the Lee-Valves into the right positions

Command Structure
VxQR
or DxMyG2400R

Number of repeats: 9 | 10

Velocity: 0 to 2500 (slider)

Pump No.: 33

If the program is not running initialise the pumps first. This can be done via the Program Management.vi. In case that no liquid is pumped into the chip make sure that the valve at the pumps are set back to the input position (wait for completion of the initialisation program).

Components:

PumpType: Cavro XL-3000HR

CCD-Camera: None

AutoSampType: No autosampler

Valve Type: Lee solenoid

Syringes:

SyringeVolG1: 50 µl

SyringeVolG2: 50 µl

SyringeVolS: 50 µl

Fill max rate G1: 50,00 µl/s

Fill max rate G2: 50,00 µl/s

Fill max rate S: 10,00 µl/s

Chip:

ChipID/2D: 1D

ChipWidth: 1420 µm

ChipDepth: 40 µm

CapillaryDiaG: 100 µm

CapillaryDiaS: 100 µm

CapillaryDiaO: 100 µm

Chip flowrate: 3,00 µl/s

Operate mode: Fast | normal

Lanes:

Thick lane width: 200 µm

Thin lane width: 50 µm

Lane width calibration: 25,00 µm

Small lane incubation delay: 6,00 s

Broad lane incubation delay: 1,00 s

Broad max pos.: 6

Broad min pos.: 1

Thin max pos.: 26

Thin min pos.: 3

No of broad pos.: 7

No of thin pos.: 28

Flow parameters:

Injection vol: 10,00 µl

Vol to T-junc.: 5,00 µl

Pressure equilibrium delay: 5,00 s

Sample fv adjustment: 0,14 µl

Sample back-suction: 0,40 µl

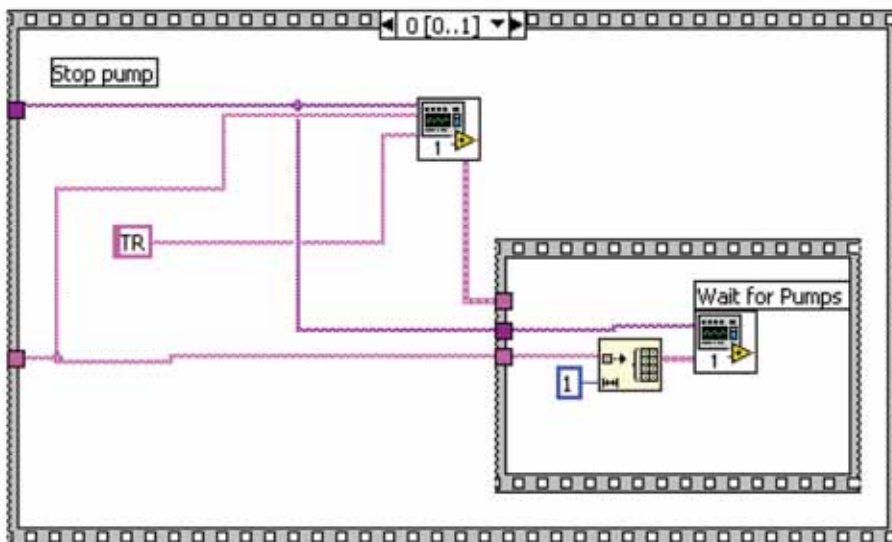
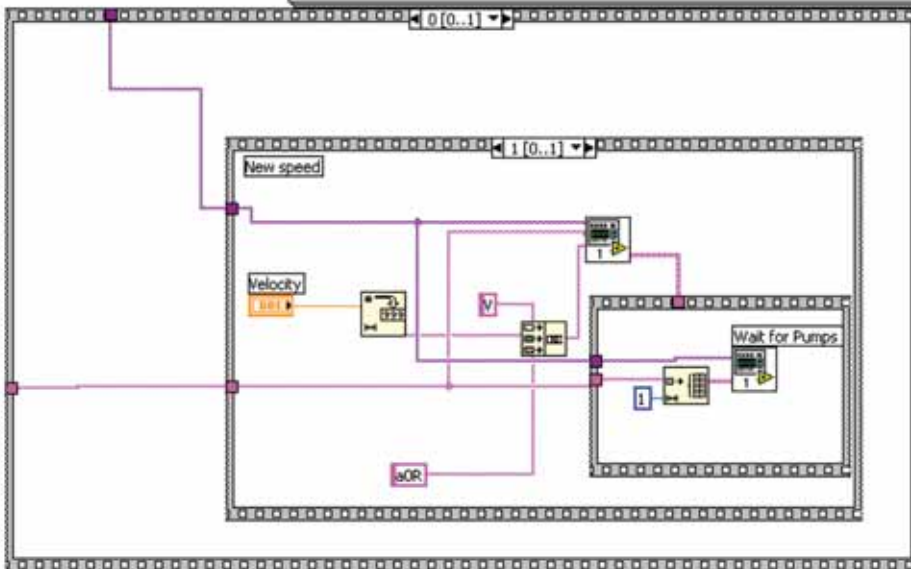
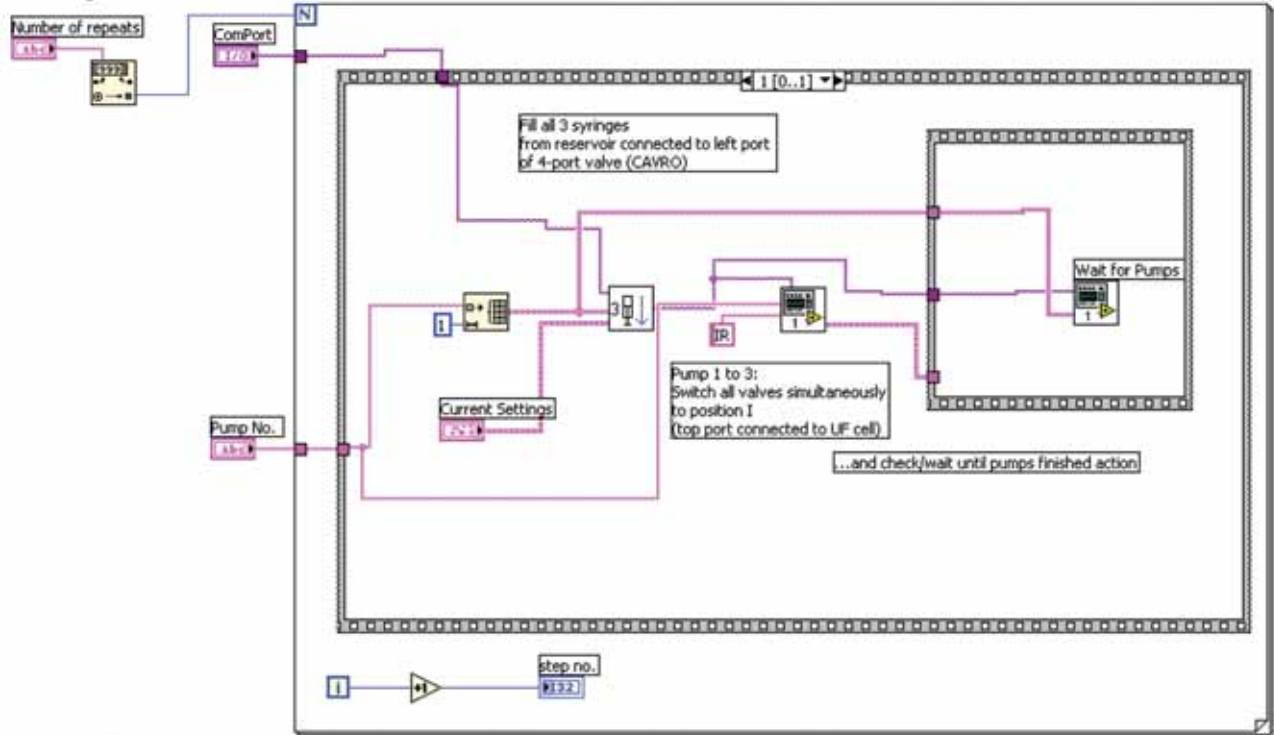
MaxFlowRate: 6,00 µl/s

Computer:

LPT Port: 378

Com Port: D

Block Diagram



init all pumps.vi

Connector Pane



Front Panel

ComPort
% COM1

INIT Pluggler Drive
full force
full force
full force

INIT Valve Direction
Clockwise

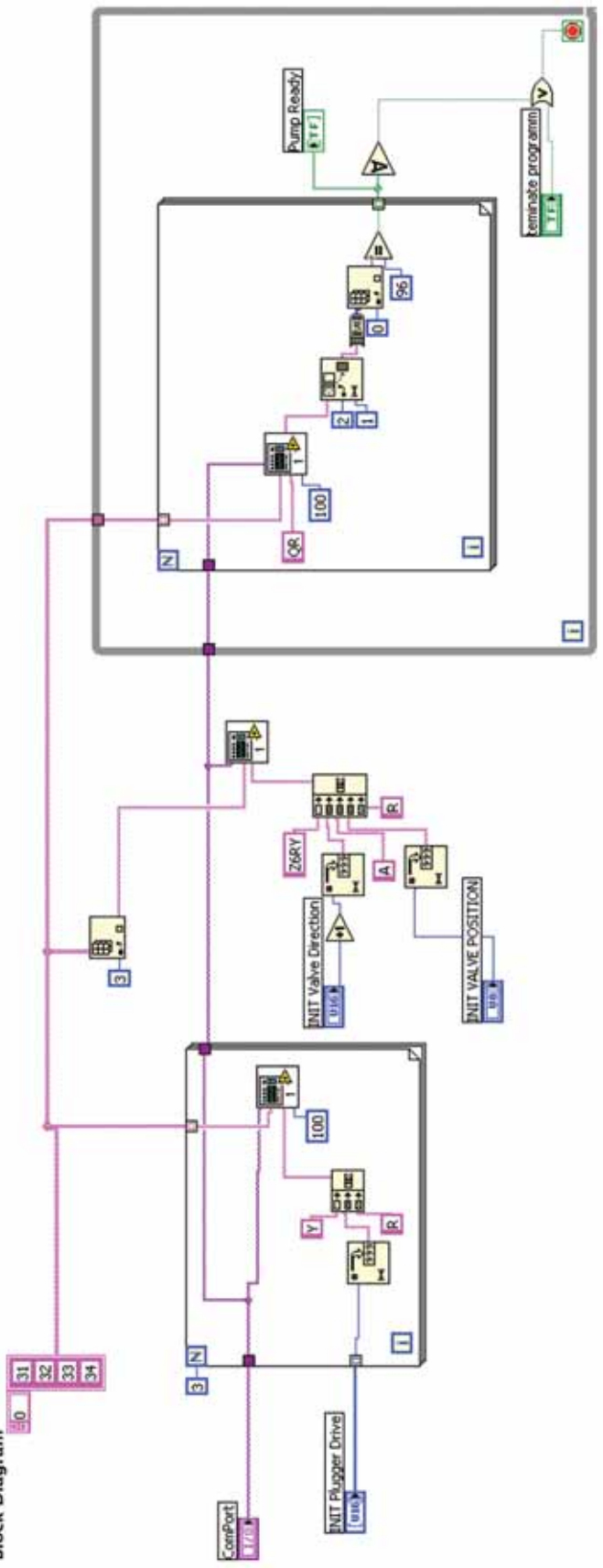
INIT VALVE POSITION
31

Pump Ready
0

terminate programm

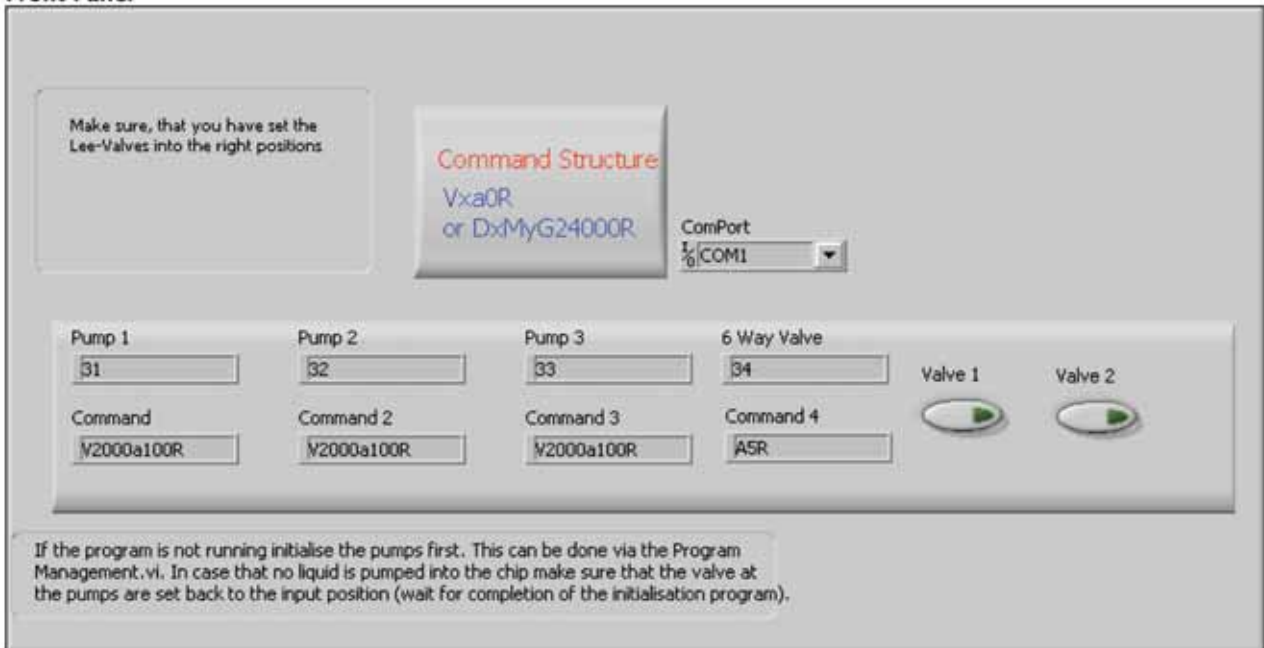
STOP

Block Diagram

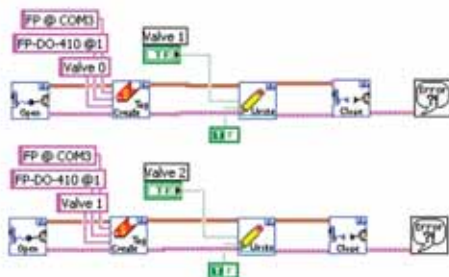
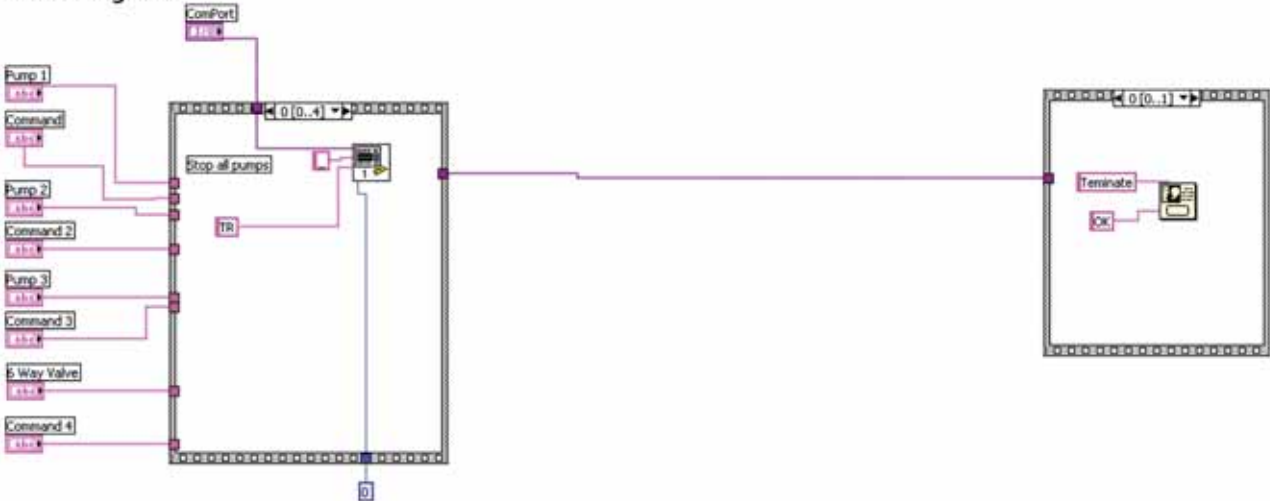


pump rate control.vi

Front Panel



Block Diagram



List of Figures

1.1	The concept of this thesis	2
2.1	Dendritic cell life cycle: In tissue resident dendritic cells take up antigens and migrate towards lymphoid organs. During this time they get matured and are then able to activate T-cells in the lymph nodes to launch an effective immune response.	10
2.2	T-cell stimulation requires three dendritic cell-derived signals: MHC/TCR interaction, a co-stimulatory signal via CD28 and a signal via the cytokine receptor.	11
2.3	Dendritic cell/cancer cell hybrid vaccination strategy	16
2.4	Schematic depiction of a hybrid resulting from DC/tumour cell fusion: It is hypothesised that the DC/tumour cell hybrid functions as antigen-presenting cell expressing TAAs on MHC class I and II alongside with co-stimulatory molecules.	16
2.5	Schematic representation of an inhomogeneous electrical field between electrodes E^+ and E^- that induces a dipole in a cell.	20
2.6	Cells in an inhomogeneous electrical field line up in pearl chains at the electrodes by dielectrophoresis	20
2.7	Schematic representation of two cell membranes (red and green)	21
2.8	Schematic representation of the electrical breakdown and coalescence of the membranes of two adjacent cells	21
3.1	Micro fusion chamber for the Eppendorf Multiporator: It consists of a casing containing two electrodes above a transparent reservoir. Connection to the Multiporator can be established by a coaxial cable via a special insert. This micro fusion chamber allows the optimisation for cell alignment and cell fusion under microscopic control.	32

3.2	Close-up view of the electrodes from the Eppendorf micro fusion chamber: The two electrodes consist of Platinum and are $200\mu m$ apart.	33
3.3	Helix chamber for the Eppendorf Multiporator: It consists of a conical core that carries the parallel wrapped electrode wires and a beaker into which the cell suspension is added. The filling volume accounts to $250\mu L$. The electrode gap width of $200\mu m$ is filled by the screwing of the core into the beaker, whereupon the cell solution is pressed upwards into the gap.	33
3.4	Situation in the Eppendorf micro fusion chamber filled with a cell suspension of $10^6 mL^{-1}$ before and after application of a low a.c. field ($500V/cm$) for 30 seconds. The used breast cancer cell line MCF-7 has been stained in red using the fluorescent cytoplasmatic Celltracker CMTMR dye. [picture by H.R. Bohnenkamp]	34
3.5	Mixture of two different breast cancer cell lines, T47D and MCF-7, stained in green with CMFDA and in red with CMTMR, respectively, in the micro fusion chamber. Many clusters of cells of the same type can be observed. However, only at sites in the cellular pearl chains, where the two cell types alternate (see marks for example) a heterologous fusion can take place. [picture by H.R. Bohnenkamp, modified]	34
3.6	Schematic diagram of the proportion of a cancer cell (green) in comparison to a dendritic cell (red): A successful two-cell fusion requires the appearance of two holes in the membranes, one in each cell. These holes, which result from a membrane breakdown due to the applied fusion pulse, have to co-localise.	35
3.7	Schematic depiction of the targeted alternating cell alignment between the electrodes of the fusion chamber. The arrangement has to be adjusted alongside the field lines, depicted here in yellow.	36
3.8	Phase contrast micrographs of PCC7-MzN mouse embryonic neuroblastoma cells on straight lines of patterned laminin. Comparison of cellular growth on different line sizes at day 4 shows that on $6\mu m$ lines cells form big clusters (a), whereas on $2\mu m$ lines monocellular lines are visible (b). Scale bar represents $100\mu m$ (pictures taken from LAUER ET AL., 2001).	38
3.9	Immobilisation approach for an arranged electrofusion chamber	39
3.10	Reaction scheme for the coupling of antibodies to a glass surface by 3-aminopropyltriethoxysilane and glutardialdehyde	43

- 3.11 Immobilisation of KG-1 cells on a APTES/glutaraldehyde-treated glass surface via a covalent coupled anti-CD34 antibody: The antibodies were immobilised in a drop shape. The picture was assembled from multiple micrographs. 44
- 3.12 Immobilisation of KG-1 cells via anti-CD34 antibody: The antibody was applied using a microstamp to a glass surface completely functionalised with APTES/glutaraldehyde. $80\mu\text{m}$ wide antibody lines show binding of multiple cells over the line width. Cell clusters could also be observed in the space between the printed antibody lines. 48
- 3.13 Scanning electron micrographs of master structures raised from negative photoresist SU-8 25 on a silicon master: A) three $30\mu\text{m}$ wide and $15\mu\text{m}$ high structures, B) $30\mu\text{m}$ wide, $15\mu\text{m}$ high, c) a $100\mu\text{m}$ wide and $25\mu\text{m}$ high structure. The results demonstrated that smaller structures can be obtained the thinner the spincoats are applied. Best results were obtained with a structure height of $15\mu\text{m}$ 51
- 3.14 Photographs of the produced master for the PDMS stamp preparation. The master was placed into a special holder for the moulding with PDMS. A) master and holder (in-house production), B) assembled, C) defect master where the photoresist lines were detached, due to improper handling such as sonication. . . 52
- 3.15 Photographs of PDMS stamps for inverse microcontact printing: A) PDMS stamp with punched holes for filling the channels, B) punched filling hole in PDMS with connection to channel, C) $15\mu\text{m}$ channel in PDMS stamp. 53
- 3.16 Fluorescent images of channels in PDMS stamps to examine the quality and filling: Channels of different widths from $30\mu\text{m}$ down to $10\mu\text{m}$ in a PDMS stamp filled with a green fluorescent fluid (na.fluorescein). 54
- 3.17 Immobilised FITC-labelled bovine serum albumin (BSA) on glass: A) Three $30\mu\text{m}$ lines of immobilised BSA are shown with only the middle line showing homogenous immobilisation. The other two protein lines show debris at the border of the line; B) Seven $15\mu\text{m}$ wide lines of immobilised BSA should be visible, but only part of the channels show protein immobilisation; C) The picture shows a curved line of immobilised FITC-labelled BSA, which probably resulted from bursting of the channel by the applied vacuum. 56
- 3.18 ^{13}C nuclear magnetic resonance spectrum of 3-aminopropyltriethoxysilane 58

3.19	Live Images and 3D maps of aminopropyltriethoxysilane functionalised lines on glass. A 10 % aminosilane solution in different solvents was reacted for 1h at 60°C with the substrate: A) 85 % ethanol (pH 4.5-5.5), B) toluol (pH not adjusted), C) in water (pH 3.45)	60
3.20	Fluorescence micrographs of immobilised proteins on glass via aminopropyltriethoxysilane and glutardialdehyde: A) BSA-FITC in a 50 μ m channel; B) BSA-FITC (bovine serum albumin) in a 30 μ m channel; C) anti-CD34-FITC antibody in a 80 μ m channel.	63
3.21	Live images (A and C) and ellipsometrical contrasts (B and D) of an immobilised antibody line (anti-CD34-FITC) (A and B) and an immobilised FITC-labelled BSA line (C and D)	64
3.22	Measured and fitted Delta and Psi data for the glass substrate (surrounding) and an FITC-labelled BSA line (named stripe 6).	65
3.23	3-dimensional film thickness map of an immobilised FITC-labelled BSA line. The z-axis gives the film thickness in nm, x- and y-axis are random units.	65
3.24	Ellipsometrical live image of an anti-CD34 antibody line	66
3.25	Diagram of direct binding of cells to antibodies and indirect binding via streptavidin/biotin linkage	67
3.26	Light microscopy pictures of the immobilisation of KG-1 to antibody lines: A) This picture shows a 20 μ m wide antibody line. This line is too wide for the binding of KG-1, thus the cells do not line up in a chain; B) shows binding of the cells to nine parallel antibody lines (15 μ m); C) the picture shows the aligning of cells in a chain bound to antibody lanes with a width of 10 μ m.	69
3.27	Coloured SEM pictures of single dendritic cells bound to an antibody line: A) shows that the chosen size of 15 μ m for the antibody line correlates with the size of the dendritic cell; B) shows a dendritic cell stretching along an antibody line; C) shows that the extensions of the DC do not protrude over the edge of the antibody line.	71

- 3.28 Scanning electron micrographs of immobilised antibody stripes and dendritic cells bound to it: A) The micrograph shows part of an immobilised antibody stripe on the right and the glass substrate on the left; B) Dendritic cells bound side by side on an antibody line; C) Coloured photo of dendritic cells on antibody lines ($15\mu m$). 72
- 3.29 Alternating arrangement of red and green KG-1 cells, stained with CMTMR (red) or CMFDA (green), respectively, opposed to the schematic representation. 73
- 3.30 Detachment of an anti-CD45 antibody from KG-1 or dendritic cells by a short drastic shift of the pH from pH 7.4 to pH 2. The unlabelled cell peak is outlined in blue (negative controlled), the stained cell peaks are depicted in red (before treatment with pH 2 (red filled) and after treatment (red outlined)). 74
- 3.31 Schematic depiction and photograph of LTCC ceramic slab with electrodes for the usage as fusion chamber in the immobilisation approach 77
- 3.32 Schematic diagram of the electrofusion chamber assembly: A) A gold structure, which comprises electrodes and lines for antibody immobilisation, is evaporated six times onto a glass substrate, the size of a microscope slide; B) A bonding layer, made of double-sided tape, is applied on top of the gold structure; C) The chamber is sealed with a acetate foil top layer. 78
- 3.33 Photolithographic chrome mask with two times six gold structures: Three different photolithographic masks were manufactured, which differ in the width of the lines for the antibodies (not visible macroscopically). 79
- 3.34 Cross sections of a bi-layer reentrant sidewall profile with LOR 3B and S1813 as imaging resist. A) The width of the photoresist structure determines the distance of the structure elements *e.g.* lines within the whole gold structure. B) The height of the lift-off resist needs to be 1.2 - 1.3 fold thicker than the metal film, which will be deposited, to obtain a discontinuous metal film. C) Undercut of the lift-off resist. 81
- 3.35 Cross section of a bi-layer reentrant sidewall profile with LOR 3B and S1813. The exposure dose was too high, with 10sec exposure time, leaving only a small rest of the lift-off resist. The photoresist structure nearly collapsed. 82

- 3.36 Gold structures on glass: A) Two times six structures of electrodes and lines for antibodies of gold on a 140mm glass wafer; B) Micrograph of the $200\mu\text{m}$ wide electrodes with five $10\mu\text{m}$ wide lines for antibodies in the space between the electrodes; C) Micrograph of the same structure than in B, showing the branching to the contact patches. 83
- 3.37 Assembly of the chamber for the immobilisation approach. The goldstructure was applied 6 times on the size of a microscope slide and the electrode structures where covered by the build-up of the electrofusion chamber: A) Microscope slide with six electrofusion chambers. B) Each electrofusion chamber can be connected and operated individually. C) Multiple gold lines for the immobilisation of the antibodies were deposited inside the electrofusion chamber. 84
- 3.38 Design drawing of the six pieces, which were used for the build-up of the electrofusion chamber. Top row: These three pieces are cut with a CO_2 laser out of double-sided tape. Bottom row: Holes for filling the electrofusion chamber and contacting the electrodes are comprised in the pieces, which seal the chamber. 85
- 3.39 Strategy for the immobilisation of antibodies onto gold lines functionalised with carboxylate-terminated SAMs 87
- 3.40 High-resolution XPS peaks for four spectral regions on activated MUA monolayers (BC1) and immobilised antibodies on MUA (BC2) 89
- 3.41 High-resolution N1s (left) and C1s (right) spectra for activated MUA monolayers (top) and immobilised antibodies on MUA (bottom). Peaks were fitted to the obtained spectrum using Unifit for Windows, Version 32-32. 90
- 3.42 Immobilisation of KG-1 cells stained with CMTMR (red) on a gold surface. The left half of the gold surface was treated with MUA and the SAM layer was activated with NHS/EDC. The right half was left untreated. Cells only bound to the functionalised part of the gold surface. 91
- 3.43 The completed electrofusion chamber can be connected via a push-pull self-latching connection system to the voltage generator from Eppendorf. 91

3.44 Microfluidic Device for patterned application of microfluids to neuronal cells developed by Thiébaud et al.: A) Photograph of the device compared with a syringe needle; B) Micrograph of the PDMS microinjector top plate. The grooves of the eight injection channels of the device are highlighted with arrows. The location of the picture frame in respect to the entire device is shown in the insert (pictures taken from THIÉBAUD, P. ET AL., 2002). 95

3.45 Microfluidic approach for an arranged electrofusion chamber 96

3.46 Microfluidic system 1: It contains channels, which end in a collective chamber. The red area highlights feed A (the input for cell solution A), blue marks feed B (cell solution B, respectively) and the output is displayed by a green mark. Neither microfluidic feed lines nor adapters for electric components are illustrated. 98

3.47 Microfluidic system 2: It contains implied trenches in the bottom plate. The red area highlights feed A (cell solution A), blue marks feed B (cell solution B) and the output is displayed by a green mark. Neither microfluidic feed lines nor adapters for electric components are illustrated. 99

3.48 Microfluidic system 1: Partial flows with different flow velocities caused by invalid dimensions of the input cross sections. 102

3.49 Microfluidic system 2: Run of the streamlines with 2-pump-operation modus . . 103

3.50 Microfluidic system 2: The simulated streamlines, coloured in red for cell suspension 1 and green for cell suspension 2, start to trundle, due to pressure rise towards the end of the chamber. 104

3.51 Microfluidic system 2: The simulated streamlines enter the microfluidic chamber via inlet A. The other streamlines, resulting from the fluid entering via inlet B have been left out to clarify the flow situation. 105

3.52 Microfluidic system 1: The coloured streamlines represent cell solution 1 (red) and cell solution 2 (green). They show a laminar flow pattern alongside the whole chamber. 106

3.53 Microfluidic system 1: The selected pictures have been extracted from a movie, which presents the final design of the microfluidic system 1, showing the chamber in 3D and the flow of the streamlines. This movie is available on the enclosed DVD. 107

- 3.54 Microfluidic system 2: The selected pictures have been extracted from a movie, which presents the final design of the microfluidic system 2, showing the chamber in 3D and the flow of the streamlines. This movie is available on the enclosed DVD. 108
- 3.55 Overview of the flow velocity inside the microfluidic system 1: The highest velocities are found in the channels and at the outlet, indicated in red. 109
- 3.56 Close-up from figure 3.55 showing the channels of the microfluidic system 1, which guide the laminar flows in the right direction. 110
- 3.57 Close-up from figure 3.55 showing the outlet of the microfluidic system 1 as vector graphic. 110
- 3.58 Simulated inflow of a fluid into the microfluidic system 2: The fluid arrives with high velocity at inlet A and is decelerated by entering the chamber. 111
- 3.59 Vector graphics system 1: The selected pictures have been extracted from a movie, which presents the flow velocity pictured as vector graphic. An animation of all cross sectional areas is shown. This movie is available on the enclosed DVD. 112
- 3.60 Vector graphics system 2: The selected pictures have been extracted from a movie, which presents the flow velocity pictured as vector graphic. An animation of all cross sectional areas is shown. This movie is available on the enclosed DVD. 113
- 3.61 Flow velocity profile in a cross sectional area situated inside the channels of microfluidic system 1, which guides the laminar flows in direction. The gradient of velocity is parabolic, which is typical for a laminar flow. Thereby, the highest flow velocity, indicated in red, can be found in the center of the channel. 114
- 3.62 Phenotypical analysis of matured DCs either brought into contact with an PMMA sample for 24h or left untreated. Shown are results of surface antigen expression after 1 day incubation (d9) compared to the expression levels on day 8 (d8). The values are presented with a mean standard deviation (SD) resulting from 3 measurements. 117
- 3.63 Positioning of the microfluidic system on a 15mm · 15mm polymer piece 118
- 3.64 Close-up of figure 3.63: The 2D design of the microfluidic system 1 was drawn with the software AutoCAD showing the chamber with feedlines for inlet A, inlet B and the outlet (from left to right). 118

- 3.65 Picture of the front part of the microfluidic system 1 burned into PMMA with the use of an excimer laser: The through holes are visible, which connect the feedlines from the bottom side with the chamber on the Top. 119
- 3.66 Sloped oversight of the microfluidic system 1 using a binocular microscope . . . 120
- 3.67 Plan view of the microfluidic system 1 using a binocular microscope 121
- 3.68 Microfluidic system 1: Photographs from the inlets B (A), the middle (B) and rear part (C) of the chamber taken using a light optical microscope. 122
- 3.69 Microfluidic system 2: Photographs from the inlets B (A), the middle (B) and the rear part (C) of the chamber taken using a light optical microscope. 123
- 3.70 Schematic depiction of the microfluidic chip for the microsystem 1 124
- 3.71 Light-Micrograph of a capillary with an ID of 0.25mm glued into a drilling, thus connecting the microfluidic channels of the microstructure with outer apparatus, such as pumps. 125
- 3.72 Cross section through a bonded microfluidic structure: A test series of channels with different widths and depths were cut with an excimer laser in PMMA. Subsequently a PMMA cover was welded on top of the microstructure under specific process conditions. 126
- 3.73 Partial records of the channels of figure 3.72 127
- 3.74 Solution for the sealing of the microfluidic chambers instead of bonding 128
- 3.75 Schematic (A) and real (B) view of the sandwich technique used for sealing the microfluidic chambers. 129
- 3.76 Sealed microfluidic chamber placed under an inverted microscope for the examination of the fusion process. The UV light is turned on to track fluorescent labelled cells (see validation section 3.2.7 for specification). 130
- 3.77 Pump station for fluid handling in combination with the microfluidic chips: The main components (pumps and valves) are controlled by an external computer (not shown). 132
- 3.78 An analogue pump station was assembled in Jülich: The SV 6-port valve is to the fore, whereas the inert valves cannot be seen. 133
- 3.79 Flowsheet of the pump station illustrating the connection of the pumps and valves to the microfluidic chip. 134

- 3.80 Screen shot of the sample only programme: This programme is an easy to use programme for the operation of only one pump at a time. The pump, pump velocity and the number of repeats are the only variables, which have to be chosen. The selected pump will then fill and empty its syringe via valve position inlet for the number of times chosen. 136
- 3.81 Screen shot of the pump rate ctrl programme: This programme allows the simultaneous operation of all three pumps, the 6-port smart valve and both inert valves. The knowledge of pump and valve commands and command structures are required for this programme. 136
- 3.82 Screen shot of the Labview pump software programmed in Jülich: This easy-to-use system combines all important operation procedures. 137
- 3.83 Microfluidic system 2: Light microscope picture of the laminar flows. One of the streams (inlet B) is stained with Na-Fluorescein. 138
- 3.84 Microfluidic system 1: The solution, which enters the microfluidic structure through inlet B, is stained with Na-Fluorescein. The pictures represent the laminar flow situation, as apparent by the distinct flows, at the entrance of the open chamber (A), in the middle of the chamber (B) and near the outlet, where the streams converge (C). 139
- 3.85 Particle flow system 1: The selected pictures have been extracted from a movie, which shows how fluorescent particles are streamed through the chamber with high speed, thus the single cell cannot be spotted. This movie is available on the enclosed DVD. 141
- 3.86 Particle flow system 2: The selected pictures have been extracted from a movie, which shows how fluorescent particles are streamed through the chamber at lower speed than in figure 3.85. This movie is available on the enclosed DVD. 142
- 3.87 Trouble-shooting 1: The selected pictures have been extracted from a movie, which shows how the standpipes of the microfluidic system 1 are plugging. This movie is available on the enclosed DVD. 143
- 3.88 Trouble-shooting 2: The selected pictures have been extracted from a movie, which shows the breakdown of the laminar flow situation with nine parallel flows in the microfluidic system 1 due to the incidence of air bubbles. This movie is available on the enclosed DVD. 144

3.89	Plugging in the feed and standpipes: The pictures show plugging of fluorescent particles in a standpipe (in focus in A) and in a feed pipe (in focus in B)	145
3.90	Ablation material, which is characterised by a high self fluorescence (A), is found near the inlets (B) and sometimes is plugging the channels (C).	146
3.91	Scanning electron microscope pictures of the microfluidic system 2: The top part of the laser-manufactured structure (A), a close-up of the outlet (B) and the distribution system of inlet B (C) can be seen.	147
3.92	Microfluidic system 2: SEM picture of the top part of the laser-manufactured structure. It should be mentioned here that the chamber has been extensively used before the micrograph was taken and ablation material was removed mechanically from the blocked inlets.	148
3.93	Open Chamber of the microfluidic system 3 characterised by enlarged inflow channels and standpipes.	150
3.94	Engineering drawing of the microfluidic chamber 3. All data is given in μm	150
3.95	Microfluidic system 3: Photographs from the inlets (A), the middle (B) and rear part (C) of the chamber.	151
3.96	Blockage of a channel inlet by fluorescent particles.	152
3.97	Microfluidic structure 3: The hydrodynamic focussing of the laminar flows is visualised by the addition of Na-Fluorescein into the solution, which enters the microfluidic structure via inlet B.	153
3.98	SEM picture showing extensive damage caused to the microfluidic structure 3 by mechanical removing of blockages	154
3.99	Microfluidic system 3 cut in PET, which shows a higher autofluorescence compared with PMMA.	155
3.100	Fluorescent polymer particles sticking to the walls of the microfluidic structure.	155
3.101	Microfluidic structure 3: A purgeline (shown in yellow) was introduced to provide more flexibility for flushing the system.	156
3.102	The pictures show the connection of the laser-machined area of the microfluidic structure to the boreholes, where the capillaries are inserted. The glue does not approximate to the entrance of the capillary. Otherwise, the risk exists that the capillary is sealed by the glue. Thus, particles can accumulate in this passage, which need regular flushing.	157

- 3.103 Microfluidic system 3 with purge line: The microfluidic structure is cut in PET and before usage will be sealed with PDMS. 158
- 3.104 Microfluidic system 3 with purge line: The picture shows the proportions of the microfluidic system in comparison to a match. 159
- 3.105 Final design of the microfluidic structure 3 with dimensions in μm 160
- 3.106 Purge line between inlet A and B. The fluid entering the system via inlet A is stained with Na-Fluorescein (green). In the normal operation mode of the microfluidic system, a flow situation with a distinct boundary (A) should prevail. However, such a stable flow situation could not be obtained and more (B) or less (C) strong cross-circuit flows were present. 161
- 3.107 3D-model of the microfluidic system 3 162
- 3.108 Tracer experiment system 3: Na-Fluorescein adds a green fluorescence to the fluid, which enters the microfluidic chamber via inlet B. With the start of the pump system, the partial flows can be observed immediately, while they disappear, when the pumps are switched off and the fluids mix by diffusion. 163
- 3.109 Microfluidic system 3: The fluid flow of inlet B is stained with Na-Fluorescein (A) and in addition, the second fluid is stained with CMTMR (B) resulting in an alternating flow of red and green partial flows. 164
- 3.110 Sketch of the microfluidic system 3 with positioning of two Platinum wires as electrodes alongside the microfluidic chamber 165
- 3.111 Engineering drawing of the microfluidic system 3 including electrodes. All dimensions are given in μm 166
- 3.112 Left: Concept of the splitter chip for the use with the microfluidic chip (on the right), to reduce the number of required pumps from nine to two. Right: Concept of the microfluidic chip based on Micronit's standard hole pattern, where nine of the ten access holes are used as inlets (in an alternating manner B-A-B) and one as outlet 170

3.113 Engineering drawing of the electrofusion chamber of the microfluidic system 4: Nine individual channels enter the chamber, each channel gives rise to one partial flow. The nine parallel flows are subsequently reduced in size by hydrodynamic focussing and enter the part of the chamber, which is flanked by electrodes (depicted in blue). The electrodes are leading to patches, where the connection to the power supply can take place. The black rectangle with a dimension of $1 \cdot 1.5\text{cm}^2$ indicates, which part of the chip will be accessible for visual inspection. 171

3.114 Engineering drawing of the 2in-1out microfluidic chip. In this design only two channels enter the chamber, resulting in two parallel laminar cell flows inside the electrofusion chamber. 172

3.115 Schematic depiction of the microfluidic system 4 with two integrated electrodes (9in-1out). 173

3.116 Schematic depiction of the reduced version of the electrofusion chip (2in-1out). . 173

3.117 Schematic depiction of the splitter chip (1in-4out (left) and 1in-5out (right)). . . 173

3.118 Microfluidic electrofusion chip with nine inlets, one outlet and two electrodes (with feed line to contact patches) alongside the rear part of the chamber for the generation of large numbers of hybrids. 174

3.119 Reduced version of the microfluidic electrofusion chip for the study of the fusion process of mammalian cells. 175

3.120 Splitter chip for the use with the microfluidic electrofusion chip to reduce the number of required pumps from nine to two. 176

3.121 Inverted photographs of the electrofusion chamber in the 9in-1out chip (left) and 2in-1out chip (right). 177

3.122 Schematic depiction of the cross sectional area of the chipholder including a ferrule (sealing rubber). 178

3.123 Chipholder from Micronit: A) The capillaries were threaded through the top plate of the chipholder and received a ferrule at their ends. B) The assembled chipholder for the splitter chip has two inlets and 9 outlets. C) Micronit's chipholder was costumised for the application with electrofusion chips and received a see-through window for observation of the fusion process. 179

3.124 The electrofusion chip with chipholder can easily be placed on an inverted microscope, whereas the splitterchip can be placed elsewhere. 180

- 3.125 Overview of the set-up for electrofusion experiments. 181
- 3.126 Fluorescent micrographs of the laminar flow situation inside a 9in-1out electrofusion chip. The electrodes in the middle of the fusion chamber appear in white, due to reflection on the gold surface. 182
- 3.127 Cell flow system 4: The selected pictures have been extracted from a movie which shows the cell flow within a 9in-1out electrofusion chip. This movie is available on the enclosed DVD. 183
- 3.128 Size distribution of MCF-7 cells: The size distribution represented a Gauss curve (yellow) with a mean cell diameter of about $15\mu m$. After different time intervals of incubation in hypoosmolar buffer ($90mOsmol/kg$) the size of the cells increased and the distribution curves were shifted to the right. 187
- 3.129 SEM pictures of dendritic cells incubated for different time intervals in hypoosmolar buffer: A) shows a dendritic cell in an isoosmolar solution. B) After an incubation of 30 minutes in a hypoosmolar buffer ($90mOsmol/kg$) the dendritic cells lost their dendrites and obtained a smoother surface. C) After 120 minutes of incubation the DCs were heavily swollen and assumed a rounded form. 188
- 3.130 Cell alignment of KG-1 cells in a standard electrofusion chamber with two electrodes with a separation distance of $200\mu m$: A) The cells were aligned by an alternating field ($500V/cm$ for $30sec$). B+C) Subsequently, a d.c. pulse of $1.8kV/cm$ is applied for $20\mu s$ and the pearl chains are stretched by the electrodeformation force. Upon removal of the field, the pearl chains assume their original shape. 190
- 3.131 Cell alignment (KG-1) by dielectrophoresis in a standard electrofusion chamber with to Platinum electrodes with a separation distance of $200\mu m$: The selected pictures have been extracted from a movie, which shows the alignment of the cells in pearl chains. This movie is available on the enclosed DVD. 191
- 3.132 Cell alignment (KG-1) by dielectrophoresis in the newly developed electrofusion chamber based on immobilisation: The selected pictures have been extracted from a movie, which shows that cell alignment was successful. This movie is available on the enclosed DVD. 192

- 3.133 Cell alignment (KG-1) by dielectrophoresis in the newly developed microfluidic electrofusion chamber: The selected pictures have been extracted from a movie, which shows the alignment of cells in flow. This movie is available on the enclosed DVD. 193
- 3.134 FACS analysis of a fusion process. Measurements before and after fusion pulse application are shown. The fusion partners are stained with CMFDA green and CMTMR orange to distinguish the two populations by means of FACS. 195
- 3.135 FACS analysis of DCs and the breast cancer cell line MCF-7. An antibody pair was found (CD71 and HLA-DR), which can be used after fusion to distinguish between the two fusion partners and hybrids by means of FACS. 196
- 3.136 Series of pictures taken within 1min , which show the lysis of KG-1 cells in the electrofusion chamber based on immobilisation. The white arrows in A) mark the cells, which were lysed by the application of one pulse of 2.5kV/cm for $25\mu\text{s}$ 198
- 3.137 Homologous fusion of T47D breast cancer cells 198
- 3.138 Fusion Phases: The selected pictures have been extracted from a movie, which shows the evolution of the fusion process between two adjacent KG-1 cells. Details from a series of images captured at times of 1 to 60sec after pulse application. This movie is available on the enclosed DVD. 199
- 3.139 Shifting of cell populations in connection with the treatment with a fusion pulse. The displacement of the populations in the FACS dot plot increases with the applied voltage. 202
- 3.140 Correction of the cell population displacement by adjusting the dot plot quadrants according to a pre-fused negative control 202
- 3.141 Activation of positive T-cells (CD3) was assessed by CD25 (α -chain of the IL-2 receptor) staining after 4 days of co-cultivation in a MLR. Shown is one representative donor out of two. The experiments were made in triplicates and results are presented as mean \pm SD. 205
- 3.142 Activation of positive T-cells (CD3) was assessed by CD71 (transferrin receptor) staining after 4 days of co-cultivation in a MLR. Shown is one representative donor out of two. The experiments were made in triplicates and results are presented as mean \pm SD. 205

3.143 Proliferation of autologous T-cells stimulated with DCs pulsed together with MCF-7 cells or DCs loaded with pulsed MCF-7. Dendritic cells loaded with a MCF-7 lysate were used as control. Shown is one representative donor out of two. 208

3.144 Expansions of different cytotoxic T-cell (CTL, CD8⁺) subsets obtained from autologous T-cell stimulation (see figure 3.143). 208

5.1 Comparison of papers reporting tumour cell/DC fusion 244

5.2 Continuation of Table from figure 5.1 245

5.3 Three representative dot plots of FACS analysis of fusion processes. 247

6.1 Three representative dot plots of FACS analysis of fusion processes. 254

List of Tables

2.1	Impact of autologous versus allogeneic fusion composition on TAA presentation	15
2.2	Scaling derived from physical parameters (L: length, T: time, M: mass)	25
3.1	Increase in cell size by incubation in hypoosmolar buffer with an osmolarity of $90mOsmol/kg$ for 30 minutes. The increase in cell volume is calculated from the cell diameter.	189
3.2	Permeabilisation of MCF-7 cells as subject to different cellular stains	195
3.3	Optimised fusion parameters for different cell types	201
3.4	Memory T-cell subsets	209
5.1	Comparison of Immobilisation and Microfluidic approach	241
7.1	Materials for the mask preparation	255
7.2	Materials for the master preparation	256
7.3	Materials for the PDMS stamp preparation	256
7.4	Materials for direct microcontact printing	257
7.5	Materials for inverse microcontact printing	257
7.6	Materials for immobilisation reaction	258
7.7	Antibodies used for immobilisation	258
7.8	Materials for ellipsometry	259
7.9	Materials for LOR processing	260
7.10	Parameters for laser processing	261
7.11	Materials for laser processing	261
7.12	Materials for laser processing	262
7.13	The Components of the Pump Station	263
7.14	Initialisation and valve commands for Cavro digital pump	264

7.15	Important commands for Cavro digital pump	265
7.16	Overview of important commands for Cavro Smart Valve	266
7.17	Additives for the connection of the microfluidic chip to the pump station and power supply	268
7.18	SPHERO fluorescent particles	268
7.19	Components for the electrofusion of mammalian cells	269
7.20	Mixed leukocyte reaction	270
7.21	Materials for the preparation of tumour cell lysate	270
7.22	Materials utilized for the autologous stimulation of T cells with lysate-pulsed dendritic cells	271
7.23	Materials for the cultivation of breast carcinoma cell lines	272
7.24	Materials for DC generation and maturation	274
7.25	Materials and solutions used for the cryopreservation of primary cells	275
7.26	Antibodies used for surface protein analysis	276
7.27	Dyes used for the intracellular labelling of mammalian cells	277
7.28	Materials for scanning electron microscopy	278
7.29	Formulation of phosphate buffered saline (PBS), which is an isotonic solution and not nutritionally complete. The pH was adjusted to 7.3. The solution was autoclaved for 30min.	278
7.30	Formulation of EDTA buffer. The pH was adjusted to 7.3. The solution was autoclaved for 30min.	278

Bibliography

Abidor, I.G. and Sowers, A.E. (1992) Kinetics and mechanism of cell membrane electrofusion. *Biophys. J.* 61, 1557-1569.

Acuto, O. and Michel, F. (2003) CD28-mediated Co-stimulation: a Quantitative Support for TCR Signalling. *Nature Reviews Immunology* 3, 939-951.

Andersson, H. and van den Berg, A. (2003) Microfluidic devices for cellomics: a review. *Sensors and Actuators B* 92, 315-325.

Armstrong, A.C., Eaton, D. and Ewing, J.C. (2001) Cellular Immunotherapy for Cancer. *British Medical Journal* 323, 1289-1293.

Bär, S. (2001) Menschenversuche mit Göttinger Gebräu? Impfstoff gegen Nierenzellkarzinom im Zwielicht. *Laborjournal* 7-8.

Bakker Schut, T.C., Kraan, Y.M., Barlag, W., de Leij, L., de Grooth, B.G. and Greve, J. (1993) Selective Electrofusion of Conjugated Cells in Flow. *Biophysical Journal* 65, 568-572.

Banchereau, J. and Steinman, R.M. (1998) Dendritic Cells and the Control of Immunity. *Nature* 392, 245-252.

Barbuto, J.A.M., Ensina, L.F.C., Neves, A.R., Bergami-Santos, P.C., Leite, K.R.M., Marques, R., Costa, F., Martins, S.C., Camara-Lopes, L.H. and Buzaid, A.C. (2004) Dendritic cell-tumor cell hybrid vaccination for metastatic cancer. *Cancer Immunol Immunother* 53, 1111-1118.

Barratt-Boyes, S.M. and Fidgor, C.G. (2004) Current issues in delivering DCs for immunotherapy. *Cytotherapy* 6, 105-110.

Barrau, C., Teissié, J. and Gabriel, B. (2004) Osmotically induced membrane tension facilitates the triggering of living cell electropermeabilization. *Bioelectrochemistry* 63, 327-332.

Belz, G.T., Smith, C.M., Bharadwaj, M., Rice, A.M. and Jackson, D.C. (2004) DCs as target for vaccine design. *Cytotherapy* 6, 88-89.

Bhatia, S.K., Shriver-Lake, Kimberly, J.P., Georger, J.H., Calvert, J.M., Bredehorst, R. and Ligler, F.S. (1989) Use of Thiol-Terminal Silanes and Heterobifunctional Crosslinkers for Immobilization of Antibodies on Silica Surfaces. *Analytical Biochemistry* 178, 408-413.

Bocchia, M., Bronte, V., Colombo, M.P., de Vicentiis, A., di Nicola, M., Forni, G., Lanata, L., Lemoli, R.M., Massaia, M., Rondelli, D., Zanon, P. and Tura, S. (2000) Antitumor vaccination: where we stand. *Haematologica* 85, 1172-1206.

Bohnenkamp, H.R. and Noll, T. (2003) Development of a standardized protocol for reproducible generation of matured monocyte-derived dendritic cells suitable for clinical application. *Cytotechnology* 42, 121-31.

Bohnenkamp, H.R., Coleman, J., Burchell, J.M., Taylor-Papadimitriou, J. and Noll, T. (2004) Breast carcinoma cell lysate-pulsed dendritic cells cross-prime MUC1-specific CD8+ T cells identified by peptide-MHC-class-I tetramers. *Cell Immunol.* 1-2, 112-125.

Bora, U., Chugh, L. and Nahar, P. (2002) Covalent immobilization of proteins onto photoactivated polystyrene microtiter plates for enzyme-linked immunosorbent assay procedures. *Journal of Immunological Methods* 268, 171-177.

Chow, W.W.Y., Lei, K.F., Shi, G., Li, W.J. and Huang, Q. (2006) Microfluidic channel fabrication by PDMS-interface bonding. *Smart Mater. Struct.* 15, 112-116.

Dörfel, D., Appel, S., Grünebach, F., Weck, M.M., Mueller, M.R., Heine, A. and Brossart, P. (2005) Processign and Presentation of HLA class I and II epitopes by dendritic cells after transfection with in vitro-transcribed MUC1 RNA. *Blood* 105, 3199-3205.

Efimenko, K., Wallace, W.E. and Genzer, J. (2002) Surface Modification of Sylgard-184 Poly(dimethyl siloxane) Networks by Ultraviolet and Ultraviolet/Ozone Treatment. *J. Colloid and Interface Science* 254, 306-315.

Friedrich, U., Stachowicz, N., Simm, A., Fuhr, G., Lucas, K. and Zimmermann U. (1998) High efficiency electrotransfection with electrodes using microsecond controlled pulses. *Bioelectrochemistry and Bioenergetics* 47, 103-111.

Gabriel, B. and Teissié, J. (1999) Time Courses of Mammalian Cell Electropermeabilization Observed

by Millisecond Imaging of Membrane Property Changes during the Pulse. *Biophysical Journal* 76, 2158-2165.

Ghallab, Y. and Badawy, W. (2004) Sensing Methods for Dielectrophoresis Phenomenon: From Bulky Instruments to Lab-on-a-Chip. *IEEE Circuits and Systems Magazine*

Gottfried, E., Krieg, R., Eichelberg, C., Andreesen, R., Mackensen, A. and Krause, S.W. (2002) Characterization of cells prepared by dendritic cell-tumor cell fusion. *Cancer Immunity* 2, 15.

Gunzer, M., Jänich, S., Varga, G. and Grabbe, S. (2001) Dendritic cells and tumor immunity. *Seminars in Immunology* 13, 291-302.

Ha, B.-Y. (2001) Stabilization and destabilization of cell membranes by multivalent ions. *Physical Review E* 64, 051902.

Haenssle, H.A., Krause, S.W., Emmert, S., Zutt, M., Kretschmer, L., Schmidberger, H., Andreesen, R. and Soruri, A. (2004) Hybrid Cell Vaccination in Metastatic Melanoma - Clinical and Immunologic Results of a Phase I/II Study. *J Immunother* 27 (2), 147-155.

Haritou, M., Yova, D., Loukas; s. (2000) Agents facilitating the electric field-induced fusion of intact rabbit erythrocytes. *Bioelectrochemistry* 52, 229-238.

Hsu, F.J., Benike, C., Fagnoni, F., Liles, T.M., Czerwinski, D. and Taida, B. (1996) Vaccination of Patients with B-cell Lymphoma using Autologous Antigen-pulsed Dendritic Cells. *Nat Med* 2, 52-58.

Huppa, J.B. and Davis, M.M. (2003) T-cell-antigen Recognition and the Immunological Synapse. *Nature Reviews Immunology* 3, 973-983.

Imura, K., Hayashi, T., Yano, Y., Kouhara, J., Ueda, Y., Nakane, K., Matsuura, Y., Takeda, T., Kawai, K. and Yamagishi, H. (2004) Immunogenic reactivity of CTLs induced by electrofusion cells of human dendritic cells and gastric cancer cells. *Gan To Kagaku Ryoho* 31 (11), 1797-1799.

Janeway, C.A., Travers, P., Walport, M. and Shlomichik, M. (2005) *Immunobiology - The immune system in health and disease*. Garland Publishing, New York.

Jantscheff, P., Spagnoli, G., Zajac, P. and Rochlitz, C.F. (2002) Cell fusion: an approach to generating constitutively proliferating human tumor antigen-presenting cells. *Cancer Immunol Immunother* 51, 367-375.

Jarozeski, M. J., Gilbert, R., Fallon, P. G. and Heller, R. (1994) Mechanically Facilitated Cell-Cell Fusion. *Biophysical Journal* 67, 1574-1581.

Jarozeski, M. J., Gilbert, R. and Heller, R. (1994) Detection and Quantification of Cell-Cell Electrofusion Products by Flow Cytometry. *Analytical Biochemistry* 216, 271-275.

Jenne, L., Arrighi, J.-F., Jonuleit, H., Saurat, J.-H. and Hauser, C. (2000) Dendritic Cells Containing Apoptotic Melanoma Cells Prime Human CD8⁺ T-cells for Efficient Tumour Cell Lysis. *Cancer Research* 60, 4446-4452.

Jiang, Z., Wang, M. and Wang, W. (1999) Influence of additives on the protoplasts electrofusion. *Bioelectrochemistry and Bioenergetics* 48, 447-451.

Kane, R.S., Takayama, S., Ostuni, E., Ingber, D.E. and Whitesides, G.M. (1999) Patterning proteins and cells using soft lithography. *Biomaterials* 20, 2363-2376.

Karsten, U., Stolley, P., Walther, I., Papsdorf, G., Weber, S., Conrad, K., Pasternak, L. and Knopp, J. (1988) Direct comparison of electric field-mediated and PEG-mediated cell fusion for the generation of antibody producing hybridomas. *Hybridoma* 7, 627-633.

Kugler, A., Stuhler, G., Walden, P., Zöller, G., Zobywalski, A., Brossart, P., Trefzer, U., Ullrich, S., Müller, C.A., Becker, V., Gross, A.J., Hemmerlein, B., Kanz, L., Müller, G.A. and Ringert, R.-H. (2000) Regression of human metastatic renal cell carcinoma after vaccination with tumour cell-dendritic cell hybrids. *Nature Medicine* 6 (3), 332-336.

Kurokawa, T., Oelke, M. and Mackensen, A. (2001) Induction and Clonal Expansion of Tumor-specific Cytotoxic T Lymphocytes from Renal Cell Carcinoma Patients after Stimulation with Autologous Dendritic Cells loaded with Tumour Cells. *Int. J. Cancer* 91, 749-756

Lanzavecchia, A. and Sallusto, F. (2001) Regulation of T-cell Immunity by Dendritic Cells. *Cell*, 106, 263-266.

Lauer, L., Klein, C. and Offenhäuser, A. (2001) Spot compliant neuronal networks by structure optimized micro-contact printing. *Biomaterials* 22, 1925-1932.

Lee, S.-W.m, Choi, J.-H. and Kim, Y.-K. (1995) Design of a biological cell fusion device. *Solid-State Sensors and Actuators* 1, 377-380.

Lin, Y.-C., Jen, C.-M., Huang, M.-Y., Wu, C.-Y. and Lin, X.-Z. (2001) Electroporation microcips for continuous gene transfection. *Sensors and Actuators B* 79, 137-143.

Lizée, G., Basha, G., Tiong, J., Julien, J.-P., Tian, M., Biron, K.E. and Jefferies, W.A. (2003) Control of dendritic cell cross-presentation by the major histocompatibility complex class I cytoplasmic domain.

Nature Immunology 4, 1065-1073.

Lopéz, E., Guerrero, R., Núñez, M.I., del Moral, R., Villalobos, M., Martínez-Galán, J., Valenzuela, M.T., Muñoz-Gámez, J.A., Olivier, F.J., Matin-Oliva, D., and Ruiz de Almodóvar, J.M. (2005) Early and late skin reactions to radiotherapy for breast cancer and their correlation with radiation-induced DNA damage in lymphocytes. *Breast Cancer Research* 7, 690-698.

Luster, A.D. (2002) The role of chemokines in linking innate and adaptive immunity. *Current Opinions in Immunology* 14, 129-135.

Mourzina, Y., Steffen, A., Kalyagin, D., Carius, R. and Offenhäusser, A. (2005) Capillary zone electrophoresis of amino acids on a hybrid poly(dimethylsiloxane)-glass chip. *Electrophoresis* 26, 1849-1860.

Naqvi, A., Nahar, P. and Gandhi, R.P. (2002) Introduction of Functional Groups onto Polypropylene and Polyethylene Surfaces for Immobilization of Enzymes. *Analytical Biochemistry* 306, 74-78.

Neumann, E., Toensing, K., Kakorin, S., Budde, P. and Frey, J. (1998) Mechanism of Electroporative Dye Uptake by Mouse B Cells. *Biophysical Journal* 74, 98-108.

Nguyen, N.-T. (2004) *Mikrofluidik - Entwurf, Herstellung und Charakterisierung*. Teubner Verlag/GWV Fachverlage GmbH, Wiesbaden.

Nguyen, X.D., Eichler, H., Dugrillon, A., Piechaczek, C., Braun, M. and Klüter, A. (2003) Flow cytometric analysis of T-cell proliferation in a mixed lymphocyte reaction with dendritic cells. *Journal of Immunological Methods* 275, 57-68.

Ohno-Shosaku, T. and Okada, Y. (1984) Facilitation of electrofusion of mouse lymphoma cells by the proteolytic action of proteases. *Biochemical and Biophysical Research Communications* 120, 138-143.

Parajuli, P., Mathupala, S. and Sloan, A.E. (2004) Systematic Comparison of Dendritic Cell-based Immunotherapeutic Strategies for Malignant Gliomas: In Vitro Induction of Cytolytic and Natural Killer-like T-cells. *Neurosurgery* 55, 1194-1204.

Pardoll, D. (2003) Does the Immune System see Tumors as foreign or self? *Annu. Rev. Immunol.* 21, 807-839.

Parkhurst, M.R., DePan, C., Riley, J.P., ROsenberg, S.A. and Shu, S. (2003) Hybrids of Dendritic Cells and Tumor Cells Generated by Electrofusion SIMultaneously Present Immunodominant Epitopes from Multiple Human Tumor-Associated Antigens in the Context of MHC Class I and Class II Molecules. *J Immunol.* 170(10),5317-25.

Piccart-Gebhart, M.J., Procter, M., Leyland-Jones, B., Goldhirsch, Ar., Untch, M., Smith, I.m Gianni, L., Baselga, J., Bell, R., Jakisch, C., Cameron, D., Dowsett, M., Barrios, C.H., Steger, G., Huang, C.-S., Andersson, M., Inbar, M., Lichinitser, M., Láng, I., Nitz, U., Iwata, H., Thomssen, C., Lohrisch, C., Suter, T.M., Rüschoff, J., Sutó, T., Greaorex, V., Ward, C., Straehle, C., McFadden, E., Dolci, S and Gelber, R.D. (2005) Trastuzumab after Adjuvant Chemotherapy in HER2-Positive Breast Cancer. *N Engl J Med* 353, 1659-1672.

Ramos, C. and Teissié, J. (2000) Electrofusion: A biophysical modification of cell membrane and a mechanism in exocytosis. *Biochimie* 82, 511-518.

Reis e Sousa, C. (2004) Activation of dendritic cells: translating innate into adaptive immunity. *Curr Opin Immunol.* 16, 21-25.

Rosenblatt, J., Kufe, D. and Avigan, D. (2005) Dendritic cell fusion vaccines for cancer immunotherapy. *Expert Opin. Biol. Ther.* 5, 703-715.

Sallusto, F., Geginat, J. and Lanzavecchia, A. (2004) Central Memory and Effector Memory T Cell Subsets: Function, Generation and Maintenance. *Annu. Rev. Immunol.* 22, 745-763.

Schmitt, J.J. and Zimmermann, U. (1989) Enhanced hybridoma production by electrofusion in strongly hypo-osmolar solutions. *Biochimica and Biophysica Acta* 983, 42-50.

Scott-Taylor, T.H., Pettengell, R.C ;larke, I., STuhler, G., La Barthe, M.C., Walden, P. and Dalglish, A.G. (2000) Human tumour and dendritic cell hybrids generated by electrofusion: potential for cancer vaccines. *Biochimica et Biophysica Acta* 1500, 265-279.

Sheikh, S.H., Abela, B.A. and Mulchandani, A. (2000) Development of a Fluorescence Immunoassay for Measurement of Paclitaxel in Human Plasma. *Analytical Biochemistry* 283, 33-38.

Shortman, K. and Liu, Y.-J. (2002) Mouse and Human Dendritic Cell Subtypes. *Nature Reviews Immunology* 2, 151-161.

Sia, S.K. and Whitesides, G.M. (2003) Microfluidic devices fabricated in poly(dimethylsiloxane) for biological studies. *Electrophoresis* 24, 3563-3576.

Song, W., Kong, H.L. and Carpenter, H. (1997) Dendritic cells genetically modified with an adenovirus vector encoding the cDNA for a model antigen induce protective and therapeutic antitumor immunity. *J Exp Med* 186, 1247-1256.

Strömberg, A., Ryttsen, F., Chiu, D.T., Davidson, M., Eriksson, P.S., Wilson, C.F., Orwar, O and

- Zare, R.N. (1999) Manipulating the genetic identity and biochemical surface properties of individual cells with electric-field-induced fusion. *PNAS* 97, 7-11.
- Strömberg, A., Karlsson, A., Ryttsén, F., Davidson, M., Chiu, D.T. and Orwar, O. (2001) Microfluidic Device for Combinatorial Fusion of Liposomes and Cells. *Anal. Chem.* 73, 126-130.
- Sugar, I.P., Förster, W. and Neumann, E. (1987) Model of cell electrofusion: Membrane electroporation, pore coalescence and percolation. *Biophysical Chemistry* 26, 321-335.
- Teissié, J., Eynard, N., Gabriel, B. and Rols, M.P. (1999) Electropermeabilization of cell membranes. *Advanced Drug Delivery Reviews* 35, 3-19.
- Teissié, J. and Ramos, C. (1998) Correlation between Electric Field Pulse Induced Long-Lived Permeabilization and Fusogenicity in Cell Membranes. *Biophysical Journal* 74, 1889-1898.
- Thiébaud, P., Lauer, L., Knoll, W. and Offenhäuser, A. (2002) PDMS device for patterned application of microfluids to neuronal cells arranged by microcontact printing. *Biosensors & Bioelectronics* 17, 87-93.
- Thurner, B., Haendle, I., Roeder, C., Dieckmann, D., Keikavoussi, P., Jonuleit, H., Bender, A., Mazcek, C., Schreiner, D., von der Driesch, P., Broecker, E.B., Steinman, R.M., Enk, A., Kämpgen, E. and Schuler, G. (1999) Vaccination with Mage-3A1 Peptide-pulsed Mature, Monocyte-derived Dendritic Cells Expands Specific Cytotoxic T-cells and Induces Regression of Some Metastases in Advanced Stage IV Melanoma. *J. Exp. Med* 190, 1660-1678.
- Tieleman, D.P. (2004) The molecular basis of electroporation. *BMC Biochemistry* 5:10
- Tfrezer, U. and Walden, P. (2003) Hybrid-Cell Vaccines for Cancer Immune Therapy. *Molecular Biotechnology* 25, 63-69.
- Tresset, G. and Takeuchi, S. (2004) A microfluidic device fo electrofusion of biological membranes. *Micro Electro Mechanical Systems, 17th IEEE International Conference on MEMS*, 25-28.
- Trevor, K.T., Cover, C., Ruiz, Y.W., Akporiaye, E.T., Hersh, E.M., Landais, D., Taylor, R.R., King, A.D. and Walters, R.E. (2004) Generation of dendritic cell-tumor cell hybrids by electrofusion for clinical vaccine application. *Cancer Immunol Immunther* 53, 705-714.
- Vermes, I., Haanen, C., Steffens-Nakken, H. and Reutelingsperger, C. (1995) A novel assay for apoptosis, FLOW cytometric detection of phosphatidylserine expression on early apoptotic cells using fluorescein labelled Annexin V. *J of Immun Methods* 184, 39-51.

Vogt, A.K., Lauer, L., Knoll, W. and Offenhäuser, A. (2003) Micropatterned Substrates for the Growth of Functional Neuronal Networks of Defined Geometry. *Biotechnol. Prog.* 19, 1562-1568.

Wang, W.S., Roh, S.I., Lee, B.C., Kang, S.K. et al. (2005) Patient-Specific Embryonic Stem Cells Derived from Human SCNT Blastocytes. *Scienceexpress*, 10.1126.

Wang, Z.-H. and Jin, G. (2004) Covalent immobilization of proteins for the biosensor based on imaging ellipsometry. *J Immunol Methods* 285, 237-243.

Weise, J.B., Maune, S., Görögh, T., Kabelitz, D., Arnold, N., Pfisterer, J., Hilpert, F. and Heiser, A. (2004) A dendritic cell based hybrid cell vaccine generated by electrofusion for immunotherapy strategies HNSCC. *Auris Nasus Larynx* 31, 149-153.

Weise, J.B., Hilpert, F., Heiser, A., Görögh, T., Meyer, J.E., Weimer, J., Krüger, C., Rosenau, A., Wieckhorst, W., Arnold, N., Pfisterer, J., Kabelitz, D. and Maune, S. (2004) Electrofusion Generates Diverse DC-tumour Cell Hybrids for Cancer Immunotherapy. *Anticancer Research* 24, 929-934.

Wooster, R. and Weber, B.L. (2003) Breast and Ovarian Cancer. *N Engl J Med* 348, 2339-47

Zimmermann, U. (1982) Electric field-mediated fusion and related electrical phenomena. *Biochim. Biophys. Acta* 694, 227-277.

Zimmermann, U. (1987) Electrofusion of cells. in Barta, A.H. and Hirshaut, Y., *Methods of hybridoma formation*, Humana Press, Clifton, New Jersey, 97-149.

Zimmermann, U., Friedrich, U., Mussauer, H., Gessner, P., Haemel, K. and Sukhorukov, V. (2000) Electromanipulation of Mammalian Cells: Fundamentals and Application. *IEEE Transactions on Plasma Science* 28, 72-82.